



MONASH University

**Use of Regenerative Ammonium Salt for
Mineral Extraction and CO₂ Mineralisation
from Victorian Brown Coal Fly Ash**

By

SeyyedeH Tahereh Hosseini Dashtikhani

M.Eng. (Chemical)

A thesis submitted in fulfilment of the requirements for the degree

Doctor of Philosophy

Department of Chemical Engineering

Monash University

November 2015

Copyright notice

© Seyyedeh Tahereh Hosseini Dashtikhani, 2015. Except as provided in the Copyright Act 1968, this thesis may not be reproduced in any form without the written permission of the author.

I certify that I have made all reasonable efforts to secure copyright permissions for third-party content included in this thesis and have not knowingly added copyright content to my work without the owner's permission.

Dedicated to:

My wonderful parents, my dearest sister and brother and my beloved husband whom I love the most because they never lose faith in me and give me endless support and encouragement through my whole life.

Contents

Abstract / Summary.....	vi
General Declaration.....	vii
Acknowledgements	ix
List of Publications.....	x
Journal Publications:	x
Refereed Conference Proceedings:.....	x
Abbreviations and Nomenclatures	xi
Abbreviations	xi
Nomenclatures	xii
List of Figures	xiii
List of Tables	xviii
List of Figures in Appendix	xx
List of Tables in Appendix	xx
Chapter 1	1
1.1 Background	1
1.2 Research aims.....	2
1.3 Thesis structure and chapter outline	4
1.3.1 Chapter 1. Introduction	4
1.3.2 Chapter 2. Literature review.....	5
1.3.3 Chapter 3. Multiple cycle leaching-carbonation using regenerative ammonium chloride and leaching kinetic modelling.....	5
1.3.4 Chapter 4. Comparison of leaching characteristics of fresh and weathered fly ash in NH ₄ Cl+HCl and sole HCl.....	5
1.3.5 Chapter 5. Mechanism of competition between Mg ²⁺ and Ca ²⁺ cations upon carbonation.....	6
1.3.6 Chapter 6. Carbonation kinetic modelling and parameter sensitivity analysis.....	6
1.3.7 Chapter 7. Simulation and techno-economic analysis of the overall process.....	6
1.3.8 Chapter 8. Conclusions and Recommendations	7
References	7
Chapter 2	8
2.1 Carbon dioxide emissions: A global concern.....	8
2.2 Mineral carbonation: A potential CO ₂ mitigation option.....	9

2.3 Use of industrial wastes for mineralisation.....	11
2.4 Coal fly ash.....	13
2.5 Different types of mineral carbonation.....	15
2.5.1 Direct carbonation.....	15
2.5.2 Indirect carbonation.....	17
2.6 Industrial mineral carbonation processes and cost estimation.....	22
2.7 Research gap.....	22
References.....	23
Chapter 3	31
3.1 Abstract.....	32
3.2 Introduction.....	32
3.3 Materials and experimental methods.....	35
3.3.1 Materials preparation.....	35
3.3.2 Materials characterisation.....	35
3.3.3 Thermodynamic equilibrium calculation.....	36
3.3.4 Single leaching conditions.....	36
3.3.5 Single carbonation conditions.....	37
3.3.6 Five cycles leaching-carbonation conditions.....	37
3.4 Results and Discussions.....	37
3.4.1 Properties of fly ashes.....	37
3.4.2 Single leaching results.....	38
3.4.3 Five leaching-carbonation cycles.....	41
3.4.3.1 Leaching results.....	41
3.4.3.2 Carbonation results.....	46
3.4.4 Kinetic modelling of magnesium leaching.....	50
3.5 Conclusion.....	54
References.....	55
Chapter 4	60
4.1 Abstract.....	61
4.2 Introduction.....	61
4.3 Materials and experimental methods.....	63
4.3.1 Materials preparation.....	63
4.3.2 Materials characterisation methodologies.....	64

4.3.3 Leaching experiments procedure	65
4.4 Results and Discussions.....	66
4.4.1 Characterisation of raw weathered fly ash	66
4.4.1.1 XRF, QXRD and SEM results	66
4.4.1.2 Mössbauer results for the speciation of iron	70
4.4.2 Sulfur removal upon sodium carbonate washing.....	72
4.4.3 Fresh and weathered fly ash leaching characteristic	72
4.4.3.1 Leaching in $\text{NH}_4\text{Cl}+\text{HCl}$	72
4.4.3.2 Leaching in sole HCl	76
4.4.4 Selective leaching of Mg and Ca over Fe, Al, Si and S by $\text{NH}_4\text{Cl} + \text{HCl}$ solution.....	78
4.5 Conclusion	83
Acknowledgment	83
References	84
Chapter 5	88
5.1 Abstract.....	89
5.2 Introduction.....	89
5.3 Materials and experimental methods	91
5.3.1 Materials.....	91
5.3.2 Characterisation of solid precipitates.....	92
5.3.3 Geochemical modelling	95
5.4 Results and Discussions.....	96
5.4.1 Effect of $\text{Mg}^{2+}/\text{Ca}^{2+}$ molar ratio and reaction time on carbonation at room temperature	96
5.4.2 Characterisation of solid precipitates formed at room temperature.....	98
5.4.2.1 The precipitates from sole Mg^{2+} leachate.....	98
5.4.2.2 The precipitates from the mixture of $\text{Mg}^{2+}+\text{Ca}^{2+}$ and sole Ca^{2+}	100
5.4.3 Effect of temperature on carbonation.....	107
5.4.4 Characterisation of solid precipitate at different temperature	109
5.5 Conclusions.....	111
References	111
Chapter 6	118
6.1 Abstract.....	119
6.2 Introduction.....	119

6.3 Materials and methodologies	121
6.3.1 Experiment methods	121
6.3.2 Modelling methods	122
6.3.2.1 Reaction network and kinetic modelling.....	122
6.3.2.2 Numerical methods.....	124
6.3.3 Methodology for sensitivity analysis	127
6.4 Results and Discussion	128
6.4.1 Calculation of the activation energies for individual reactions	128
6.4.2 Calculation of the reaction constants and orders for individual reactions.....	130
6.4.3 Concentration profiles for individual species at the Mg^{2+}/Ca^{2+} molar ratio of 1 .	134
6.4.4 Sensitivity analysis	135
6.4.4.1 Effect of the initial Mg^{2+} concentration	135
6.4.4.2 Effect of the initial Ca^{2+} concentration.....	137
6.4.4.3 Effect of the initial NH_4OH concentration	138
6.4.4.4 Effect of the initial CO_2 partial pressure	141
6.4. Conclusions.....	143
References	144
Chapter 7	150
7.1 Abstract.....	151
7.2 Introduction.....	151
7.3 Methodology	154
7.3.1 Process description	154
7.3.2 Model development	156
7.3.3 Four proposed scenarios with different process integration	157
7.3.4 Cost estimation methodology	160
7.4 Results and Discussion	162
7.4.1 Comparison of leaching agents in Scenarios 1 and 2.....	162
7.4.2 Comparison of different process integrations in Scenarios 1, 3 and 4.....	164
7.4.3 Economic analysis	167
7.4.3.1 Operating and capital costs	167
7.4.3.2 Effects of HCl amount and flow rate.....	170
7.4.3.3 Effects of fly ash composition.....	172

7.4.3.4 Comparison of CO ₂ capture capacity and cost with other mineral carbonation processes	172
7.4.3.5 Modified cost for Australian context	173
7.4.4 Product utilisation	177
7.4.4.1 NPV, IRR and payback period analysis	177
7.4.4.2 Sensitivity analysis of the effects of the major variables on the NPV, IRR and payback period	179
7.5 Conclusions	181
Acknowledgment	182
References	182
Chapter 8	187
8.1 Conclusions	187
8.1.1 Multiple cycle leaching-carbonation	188
8.1.2 Leaching kinetic modelling	188
8.1.3 Properties and leaching propensity of weathered fly ash	188
8.1.4 Selective leaching of Mg and Ca by NH ₄ Cl+HCl solution	189
8.1.5 Effect of Mg ²⁺ /Ca ²⁺ molar ratio and reaction time on carbonation	189
8.1.6 Composition of carbonate precipitates	189
8.1.7 Effect of temperature on carbonation	189
8.1.8 Techno-economic analysis of different scenarios	190
8.2 Recommendations	190
8.2.1 Investigating the leaching capability and crystallisation affinity of other ammonia salts	190
8.2.2 Pilot scale research	191
8.2.3 Research on application or purification of carbonation products	191
8.2.4 Research on regeneration of HCl	191
8.2.5 Utilisation of other industrial wastes through this process	191
Appendix A	I
Supplementary material – Chapter 5	I
Appendix B	III
Supplementary material – Chapter 6	III
Appendix C	X
Supplementary material – Chapter 7	X
Appendix D	XV

Abstract / Summary

In Victoria, brown coal combustion is the single largest source for energy, meeting greater than 85% of the electricity needs. However this produces approximately 1.3 million tonnes of fly ash annually, which is predominantly dumped into ash ponds. The brown coal fly ash is rich in alkali and alkaline earth metals and transition metals with little aluminium and silicon. Industrial wastes such as fly ash are being considered for CO₂ mineralisation as part of the strategy for carbon dioxide capture, storage and utilisation (CCSU). This process also converts the valueless wastes, into value-added products such as magnesium carbonate and calcium carbonate to replace dolomite in industrial applications. A cost-effective carbon capture process is fundamental for the sustainability of brown coal in the carbon-constrained future. With the continuous increase in the amount of fly ash generated, there is an increasing demand in the use of vast land for landfill, which simultaneously contaminates soil, ground and water. To date, the majority of studies on fly ash utilisation have focused on direct route (single stage leaching and carbonation in the same reactor) under high CO₂ partial pressure with a long reaction time. However, there are a limited number of studies on utilisation of brown coal fly ash through the indirect mineral carbonation route, *i.e.* using separate leaching and carbonation steps.

The scope of this thesis includes, firstly establishing a closed-loop multi-step leaching-carbonation process using regenerative ammonium chloride as the leaching reagent. This process allows efficient extraction of magnesium and calcium from Victorian brown coal fly ash under relatively mild operating condition (<80°C). Secondly, optimising the leaching condition to achieve highest Mg²⁺ and Ca²⁺ extraction yields and detailed modelling on the kinetics of leaching reaction was also conducted. Thirdly, extensive investigations on chemical and morphological changes of weathered fly ash *via* a variety of analytical instruments. The motivation was to understand the weathering process in ash pond and how the weathering affects the mineral carbonation process. In this part, modification of ammonium chloride solution by combining with acid *via* pH control leaching was conducted so as to improve both the extraction yield and selectivity of magnesium and calcium over other metals.

Thirdly, to clarify the competition of Mg²⁺ and Ca²⁺ ions in the leachate upon carbonation, a synthetic leachate was employed to examine the effects of variables including Mg²⁺/Ca²⁺ ratio, reaction time and temperature on the carbonation rate and precipitate composition. Based on the experimental data, a mathematical kinetic model was further developed to quantitatively clarify the interaction and competition between Mg²⁺ and Ca²⁺ cations in the leachate upon carbonation. Finally, a comprehensive energy and techno-economic analysis was conducted to identify the most promising process configurations in terms of energy consumption, product yield and cost.

General Declaration

Monash University

Institute of Graduate Research

Declaration for thesis based or partially based on conjointly published or unpublished work

In accordance with Monash University Doctorate Regulation 17.2 Doctor of Philosophy and Research Master's regulations the following declarations are made:

I hereby declare that this thesis contains no material which has been accepted for the award of any other degree or diploma at any university or equivalent institution and that, to the best of my knowledge and belief, this thesis contains no material previously published or written by another person, except where due reference is made in the text of the thesis.

This thesis includes three original papers published in peer reviewed journals and two submitted journal articles. The core theme of the thesis is the utilisation of Victorian brown coal fly ash using mineral carbonation. The ideas, development and writing up of all papers in the thesis were the principle responsibility of myself; the candidate, working within the Department of Chemical Engineering under the supervision of Dr Lian Zhang, A/Prof Cordelia Selomulya and Dr Nawshad Haque from Mineral resources division in CSIRO.

The inclusion of co-authors reflects the fact that the work came from active collaboration between researchers and acknowledges the input into team-based research.

In the case of the five chapters listed below, my contribution to the work involved the following:

Thesis Chapter	Publication title	Publication status	Nature and extent of candidate's contribution
3	Indirect Carbonation of Victorian Brown Coal Fly Ash for CO ₂ Sequestration: Multiple-Cycle Leaching-Carbonation and Magnesium Leaching Kinetic Modelling	Energy & Fuels, 2014, 28(10), pp 6481–6493	Experiment and analysis work and writing up the paper
4	Chemical and Morphological Changes of weathered Victorian Brown Coal Fly Ash and its Leaching Characteristic upon the Leaching in Ammonia Chloride and Hydrochloric Acid	Hydrometallurgy, 2015, 157, pp 22-32	Experiment and analysis work and writing up the paper
5	Investigating the Effect of Mg ²⁺ /Ca ²⁺ Molar Ratio on the Carbonate Speciation during the Mild Mineral Carbonation Process at Atmospheric Pressure	Energy & Fuels, 2015, 29 (11), pp 7483–7496	Experiment and analysis work and writing up the paper
6	Chemical Kinetic Modelling and Parameter Sensitivity Analysis for the Carbonation of Ca ²⁺ and Mg ²⁺ Under Ambient Conditions	Submitted to Chemical Engineering Journal	Kinetic modelling, writing code in MATLAB and writing up the paper
7	Mineral Carbonation of Victorian Brown Coal Fly Ash Using Regenerative Ammonium Chloride- Process Simulation and Techno-economic Analysis	Submitted to Applied Energy	Simulation, techno-economic analysis and writing up the paper

I have re-numbered sections of submitted or published papers in order to generate a consistent presentation within the thesis.

Signed: 

Date:

.....12/11/2015.....

Acknowledgements

I would like to specially thank my supervisor Dr Lian Zhang for his great support, advice and encouragement from the start of this project. You have been an excellent supervisor throughout the whole PhD work and it has been a pleasure to work with you. Also I would like to express my deepest gratitude to my co-supervisors associated professor Cordelia Selomulya and Dr Nawshad Haque in CSIRO for their valueless advice and support through my PhD study. Pursuing this PhD degree in Monash University improved my knowledge and way of my life a lot and I am very grateful to give this opportunity to me.

I would like to acknowledge the financial support from Monash University and CSIRO funding and scholarship. Without this funding the research would not have been possible.

I also acknowledge my colleagues Billy Han and Lynn Eng for helping me to do some parts of experiments, Teck kwang Choo for being available anytime I needed his help, Bai-qian Dai, Jian Zhang, Wirhan Prationo and Anthony De Girolamo to be good friends and share their experiences with me. I would like to thank Mr Jim Siemon from Latrobe magnesium Ltd for providing fly ash samples and kindly devoting his time to answer my questions. I would like to extend my appreciation to the support and assistance I received from Dr. Shahnaz Mansouri during my early candidature days. An acknowledgement to academic and general staff of Monash university especially Ms Lilyanne price, Ms Jill Crisfield, Ms Kim Phu, Mr Harry Bouwmeester and Mr Ross Ellingham. To my lovely friends in department, Ezzatollah Shamsaei, Shahrouz Taranejoo, Zahra Abbasi, Soroush Shakiba, Azadeh Nilghaz, Ali Bahmanpour, Joanne Tanner, Iman Ghanim and Jia Tang who encouraged me and supported me during the PhD journey.

I would like to thank my beloved mother and father. Their constant support and belief throughout my life helped me to be successful in all parts of my life. Thank you to my dearest sister and brother to support me and believe me, without you I couldn't achieve any success in my life. Finally, I would like to thank Mehdi, my best friend and best husband ever. You have supported me and encouraged me during all difficult moments of my work. Without you and your encouragement I couldn't survive these past three and half years. Also thank you for being my co-worker and sharing your chemical engineering and mathematical modelling knowledge with me.

List of Publications

Journal Publications:

- T. Hosseini**, C. Selomulya, N. Haque, L. Zhang, Indirect Carbonation of Victorian Brown Coal Fly Ash for CO₂ Sequestration: Multiple-Cycle Leaching-Carbonation and Magnesium Leaching Kinetic Modelling, *Energy & Fuels*, 2014, 28(10), pp 6481–6493.
- T. Hosseini**, C. Selomulya, N. Haque, L. Zhang, Chemical and Morphological Changes of Weathered Victorian Brown Coal Fly Ash and its Leaching Characteristic upon the Leaching in Ammonia Chloride and Hydrochloric Acid, *Hydrometallurgy*, 2015, 157, pp 22-32.
- T. Hosseini**, C. Selomulya, N. Haque, L. Zhang, Investigating the Effect of Mg²⁺/Ca²⁺ Molar Ratio on the Carbonate Speciation during the Mild Mineral Carbonation Process at Atmospheric Pressure, *Energy & Fuels*, 2015, 29 (11), pp 7483–7496.

Refereed Conference Proceedings:

- T. Hosseini**, C. Selomulya, N. Haque, L. Zhang, Investigating the mineral carbonation of Mg and Ca-rich leachate for utilisation of Victorian brown coal fly ash, APCChE incorporating Chemeca, 27 September – 1 October 2015, Melbourne, Australia.
- T. Hosseini**, C. Selomulya, N. Haque, L. Zhang, The leaching behaviour of alkaline metals in weathered Victorian brown coal fly using hydrochloric acid and ammonium chloride, Chemeca, 27 September – 1 October 2014, Perth, Australia.
- T. Hosseini**, C. Selomulya, N. Haque, L. Zhang, Comparison of magnesium oxide extraction from Victorian brown coal fly ash and steel-making slag using regenerative ammonium chloride, Chemeca, 27 September – 1 October 2013, Brisbane, Australia.
- T. Hosseini**, C. Selomulya, N. Haque, L. Zhang, Using regenerative ammonium salts to extract and purify magnesium oxide from Victorian brown coal fly ash, WOCA 2013, Kentucky, USA.

Abbreviations and Nomenclatures

Abbreviations

Al	Aluminium
APEA	Aspen process economic analyser
Ca	Calcium
CaCO ₃	Calcium carbonate
CaSO ₄	Calcium ferrite
CCS	Carbon capture and storage
CCSU	Carbon capture, storage and utilisation
CO ₂	Carbon dioxide
DEC	Direct equipment cost
E _a	Activation energy
EPC	Equipment purchase cost
ESP	Electrostatic precipitator
Fe	Iron
GA	Genetic algorithm
GHG	Greenhouse gas
HCl	Hydrochloric acid
Mg	Magnesium
NH ₄ Cl	Ammonium chloride
NH ₄ OH	Ammonium hydroxide
MS	Mössbauer Spectroscopy
MSWI	Municipal Solid Waste Incinerator
NPV	Net present value
PCM	Progressive conversion model
QXRD	Quantitative X-Ray Diffraction
RStoic	Stoichiometric reactor
RT	Room temperature
S	Sulphur
SCM	Shrinking core model
SEM	Scanning Electron Microscopy
SEM/BSE	Backscattered electron of Scanning Electron Microscopy
TGA	Thermogravimetric analysis
XRD	X-Ray Diffraction
XRF	X-Ray Fluorescence

Nomenclatures

a	he stoichiometric coefficient of the reagent in the leaching reaction
A	Fluid in leaching kinetic modelling
B	Solid particle in leaching kinetic modelling
C_A	Concentration (mol/l)
D	Diffusion constant
h	Hour
IAP	Ion activity product
J	Energy (Joule)
k	Reaction rate constant
K_C	The kinetic constant in leaching kinetic modelling
K_{eq}	Equilibrium constant
K_{sp}	Solubility constant
kV	kilovolts
ln	Natural logarithm
L/S	Liquid to solid ratio (g/mL)
M	Molar
mA	Milliampere
M_B	The molecular weight of solid
m	Reaction power
min	minute/ minutes
n	Reaction power
r_0	The initial radius of the solid particle
R^2	Correlation coefficient
W_i	Weight percentage of species i
SI	Saturation index
wt%	Weight percentage
T	Temperature
t	Time
X	Conversion
θ	Theta (notation for angle measured in degrees (°))
γ	Gamma rays
ρ_B	The density of solid
τ_{50}	Reaction time required to reach 50wt% precipitation extent
ΔH	Enthalpy of formation

List of Figures

Chapter 1

Figure 1.1 Proposed closed-loop process in this research

Chapter 2

Figure 2.1 Annual levels of greenhouse gases represented as CO₂-equivalent emissions

Figure 2.2 A schematic overview of a generic mineral carbonation process

Figure 2.3 Conversion of different carbonates during carbonation at different temperatures.

Chapter 3

Figure 3.1 XRD spectra for Hazelwood fly ash and Yallourn fly ash

Figure 3.2 Effect of time and temperature on leaching of magnesium with NH₄Cl 4M, L/S=6, Solid lines represent leaching from pure MgO and dashed lines refer to Hazelwood Fly ash

Figure 3.3 Derivative Mass loss of dried residue against temperature running TGA (Pure MgO leaching at T=80°C, t=1 h)

Figure 3.4 Theoretical and Practical ammonia recovery, dashed lines are related to theoretical ammonia recovery and solid lines corresponds to practical ammonia recovery (Pure MgO leaching, NH₄Cl 4M and L/S=6)

Figure 3.5 Leaching% for Mg during five cycle leaching-carbonation at optimum condition (T=80°C, t=30 min). a) Pure MgO, MgO + CaO and MgO + Fe₂O₃. b) Hazelwood and Yallourn fly ash

Figure 3.6 Leaching% for Ca during five cycle leaching-carbonation at optimum condition (T=80°C, t=30 min), in MgO + CaO, Hazelwood and Yallourn fly ash

Figure 3.7 Thermodynamic equilibrium calculation for different Mg and Ca bearing species in ammonium chloride solution

Figure 3.8 XRD results for first cycle leaching residue and carbonate before and after washing for pure MgO

Figure 3.9 Loss percentage of NH₄Cl at each cycle breaking down to crystallised and complex formed for MgO, MgO + CaO, MgO + Fe₂O₃ and Hazelwood fly ash. Water washing was done at RT, L/S=10 and t=1h

Figure 3.10 Carbonation% for Mg during five cycle leaching-carbonation at optimum condition (T=RT, t=20 min). a) Pure MgO, MgO + CaO and MgO + Fe₂O₃. b) Hazelwood and Yallourn fly ash.

Figure 3.11 Carbonation % for Ca during five cycle leaching-carbonation at optimum condition (T=RT, t=20 min), in MgO + CaO, Hazelwood and Yallourn fly ash

Figure 3.12 SEM images of carbonate obtained from first and last cycle of multiple cycle leaching-carbonation. a) Pure MgO b) MgO + CaO c) MgO + Fe₂O₃ and d) Hazelwood fly ash

Figure 3.13 Effect of time and temperature on leaching of calcium from Hazelwood fly ash

Figure 3.14 Plots for a) pseudo-second order reaction for first 30 minutes of reaction and b) Product layer diffusion for last 30 minutes of reaction.

Figure 3.15 An Arrhenius plot for leaching of MgO with ammonium chloride using pseudo-second order reaction model

Figure 3.16 K values fitting second order model for different cycles of Hazelwood fly ash

Chapter 4

Figure 4.1 Measured and fitted XRD pattern by Siroquant software for fresh and weathered fly ash

Figure 4.2 Composition of fresh fly ash, synthesised fly ash 1 (from synthetic weathering of fresh fly ash), weathered fly ash and synthesised fly ash 2 (from synthetic weathering of weathered fly ash) calculated by QXRD and internal standard method

Figure 4.3 BSE image (magnification 4000 X) and EDX elemental maps of representative particle of weathered fly ash. Elemental maps of Mg (red), Ca (Light blue), O (light green), Si (dark green), Al (Purple) and K (dark blue)

Figure 4.4 Mössbauer spectroscopy fitting results a) fresh fly ash; b) weathered fly ash, 3 sextets + 2 doublets

Figure 4.5 Percentage of different minerals in crystalline phase (Amorphous phase was not considered) before and after sodium carbonate washing of weathered fly ash calculated by QXRD.

Figure 4.6 Leaching yields of Mg and Ca (target elements) and Fe, Al, Si and S (interfering elements) from fresh fly ash and weathered fly ash using NH_4Cl 4M, $T=80^\circ\text{C}$ and $t=30$ min at a) pH 5-5.5 and b) <4.5

Figure 4.7 Leaching of major elements from weathered fly ash as a function of leaching time (Ammonium chloride pH controlled condition $\text{pH}<4.5$, $T=80^\circ\text{C}$)

Figure 4.8 Leaching of major elements from weathered fly ash as a function of temperature (Ammonium chloride pH controlled condition $\text{pH}<4.5$, $t=40$ min)

Figure 4.9 Total Fe in each area before and after leaching, taken from Mössbauer spectra

Figure 4.10 Mössbauer spectroscopy fitting results $\text{NH}_4\text{Cl}+\text{HCl}$ leached residue

Figure 4.11 Leaching yields of a) Mg and Ca (target elements) and b) Fe, Al, Si and S (Interfering elements) as a function of initial L/S ratio from weathered fly ash using NH_4Cl 4M, $T=\text{RT}$ and $t=40$ min at $\text{pH}<4.5$

Figure 4.12 Leaching yields of Mg, Ca, Fe, Al, Si and S from fresh fly ash and weathered fly ash using HCl 1M without control pH ($T=\text{RT}$ and $t=30$ min and $L/S=6$)

Figure 4.13 Effect of temperature on hydrochloric acid leaching of Mg, Ca and Fe from weathered fly ash ($L/S = 6$, $t=30$ min, $\text{HCl} = 1\text{M}$)

Figure 4.14 Leaching behaviour of a) Mg and Ca and b) other metals Fe, Si and Al in different pH of $\text{NH}_4\text{Cl}+\text{HCl}$ and sole HCl solution

Figure 4.15 BSE images magnification 5000 X of typical particles L1 and L2 obtained from $\text{NH}_4\text{Cl}+\text{HCl}$ (top) and L3 and L4 from sole HCl (bottom) leaching residue of weathered fly ash

Chapter 5

Figure 5.1 Comparison of QXRD results with actual mass percentages for two pure oxides in their mixtures, a) Fe_2O_3 and b) SiO_2 at different mixing ratios

Figure 5.2 Amorphous percentage inside fly ash sample based on different amount of internal standard

Figure 5.3 a) Mg and b) Ca carbonation yield of different $\text{Mg}^{2+}/\text{Ca}^{2+}$ ratio at room temperature as a function of time

Figure 5.4 Correlation between the molar ratio of $\text{Mg}^{2+}/(\text{Mg}^{2+}+\text{Ca}^{2+})$ and $1/\tau_{50}$ for the precipitation of two cations.

Figure 5.5 XRD pattern for the carbonation precipitate of sole Mg^{2+} after 10 min reaction time, Unfitted with potential Mg-bearing minerals from MDI Jade database

Figure 5.6 Measured and calculated XRD patterns for the carbonation of different molar ratios of $\text{Mg}^{2+}/\text{Ca}^{2+}$ at 5 min reaction time (V : Vaterite, C : Calcite and Magnesian calcite, A : Aragonite)

Figure 5.7 The enlarged XRD patterns for magnesian calcite peak positions for different $\text{Mg}^{2+}/\text{Ca}^{2+}$ ratios compared to pure calcite after 10 min reaction time

Figure 5.8 Solid precipitate composition of carbonation of a) $\text{Mg}^{2+}/\text{Ca}^{2+}=2/1$, b) $\text{Mg}^{2+}/\text{Ca}^{2+}=1/1$, c) $\text{Mg}^{2+}/\text{Ca}^{2+}=1/2$, d) Sole Ca^{2+} , at room temperature calculated by QXRD and internal standard method.

Figure 5.9 Percent of a) amorphous phase and b) magnesian calcite in precipitates formed from the carbonation of different ratios of $\text{Mg}^{2+}/\text{Ca}^{2+}$ as a function of reaction time

Figure 5.10 The mass fraction of MgCO_3 in magnesian calcite for different ratios of $\text{Mg}^{2+}/\text{Ca}^{2+}$ as a function of reaction time

Figure 5.11 TGA - DTG mass loss curves of solid carbonate precipitates compared with pure MgCO_3 and $\text{Mg}(\text{OH})_2$ decomposition after 20 min reaction time

Figure 5.12 Effect of temperature and time on a) Mg and b) Ca carbonation for case 3 ($\text{Mg}^{2+}/\text{Ca}^{2+}$ equal to 1/1)

Figure 5.13 Influence of temperature on the $1/\tau_{50}$ (carbonation rate to achieve 50wt% precipitation extents) of two cations at a molar ratio of 1 in solution

Figure 5.14 Solid precipitate composition of carbonation of $\text{Mg}^{2+}/\text{Ca}^{2+}=1/1$ at different temperatures a) 25°C, b) 40°C, c) 60°C and d) 80°C calculated by QXRD and internal standard method.

Figure 5.15 Mass fractions of amorphous, magnesian calcite and aragonite in solid precipitate as a function of temperature at the fixed reaction time of 10 min

Chapter 6

Figure 6.1 A simplified flowchart for the kinetic modelling steps and methods

Figure 6.2 Comparison of a) Mg^{2+} and b) Ca^{2+} actual experimental precipitation yield (%) and predicted precipitation yield (%) calculated by model at different temperatures and a fixed $\text{Mg}^{2+}/\text{Ca}^{2+}$ molar ratio of 1

Figure 6.3 Comparison of Mg^{2+} (left panel) and Ca^{2+} (right panel) carbonation for *a)* $Mg^{2+}/Ca^{2+}=2/1$ and *b)* $Mg^{2+}/Ca^{2+}=1/2$ from experimental data (data points) and modelling data (solid lines), Experimental data are collected at room temperature.

Figure 6.4 The mass fraction of magnesian calcite in the total precipitate as a function of time for Mg^{2+}/Ca^{2+} ratio of 2/1, 1/1 and 1/2 calculated by experimental (points) and modelling data (solid lines). Experimental data were collected at room temperature.

Figure 6.5 *a)* Experimental (points) and predicted pH and concentrations (line) of *b)* CO_2 (aq) and CO_3^{2-} , *c)* HCO_3^- , *d)* NH_4^+ and NH_4OH , *e)* Mg^{2+} , $MgCO_3$ and $Mg_NCa_{(1-N)}CO_3$, *f)* Ca^{2+} , $CaCO_3$ and $Mg_NCa_{(1-N)}CO_3$.

Figure 6.6 Concentrations of *a)* Mg/Ca-bearing species and *b)* NH_4^+ , NH_4OH and HCO_3^- as a function of initial Mg^{2+} concentration in the solution at 30 min reaction time (temperature, Ca^{2+} and NH_4OH concentration and CO_2 pressure remained constant at room temperature, 0.68 and 3.18 mol/L and 1 atm respectively)

Figure 6.7 Concentrations of different Mg- and Ca-bearing species as a function of initial Ca^{2+} concentration in the leachate in 30 min (Other parameters were fixed as room temperature, initial Mg^{2+} 0.68mol/L, initial NH_4OH 3.18mol/L and CO_2 pressure 1 atm)

Figure 6.8 Concentrations of Mg- and Ca-bearing species in the solution at different NH_4OH concentrations at 30 min reaction time (equal Mg^{2+} and Ca^{2+} concentrations of 0.68 mol/L, room temperature and atmospheric CO_2 pressure)

Figure 6.9 Concentration profile of *a)* NH_4OH , *b)* NH_4^+ , *c)* HCO_3^- , *d)* $MgCO_3$, *e)* $CaCO_3$ and *f)* $Mg_NCa_{(1-N)}CO_3$ upon the change of the initial ammonia concentration by a factor of 2, 4, 1/2 and 1/4. (equal Mg^{2+} and Ca^{2+} concentrations of 0.68 mol/L, CO_2 pressure of 1 atm, room temperature and x refers to the ammonia concentration at reference case (3.18 mol/L))

Figure 6.10 Concentrations of different Mg- and Ca-bearing species as a function of the initial CO_2 pressure in 30 min (equal Mg^{2+} and Ca^{2+} concentrations of 0.68 mol/L, room temperature and NH_4OH concentration of 3.18 mol/L)

Figure 6.11 Concentration profile for *a)* HCO_3^- , *b)* CO_3^{2-} , *c)* CO_2 (aq), *d)* $MgCO_3$, *e)* $CaCO_3$ and *f)* $Mg_NCa_{(1-N)}CO_3$ at different initial CO_2 pressure (Equimolar Mg^{2+} and Ca^{2+} concentrations (0.68 mol/L), room temperature, NH_4OH concentration of 3.18 mol/L)

Chapter 7

Figure 7.1 Proposed block flow diagram and system boundary for mineral carbonation of Victorian brown coal fly ash

Figure 7.2 Simplified diagram for Scenario 1 (NH_4Cl leaching), Scenario 2 ($NH_4Cl+HCl$ leaching), Scenario 3 (NH_4Cl leaching with leaching waste recycling) and Scenario 4 (Multiple cycle leaching)

Figure 7.3 Aspen Plus flowsheet for Scenario 1

Figure 7.4 Aspen Plus flowsheet for Scenario 2

Figure 7.5 Product yield as a function of the fresh fly ash flow rate in the case of recycling the leaching waste (Scenario 3) compared with the case without recycling (Scenario 1-indicated by two single points at 25t/h)

Figure 7.6 Chemical composition of the solid waste obtained from the final leaching stage of scenario 4

Figure 7.7 Comparison of the amount of products and chemicals used for Scenarios 1, 2 and 4

Figure 7.8 Breakdown of the capital costs for different scenarios

Figure 7.9 Total operating cost and breakdown for the operating items per year in the evaluated scenarios

Figure 7.10 Chemicals cost per tonne of fly ash or per tonne of product as a function of the HCl flow rate

Figure 7.11 Comparison of the *a*) capital cost and *b*) operating cost calculated from the Aspen process economic analyser (APEA) and the new cost alternative method for the different scenarios

Figure 7.12 Production cost sensitivity to the economic parameters for Scenario 1

Figure 7.13 Cumulative discounted cash flow analysis over the lifetime of the project for Scenario 1 (NH₄Cl leaching), Scenario 3 (waste recycling) and Scenario 4 (multi-stage leaching)

Figure 7.14 Sensitivity analysis on the effects of the production cost, selling price of the product and capital cost on the a) NPV; b) IRR; and c) Payback period for Scenario 1

List of Tables

Chapter 2

Table 2.1 Potential CO₂ sequestration capacity on the basis on elementary composition of selected residues

Table 2.2 Fly ash generation and utilisation in different countries

Table 2.3 Elemental quantification of Australian Brown and Black Coal Fly Ash

Table 2.4 Direct mineral carbonation results for slag and fly ash from selected literature

Chapter 3

Table 3.1 Waste minerals elemental quantification (XRF)

Table 3.2 NH₄Cl concentration at start point of each cycle for MgO, MgO+CaO, MgO+Fe₂O₃, Hazelwood Fly ash

Table 3.3 Elemental point analysis of representative precipitates particles obtained from first and last cycle of five cycle leaching carbonation of pure MgO, MgO+CaO, MgO+Fe₂O₃ and Hazelwood fly ash determined by EDX

Table 3.4 Different Mg and Ca-bearing minerals detected by XRD for the first and last cycle of carbonation obtained from multiple cycle leaching carbonation of pure MgO, MgO+CaO, MgO+Fe₂O₃ and Hazelwood fly ash

Table 3.5 Dissolution rate and R² using Reaction controlled model, Diffusion control model and Mixed reaction and diffusion control model

Chapter 4

Table 4.1 Summary of leaching experiments conditions carried out for fly ash

Table 4.2 Elemental Quantification of major elements in fresh fly ash, weathered fly ash, synthesised fly ash 1 (from synthetic weathering of fresh fly ash) and synthesised fly ash 2 (from synthetic weathering of weathered fly ash)

Table 4.3 Hyperfine parameters determined by Mössbauer spectrum fitting for fresh and weathered fly ash

Table 4.4 XRD quantification of NH₄Cl+HCl and sole HCl residues from leaching of weathered fly ash

Table 4.5 Elemental composition of representative leaching residue particles L1 and L2 (NH₄Cl+HCl leached) and L2 and L3 (HCl leached) determined by EDX

Chapter 5

Table 5.1 Summary of different ratios of Mg²⁺/Ca²⁺ in carbonation experiments

Table 5.2 Log IAP and Saturation index (SI) calculated by MINTEQ for possible minerals in precipitate obtained from carbonation of sole Mg²⁺

Table 5.3 Chi-square value for selected Siroquant fitting

Table 5.4 XRD fitting parameters of major peak at ($2\theta\sim 28.5-31$) extracted from JADE for precipitates at different Mg^{2+}/Ca^{2+} ratios and sole Ca at 10 min reaction time

Table 5.5 Comparison of QXRD results and XRF results for the MgO contents in the carbonate precipitates formed from different Mg^{2+}/Ca^{2+} ratios at 30 min reaction time

Chapter 6

Table 6.1 Equilibrium constants for reactions 1 to 10

Table 6.2 Sensitivity analysis parameters

Table 6.3 Activation energies of each reaction estimated by GA compared with literature

Table 6.4 Kinetic parameters fitted by experimental data obtained at different Mg^{2+}/Ca^{2+} ratios and comparison with the other carbonation models reported in literature

Chapter 7

Table 7.1 Typical compositions of Hazelwood fly ash

Table 7.2 Assumptions used within the Aspen plus simulation for the unit operations

Table 7.3 Economic inputs to Aspen process economic analyser (APEA)

Table 7.4 Material and energy balance for Scenarios 1 (NH_4Cl leaching) and 2 ($NH_4Cl+HCl$ leaching)

Table 7.5 Chemical consumption and purchasing cost of the evaluated scenarios

Table 7.6 Operating cost per tonne of fly ash as well as the produced and captured CO_2 for the different scenarios evaluated

Table 7.7 Comparison of the operational parameters and cost of the lowest and highest HCl flow rates evaluated in this study

Table 7.8 Comparison of the operational parameters and cost of fresh and weathered fly ash leaching using NH_4Cl as the leaching agent (Scenario 1)

Table 7.9 Comparison of the CO_2 capture capacity of various fly ashes with Victorian brown coal fly ash

Table 7.10 Capital cost of Scenario 1 (NH_4Cl leaching) using the new cost alternative based on the Australian local market price

Table 7.11 Operating cost of Scenario 1 (NH_4Cl leaching) using the new cost alternative based on the Australian local market price

Table 7.12 Financial indices calculated using the cash flow analysis for Scenario 1 (NH_4Cl leaching), Scenario 3 (waste recycling) and Scenario 4 (multi-stage leaching)

List of Figures in Appendix

Figure A.1 XRD spectrum for Fe_2O_3 and SiO_2 mixture at different mass ratios (From top to bottom $\text{SiO}_2 + 2.5\%$, 5% , 10% and $20\% \text{Fe}_2\text{O}_3$); black solid line represents observed data and red dot line shows Siroquant fitting

Figure A.2 XRD spectrum for fly ash mixed with different proportions of corundum

Figure C.1 Aspen simulation for scenario 2 ($\text{NH}_4\text{Cl} + \text{HCl}$ leaching)

Figure C.2 Aspen simulation for scenario 3 (leaching waste recycling)

Figure C.3 Aspen simulation for scenario 4 (multi-stage leaching)

List of Tables in Appendix

Table A.1 QXRD and XRF results of fly ash mixed with different percentage of Al_2O_3 and amorphous amount calculated

Table C.1 Pump sizing and detailed design for the first scenario

Table C.2 Reactor sizing and detailed design for the based case scenario

Table C.3 Separation unit sizing and detailed design for the based case scenario

Table C.4 Vessel sizing and detailed design for the based case scenario

Chapter 1

Introduction

1.1 Background

Fossil fuels are expected to remain as the main energy source for the foreseeable future. It is postulated that the current global warming is the result of an increase in anthropogenic greenhouse gas (GHG) emissions, particularly CO₂ emission from fossil fuel combustion [1]. The reduction of CO₂ emissions in process industries is challenging. Carbon Capture Storage (CCS) can be defined as the separation and capture of CO₂ produced at stationary sources, followed by transport and storage in geological reservoirs or the ocean in order to prevent its emission to the atmosphere [2]. Among all of these methods to sequester CO₂, mineral carbonation is one of the most promising processes, in which the CO₂ reacts with minerals or industrial waste to produce thermodynamically stable carbonates [3].

Mineral carbonation technologies can be divided into two main categories: single step (direct) and multiple steps (indirect) carbonation. Direct method involves the reaction of a feedstock material with CO₂, which is usually injected in a reactor maintained at a controlled temperature and pressure. Minerals require energy-intensive pre-treatments, such as fine grinding, heat treatments, and chemical activation to provide adequate conversions and reaction kinetics [4]. Indirect carbonation has also been developed where chemicals are used to first extract the reactive components (*e.g.* pure metal oxide) from the feedstock, which subsequently react with CO₂ for carbonation.

This technology involves the precipitation of stable carbonate compounds, such as calcium carbonate (CaCO₃) and magnesium carbonate (MgCO₃). Many natural minerals containing large amounts of primary cations (Ca²⁺ and/or Mg²⁺), such as olivine (Mg,Fe)₂SiO₄ and wollastonite (CaSiO₃) as well as certain industrial wastes, such as fly ash, blast furnace and steel-making slag have been evaluated for use as raw materials for mineral carbonation [5].

To date, most of the research on the utilisation of waste minerals using indirect mineral carbonation have been focused on optimising the conditions for leaching and the subsequent

carbonation. Considering the broad variation of the properties of industrial wastes, it is still with doubt that the methods developed in the literature are applicable to any new sample. In addition, there has been little research regarding the effect of impurities on the whole process and the quality of the final products. Nearly all the works described in literature were based on the usage of single stage processes and fresh reagents that differ from industry where recycling of reagents needs to be maximised to ensure cost-effectiveness and minimum impact to the ecological system.

Considering the increasing trend of demand for fly ash in different applications, the landfilled fly ash, as a supplement to the fresh ash derived from a power plant, has also been considered so as to empty the historical ash landfilled sites. There has been no information available on the properties of weathered Victorian brown coal fly ash stored in the landfills and its potential for utilisation through CO₂ sequestration process. CCS has been in operation in various industries for several decades but it is still an emerging technology in the power generation sector which rarely has been commercialised in large scale. Energy consumption, reaction rate, thermodynamics and high cost of material handling are the crucial factors hindering the commercialisation of this technology [5-7]. Two of the main issues that needs to be overcome for full scale application of this technology are the high cost of leaching agent and energy requirements associated with industrial waste-to-carbonate pathway [8]. In order to make such a process economically and environmentally sustainable, the chemicals used in the process should be regenerated within the process itself [9].

This work focuses on the utilisation of Victorian brown coal fly ash using regenerative ammonium salts. The aim of this PhD research program is to maximise the extraction of magnesium and calcium out of these zero-value wastes, and subsequently to achieve a stable and permanent CO₂ capture/storage using the extracted alkaline earth metal cations and to simultaneously produce value-added solid production including carbonate and cement additive. Three phases were proposed for the research program: the first phase focusing on batch-scale experimental investigation to separately optimise the conditions for two single steps, leaching and carbonation upon multiple cycle tests, other than a single once-through test; the second phase clarifying the reaction mechanisms and kinetics underpinning the two sub-processes; and the final phase concentrating on the techno-economic analyses to address the costs to identify the most promising configuration of the developed process.

1.2 Research aims

The overall aim of this project was to develop a process under mild operating condition (*i.e.* Temperatures 25-80°C and atmospheric pressure) for the cost-effective and efficient utilisation of Victorian brown coal fly ash. This process relies on capturing CO₂ produced from coal

combustion in power plants *via* a two-step indirect CO₂ mineralisation route to convert these zero-value wastes to value-added high-purity products. The specific aims are summarised as:

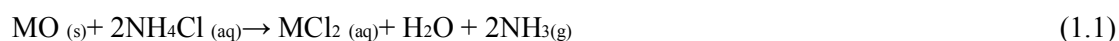
1- Experimental investigation to optimise the conditions for maximum extraction yields of both Mg²⁺ and Ca²⁺ from mineral wastes, the carbonation of the extracted Mg²⁺ and Ca²⁺ cations, and the mass flow of overall and individual elements upon the integration of leaching and carbonation steps in the closed circuit for multiple cycling.

2- Experimental investigation to understand weathered fly ash properties and its leaching characteristic in NH₄Cl+HCl and sole HCl solution. This study was conducted to assess if the weathered fly ash could replace fresh fly ash in mineral carbonation process. Additionally, the modification of ammonium chloride leaching capability was assessed by combining it with HCl doping to improve both the extraction yields and selectivity of calcium and magnesium.

3- Clarification of the reaction mechanisms and kinetics underpinning the two-sub processes: leaching and carbonation. The reaction mechanisms to be clarified, include the competition between CaO and MgO upon leaching, and the competition of their respective cations upon carbonation in the aqueous system, as a function of the variables including temperature, Mg²⁺/Ca²⁺ ratio, reaction time, mass flow rate of each cation and reagent loss upon multiple recycle.

4- Process simulation and techno-economic analysis of the different configurations of the process mentioned above to address the cost and viability of this process from an operating and economical viewpoint.

A closed loop process shown in **Figure 1.1** forms the scope of this project. It consists of two sequential stages: leaching and carbonation. Reactions (1.1) and (1.2) can be employed for the extraction of alkaline earth metals from metal sources by leaching and the carbonation reaction. In these two reactions, M refers to the alkaline earth metals (Ca²⁺ and Mg²⁺) in fly ash.



In the leaching stage of the proposed process in **Figure 1.1**, ammonium chloride was used to dissolve MgO and CaO by reaction (1.1). The released ammonia gas was captured in a water tank. After the solid-liquid separation, two phases were achieved, the solid phase rich in the unreacted elements and a liquid phase (leachate) rich in Mg²⁺ and Ca²⁺ in the chloride form. By adjusting the pH of the leachate through the use of ammonia water (ammonia, generated from leaching step) and the continuous injection of CO₂ into the aqueous solution, MgCl₂ and CaCl₂ were expected to precipitate as solid carbonate, while also ensuring NH₄Cl to be regenerated for next round. These two sequential reactions form a closed loop in which the only inputs are,

industrial wastes ash and CO₂ discharged from power plant as flue gas, while the ammonium salt theoretically remains in the loop without consumption.

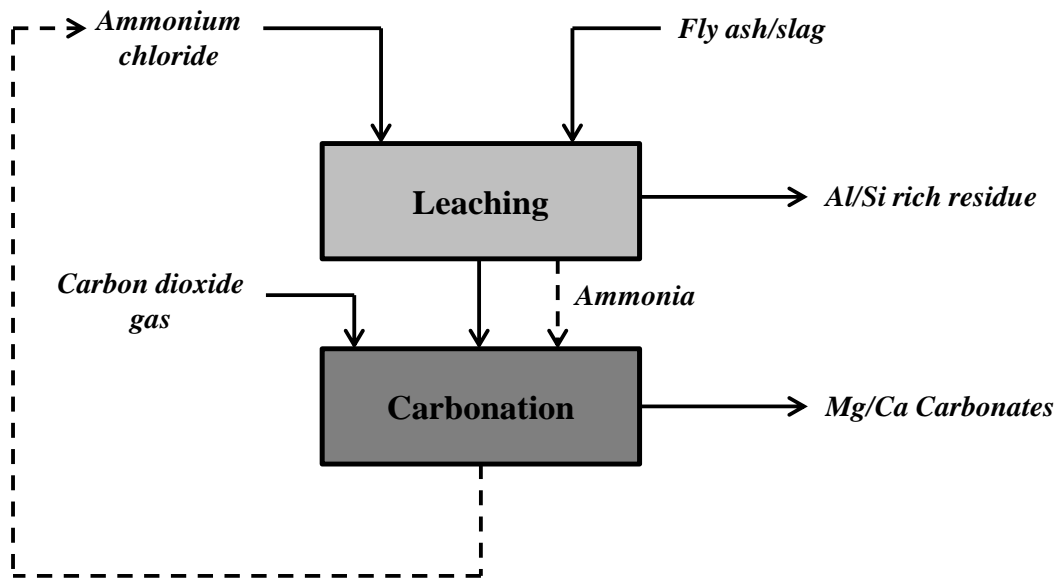


Figure 1.1 Proposed closed-loop process in this research

The advantages of the proposed process are:

- *Higher economic profit*

The project is highly cost-effective because a zero-value waste is the raw material that is used. The ammonium salt as leaching reagents can be regenerated during this process to be used in closed loop. Ammonia, required for carbonation step can be recovered through leaching step. Moreover, the carbonate and leaching residues are expected to be used in value-added ways, which further increase the economic profit of the process.

- *Environmental friendliness*

No waste gases or solutions will be released thus the proposed process is very environmentally benign. Moreover, the coal combustion-derived CO₂ will be used as a reactant in carbonation step to convert dissolved ions to carbonate forms which, in turn, will remarkably reduce the greenhouse gas emissions to atmosphere. Such an effort would return a large profit as a carbon credit to the brown coal industry.

1.3 Thesis structure and chapter outline

This thesis is organised into eight sections:

1.3.1 Chapter 1. Introduction

This section contains a brief background for the motivation of this thesis, the research aims for the thesis and an outline of the thesis structure.

1.3.2 Chapter 2. Literature review

This chapter reviews the main approaches to reduce the atmospheric CO₂ concentration. The advantages and updates on the progress of mineral carbonation are introduced. The literature review with research gaps are then identified in relation to the thesis chapters that address them.

1.3.3 Chapter 3. Multiple cycle leaching-carbonation using regenerative ammonium chloride and leaching kinetic modelling

In this chapter, a closed-loop multi-step process which allows leaching and carbonation of magnesium and calcium from Victorian brown coal fly ash was examined. Properties of two types of fly ash were studied, multiple locked circuits were adopted to assess the leaching capability of regenerated ammonium salt as well as the accumulation of impurities upon recycling. In comparison to fly ash, pure oxide compounds of MgO, CaO and Fe₂O₃ and their mixtures were also examined in the multi-cycle mode to evaluate the influence of impurities in fly ash on the extraction of target oxides. Finally, a detailed kinetic modelling on the leaching of magnesium from pure oxide and fly ash was conducted by assessing the applicability of various models, so as to provide an accurate model for future scale-up.

This chapter has been published as a journal article: **T. Hosseini**, C. Selomulya, N. Haque, L. Zhang, Indirect Carbonation of Victorian Brown Coal Fly Ash for CO₂ Sequestration: Multiple-Cycle Leaching-Carbonation and Magnesium Leaching Kinetic Modelling, *Energy & Fuels*, 2014, 28(10), pp 6481–6493.

1.3.4 Chapter 4. Comparison of leaching characteristics of fresh and weathered fly ash in NH₄Cl+HCl and sole HCl

This chapter comprises an extensive investigation on the chemical and morphological changes of weathered fly ash through the use of a variety of advanced instruments. The motivation for this work was to examine if the weathered fly ash could replace fresh fly ash in the mineral carbonation process. The effect of weathering process on the modes of occurrence of alkaline earth metals in a fly ash and its leaching behaviour in acidic reagent prior to carbonation was examined. In addition, modification of ammonium chloride upon the addition of hydrochloric acid was studied and compared with hydrochloric acid to increase the extraction yields and selectivity of the two target metal oxides.

This chapter has been published as a journal article: **T. Hosseini**, C. Selomulya, N. Haque, L. Zhang, Chemical and Morphological Changes of Weathered Victorian Brown Coal Fly Ash and its Leaching Characteristic upon the Leaching in Ammonia Chloride and Hydrochloric Acid, *Hydrometallurgy*, 2015, 157, pp 22-32.

1.3.5 Chapter 5. Mechanism of competition between Mg^{2+} and Ca^{2+} cations upon carbonation

This chapter aims to clarify the competition between Mg^{2+} and Ca^{2+} cations upon carbonation and effect of such a competition on carbonation rate and speciation of the resulting carbonate precipitates. The characteristics and Mg^{2+} and Ca^{2+} content of fly ash differ substantially according to the coal type and combustion condition. Therefore it is critical to reveal the effect of different parameters on carbonation rate and chemical speciation of solid precipitates so as to optimise the operating condition for the carbonation process.

This chapter has been published as a journal article: **T. Hosseini**, C. Selomulya, N. Haque, L. Zhang, Investigating the Effect of Mg^{2+}/Ca^{2+} Molar Ratio on the Carbonate Speciation during the Mild Mineral Carbonation Process at Atmospheric Pressure, *Energy & Fuels*, 2015, 29 (11), pp 7483–7496.

1.3.6 Chapter 6. Carbonation kinetic modelling and parameter sensitivity analysis

In this chapter, carbonation experimental data achieved at different Mg^{2+}/Ca^{2+} ratio, time and temperature were used to validate a kinetic model for the carbonation under mild operating condition. Due to the complexity of reactions occurring in parallel, and the significant inter-influence of Mg^{2+}/Ca^{2+} ratio on carbonation rate, none of the available kinetic models can predict Mg^{2+} and Ca^{2+} behaviour in the solution and formation of magnesium calcite ($Mg_NCa_{(1-N)}CO_3$). For this reason, a kinetic model with the aid of numerical and optimisation calculation technique was developed. This work is currently submitted to “Chemical Engineering Journal”.

1.3.7 Chapter 7. Simulation and techno-economic analysis of the overall process

The aim of this chapter was to identify the most promising process configurations in terms of energy consumption, product yield and costs. For these purposes, a comprehensive energy and techno-economic analysis has been carried out to examine the technical and economic performance of four different scenarios, based on the experimental data gathered in lab-scale experiments. The concepts based on experimental data were modelled and simulated using process flow-sheet software Aspen Plus®. Accordingly, the mass and energy balances were used to assess the economic analysis using Aspen process economic analyser. Finally, the cost of this process was compared with the other CCS methods. This work is currently submitted to “Applied Energy” Journal.

1.3.8 Chapter 8. Conclusions and Recommendations

The major findings of this thesis and the unexplored areas recommended for future investigation are presented in this chapter.

References

- [1] Bobicki, E.R.; Liu, Q.; Xu, Z.; and Zeng, H. Carbon capture and storage using alkaline industrial wastes. *Prog. Energ. Combust. Science* **2012**, 38(2), 302-320.
- [2] Damen, K.; Van Troost, M.; Faaij, A.; Turkenburg, W. A comparison of electricity and hydrogen production systems with CO₂ capture and storage. Part A: Review and selection of promising conversion and capture technologies, *Prog. Energ. Combust. Science* **2006**, 32, 215-246.
- [3] Eloneva, S.; Teir, S.; Salminen, J.; Fogelholm, C.J.; Zevenhoven, R. Fixation of CO₂ by carbonating calcium derived from blast furnace slag. *Energy* **2008**, 33, 1461-1467.
- [4] Sanna, A.; Dri, M.; Hall, M.R.; Maroto-Valer, M. Waste materials for carbon capture and storage by mineralisation (CCSM) – A UK perspective, *Appl. Energy* **2012**, 99, 545-554.
- [5] Lee, M.G.; Jang, Y.N.; Ryu, K.W.; Kim, W.; Bang, J.H., Mineral carbonation of flue gas desulfurisation gypsum for CO₂ sequestration, *Energy* **2012**, 47, 370-377.
- [6] Sanna, A.; Uibu, M.; Caramanna, G.; Kuusik, R.; MarotoValer, M.M. A Review of Mineral Carbonation Technologies to Sequester CO₂. *Chem. Soc. Rev.* **2014**, 43, 8049–8080.
- [7] Santos, R.M.; Van Bouwel, J.; Vandavelde, E.; Mertens, G.; Elsen, J.; Van Gerven, T. Integrated mineral carbonation reactor technology for sustainable carbon dioxide sequestration: ‘CO₂ energy reactor’, *Energy Procedia* **2013**, 37, 5884 – 5891.
- [8] Leung, D.Y.C; Caramanna, G; Maroto-Valer M.M. An overview of current status of carbon dioxide capture and storage technologies, *Renew. Sust. Energ. Rev.* **2014**, 39, 426–443.
- [9] Wang, X; Maroto-Valer, M.M. Optimisation of carbon dioxide capture and storage with mineralisation using recyclable ammonium salts, *Energy* **2013**, 51, 431-438.

Chapter 2

Literature review

This chapter reviews in detail the researches carried out so far on utilisation of industrial waste through the mineralisation scheme. Mineral carbonation of industrial wastes is deemed advantageous, due to its possibility of converting value-less waste into value-added by-products and permanent nature of carbon capture. To date, various types of minerals rich in alkaline earth metals, either natural minerals or industrial waste have been tested for their carbonation propensities.

2.1 Carbon dioxide emissions: A global concern

The population explosion and industrial growth are the traits of present day society, which require more electricity generated from the coal-based thermal power plants. Coal provides 30.3% of global primary energy needs and generates 42% of the world's electricity [1]. Coal combustion is facing significant challenges due to its high carbon emission rate. Generation of electricity and heat was by far the largest producer of CO₂ emissions and was responsible for 41% of the world CO₂ emissions in 2010. Countries such as Australia, China, India, Poland and South Africa produce between 68% and 94% of their electricity and heat through the combustion of coal [2].

Atmospheric carbon dioxide levels have increased from ~280 ppm before industrialisation to the level of 389 ppm in 2010 [3]. Carbon dioxide is a greenhouse gas (together with methane, nitrous oxide, CFC's and many more, including water vapour). An increase of GHG's in the atmosphere has been attributed to causing an increase in the global mean temperature [4]. In fact, the impact of CO₂ emissions is much larger than the impact of other GHG's, as displayed in **Figure 2.1**.

If no proactive mitigative action was taken, energy-related CO₂ emissions would likely to be 40-110% higher in 2030 than they were in 2000 (23.5 Gt CO₂ per annum), resulting in a global mean temperature rise by 1.8-4°C. It is recognised that a temperature increase in such a

magnitude would have wide-ranging and drastic implications for water and food availability, human health, ecosystems, coastlines and biodiversity [5,6].

In order to prevent a major climate change, the atmospheric CO₂ concentration should be stabilised by either increasing the CO₂ up-take from the atmosphere or reducing the CO₂ emissions. Three major approaches for the reduction of CO₂ emissions can be classified: (1) Reduction of the energy consumption based on fossil fuels, (2) Energy generation by non-fossil sources such as solar, wind, biomass, and nuclear energy and (3) Carbon capture and storage (CCS).

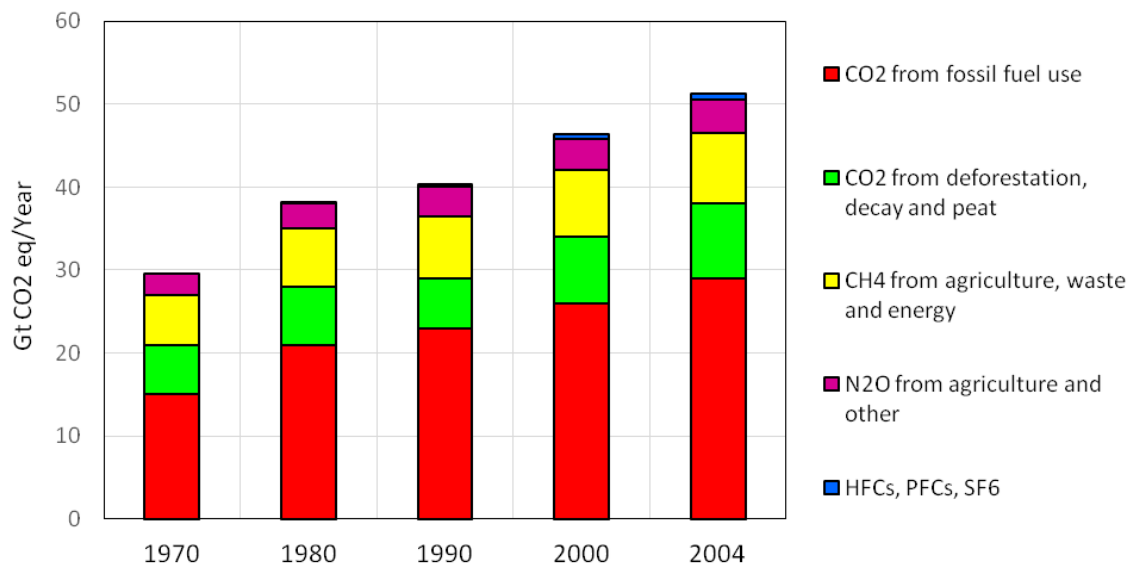


Figure 2.1 Annual levels of greenhouse gases represented as CO₂-equivalent emissions [4]

2.2 Mineral carbonation: A potential CO₂ mitigation option

Fossil fuels are expected to remain as the main energy source in the foreseeable future. The available reserves of oil, gas, and particularly coal are still large enough to provide energy to the world for the coming decades. In addition, renewable fuels will remain relatively expensive in the near future and energy saving will not have an impact large enough to substantially reduce the amount of CO₂ emitted into the atmosphere. Therefore, carbon capture and storage technologies such as mineral carbonation have been investigated intensively to reduce CO₂ emissions in the short term, so as to enable a transition to a sustainable future based on non-fossil energy sources [7].

Mineral carbonation is a relatively new CO₂ mitigation option. The idea was originally proposed in 1990 [8] and the first study on this concept was published in 1995 [9]. This process is based on industrial imitation of the natural weathering processes. In weathering processes, eroded rock surfaces come into contact with rainwater saturated with dissolved atmospheric CO₂.

Subsequently, soluble elements dissolve into the water and eventually, carbonate minerals form. If these weathering or carbonation processes could be enhanced and industrially applied, they could be used to bind gaseous carbon dioxide into a solid carbonate that is chemically stable.

Mineral carbonation has a number of advantages over the other carbon storage techniques such as:

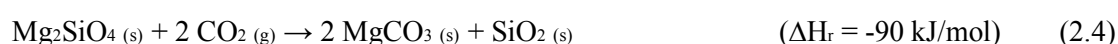
- Mineral carbonation is a chemical sequestration route, of which the formed products are thermodynamically stable and environmentally benign. The formed mineral carbonates are end-products of geologic processes and are known to be stable over geological time periods. Therefore, the storage of CO₂ is permanent and inherently safe.
- The potential CO₂ sequestration capacity of mineral carbonation is very large. Sufficient minerals can potentially be mined worldwide to sequester future CO₂ emitted from fossil fuel combustion.
- The carbonation reaction is exothermic. The reaction energy may potentially be recovered [9].

Both alkali (*e.g.*, Na, K) and alkaline earth (*e.g.*, Ca, Mg) metals as well as a number of other metals (*e.g.*, Mn, Fe, Co, Ni, Cu, and Zn) can potentially be carbonated. However, most of the latter elements are either too rare or too valuable to be suitable as feedstock for mineral carbonation. Alkali metals are unsuitable, since alkali (bi) carbonates are highly soluble for long-term CO₂ sequestration. Of the alkaline earth metals, calcium and magnesium are by far the most common in nature and most suitable elements to be carbonated for CO₂ sequestration purposes.

The simplest carbonation reactions for calcium and magnesium minerals are:



These carbonation reactions are exothermic, since carbonate is the lowest energy-state of carbon. However, calcium and magnesium rarely occur as binary oxides in nature. They are typically found in silicate minerals. In principle, these minerals are also capable of being carbonated because carbonic acid is a stronger acid than silicic acid (H₄SiO₄). Therefore, silica present in the mineral is exchanged with carbonate and the mineral is carbonated. These reactions are still exothermic, but to a lesser extent than the carbonation of pure oxides [7], as shown below:



2.3 Use of industrial wastes for mineralisation

Two types of feedstock for mineral CO₂ carbonation can be classified: mineral ores (primary minerals) and industrial wastes (secondary materials). Nature is the primary source for calcium and magnesium oxide and silicates, and only mining activities produce the large amount of feedstock required [10,11]. The main Mg-rich rocks are olivine ((Mg,Fe)₂SiO₄) and serpentinites (Mg₃Si₂O₅(OH)₄). The main Ca-containing candidate ore are wollastonite (CaSiO₃) and basalt which is a mixture of different minerals [12]. The industrial solid wastes rich in magnesium or calcium could be an alternative source of oxide or silicates for CO₂ sequestration [13].

The principal idea of an industrial mineral carbonation process and the material streams involved are given in **Figure 2.2**, Carbon dioxide is supplied from a source emitting a relatively high concentration of CO₂. In addition to CO₂, a source of magnesium or calcium is required and that can be supplied from a mine or alternatively from an industrial waste product rich in either Ca or Mg [14].

Alkaline waste residues have some distinct advantages over natural minerals. Mining operation is not required and the comminution of raw materials is avoided [10]. In most cases these zero-value wastes are generated in industrial areas near the point source of CO₂ emissions, greatly reducing the cost for transportation of either CO₂ or mineral carbonation feedstock. Alkaline waste residues are, in general, highly reactive and do not require pre-treatment to achieve high carbonate conversions [15]. In addition, the carbonation of alkaline waste residues allows them to be stored safely, reused or sold as value-added by-products.

A variety of alkaline waste residues have been tested for mineral carbonation purposes, including different types of coal ashes, steel-making slags, cements wastes, mining and mineral processing wastes and alkaline paper mill wastes. The carbon sequestration capacities of these wastes vary and largely depend on the content of calcium and/or magnesium and their accessibility in the mineral phases present. For example, a waste containing a large percentage of free magnesium oxide is carbonated more readily than a waste with the same magnesium content, but in the form of silicates. However, it is difficult to compare the desirability and efficiency of different alkaline wastes for mineral carbon sequestration [3]. The maximum sequestration capacity of some typical residues based on total elementary composition is determined and summarised in **Table 2.1**. It is assumed that all magnesium and calcium can be liberated from the matrix and carbonated [16].

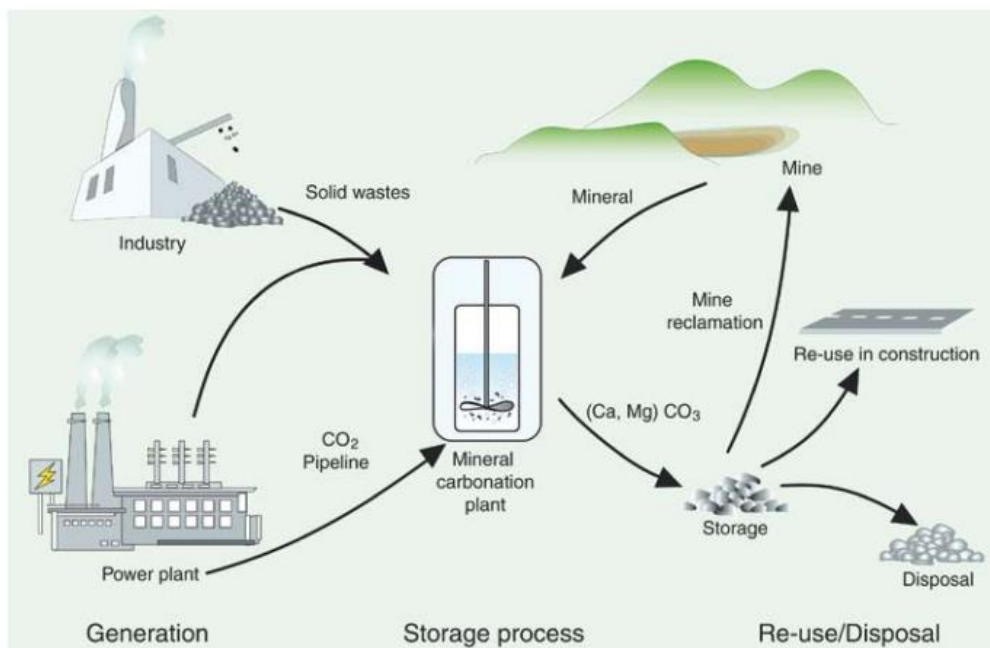


Figure 2.2 A schematic overview of a generic mineral carbonation process [4]

Table 2.1 Potential CO₂ sequestration capacity on the basis of elementary composition of selected residues [16]

Residue	Ca (g/kg)	Mg (g/kg)	CO ₂ (g/kg)
Carbon enriched fly ash	6.9	2.8	12.6
Coal fly ash	38.1	9.2	58.6
Electricity bottom ash	69.6	11.3	96.8
MSWI fly ash	119.1	13.5	155.2
Steel slag	222-315.5	45-73.1	325.2-407.1

On the assumption of 32 wt% CaO and 29 wt% MgO in Victorian Brown coal fly ash (data shown in **Table 3.1** in chapter 3), the carbonation reaction is expected to capture 278 kg CO₂ per tonne of raw fly ash, which is equivalent to a total amount of 0.36 million tonnes CO₂ captured per annum, based on the yield of approximately 1.3 million tonne for fly ash produced annually in the Latrobe Valley. Although these numbers are much smaller than the total amount of CO₂ released in the Latrobe Valley, it is expected that the industrial mineral wastes can act as supplement to the natural minerals for CO₂ capture. Our study here is also expected to act as ‘icebreaker’ for introducing CO₂ permanent mineralisation technology that eventually may be picked up by the power producers.

2.4 Coal fly ash

Fly ash is a by-product from the combustion of pulverised coal in the power generating plants. Coal fly ash is an abundant solid waste, production of which is expected to increase as a result of the world's increasing reliance on coal-fired power generation over the next few decades [17,18]. In 2000, only 20% of the total global coal fly ash production (600 million tonnes) was used beneficially, mostly in the cement industry [19].

Each year, a large mass of fly ash is collected in storage ponds, which emphasises the need for the investigation of large-scale applications for this waste product. Over the last few decades, fly ash has attracted attention as a potential source in the mineral sequestration process, which involves the capture and storage of atmospheric CO₂ in alkaline materials [20-23]. The utilisation of fly ash to capture and fix CO₂ has an added advantage that it assists in the management of this potentially hazardous waste. Since the carbonation process helps to alter the chemical stability of the fly ash, the leachability of heavy metals such as Pb and Zn tends to reduce after carbonation [24,25]. This allows a safe disposal of carbonated fly ash into landfills. **Table 2.2** lists the annual yield and utilisation percentage of the fly ash for different countries. Worldwide, more than 65% of fly ash produced from coal power stations is disposed of in landfills and ash ponds [26].

Table 2.2 Fly ash generation and utilisation in different countries [26]

Country	Annual Ash Production, MT	Ash Utilisation (%)
India	112	38
China	100	45
USA	75	65
Germany	40	85
UK	15	50
Australia	10	85
Canada	6	75
France	3	85
Denmark	2	100
Italy	2	100
Netherland	2	100

Elemental chemical composition of fly ash is highly variable. The variability is directly related to the source of the coal, its pre-treatment, and the operation of the plant burning the coal. The major elements in typical fly ash are: Si, Al, Ca, C, Mg, K, Na, S, Ti, P and Mn. Most of these major elements exist in the core of the fly ash which is relatively stable. This is probably because they are not volatilised in the combustion process [27].

In Australia, Victorian brown coal is the single largest source meeting >85% of the electricity need in the State of Victoria, which in the meanwhile yields approximately 1.3 million

tonnes fly ash annually [28,29]. The ash forming constituents in brown coal are mainly magnesium, sodium, calcium and iron, which transform into fly ash during the combustion process. New South Wales and Queensland produce 95% of the total production of raw black coal. The ash from black coal is mainly composed of discrete mineral particles such as quartz, gypsum and glassy species [30,31].

Table 2.3 shows the quantification of elements present in fly ash produced from combustion of different kinds of Australian brown and black coals. As can be seen, Victorian brown coal fly ash is dominated by MgO, CaO and Fe₂O₃ whereas black coal fly ash is rich in SiO₂ and Al₂O₃.

Table 2.3 Elemental quantification of Australian brown and black coal fly ash [32,33]

Species	Victorian Brown Coal Fly ash			Australian Black Coal Fly ash	
	Hazelwood 1	Hazelwood 2	Yallourn	Awaba	Collie
	wt %	wt %	wt %	wt %	wt %
SiO ₂	5.36	2.11	11.3	64.6	52.3
Al ₂ O ₃	2.6	2.14	6.98	26.4	33.8
CaO	30	27.4	8.49	0.5	1.9
MgO	25.8	23.5	23	0.6	1.3
Fe ₂ O ₃	11.2	9.66	43.9	3.4	15.4
Na ₂ O	6.58	8.91	1.01	0.2	0.63
K ₂ O	0.48	0.46	0.32	2.6	0.88
SO ₃	15.1	22.8	2.63	0.4	0.1

The pH of the ash–water system is controlled by the ratio between ubiquitous Ca and S concentrations in fly ash [34], although other minor alkalis or alkaline earth cations such as Mg may also contribute to the balance [35]. The occurrence and levels of Ca-bearing phases in ash are intimately related to the depositional environment of coal. Based on Ca/S balance and the pH, fly ash can be categorised into three major groups:

- **Strongly alkaline ashes:** free-lime dissolution dominates the leaching process, with pH values typically in the pH 11–13 range [36] and large amounts of Ca in the leachates. Ca prevails over S (Ca/S >> 1).

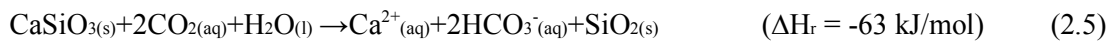
- **Mildly alkaline ashes:** anhydrite dissolution dominates the leaching process, with moderately low Ca levels and balanced Ca/S ratios that give rise to mildly alkaline conditions (pH 8–9) [34].

- **Acidic fly ash:** depleted in CaO and MgO in relation to the sulphate content [35] and therefore retaining its original acid characteristics, as the acidic components concentrated on the surface of fly ash particles are initially brought into solution as sulfuric acid [37].

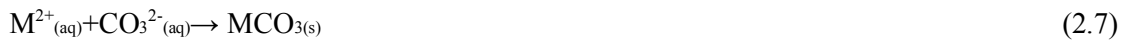
Abundant alkali (Na, K), alkaline earth metals (Ca, Mg) and iron (Fe) makes brown coal fly strongly alkaline fly ash which is unsuitable to be used as additive to cement, but a good candidate for mineral carbonation.

2.5 Different types of mineral carbonation

Carbonation can occur naturally. Natural carbonation is also well known as “weathering”, which eventually removes CO₂ from the atmosphere by neutralising the acid with mineral alkalinity. Natural weathering occurs by the reaction between natural alkaline silicates and atmospheric CO₂, as shown in Equations (2.5) and (2.6):



Atmospheric CO₂ dissolves in rainwater, producing weak carbonic acid, and becomes slightly acidic by nature. Calcium and magnesium silicates are therefore leached from the mineral matrix after coming in contact with the rainwater. Rainwater thus carries the leached Ca²⁺ and Mg²⁺ to rivers and subsequently to the ocean, where these two cations precipitate and form solid carbonates (M²⁺ represents alkaline earth metal element) as shown in Equation (2.7). However, the kinetics of natural carbonation is extremely slow, due to the relatively low CO₂ concentration, about 0.03–0.06% [12, 38].



Accelerated carbonation involves alkaline materials reacting with high-purity CO₂ in the presence of moisture to accelerate the reaction to a timescale of a few minutes or hours [39]. Accelerated carbonation has been classified as: *direct carbonation*, where carbonation occurs in a single process step, and *indirect carbonation*, where alkaline earth metal is first extracted from the mineral matrix and subsequently carbonated [40].

2.5.1 Direct carbonation

This process typically occurs at temperatures above 100°C and high CO₂ pressure (10-20 bar), to allow the breakage of metal silicate bonds for the release of metallic species and improve the reaction kinetic [3]. There are two main forms of direct carbonation: *gas-solid carbonation* and *aqueous carbonation*. Gas-solid carbonation has the potential to produce high temperature steam that can be used to generate electricity while fixing CO₂ [41]. For common natural silicate minerals, this temperature limit ranges from 170°C to 410°C [42]. Unfortunately, even under high pressure and temperature, direct gas-solid reactions are too slow to be practical for calcium and magnesium silicates. Instead, the calcium and magnesium containing oxides or hydroxides, are more reactive [5,42].

Huijgen et al. (2005) performed the carbonation of steel slag slurries at a 10:1 water/solid ratio. A 70% Ca^{2+} carbonation conversion was obtained under the conditions, 20 bar and 200°C in a 100% CO_2 atmosphere [43]. Bhatia and Perlmutter (1983) investigated the kinetics of CaO carbonation by modified TGA experiments performed in a CO_2 stream at different operating temperatures, confirming 70% calcium carbonation conversion at 500°C [44]. A different approach was followed by Abanades et al. (2004), proposed the use of CaO in a fluidised bed to capture CO_2 directly from combustion gases; up to 70% carbonation conversion was obtained for the fresh material. However, a reduction in the conversion yield was observed after several carbonation-calcination cycles [45].

Direct aqueous mineral carbonation involves the reaction of CO_2 with alkaline minerals in an aqueous suspension in a single stage [41]. Same as gas-solid direct carbonation, the elevated pressure and temperature enhances mineral carbonation efficiency but it has an upper limit. The carbonation reaction rate can be further accelerated by adding acids or other chemical activators [46], and through the use of various pre-treatment techniques, such as crushing the particles. Unfortunately, the pre-treatments tend to be very energy-intensive. As a result, the direct aqueous carbonation process is still too expensive to be applied on a large scale [41].

The direct aqueous carbonation of industrial wastes rich in Mg and Ca, including steel-making slags under ambient condition as well as elevated temperature and pressure have been reported [10,47-50]. Li et al (2012) achieved a sequestration of 6.93g CO_2 /100 g slag under ambient condition, using ammonium chloride solution over 2 h reaction time [49]. Cheng et al. (2013) studied the direct carbonation of basic oxygen furnace slag (BOFS) using the same condition as above, 89.4% magnesium carbonated [50]. Results confirmed that higher Ca or Mg content are more reactive, especially if the Ca or Mg are present primarily as free oxide or hydroxide as opposed to silicate [47,50].

Research on the mineral carbonation of coal fly ash has been focused mainly on the direct aqueous method at ambient temperature, but high initial CO_2 pressure and long reaction rate (about 1 day) with either water or brine as the reaction medium. Montes-Hernandez et al. (2009) achieved a carbonate conversion of 82% and a carbon sequestration capacity of 26 kg CO_2 /t ash at 30°C and 10 bar initial CO_2 pressure over 18 h in water [20]. Uliasz-Bochenczyk et al. (2009) found a maximum carbon sequestration capacity of 7.85 g CO_2 /100 g ash at ambient temperature and 10 bar CO_2 initial pressure over 24 h in water [51]. It was concluded that the efficient carbonation of fly ash using the direct aqueous method could be reached at ambient temperature, elevated initial pressure of CO_2 (~ 10 bar) and the reaction time up to about 24 hours. **Table 2.4** summarises the selected works using fly ash as feedstock for the aqueous direct carbonation.

Table 2.4 Direct mineral carbonation results for slag and fly ash from selected literature

Literature Reference	Type of Direct Carbonation	Type of solution	condition	Reaction Time	Result
Muriithi et al. [52]	Aqueous	Brine	90°C, 4 Mpa	2 h	60% Ca carbonated
Ukwattage et al [53]	Aqueous	Water	4°C, 2-6 Mpa	0-10 h	0.0489-0.0546 moles CaCO ₃ was carbonated
Bauer et al. [54]	Aqueous	Semi-dry process Water	25-80°C, 0.15 atm	120 min	52.8% carbonation efficiency
Montes-Hernandez et al. [20]	Aqueous	Water	30°C , 10 bar	2 h	82% Mg carbonated 2.6 g CO ₂ /100 g fly ash
Uliasz-Bochenczyk et al. [51]	Aqueous	Water	Ambient temperature, 10 bar	24 h	7.85 g CO ₂ /100 g ash

The main barriers to the industrial deployment of this process is the low reaction yield and slow reaction kinetics [55]. The solid particle dissolution process generally follows: (1) diffusion through a fluid film surrounding the particle, (2) diffusion through a solid product layer on the particle surface, or (3) chemical reaction at the particle surface [56]. The rate of the overall process is controlled by the slowest of these sequential steps. Dissolution of mineral is the rate-limiting step in the direct aqueous mineral carbonation system, mainly due to the absence of protons at the pH close to 7 [55]. The mechanisms of direct aqueous mineral carbonation are well understood. These mechanisms indicate that increasing the dissolution rate of Ca/Mg oxide in the solution could lead to the acceleration on the overall carbonation reaction [57]. Guthrie et al., (2001) concluded that, the dissolution of magnesium silicate is the most important step that probably determines the overall reaction rate [57]. Wu et al. (2001) concluded that, the rate-determining steps for the carbonation of wollastonite are the dissolution of calcium from the matrix and its carbonation in aqueous solution [58]. In these cases, the carbonation reaction rate could not be determined accurately because the dissolution reaction occurs simultaneously with carbonation reaction in the same reactor.

2.5.2 Indirect carbonation

The realisation that aqueous carbonation could be improved by dividing the process into separate dissolution and carbonation step has resulted in a considerable amount of studies [23,59,60]. Indirect carbonation typically involves a prior extraction step into an aqueous phase first, and the resultant solution is bubbled with CO₂ for carbonation.

An advantage of indirect carbonation is that it allows pure carbonates to be produced, because impurities, such as silica and iron, can be removed prior to the carbonate precipitation [13]. A number of technologies are available for extracting the reactive components from the minerals and industrial wastes, including *acid extraction*, *molten salt process*, *bioleaching*, *ammonia extraction* and *caustic extraction*.

Various extraction reagents have been investigated for indirect aqueous mineral carbonation of industrial wastes and natural minerals, including strong acids (nitric acid, sulphuric acid) [61], ammonium salts (ammonium chloride, ammonium nitrate and ammonium sulphate) [23,60,62] and weak acid (acetic acid). Teir et al. (2007) found that, acetic acid (CH_3COOH) and formic acid (HCOOH) are strong enough to leach significant amount of magnesium from serpentine [63]. Wand and Maroto-Valer (2013) proposed a pH-swing mineral carbonation process using ammonium salts [64]. At 100°C , 1.4 M aqueous solution of NH_4HSO_4 was found to extract 100% Mg from serpentine in three hours. The main drawback of the aqueous pH swing, ammonium-based process is that a large amount of water needs to be separated from the salts during the regeneration step [55]. Although not ready for commercialisation, the ammonia extraction process appears to be a promising technique given the potential for reagent recovery and the selectivity of the leaching reagents. According to Teir et al. (2007), the ammonium salt solutions were the only solvents tested that seemed to extract magnesium selectively; no measurable iron or silicon concentration was found in the salt solutions after filtration. Calcium and magnesium can be extracted efficiently from steel-making slag using weak acid or ammonia salts under even mild conditions [63].

Kodama et al. (2006) [60] found that at 80°C and atmospheric pressure, ~60% of calcium was extracted from steel-making slag with a 99% selectivity using ammonium chloride as the leaching reagent. Conversion of the extracted calcium to carbonate was 70% and the calcium carbonate produced had a purity of 98%. Eloneva et al. (2012) studied mineral carbonation of steel-making slags using different ammonium salts, including ammonium chloride, ammonium nitrate and ammonium acetate. These ammonium salts effectively dissolved 50-80% Ca at 30°C and atmospheric pressure. Pure calcium carbonate was precipitated by bubbling CO_2 at 30°C with conversion efficiencies of 50-70%. However, the ammonium loss was found considerable [62]. Ammonium loss took place due to the vapourisation loss during the leaching process and the crystallisation of ammonia. Wang et al. (2012) performed research on the crystallisation kinetic of ammonium chloride in a ternary aqueous solution of NH_4Cl - MgCl_2 - H_2O . Their result indicated that, the crystallisation tendency of ammonium chloride was enhanced in the solution with a high MgCl_2 concentration and the elevation of reaction [65]. During the leaching process, ammonium chloride dissolves magnesium/calcium oxide and causes the increase of magnesium/calcium chloride concentration in the leachate, which in turn accelerates the

crystallisation of ammonium chloride. Sun et al. (2011) investigated the leaching and carbonation behaviour of steel-making slag using ammonium chloride [23]. The high purity (96±2%) calcium carbonate was obtained under the optimised carbonation condition (initial pressure 10 bar, 60°C, 400 rpm and 1 h duration).

There are limited numbers of researches on indirect carbonation of fly ash. Studies have mainly focused on the direct aqueous carbonation route under mild process conditions with either water or brine as the reaction medium [55], or by natural weathering over a longer period of time [52]. Sun et al. (2012) investigated the sequestration of CO₂ by indirect mineralisation using Victorian brown coal fly ash. The leaching conditions including 6% (v/v) acetic acid and a stirring duration of 1 h were used for the ash leaching at ambient conditions. The results confirmed the extraction of the majority of calcium and magnesium into the leachate, and a large CO₂ capture capacity of fly ash under the mild conditions examined. Also, the carbonation yield of magnesium in the Victorian brown coal fly ash sample being tested was maximised at 60°C. It was also found that, increasing temperature negated the calcium carbonation yield [29]. **Figure 2.3** plotted the fraction of each cation converted to carbonate/bicarbonate versus carbonation temperature. They found that the bubbling of gaseous CO₂ into the leachate is initiated by its dissolution to form HCO₃⁻ by Equation (2.8), which subsequently dissolves to form CO₃²⁻ by Equation (2.9). For the CO₃²⁻ anion formed, its stabilisation follows reaction (2.10) for the formation of calcium carbonate. Such a reaction is exothermic and hence, it is depreciated at elevated temperatures. In contrast, for Mg²⁺ ion, it initially reacts with HCO₃⁻ rather than CO₃²⁻ to form Mg bicarbonate which is highly water-soluble, according to Equation (2.11). Upon heating, the resulting bicarbonate is expected to decompose into carbonate and release one mole of CO₂ as gas by Equation (2.12) [29]



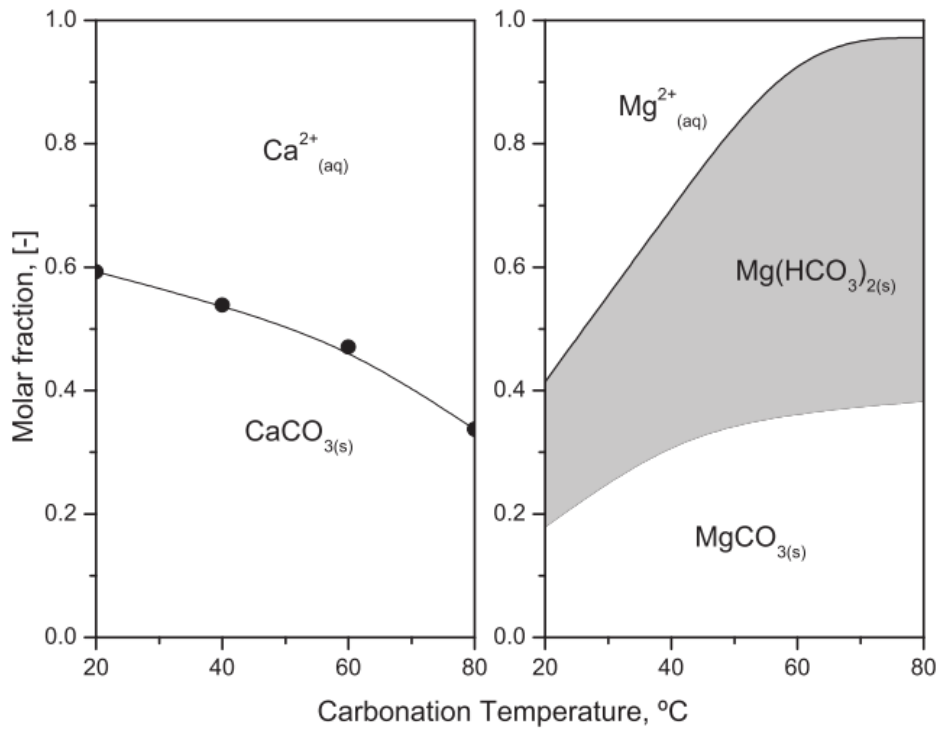


Figure 2.3 Conversion of different carbonates during carbonation at different temperatures [29].

Jo et al., (2012) examined the factors affecting mineral carbonation of fly ash in the aqueous solution, under ambient conditions. Based on their results, the CO_2 sequestration capacity of coal fly ash was approximately 0.008 kg of CO_2 per kg of fly ash under the experimental conditions tested (CaO content: 7 wt.% in the ash, solid dosage: 100 g/L, CO_2 flow rate: 2 mL/min, and solvent: deionised water) [66]. The leaching and carbonation performances of indirect mineral carbonation were investigated by Han et al. (2015). They used coal fly ash (FA) as the raw source and water as the solvent. The overall CO_2 storage capacity of FA suspended solution was 31.1 mg CO_2 /g FA [67].

Most of the literatures about fly ash have focused on the leaching behaviour of various target metals from different types of fly ash [68-70]. Fly ash characteristic is strongly dependent on its composition. The type of leaching reagent used depends on the target metal and the abundance of the particular metal of interest in the fly ash. The amount of particular metal that can be extracted from fly ash depends on the factors such as leaching reagent concentration, leaching time, liquid to solid ratio, temperature and the particle size of the solid [71].

The reaction mechanism in which an acid leaching progress normally follows is the shrinking core model [72]. According to the shrinking-core model, reactions take place at the outer surface of the un-reacted particle and heterogeneous reactions are controlled by one of the

following mechanisms. The rate of the process is controlled by the slowest of these sequential steps [54]:

- *Film diffusion control*: diffusion of the fluid reactant from the bulk fluid film to the surface of the solid, represented by:

$$kt = x \quad (2.13)$$

- *Reaction control*: reaction on the surface between the fluid reactant and the solid, represented by:

$$kt = 1 - (1 - x)^{1/3} \quad (2.14)$$

- *Product layer diffusion*: diffusion of the products of reaction from the surface of the solid through the fluid film back into the bulk fluid (without ash layer), represented by:

$$kt = 1 - 3(1 - x)^{2/3} + 2(1 - x) \quad (2.15)$$

Where, k is the reaction rate constant and x the fraction transformed for the product phase at time t . Ranjitham et al. (1990), Raschman (2000) and Atashi et al. (2010) carried out leaching of calcined magnesite using ammonium chloride [73-75]. They concluded that the leaching process is controlled by the chemical reaction of MgO with NH_4^+ ions at the liquid–solid interface. Based on the Arrhenius kinetic rate, their activation energies for their experiments were 43.2, 57.8 and 42.3 kJ/mol for different magnesite. Glaser et al. (1988) investigated the leaching kinetic of pure MgO using ammonium chloride and their results confirmed that the chemical reaction controls the overall process and the activation energy was found to be 39 kJ/mol [76]. The dissolution rate seemed to be limited by the product layer diffusion for serpentine in the HCl solution [63].

Kinetic analysis carried out by Chang et al. (2013) [50] showed that, the diffusion process through the ash layer can accurately represent the kinetic for the direct carbonation of steel-making slag. Sun et al. (2011) reached the same conclusion as above and showed that the carbonation reaction is limited by diffusion through slag layer [23]. The pseudo-second-order kinetic model was used to model the CO_2 capture by Sun et al. (2012) [29]. Based on their results, the calculated apparent activation energy was found to be 12.7 kJ/mol with a relative variance R^2 of 0.96 for the carbonation of calcium and magnesium ions in the brown coal fly ash leachate. In their work, the carbonation process was assumed as a single reaction and apparent rate constant for the whole process was calculated [29].

2.6 Industrial mineral carbonation processes and cost estimation

At this stage, there is very limited research on this aspect [77]. Due to the lack of commercial applications, mineral carbonation cost estimates reported in literature were mostly based on laboratory or pilot-scale experiments [55]. A pilot-scale direct mineral carbonation process was developed and tested by reacting coal fly ash with flue gases in a fluidised bed reactor at a 2120 MW coal-fired power plant in the USA. A preliminary economic analysis of the process showed that, the CO₂ capture from a 532 MW power plant would cost about \$11–21 per tonne of CO₂ assuming a sequestration capacity of 0.1–0.2 tonne CO₂ per tonne of fly ash [78]. However, the other analysis suggests a range from \$50 to \$300 per tonne of CO₂ sequestered [55]. The high cost of the leaching reagent and energy requirements associated with industrial wastes-to-carbonates pathways is one of the major issues hindering the application of indirect route [79]. In order to make such a process economically and environmentally sustainable, the chemicals used in the process should be regenerated within the process itself [64]. In addition, the final products should be used in a value-added way as well. However, the literature to date indicates that in the coming decades mineral carbonation can play an important role in decarbonising the power and industrial sector [55]. Mineral carbonation demonstration plants of up to 1Mt CO₂ per annum may be operational as early as 2020 [80].

2.7 Research gap

Natural minerals are rather constant in properties and they have been researched intensively in the literature. However, fly ash is rather heterogeneous in property, and there are not generalised methods regarding the leaching and carbonation for the use of any specific industrial wastes. Considering the broad variation of the properties of industrial wastes, it is with doubt that the methods developed in the literature are applicable to any new sample. In addition, there has been little research on the fates of impure metals and their effect on the whole process and the quality of final products.

To date, the majority of researches on fly ash utilisation have focused on direct carbonation which requires a high CO₂ partial pressure and a rather long reaction time. In order to extract certain elements with a higher selectivity under mild condition, the indirect method with an initial selective extraction of the metals of interest is highly preferred. However, the reports on fly ash by indirect method are much limited. Moreover, in the existing literatures on this area, the research target was only set at optimising the conditions for the once-through single leaching and carbonation stages, whereas the integration of these two steps and the recovery of leaching reagent has yet to be discussed.

Compared to coal fly ash, the other industrial wastes such as steel-making slag have been examined widely by both direct and indirect carbonation methods. Among these two methods, the indirect carbonation seems more attractive, because of its larger capacity to capture CO₂ per tonne of solid waste and the lower operating cost than the direct carbonation method. There are also some studies that have applied regenerative ammonium salts to extract calcium or magnesium out of steel-making slag, however, none of them were successful to extract both of magnesium and calcium simultaneously. For example Kodama et al. (2006) [59] was only able to extract calcium with 99% selectivity from steel-making slag using ammonium chloride as the leaching agent. They used the calcination process prior to the leaching step. The energy required for overall process was estimated to be approximately 300 kWh/t CO₂, which is highly energy-intensive. Moreover, the loss of leaching reagent during the process and the recyclability of the regenerated ammonium salt has not yet been reported. Furthermore, the reaction mechanism and modelling of the overall process, as well as a detailed techno-economic analysis are still lacking to assist in the scale-up of the developed process from laboratory to industry.

References

- [1] World Coal Association, Based on 2011 IEA and BP data published in 2012.
- [2] Olivier, J.; Janssens-Maenhout, G. (IEA), CO₂ Emissions from Fuel Combustion, **2012**.
- [3] Bobicki, E.R.; Liu, Q.; Xu, Z.; and Zeng, H. Carbon capture and storage using alkaline industrial wastes. *Prog. Energ. Combust. Science* **2012**. 38(2), 302-320.
- [4] IPCC. Climate Change 2007: Mitigation of Climate Change. Contribution of Working Group III to the Fourth Assessment Report of the Intergovernmental Panel on Climate Change. Cambridge, United Kingdom and New York (NY), USA: Cambridge University Press, **2007**.
- [5] Metz, B.; Davidson, O.R.; Bosch, P.R.; Dave, R.; Meyer, L.A. Climate change mitigation. Contribution of working group III to the fourth assessment report of the intergovernmental panel on climate change. Cambridge, UK and New York, NY, USA: Cambridge University Press, **2007**.
- [6] Solomon, S.; Qin, D.; Manning, M.; Chen, Z.; Marquis, M.; Averyt, K.B. Climate change: the physical science basis. Contribution of working group I to the fourth assessment report of the intergovernmental panel on climate change. Cambridge, UK and New York, NY, USA: Cambridge University Press, **2007**.
- [7] Wouter, J.; Huijgen, J. Carbon Dioxide Sequestration by Mineral Carbonation. Thesis, Energy research Centre of the Netherlands, The Netherlands, **2005**.

- [8] Seifritz, W. CO₂ disposal by means of silicates, *Nature* **1990**, 345, 486.
- [9] Lackner, K.S.; Wendt, C.H.; Butt, D.P.; Joyce, E.L.; Sharp, D.H. Carbon dioxide disposal in carbonate minerals. *Energy* **1995**, 20, 1153-1170.
- [10] Huijgen, W.J.J.; Witkamp, G.J.; Comans, R.N.J. Mineral CO₂ sequestration by steel slag carbonation. *Environ. Sci. Technol.* **2005**, 39(24), 9676–9682.
- [11] Teir, S. Fixation of carbon dioxide by producing carbonates from minerals and steelmaking slags. PhD (Eng) thesis. Helsinki University of Technology Espoo, Finland, **2008**.
- [12] Lackner, K.S. Carbonate chemistry for sequestering fossil carbon, *Annu. Rev. Energ. Env.* **2002**, 27, 193-232.
- [13] Eloneva, S.; Teir, S.; Salminen, J.; Fogelholm, C.J.; Zevenhoven, R. Fixation of CO₂ by carbonating calcium derived from blast furnace slag. *Energy* **2008**, 33, 1461-1467.
- [14] IPCC, Special Report on Carbon Dioxide Capture and Storage. Prepared by Working Group III of the Intergovernmental Panel on Climate Change, NY, USA: Cambridge University Press, Cambridge, United Kingdom and New York, **2005**.
- [15] Bertos, M.F.; Simons, S.J.R.; Hills, C.D.; Carey, P.J. A review of accelerated carbonation technology in the treatment of cement-based materials and sequestration of CO₂. *J. Hazard. Mater.* **2004**, 112(3), 193–205.
- [16] Huijgen, W.J.J.; Comans, R.N.J. Carbon dioxide sequestration by mineral carbonation, literature review; Energy research Centre of the Netherlands, ECN-C-03-016, Petten, The Netherlands, **2003**.
- [17] Wu, C.V.; Yu, H.F.; Zhang, H.F. Extraction of aluminium by pressure acid-leaching method from coal fly ash, *T. Nonferr. Metal. Soc.* **2012**, 22, 2282-2288.
- [18] Neupane, G.; Donahoe, R.J. Leachability of elements in alkaline and acidic coal fly ash samples during batch and column leaching tests, *Fuel* **2013**, 104, 758-770.
- [19] Malhotra, V.M. Making concrete greener with fly ash. *Concr. Int.* **1999**, 21(5), 61-66.
- [20] Montes-Hernandez, G.; Pérez-López, R.; Renard, F.; Nieto, J.M.; Charlet, L. Mineral sequestration of CO₂ by aqueous carbonation of coal combustion fly-ash. *J. Hazard. Mater.* **2009**, 161(2-3), 1347-1354.
- [21] Nyambura, M.G.; Mugeru, W.G.; Felicia, P.L.; Gathura, N.P. Carbonation of brine impacted fractionated coal fly ash: implications for CO₂ sequestration. *J. Environ. Manag.* **2011**, 92, 655-664.

- [22] Jo, H.Y.; Ahn, J.H.; Jo, H. Evaluation of the CO₂ sequestration capacity for coal fly ash using a flow-through column reactor under ambient conditions, *J. Hazard. Mater.* **2012**, 242-242, 127-136.
- [23] Sun, Y.; Yao, M.S.; Zhang, J.P.; Yang, G. Indirect CO₂ mineral sequestration by steelmaking slag with NH₄Cl as leaching solution, *Chem. Eng. J.* **2011**, 173(2), 437-445.
- [24] Van Gerven, T.; Van Keer, E.; Arickx, S.; Jaspers, M.; Wauters, G.; Vandecasteele, C. Carbonation of MSWI bottom ash to decrease heavy metal leaching, in view of recycling. *Waste Manag.* **2005**, 25, 291-300.
- [25] Meima, J.A.; Van der Eeijden, R.D.; Eighmy, T.T.; Comans, R.N.J. Carbonation process in municipal solid waste incinerator bottom ash and their effect on the leaching of Copper and Molybdenum. *Appl. Geochem.* **2002**, 17, 1503-1513.
- [26] Alam, J.; Akhtar, M.N. Fly ash utilisation in different sectors in Indian scenario, *International Journal of emerging trends in Engineering and Development* **2011**, 1.
- [27] EI-Mogazi, E.; Lisk, D.; Weinstein, L. A Review of Physical, Chemical and Biological Properties of Fly ash and Effects on Agricultural Ecosystems, *Sci. Tot. Environ.* **1988**, 74, 1-37.
- [28] Ward, C.R.; French, D. Fly ash Characteristic and Feed Coal properties, Cooperative research centre for coal in sustainable development, **2003**.
- [29] Sun, Y.; Parikh, V.; Zhang, L. Sequestration of carbon dioxide by indirect mineralisation using Victorian brown coal fly ash, *J. Hazard. Mater.* **2012**, 209-210, 458-466.
- [30] Hayashi, J.; Li, C. Chapter 2- Structure and properties of Victorian Brown Coal, *Advances in science of Victorian Brown Coal*, **2004**, 11-84.
- [31] Ranjith, P.G. Jasinge, D. Choi, S.K. The effect of CO₂ saturation on mechanical properties of Australian black coal using acoustic emission, *Fuel* **2010**, 89 (8), 2110-2117.
- [32] Black, C.; Brockway, D.; Hodges, S.; Milner, A. Utilisation of Latrobe Valley Brown coal Fly-Ash, in Gippsland Basin Symposium, **1992**.
- [33] Fansuri, H.; Pritchard, D.; Zhang, D.K. Manufacture of low-grade zeolites from fly ash for fertiliser application, Centre for Fuels and Energy, Curtin University of Technology, **2008**.
- [34] Querol, X.; Umaña, J.C.; Alastuey, A.; Ayora, C.; Lopez-Soler, A.; Plana, F. Extraction of soluble major and trace elements from fly ash in open and closed leaching systems. *Fuel* **2001**. 80, 801-813.

- [35] Ward, C.R.; French, D.; Jankowski, J.; Dubikova, M.; Li, Z.; Riley, K.W., Element mobility from fresh and long-stored acidic fly ashes associated with an Australian power station, *Int. J. Coal Geol.* **2009**, 80, 224-236.
- [36] Van der Sloot, H.A.; Heasman, L.; Quevauviller, P. Harmonisation of Leaching/Extraction Tests, Studies in Environmental Science, Volume 70, Amsterdam, Elsevier, **1997**.
- [37] Swaine, D.J. Trace Elements in Coal, London, Butterworth-Heinemann Ltd. **1990**.
- [38] Costa, G. Accelerated Carbonation of Minerals and Industrial Residues for Carbon Dioxide Storage, Università Degli Studi Di Roma, **2009**.
- [39] Lim, M.; Han, G.C.; Ahn, J.W.; You, K.S. Environmental Remediation and Conversion of Carbon Dioxide (CO₂) into Useful Green Products by Accelerated Carbonation Technology. *Int. J. Environ. Res. Public Health*, **2010**, 7, 203–228.
- [40] Pan, S.Y.; Chang, E.E.; Chiang, P.C. CO₂ Capture by Accelerated Carbonation of Alkaline Wastes: A Review on Its Principles and Applications, *Aerosol Air Qual Res.* **2012**, 12, 770–791.
- [41] Sipilä, J.; Teir, S.; Zevenhoven, R. Carbon dioxide sequestration by mineral carbonation: literature review update 2005-2007. Turku, Finland, Abo Akademi University, Faculty of Technology, Heat Engineering Laboratory, **2008**.
- [42] Lackner, K.S.; Butt, D.P.; Wendt, C.H. Progress on binding CO₂ in mineral substrates. *Energy Convers. Manag.* **1997**, 38, 259-264.
- [43] Huijgen, W.J.J.; Witkamp, G. J; Comans, R.N.J. Mineral CO₂ Sequestration in Alkaline Solid Residues; Report ECN SF ECN-RX--04-079: Petten, The Netherlands, **2004**.
- [44] Bhatia, S.K.; Perlmutter, D.D., Effect of the product layer on the kinetics of the CO₂-lime reaction. *AIChE J.* **1983**, 29, 79-86.
- [45] Abanades, J.C.; Anthony, E.J.; Lu, D.Y.; Salvador, C. Capture of CO₂ from combustion gases in a fluidised bed of CaO, *AIChE J.* **2004**, 50, 1614-1622.
- [46] Maroto-Valer, M.M.; Kuchta, M.E.; Zhang, Y.; Andrésen, J.M.; Fauth, D.J. Comparison of physical and chemical activation of serpentine for enhanced CO₂ sequestration. *J. Am. Chem. Soc. Division of Fuel Chemistry* **2004**, 49(1), 373-375.
- [47] Bonenfant, D.; Kharoune, L.; Sauvé, S.; Hausler, R.; Niquette, P.; Mimeault, M. CO₂ sequestration potential of steel slags at ambient pressure and temperature. *Ind. Eng. Chem. Res.* **2008**, 47, 7610-7616.

- [48] Lekakh, S.N.; Rawlins, C.H.; Robertson, D.G.C.; Richards, V.L.; Peaslee, K.D. Kinetics of aqueous leaching and carbonisation of steelmaking slag. *Metall. Mater. Trans.* **2008**, *39*, 125-134.
- [49] Li, J.L.; Zhang, H.N.; Xu, A.J.; Cui, J.; He, D.F.; Tian, N.Y. Theoretical and Experimental on Carbon Dioxide Degree of Steel Slag. *J. Iron Steel. Res. Int.* **2012**, *19*(12), 29-32
- [50] Chang, E.E.; Chiu, A.C.; Pan, Y.P.; Chen, Y.H.; Tan, C.S.; Chiang, P.C. Carbonation of basic oxygen furnace slag with metalworking wastewater in a slurry reactor. *Int. J. Greenh. Gas Control* **2013**, *12*, 382-389.
- [51] Uliasz-Bochenczyk, A.; Mokrzycki, E.; Piotrowski, Z.; Pomyka, R. Estimation of CO₂ sequestration potential via mineral carbonation in fly ash from lignite combustion in Poland. *Energy Procedia* **2009**, *1*, 4873-4879.
- [52] Muriithi, G.N.; Petrik, L.F.; Fatoba, O.; Gitari, W.M.; Doucet, F.J.; Nel, J.; Nyale, S. M.; Chuks, P.E.; *J. Environ. Manag.* **2013**, *127*, 212–220.
- [53] Ukwattage, N.L.; Ranjith, P.G.; Wang S.H. Investigation of the potential of coal combustion fly ash for mineral sequestration of CO₂ by accelerated carbonation, *Energy* **2013**, *52*, 230-236.
- [54] Bauer, M.; Gassen, N.; Stanjek, H.; Peiffer, S. Carbonation of lignite fly ash at ambient T and P in a semi-dry reaction system for CO₂ sequestration, *Appl. Geochemistry* **2011**, *26*, 1502–1512.
- [55] Sanna, A.; Uibu, M.; Caramanna, G.; Kuusik, R; MarotoValer, M.M. A Review of Mineral Carbonation Technologies to Sequester CO₂. *Chem. Soc. Rev.* **2014**, *43*, 8049–8080.
- [56] Levenspiel O., *Chemical Reaction Engineering*, 2nd edition, John Wiley and Sons, New York, USA, **1972**.
- [57] Guthrie, G. D.; Carey, J. W.; Bergfeld, D.; Byler, D.; Chipera, S.; Ziock, H. J. & Lackner, K. S. Geochemical aspects of the carbonation of magnesium silicates in an aqueous medium, NETL Conference on Carbon Sequestration, **2001**.
- [58] Wu, J.C.S.; Sheen, J.D.; Chen, S.Y.; Fan, Y.C. Feasibility of CO₂ fixation via artificial rock weathering, *Ind. Eng. Chem. Res.* *40*/18, **2001**, 3902-3905.
- [59] Pundsack, F.L.; Somerville, N.J. Recovery of Silica, Iron Oxide and Magnesium Carbonate from the Treatment of Serpentine with Ammonium Bisulfate, Johns-Manville Corporation, New York, **1963**.

- [60] Kodama, S.; Nishimoto, T.; Yamamoto, N.; Yogo, K.; Yamada, K. Development of a new pH-swing CO₂ mineralisation process with a recyclable reaction solution. *Energy* **2006**, 33(5), 776-784.
- [61] Doucet, F.J., Effective CO₂-specific sequestration capacity of steel slags and variability in their leaching behaviour in view of industrial mineral carbonation. *Miner. Eng.* **2010**, 23, 262-269.
- [62] Eloneva, S.; Said, A.; Fogelholm, C.J.; Zevenhoven, R. Preliminary assessment of a method utilising carbon dioxide and steelmaking slags to produce precipitated calcium carbonate, *Appl. Energy* **2012**, 90, 329–334.
- [63] Teir, S.; Revitzer, H.; Eloneva, S.; Fogelholm, C.J.; Zevenhoven, R. Dissolution of natural serpentinite in mineral and organic acids, *Int. J. Miner. Process.* **2007**, 83, 36–46.
- [64] Wang, X; Maroto-Valer, M.M Optimisation of carbon dioxide capture and storage with mineralisation using recyclable ammonium salts, *Energy* **2013**, 51, 431-438.
- [65] Wang, D.; Li, Z. Study of crystallisation kinetics of ammonium carnallite and Ammonium Chloride in the NH₄Cl-MgCl₂-H₂O System, *Ind. Eng. Chem. Res.* **2012**, 51, 2397-2406.
- [66] Jo, H.; Ahn, J.; Jo, H. Evaluation of the CO₂ sequestration capacity for coal fly ash using a flow-through column reactor under ambient conditions, *J. Hazard. Mater.* **2012**, 241–242, 127-136.
- [67] Han, S.J; Im, H.J.; Wee, J.H. Leaching and indirect mineral carbonation performance of coal fly ash-water solution system, *Appl. Energy* **2015**, 142, 274–282
- [68] Huang, K.; Inoue, K.; Harada, H. Leaching of heavy metals by citric acid from fly ash generated in municipal waste incineration plants, *J. Mater. Cycles Waste Manag.* **2011**, 13, 118-126.
- [69] Kersch, C.; Pereto Ortiza, S.; Woerlee, G.F.; Witkamp, G.J., Leachability of metals from fly ash: leaching tests before and after extraction with supercritical CO₂ and extractants, *Hydrometallurgy* **2004**, 72, 119-127.
- [70] Soco, E.; Kalemkiewicz, J. Investigations of sequential leaching behaviour of Cu and Zn from coal fly ash and their mobility in environmental conditions, *J. Hazard. Mater.* **2007**, 145, 482-487.
- [71] Ahmaruzzaman M., A review on the utilisation of fly ash, *Prog. Energ. Combust. Science* **2010**, 36, 327–363.
- [72] Iyer, R. The surface chemistry of leaching coal fly ash, *J. Hazard. Mater.* **2002**, 93, 321–329.

- [73] Ranjitham, A.M.; Khangaonkar, P.R. Leaching Behaviour of Calcined Magnesite with Ammonium Chloride Solutions, *Hydrometallurgy* **1990**, 23, 177-189.
- [74] Raschman, P. Leaching of calcined magnesite using ammonium chloride at constant pH, *Hydrometallurgy* **2000**, 56, 109-123.
- [75] Atashi, H.; Fazlollahi, F.; tehranirad, S. Leaching Kinetics of Calcined Magnesite in Ammonium Chloride Solutions. *Aust. J. Basic Appl. Sci.* **2010**, 4, 5956-5962.
- [76] Glaser, V.; Vidensky, J.; Kuzela, M. Kinetics of the reaction between magnesium oxide and ammonium chloride solution, *Collect. Czech. Chem. Commun.* **1988**. 1711–1717.
- [77] Huijgen, W.J.J.; Comans, R.N.J. Mineral CO₂ sequestration by carbonation of industrial residues, Literature review and selection of residues, **2005**.
- [78] Reddy, K. J.; John, S.; Weber, H.; Argyle, M.D.; Bhattacharyya, P.; Taylor, D.T.; Christensen, M.; Foulke, T.; Fahlsing, P. *Energy Procedia* **2011**, 4, 1574–1583.
- [79] Leung, D.Y.C; Caramanna, G; Maroto-Valer M.M., An overview of current status of carbon dioxide capture and storage technologies, *Renew. Sust. Energ. Rev.* **2014**, 39, 426-443.
- [80] Zevenhoven, R.; Fagerlund, J.; Joel S.K.; CO₂ mineral sequestration: developments toward large-scale application. *Greenhouse Gases Science and Technology* **2011**, 1, 48-57.

Monash University

Declaration for Thesis Chapter 3

Declaration by candidate

In the case of Chapter 3, the nature and extent of my contribution to the work was the following:

Nature of contribution	Extent of contribution (%)
Experimental design and conduct, analysis of results and writing up.	95 %

The following co-authors contributed to the work. If co-authors are students at Monash University, the extent of their contribution in percentage terms must be stated:

Name	Nature of contribution	Extent of contribution (%) for student co-authors only
Yi Lynn Eng	Experimental work	5%
Lian Zhang	Experimental design, key ideas, reviewing and editing paper	Supervisor
Cordelia Selomulya	Editing paper	Supervisor
Nawshad Haque	Comments on my work	Supervisor

The undersigned hereby certify that the above declaration correctly reflects the nature and extent of the candidate's and co-authors' contributions to this work*.

Candidate's Signature		Date 12/11/2015
-----------------------	---	--------------------

Main Supervisor's Signature		Date 12/11/2015
-----------------------------	---	--------------------

*Note: Where the responsible author is not the candidate's main supervisor, the main supervisor should consult with the responsible author to agree on the respective contributions of the authors.

Chapter 3

Multiple cycle leaching-carbonation and leaching kinetic modelling

The literature review on chapter 2 has shown the necessity of establishing a closed-loop multi-stage leaching-carbonation using regenerative ammonium chloride as leaching agent. This process allows an efficient and selective extraction of magnesium and calcium from Victorian brown coal fly ash, under the mild operating condition ($< 80^{\circ}\text{C}$ and atmospheric pressure). The leaching process was optimised by changing the effective parameters such as time and temperature to maximise the extraction of the target elements (Mg and Ca). Ultimately, detailed modelling on kinetic of leaching reaction was also conducted. This chapter has been reformatted from the following published manuscript: **T. Hosseini**, C. Selomulya, N. Haque, L. Zhang, Indirect Carbonation of Victorian Brown Coal Fly Ash for CO_2 Sequestration: Multiple-Cycle Leaching-Carbonation and Magnesium Leaching Kinetic Modelling, *Energy & Fuels*, 2014, 28(10), pp 6481–6493.

3.1 Abstract

In this chapter, a closed-loop multi-step process which allows leaching and precipitation of magnesium and calcium as carbonate from Victorian brown coal fly ash has been examined. Victorian brown coal fly ash has a distinctively high concentration of alkaline earth metals and low amounts of aluminium and silica. The main objective here is to clarify the dissolution kinetics of magnesium and calcium in regenerative ammonium chloride and subsequently carbonation of dissolved cations. Instead of a once-through test with fresh ammonium chloride, a multiple locked circuits were adopted to assess the leaching capability of regenerated ammonium salt, as well as the accumulation of impurities upon the recycling and reuse of the leaching agent. As has been revealed, upon increasing cycles of ammonium chloride use, the extraction yields of both target cations decreased significantly. Their extraction by ammonium chloride was favoured by the presence of oxide form in the original ash sample, with the extraction of calcium occurring much faster than that of magnesium. Both phenomena were in agreement with the thermodynamic equilibrium prediction on the lowest Gibbs function for the dissolution of oxides, especially calcium oxide in ammonium chloride solution. Carbonation results dropped gradually upon the increase in the cycle number meanwhile size and morphology of precipitates were changed from first to last cycle. By fitting the observed results with a shrinking core model, it was shown that the extraction of Mg^{2+} followed a pseudo-second order reaction with a non-constant ammonium chloride concentration in the film layer on the surface of a solid particle. The activation energy of 20.7 kJ/mol was obtained for the dissolution of magnesium from both Hazelwood fly ash and pure MgO in ammonium chloride solution.

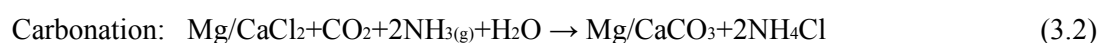
3.2 Introduction

Mineral carbonation or mineralisation is one of the most promising processes for carbon capture, storage, and utilisation (CCSU) to combat the climate change. In this process, carbon dioxide (CO_2) reacts with alkaline oxides or hydroxides, specifically magnesium and/or calcium in natural minerals or industrial waste to convert into thermodynamically stable carbonates, thus avoiding the necessity of the costly monitoring of CO_2 leakage during transportation and storage [1].

Mineral carbonation technologies can be divided into single-step (direct) and multiple-step (indirect) categories. The single-step method involves a direct reaction of feedstock material with CO_2 in a single reactor maintained at controlled temperature and pressure which generally fall in the range of 100-500°C and 10-20 bar, respectively [2]. In contrast, the multi-step indirect carbonation is initiated by the dissolution of a mineral species in an aqueous media to extract the alkaline earth metals within it. The resulting cations are subsequently carbonated through

bubbling the CO₂-containing flue gas into the leachate. Both leaching and carbonation take place under relatively mild conditions, *e.g.* 20-80°C and 1-5 bar.

The leaching media for the dissolution of calcium and magnesium in minerals are either strong or weak acidic reagents, ammonium salts, or alkaline solutions [3]. Of those, the ammonium extraction process appears to be a favourable technique, given its potential for reagent recovery and the relatively large selectivity of magnesium and calcium over other elements [4], as demonstrated by the reactions below:



To date, various types of minerals rich in alkaline earth metals, either natural species or man-made industry waste have been tested for their carbonation propensities. These include serpentine [5], olivine and wollastonite [6], fly ash derived from coal combustion and municipal solid waste incineration (MSWI) [3,7] blast furnace, and steel-making slag [1,8]. Brown coal fly ash is a potentially appropriate source as it is rich in magnesium and/or calcium. The fly ash is generated on-site with CO₂ together in a power plant. It possesses a particle size distribution with the majority falling in the micron even sub-micron scale, thereby requiring no comminution prior to utilisation. In addition, the conversion of fly ash from zero value waste into value-added high-purity carbonates could create extra income stream for power plants, thereby offsetting the carbon tax to be implemented in the carbon-constrained future [9-12,3]. The capacity to sequester CO₂ for fly ash depends directly on the proportion of binary oxides (CaO and MgO) and/or hydroxides (Ca(OH)₂) and Mg(OH)₂) contained in the waste matrix. For example, a fly ash containing a high percentage of free magnesium in oxide form can be carbonated more readily than a fly ash with the same magnesium content, but in the form of silicates. Thus it is difficult to directly compare the efficiency of various fly ashes for mineral carbon sequestration [13].

Brown coal is the single largest energy source in the state of Victoria, Australia, meeting >85% of its electricity need. The combustion of brown coal yields up to 1.3 million tonnes fly ash annually, nearly all of which were simply dumped in ash ponds. Victorian brown coal fly ash has a chemical composition dominated by magnesium, calcium, iron and sulfur and is classified as being a strongly alkaline fly ash that is not suitable as cement's additive [3]. Due to its high moisture content, the brown coal combustion generates a high CO₂ emission rate relative to the high - rank black coal and natural gas in Australia [14]. A cost-effective carbon capture process is pivotal for the sustainability of brown coal in the carbon-constrained future. Moreover, with the continuous increase in the amount of fly ash generated, it incurs the increasing demand on the use of vast land for landfill, which also contaminates the soil, ground and water simultaneously [15]. On the assumption of total conversion of magnesium and calcium to

carbonate in a typical Victorian brown coal fly ash with around 32% CaO and 29% MgO (**Table 3-1**), the carbonation reaction is expected to capture 278 kg CO₂ per tonne of raw fly ash, which is equivalent to a total amount of 0.36 million tonnes CO₂ captured per annum. Sun et al. (2012) compared the CO₂ sequestration capacity of Victorian brown coal fly ash with other fly ashes and found 264 kg CO₂ per tonne of raw fly ash at 60 °C, 10 bar and 1 h reaction time which is higher than lignite and black coal fly ashes [3]. Although this number is much smaller than that total amount of CO₂ released, it is expected that the industrial mineral wastes can act as supplement to the natural minerals for CO₂ capture.

Considering the broad variation of fly ash properties, the methods developed in the literature are generally not applicable to different samples. To date, the majority of studies on fly ash utilisation have focused on direct carbonation under a high CO₂ partial pressure with a rather long reaction time [16-18]. However, reports on utilisation of coal fly ash are limited with the research target set only to optimise the conditions for once-through leaching and carbonation stages. The integration of leaching and carbonation stages, and the recovery of leaching reagent are yet to be discussed. Moreover, the mechanisms underpinning the dissolution of magnesium upon leaching of fly ash are rarely reported [19]. Few papers reported leaching kinetics of different elements including Al, Fe, Ca and trace elements like Cr, Zn, As from coal fly ash [20,21].

Elemental leaching from fly ash is a complex process, which involves dissolution, diffusion, adsorption, and mineral precipitation. Leaching of ash takes place through dissolution of constituents inside or on the surface of ash particle and transport through the pore structure to the surrounding solution. For solid–fluid reactions, the shrinking core kinetic model has been used widely [22]. Ranjitham et al. [23], Raschman [24] and Atashi et al. [25] have successfully applied this model to the leaching kinetic of calcined magnesite in ammonium chloride with a concentration of about 1 M. Paul et al. indicated that the kinetic of acid consumption for different types of Turkish fly ashes consist of an initially fast process followed by a slower period [19]. To reiterate, all these studies only focused on the once-through fresh leaching reagent.

In this study, two types of Victorian brown coal fly ash were tested in multiple cycles of the leaching-carbonation closed loop using regenerative ammonium chloride as the leaching reagent. The aim is to clarify the extraction and carbonation mechanisms of magnesium (as well as calcium) in an industrially relevant process. That is, rather than the use of fresh reagent for once-through investigation, a multi-cycle experiment has been conducted to reveal the recyclability of a regenerative reagent, ammonia chloride. As comparison to fly ash, pure oxide compounds of predominant elements (MgO, CaO and Fe₂O₃) and their mixtures were also examined in the multi-cycle mode to evaluate the influence of impurities in fly ash on the extraction of target oxides. Furthermore, a detailed modelling on the leaching of magnesium

from pure oxide and fly ash was conducted by assessing the applicability of various models, so as to provide an accurate model for future scale-up.

3.3 Materials and experimental methods

3.3.1 Materials preparation

Two coal fly ash samples were collected as dry powders from the electrostatic precipitator in International Power Hazelwood, and Energy Australia Yallourn power plant located at the Latrobe Valley, Victoria, Australia. Once being delivered to the laboratory, each fly ash sample was initially washed with water with liquid to solid ratio of 10 to remove the unburnt carbon and water-soluble species such as sodium and potassium sulfate. Subsequently, the water-washed fly ash samples were dried in oven at 120°C overnight and crushed mildly below 150 µm prior to use. Pure MgO and CaO samples were prepared by calcination of magnesium carbonate and calcium carbonate (purchased from Sigma-Aldrich), respectively. The temperature and time for calcination in a muffle furnace were fixed at 800°C and 12 h, respectively [23]. The resulting MgO and CaO obtained were analysed by thermogravimetric analysis (TGA) to ensure a complete calcination of the carbonates. Pure Fe₂O₃ was purchased from Sigma-Aldrich in oxide form. In addition, the analytical grade ammonium chloride was purchased from Merck with a purity of 98%.

For the comparison to fly ash samples, the pure oxide and their mixtures were also tested on multiple leaching-carbonation cycles, including pure MgO, mixtures of MgO+CaO (mass ratio 1:1), and mixtures of MgO+Fe₂O₃ (mass ratio 1:4). These ratios were selected based on molecular weights and weight percentages of these metals in the two fly ash samples.

3.3.2 Materials characterisation

The elemental composition of a raw sample, its leaching residues, and precipitated carbonates were determined by a pre-calibrated X-ray fluorescence spectroscopy (XRF, Spectro iQ II). About 3-4 g of a representative sample was finely ground and stored in a sample holder for the XRF analysis. The leaching percentage of each element was calculated based on the difference between its mass in raw washed sample and solid residue after drying. The produced carbonates were dried overnight at 105°C and weighted to determine the conversion. The mineralogical composition of raw fly ash and few leaching residues and carbonates were determined by X-ray diffraction analysis (XRD, Rigaku, Miniflex), under scanning speed 1°/min from 2 to 90°, 40 kV and 15 mA. The peak identification was achieved by search-match function in the JADE software.

Scanning electron microscopy (SEM) was employed for morphology observation of carbonate precipitates. The sample powder was dispersed into carbon-taped sample holder stub and platinum coated. Each carbonate precipitate was characterised by randomly selecting 3-4 fields of view and examining all the fly ash particles observed within the selected fields. The SEM microscopes used are a JEOL JSM-7001F equipped with energy dispersive X-ray spectroscopy (EDX). SEM imaging studies were performed at 15 kV at a working distance of 10 mm.

3.3.3 Thermodynamic equilibrium calculation

The different species and phases, which were known to be existed, were specified into the reaction equation module of HSC Chemistry 7.1 to calculate multi-component equilibrium compositions for the heterogeneous systems. The heat capacity, enthalpy, entropy and Gibbs energy of a single species and reactions system of pure substances were provided by the built-in database in the HSC Chemistry [26]. The Gibbs free energy of the reactions of various Mg and Ca-bearing species with ammonium chloride were calculated at a wide temperature range.

3.3.4 Single leaching conditions

For each run, 10 g of a sample in dried powder form was mixed with 60 ml, 4 M ammonium chloride at a liquid to solid ratio of 6. The liquid to solid ratio and ammonium chloride concentration were fixed throughout this study. Instead, a broad range of temperature (25, 40, 60 and 80°C) and time (10-60 min) was varied and three replications were carried out for each condition. The temperature was not increased further due to the limitation of operation at higher temperatures in industry and to avoid evaporation of aqueous solutions that might increase the concentration of ammonium chloride, thus causing the dissolved ammonium chloride to precipitate back in leaching residue. In addition, the study on leaching behaviour of calcined magnesite carried out by Ranjitham and Khangaonkar showed insignificant change of leaching progress at temperatures above 80°C [23].

Batch leaching tests were performed in a glass sealed beaker equipped with two connections, one for feeding air of 1 L/min, while another tube is to release ammonia vapour that is then trapped in a conical flask containing distilled water. The reaction temperature (40-80°C) was controlled by immersing the reactor in a thermostat-controlled water bath. A magnetic stirrer bar with a stirring speed of 350 rpm enabled the solution to be fully agitated with minimal spillage. The resulting residue after filtration were dried at 120°C overnight in an oven, weighed and quantified by XRF for elemental compositions to determine the leaching percentages of individual elements, particularly magnesium and calcium. The resulting ammonium water was titrated by acetic acid (1 M) to determine the amount of the ammonia recovered from the leaching step.

3.3.5 Single carbonation conditions

Following each leaching experiment, the resulting leachate is subsequently carbonated by the conditions of the pH of the 9-10 [8] through the doping of ammonia water (NH_3 , generated from leaching step), a continuous injection of pure CO_2 at 15 L/min and 20 min. The amount of ammonia added in the carbonation tank is exactly the same as that evaporated from the leaching step to ensure a closure of the whole process in NH_3 balance. These conditions were optimised in our previous works. According to reactions (3.1) and (3.2) the Mg^{2+} and Ca^{2+} cations in the leachate are expected to fully precipitate out as solid carbonate, which in turn results in the regeneration of ammonia chloride to be used in next round. The resulting carbonate was filtered and dried overnight in the oven, and its mass was recorded.

3.3.6 Five cycles leaching-carbonation conditions

Once a cycle of leaching-carbonation is finished, the regenerated ammonia chloride was tested again for a total of five cycles in this study. The experiments for all the leaching and carbonate exactly follow the above-mentioned conditions, except that a few amount of fresh hydrochloric acid (2 M) was doped into the regenerated chloride to reduce its pH back to the original value of 4.5. The increase in the pH of ammonia chloride is attributed to the accumulation of un-reacted alkali and alkaline earth metal cations after carbonation.

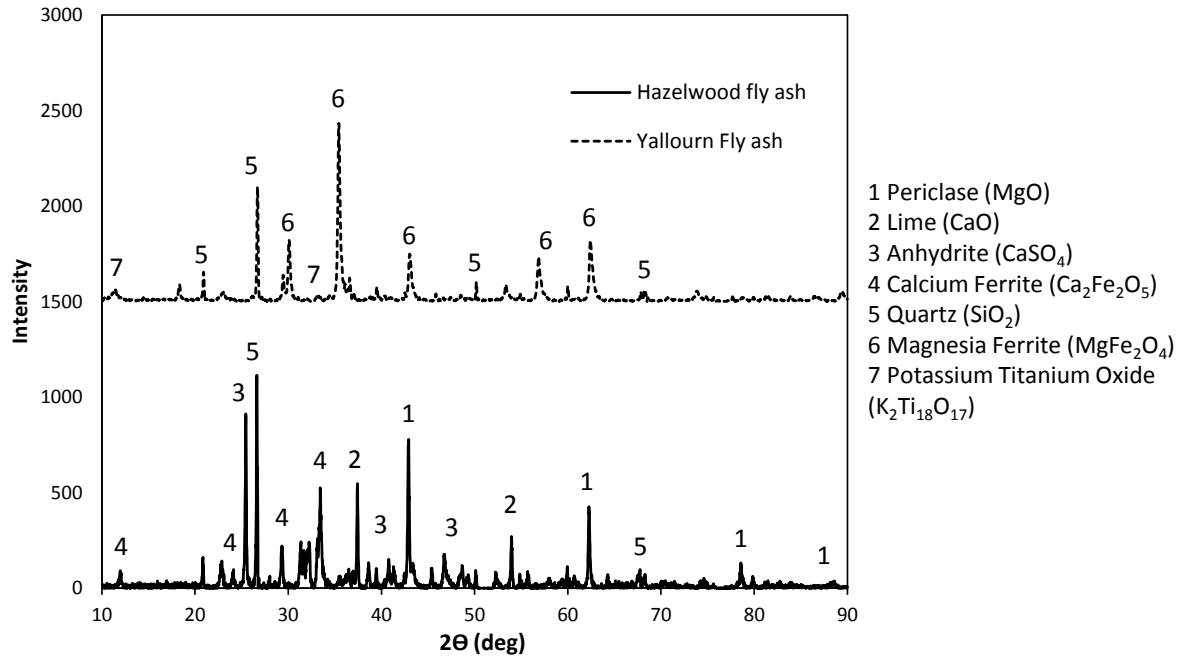
3.4 Results and Discussions

3.4.1 Properties of fly ashes

Table 3.1 tabulates XRF results in the oxide forms for the as-received and washed Hazelwood and Yallourn fly ash samples. The major elements are Mg, Ca and Fe. Hazelwood fly ash is rich in MgO and CaO (29.3% and 32.4%, respectively) and includes 14% Fe_2O_3 , whereas the predominant elements in Yallourn fly ash are Fe_2O_3 and MgO (42.3% and 27.9%, respectively) with only 9.4% CaO. **Figure 3.1** depicts the XRD spectra for Hazelwood and Yallourn fly ash. As can be seen, periclase (MgO) is the only Mg-bearing crystal species in Hazelwood fly ash, which is accompanied by Ca-bearing species including anhydrite (CaSO_4), lime (CaO), calcium ferrite (CaFe_2O_4) and silicate. Only two major crystalline phases were found in Yallourn fly ash, with magnesia ferrite showing the strongest intensity and quartz with a medium peak height. Interestingly, calcium (9.4% in its oxide form) in Yallourn fly ash was present as an amorphous structure that was undetectable by XRD analysis.

Table 3.1 Waste minerals elemental quantification (XRF)

	Composition (%)								
	SiO ₂	Al ₂ O ₃	Fe ₂ O ₃	CaO	MgO	Na ₂ O	K ₂ O	P ₂ O ₅	SO ₃
Hazelwood fly ash	5.82	3.01	14	32.4	29.3	0.2	0.17	0.41	12.8
Yallourn fly ash	8.92	5.92	42.3	9.4	27.9	0.56	0.16	0.11	2.84

**Figure 3.1** XRD spectra for Hazelwood fly ash and Yallourn fly ash

3.4.2 Single leaching results

The solid lines in **Figure 3.2** illustrate the leaching percentage of pure MgO as a function of temperature and time. In contrast, the dashed lines show the magnesium leaching percentage from Hazelwood fly ash. The error bars refer to standard deviations from measured values of three replicates. The nearly identical results for magnesium extraction from both pure MgO and Hazelwood fly ash can be confirmed for the same condition. This substantiates the presence of the majority of magnesium as free oxide in Hazelwood fly ash and insignificant influence of impurities and the other forms of magnesium in this fly ash, if any. The leaching temperature was influential as it improved the equilibrium fraction of magnesium leached in 1 h from around 20% at 25 °C to 32% at 80 °C. The increasing trend of temperature is consistent with observation of Ranjitham and Khangaonkar on sensitivity of leaching of calcined magnesite with temperature up to 80°C. However they achieved around 43% magnesium extraction at 80°C and 30 min

reaction time with L/S equal to 20. The lower pH of their solution emerges from using significant amount of leaching agent is the likely cause of discrepancy [23].

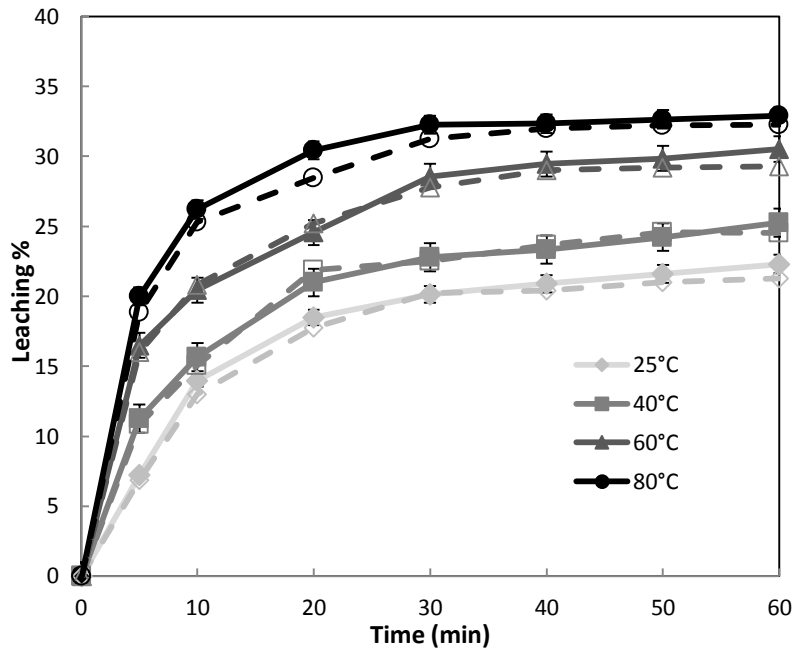


Figure 3.2 Effect of time and temperature on leaching of magnesium with NH_4Cl 4M, L/S=6. Solid lines represent leaching from pure MgO and dashed lines refer to Hazelwood Fly ash

At a given temperature, the leaching fraction of magnesium increased exponentially over time, reaching its maximum at around 30 min. The leaching of magnesium was nearly ceased from 30 min onwards. The probable explanation for this phenomenon is the crystallisation of ammonium chloride and the possible reaction of free Mg^{2+} with OH^- from ammonium hydroxide on the surface of ash at high pH, creating a passive layer on the surface of particles to block the continued leaching of magnesium.

To validate the above proposed hypothesis, the thermal decomposition of leaching residue obtained from condition of 80°C and 1 h for the use of pure MgO was conducted by TGA, at a heating rate of 5°C/min from room temperature to 800°C. **Figure 3.3** illustrates a three-step mass loss for the residue tested. The first loss was commenced before 200°C, which can be assigned as to hydrate; the second one at around 330°C is attributed to the decomposition of ammonium chloride crystals which is 338°C for the pure compound [27]; whereas the last one at about 490°C was due to the decomposition of magnesium hydroxide. A significant decrease in weight of leaching residue after washing with water was another proof for the existence of ammonium chloride crystal, which accounted for around 48% of the total residue. Such phenomenon has been confirmed by Wang et.al [28] who has observed that the crystallisation of NH_4Cl occurs from the NH_4Cl -rich solution when the concentration of MgCl_2 within it is increased up to 2.5–2.7 mol/L. The concentration of MgCl_2 in the leachate achieved in our study reaches 2.62 mol/L, which just falls in the above range.

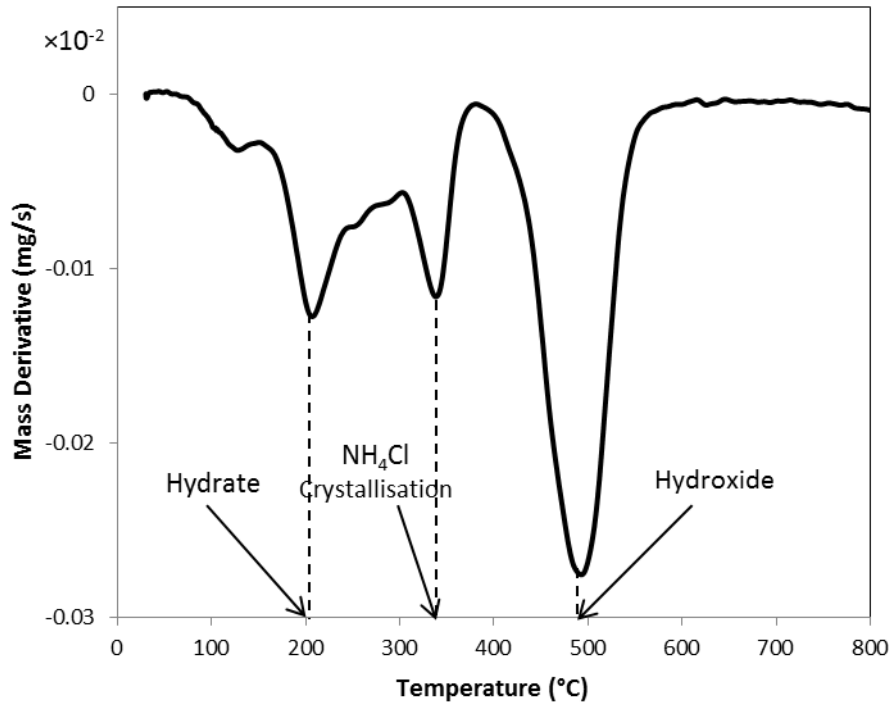


Figure 3.3 Derivative Mass loss of dried residue against temperature running TGA (Pure MgO leaching at $T=80^{\circ}\text{C}$, $t=1\text{ h}$)

The theoretical and practical ammonia recovery as a function of leaching time and temperature are presented in **Figure 3.4**. The theoretical ammonia recovery was calculated according to Equation (3.1), based on the amount of magnesium cation extracted. Increasing temperature favours the recovery of ammonia. This was expected since the solubility of ammonia will decrease at elevated temperatures. However, the practical ammonia recovery is much lower than the corresponding theoretical value, indicating that a certain fraction of evaporated ammonia gas is still present in the leachate. This may not be a big issue as the ammonia is essential for the subsequent carbonation of the dissolved Ca^{2+} and Mg^{2+} cations.

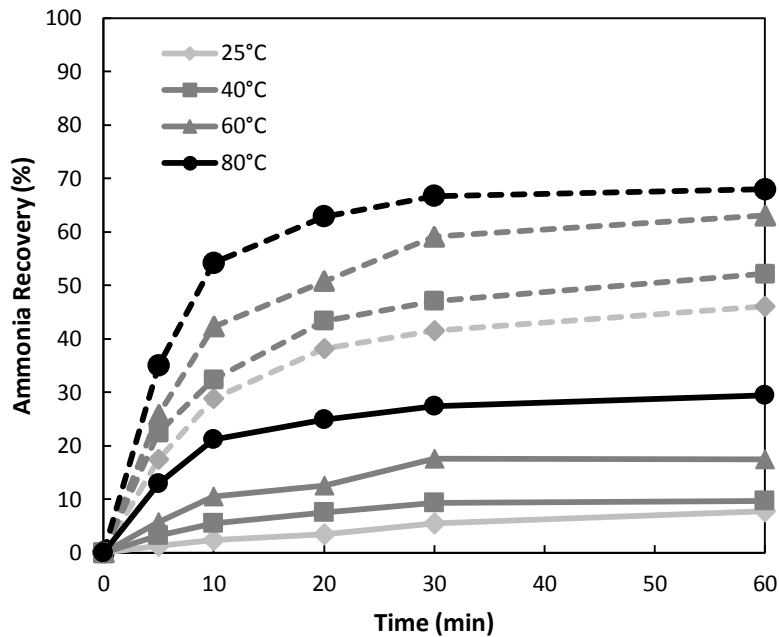


Figure 3.4 Theoretical and Practical ammonia recovery, dashed lines are related to theoretical ammonia recovery and solid lines corresponds to practical ammonia recovery (Pure MgO leaching, NH_4Cl 4M and L/S=6)

3.4.3 Five leaching-carbonation cycles

3.4.3.1 Leaching results

The leaching percentages of magnesium in pure oxide compounds upon the reuse of ammonia chloride in the five cycles are presented in the panel (a) of **Figure 3.5**, where the panel (b) shows the results of the two fly ashes tested. For pure oxide mixtures, the extraction yield of magnesium is relatively constant for the three mixtures, regardless of the cycle number. This is an indicator of the independence of the magnesium extraction on the mass of MgO in the solid sample mixtures. For all of the pure oxide mixtures, total mass of solid added to the same volume of ammonium chloride is 10 g while mass of MgO is not the same. For each pure species, upon the increase on cycle number, the extraction yield of magnesium drops slowly from ~35% in first cycle to 30% in the fifth cycle. A similar observation was confirmed for Hazelwood fly ash. However, for Yallourn fly ash, the leaching yield of magnesium reached only 25% in the first three cycles. Its leaching and carbonation were fully stopped from the third cycle (results for fourth and fifth cycle are not shown). This should be due mainly to a strong association of most of magnesium with iron in the form of magnesia ferrite in this fly ash. Accordingly, the ammonia salt was too weak to break the strong association of MgO and Fe_2O_3 .

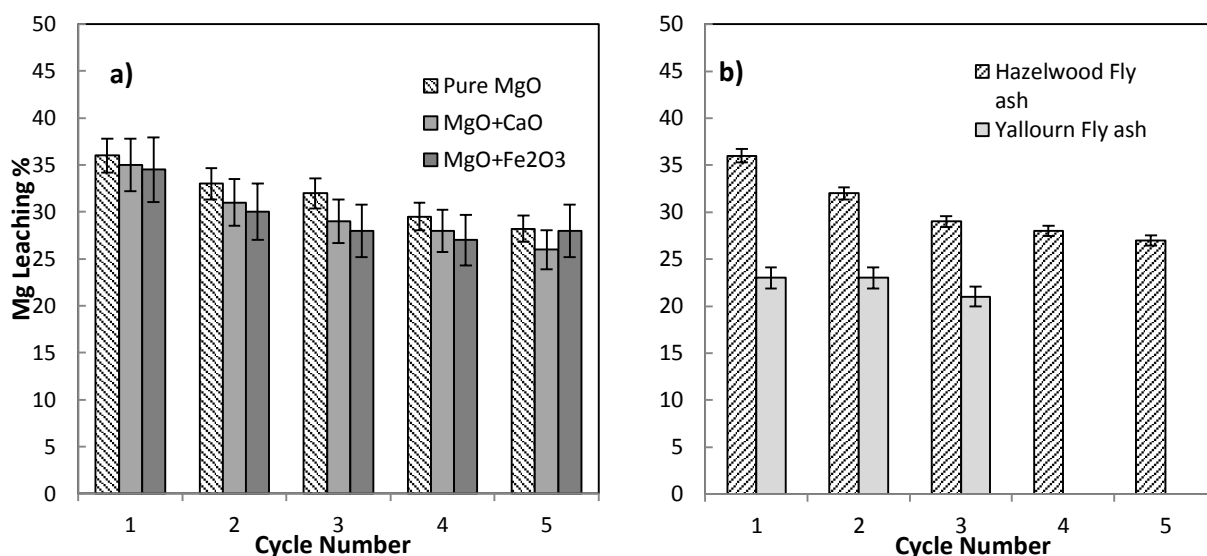


Figure 3.5 Leaching% for Mg during five cycle leaching-carbonation at optimum condition ($T=80^{\circ}\text{C}$, $t=30$ min). (a) Pure MgO, MgO + CaO and MgO + Fe₂O₃. (b) Hazelwood and Yallourn fly ash

The leaching percentage of calcium from the MgO+CaO mixtures has also been compared to the two fly ash samples. The results are presented in **Figure 3.6**. Compared to a rather constant extraction yield of around 80% for calcium from the MgO+CaO mixture, the leaching yield of calcium out of two fly ashes is much lower and decreases dramatically upon increasing the cycle number. The calcium leaching yields from two fly ash samples reach 32% for the first cycle and only 10% at the fifth cycle for Hazelwood fly ash, and from 37% to 3% for Yallourn fly ash during the three cycles tested. This was attributed to different modes of occurrence of calcium in two fly ash samples, *i.e.* abundance of mixture of anhydrite, lime and calcium ferrite in Hazelwood fly ash, and undetectable amorphous calcium aluminosilicate in Yallourn coal fly ash.

The dissolution rate of both magnesium and calcium bearing species in ammonium chloride were compared using thermodynamic equilibrium calculation (**Figure 3.7**). For the dissolution of MgO in ammonium chloride its ΔG turns negative from 80°C onwards, suggesting the spontaneity of the forward reaction to occur at this temperature. This is consistent with our results for the leaching of pure MgO and Hazelwood fly ash summarised in **Figure 3.2**. The lower magnesium leaching percentage of Yallourn fly ash rich in magnesia ferrite can also be explained by the positive ΔG for this reaction from room temperature to 200°C in **Figure 3.7**. For both calcium oxide and portlandite ($\text{Ca}(\text{OH})_2$), their dissolution ΔG is always the lowest than the other Ca-/Mg-bearing compounds, substantiating the spontaneous dissolution of these two species in ammonium chloride at every temperature. This supports the experimental observation

for higher calcium extraction percentage from the mixture of MgO+CaO than the two real fly ash samples.

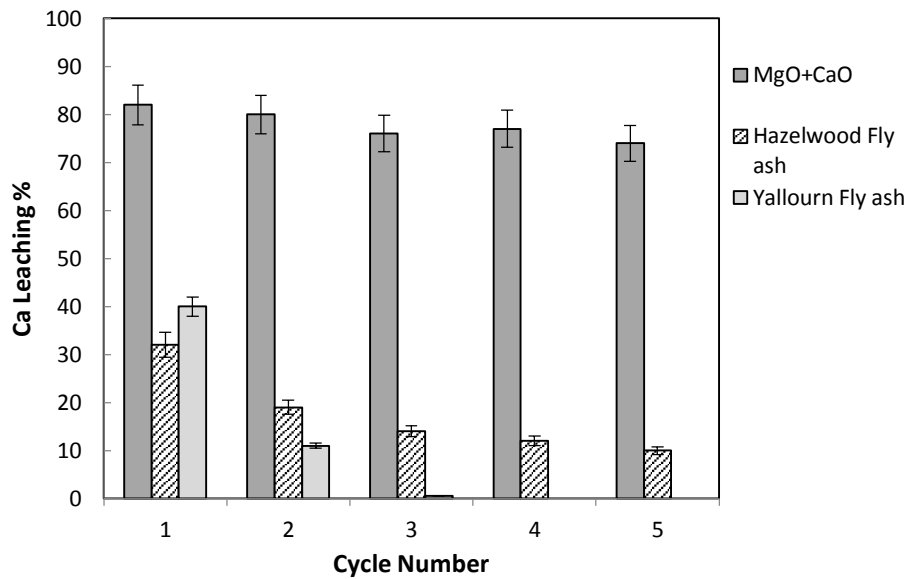


Figure 3.6 Leaching% for Ca during five cycle leaching-carbonation at optimum condition ($T=80^{\circ}\text{C}$, $t=30$ min), in MgO + CaO, Hazelwood and Yallourn fly ash

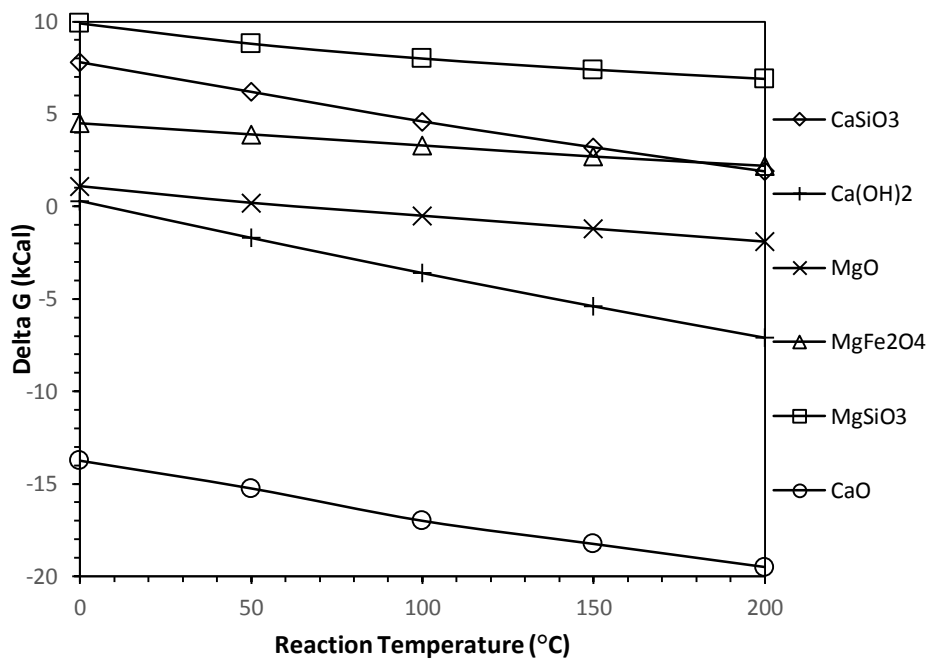


Figure 3.7 Thermodynamic equilibrium calculations for different Mg and Ca bearing species in ammonium chloride solution

The decreasing trend upon the five cycles suggests that ammonium chloride leaching capability has been declined upon recycling. It is hypothesised that increasing the concentration of dissolved magnesium and calcium ions in leachate favoured two side reactions: 1-reaction of

ammonium chloride with dissolved Mg^{2+} cation to form a complex precipitate, 2-ammonium chloride crystallisation during carbonation. The second hypothesis has been proven by the leaching residue mass loss profile upon heating in **Figure 3.3**. To further support the first hypothesis, XRD analysis results for the leaching residue and carbonate from first cycle of multiple cycle leaching-carbonation of pure MgO are presented in **Figure 3.8**. The presence of magnesium-chloride complex in leaching residues has been confirmed, which are also water-soluble upon washing the leaching residues. Similarly, the ammonium chloride crystals in carbonate products were confirmed too, which, again vanished upon water washing. The similar results were confirmed for the leaching residues and carbonates generated in the other cycles (XRD data not shown). Moreover, based on the assumption of producing one mole of Mg-Cl complex upon consumption of one mole of ammonium chloride, the weight loss after washing can be further derived for the fractionation of ammonium chloride complex coupled with dissolved magnesium. The results are depicted in **Figure 3.9**. For the pure MgO and its mixture with CaO, the crystallisation extent of ammonium chloride is more significant than the fraction of solid complex formed. The crystallisation extent also increases noticeably upon increasing the cycle number. Such a trend was however not found for the solid complex. In contrast, the solid complex formed has a comparable and even higher fraction than that of ammonium chloride crystal for the pure mixture of MgO+Fe₂O₃ and Hazelwood fly ash. This suggests that Fe₂O₃ and other impurities in fly ash are in favour of the combination of ammonium and MgO into complex solid. This explains the extremely low extraction yield for magnesium out of MgO+Fe₂O₃ mixture and Yallourn coal fly ash. Moreover, the concentration of ammonium chloride at each cycle were also calculated and summarised in **Table 3.2**. As can be seen, for all of the four leachates examined, ammonium chloride concentration was decreased gradually from first cycle to last cycle. It is another direct evidence for loss of ammonium chloride from the solution upon recycling.

Table 3.2 NH₄Cl concentration at start point of each cycle for MgO, MgO+CaO, MgO+Fe₂O₃, Hazelwood Fly ash

Cycle	NH ₄ Cl Concentration (M)			
	MgO	MgO+CaO	MgO+Fe ₂ O ₃	Hazelwood Fly ash
1	4	4	4	4
2	3.47	3.52	3.58	3.38
3	3.02	3.04	3.01	2.99
4	2.81	2.84	2.86	2.85
5	2.67	2.73	2.76	2.72

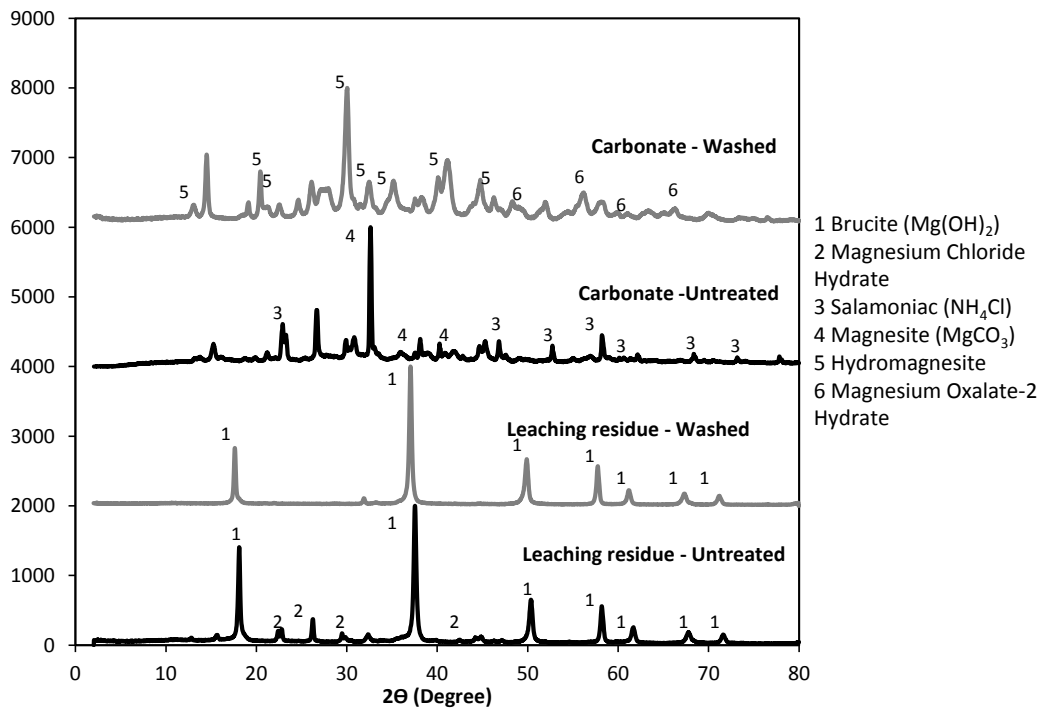


Figure 3.8 XRD results for first cycle leaching residue and carbonate before and after washing for pure MgO

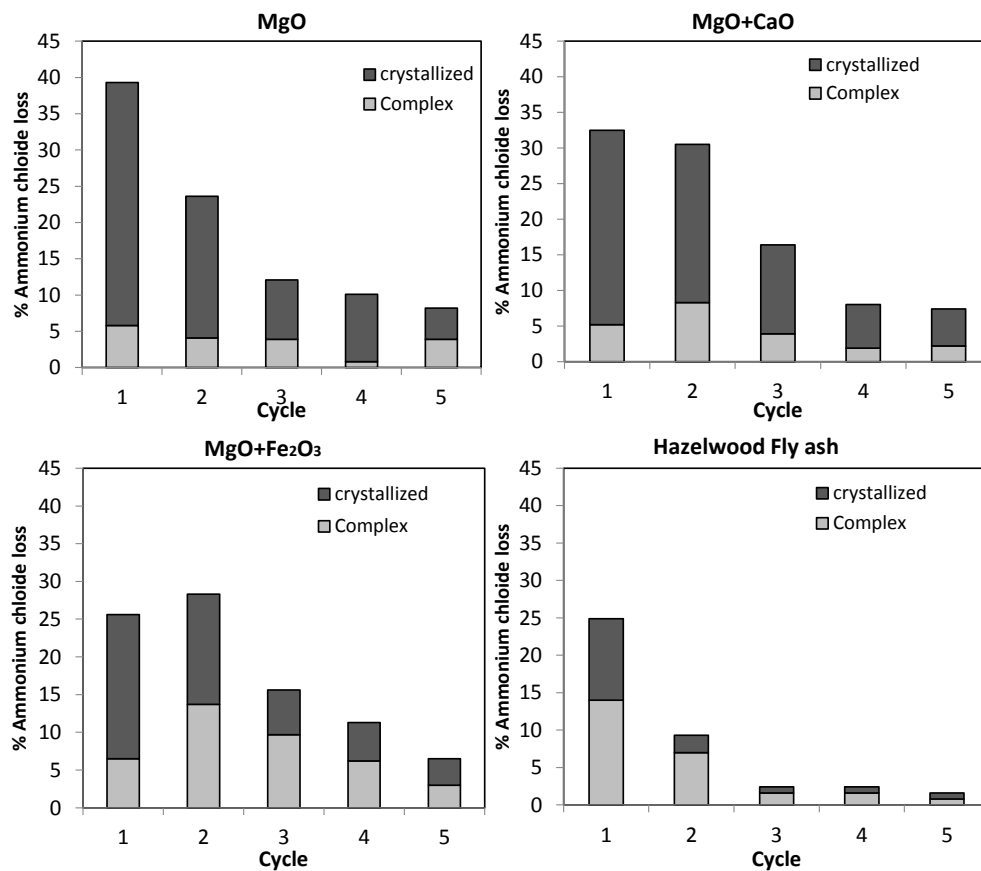


Figure 3.9 Loss percentage of NH_4Cl at each cycle breaking down to crystallised and complex formed for MgO, MgO+CaO, MgO+Fe₂O₃ and Hazelwood fly ash. Water washing was done at RT, L/S=10 and t=1h

3.4.3.2 Carbonation results

Figure 3.10 demonstrates the carbonation percentage of Mg from the leachates of (a) different mixtures of pure oxides and (b) two fly ashes. The panel (a) indicates that, irrespective of the oxide mixture type, the carbonation percentage of magnesium reaches nearly 100% at the first cycle, and drops gradually upon the increase in the cycle number. For the two fly ash samples in the panel (b), magnesium in the Hazelwood Fly ash leachate was nearly fully carbonated in the first cycle. Its carbonation yield, however, was dropped quickly to only 50% in the fifth round. This is clearly faster than the pure oxide compounds shown in the panel (a). Moreover, the performance of Yallourn fly ash leachate is even worse, with the carbonation degrees for Mg^{2+} cations decreasing sharply from 31% in first cycle to nearly zero in the third cycle. These results link with the afore-mentioned phenomenon on the loss of ammonium and magnesium into solid complex and crystallisation species in the leaching residues.

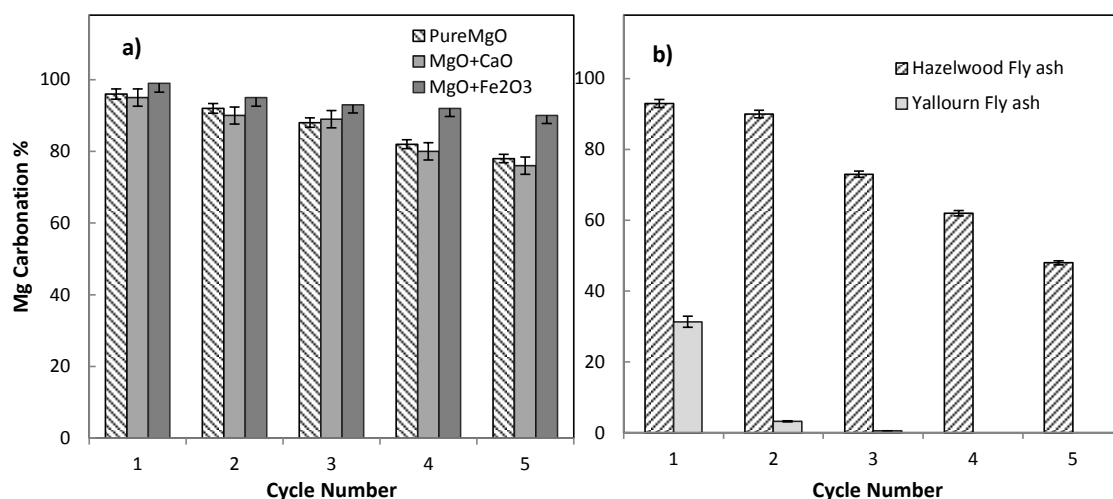


Figure 3.10 Carbonation% for Mg during five cycle leaching-carbonation at optimum condition ($T=RT$, $t=20$ min). (a) Pure MgO, MgO + CaO and MgO + Fe₂O₃. (b) Hazelwood and Yallourn fly ash.

The carbonation percentage of calcium in MgO+CaO, Hazelwood fly ash and Yallourn fly ash are presented in **Figure 3.11**. Compared to Mg^{2+} cation in the leachate from the mixture of MgO+CaO, Ca^{2+} cation showed a slightly low carbonation extent, with a similar trend of decreasing slightly from 90% in first cycle to 76% in last cycle. The Ca^{2+} cation in the leachate of Hazelwood fly ash shows the same calcium carbonation behaviour as the mixture of oxide (MgO+CaO) in the first and second cycles. However, its carbonation extent was decreased sharply after second cycle and reached 32% at the fifth cycle. Similarly, the Yallourn fly ash carbonation percentage is the lowest among the samples tested, dropping from 40% to a negligible value at the third cycle.

Availability of calcium and magnesium seems to be significant factors influencing carbonation with pH, temperature and CO₂ pressure [29]. Competition between ions present in solution can influence the nature and morphology of precipitated carbonates [30]. **Figure 3.12** and **Table 3.3** correspond to a suite of typical SEM images and their elemental point analysis of the carbonate precipitates from the first and last cycle of (a) pure MgO, (b) MgO+CaO, (c) MgO + Fe₂O₃ and (d) Hazelwood fly ash. Being complementary to the SEM observation, XRD results on the major Mg and Ca-bearing carbonate minerals are summarised in **Table 3.4**.

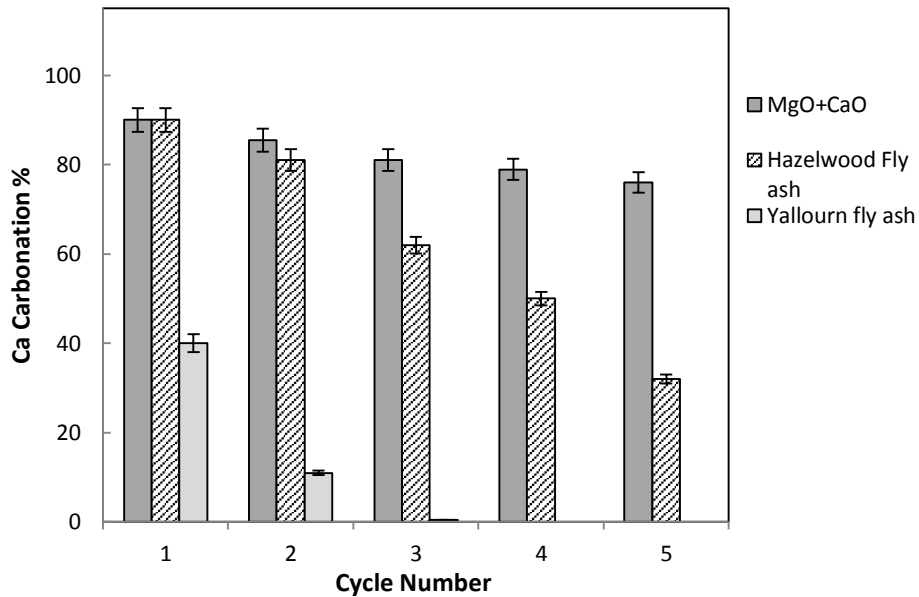


Figure 3.11 Carbonation % for Ca during five cycle leaching-carbonation at optimum condition (T=RT, t=20 min), in MgO + CaO, Hazelwood and Yallourn fly ash

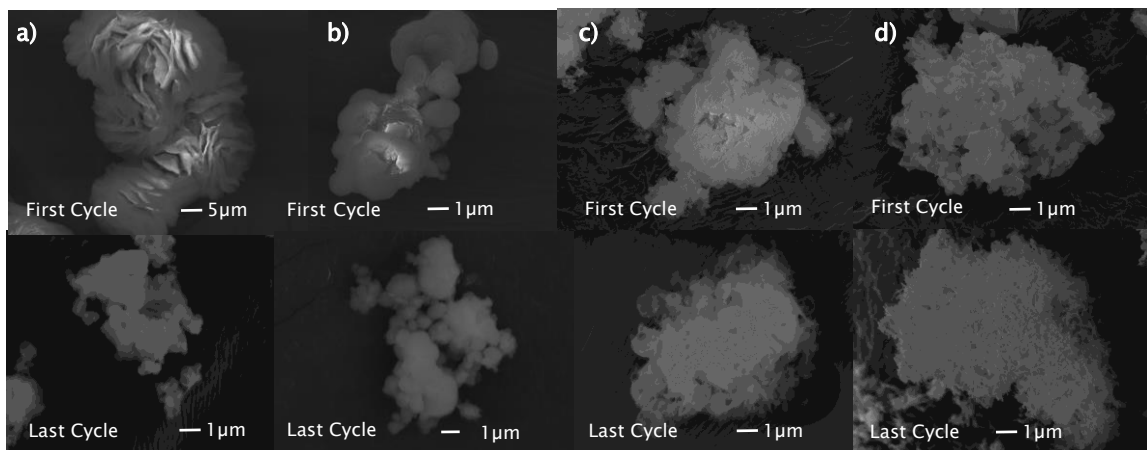


Figure 3.12 SEM images of carbonate obtained from first and last cycle of multiple cycle leaching- carbonation. (a) Pure MgO (b) MgO+CaO (c) MgO+Fe₂O₃ and (d) Hazelwood fly ash

In the case of pure MgO as demonstrated in the **Figure 3.12 (a)**, the first cycle carbonate is dominated by discrete rosettes of magnesite (MgCO₃). Under natural conditions hydromagnesite or other meta-stable phases like nesquehonite and lansfordite may form depending on the

availability of the Mg^{2+} ions in solution in relation to the availability of other cations such as Ca^{2+} [31]. In addition, transformation of nesquehonite to magnesite or amorphous magnesium carbonate at 70-100°C was reported by Hollingbery et al. (2010) which may occur during drying in the oven at temperature around 110°C [32]. Instead, the last cycle precipitates showed aggregates of small round particles. Such a discrepancy should be caused by the decreased concentration of magnesium cation in the leachate in the last cycle, which preferred to precipitate into small crystals that are too dilute to agglomerate together. This is consistent with observation of Case et al. (2011) that concluded higher concentration of magnesium ion in solution along with adding substrate increases nucleation rate of magnesium precipitates [33]. Among the minerals formed in the MgO-CO₂-H₂O systems, the anhydrous phase, magnesite (MgCO₃) is the only thermodynamically stable mineral at room temperature. However, magnesium carbonation needs initial central nuclei which the rate of precipitation can be accelerated by presence of other elements or formation of hydroxide act as substrate for nucleation growth [34].

Table 3.3 Elemental point analysis of representative precipitates particles obtained from first and last cycle of five cycle leaching carbonation of pure MgO, MgO+CaO, MgO+Fe₂O₃ and Hazelwood fly ash determined by EDX

Sample	Cycle	Elemental Composition (wt%)					
		Ca	Mg	Fe	S	Cl	O
Pure MgO	First	-	26	-	-	21	53
	Last	-	4	-	-	8	68
MgO+CaO	First	34	2	-	-	8	56
	Last	14	20	-	-	13	53
MgO+Fe ₂ O ₃	First	-	24	-	-	20	56
	Last	-	30	-	-	5	65
Hazelwood fly ash	First	16	20	-	-	13	51
	Last	23	14	-	2	7	54

Regarding the case of MgO+CaO mixture, its carbonate precipitates in **Figure 3.12 (b)** suggest the polymorph of round particles for the first cycle while in the last cycle aggregate of rhombohedral platy particles were observed. EDX mapping showed scattered magnesium particles between calcium particles. Strong peaks of magnesite and lansfordite in XRD spectra suggests diffusion of magnesium ions to internal layers of calcite lattice. The sensitivity of calcium carbonate crystallisation to the presence of magnesium ions has been reported by several investigators [30,35]. Roques and Girou (1974) have reported that calcium carbonate precipitation was markedly reduced by presence of small amount of magnesium ions in the

solution. The ions of Mg stabilise amorphous, unstable and hydrated phases and so decrease the quantity of well crystallised carbonates [36].

The crystalline structures of carbonate precipitates from first and last cycle of MgO+Fe₂O₃ are present in **Figure 3.12 (c)**. In comparison to the precipitates from MgO leachate (**Figure 3.12 (a)**), the presence of iron in the leachate apparently changed the morphology of the magnesium carbonate particles to a relatively porous structure. However there is no significant difference observed between the first and last cycle. The smallest drop in the carbonation extent of MgO+Fe₂O₃ from first to last cycle in comparison to other mixtures is consistent with negligible change in carbonation morphology of magnesium through recycling. This can be attributed to inferior concentration of magnesium ion in the leachate and low tendency of iron to compete with magnesium to form carbonate or precipitate at the pH range of 7-9.5.

Carbonate precipitates obtained from first and last cycle leaching-carbonation of Hazelwood fly ash is present in panel *(d)* of **Figure 3.12**. As can be seen, significant changes occurs for the particle shape as the cycle number shifts from first to last. First cycle precipitates shows randomly oriented polycrystalline aggregates while at the last cycle formation of sub-micron rod shape particles coalesced and settled in the irregular shaped agglomerates was observed. XRD results for the first cycle precipitates showed incorporation of both magnesium and calcium in the crystal lattice in the form of calcite magnesian ((Ca,Mg)CO₃). Calcium sulfate peak in the last cycle XRD spectra shows affinity of calcium ion to react with high concentration of sulfate ion in the leachate to form solid precipitate. Bischoff and Fyfe (1968) reported inhibition of calcite formation strongly by presence of magnesium and less strongly by sulfate ions [35]. The increased concentration of interfering ions concentration in leachate upon recycling clearly affected the morphology of carbonate.

Table 3.4 Different Mg and Ca-bearing minerals detected by XRD for the first and last cycle of carbonation obtained from multiple cycle leaching carbonation of pure MgO, MgO+CaO, MgO+Fe₂O₃ and Hazelwood fly ash

Cycle	Pure MgO	MgO+CaO	MgO+Fe ₂ O ₃	Hazelwood fly ash
First cycle	Magnesite (MgCO ₃)	Magnesite (MgCO ₃) Lansfordite MgCO ₃ .5(H ₂ O) Calcite (CaCO ₃)	Magnesite (MgCO ₃)	Magnesian calcite (Ca, Mg)CO ₃
Last cycle	Hydromagnesite Mg ₅ (CO ₃) ₄ (OH) ₂ .4(H ₂ O)	Magnesite (MgCO ₃) Lansfordite, MgCO ₃ .5(H ₂ O) Calcite (CaCO ₃)	Magnesite (MgCO ₃)	Magnesite (MgCO ₃) Calcite (CaCO ₃) Calcium sulfate (CaSO ₄)

3.4.4 Kinetic modelling of magnesium leaching

In comparison to an obvious time-dependence of the leaching of magnesium in **Figure 3.2**, the leaching of calcium in the form of oxide is much faster, which was proven in **Figure 3.13** to be finished in less than 5 min, irrespective of the leaching temperature. Clearly, the leaching of calcium in the form of oxide is mainly thermodynamically controlled, whereas its reaction rate is fast enough. In other words, for the co-existence of magnesium and calcium in a sample such as Hazelwood fly ash, the leaching of magnesium out of the solid matrix is the limiting step for the overall extraction. In this sense, the kinetic modelling for magnesium was further performed in this paper.

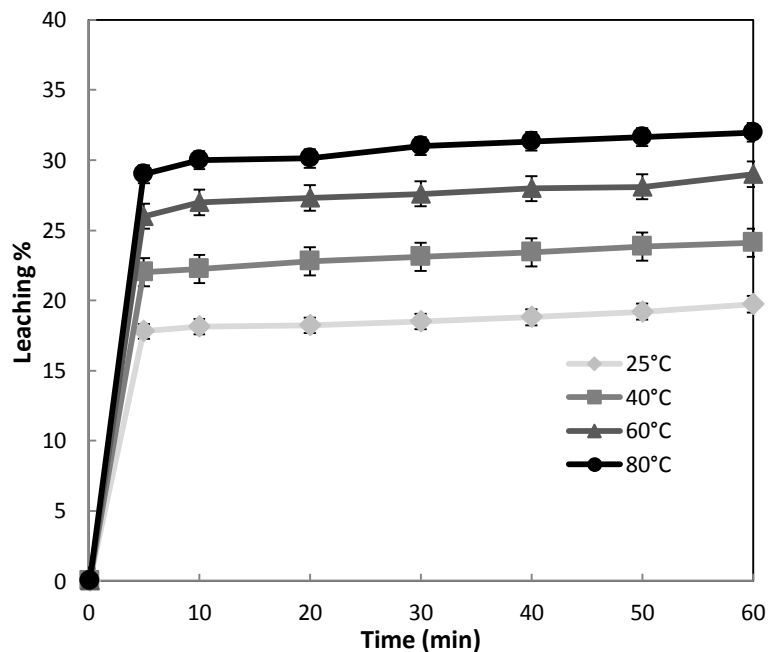


Figure 3.13 Effect of time and temperature on leaching of calcium from Hazelwood fly ash

For the non-catalytic reaction of particles with surrounding fluid, we consider two simple idealised models, the progressive-conversion model (PCM) and the shrinking unreacted-core model (SCM). In PSM it is assumed that reactant enters and react through the particle at all times thus solid reactant is converted continuously and progressively throughout the particles. SCM shows reaction occurs first at the outer skin of particle and the reaction zone then moves into the solid and leaving behind partly or completely converted material and inert solid which can precipitate back on surface of particle. Thus, at any time during reaction there exists an unreacted core of material which shrinks in size. Back to **Figure 3.2**, it is clear that the leaching process was controlled either by diffusion of reactant through solution boundary, or through a solid product layer, or by the surface chemical reaction rate [22]. Therefore, the shrinking core model for magnesium leaching is considered here. In the model, a solid particle B immersed in a fluid A reacts with the fluid by the equation (3.3):



Assuming MgO as solid B , ammonium chloride as fluid A and according to equation (3.1) the stoichiometric coefficient of a can be set as 2. When the first order surface chemical reaction is the slowest step, the following expression of the shrinking core model can be used to describe the dissolution kinetics:

$$1 - (1 - X_B)^{\frac{1}{3}} = \frac{K_C M_B C_A}{\rho_B a r_0} = K_r t \quad (3.4)$$

Vice versa, in the case that the diffusion of magnesium ion through ash layer is the rate controlling step, the following equation can be used:

$$1 - \frac{2}{3} X_B - (1 - X_B)^{2/3} = \frac{2DM_B V_A}{\rho_B a r_0^2} t = K_d t \quad (3.5)$$

In Equations (3.4) and (3.5), X_B is the fraction of solid reacted, K_C the kinetic constant, M_B the molecular weight of the solid, C_A the concentration of dissolved lixiviant A in the bulk of solution, ρ_B the density of solid, a the stoichiometric coefficient of the reagent in the leaching reaction, r_0 the initial radius of the solid particle, t the reaction time, D the diffusion coefficient in the porous product layer, and K_r, K_d are the rate constants which are calculated from equations (3.4) and (3.5) respectively [37].

The rate of dissolution of magnesium was tested against diffusion control (Equation 3.4) and chemical control (Equation 3.5). For this purpose, the left sides of these equations were plotted with respect to reaction time. The fitting level of these models was evaluated using correlation coefficient (R^2) values. The slopes of these plots were used as the apparent rate constants (K_r and K_d). **Table 3.5** summaries the diffusion control and chemical control models of leaching reaction in terms of rate constant and correlation coefficient. Clearly, the correlation coefficients are mostly below 0.8, which are too poor to be accepted. In other words, the above approaches based on the classical shrinking core model are inaccurate. A careful examination of leaching results in **Figure 3.2** reveals that the magnesium concentration in the bulk liquid solution initially increased very fast and then levelled off at an equilibrium value in each temperature. Furthermore, the previous discussions have confirmed the crystallisation of ammonium chloride and the formation of complex mixture as solid residues. They grow steadily upon the gradual dissolution of magnesium into the leachate. As a result, the resistance against diffusions of ions through the boundary should increase gradually, which eventually lead to the full termination of the reaction. For simplification, the leaching of magnesium was simulated by two steps, first 30 min for step 1 and the remaining 30 min for step 2 where the leaching is rather stopped.

Table 3.5 Dissolution rate and R^2 using Reaction controlled model, Diffusion control model and Mixed reaction and diffusion control model

T(°C)	Reaction Controlled Model		Diffusion Controlled Model	
	R^2	$K_r \times 10^3(\text{min}^{-1})$	R^2	$K_d \times 10^4(\text{min}^{-1})$
25	0.7482	1.142	0.8458	2.944
40	0.7543	1.333	0.8551	4.010
60	0.7054	1.663	0.7973	5.984
80	0.5779	1.728	0.6104	6.676

The kinetic data for the first step were matched well by the fitting of an empirical pseudo-second order reaction with non-constant ammonium chloride concentration in the outer surface of MgO particles, as presented in Equation (3.6). This model is also consistent with stoichiometric the coefficient of ammonium chloride in the Equation (3.1) and decreasing trend of the magnesium leaching results from multiple cycle leaching-carbonation of pure MgO and Hazelwood fly ash presented in **Figure 3.5**. To reiterate, the reason for a decreased extraction of magnesium upon multiple cycles is due to the decreased concentration of free ammonium chloride. To reflect this point, the concentration of ammonium chloride was introduced into the left hand side of the Equation (3.6), as a non-constant term and as a function of time and temperature. By further dividing both left and right hand sides with C_A , concentration of ammonium chloride at time t, the effect of the initial concentration of ammonium chloride on leaching is further added into to the model. C_A can be substituted in terms of initial concentration and conversion.

$$\frac{(1 - X_B)^{-1}}{C_{A0} - 2C_{B0}X_B} = \frac{K_C M_B}{\rho_B a r_0} = K_r t \quad (3.6)$$

The diffusion control model presented in equation (3.5) was proven to fit the kinetic data for the second step satisfactorily. In summary, **Figure 3.14** shows the R^2 values of two proposed models for (a) first step and (b) diffusion control model for second step. One can see the much better correlation coefficients for the newly developed model. The Arrhenius plots of $\ln(K)$ versus the reciprocal of temperature for pseudo-second order reaction model (Equation 3.6) further indicates an activation energy of 20.7 kJ/mol for the leaching of magnesium in the first 30 min, as demonstrated in **Figure 3.15**. Ranjitham et al. [23], Raschman [24] and Atashi et al. [25] reported activation energies of 43.2, 48.5 and 42.2 kJ/mol respectively for the leaching of calcined magnesite which are relatively higher than our result. Luo et al. (2013) [38] concluded activation energies of 32, 28 and 19 kJ/mol for dissolution of aluminium, calcium and iron

respectively from calcined Chinese coal fly ash in hydrochloric acid which is comparable with present work. **Figure 3.16**, further demonstrates a linear dependence of the K value on the initial/free concentration of ammonium chloride for the leaching of magnesium from Hazelwood fly ash/pure MgO. This further confirmed the applicability of this model for predicting magnesium leaching kinetic in the multiple cycle leaching-carbonation.

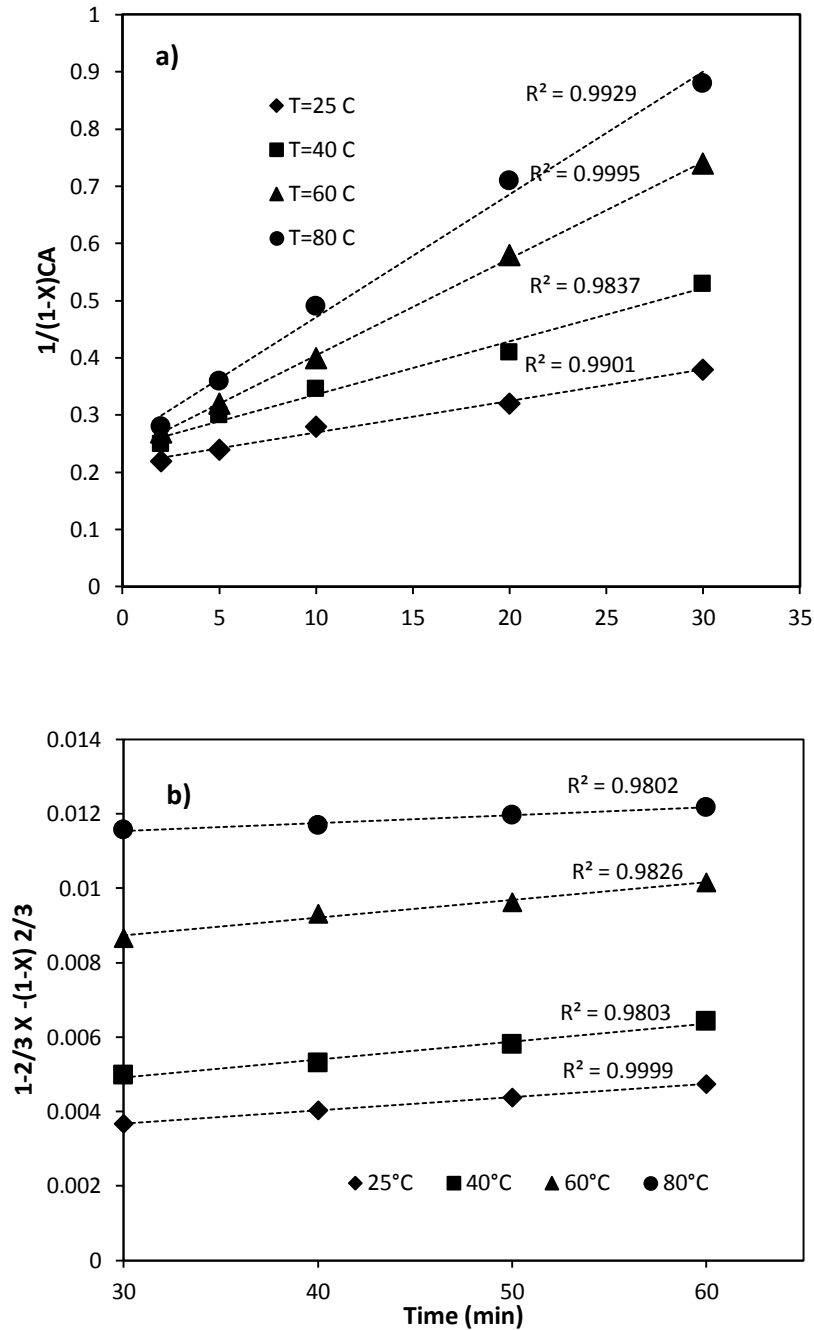


Figure 3.14 Plots for (a) pseudo-second order reaction for first 30 minutes of reaction and (b) Product layer diffusion for last 30 minutes of reaction.

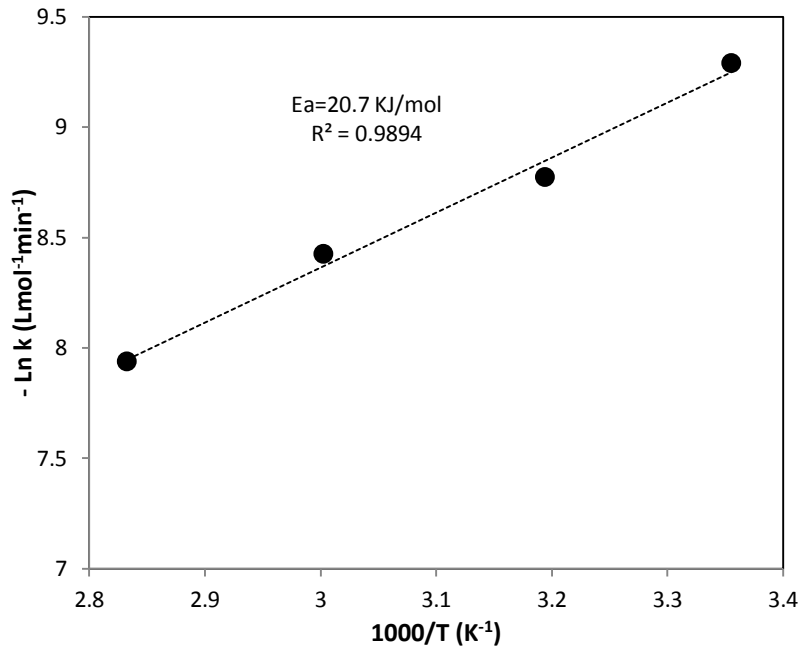


Figure 3.15 An Arrhenius plot for leaching of MgO with ammonium chloride using pseudo-second order reaction model

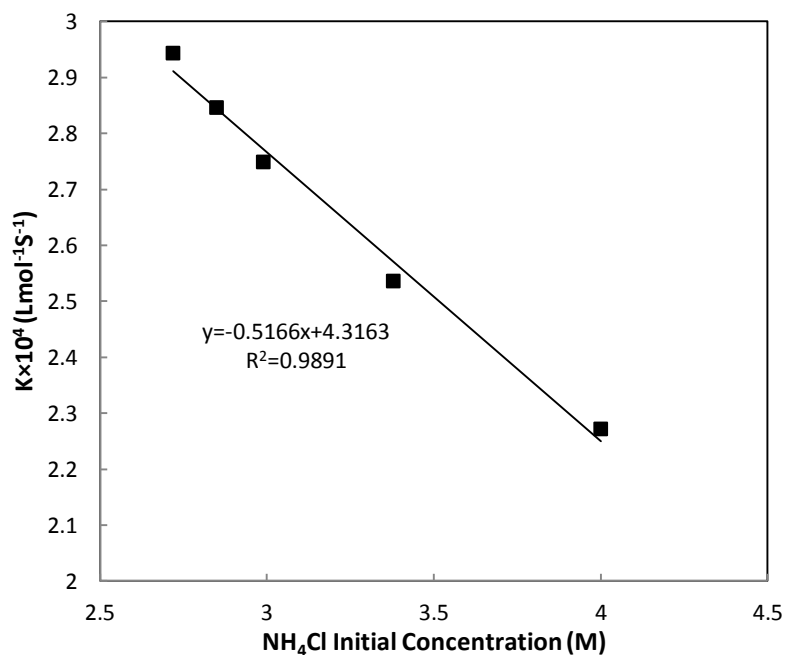


Figure 3.16 K values fitting second order model for different cycles of Hazelwood fly ash

3.5 Conclusion

A comprehensive investigation on the leaching propensity of dominant oxides (MgO and CaO) in two different types of brown coal fly ash (Hazelwood and Yallourn) using ammonium chloride has been conducted. Apart from the parametric investigation over the influence of time and temperature on the once-through leaching experiment, five closed leaching-carbonation loops have been performed to explore the reusability of the leaching reagent, as well as the accumulation of impurities upon recycling. The optimum conditions for leaching of magnesium

from pure MgO within the range studied here were found to be at 80°C, reaction time of 30 min, liquid/solid ratio of 6, and ammonium chloride concentration of 4 M.

Identical results for magnesium leaching yields have been observed for all samples, except for Yallourn coal fly ash with a chemically stable magnesia ferrite (MgFe₂O₄). Leaching and carbonation percentage of magnesium and calcium decreased upon increasing cycle number, due to the loss of ammonium chloride by crystallisation and its interaction with dissolved magnesium forming complex precipitates. The leaching of calcium in the form of oxide is much faster than magnesium, which can be finished in less than 5 min at a given temperature. Instead, the leaching of magnesium in Hazelwood fly ash was slow in the first 30 min, following a pseudo- second order reaction with a non-constant ammonium chloride concentration, while the kinetic data for the second step showed a good fit to the diffusion-controlled process. The activation energy for the leaching of MgO was found to be about 20.7 kJ/mol from the start of reaction toward 30 min after reaction which is consistent with the value obtained for the reaction control kinetic modelling.

References

- [1] Eloneva, S.; Teir, S.; Salminen, J.; Fogelholm, C.J.; Zevenhoven, R. Fixation of CO₂ by carbonating calcium derived from blast furnace slag. *Energy* **2008**, 33, 1461-1467.
- [2] Sanna, A.; Dri, M.; Hall, M.R.; Maroto-Valer, M.; Waste materials for carbon capture and storage by mineralisation (CCSM) – A UK perspective. *Appl. Energ.* **2012**, 99, 545-554.
- [3] Sun, Y.; Parikh, V.; Zhang, L; Sequestration of carbon dioxide by indirect mineralisation using Victorian brown coal fly ash, *J. Hazard. Mater.* **2012**, 209-210, 458-466.
- [4] Teir, S.; Revitzer, H.; Eloneva, S.; Fogelholm, C.J.; Zevenhoven, R.; Dissolution of natural serpentinite in mineral and organic acids, *Int. J. Miner. Process.* **2007**, 83, 36–46.
- [5] Maroto-Valer, M.M.; Kuchta, M.E.; Zhang, Y.; Andréßen, J.M.; Fauth, D.J. Comparison of physical and chemical activation of serpentinite for enhanced CO₂ sequestration. *Am. Chem. S. Div. Fuel. Chem.* **2004**, 49(1), 373-375.
- [6] Gerdemann, S.J.; O'Connor, W.K.; Dahlin, D.C.; Penner, L.R.; Rush H. Ex Situ Aqueous Mineral Carbonation. *Env. Sci. Technol.* **2007**, 41, 2587-2593.
- [7] Hong, K.J.; Tokunaga, S.; Kajiuchi, T. Extraction of heavy metals from MSW incinerator fly ash using saponins, *J. Hazard. Mater.* **2000**, 75, 57-73.
- [8] Sun, Y.; Yao, M.S.; Zhang, J.P.; and Yang, G.; Indirect CO₂ mineral sequestration by steelmaking slag with NH₄Cl as leaching solution. *Chem. Eng. J.* **2011**. 173(2), 437-445.

- [9] Nyambura, M.G.; Mugeru, W.G.; Felicia, P.L.; Gathura, N.P. Carbonation of brine impacted fractionated coal fly ash: implications for CO₂ sequestration. *J. Environ. Manage.* **2011**, *92*, 655-664.
- [10] Montes-Hernandez, G.; Pérez-López, R.; Renard, F.; Nieto, J.M.; Charlet, L. Mineral sequestration of CO₂ by aqueous carbonation of coal combustion fly-ash. *J. Hazard. Mater.* **2009**, *161*(2-3), 1347-1354.
- [11] Huijgen, W.J.J.; Witkamp, G.J.; Comans, R.N.J. Mineral CO₂ sequestration by steel slag carbonation. *Env. Sci. Technol.* **2005**, *39*(24), 9676–9682.
- [12] Bonenfant, D.; Kharoune, L.; Sauvé, S.; Hausler, R.; Niquette, P.; Mimeault, M. CO₂ Sequestration potential of steel slags at ambient temperature and pressure. *Ind. Eng. Chem. Res.* **2008**, *47* (20), 7610-7616.
- [13] Bobicki, E.R.; Liu, Q.; Xu, Z.; Zeng, H.; Carbon capture and storage using alkaline industrial wastes. *Progress. Energ. Combust.* **2012**, *308*, 302-320.
- [14] Johnson, T.R. Future Options for Brown Coal based Electricity Generation - the role of IDGCC. *Future Options for Brown Coal based Electricity Generation.* **2003**, 371-380.
- [15] Wu, C.Y.; Yu, H.F.; Extraction of aluminum by pressure acid-leaching method from coal fly ash. *Trans. Nonferrous Met. Soc. China.* **2012**, *22*, 2282-2288.
- [16] Huang, K.; Inoue, K.; Harada, H. Leaching of heavy metals by citric acid from fly ash generated in municipal waste incineration plants. *J. Mater. Cycles Waste Manage.* **2011**, *13*, 118-126.
- [17] Kersch, C; Pereto; Ortiza S.; Woerlee, G.F.; Witkampa, G.J. Leachability of metals from fly ash: leaching tests before and after extraction with supercritical CO₂ and extractants. *Hydrometallurgy* **2004**, *72*, 119-127.
- [18] Soco, E.; Kalemkiewicz, J. Investigations of sequential leaching behaviour of Cu and Zn from coal fly ash and their mobility in environmental conditions. *J. Hazard. Mater.* **2007**, *145*, 482-487.
- [19] Paul, M.; Seferinoglu, M.; Ayçik, G.A.; Sandström, A.; Paul, J. Acid leaching of coal and coal-ash: kinetics and dominant ions. American Chemical Society, *228th National Meeting Conference proceeding*, **2004**.
- [20] Seidel, A.; Zimmels, Y. Mechanism and kinetics of aluminum and iron leaching from coal fly ash by sulfuric acid. *Chem. Eng. Sci.* **1998**, *53*(22), 3835-3852.
- [21] Zhu, Z. Characterisation and modelling of toxic fly ash constituents in the environment, PhD Thesis, University of Tennessee, USA. **2011**.

- [22] Levenspiel, O. *Chemical Reaction Engineering*; John Wiley and Sons: New York, U.S.A., **1972**.
- [23] Ranjitham, A.M.; Khangaonkar, P.R. Leaching Behaviour of Calcined Magnesite with Ammonium Chloride Solutions. *Hydrometallurgy* **1990**, 23, 177-189.
- [24] Raschman, P. Leaching of calcined magnesite using ammonium chloride at constant pH. *Hydrometallurgy* **2000**, 56, 109-123.
- [25] Atashi, H.; Fazlollahi, F.; Tehranirad, S. Leaching Kinetics of Calcined Magnesite in Ammonium Chloride Solutions. *Aust. J. Basic Appl. Sci.* **2010**, 4, 5956-5962.
- [26] Pickles, C.A.; Thermodynamic modelling of the formation of zinc- manganese ferrite spinel in electric arc furnace dust, *J. Hazard. Mater.* **2010**, 179, 309–317.
- [27] <http://www.chem.unep.ch/irptc/sids/OECD/SIDS/12125029.pdf>
- [28] Wang, D.; Li, Z.; Study of Crystallisation Kinetics of Ammonium Carnallite and Ammonium Chloride in the $\text{NH}_4\text{Cl-MgCl}_2\text{-H}_2\text{O}$ System. *Ind. Eng. Chem. Res.* **2012**, 51, 2397-2406.
- [29] Han, Y.S; Hadiko, G.; Fuji, M.; Takahashi, M.; Effect of flow rate and CO_2 content on the phase and morphology of CaCO_3 prepared by bubbling method, *J. Cryst. Growth* **2005**, 276, 541.
- [30] Reddy, M.M.; Nancollas G.H; The crystallisation of calcium carbonate: iv. The effect of magnesium, strontium and sulfate ions. *J. Cryst. Growth* **1976**, 35, 33-38.
- [31] Frost, R.L.; Hales, M.C.; Locke, A.J.; Kristof, J.; Horvath, E.; Vagvolgyi, Controlled rate thermal analysis of hydromagnesite. *J. Therm. Anal. Calorim.* **2008**, 92, 893-897.
- [32] Hollingbery, L.A.; Hull, T.R.; The thermal decomposition of Huntite and Hydromagnesite - A Review. *Thermochim. Acta* **2010**, 509, 1–11.
- [33] Case, D.H.; Wang, F.; Giammar, D.E.; Precipitation of Magnesium Carbonates as a Function of Temperature, Solution Composition, and Presence of a Silicate Mineral Substrate. *Environ. Eng. Sci.* **2011**, 28, 881-889.
- [34] Langmuir, D.; Stability of Carbonates in the System $\text{MgO-CO}_2\text{-H}_2\text{O}$, *J. Geol.* **1965**, 73, 73.
- [35] Bischoff, J.L.; Fyfe, W.S., Catalysis, inhibition and the calcite-aragonite problem. *Am. J. Sci.* **1968**, 266, 65-79.
- [36] Roques, H.; Girou, A., Kinetics of the formation conditions of carbonate tartars, *Water res.* **1974**, 8, 907-920.

- [37] Dehghan, R.; Noaparast, M.; Kolahdoozan, M. Leaching and kinetic modelling of low-grade calcareous sphalerite in acidic ferric chloride solution. *Hydrometallurgy* **2009**, 96, 275–282.
- [38] Luo, Q.; Chen, G.; Sun, Y.; Ye, Y.; Qiao, X.; Yu, J. Dissolution kinetics of aluminum, calcium and iron from circulating fluidised bed combustion fly ash with hydrochloric acid. *Ind. Eng. Chem. Res.* **2013**, 52, 18184-18191.

Monash University

Declaration for Thesis Chapter 4

Declaration by candidate

In the case of Chapter 4, the nature and extent of my contribution to the work was the following:

Nature of contribution	Extent of contribution (%)
Experimental design and conduct, writing up	90 %

The following co-authors contributed to the work. If co-authors are students at Monash University, the extent of their contribution in percentage terms must be stated:

Name	Nature of contribution	Extent of contribution (%) for student co-authors only
Boyoung Han	Experimental work	8%
John Cashion	Mössbauer Spectroscopy analysis	2%
Lian Zhang	Experimental design, key ideas, reviewing and editing paper	Supervisor
Cordelia Selomulya	Editing paper	Supervisor
Nawshad Haque	Comments on my work	Supervisor

The undersigned hereby certify that the above declaration correctly reflects the nature and extent of the candidate's and co-authors' contributions to this work*.

Candidate's Signature		Date 12/11/2015
--------------------------	---	--------------------

Main Supervisor's Signature		Date 12/11/2015
-----------------------------------	---	--------------------

*Note: Where the responsible author is not the candidate's main supervisor, the main supervisor should consult with the responsible author to agree on the respective contributions of the authors.

Chapter 4

Comparison of leaching characteristics of fresh and weathered fly ash in $\text{NH}_4\text{Cl}+\text{HCl}$ and sole HCl

In Chapter 3, a closed-loop multi-stage process was developed to utilise fresh fly ash collected directly from the electrostatic precipitator. It was shown that around 36% and 33% of magnesium and calcium could be extracted using NH_4Cl as leaching agent. Here, first, intensive investigation on chemical and morphological changes of weathered fly ash was carried out to assess if the weathered fly ash could replace fresh fly ash in mineral carbonation scheme. Then, NH_4Cl solution was modified by combining with HCl via pH-control leaching so as to improve both the extraction yield and selectivity of magnesium and calcium over other impurities prior to the carbonation. This chapter has been reformatted from the following published manuscript: **T. Hosseini**, C. Selomulya, N. Haque, L. Zhang, Chemical and Morphological Changes of Weathered Victorian Brown Coal Fly Ash and its Leaching Characteristic upon the Leaching in Ammonia Chloride and Hydrochloric Acid, *Hydrometallurgy*, 2015, 157, pp 22-32.

4.1 Abstract

In this paper, the properties and leaching propensity of weathered Victorian brown coal fly ash have been investigated. This study was conducted to assess if the weathered ash could replace fresh fly ash in mineral carbonation process. Through the use of a variety of advanced instruments, the mineralogical properties of weathered fly ash have been investigated. In addition, the leaching of such a fly ash in the mixture of ammonium chloride and sole hydrochloric acid has been examined. As has been confirmed, the weathered fly ash is dominated by hydrates and carbonates which were formed in aqueous landfilling system. These species were mostly poorly crystallised, and even loosely agglomerated into clusters in the weathered fly ash. Irrespective of the leaching reagent, the target Ca and Mg in weathered fly ash were more easily extracted than in the fresh ash counterpart under the same leaching conditions. In addition, for the use of either leaching agent, the temperature and time played little or marginal role on the extraction of target Ca and Mg out of the weathered fly ash sample. Decreasing the pH of the leaching agent is beneficial in enhancing the extraction of Ca and Mg, at a cost of a gradually lowered selectivity due to the simultaneous elution of impure elements. The optimum pH value was found to be around 4 for the mixture of $\text{NH}_4\text{Cl}+\text{HCl}$, which maximised the extraction yields of Ca and Mg close to ~70% at a minimal elution of the impurities. This is attributed to the buffering property of NH_3 and its complexing capability to prevent the dissolution of impure elements. Instead, the use of sole HCl even at the same pH value as the mixture of $\text{NH}_4\text{Cl}+\text{HCl}$ resulted in a deep penetration of protons into particle inside, the intense breakage of ash cluster, and hence, the simultaneous dissolution of plenty of impurities.

4.2 Introduction

Coal-fired power stations around the world produce enormous quantities of coal fly ash annually. Since the consumption of fly ash to make value-added products is poorly low, the large amount of fly ash is disposed in storage ponds [1]. This induces the environmental concerns related to land and subsurface water contamination upon the dissolution of toxic and non-degradable elements [2].

The management of long-term fly ash disposal or its utilisation needs proper understanding of the weathered fly ash properties [3]. Regarding the coal ash characteristics, they vary broadly with the properties of the raw coal, combustion technology used to generate electricity, as well as the wet processing and environmental exposure in storage [2]. Natural weathering process occurs via hydration, carbonation, dissolution and so forth, leading to the changes in physical, chemical and mineralogical properties of a fly ash sample [1,3,4]. Upon the decrease of the pH of

fly ash-water slurry, it has been confirmed that the soluble salt content was reduced remarkably as well [5,6].

The utilisation of coal fly ash has been receiving increased attention, since it is an effective means of reducing the amount of this waste product that otherwise has to be landfilled. Considering the increasing trend of demand for fly ash in different applications, the landfilled fly ash, as a supplement to the fresh ash derived from a power plant, has also been considered so as to empty the historical ash landfilled site [7]. Compared to the conventional methods such as the use of fly ash as additive to cement, the use of fly ash to supplement natural minerals for CO₂ mineralisation has been receiving increased attention [8-11]. The brown coal fly ash is unsuitable for cement industry, because it is predominated by alkali and alkaline earth metals that are highly soluble in rain water [12]. Regarding the CO₂ mineralisation process, one primary method, namely indirect carbonation is to first separate alkaline earth metals via aqueous leaching out of solid fly ash. The resulting leachate is subsequently bubbled with CO₂ - bearing flue gas to precipitate the alkaline earth cations out as carbonates [13]. For such a purpose, the fly ash rich in alkaline earth metals collected from brown coal combustion process is an ideal source.

As a continuation of our previous works focusing on the use of dried fresh fly ash collected from the electrostatic precipitator in a Victorian brown coal combustion power plant [12], this paper aims to further examine the applicability of weathered Victorian brown coal fly ash upon indirect leaching process. The motivation of us lies in the fact that the Victorian brown coal fly ash has been stored in ash pond for the past decades, which thus possesses a huge amount and potentially distinct properties when compared with the fresh fly ash. It raises the concern if the results based on fresh fly ash can be applied to its weathered counterpart. It is still unclear how the weathering would affect the modes of occurrence of alkaline earth metals in a fly ash and their leaching behaviour in acidic reagent prior to carbonation. As far as the authors are aware, there are very limited papers that have touched down the leaching characteristics of different types of weathered fly ash [14-17]. In particular, there is no information available on the properties of weathered Victorian brown coal fly ash and its potential for utilisation through CO₂ sequestration process.

In principle, the use of ammonium salt for the leaching process is superior over acidic leaching, since it can be recovered readily and reused in a closed loop [18]. However, ammonia and ammonium ion constitute a pH buffer solution which is not in favour of the extraction of alkaline earth metals requiring a low pH for the solution. On the other hand, the use of strong acids such as hydrochloric acid has been reported to improve the extraction yields of target elements. However, the selectivity of target elements is usually poor, because the undesirable elements are also extracted simultaneously [19]. In this paper, we modified the ammonium chloride solution by combining with acid via pH control leaching, so as to improve both the

extraction yields and selectivity of calcium and magnesium over other metals in a fly ash matrix. A one-year old weathered Hazelwood fly ash was used for such a test. Initially, it was compared with the fresh ash sample collected from the electrostatic precipitator (ESP) of the same power plant. For such a purpose, the modes of occurrence of individual metals in both fly ash samples were characterised by quantitative X-ray diffraction (QXRD) for mineralogical identification and quantification. Subsequently, the leaching characteristics of the two fly ash samples in ammonia chloride solution, with and without pH control using sole hydrochloric acid (HCl) were examined. The aim here is to maximise both leaching yields and selectivity of magnesium and calcium from weathered Victorian brown coal fly ash. The optimisation of process parameters including temperature and time has been conducted intensively. The results achieved are expected to shed light in understanding the mechanisms underpinning the synergetic interaction between ammonia chloride and hydrochloric acid in the extraction of individual elements out of ash matrix, and in broadening the methods for a value-added utilisation of landfilled Victorian brown coal fly ash, an otherwise valueless waste which is of environmental concern.

4.3 Materials and experimental methods

4.3.1 Materials preparation

The fresh coal fly ash sample was collected as dry powders from the ESP in International Power Hazelwood power plant located at the Latrobe Valley, Victoria, Australia. One-year old wet weathered fly ash was collected from the top of the ash pond in the same power plant, and dried in ambient air prior to being tested. Although the ash from different depths of the ash pond was not sampled, it is presumed that the top surface ash collected is representative, since its properties, as the properties of the sample used in this study are broadly in agreement with the previously reported ash pond samples [15].

In order to estimate the degree of weathering of the fly ash collected from ash dump, two complementary experiments were performed on the fresh and weathered fly ash. Simulated weathering was considered a tool allows the changes occurring in ash particle structure to be produced. One part of fresh fly ash (from ESP) and weathered fly ash (from ash pond) underwent two-week treatment under conditions simulating the deposition on landfill site in natural environment, including contact with water and air. Obtained samples (herein after synthesised fly ash 1 and 2 respectively) were dried overnight in the oven at 110°C and analysed by XRF and QXRD.

A portion of fly ash was prewashed with sodium carbonate solution (0.3 M) to remove sulfur and soluble salts. A 100 g sample of dried fly ash was mixed together with sodium carbonate solution in a beaker and stirred at room temperature for around 1 hour. This is to ensure the

production of high-purity carbonate that could be used as a value-added product. The sulfur in fly ash (mainly in form of calcium sulfate) was washed by sodium carbonate according to the following equation [20]:



After vacuum filtration, the filter cake was dried in oven at 120°C overnight and analysed by both XRF and XRD.

4.3.2 Materials characterisation methodologies

The elemental composition of a raw and sodium carbonate washed fly ash and leaching residues were determined by a pre-calibrated X-ray fluorescence spectroscopy (XRF, Spectro iQ II). The leaching percentage of each element was calculated based on the difference between its mass in raw washed sample and leaching residue after drying.

The mineralogical composition of fly ash samples and its leaching residues were determined by X-ray diffraction analysis (XRD, Rigaku, MiniFlex 600), under the condition of scanning speed 1°/min from 2 to 90°, 40 kV and 15 mA. The peak identification and crystalline mineral phase quantification was achieved by Siroquant. Based on the Rietveld method, Siroquant generates a synthetic X-ray pattern from crystallographic information of the built-in mineral database and adjusts the pattern interactively through refinement procedure to minimise the chi-square value [21]. To quantify the amount of amorphous species within a sample, 20 wt% corundum (Sigma–Aldrich >99.5%, powder) was added as internal standard into a sample and the mixture was re-measured by XRD, following the method proposed elsewhere [22].

The cross-sectional scanning electron microscopy (SEM) images of particles was observed by mounting the sample in epoxy resin and polishing using silicon carbide and diamond papers. Each fly ash sample was characterised by randomly selecting 3-4 fields of view and examining all the fly ash particles observed within the selected fields. The SEM microscopes used are a JEOL JSM-7001F equipped with backscattered electron detectors (BSE) coupled with Energy Dispersive X-ray Spectroscopy (EDX). SEM imaging studies were performed at 15 kV at a working distance of 10 mm.

Iron Mössbauer spectroscopy analyses were also conducted. Approximate loadings of 60-94 mg/cm² were weighed out into piston type perspex absorber holders for the Mössbauer analyses. The experiments were carried out with both the source and absorber at room temperature with a high and low velocity resolution. The samples were exposed to a beam of γ radiation. The γ ray emitted by the source pass through an absorber and the transmitted gamma rays are detected by a radiation detector. In the resulting spectra, γ -ray intensity was plotted as a function of the source velocity. All spectra have been fitted with Voigtian line-shapes, which is

a Lorentzian with Gaussian broadening due to variation in the local coordination of the iron atoms.

4.3.3 Leaching experiments procedure

Since the kinetics of leaching of minerals is highly dependent upon the activity of hydrogen ion (i.e. H^+) in a leachate, the influence of leachate pH was examined here. The pH of a leachate was varied by either using ammonium chloride solution which has its pH regulated by continuously dropping HCl, namely the mixture of $NH_4Cl+HCl$ at the two pH ranges (5-5.5 and <4.5), or the use of sole HCl without pH control. In both series of leaching experiments, the initial condition was selected based on optimised condition found in our previous work [12]. To maximise both yield and selectivity of calcium and magnesium, the weathered fly ash leaching condition was further varied for different final pH in the leaching system of $NH_4Cl+HCl$ and sole HCl. The leaching conditions are summarised in **Table 4.1**.

Batch leaching tests were performed in a glass sealed beaker equipped with four connections, one for feeding air of 1 L/min, one tube for the release of ammonia vapour to be trapped in a conical flask containing distilled water, one connection for pH meter entrance and another one for acid injection to solution. The pH was controlled at pre-set value over the entire testing period by continuous measurement and automatic doping of acid into the leachate. Reaction temperature was controlled by having the reactor immersed in a thermostat controlled water bath. After the temperature reached its set point, 10 g of sodium carbonate washed fly ash was added to the solution. A magnetic stirrer bar with a stirring speed of 350 rpm enabled the solution to be fully agitated with minimal spillage. The resulting residue after filtration were dried at 120°C overnight in an oven, weighed and quantified by XRF for elemental compositions to determine the leaching percentages of individual elements, particularly magnesium and calcium

Table 4.1 Summary of leaching experiments conditions carried out for fly ash

Material	Leaching agent	Condition	pH range	Description
Weathered and fresh fly ash		T=80°C, t=30 min L/S=6, 60 ml NH ₄ Cl 4M HCl 4M added during leaching	pH ~5-5.5 pH < 4.5	Comparison of leaching characteristic of fresh and weathered fly ash
Weathered fly ash	NH ₄ Cl+HCl	T=25, 40, 60, 80°C t=30, 40, 50, 60 min Initial L/S= 2, 3, 4, 5, 6 ml	pH < 4.5	Optimisation of condition
Weathered fly ash		T=25°C t=40 min Initial L/S=6	0.5- ~6	Effect of pH and selectivity
Weathered and fresh fly ash		T=25°C t=30min 60 mL HCl 1M, L/S=6	Without control pH	Comparison of leaching characteristic of fresh and weathered fly ash
Weathered fly ash	Sole HCl	T=25, 40, 60, 80°C T=30, 40, 50, 60 min	Without control pH	Optimisation of condition
Weathered fly ash		T=25°C t=30min 60 mL HCl 1M, L/S=6	0.5- ~6	Effect of pH and selectivity

4.4 Results and Discussions

4.4.1 Characterisation of raw weathered fly ash

4.4.1.1 XRF, QXRD and SEM results

Table 4.2 tabulates the composition of raw fresh fly ash, weathered fly ash and synthesised fly ash 1 and 2. It has been ordered by age of the fly ash samples from youngest (fresh fly ash) to oldest (synthesised 2). It can be found that the major elements available in both fly ashes are Mg, Ca, Fe and S. The total amounts of each species in both fly ashes are quite similar with a deviation of $\pm 3\%$ for each element. This confirms that these samples are derived from the identical coal, although they underwent natural or simulated weathering. The noticeable change is in the amount of sulfur that showed decrement by weathering process regardless of the type of weathering. In addition to that, iron was increased from 14% in fresh fly ash to 17.2% in synthesised fly ash 2.

Full-pattern fitting and major peaks identification for QXRD analysis of fresh and weathered fly ash are summarised in **Figure 4.1**. Note that, a Chi-square value of 4.63 and 20.44 has been achieved for the fresh and weathered fly ash, respectively.

Table 4.2 Elemental Quantification of major elements in the fresh fly ash, weathered fly ash, synthesised fly ash 1 (from synthetic weathering of fresh fly ash) and synthesised fly ash 2 (from synthetic weathering of weathered fly ash)

Elements	Elemental composition (wt%)			
	Fresh fly ash	Synthesised fly ash 1	Weathered fly ash	Synthesised fly ash 2
SiO ₂	5.82	5.62	3.86	4.09
Al ₂ O ₃	3.01	2.54	3.65	3.36
Fe ₂ O ₃	14	17.14	16.8	17.2
CaO	32.4	33.72	30.97	31.19
MgO	29.3	29.29	32.51	32.1
Na ₂ O	0.2	0.24	2.35	2.21
K ₂ O	0.17	0.18	0.15	0.15
SO ₃	12.8	8.63	9.44	9.23

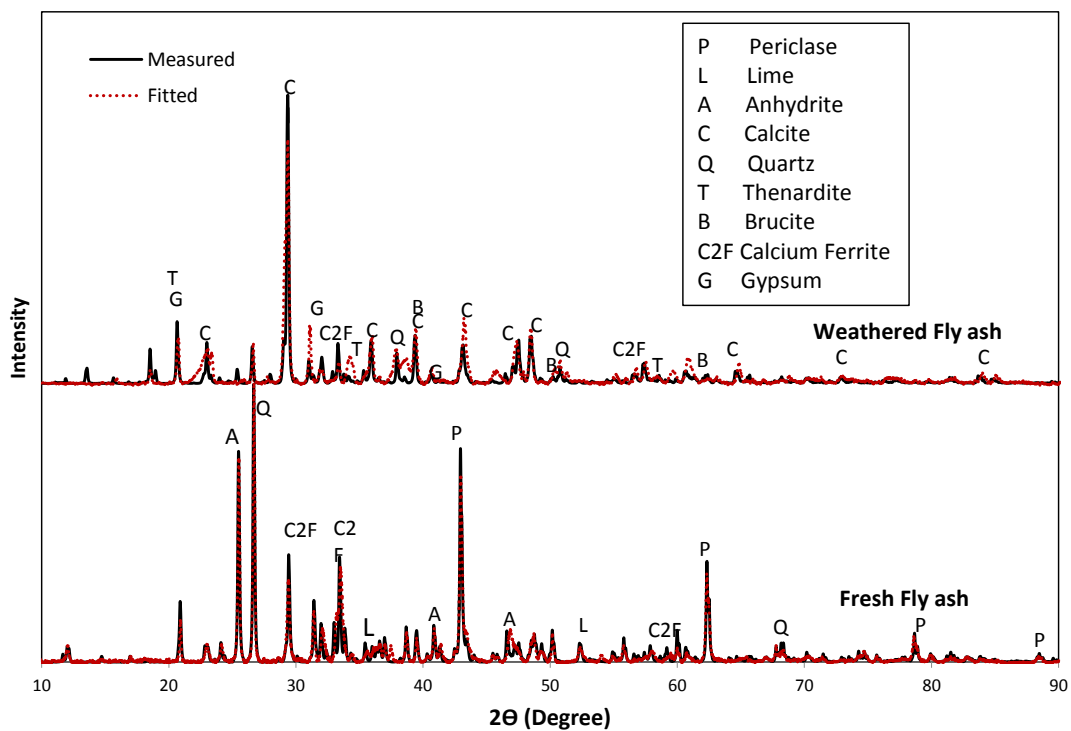


Figure 4.1 Measured and fitted XRD pattern by Siroquant software for the fresh and weathered fly ash

The abundance of individual mineralogical species in fresh fly ash, weathered fly ash and synthetic fly ash 1 and 2 determined by QXRD is summarised in **Figure 4.2**. For the fresh fly ash, the amorphous species only accounts for 3.75 wt%, suggesting the high crystallisation extent of the mineral species within it. Periclase (MgO) is the only Mg-bearing species while anhydrite (CaSO₄), C₂F (Ca₂Fe₂O₅) and a few amount of calcite (CaCO₃) are the major Ca-bearing species within it. Moreover, quartz (SiO₂) was found to be the major form for silicon within the fresh dried ash sample. XRD results for synthesised fly ash 1 showed partial weathering of this fly ash. As has been confirmed, the changes on the ash properties occurred quickly, leading to the increase in the amount of amorphous species, hydrated compound and carbonate as well. In the meanwhile the amount of anhydrous sulfate was decreased considerably and gypsum (CaSO₄(H₂O)₂) formed instead. For the weathered fly ash, the quantity of its amorphous species was increased to 62.1wt%, which is a clear sign of the strong secondary reactions occurred in the aqueous system during long-term disposal of fly ash. The increased amount for calcite suggested the complete carbonation reaction in the landfill. The amount of periclase (MgO) was reduced significantly, which was replaced by abundant brucite (Mg(OH)₂) and nesquehonite (MgCO₃·3H₂O). For anhydrite, quartz (SiO₂) and C₄AF (Ca₂Fe_{0.28}Al_{1.72}O₅) which were the predominant Si and Al bearing species in the fresh fly ash, their quantities were reduced to a trivial level in the weathered fly ash. Clearly, most of these species interacted in the aqueous system to convert into poorly crystalline species that are undetectable by XRD. Negligible changes of composition upon second synthetic weathering process suggested that weathered fly ash is completely weathered and there is no more potential to change its composition upon weathering.

The typical cross-sectional image observed by SEM suggests a strong affinity of various species together within the weathered fly ash, as illustrated in **Figure 4.3**. X-ray mapping shows that this particle consists of multiple elements including Ca, Mg, O, Si and S. The particle of quartz (SiO₂) on top part of the particles was observed while the particles around the corners are rich in Ca bounded with evenly dispersed O and C in the form of calcite which is the most predominant mineral in XRD spectra. Mg is dispersed mostly in the middle parts and associated with C and O to form hydroxide or carbonate forms specially brucite or nesquehonite.

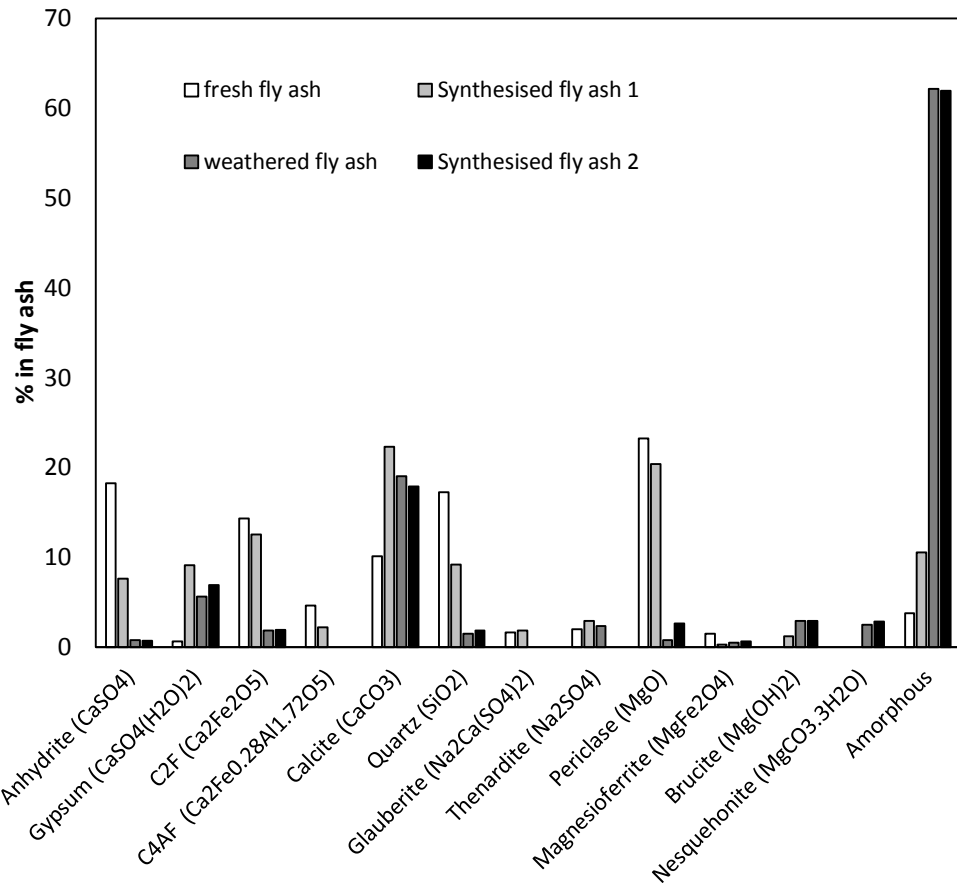


Figure 4.2 Composition of fresh fly ash, synthesised fly ash 1 (from synthetic weathering of fresh fly ash), weathered fly ash and synthesised fly ash 2 (from synthetic weathering of weathered fly ash) calculated by QXRD and internal standard method

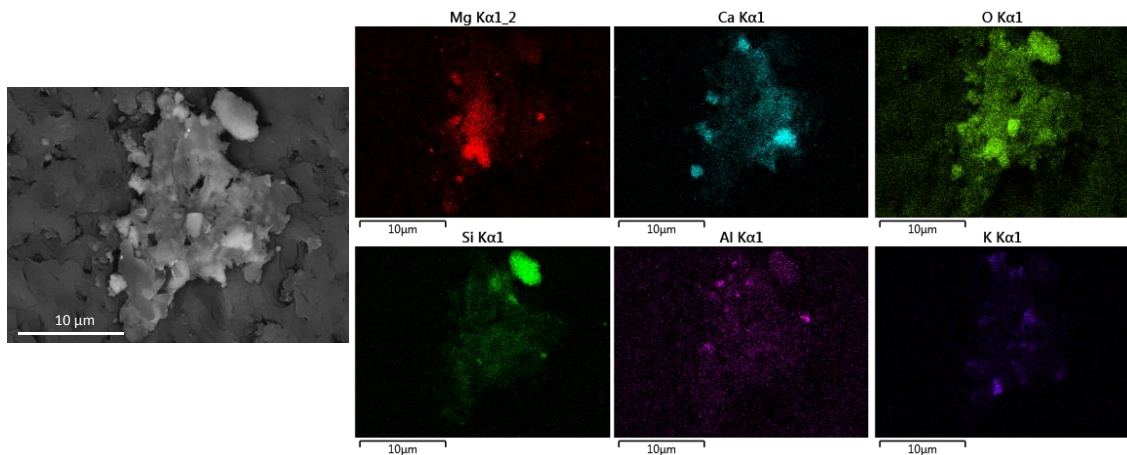


Figure 4.3 BSE image (magnification 4000 X) and EDX elemental maps of representative particle of weathered fly ash. Elemental maps of Mg (red), Ca (Light blue), O (light green), Si (dark green), Al (Purple) and K (dark blue)

4.4.1.2 Mössbauer results for the speciation of iron

As suggested by QXRD results in **Figure 4.2**, iron in a fly ash sample is mostly bound to other elements which potentially increase the difficulty for the extraction of target magnesium or calcium. The exact lattice position of the iron ions, however, is difficult to determine. The Mössbauer provides an excellent spectroscopic method for studying iron cation positions in different minerals [23]. The fitted Mössbauer spectra for fresh and weathered fly ash are illustrated in **Figure 4.4**. All the hyperfine parameters are summarised in **Table 4.3** and *Area%* refers to proportion of total iron in each of the phases.

Each of the full spectra in **Figure 4.4** consists of a relatively weak, poorly structured magnetic component and a much stronger non-magnetic component in the centre of the spectrum. The weak sharp features visible at -8, +5.5 and +8.8 mm/s fitted in light blue, which are the signature peaks of hematite (Fe_2O_3). The remainder of the magnetic sub-spectrum, as fitted in red, can be assigned as aluminium substituted calcium ferrite, CAF ($\text{Ca}_2\text{Fe}_{2-x}\text{Al}_x\text{O}_5$), and/or magnesioferrite, MAF ($\text{MgFe}_{2-x}\text{Al}_x\text{O}_4$). The central doublet in all spectra was not symmetrical, indicating the co-existence of two or more doublets with slightly different centres (isomer shifts). The quadrupole splitting < 0.75 mm/s were classified as magnesioferrite and those > 0.75 mm/s were classified as spinel (also possibly including iron substituted periclase, $\text{MgO}:\text{Fe}^{3+}$ which has the same parameters). Any possible superparamagnetic CAF would have a quadrupole splitting of ~ 1.5 mm/s [24]. From **Table 4.3**, one can clearly see that most of the iron in fresh fly ash is in the magnesioferrite phase (39%) while around 50% of total iron in the weathered fly ash is in the MAF/CAF phase. This indicates the interaction between dissolved aluminium and magnesioferrite in the aqueous system. The other species including hematite (HEM) and double 2 for a spinel structures are highly stable and resistant against weathering. This is consistent with the previous observation [25].

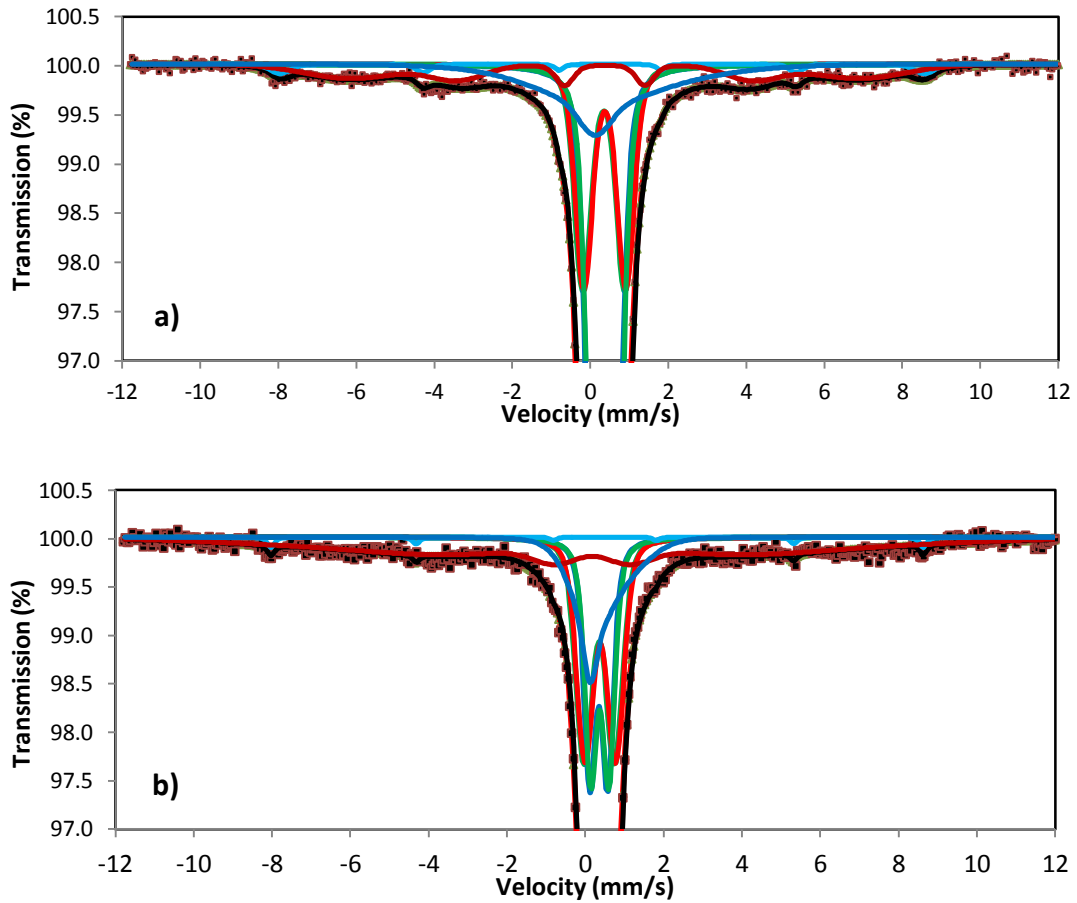


Figure 4.4 Mössbauer spectroscopy fitting results *a)* fresh fly ash; *b)* weathered fly ash. 3 sextets+2 doublets

Table 4.3 Hyperfine parameters determined by Mössbauer spectrum fitting for fresh and weathered fly ash

Sample	Sextets				Doublet 1 (magnesioferrite)			Doublet 2 (spinel)		
	IS	QS (ϵ)	Area	phase	IS	QS (ϵ)	Area	IS	QS (ϵ)	Area
	mm/s	mm/s	%		mm/s	mm/s	%	mm/s	mm/s	%
Fresh FA	0.40	-0.12	2	HEM	0.35	0.58	39	0.34	1.05	24
	0.29	0	8	CAF/MAF						
	0.35	0	17	MAF						
	0.35	0.25	9	MAF						
Weathered FA	0.38	-0.1	1.3	HEM	0.35	0.46	22	0.36	0.78	27
	0.16	0	31	CAF/MAF						
	0.35	0.25	18	MAF						

4.4.2 Sulfur removal upon sodium carbonate washing

In **Figure 4.5**, the QXRD results for raw and sodium carbonate washed weathered fly ash is presented. Note that, the amorphous amount was not considered here. It is obvious that huge amounts of anhydrite and gypsum were removed and replaced by calcite formed upon Equation (4.1). In addition, the amount of thenardite (Na_2SO_4) was found remaining unchanged, which implies that such a water-soluble species should be highly embedded within the fly ash matrix and hence, it was not easily accessed during the sodium carbonate washing process.

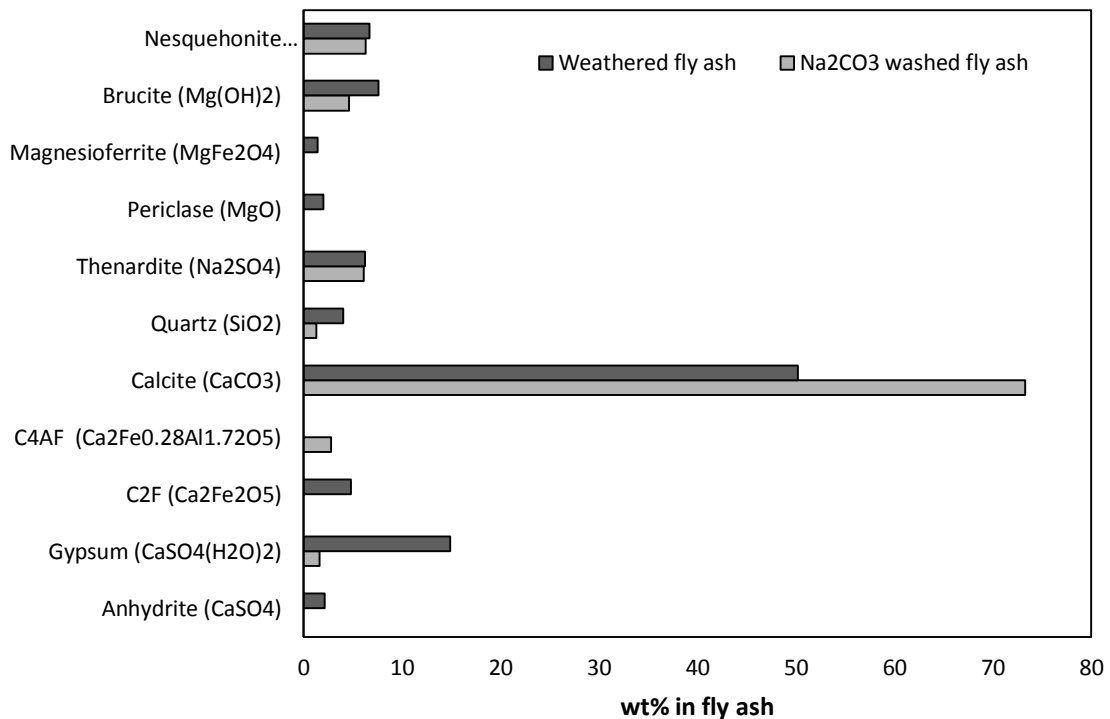


Figure 4.5 Percentage of different minerals in crystalline phase (Amorphous phase was not considered) before and after sodium carbonate washing of weathered fly ash calculated by QXRD.

4.4.3 Fresh and weathered fly ash leaching characteristic

4.4.3.1 Leaching in $\text{NH}_4\text{Cl}+\text{HCl}$

Figure 4.6 a and **b** illustrate the extraction of target elements (Mg and Ca) and interfering ions (Fe, Al, Si and S) from sodium carbonate washed fresh and weathered fly ashes in the mixture of NH_4Cl and HCl at the two pH ranges of 5-5.5 and <4.5, respectively. The leaching temperature and time were fixed at 25°C and 30 min here. As can be seen, the leaching yields of all elements from weathered fly ash are slightly higher than the respective elements in fresh fly ash. The leaching yields of individual element also show notable dependence upon pH for a more efficient dissolution of all the elements at lower pH, as expected. At the pH range of 5-5.5, 43%

Mg, 45% Ca and 13% Fe were extracted from weathered fly ash, which were further increased to 57%, 62% and 18% upon decreasing the pH to <4.5.

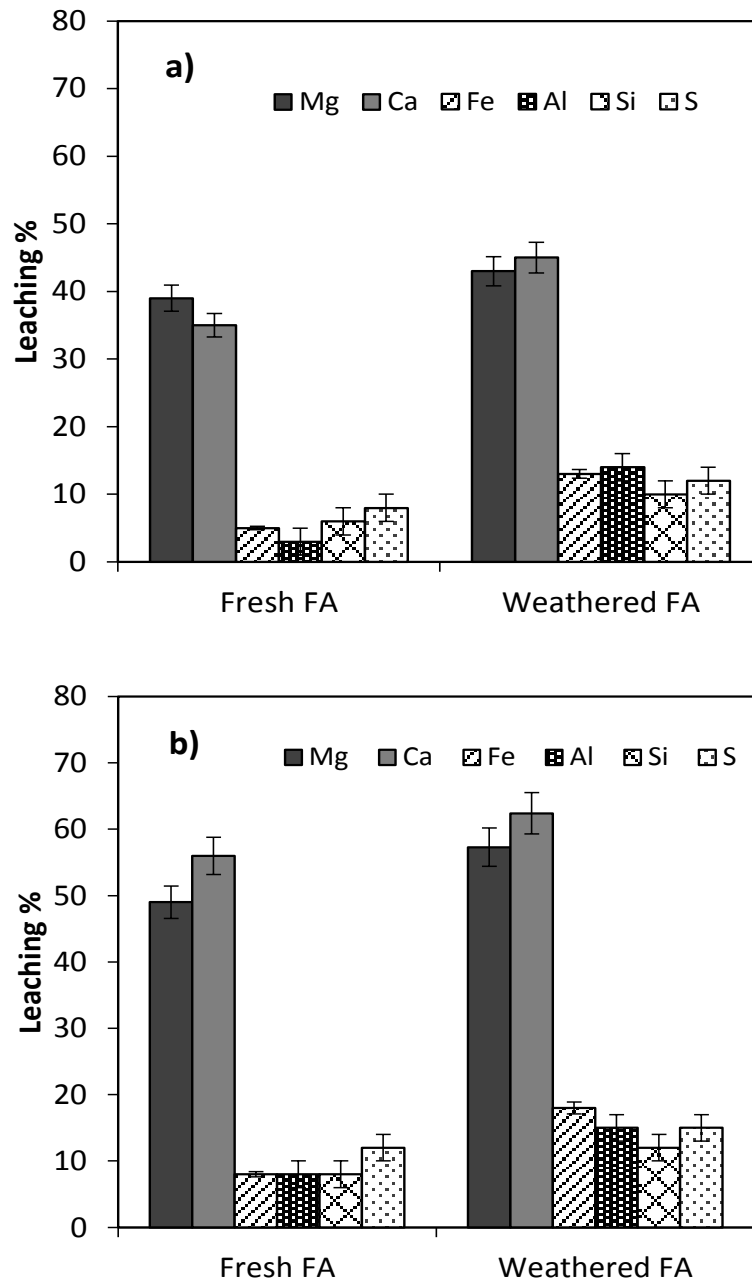


Figure 4.6 Leaching yields of Mg and Ca (target elements) and Fe, Al, Si and S (interfering elements) from fresh fly ash and weathered fly ash using NH_4Cl 4M, $T=80^\circ\text{C}$ and $t=30$ min at a) pH 5-5.5 and b) <4.5

The influences of leaching time and temperature were examined and plotted in **Figures 4.7** and **4.8**, respectively. Note that, all the experiments in these two figures were conducted under the pH – control for a final pH < 4.5 for the leachate. As evident in **Figure 4.7**, the influence of leaching time varies with the elemental type. Instead, the influence of temperature is insignificant for all the elements, as demonstrated in **Figure 4.8**. From **Figure 4.7** it is clear that the leaching time of approximately 40 min at 80°C is sufficient to maximise the extraction of target Mg and

Ca out of the weathered fly ash, reaching 65% and 70% respectively. Interestingly, such values are just slightly higher than the room temperature results shown in **Figure 4.6 b**, 59% and 62% for Ca and Mg respectively. Again, this witnesses an insignificant influence of the leaching temperature. For the interfering elements including Al, Si and S, the increment on their elution yields with leaching time is less than that observed for the two target elements. This reflects a rather refractory association of these elements in the washed fly ash. To reiterate, the unwashed thenardite (as shown in **Figure 4.5**) should be highly embedded within the amorphous matrix of the fly ash, otherwise it should be extracted readily upon either washing by sodium carbonate or $\text{NH}_4\text{Cl}/\text{HCl}$. For both Al and Si, the majority should be present as host species for the affiliation of others to form amorphous species.

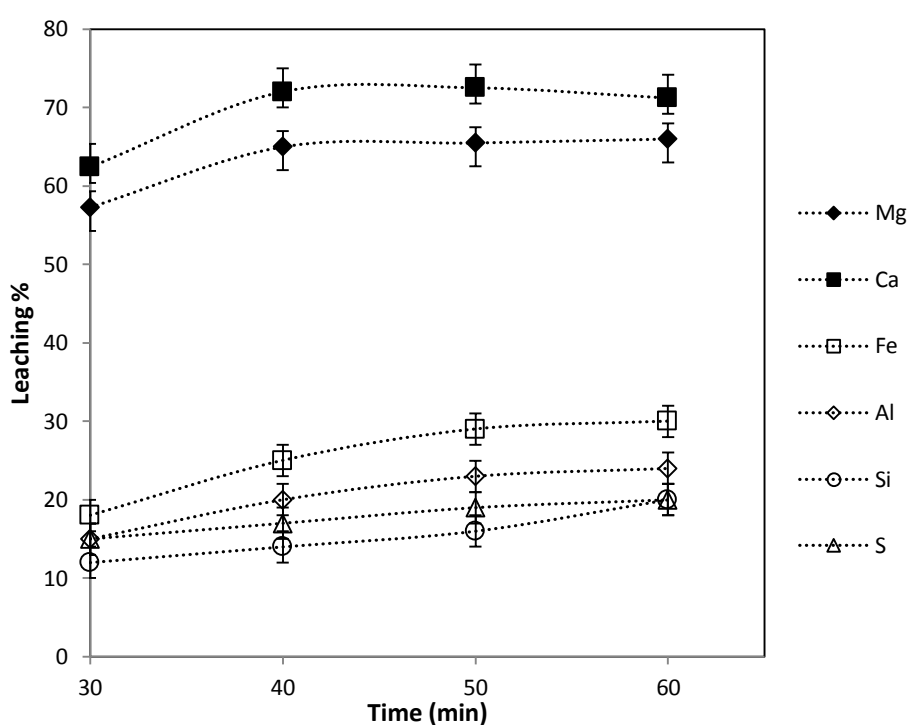


Figure 4.7 Leaching of major elements from weathered fly ash as a function of leaching time (Ammonium chloride pH controlled condition $\text{pH} < 4.5$, $T = 80^\circ\text{C}$)

Fe leaching is more time-dependent, reaching approximately 30 *wt%* in 50 min. The quantified speciation information for iron before and after leaching is summarised in **Figure 4.9**. Note that, the original Mössbauer spectroscopy spectra and the respective fitting curves are plotted in **Figure 4.10**. **Figure 4.9** indicates that, hematite is least eluted upon the leaching, whereas the percentages of the 30-50T CAF/MAF and the <10 T MAF species were reduced dramatically after the leaching. Since the percentages of the other two were increased, it is inferable that, calcium in the CAF was preferentially extracted over the MAF and

magnesioferrite upon the attack from the mixed NH_4Cl and HCl reagent. The difficulty for the breakage of the latter two species in acid has been reported previously [26].

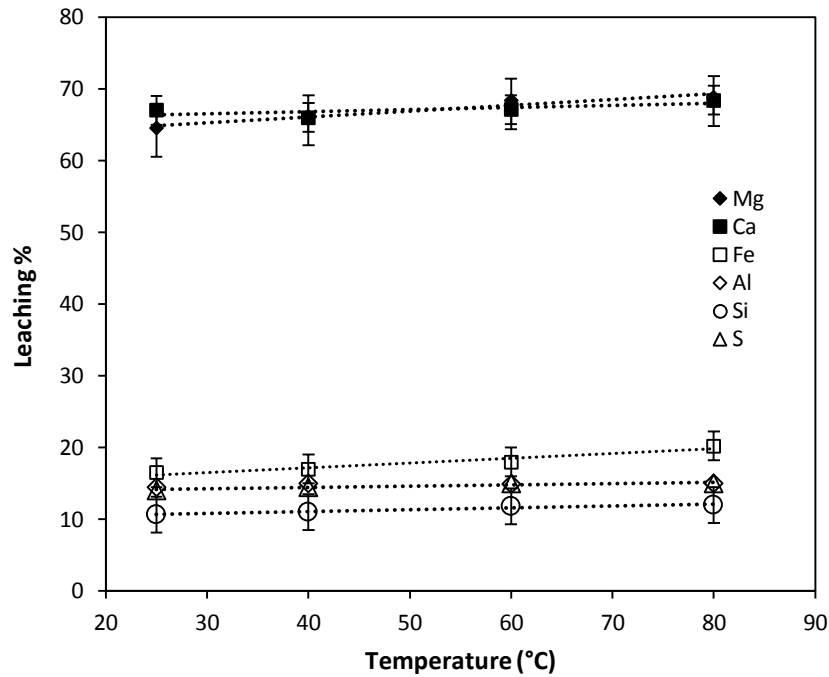


Figure 4.8 Leaching of major elements from weathered fly ash as a function of temperature (Ammonium chloride pH controlled condition $\text{pH} < 4.5$, $t = 40$ min)

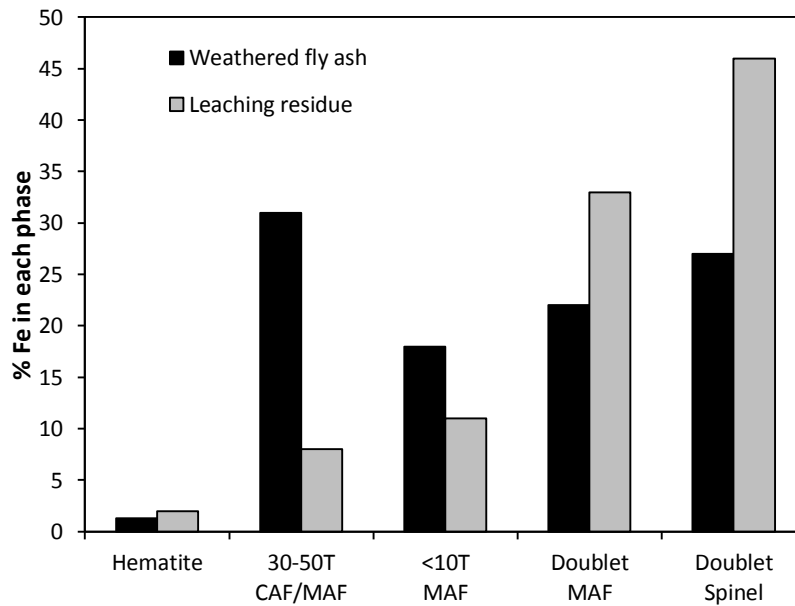


Figure 4.9 Total Fe in each area before and after leaching, taken from Mössbauer spectra

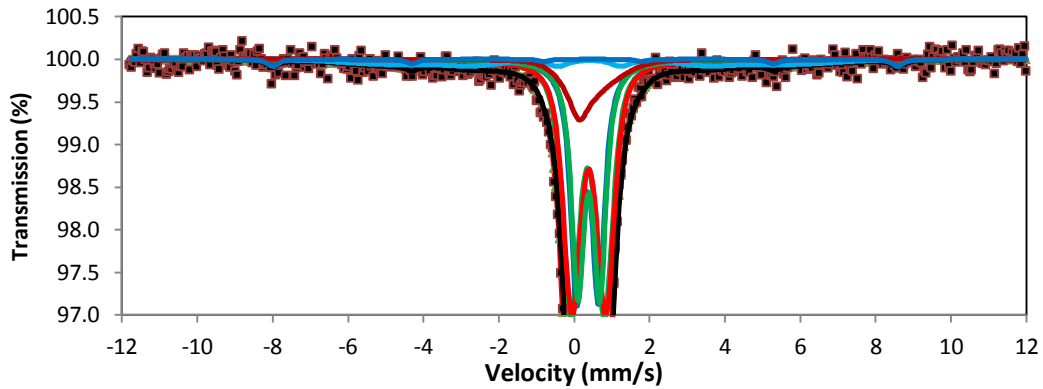


Figure 4.10 Mössbauer spectroscopy fitting results $\text{NH}_4\text{Cl}+\text{HCl}$ leached residue

The influence of liquid to solid (L/S) ratio was examined for the leaching of the weathered fly ash. As demonstrated in **Figure 4.11**, the optimum L/S ratio was found to be 4. A lower L/S ratio resulted in a rapid increase in the extraction of interfering elements, whereas the extraction of two target elements was reduced.

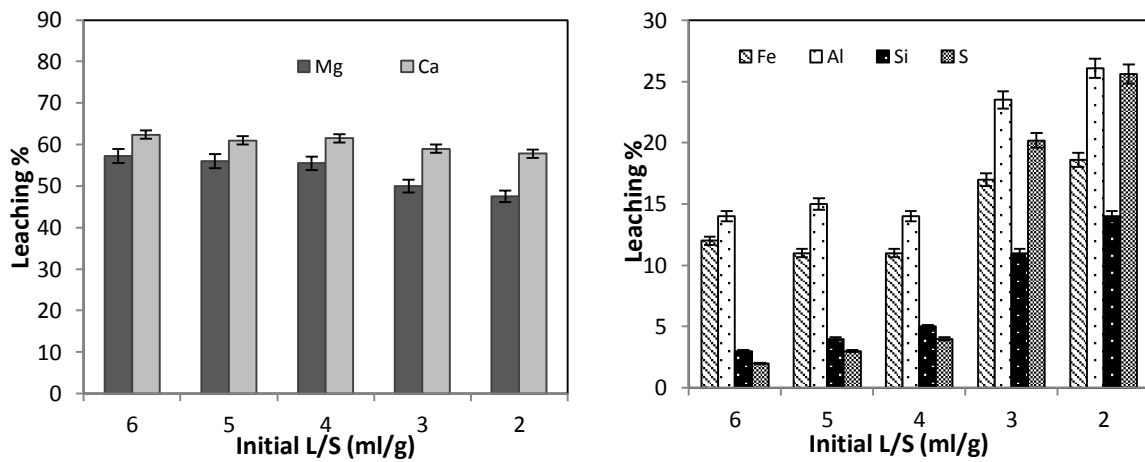


Figure 4.11 Leaching yields of a) Mg and Ca (target elements) and b) Fe, Al, Si and S (Interfering elements) as a function of initial L/S ratio from weathered fly ash using NH_4Cl 4M, $T=\text{RT}$ and $t=40$ min at $\text{pH}<4.5$

4.4.3.2 Leaching in sole HCl

Leaching experiments were further conducted using pure HCl (without pH control) to increase the extraction yields of the two target elements. Despite a very low pH of around 0.8 for HCl used, its pH was increased quickly to ~ 7 once mixed with fly ash. Subsequently, the pH of the leachate fluctuated and was stabilised at ~ 6 in 10 minutes. In light of this, the results of using HCl can be compared with the pH-controlled leaching experiments using $\text{NH}_4\text{Cl}+\text{HCl}$ for a final pH value of 5-5.5. **Figure 4.12** shows the leaching yields of major and interfering elements in sole HCl 1 M. Similar to the pH controlled condition for the use of ammonia chloride (**Figure 4.6 a**), the leaching of both major and interfering ions from weathered fly ash is slightly

higher than fresh fly ash. About 43% and 44% of Mg and Ca were extracted from weathered fly ash, relative to 41% and 41% respectively from fresh fly ash. This further indicates the abundant amorphous species in weathered fly ash are easier to be cracked than the highly crystallised species in the fresh ash. In other words, the weathering of fly ash is beneficial in improving its leaching propensity. The effect of temperature on the leaching of Mg, Ca and Fe in sole HCl was further examined and demonstrated in **Figure 4.13**. Again, similar with the leaching results for $\text{NH}_4\text{Cl}+\text{HCl}$ in **Figure 4.8**, the temperature is insignificant on the extraction rates of Mg and Ca while the leaching of interfering ions was enhanced slightly.

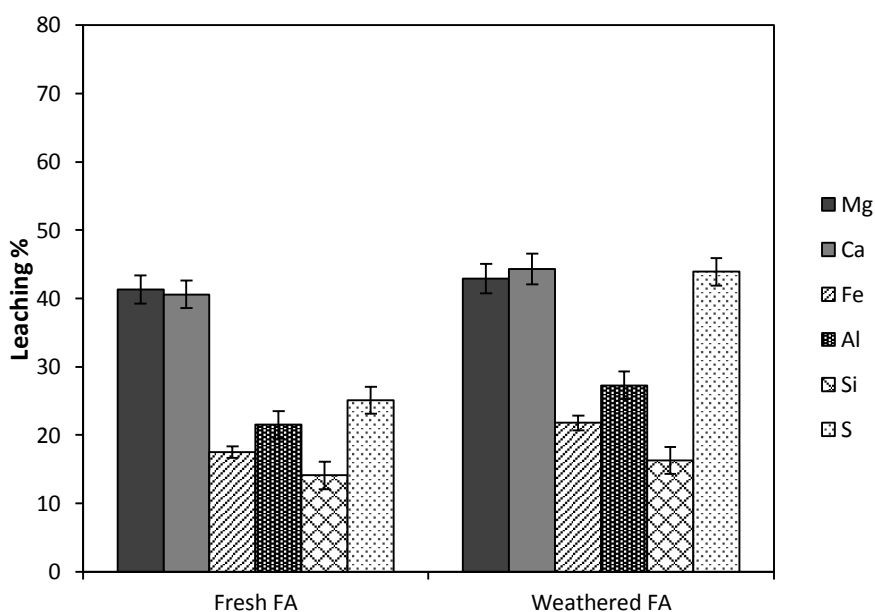


Figure 4.12 Leaching yields of Mg, Ca, Fe, Al, Si and S from fresh fly ash and weathered fly ash using HCl 1M without control pH (T=RT and t=30 min and L/S=6)

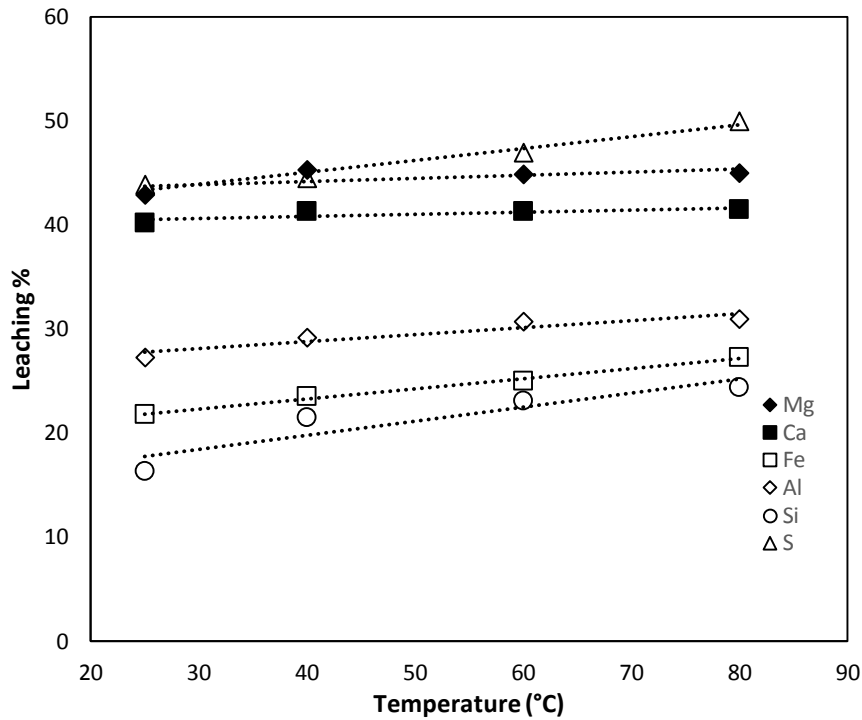


Figure 4.13 Effect of temperature on hydrochloric acid leaching of Mg, Ca and Fe from weathered fly ash (L/S = 6, t=30 min, HCl=1M)

4.4.4 Selective leaching of Mg and Ca over Fe, Al, Si and S by NH₄Cl + HCl solution

The effect of pH on leaching behaviour of individual elements from weathered fly ash was further investigated in the two leaching systems of NH₄Cl+HCl and sole HCl. Note that, both two systems were pH controlled at various values show as x-axis in **Figure 4.14**. The results for both two leaching systems were also plotted in each panel for the comparison purpose.

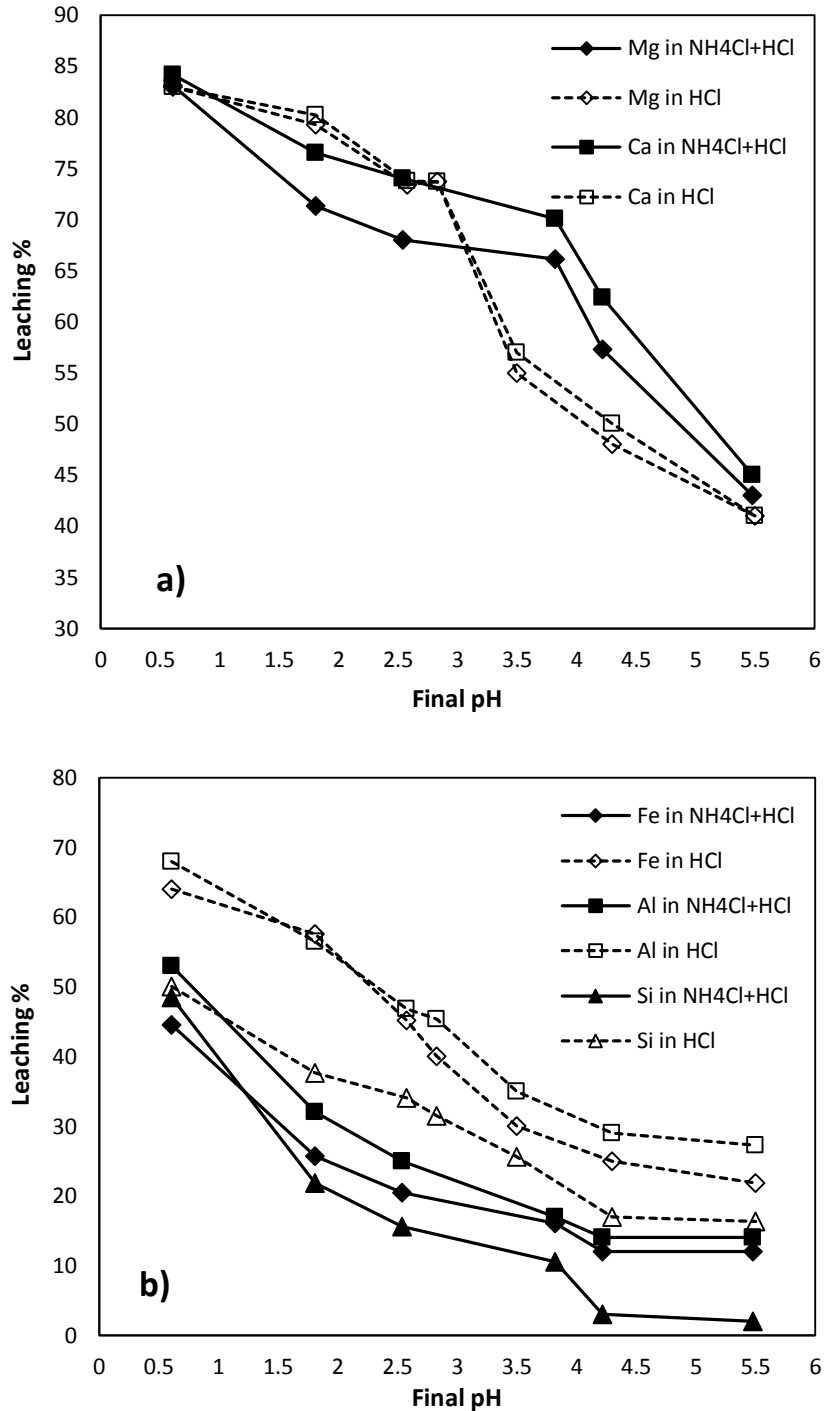


Figure 4.14 Leaching behaviour of a) Mg and Ca and b) other metals Fe, Si and Al in different pH of NH₄Cl+HCl and sole HCl solution

As expected, decreasing pH resulted in a rapid increase in the dissolution of all the metals in both NH₄Cl+HCl and sole HCl solution. However, the two leaching systems performed considerably different upon the variation of pH. For the two target elements Ca and Mg shown in panel a, although the sole HCl is slightly better in terms of the yields of the two elements below the pH of 3.0, the use of NH₄Cl+HCl solution is clearly superior at the higher pH values,

leading to the extraction of 71% Mg and 66% Ca relative to only 50% of the two metals extracted in sole HCl at the same pH value of 4. With a further increase of pH from 4 to 5.5, the discrepancy between the two leaching systems was decreased and eventually vanished. For the interfering elements shown in panel *b*, increasing the pH value of the leachate is clearly beneficial in reducing their yields, which were stabilised at the pH of ~4.5 for both two leaching systems. Clearly, the pH value of 4.5 is the optimum/maximum value to be chosen for either leaching system. Moreover, the use of NH₄Cl+HCl was confirmed superior against the sole HCl in the leaching of impure elements. In other words, the use of NH₄Cl+HCl mixture facilitates a selective leaching of Ca and Mg over other elements out of fly ash.

It is inferred that cationic metal ions are chemically adsorbed on the surface of fly ash particles, especially weathered fly ash and hence, they are highly reactive. The release of metallic ions aqueous solution is assisted by the aid of hydrogen ions of acids or salts according to a cation exchange mechanism [27]. Therefore, maintaining a high level of in the leach liquor using HCl is in favour of enhancing the reaction kinetics. For the fly ash studied here, the H⁺ ion should penetrate into its internal layers to break the refractory associations such as CAF. Consequently, the elution of both target and interfering ions was improved. The positive role of NH₄Cl here is easier pH adjustment and restricting H⁺ concentration through its buffer property [28]. Though HCl was added drop-wise to both NH₄Cl and HCl solution but fluctuation of pH from ~1 to 5 in the case of sole HCl could favours partial dissolution of substantial amount of iron, silicon and sulfur which can be released into the solution at lower pH range.

In addition, ammonium chloride has proven to be able to isolate metals or groups of metals from a polymetallic solution. As has been mentioned by Smith and Martell (1974), ammonia can selectively form a complex with magnesium and calcium and no other ions in a solution [29]. The addition of an ammonium salt increases the solubility of the complexed species of Mg and Ca, which thus allows a much broader range of pH where the interfering ions precipitate rather dissolving into the leachate. Lalancette et al. (2014) has used hydrochloric acid as the leaching agent to dissolve desirable ions like magnesium, zinc and arsenic. Consequently they used ammonium chloride as complex agent to precipitate iron and prevent co-precipitation of other ions [30].

The QXRD results for weathered fly ash NH₄Cl+HCl and HCl leached residues are tabulated in **Table 4.4**. The leaching residues were obtained from the same final pH (around 5.5) for both leaching systems under the same experiment condition, (80°C, 30 min and L/S ratio of 6). The results confirmed the formation of new minerals including ettringite (Ca₆Al₂(SO₄)₃(OH)₁₂.26H₂O), tschermigite (NH₄Al(SO₄)₂.12(H₂O)) and mascagnite ((NH₄)₂SO₄) in NH₄Cl+HCl system. It is evident that ammonium chloride inhibited the dissolution of Al and Si into the leachate through precipitation. No differences were observed in

terms of amorphous amounts from two leaching reagents. It is also clear that there is more amorphous present in the leaching residue, around 71%, compared to only 62% in the original fly ash.

Table 4.4 XRD quantification of NH₄Cl+HCl and sole HCl residues from leaching of weathered fly ash

Minerals	Composition (wt%)	
	NH ₄ Cl leached residue	HCl leached residue
Anhydrite (CaSO ₄)	-	0.6
Gypsum (CaSO ₄ (H ₂ O) ₂)	1.0	1.2
C ₂ F (Ca ₂ Fe ₂ O ₅)	-	2.2
C ₄ AF (Ca ₂ Fe _{0.28} Al _{1.72} O ₅)	-	0.3
Calcite (CaCO ₃)	11.5	15.8
Quartz (SiO ₂)	1.2	1.2
Cristobalite (SiO ₂)	0.3	0.4
Thenardite (Na ₂ SO ₄)	-	1.6
Magnesioferrite (MgFe ₂ O ₄)	-	1.8
Brucite (Mg(OH) ₂)	0.4	0.8
Nesquehonite (MgCO ₃ .3H ₂ O)	0.7	0.7
Hematite (Fe ₂ O ₃)	-	1.6
Etringite (Ca ₆ Al ₂ (SO ₄) ₃ (OH) ₁₂ .26H ₂ O)	0.6	-
Tschermigite (NH ₄ AlSO ₄ .12(H ₂ O))	1.2	-
Magnesite (MgCO ₃)	10.2	-
Mascagnite (NH ₄ (SO ₄) ₂)	0.7	-
Amorphous amount	71.8%	71.6%

The SEM cross-sectional images taken from NH₄Cl+HCl and sole HCl leaching residues further show the different particle compositions. **Figure 4.15 a** shows SEM images of typical particles (L1 and L2) in NH₄Cl+HCl leaching residue while part *b* demonstrates the representative particles from HCl leaching residue (L3 and L4). Elemental composition of closed area on surface of particles calculated from EDX analysis is summarised in **Table 4.5**. The particle L1 shown is the combination of Fe, Ca and Mg that might be mixture of CAF, MAF or hematite in amorphous form. Abundance of O and C in all of the particles confirms the presence of oxide, hydroxide or carbonates of Mg. L2 shows significant amount of Fe, Mg, Si and Al which can be attributed to quartz, hematite or magnesioferrite along with magnesium hydroxide or carbonates. Both two particles are rather dense with fewer pores inside, indicating a weak

penetration of ammonium ion into the particle for the extraction of the elements embedded in depth. Instead, L3 shows a large cluster which are composed of fine agglomerates that are made up of Fe, C, O and Mg. Brucite, periclase, nesquehonite, magnesioferrite and hematite are possible minerals existing in this particle. The rather loose packing of the particle aggregates indicates the breakage of original coarse particles upon the severe attack of protons. The particle L4 is different in shape and texture, which is flat in shape and is exclusively made up of Al, Fe and Mg. It can be inferred as Fe-bearing spinel that is even difficult to dissolve in sole acid [26].

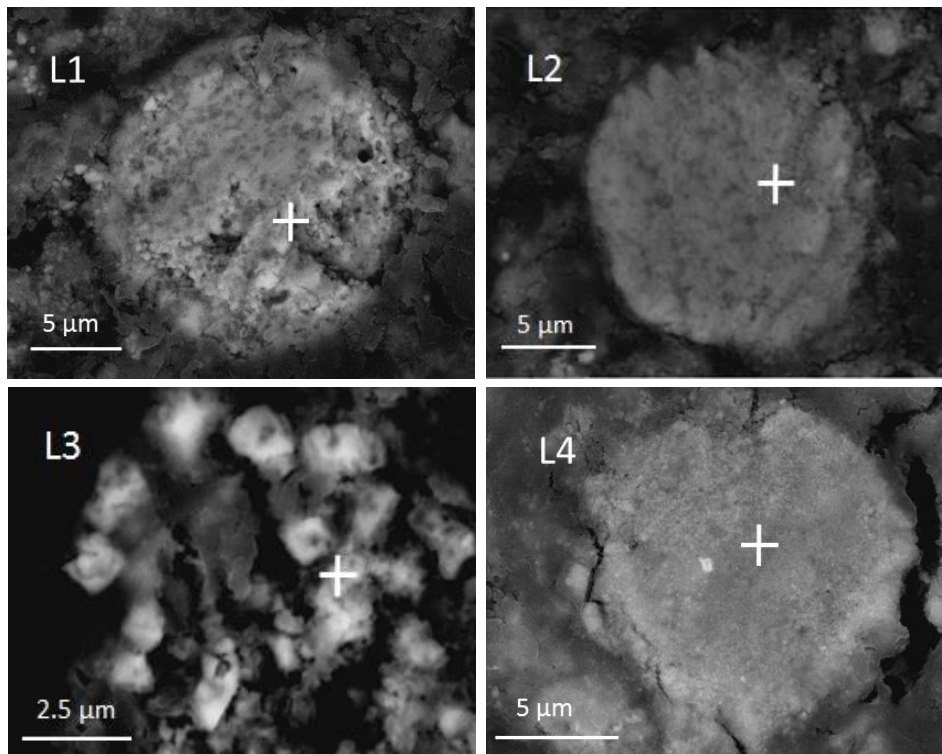


Figure 4.15 BSE images magnification 5000 X of typical particles L1 and L2 obtained from $\text{NH}_4\text{Cl}+\text{HCl}$ (top) and L3 and L4 from sole HCl (bottom) leaching residue of weathered fly ash

Table 4.5 Elemental composition of representative leaching residue particles L1 and L2 ($\text{NH}_4\text{Cl}+\text{HCl}$ leached) and L2 and L3 (HCl leached) determined by EDX

Sample	Size (μm)	Elemental Composition (wt%)								
		Ca	Mg	Fe	Si	Al	S	Cl	Na	O
L1	10-15	23	13	28	+	3	+	+	ND	32
L2	10-15	3	9	33	8	6	+	2	+	38
L3	10-15	2	6	53	3	5	ND	2	ND	24
L4	8-10	2	15	15	+	18	+	+	ND	44

+: Not significant, ND: Not detected

4.5 Conclusion

This study for the first time has examined the properties and leaching propensity of weathered Victorian brown coal fly ash collected from ash pond. The leaching conditions for the target metals Ca and Mg were also optimised. The major conclusions achieved are summarised as follows:

- 1) In comparison to fresh fly ash rich in oxides, the weathered fly ash is dominated by hydrates and carbonate forms which were formed in aqueous landfilling system. These species were mostly poorly crystallised, and even loosely agglomerated into clusters. Irrespective of the leaching reagent, the target Ca and Mg in weathered fly ash were more easily extracted than in the fresh ash counterpart under the same leaching conditions, due to the association of these two metals with amorphous species.
- 2) For the use of either leaching agent, the temperature and time played little or marginal role on the extraction of target Ca and Mg out of the weathered fly ash sample. In contrast, the liquid to solid ratio is crucial. The optimum value of 4 was found beneficial for maximising the selectivity of Ca and Mg.
- 3) The optimum pH value was found to be around 4 for the mixture of $\text{NH}_4\text{Cl}+\text{HCl}$, which reduced the extraction yields of impure elements to the lowest value, whereas the leaching extent of two target elements was still reasonably high, ~70 %. However, this is not the case observed for the sole HCl, the use of which resulted in a lower selectivity of Ca and Mg at the pH of 4
- 4) The use of $\text{NH}_4\text{Cl}+\text{HCl}$ is superior over sole HCl, due to the buffering property of NH_3 and its complexing capability to prevent the dissolution of impure elements. Instead, the use of sole HCl even at the same pH value as the mixture of $\text{NH}_4\text{Cl}+\text{HCl}$ resulted in a deep penetration of protons into particle inside, the intense breakage of ash cluster, and hence, the simultaneous dissolution of plenty of impure elements.

Acknowledgment

This project was supported by the Faculty of Engineering of Monash University for 2012-13 seed grant. The first author is grateful to Monash Research Graduate School (MRGS) for PhD tuition fee award and CSIRO Flagship scholarship. The invaluable comments from Jim Siemon in Latrobe Magnesium Co. Ltd are also acknowledged.

References

- [1] Yeheyis, M.; Shang, J.; Yanful, E. Chemical and mineralogical transformations of coal fly ash after landfilling. World of coal ash (WOCA) conference. May 4-7, Lexington, USA. **2009**.
- [2] Ahmaruzzaman M. A review on the utilisation of fly ash. *Prog. Energ. Combust.* **2010**, 36, 327–363.
- [3] Eze, C.P.; Nyale, S.M.; Akinyeye, R.O.; Gitari, W.M.; Akinyemi, S.A.; Fatoba, O.O; Petrik, L.F. Chemical, mineralogical and morphological changes in weathered coal fly ash: A case study of a brine impacted wet ash dump. *J. Environ. Manage.* **2013**, 129, 479-492.
- [4] Muriithi, G.N.; Petrik, L.F.; Fatoba, O.; Gitari, W.M.; Doucet, F.J.; Nel, L.; Nyale, S. M.; Chucks, P.E. Comparison of CO₂ capture by ex-situ accelerated carbonation and in in-situ naturally weathered coal fly ash. *J. Environ. Manage.* **2013**, 127, 212-220.
- [5] Baba, A.; Gurdal, G.; Sengunalp, F.; Ozay, O. Effects of leachant temperature and pH on leachability of metals from fly ash. A case study: Can thermal power plant, province of Canakkale, Turkey. *Environ. Monit. Assess.* **2008**, 139, 287-298.
- [6] Ward, C.; French, D.; Jankowski, D.; Dubikova, M.; Li, Z.; Riley, K. Element mobility from fresh and long-stored acidic fly ashes associated with an Australian power station, *Int. J. Coal Geol.* **2009**, 80, 224-236.
- [7] Baker, L.; Gupta, A.; Gasiorowski, S. Triboelectrostatic beneficiation of landfilled fly ash, In: World of Coal Ash (WOCA) Conference. May 5-7, Nashville, USA, **2015**.
- [8] Jo, H.Y.; Ahn, J.H.; Jo, H. Evaluation of the CO₂ sequestration capacity for coal fly ash using a flow-through column reactor under ambient conditions. *J. Hazard. Mater.* **2012**, 242, 127-136.
- [9] Montes-Hernandez, G.; Pérez-López, R.; Renard, F.; Nieto, J.M.; Charlet, L. Mineral sequestration of CO₂ by aqueous carbonation of coal combustion fly-ash. *J. Hazard. Mater.* **2009**, 161(2-3), 1347-1354.
- [10] Nyambura, M.G.; Mugeru, W.G.; Felicia, P.L.; Gathura, N.P. Carbonation of brine impacted fractionated coal fly ash: implications for CO₂ sequestration. *J. Environ. Manage.* **2011**, 92, 655-664.
- [11] Sun, Y.; Yao, M.S.; Zhang, J.P.; and Yang, G. Indirect CO₂ mineral sequestration by steelmaking slag with NH₄Cl as leaching solution. *Chem. Eng. J.* **2011**, 173(2), 437-445.

- [12] Hosseini, T.; Selomulya, C.; Haque N.; Zhang L. Indirect Carbonation of Victorian Brown Coal Fly Ash for CO₂ Sequestration: Multiple-Cycle Leaching-Carbonation and Magnesium Leaching Kinetic Modelling. *Energ. Fuel.* **2014**, 28(10), 6481-6493.
- [13] Sun, Y., Parikh, V., Zhang, L., Sequestration of carbon dioxide by indirect mineralisation using Victorian brown coal fly ash, *J. Hazard. Mater.* **2012**, 209-210, 458-466.
- [14] Andrade, A.; Coenegracht, Y.M.A; Hollman, G.G.; Janssen-Jurkovicova, M.; Pietersen, H.S.; Vriend, S.P.; Schuiling, R.D. Leaching characteristics of fly ash after four years of natural weathering, MRS online proceeding library 178, **1990**.
- [15] Mudd, G.M.; Kodikara J. Field Studies of the Leachability of Aged Brown Coal Ash. *J. Hazard. Mater.* **2000**, 76 (2-3), 159-192.
- [16] Singh, R.K.; Gupta, N.C.; Guha, B.K. pH dependence leaching characteristics of selected metals from coal fly ash and its impact on ground water quality. *Int. J. Chem. Environ. Eng.* **2014**, 5, 218-222.
- [17] Zygadło M., Woźniak, M., Processes of coal fly ash weathering in waste deposits. *Environ. Prot. Eng.* **2010**, 36 (2), 17-29.
- [18] Teir, S.; Revitzer, H.; Eloneva, S.; Fogelholm, C.J.; Zevenhoven, R. Dissolution of natural serpentinite in mineral and organic acids. *Int. J. Miner. Process.* **2007**, 83, 36–46.
- [19] Berry E.E.; Hemmings R.T.; Golden D.M. Enhanced resource recovery by beneficiation and direct acid leaching of fly ash, MRS online proceedings library 86, **1986**.
- [20] Sharma, B.K. Soil and noise pollution. Goel publishing house, Meerut, **2001**.
- [21] Ward, C.R.; Taylor, J.C.; Cohen, D.R. Quantitative mineralogy of sandstones by x-ray diffractometry and normative analysis. *J. Sediment. Res.* **1995**, 69(5), 1050-1062.
- [22] Williams, R.P.; Van Riessen, A. Determination of the reactive component of fly ashes for geopolymer production using XRF and XRD. *Fuel* **2010**, 89(12), 3683-3692.
- [23] Taylor, G.R.; Ruotsala, A.P.; Keeling, R.O. Analysis of iron in layer silicates by Mössbauer spectroscopy. *Clay. Clay. Miner.* **1968**, 16, 381-391.
- [24] Murad, E.; Cashion, J. Mössbauer Spectroscopy of Environmental Materials and Their Industrial Utilisation, Kluwer Academic Publishers, Dordrecht, **2004**.
- [25] Kukier, U.; Ishak, C.F.; Sumner, M.E.; Miller, W.P. Composition and element solubility of magnetic and non-magnetic fly ash fractions. *Environ. Pollut.* **2003**, 123, 255–266.

- [26] Choo, T.K.; Song, Y.; Zhang, L.; Selomulya, C.; Zhang, L. Mechanisms underpinning the Mobilisation of Iron and Magnesium Cations from Victorian Brown Coal Fly Ash. *Energ. Fuel* **2014**, 28 (6), 4051-4061.
- [27] Huang, K.; Inoue, K.; Harada, H.; Kawakita, H.; Ohto, K. Leaching of heavy metals by citric acid from fly ash generated in municipal waste incineration plants. *J. Mater. Cycles Waste Manag.* **2011**, 13, 118–126.
- [28] Künkül, A.; Gülezgin, A.; Demirkiran, N. Investigation of the use of ammonium acetate as an alternative lixiviant in the leaching of malachite ore, Scientific Paper, Inonu University, Malatya, Turkey, 2013.
- [29] Smith, R.M.; Martell, A.E. Critical stability constants, Volume 4: Inorganic complexes. Plenum Press, New York, **1974**.
- [30] Lalancette, J.M. ; Dubreuil, B. ; Lemieux, D. Method for selective precipitation of iron, arsenic and antimony, US Patent 2014/0120012, **2014**.

Monash University

Declaration for Thesis Chapter 5

Declaration by candidate

In the case of Chapter 5, the nature and extent of my contribution to the work was the following:

Nature of contribution	Extent of contribution (%)
Experimental design and conduct, writing up	96 %

The following co-authors contributed to the work. If co-authors are students at Monash University, the extent of their contribution in percentage terms must be stated:

Name	Nature of contribution	Extent of contribution (%) for student co-authors only
Dashen Dong	QXRD reliability experiments	2%
Wang Zhao	QXRD reliability experiments	2%
Lian Zhang	Experimental design, key ideas, reviewing and editing paper	Supervisor
Cordelia Selomulya	Editing paper, comments and feedback	Supervisor
Nawshad Haque	Editing paper, comments and feedback	Supervisor

The undersigned hereby certify that the above declaration correctly reflects the nature and extent of the candidate's and co-authors' contributions to this work*.

Candidate's
Signature

		Date 12/11/2015
--	--	--------------------

Main
Supervisor's
Signature

		Date 12/11/2015
--	---	--------------------

*Note: Where the responsible author is not the candidate's main supervisor, the main supervisor should consult with the responsible author to agree on the respective contributions of the authors.

Chapter 5

Mechanism of competition between Mg^{2+} and Ca^{2+} upon carbonation

In Chapter 4, leaching propensities of fresh and weathered fly ash in the $NH_4Cl+HCl$ and sole HCl were examined and it was found that $NH_4Cl+HCl$ showed higher selectivity of magnesium and calcium over other impurities. Given the fact that concentration of magnesium and calcium in the leachate varies broadly upon change in the fly ash type and leaching reagent, the competition between the two cations Ca^{2+} and Mg^{2+} extracted in the leachate can be regarded as the most critical parameter affecting their carbonation rate, as well as the final carbonate product properties. In this chapter, the carbonation capacity of a leachate rich in Mg^{2+} and Ca^{2+} at varying Mg^{2+}/Ca^{2+} ratio was examined to clarify the competition between the carbonation of two cations and speciation of the resulting carbonate precipitate upon mineral carbonation process. This chapter has been reformatted from the following published manuscript: **T. Hosseini**, C. Selomulya, N. Haque, L. Zhang, Investigating the Effect of Mg^{2+}/Ca^{2+} Molar Ratio on the Carbonate Speciation during the Mild Mineral Carbonation Process at Atmospheric Pressure, *Energy & Fuels*, 2015, 29 (11), PP 7483-7496.

5.1 Abstract

Aqueous mineral carbonation of industrial wastes like fly ash is a promising sequestration technology to reduce CO₂ emission in the small/medium-sized plants. In this paper, the carbonation capacity of a leachate rich in Mg²⁺ and Ca²⁺ contents was examined to clarify the competition between the carbonation of these two cations and the speciation of the resulting carbonate precipitate, under the mild carbonation conditions using 20-80°C and atmospheric pressure. As has been confirmed, the carbonation precipitation of the two cations was completed in 30-40 min. At room temperature, increasing the Mg²⁺/Ca²⁺ molar ratio was in favour of the carbonation rate of Mg²⁺, which is maximised at the Mg²⁺/Ca²⁺ molar ratio of 2. In contrast, the carbonation rate of Ca²⁺ was decreased monotonically, due to the competition from Mg²⁺. For both two cations, their carbonation rate was maximised at 60°C. Compared to the formation of predominant calcite and vaterite in the presence of sole Ca²⁺ in the leachate, the co-existence of two cations resulted in the preferential formation of amorphous species, aragonite and magnesian calcite. The quantity of amorphous phase was increased remarkably upon increasing the Mg²⁺/Ca²⁺ molar ratio at room temperature. Increase in carbonation temperature further deteriorated the crystallisation of carbonation precipitate, resulting in the increase of the amount of amorphous species, and the phase change of calcium carbonate from calcite to aragonite.

5.2 Introduction

Mineral carbonation is a process that involves the sequestration of CO₂ by converting the Ca- and/or Mg-bearing solid residue wastes into carbonates which are thermodynamically stable [1-3]. The main drawback of mineral carbonation technologies that use natural mineral resources such as serpentine, wollastonite and olivine as feedstock is the large effort that has been exerted in mining and milling of raw material to achieve small size and large specific surface area [4]. The utilisation of alkaline solid wastes such as fly ash has several advantages, including a low cost of sequestration, close proximity to the place which CO₂ is emitted, and the abundance of fine and uniform particle size which circumvent the comminution cost. Moreover, alkaline solid wastes are typically more reactive with CO₂ than natural minerals due to their chemical instability [5].

Fly ash is a valueless waste derived from the combustion of coal and municipal solid wastes (MSW), containing magnesium (Mg) and calcium (Ca) at varying proportions. The characteristics of fly ash differ substantially according to the coal type and combustion conditions. Fly ash derived from low-rank lignite or sub-bituminous coal generally consists of more than 20% CaO and MgO in total, which are essential for mineral carbonation [6]. The

typical Victorian brown coal fly ash, from Victoria, Australia is composed of 29.3% MgO and 32.4% of CaO, which has proven to be an appropriate feedstock for mineral carbonation [7,8].

Since the fly ash rich in alkali and alkaline earth metals are unsuitable for being used as additive into the cement, the use of this kind of fly ash to supplement natural minerals for CO₂ mineralisation has been receiving increased attention [9-11]. To date, the majority of studies on fly ash utilisation has focused on direct carbonation under a high CO₂ partial pressure with a rather long reaction time [10,12]. Little work has been done on an indirect carbonation fashion, *i.e.*, a prior leaching for the extraction of Ca and Mg into an aqueous leachate with subsequent precipitation of solid carbonate by contacting the liquor with a CO₂-laden flue gas [11,13,14]. The advantages of this method lies in the fact that mild conditions (25–80°C and atmospheric pressure) are good enough for both leaching and carbonation. The resulting carbonation products are also of high-purity that can be used as a substitution for the natural carbonates.

To date, the majority of works on the indirect carbonation of industrial wastes focused on the optimisation of process condition to maximise the yield of calcium carbonate, due to the less amount of Mg in the certain solid wastes [4,5,9,15]. In the case of solid wastes with a high Ca/Mg ratio, such as steel making slag, it is mostly preferred to minimise Mg contamination in the leachate and consequently achieve high purity calcium carbonate by adjusting the leaching or carbonation parameters [16-18]. In some cases, however, studies on the carbonation of aqueous resources including sea water, subsurface brine and industrial effluents have focused on the carbonation of both Ca²⁺ and Mg²⁺ [19,20]. Although over 90% of the Mg²⁺ and Ca²⁺ in sea water can precipitate in their carbonate forms through raising the pH of the leachate or CO₂ partial pressure [21] the co-existence of Mg²⁺ and Ca²⁺ in the leachate has proven to exert a remarkable effort on the precipitation behaviour of Ca²⁺ [21-24]. Roques and Girou (1974) have reported that Ca²⁺ precipitation extent was significantly reduced by the presence of even a small amount of Mg²⁺ in the leachate. They concluded that, the cations having atomic radii smaller than that of Ca²⁺ and hydration energy higher than Ca²⁺ can orient to aragonite (CaCO₃), a deposit normally made up of calcite [21]. Kitano (1976) has observed that the initial concentration ratio of Mg²⁺/Ca²⁺ greater than three yielded a precipitate which is composed mainly of aragonite (CaCO₃) [23].

Although a limited number of studies have been mentioned about the co-precipitation of Mg²⁺ and Ca²⁺ in aqueous mineral carbonation process, the competition of Mg²⁺ and Ca²⁺ cations on the carbonation rate and carbonate precipitate composition has yet to be achieved. This is the motivation for this study. Given the fact that the compositions of both calcium and magnesium in fly ash varies broadly, the competition between the two cations Ca²⁺ and Mg²⁺ extracted in the leachate can be regarded as the most critical parameter affecting their carbonation rate, as well as the final carbonate product properties. In light of this, we have varied the Ca²⁺/Mg²⁺ ratio

between two extremes for pure Ca^{2+} or Mg^{2+} cation to examine their competition in the carbonation process. The pure CaCl_2 and MgCl_2 solutions were used to mimic the leachates achieved from leaching processes of Mg and Ca-rich industrial wastes or natural minerals which usually have a broad Ca^{2+} to Mg^{2+} molar ratio upon the variation of the feedstock. In addition, the carbonation of the mixed solutions was conducted as a function of reaction temperature and time at atmospheric pressure. Here the partial pressure of CO_2 and its flow rate was fixed at a bar and 15 L/min, which were large enough to eliminate both external and internal diffusion resistance. By doing this, the effect of CO_2 partial pressure was ruled out in this study. The precipitated solid products from carbonation process were analysed delicately using quantitative X-ray diffraction (QXRD), so as to establish the mineral phase diagram for both two cations upon atmospheric carbonation. The accuracy of the QXRD has been validated through the use of pure compounds mixtures. An internal standard method was also established by use for the QXRD to quantify the amount of both amorphous and individual crystallised species. This study aims to provide an overall mineral phase diagram for mild indirect carbonation, and therefore, enhance the understanding on properties of carbonate upon the competition between two cations, and their potential value-added utilisation as well.

5.3 Materials and experimental methods

5.3.1 Materials

Experiments were performed using mixtures of MgCl_2 and CaCl_2 solutions to mimic fly ash leachates. Analytical grade reagents $\text{MgCl}_2 \cdot 6\text{H}_2\text{O}$, $\text{CaCl}_2 \cdot 2\text{H}_2\text{O}$ and aqueous ammonia (28%) were used as the source of Mg^{2+} , Ca^{2+} and pH swing agent, respectively. The carbonation experiments conditions are summarised in **Table 5.1**. The first and last experiments correspond to two extremes for the presence of sole Mg^{2+} and Ca^{2+} in the solution, respectively. The initial concentration of MgCl_2 0.065 g/mL (Mg^{2+} 0.0163 g/mL), was chosen based on the leachate achieved from the leaching of a brown coal fly ash in ammonium chloride solution in our previous work [7]. For all of the remaining experiments, the concentration of Mg^{2+} remained constant where Ca^{2+} with different ratio relative to Mg^{2+} was added to the solution. An extra set of complementary experiments were conducted at a $\text{Mg}^{2+}/\text{Ca}^{2+}$ molar ratio of 1 to clarify the effect of temperature on carbonation yield and the quantity of precipitates. Note that, the concentration range for Mg^{2+} and Ca^{2+} in the simulated leachates studied here is broadly consistent with the respective ranges for the man-made mineral-derived leachates that have been studied [8,11,25].

For each carbonation experiment, the pre-determined amount of $\text{MgCl}_2 \cdot 6\text{H}_2\text{O}$ and $\text{CaCl}_2 \cdot 2\text{H}_2\text{O}$ were dissolved in distilled water. Before carbonation, 16 mL ammonia solution

(28%) was added into synthesised solution to adjust the pH value to 10-11. The resulting solution was placed immediately into a sealed glass beaker under magnetic stirring at 400 rpm. Gas inlet and outlet tubes allowed a continuous pure CO₂ gas stream with a constant flow rate of 15 L/min at atmospheric pressure. This rate has been confirmed to be the optimum value in terms of eliminating the external diffusion resistance. It is also high enough to stir the leachate thoroughly to eliminate the internal diffusion, but causes no splash of the solution. In theory, the optimised flow rate depends on size of reactor, volume of solution and pH [5]. The role of CO₂ partial pressure is out of scope for this study. Moreover, although the flow rate of CO₂ is influential in affecting the carbonation rate, it has been confirmed affecting little on the final yield and properties of the final carbonate products [26].

Table 5.1 Summary of different ratios of Mg²⁺/Ca²⁺ in carbonation experiments

Case	Material	[Mg ²⁺]/[Ca ²⁺]	Concentration	Description
1	MgCl ₂ .6H ₂ O	[Mg ²⁺]/[Ca ²⁺]=1/0	MgCl ₂ (0.0646 g/ml)	Only Mg ²⁺ in solution
2	MgCl ₂ .6H ₂ O + CaCl ₂ .2H ₂ O	[Mg ²⁺]/[Ca ²⁺]=2/1	MgCl ₂ (0.0646 g/ml)+ CaCl ₂ (0.03762 g/ml)	[Mg ²⁺] kept constant in the solution and CaCl ₂ was doubled in each case.
3	MgCl ₂ .6H ₂ O + CaCl ₂ .2H ₂ O	[Mg ²⁺]/[Ca ²⁺]=1/1	MgCl ₂ (0.0646 g/ml)+ CaCl ₂ (0.07524 g/ml)	
4	MgCl ₂ .6H ₂ O + CaCl ₂ .2H ₂ O	[Mg ²⁺]/[Ca ²⁺]=1/2	MgCl ₂ (0.0646 g/ml)+ CaCl ₂ (0.15048 g/ml)	
5	CaCl ₂ .2H ₂ O	[Mg ²⁺]/[Ca ²⁺]=0/1	CaCl ₂ (0.07524 g/ml)	

The aqueous carbonation experiments were conducted with a reaction time up to 1 h. Eventually, the solution was filtered using a vacuum filter and the resulting solid powders were dried at 110°C overnight and stored. The solid dry residue was further washed with distilled water for around 1 h at a liquid to solid ratio of 10 to remove any crystallised ammonium chloride [7].

5.3.2 Characterisation of solid precipitates

The elemental compositions of carbonate precipitates were determined using a pre-calibrated X-ray fluorescence spectroscopy (XRF, Spectro iQ II). The X-ray diffraction (XRD, Rigaku, Miniflex 600) pattern for each precipitate was recorded from 2 to 90° 2θ at 40 kV and 15 mA using a rate of 2°/min with Cu Kα radiation. Mineral identification was conducted in

MDI Jade 6, whereas QXRD was performed using Siroquant V.4.0. Through the least-squares fitting refinement of the Rietveld parameters, Siroquant is able to create a theoretical XRD profile to fit the measured XRD pattern, through iteratively minimising the chi-square. The Rietveld method has been applied successfully to determine crystalline phase composition of pure and complex substances. It was applied successfully to analyse NIST fly ash standard reference material and the total average error was found to be only 4% [27]. In this study we also ground each carbonate precipitate down to $<10\ \mu\text{m}$ through the use of a SPEX Mixer/Mill 8000D. The adequate reduction of particle size will eliminate preferred orientation and obtain a uniformly sized, randomly oriented fine power specimen which accurately reflects the structure and composition of phases [28]. In order to validate the QXRD results in the quantification of oxide compositions, the mixtures of super-pure silica (SiO_2 , $>99\%$, Sigma-Aldrich) was mixed with iron oxide (Fe_2O_3 , $>99\%$ Sigma-Aldrich) at different mass ratios and were analysed by the QXRD first. **Figure A.1** in appendix provides the measured XRD patterns for the mixtures and their respective fitting curves. Based on the Rietveld method, the QXRD is further able to deliver the mass percentage of these two oxides. **Figure 5.1** is the corresponding scatter charts for the comparison of QXRD results and the actual values for different mixtures of SiO_2 and Fe_2O_3 . Clearly, one can see a good accuracy for the QXRD, yielding a linear regression R^2 value of 0.8085 and 0.9692 for SiO_2 and Fe_2O_3 , respectively. This echoes a chi-square error no larger than 50 for the QXRD fitting in **Figure A.1** in appendix A.

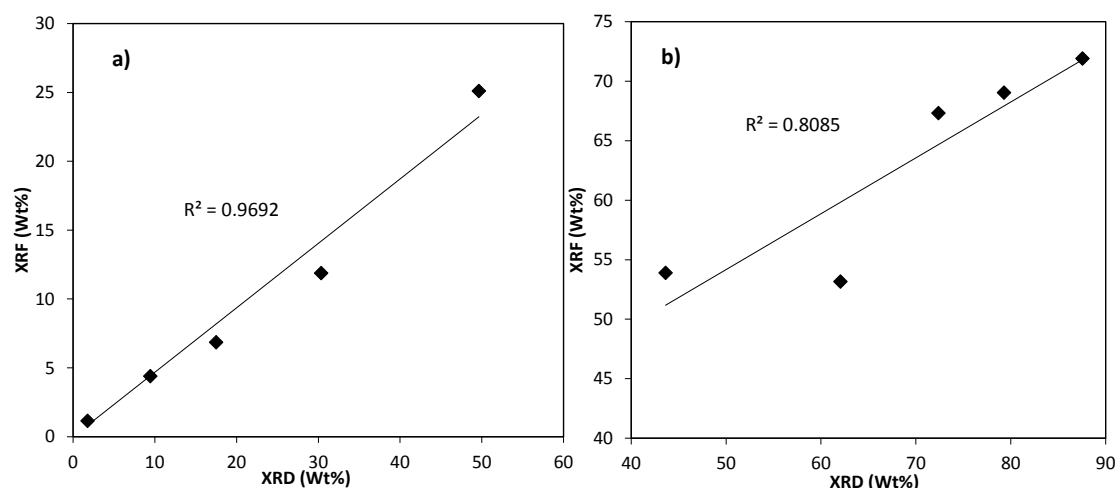


Figure 5.1 Comparison of QXRD results with actual mass percentages for two pure oxides in their mixtures, *a)* Fe_2O_3 and *b)* SiO_2 at different mixing ratios

Based on the fact that the amorphous species is undetectable in XRD, we further extend the QXRD methodology for the quantification of the amount of species, through the use of an internal standard, high-purity corundum $\alpha\text{-Al}_2\text{O}_3$ crystal powder (Sigma-Aldrich $>99.5\%$, powder). The amount of amorphous species upon QXRD analysis was determined based on the

mass percentage ($W_{Al_2O_3, QXR D}$) of internal standard, corundum quantified by QXR D, by Equation (5.1) [29-31]:

$$W_{Al_2O_3, Q-XRD} = \left(\frac{W_{Al_2O_3} \times 100}{(100 - W_{Al_2O_3} \times 100 - X)} \right) \times 100 \quad (5.1)$$

Where $W_{Al_2O_3}$ is the original mass percentage of Al_2O_3 added into its mixture with the real sample to be analysed, and X stands for the about mass of amorphous species in the sample with a mass of $100 - W_{Al_2O_3} \times 100$. The value of $W_{Al_2O_3, Q-XRD}$ must be larger than that for $W_{Al_2O_3}$, due to the presence of amorphous species which cannot be detected by the XRD.

Figure 5.2 demonstrates a variation of the quantity of the amorphous species with the amount of the internal standard added in a real fly ash samples collected from a coal-fired power plant. The elemental composition of the fly ash sample mixed with different ratios of corundum calculated by XRD and XRF as well as amorphous amounts calculated by Equation (5.1) are presented in **Table A.1** in Appendix A. The XRD patterns for its mixture with corundum are given in **Figure A.2**. It is clear that a minimum amount of 10wt% is essential for the internal standard, otherwise its peaks are strongly superimposed by the species in the fly ash sample, as demonstrated in **Figure A.2**. To maximise the accuracy of the QXR D results, we hereafter fixed the internal standard amount at 20 wt%. Such a value has also proven highly accurate elsewhere [32]. It is also noteworthy that the amorphous fraction (~61 wt%) is broadly consistent with that was reported for a NIST fly ash reference sample [27]. This is another evidence supporting the high accuracy of the QXR D method developed here.

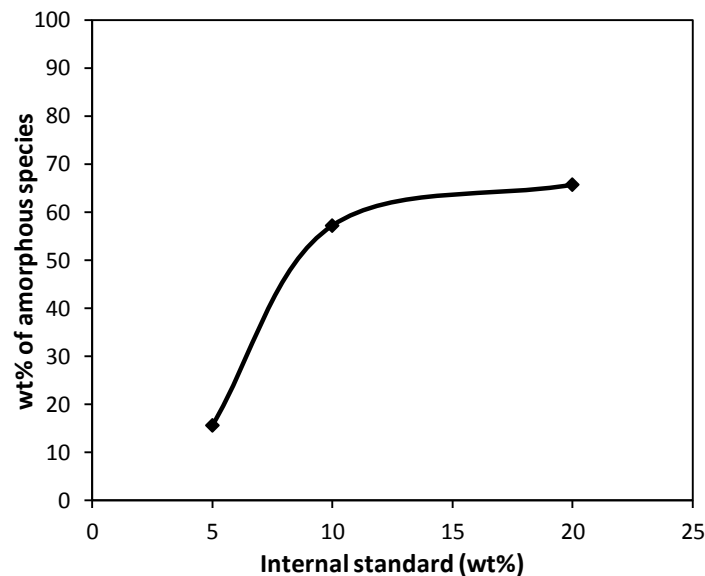


Figure 5.2 Amorphous percentage inside fly ash sample based on different amount of internal standard

The thermal characteristics of carbonation precipitate and loss on ignition (LOI) were examined with a thermogravimetric analyser (TGA, Shimadzu). Approximately 5-10 mg of the solid precipitate were placed inside a quartz crucible, and heated at a heating rate of 50°C/min in a nitrogen flow rate of 100 mL/min.

The following equations were used to calculate the Mg and Ca% precipitated:

$$\text{Mg \%} = \frac{(W_{ws} - \text{LOI}) \times \text{Mg(XRF\%)}}{W_{\text{Mg}}} \times 100 \quad (5.2)$$

$$\text{Ca \%} = \frac{(W_{ws} - \text{LOI}) \times \text{Ca (XRF\%)}}{W_{\text{Ca}}} \times 100 \quad (5.3)$$

In above equations, W_{ws} refers to the weight of a solid precipitate after washing by water to remove ammonia chloride residue, W_{Mg} and W_{Ca} are the absolute amount of Mg^{2+} and Ca^{2+} , respectively, which were calculated based on their concentration in the leachate. Calcium carbonation conversion for some cases was also calculated based on the following equation and was compared with results from Equation (5.3). The error was around 2-3% which can confirm the presence of the whole Ca in the carbonate form.

$$\text{Ca \%} = \frac{\frac{\text{CO}_2 \text{ (wt\%)}}{100 - \text{CO}_2 \text{ (wt\%)}} \times \frac{\text{MW}_{\text{Ca}}}{\text{MW}_{\text{CO}_2}}}{W_{\text{Ca}}} \quad (5.4)$$

The CO_2 (wt%) in Equation (5.4) was derived from the weight loss observed in TGA at temperature range of ~620-780°C, which is the characteristic temperature for the decomposition of calcium carbonate. MW_{Ca} and MW_{CO_2} are the molar weights of Ca and CO_2 in kg/mol respectively, and W_{Ca} is the total Ca content of leachate in kg/kg [33].

5.3.3 Geochemical modelling

Thermodynamic equilibrium speciation modelling was carried out using Visual MINTEQ, a windows version of the MINTEQA2 geochemical speciation code. VMINTEQ is an equilibrium speciation model that is useful for calculating the equilibrium mass distribution among dissolved species and multiple solid phases under a variety of conditions including a gas phase with constant partial pressure [34]. The degree of under-saturation or over-saturation of a leachate with respect to a particular mineral is determined as saturation index (SI), according to the Equation (5.5):

$$SI = \log \frac{IAP}{K_{sp}} \quad (5.5)$$

Where IAP is the ion activity product and K_{sp} is the solubility constant for a particular mineral [35]. In the case of the SI value greater than zero, the leachate solution deemed oversaturated with respect to that particular mineral, and that mineral will spontaneously precipitate. In this study, the dissolved concentration of each species was set as input for the

modelling. The partial pressure of CO₂ was introduced as a fixed parameter, and a pH value of 11 was chosen for the carbonation reaction. The Davis method was used to estimate the fugacity coefficients.

5.4 Results and Discussions

5.4.1 Effect of Mg²⁺/Ca²⁺ molar ratio and reaction time on carbonation at room temperature

Figure 5.3 *a* and *b* depicts the precipitation rate of Mg²⁺ and Ca²⁺ cations as a function of the molar ratio of Mg²⁺/Ca²⁺ at room temperature, respectively. The data show that regardless of the molar ratio of Mg²⁺ to Ca²⁺, the precipitation rate of two cations was increased exponentially over time, and was completed in 40 min. This is consistent with our previous findings for tests on real leachates derived from ammonia chloride leaching of fly ash [7]. Moreover, the molar ratio of two cations was found to play a noticeable role on the precipitation rate of each cation. For the sole Mg²⁺ cation in panel *a*, it shows the slowest precipitation rate, whereas the case for a molar Mg²⁺/Ca²⁺ ratio of 2 exhibits the fastest precipitation rate. More interestingly, upon the decrease on the molar ratio of Mg²⁺ to Ca²⁺, the precipitation rate of Mg²⁺ was decreased considerably. The results for Ca²⁺ in panel *b* show an opposite trend. That is, the existence of sole Ca²⁺ in the leachate exhibits the highest precipitation rate, whereas its precipitation rate decreases quickly upon increasing the molar ratio of Mg²⁺ to Ca²⁺ in the leachate.

To further quantitatively compare the precipitation rates of two cations in different cases, a parameter, $1/\tau_{50}$ for the reverse of the reaction time required to reach a 50wt% precipitation extent was plotted versus the molar ratio of Mg²⁺ to (Mg²⁺+Ca²⁺) and shown in **Figure 5.4**. Such a ratio was used as *x*-axis to avoid the appearance of infinity for the molar ratio of Mg²⁺/Ca²⁺ in the case of sole Mg²⁺. Here, a value of zero for Mg²⁺/(Mg²⁺+Ca²⁺) refers to the case of sole Ca²⁺ in the leachate, whereas the unity value denotes the case of sole Mg²⁺ for carbonation reaction. The values of τ_{50} were inferred from the simulated curves in the two panels in **Figure 5.3**. Clearly, the precipitation rate of Ca²⁺ decreases monotonically upon introducing and increasing the Mg²⁺ cation in the leachate. This is a direct sign of the competition between the two cations in reacting with CO₂ dissolved into the leachate. On the contrary, the precipitation rate of Mg²⁺ reaches a peak at the value of 0.67 for the molar ratio of Mg²⁺/(Mg²⁺+Ca²⁺), which corresponds to the case when concentration of Mg²⁺ is twice that of Ca²⁺ in the leachate. The precipitation rate of Mg²⁺ at such a peak value is even higher than that of Ca²⁺. Such a unique phenomenon can be explained by the promoting effect of Ca²⁺ on the carbonation rate of Mg²⁺ when they co-exist. There have been several studies to support this phenomenon. Calcite in a supersaturated solution can

precipitate by nucleation in an early stage and subsequent growth in later stages. The presence of Mg^{2+} in the solution, however, inhibits the calcite nucleation kinetics by poisoning the active growth sites of the pre-critical nuclei through the incorporation of Mg^{2+} into the calcite lattice [9, 36-38]. Both the rate of the diffusion and the composition of the products are also strongly dependent on the initial Mg^{2+}/Ca^{2+} in the solution [39]. Upon further increasing of the Ca^{2+} concentration over the optimum value for the peak precipitation rate of Mg^{2+} , Ca^{2+} competes with Mg^{2+} and attracts CO_3^{2-} and HCO_3^- more readily, thereby leading to a longer equilibrium time for Mg^{2+} precipitation.

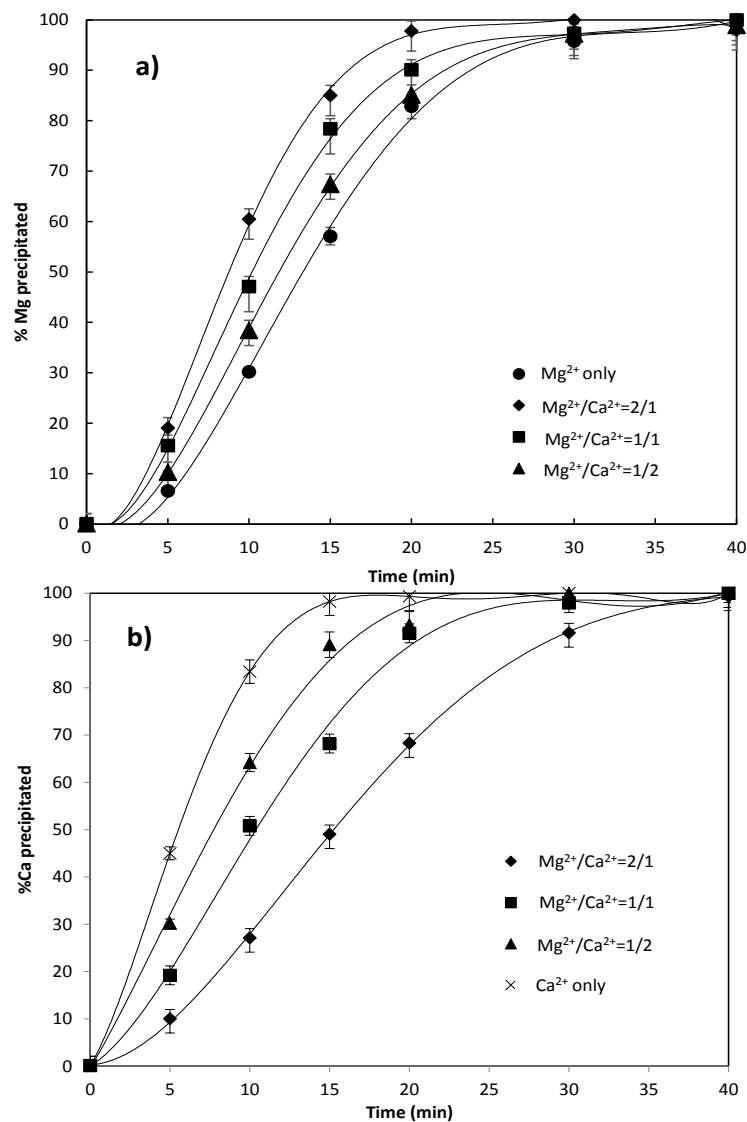


Figure 5.3 a) Mg and b) Ca carbonation yield of different Mg^{2+}/Ca^{2+} ratios at room temperature as a function of time

The monotonic decrease on the precipitation rate of Ca^{2+} upon the increase of Mg^{2+} concentration is not unusual. Fernandez-Diaz et al. (1996) have reported inhibition of calcite

crystal growth in presence of Mg with concentration higher than 25 mg/kg. This has been attributed to the incorporation of Mg^{2+} cation into the calcite crystal lattice and a 20% higher dehydration energy of Mg^{2+} than Ca^{2+} resulting in a slower growth of calcite nuclei [36]. Moreover, it was found that the variation in the Mg^{2+} carbonation rate is rather narrower than that for Ca^{2+} , which is a strong indicator for a greater inhibition influence of Mg^{2+} on calcite formation. For the case of the concentration of Mg^{2+} equalling twice that of Ca^{2+} , the promotion effect of Ca^{2+} on Mg^{2+} is clearly much greater than the reserve inhibitory influence of Mg^{2+} on Ca^{2+} , therefore, the precipitation rate of Mg^{2+} is nearly double that of Ca^{2+} .

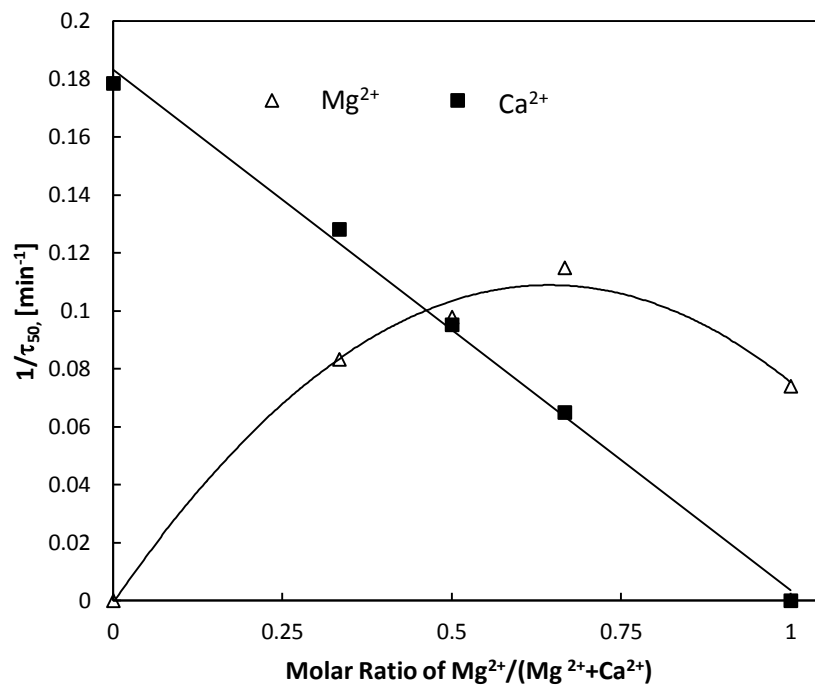


Figure 5.4 Correlation between the molar ratio of $Mg^{2+}/(Mg^{2+}+Ca^{2+})$ and $1/\tau_{50}$ for the precipitation of two cations.

5.4.2 Characterisation of solid precipitates formed at room temperature

5.4.2.1 The precipitates from sole Mg^{2+} leachate

Carbonation of sole Mg^{2+} resulted in the formation of an unidentified precipitate, the XRD pattern of which cannot be matched by any database we have. As an instance, XRD pattern for the precipitate obtained after 10 min reaction time as well as standard database in MDI Jade software with unmatched potential Mg - bearing components is depicted in **Figure 5.5**. For the Mg^{2+} - CO_2 - H_2O system, the thermodynamically stable phase is either magnesite ($MgCO_3$) or brucite ($Mg(OH)_2$). However, in practice, these two species are mostly preceded or usurped by the metastable phases [40]. Several unidentified magnesium carbonates have been detected, some of which possess amorphous structures [41,42]. Botha and Strydom (2001) obtained an unidentified structure, which shows similarities to hydromagnesite ($Mg_5(CO_3)_4(OH)_2 \cdot 4H_2O$) and

appears to be an intermediate phase between nesquehonite ($\text{MgCO}_3 \cdot 3\text{H}_2\text{O}$) and hydromagnesite ($\text{Mg}_5(\text{CO}_3)_4(\text{OH})_2 \cdot 4\text{H}_2\text{O}$). They have confirmed that, the carbonate product dried at 80-120°C is unidentified amorphous, which is consistent with our experimental observations here [41].

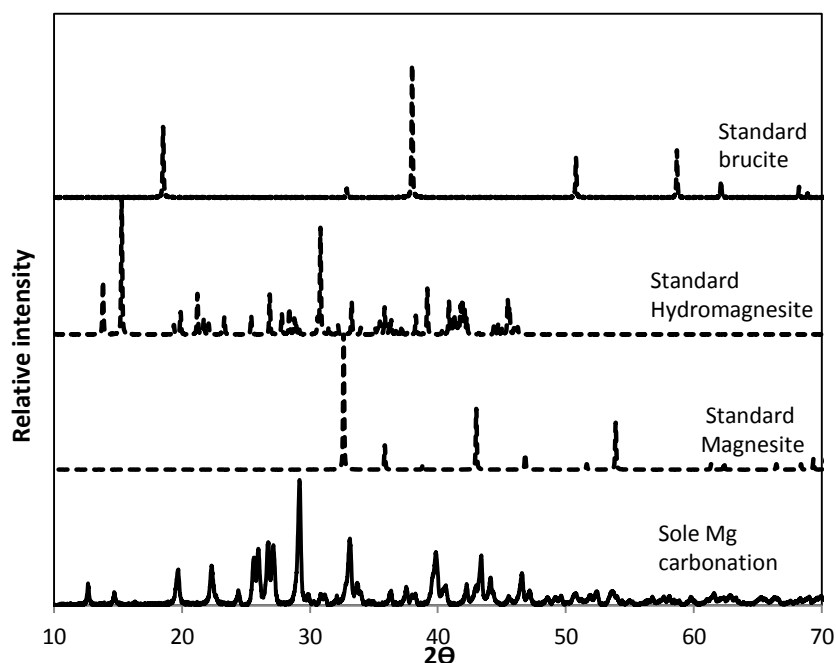


Figure 5.5 XRD pattern for the carbonation precipitate of sole Mg^{2+} after 10 min reaction time, Unfitted with potential Mg- bearing minerals from MDI Jade database

The precipitation potential of minerals that could form in Mg - H_2O - CO_2 system was further assessed by MINTEQA and demonstrated in **Table 5.2**. As can be seen, four species including artinite ($\text{Mg}_2(\text{CO}_3)(\text{OH})_2 \cdot 3\text{H}_2\text{O}$), hydromagnesite ($\text{Mg}_5(\text{CO}_3)_4(\text{OH})_2 \cdot 4\text{H}_2\text{O}$), magnesite (MgCO_3) and nesquehonite ($\text{MgCO}_3 \cdot 3\text{H}_2\text{O}$) can thermodynamically be formed and precipitate under the experimental conditions employed here. However, none of them have been confirmed by the XRD analysis. This hints that the unknown species such as metastable hydrated magnesium carbonate phases could be formed instead. Metastable phases interfere with the production of magnesite or well-ordered crystals due to their fast nucleation and growth rate compared to magnesite crystals [43]. Metastable arrangements are common when minerals are grown rapidly at low temperature [44].

Table 5.2 Log IAP and Saturation index (SI) calculated by MINTEQA for possible minerals in precipitate obtained from carbonation of sole Mg^{2+}

Mineral	Log IAP	SI
Artinite ($Mg_2(CO_3)(OH)_2 \cdot 3H_2O$)	12.758	3.158
Brucite ($Mg(OH)_2$)	15.453	-1.647
Hydromagnesite ($Mg_5(CO_3)_4(OH)_2 \cdot 4H_2O$)	4.671	13.437
Magnesite ($MgCO_3$)	-2.696	4.764
Nesquehonite ($MgCO_3 \cdot 3H_2O$)	-2.696	1.974
Periclase (MgO)	15.453	-6.131

5.4.2.2 The precipitates from the mixture of $Mg^{2+}+Ca^{2+}$ and sole Ca^{2+}

The measured XRD patterns for the precipitates formed from the co-existence of two cations and sole Ca^{2+} have been matched satisfactorily by Siroquant. As an example, the measured and fitted XRD patterns for the precipitates obtained at 5 min of different Mg^{2+}/Ca^{2+} ratios (except sole Mg^{2+}) carbonation is presented in **Figure 5.6**. The chi-square values for the final fitting of XRD patterns for the reaction times of 5 and 60 min areas summarised in **Table 5.3**, suggesting that all the errors have been minimised to a very low and acceptable level [45].

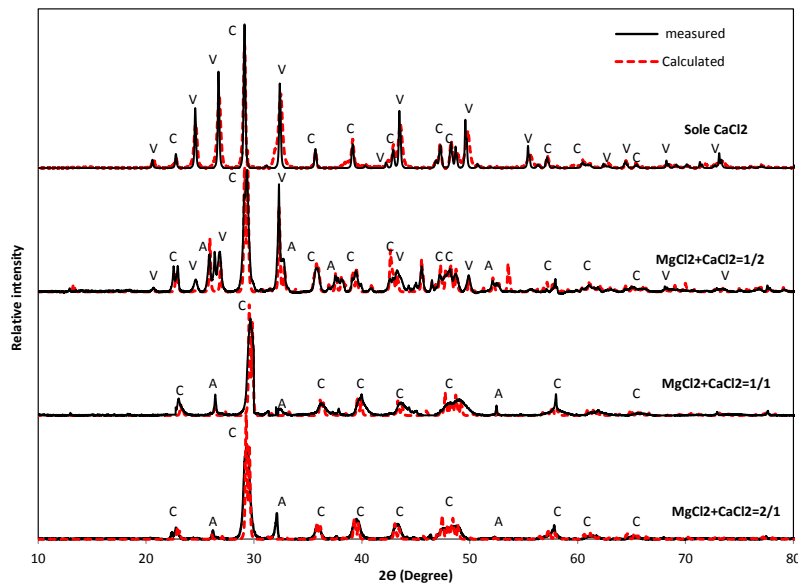
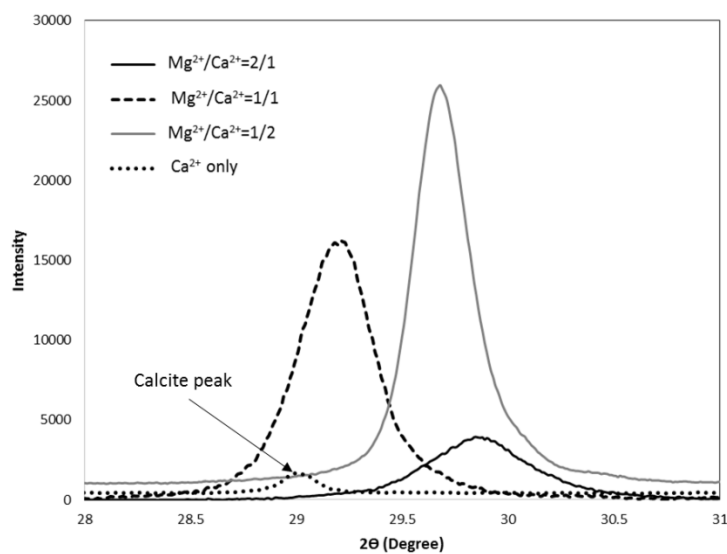


Figure 5.6 Measured and calculated XRD patterns for the carbonation of different molar ratios of Mg^{2+}/Ca^{2+} at 5 min reaction time (V : Vaterite, C : Calcite and Magnesian calcite, A : Aragonite)

Table 5.3 Chi-square value for selected Siroquant fitting

Case	Chi-squared value	
	t=5 min	T=60 min
Mg ²⁺ /Ca ²⁺ =2/1	11.9	18
Mg ²⁺ /Ca ²⁺ =1/1	8.1	22.8
Mg ²⁺ /Ca ²⁺ =1/2	27.1	17.9
Sole Ca ²⁺	9.7	9.3

Presence of sole Ca²⁺ in the solution led to the formation of different polymorphs of pure Ca-carbonates, calcite (CaCO₃), aragonite (CaCO₃) and vaterite (CaCO₃). Calcite is generally the most common mineral species formed in most of the Ca-bearing solution [46]. Examination of the XRD patterns from co-precipitation of Mg²⁺ and Ca²⁺ revealed the broadening of the peak positioned ~29-30.5°, which overlaps with calcite, dolomite (CaMg(CO₃)₂) and magnesian calcite (Mg_nCa_{1-n}CO₃, typically n<<1) on the same *hkl* plane of 104. The Rietveld refinement using both calcite and magnesian calcite showed better fitting and lower chi-square value compared to the sole presence of any of the three phases mentioned above. Diagnostic X-Ray spacing and typical diffractogram are another two criteria that can be used to differentiate calcite from dolomite. The peak at ~28.5-29.5° with a space diameter of ~0.304 nm represents calcite. A skewing or displacement of calcite peak towards lower spacing will denote the presence of magnesian calcite as well. Generally, the presence of magnesian calcite shifts the overlapped calcite and magnesian calcite peak toward higher 2θ. This is evident in **Figure 5.7** which displays the enlarged XRD pattern of (28-31°) for magnesian calcite peak positions formed at different Mg²⁺/Ca²⁺ ratios after 10 min reaction time. The calcite peak from carbonation of sole Ca²⁺ is also presented for comparison.

**Figure 5.7** The enlarged XRD patterns for magnesian calcite peak positions for different Mg²⁺/Ca²⁺ ratios compared to pure calcite after 10 min reaction time

The main feature of dolomite is that occurs at higher 2θ ($\sim 30.6-31.4^\circ$) compared to calcite and magnesian calcite with a space diameter of 0.289 nm [57]. In this study, the differentiation of these species has been successfully performed through the use of two software programs. As depicted in **Table 5.4**, it is clear that the 2θ for mixture of Mg and Ca has been shifted to higher angles and lower spacing upon the increase on the molar ratio of Mg^{2+} to Ca^{2+} in the leachate. Such a distinct feature echoes the presence of magnesian calcite in the samples. In addition, it is noteworthy that dolomite ($\text{CaMg}(\text{CO}_3)_2$) peak was not observed in any of the $\text{Mg}^{2+}/\text{Ca}^{2+}$ ratio in the leachate. Dolomite occurs mostly at earth surfaces through a dissolution-precipitation reaction in which a calcium carbonate precursor is replaced by dolomite through interaction with magnesium rich solution [39]. In the aqueous environment, hydration of magnesium and cation ordering prevent dolomite precipitation and metastable magnesian calcite forms instead. Increase in pressure favours dolomitisation of magnesian calcite due to tendency of atoms to approach an ideal arrangement [37].

The Phase diagram derived from QXRD for all the precipitates formed as a function of reaction time are summarised in **Figure 5.8 a-d**. From panel *c* and *d* related to least $\text{Mg}^{2+}/\text{Ca}^{2+}$ ratio and sole Ca^{2+} , respectively, the metastable form of CaCO_3 , vaterite was detected and it is even predominant in the sole Ca^{2+} case. Calcite is the second largest Ca-bearing species for calcium. The presence of Mg^{2+} in the leachate ($\text{Mg}^{2+}/\text{Ca}^{2+}$ molar ratio of 1/2) led to the transformation of whole vaterite to calcite toward the end of the reaction time. Upon the increase of the $\text{Mg}^{2+}/\text{Ca}^{2+}$ ratio in the leachate, the fractions of aragonite, magnesian calcite and even the amorphous species were increased remarkably. The increased formation of aragonite growth with increasing Mg^{2+} concentrations was also observed by Boyd et al. (2014) [38].

Table 5.4 XRD fitting parameters of major peak at ($2\theta \sim 28.5-31$) extracted from JADE for precipitates at different $\text{Mg}^{2+}/\text{Ca}^{2+}$ ratios and sole Ca^{2+} at 10 min reaction time

Case	2θ	$d(\text{\AA})$	Centroid	Skew	FWHM	Breadth
$\text{Mg}^{2+}/\text{Ca}^{2+}=2/1$	29.861	2.9897	29.861	-0.004	0.584	0.739
$\text{Mg}^{2+}/\text{Ca}^{2+}=1/1$	29.183	3.0575	29.189	-0.056	0.418	0.522
$\text{Mg}^{2+}/\text{Ca}^{2+}=1/2$	29.645	3.011	29.668	-0.31	0.284	0.384
Sole Ca^{2+}	28.997	3.0768	28.988	0.219	0.153	0.211

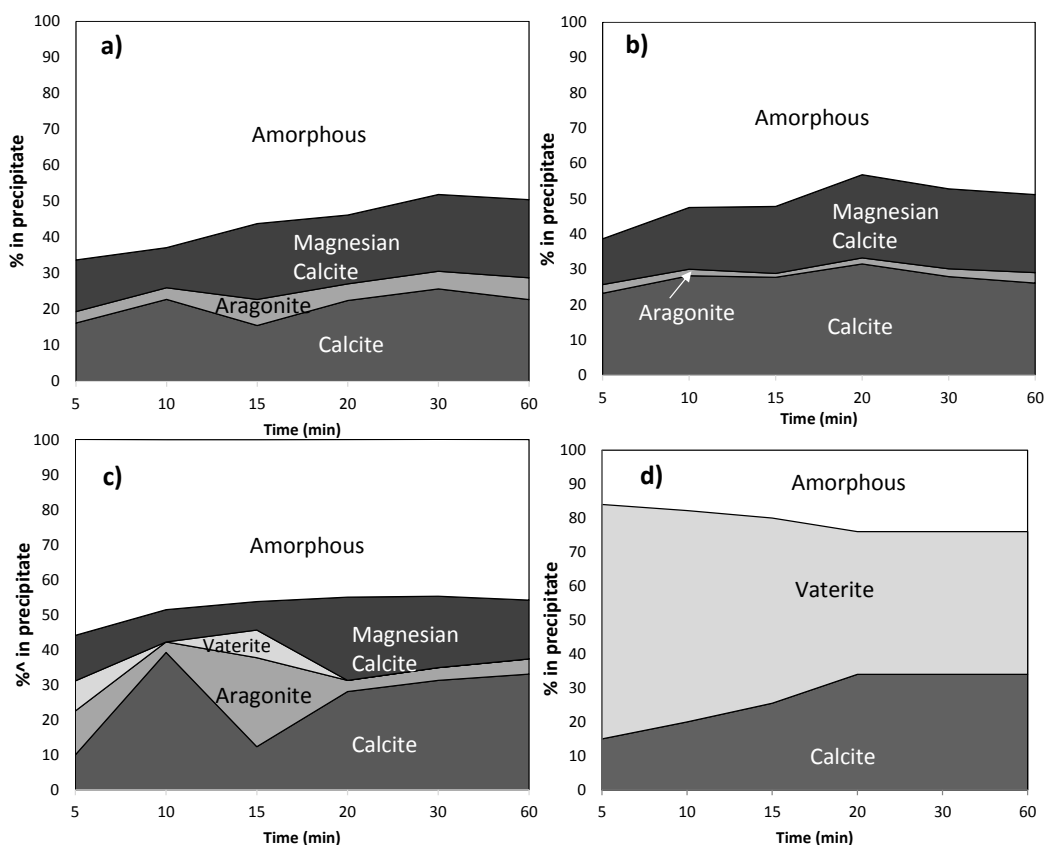


Figure 5.8. Solid precipitate composition of carbonation of *a)* $Mg^{2+}/Ca^{2+}=2/1$, *b)* $Mg^{2+}/Ca^{2+}=1/1$, *c)* $Mg^{2+}/Ca^{2+}=1/2$, *d)* Sole Ca^{2+} , at room temperature calculated by QXRD and internal standard method.

Figure 5.9 further demonstrates the percentages of two major compounds, *a)* amorphous phase and *b)* magnesian calcite in solid precipitates as a function of the Mg^{2+}/Ca^{2+} molar ratio and reaction time at room temperature. For the amorphous species depicted in panel *a*, its amount formed in the case of sole Ca^{2+} is the lowest, reaching the maximum of $\sim 20\text{ wt}\%$ at around 10 min and stabilised afterwards. Upon the increase of the Mg^{2+}/Ca^{2+} in the leachate, the amount of amorphous formed was increased dramatically in the first 10 min, reaching around $50\text{ wt}\%$ and $65\text{ wt}\%$ for the two medium Mg^{2+}/Ca^{2+} ratios and the highest one, respectively. Xu et al. (2013) have also confirmed exclusive formation of amorphous magnesian calcite and magnesite in high Mg^{2+}/Ca^{2+} ratios and sole Mg^{2+} leachate, respectively [48]. With respect to magnesian calcite shown in panel *b*, it was found that the Mg^{2+}/Ca^{2+} ratio of 1/1 is the optimum ratio for the maximised formation of this species in the carbonate precipitate. Its amount was maximised in 20 min, irrespective of the Mg^{2+}/Ca^{2+} molar ratio in the leachate. Upon the further increase of time, this species levels off for the cases of Mg^{2+}/Ca^{2+} equalling 1 and 2. However, it decreases continuously for the case with the least Mg^{2+}/Ca^{2+} ratio. This phenomenon indicates a complicated reordering of the magnesian calcite crystal lattice in the leachate. It is very likely

that a portion of Mg^{2+} could elute out of the calcite matrix upon increasing its residence time in the leachate.

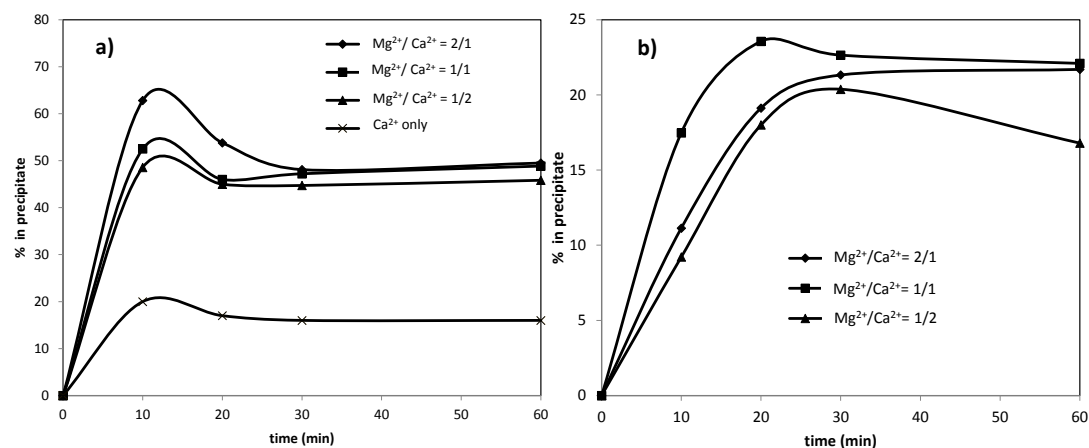


Figure 5.9 Percent of **a)** amorphous phase and **b)** magnesian calcite in precipitates formed from the carbonation of different ratios of $\text{Mg}^{2+}/\text{Ca}^{2+}$ as a function of reaction time

To further clarify this phenomenon, the percentage of MgCO_3 or n in magnesian calcite formula ($\text{Mg}_n\text{Ca}_{1-n}\text{CO}_3$) as a function of time for various $\text{Mg}^{2+}/\text{Ca}^{2+}$ molar ratios is further shown in **Figure 5.10**. This percentage was estimated from a semi-quantitative method, based on the position of magnesian calcite peak respect to the calcite peak [47]. Regarding the optimum $\text{Mg}^{2+}/\text{Ca}^{2+}$ of 1 discussed above, a lowest MgCO_3 content was confirmed in its magnesian calcite, which reaches only 15wt% in 20 min. Such a value is close to around 17wt% observed for $\text{Mg}^{2+}/\text{Ca}^{2+}$ of 1/2 but lower than the case of the molar ratio of $\text{Mg}^{2+}/\text{Ca}^{2+}$ equalling 2. This fluctuation suggests that under certain conditions, the Mg^{2+} is trapped in the calcite crystal lattice, leading to the increase in the solubility of the solid precipitate due to the creation of strains on the crystalline structure [49]. Moreover, irrespective of the $\text{Mg}^{2+}/\text{Ca}^{2+}$ molar ratio, the fraction of MgCO_3 in magnesian calcite reached plateau at $\sim 10\%$ MgCO_3 in the calcite lattice. Such a value has been confirmed to be the highest limit for the amount of MgCO_3 in a thermodynamically stable magnesian calcite [50]. In marine environments co-precipitation of magnesium generally results in calcite with up to $\sim 10\%$ MgCO_3 whereas in natural skeletal calcite, the magnesium content can increase up to $\sim 30\%$ [51]. However, crystallisation experiments using artificial or real seawater produced calcite with magnesium content up to 22% along with other carbonate phases have been reported in literature [52]. The Mg content in inorganically formed calcite is limited due to the formation of aragonite, the saturation degree of calcite lattice and reaction temperature as well [51].

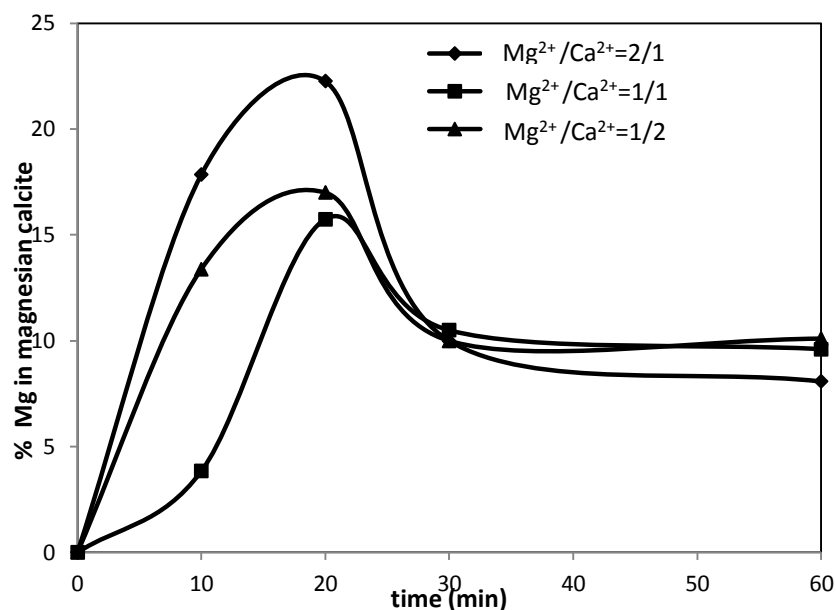


Figure 5.10 The mass fraction of MgCO_3 in magnesian calcite for different ratios of Mg/Ca as a function of reaction time

In addition, to reveal the probable structure for the abundant amorphous species observed in the **Figures 5.8** and **5.9**, TG-DTG analysis of the thermal behaviour of carbonation precipitates was further conducted for the samples received after 20 min carbonation. The results are depicted in **Figure 5.11**. In the lower panel of this figure are the DTG curves for pure MgCO_3 and $\text{Mg}(\text{OH})_2$. Clearly, the carbonate precipitates formed from the leachate rich in Mg^{2+} (*i.e.* $\text{Mg}^{2+}/\text{Ca}^{2+}=1$ and 2) show the closer resemblance with $\text{Mg}(\text{OH})_2$ in terms of the decomposition temperatures, implying the strong hydration extent of these precipitate. The peak for MgCO_3 is rather small, suggestive of the minor content for this crystal species in these precipitates. Moreover, the mass loss curves for each $\text{Mg}^{2+}/\text{Ca}^{2+}$ ratio are close in decomposition temperatures but different in the weight loss, suggesting the presence of different moles of CO_2 and H_2O molecules in the solid precipitates. The weight loss between temperature $\sim 600\text{--}800^\circ\text{C}$ is contributed mainly by the decomposition of CaCO_3 [53]. Increasing the $\text{Mg}^{2+}/\text{Ca}^{2+}$ ratio slightly reduced the calcium carbonate decomposition temperature, which should be attributed to the association of calcite with magnesium. At this temperature range, the weight loss percentage for the case of $\text{Mg}^{2+}/\text{Ca}^{2+}$ ratio equalling 1/2 is most significant, due to the presence of larger amount of calcium carbonate polymorphs along with calcium carbonate- rich magnesian calcite in the solid residue. For the broad temperature range of $\sim 200\text{--}600^\circ\text{C}$, it can be due to the release of chemically bound water or carbon dioxide from a general formula of $(\text{MgO})_x(\text{CO}_2)_y(\text{H}_2\text{O})_n$ for hydrated-Mg carbonates in the amorphous form. The large discrepancy between QXRD and

XRF in the quantification of MgO content, as tabulated in **Table 5.5** confirmed the abundance of amorphous Mg-bearing species that cannot be detected by XRD.

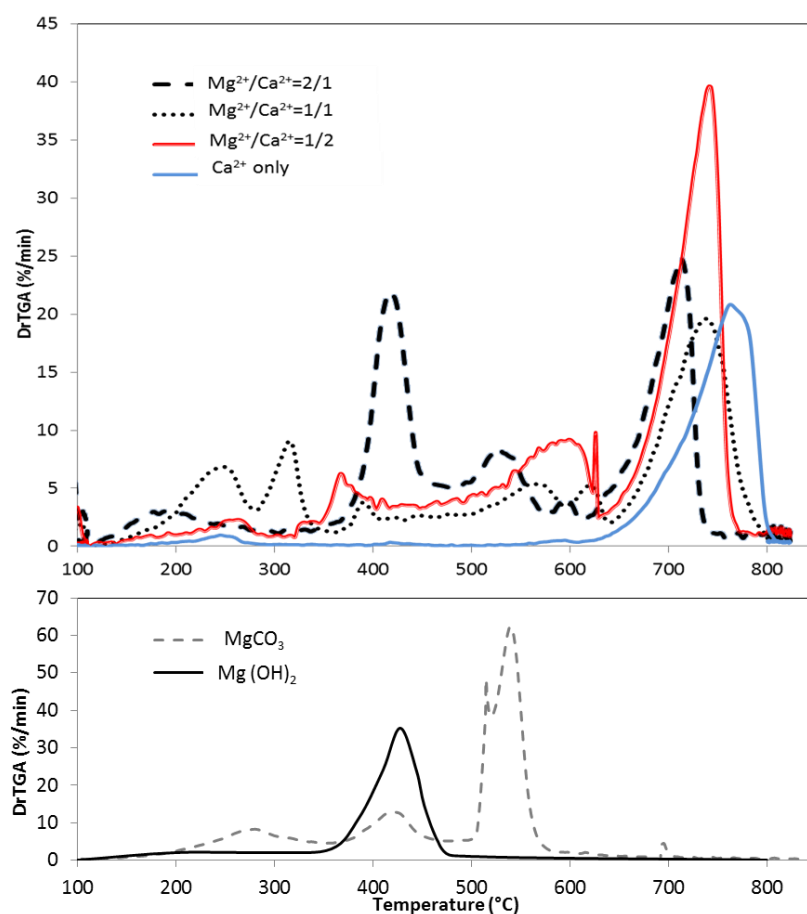


Figure 5.11 TGA - DTG mass loss curves of solid carbonate precipitates compared with pure MgCO₃ and Mg(OH)₂ decomposition after 20 min reaction time

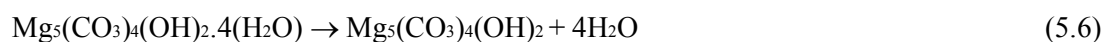
Table 5.5 Comparison of QXRD results and XRF results for the MgO contents in the carbonate precipitates formed from different Mg²⁺/Ca²⁺ ratios at 30 min reaction time

Mg ²⁺ /Ca ²⁺ ratio	XRF (wt%)	QXRD (wt%)	Chi-square value for QXRD
Mg ²⁺ /Ca ²⁺ =2/1	59.8	7.18	36.14
Mg ²⁺ /Ca ²⁺ =1/1	33.5	6.7	23.84
Mg ²⁺ /Ca ²⁺ =1/2	28.9	5.5	17.01

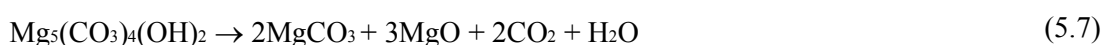
Three major peaks were observed for the precipitate from the case of Mg²⁺/Ca²⁺ ratio of 2/1. These temperatures closely resemble the presence of nesquehonite (MgCO₃.3H₂O). For nesquehonite, the first peak observed at around 200°C attributed to the loss of two water molecules of water. Another endothermic peak detected at 440°C is related to the loss of the

remaining water molecule. And finally at $\sim 550^\circ\text{C}$, de-carbonation of magnesium carbonate takes place [54].

The decomposition curve for the $\text{Mg}^{2+}/\text{Ca}^{2+}$ ratio of 1/1 resembles the presence of hydromagnesite ($\text{Mg}_5(\text{CO}_3)_4(\text{OH})_2 \cdot 4\text{H}_2\text{O}$). Todor (1976) reported that between 210°C and 395°C , the four water molecules of hydromagnesite are released according to Equation (5.6).



Following the loss of the four water molecules, the loss of a carbon dioxide molecule occurs between 395°C and 460°C , which is further followed by a reorganisation of the crystal structure. Between 460°C and 515°C a fifth molecule of water is released due to the decomposition of the hydroxide group and a further carbon dioxide molecule:



Finally over the temperature range of 515°C to 640°C a further two carbon dioxide molecules are released to leave a magnesium oxide residue [55].



5.4.3 Effect of temperature on carbonation

Figure 5.12 illustrates the influence of temperature on the precipitation rate of two cations for the $\text{Mg}^{2+}/\text{Ca}^{2+}$ molar ratio of 1. For each cation, its precipitation rate was increased remarkably upon the elevation of the carbonation temperature. Compared to the duration of 30 min required at room temperature, the completion of carbonation was shortened to 20 min at the other three temperatures. However, for the three high temperatures tested, the carbonation rate of each cation was not increased monotonically upon the rise of the reaction temperature. For Mg^{2+} shown in panel *a*, its carbonation rate was maximised at 60°C , and slightly reduced at 80°C , especially before the residence time of 10 min. The similar phenomenon was observed for Ca^{2+} for a maximum carbonation rate at 60°C , as evident in panel *b*. This is consistent with our previous observation using coal fly ash-derived leachate [8]. The reaction temperature affects several parameters including reaction rate and CO_2 solubility simultaneously. Although the carbonation reaction rate is favoured upon the rise of reaction temperature, the solubility of CO_2 decreases oppositely. Moreover, due to the exothermicity of carbonation reaction, the equilibrium constant based on Le Chatelier's principle is decreased upon the elevation of temperature [56]. To further quantitatively compare the precipitation rates of two cations at different temperature, $1/\tau_{50}$ as the reverse of the reaction time required to reach a 50wt% precipitation extent was plotted versus the temperature and shown in **Figure 5.13**. This figure indicates that except room temperature, the rate of Ca^{2+} is nearly twice higher than that of Mg^{2+} at each of the other three temperatures.

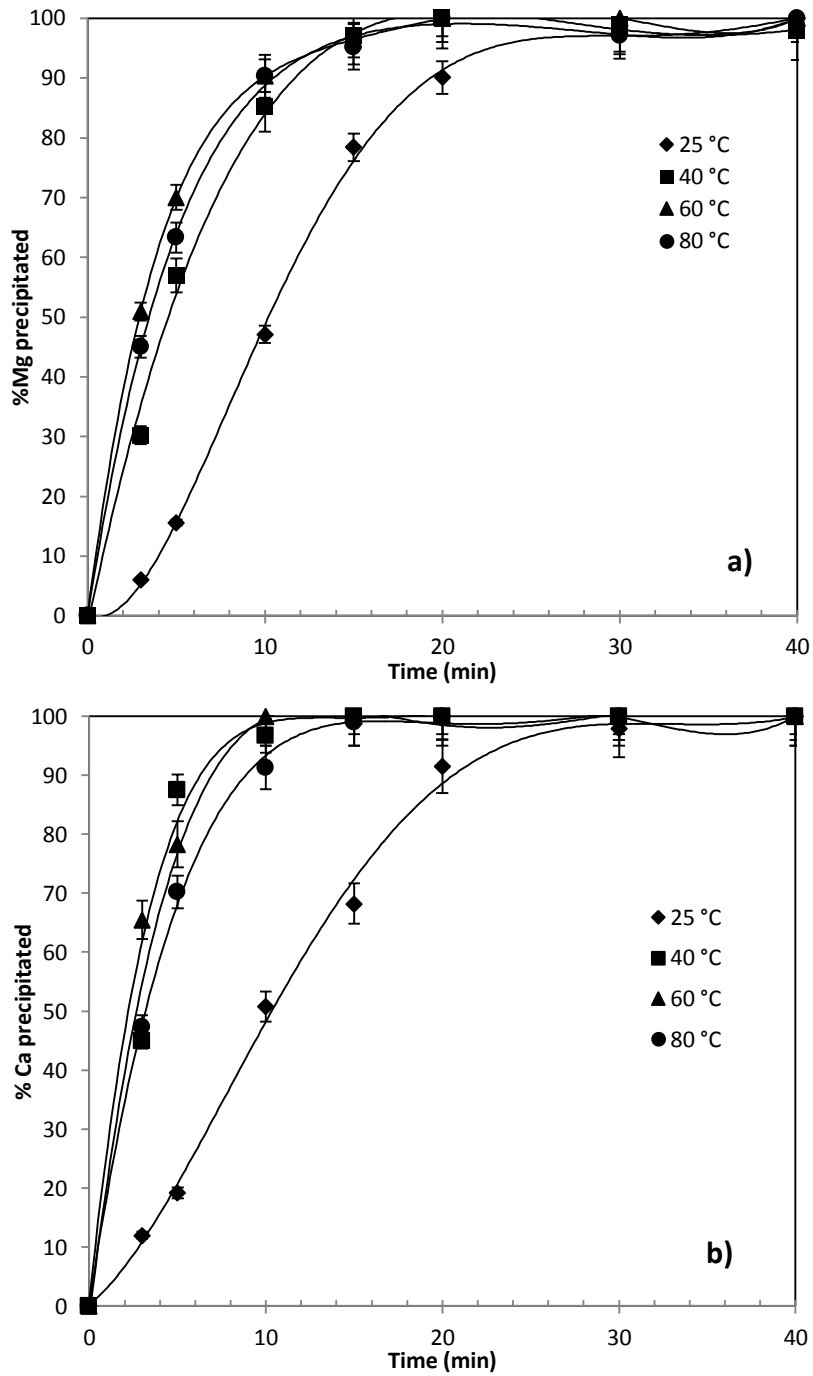


Figure 5.12 Effect of temperature and time on *a)* Mg and *b)* Ca carbonation for the Mg^{2+}/Ca^{2+} equal to 1/1

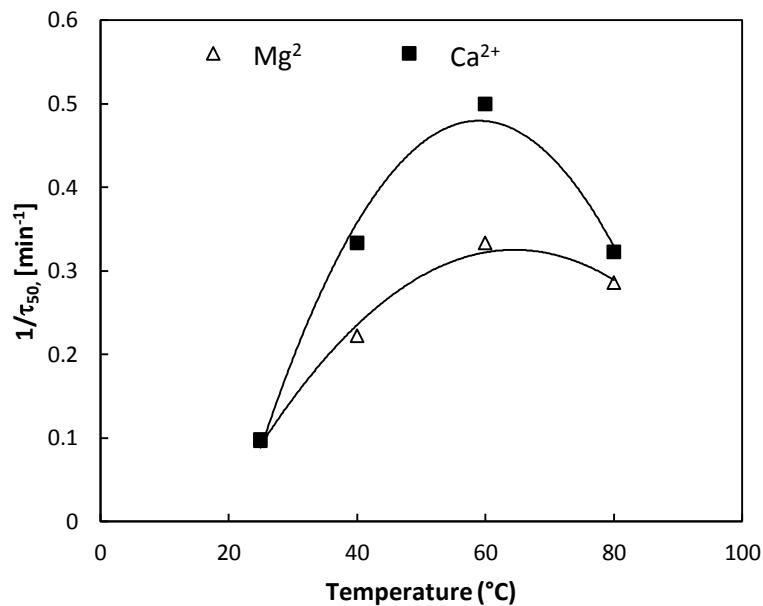


Figure 5.13 Influence of temperature on the $1/\tau_{50}$ (carbonation rate to achieve 50wt% precipitation extents) of two cations at a molar ratio of 1 in solution

5.4.4 Characterisation of solid precipitate at different temperature

The time-dependent composition of carbonate precipitates at different temperatures are illustrated in **Figure 5.14 a-d**. This figure shows that compared to the reaction time, increasing the carbonation temperature is more influential in altering the mineral speciation. **Figure 5.15** further plots the variation of the percentages of individual species as a function of reaction temperature, with the time fixed at 10 min. Increasing temperature led to the loss of crystals and the transformation of crystals to the amorphous phase. For the dominant calcite formed at room temperature, the decrease in its amount is accompanied by the increase in the fraction of its counterpart, aragonite which exhibits the highest amount at 60°C. This indicates the reordering of calcium carbonate crystal lattice structure at the elevated temperatures. Compared to the calcite bearing a trigonal-rhombohedral structure, aragonite is in an orthorhombic system with acicular crystals and easily fragile as well. Such an observation has also been confirmed by Rodriguez-Blanco et al. (2011) who have confirmed that, at temperatures $< 30^{\circ}\text{C}$, pure amorphous calcium carbonate (ACC) converts into calcite via vaterite; while at temperatures $> 40^{\circ}\text{C}$ the pure ACC is prone to transfer into aragonite via vaterite [57]. Another obvious change is the reduction on the amount of magnesian calcite upon the rise of the reaction temperature up to 60°C. Such a change should be partially caused by the above - mentioned change on the lattice structure of calcium carbonate. The lattice structure of aragonite is not easily accessible to Mg^{2+} [38]. Consequently, the carbonation of Mg^{2+} alone is promoted, which has the propensity to form amorphous structure as discussed before. Apparently, at 60°C, the formation of aragonite and

amorphous Mg-bearing carbonates are the main reasons for achieving the highest carbonation rate at this temperature.

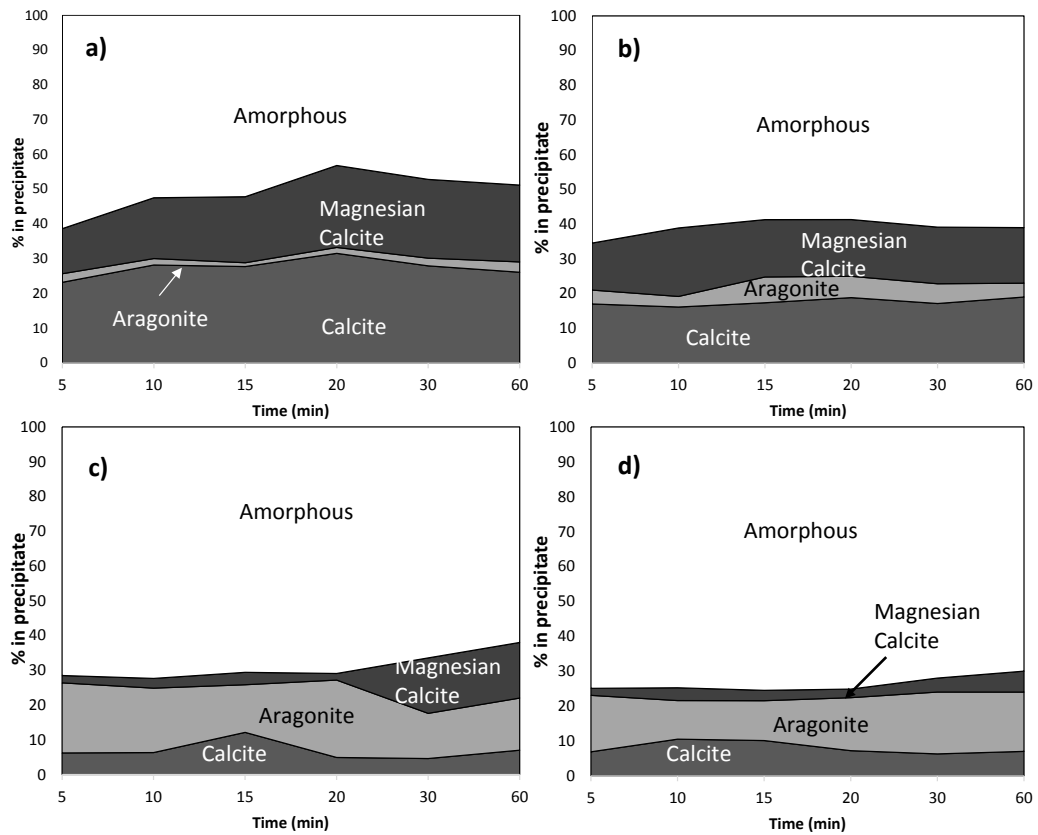


Figure 5.14 Solid precipitate composition of carbonation of Mg/Ca=1/1 at different temperatures *a)* 25 °C, *b)* 40 °C, *c)* 60 °C and *d)* 80 °C calculated by QXRD and internal standard method.

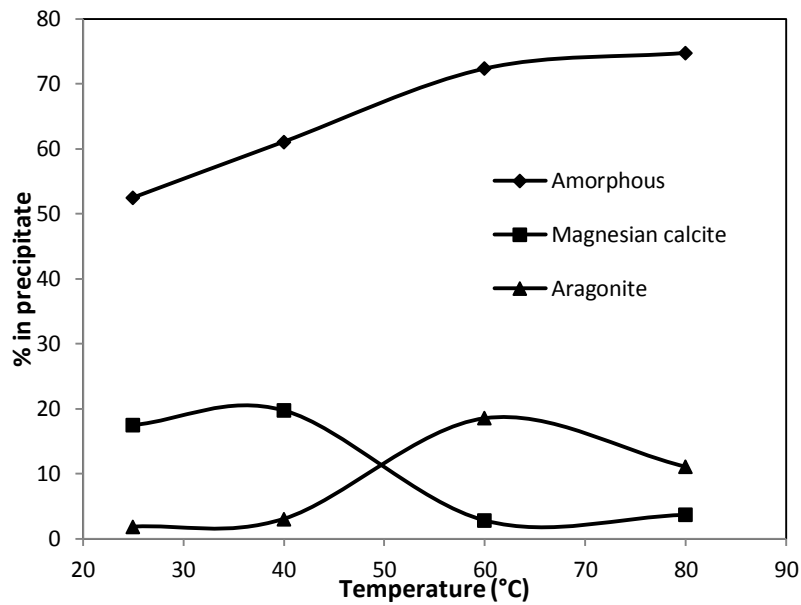


Figure 5.15 Mass fractions of amorphous, magnesian calcite and aragonite in solid precipitate as a function of temperature at the fixed reaction time of 10 min

5.5 Conclusions

This paper has investigated the competition between Ca^{2+} and Mg^{2+} ions during the mild carbonation process, and its impacts on the optimum conditions and carbonate precipitate structure. The major conclusions can be drawn as follows:

- 1) Under the ambient conditions, an initial pH of ~11, and CO_2 flow rate of 15 L/min (large enough to eliminate the diffusion resistance in this study), the carbonation of sole Ca^{2+} or Mg^{2+} can be completed in 10 min and 30 min, respectively. Upon the blending of two cations and the increase in the $\text{Mg}^{2+}/\text{Ca}^{2+}$ molar ratio, the carbonation time for Ca^{2+} was increased. In contrary, the time was shortened noticeably for Mg^{2+} . In terms of the carbonation reactivity, the reactivity of Ca^{2+} was decreased linearly upon increasing the $\text{Mg}^{2+}/\text{Ca}^{2+}$ ratio, whereas Mg^{2+} achieved its maximum reactivity at $\text{Mg}^{2+}/\text{Ca}^{2+}$ molar ratio of 2. This is due to the trapping of Mg^{2+} into the calcite lattice to form magnesian calcite.
- 2) With regard to the structure of carbonation precipitate, the metastable phase of vaterite is predominant for the case of sole Ca^{2+} , which is mainly formed upon the shell damage of aragonite. The amorphous phase accounts for less than 20wt% of the total carbonate. In contrast, the carbonate formed from sole Mg^{2+} is mainly unidentifiable upon XRD speciation, which is presumably hydromagnesite. The blending of Ca^{2+} and Mg^{2+} induced the formation of magnesian calcite caused by the substitution of a portion of Ca^{2+} by Mg^{2+} in calcite lattice. The formation of this complex is also favoured upon increasing the $\text{Ca}^{2+}/\text{Mg}^{2+}$ molar ratio.
- 3) Increasing the temperature is in favour of the carbonation of both ions particularly Ca^{2+} before 60°C. The increase of temperature from 60°C results in the reduction of the carbonation reactivity of Mg^{2+} , due to the decreased solubility of CO_2 . Upon the elevation of reaction temperature, the Ca - bearing carbonate changes its crystal from trigonal - rhombohedral calcite to orthorhombic aragonite. The resulting aragonite is not in favour of the formation of magnesian calcite. As a result, the amorphous structure dominated by Mg^{2+} is dominant in the high temperature carbonate precipitate.

References

- [1] Lackner, K.S.; Wendt, C.H.; Butt, D.P.; Joyce, E.L.; Sharp, D.H. Carbon dioxide disposal in carbonate minerals. *Energy* **1995**, *20*, 153–1170.

- [2] Baciocchi, R.; Polettini, A.; Pomi, R.; Prigiobbe, V.; Zedwitz, V.N.; Steinfeld, A. CO₂ sequestration by direct gas-solid carbonation of air pollution control (APC) residues. *Energ. Fuel* **2006**, 20, 1933–1940.
- [3] Hänchen, M.; Prigiobbe, V.; Storti, G.; Seward, T.M.; Mazzotti, M. Dissolution kinetics of forsteritic olivine at 90 – 150 °C including effects of the presence of CO₂. *Geochim. Cosmochim. Acta* **2006**, 70, 4403–4416.
- [4] Mayoral, M.C.; Andrés, J.M.; Gimeno, M.P. Optimisation of mineral carbonation process for CO₂ sequestration by lime-rich coal ashes. *Fuel* **2013**, 106, 448–454.
- [5] Jo, H.Y.; Kim, J.H.; Lee, Y.J.; Lee, M.; Choh, S.J. Evaluation of factors affecting mineral carbonation of CO₂ using coal fly ash in aqueous solutions under ambient conditions. *Chem. Eng. J.* **2012**, 183, 77– 87.
- [6] Wee, J.H. A review on carbon dioxide capture and storage technology using coal fly ash. *Appl. Energ.* **2013**, 106, 143–151.
- [7] Hosseini, T.; Selomulya, C.; Haque, N.; Zhang, L. Indirect carbonation of Victorian brown coal fly ash for CO₂ sequestration: Multiple-cycle leaching-carbonation and magnesium leaching kinetic modelling. *Energy Fuel* **2014**, 28 (10), 6481–6493.
- [8] Sun, Y.; Parikh, V.; Zhang, L; Sequestration of carbon dioxide by indirect mineralisation using Victorian brown coal fly ash. *J. Hazard. Mater.* **2012**, 209-210, 458-466.
- [9] Montes-Hernandez, G.; Pérez-López, R.; Renard, F.; Nieto, J.M.; Charlet L. Mineral sequestration of CO₂ by aqueous carbonation of coal combustion fly-ash. *J. Hazard. Mater.* **2009**, 161(2-3), 1347-1354.
- [10] Nyambura, M.G.; Mugeru, W.G.; Felicia, P.L.; Gathura, N.P.; Carbonation of brine impacted fractionated coal fly ash: implications for CO₂ sequestration. *J. Environ. Manage.* **2011**, 92, 655-664.
- [11] Sun, Y.; Yao, M.S.; Zhang, J.P.; Yang, G. Indirect CO₂ mineral sequestration by steelmaking slag with NH₄Cl as leaching solution. *Chem. Eng. J.* **2011**, 173(2), 437-445.
- [12] Uliasz-Bochenczyk, A.; Mokrzycki, E.; Piotrowski, Z.; Pomyka, R.; Estimation of CO₂ sequestration potential via mineral carbonation in fly ash from lignite combustion in Poland. *Energy Procedia* **2009**, 1, 4873-4879.
- [13] Pundsack, F.L.; Somerville, N.J. Recovery of Silica, Iron Oxide and Magnesium Carbonate from the Treatment of Serpentine with Ammonium Bisulfate; Johns-Manville Corporation, New York, **1963**.

- [14] Kodama, S.; Nishimoto, T.; Yamamoto, N.; Yogo, K.; Yamada, K. Development of a new pH-swing CO₂ mineralisation process with a recyclable reaction solution. *Energy* **2006**, 33(5), 776-784.
- [15] Jo, H.Y.; Ahn, J.H.; Jo, H. Evaluation of the CO₂ sequestration capacity for coal fly ash using a flow-through column reactor under ambient conditions. *J. Hazard. Mater.* **2012**, 241–242, 127–136.
- [16] Dri, M.; Sanna, A.; Maroto-Valer, M. Dissolution of steel slag and recycled concrete aggregate in ammonium bisulfate for CO₂ mineral carbonation. *Fuel Process. Technol.* **2013**, 113, 114–122.
- [17] Huijgen, W.J.J.; Comans, R.N.J. Carbonation of steel slag for CO₂ sequestration: Leaching of products and reaction mechanisms. *Environ. Sci. Technol.* **2006**, 40, 2790-2796.
- [18] Teir, S.; Eloneva, S.; Fogelholm, C.J.; Zevenhoven, R. Dissolution of steelmaking slags in acetic acid for precipitated calcium carbonate production. *Energy* **2007**, 32, 528–539.
- [19] Wang, W.; Liu, X.; Wang, P.; Zheng, Y.; Wang, M. Enhancement of CO₂ mineralisation in Ca²⁺/Mg²⁺-rich aqueous solutions using insoluble amine. *Ind. Eng. Chem. Res.* **2013**, 52, 8028–8033.
- [20] Ainscow, W.S.; Gadgil, B.B. Process for producing magnesium oxide. U.S. Patent 4,720,375, January, **1988**.
- [21] Roques, H.; Girou, A. Kinetics of the formation conditions of carbonate tartars. *Water res.* **1974**, 8, 907-920.
- [22] Reddy, M.M.; Nancollas, G.H. The crystallisation of calcium carbonate: iv. The effect of magnesium, strontium and sulfate ions. *J. Cryst. Growth* **1976**, 35, 33-38.
- [23] Kitano, Y. A study of the polymorphic formation of calcium carbonate in thermal springs with an emphasis on the effect of temperature. *Bull. Chem. Soc. Japan* **1962**, 35, 1980-1985.
- [24] Bischoff, J.L.; Fyfe, W.S. Catalysis, inhibition and the calcite-aragonite problem. *Am. J. Sci.* **1968**, 266, 65-79.
- [25] Yoo, K.; Kim, B.S.; Kim, M.S.; Lee, J.C.; Jeong, J. Dissolution of Magnesium from Serpentine Mineral in Sulfuric Acid Solution, *Mater. Trans.* **2009**, 50, 1225-1230.
- [26] Rendek, E.; Ducom, G.; Germain, P.; Carbon dioxide sequestration in municipal solid waste incinerator (MSWI) bottom ash, *J. Hazard. Mater.* **2006**, B12, 873–879.

- [27] Winburn, R. S.; Grier, D. G.; McCarthy, G. J.; Peterson, R. B. Rietveld quantitative X-ray diffraction analysis of NIST fly ash standard reference materials. *Powder Diffr.* **2000**, 15(3), 163-172.
- [28] Hillier, S. Accurate quantitative analysis of clay and other minerals in sandstones by XRD; comparison of a Rietveld and a reference intensity ratio (RIR) method and the importance of sample preparation. *Clay Miner.* **2000**, 35(1), 291-302.
- [29] Ward, C. R.; Taylor, J. C.; Cohen, D. R. Quantitative mineralogy of sandstones by x-ray diffractometry and normative analysis. *J. Sediment. Res.* **1999**, 69(5), 1050-1062.
- [30] Williams, R.P.; Van Riessen, A. Determination of the reactive component of fly ashes for geopolymer production using XRF and XRD. *Fuel* **2010**, 89(12), 3683-3692.
- [31] Chancey, R.T.; Stutzman, P.; Juenger, M.C.G.; Fowler, D.W. Comprehensive phase characterisation of crystalline and amorphous phases of a Class F fly ash. *Cem. Concr. Res.* **2010**, 40(1), 146-156.
- [32] Ward, C.R.; Taylor, J.C. Quantitative mineralogical analysis of coals from the Callide Basin, Queensland, Australia using X-ray diffractometry and normative interpretation. *Int. J. Coal Geol.* **1996**, 30(3), 211-229.
- [33] Chang, E.-E.; Chen, C.-H.; Chen, Y.-H.; Pan, S.-Y.; Chiang, P.-C. Performance evaluation for carbonation of steel-making slags in a slurry reactor. *J. Hazard. Mater.* **2011**, 186, 558–564.
- [34] Website of United states Environmental protection agency. Exposure assessment model: MINTEQ2.
- [35] Drever, J.I. The geochemistry of natural waters: surface and groundwater environments. 3rd ed. New Jersey: Prentice Hall. **1997**.
- [36] Fernandez-Diaz, L.; Putnis, A. The role of magnesium in the crystallisation of calcite and aragonite in a porous medium. *J. Sediment. Res.* **1996**, 66(3), 482-491.
- [37] Althoff, P.L. Structural refinements of dolomite and a magnesian calcite and implications for dolomite formation in the marine environment. *Am. Mineral.* **1977**, 62 (7–8), 772–783.
- [38] Boyd, V.; Yoon, H.; Zhang, C.; Oostrom, M.; Hess, N.; Fouke, B.; Valocchi, A.J.; Werth, C.J. Influence of Mg^{2+} on $CaCO_3$ precipitation during subsurface reactive transport in a homogeneous silicon-etched pore network. *Geochimica et Cosmochimica Acta* **2014**, 135, 321–335.

- [39] Kaczmarek, S.E.; Sibley, D.F. On the evolution of dolomite stoichiometry and cation order during high-temperature synthesis experiments: an alternative model for the geochemical evolution of natural dolomites. *Sediment. Geol.* **2011**, *240*, 30–40.
- [40] Hanchen, M.; Prigiobbe, V.; Baciocchi, R.; and Mazzotti, M. Precipitation in the Mg-carbonate system-effects of temperature and CO₂ pressure. *Chem. Eng. Sci.* **2008**, *63*, 1012.
- [41] Botha, A.; Strydom, C.A. Preparation of a magnesium hydroxy carbonate from magnesium hydroxide. *Hydrometallurgy* **2001**, *62*, 175-183.
- [42] Botha, A.; Strydom, C.A. DTA and FT-IR analysis of the rehydration of basic magnesium carbonate. *J. Therm. Anal. Cal.* **2003**, *71*, 987-995.
- [43] Swanson, E. J.; Fricker, K. J.; Sun, M.; Park, A.-H. A. Directed Precipitation of Hydrated and Anhydrous Magnesium Carbonates for Carbon Storage. *Phys. Chem. Chem. Phys.* **2014**, *16*, 23-40.
- [44] Fyfe, W.S. *Geochemistry of Solids*. McGraw-Hill, New York. **1964**.
- [45] Toby, H.B. R factors in Rietveld analysis: How good is good enough? *Powder Diffr.* **2006**, *21* (1), 67-70.
- [46] Morse, J.W.; Arvidson, R.S.; Lüttge, A. Calcium carbonate formation and dissolution. *Chem. Rev.* **2007**, *107* (2), 342–382.
- [47] St. Arnaud, R.J.; Herbillon, A.J. Occurrence and genesis of secondary magnesium-bearing calcite in soil. *Geoderma.* **1973**, *9*, 279-298.
- [48] Xu, J.; Yan, C.; Zhang, F.; Konishi, H.; Xu, H.; Teng, H.H. *Testing the cation-hydration effect on the crystallisation of Ca–Mg–CO₃ systems*; Proceedings of the national academy of sciences of the United States of America, 2013.
- [49] Santos, R.M.; Van Bouwel, J.; Vandavelde, E.; Mertens, G.; Elsen, J.; Van Gerven, T. Accelerated mineral carbonation of stainless steel slags for CO₂ storage and waste valorisation: Effect of process parameters on geochemical properties. *Int. J. Greenh. Gas Con.* **2013**, *17*, 32–45
- [50] Long, X.; Ma, Y.; Qi, L. In vitro synthesis of high Mg calcite under ambient conditions and its implication for biomineralisation process. *Cryst. Growth Des.* **2011**, *11*, 2866–2873.
- [51] Prieto, M; Stoll, H. *Ion Partitioning in Ambient-Temperature Aqueous Systems*. EMU Notes in Mineralogy, ISBN 978-0903056-26-7, 2011.

- [52] Ma, Y.R.; Cohen, S.R.; Addadi, L.; Weiner, S. Sea urchin tooth design: an “all-calcite” polycrystalline reinforced fiber composite for grinding rocks. *Adv. Mater.* **2008**, *20*, 1555–1559.
- [53] Vassilev, S.V.; Vassileva, C.G. Central methods for characterisation of composition of fly ashes from coal-fired power stations: A critical overview, *Energ. Fuel* **2005**, *19*, 1084-1098.
- [54] Lanas, J. Alvarez, J.I. Dolomitic lime: thermal decomposition of nesquehonite. *Thermochim. Acta* **2004**, *421*, 123–132.
- [55] Todor, D.N. *Thermal analysis of minerals*. Abacus Press, Kent, England, **1976**.
- [56] Chang, E.E.; Pan, S.Y.; Chen, Y.H.; Tan, C.S.; Chian, P.C. Accelerated carbonation of steelmaking slags in a high-gravity rotating packed bed. *J. Hazard. Mater.* **2012**, *227–228*, 97–106.
- [57] Rodriguez-Blanco, J.D.; Shaw, S.; Benning, LG. The kinetics and mechanisms of amorphous calcium carbonate (ACC) crystallisation to calcite, via vaterite. *Nanosci.* **2011**, *3*, 265-271.

Monash University

Declaration for Thesis Chapter 6

Declaration by candidate

In the case of Chapter 6, the nature and extent of my contribution to the work was the following:

Nature of contribution	Extent of contribution (%)
Design, key ideas, writing up code in MATLAB, writing up	90 %

The following co-authors contributed to the work. If co-authors are students at Monash University, the extent of their contribution in percentage terms must be stated:

Name	Nature of contribution	Extent of contribution (%) for student co-authors only
Lian Zhang	Reviewing and editing, comments and feedback	Supervisor
Cordelia Selomulya	Comments and editing	Supervisor
Nawshad Haque	Comments and editing	Supervisor
Mahdi Daneshpayeh	Writing up codes in MATLAB	10 %

The undersigned hereby certify that the above declaration correctly reflects the nature and extent of the candidate's and co-authors' contributions to this work*.

Candidate's Signature		Date 12/11/2015
--------------------------	---	--------------------

Main Supervisor's Signature		Date 12/11/2015
-----------------------------------	---	--------------------

*Note: Where the responsible author is not the candidate's main supervisor, the main supervisor should consult with the responsible author to agree on the respective contributions of the authors.

Chapter 6

Carbonation kinetic modelling and parameter sensitivity analysis

In chapter 5, carbonation rate and competition of Mg^{2+} and Ca^{2+} upon carbonation was examined. It was found that, the presence of Mg^{2+} in the leachate can affect the Ca^{2+} carbonation rate and even the morphology of $CaCO_3$ formed. Due to the complexity of the reactions, none of the published kinetic models for Mg^{2+} and Ca^{2+} carbonation is appropriate for the system we studied. This necessitates the estimation of optimum kinetic parameters with the aid of simulation and optimisation techniques. In this chapter, the experimental data from chapter 5 were used to develop and validate a kinetic model that suits the experimental system we examined here. This model takes into account the interaction between Mg^{2+} and Ca^{2+} cations upon carbonation in an aqueous system. This chapter has been reformatted from the following submitted manuscript to Chemical Engineering Journal: **T. Hosseini**, M. Daneshpayeh, C. Selomulya, N. Haque, L. Zhang, Chemical Kinetic Modelling and Parameter Sensitivity Analysis for the Carbonation of Ca^{2+} and Mg^{2+} Under ambient conditions.

6.1 Abstract

A reaction model was developed to predict kinetic parameters and competition of Mg^{2+} and Ca^{2+} ions during carbonation in mild conditions, *i.e.* ambient temperature and up to 3 atm for the CO_2 partial pressure. The experimental carbonation results at different temperatures, $\text{Mg}^{2+}/\text{Ca}^{2+}$ ratios, and atmospheric pressure were used to validate and predict the kinetic parameters of individual reactions in the aqueous phase by applying genetic algorithm and reactor modelling. This model showed a good agreement with experimental results, and satisfactorily predicted the competition between Mg^{2+} and Ca^{2+} and the formation of magnesian calcite ($\text{Mg}_N\text{Ca}_{(1-N)}\text{CO}_3$). In addition, a sensitivity analysis was conducted based on the validated kinetic model to maximise the precipitation rates of Mg^{2+} and Ca^{2+} . It was found that the final yield for magnesian calcite is the highest for the $\text{Mg}^{2+}/\text{Ca}^{2+}$ molar ratio of 1, referring to an equal concentration for two cations in the leachate. This suggests the strongest synergy between both cations for their co-precipitation. The optimum ammonia amount used as a pH-swing agent was found to be equal to the amount of ammonia released from the leaching stage in a closed loop leaching-carbonation. This amount of ammonia led to $\sim 100\%$ Mg^{2+} and Ca^{2+} precipitation along with the highest magnesian calcite precipitation yield. Upon the rise of the CO_2 partial pressure from 0.1 to 1 atm, the overall carbonation time is shortened from over one hour to ~ 20 minutes to reach an equilibrium which resulted in the precipitation of the whole Mg^{2+} and Ca^{2+} . An initial CO_2 partial pressure of 2 atm is essential to maximise the co-precipitation of both cations in the magnesian calcite form.

6.2 Introduction

Various researchers have investigated the mineral carbonation of CO_2 as a practical approach to reduce CO_2 emission in the atmosphere using natural minerals and industrial wastes as feedstocks [1-3]. The capacity to sequester CO_2 for these alkaline residues depends directly on the proportions of Mg^{2+} and Ca^{2+} and their forms in the original mineral and its derivatives. Investigation on mineral carbonation has been shifted towards aqueous mineral carbonation to accelerate the overall reaction rate with two distinct options [4]. The first option comprises a single-step reaction of the feedstock material with CO_2 , which is usually injected in a reactor under a controlled temperature and pressure [5]. Natural mineral processing requires energy-intensive feed pre-treatments, such as comminution and chemical activation to provide adequate conversions and reaction kinetics [6]. The second one, to which this work belongs, seeks to develop an indirect process with two sequential steps that can be optimised separately [3]. The initial step involves the dissolution of Mg^{2+} and Ca^{2+} - bearing solids under acidic attack, followed by carbonation of the resultant two cations in a basic environment.

The chemical reaction rate is generally the limit for the implementation of mineral carbonation on an industrial scale [7]. The direct aqueous mineral carbonation process consists of three steps occurring sequentially. Initially, CO₂ dissolves in the water phase, which in turn decreases the pH of the solution. Subsequently, Ca/Mg in the feedstock matrix is leached out into the solution. Finally, upon the substitution of proton in the leachate, Ca²⁺ and Mg²⁺ cations precipitate as carbonate precipitates [8]. The mechanisms of direct aqueous mineral carbonation have been studied extensively [9,10]. In general, increasing the rate for the initial dissolution of Ca/Mg is beneficial for accelerating the overall carbonation reaction rate. Guthrie et al. (2001) concluded that, the dissolution of magnesium silicate is a limiting step that determines the overall reaction rate for the mineral carbonation using this natural mineral [11]. Wu et al. (2001) concluded that the limiting step for the carbonation of wollastonite is the dissolution of calcium from the matrix [12]. In these studies, the kinetic of carbonation reaction cannot be determined separately since it is coupled with the initial dissolution reaction in the reactor.

In addition to the natural minerals, the industrial wastes rich in calcium and magnesium have been examined for mineral carbonation, including lignite fly ashes and slags [13-16]. Using industrial wastes reduces the need for natural minerals, and converts a problematic industrial waste into value-added products [17]. The two-step pH swing process using regenerative ammonium salt is a promising technique to utilise industrial wastes under the mild operating conditions [17,18]. This process involves the use of regenerative ammonia chloride (NH₄Cl) to initially extract the magnesium/calcium in the oxide/hydroxide forms out of the solid matrix, *via* the substitution reaction of NH₄⁺ + Ca/MgO = NH_{3(g)} + Ca²⁺/Mg^{2+(aq)} [19]. The resulting Ca²⁺ and Mg²⁺ cations are subsequently carbonated in a separate reactor *via* a continuous bubbling of CO₂ - containing flue gas and ammonia (NH₃) for the pH control, following the reaction equation of Ca²⁺/Mg²⁺ + CO_{2(g)} + NH_{3(g)} = Ca/MgCO₃ + NH_{4⁺(aq)} [20]. Only a few of indirect mineral carbonation studies have coupled experimental and kinetic modelling approaches to examine the competition between the two cations and its influence on the final carbonate product properties. In the past, most of the kinetic studies heavily focused on the Ca²⁺- rich leachate with a negligible Mg²⁺ content [17,21]. This is mainly because the industrial wastes tested are lean in magnesium. Sun et al. (2012) used a pseudo-second order kinetic model to simulate the CO₂ capture rate in a leachate derived from Victorian brown coal fly ash. The apparent activation energy was reported to be 12.7 kJ/mol, with a relative variance R² of 0.96 for the carbonation of Ca²⁺ and Mg²⁺ ions under a carbonation pressure up to 10 atm [22]. The extension of their work to the atmospheric pressure is, however, uncertain. In our previous works [20], it has been revealed that the competition of Ca²⁺ and Mg²⁺ ions is significant upon carbonation in atmospheric pressure. The carbonation rate of Ca²⁺ was slowed and the solubility of the resulting calcium carbonate was enhanced upon the existence of Mg²⁺ in the leachate. In contrast, the formation of

magnesian calcite ($\text{Mg}_N\text{Ca}_{(1-N)}\text{CO}_3$) was enhanced upon the co-existence of Ca^{2+} and Mg^{2+} in the leachate, which in turn accelerated the precipitation rate of Mg^{2+} . These two phenomena have yet to be clarified using a modelling approach.

This study aims to establish a kinetic model for the Mg - Ca - CO_2 - NH_3 - H_2O system to describe the apparent kinetics of Mg^{2+} and Ca^{2+} carbonation in the atmospheric pressure, in particular, in the co-existence and competition of the two cations together in a leachate. After the validation with experimental data, the established model was used to derive the reaction constant (k values) through the use of the genetic algorithm (GA) optimisation method. Subsequently, a sensitivity analysis was conducted to quantitatively evaluate the influences of a variety of key operating parameters on the overall carbonation rate, the yields and compositions of the resulting carbonate precipitate. The results are expected to help the design and sizing of the carbonation reactor, reveal the optimum operating conditions, and eventually promote the deployment of this low-emission carbon capture, storage and utilisation technology.

6.3 Materials and methodologies

6.3.1 Experiment methods

The carbonation experiments have been performed through the use of 50 mL of the mixtures of MgCl_2 and CaCl_2 solutions to mimic fly ash leachates. Analytical grade reagents $\text{MgCl}_2 \cdot 6\text{H}_2\text{O}$, $\text{CaCl}_2 \cdot 2\text{H}_2\text{O}$ and 16 mL aqueous ammonia (28%) were used as the source of Mg^{2+} , Ca^{2+} and pH swing agent, respectively. The amount of the aqueous ammonia added to the leachate was the same as that recovered from the leaching stage to ensure a closed loop for this reagent. The initial concentration of Mg^{2+} , 0.68 mol/L was chosen based on the leachate derived from a brown coal fly ash in ammonium chloride [19]. For all of the remaining experiments, the concentration of Mg^{2+} remained constant whereas the concentration of Ca^{2+} was varied to achieve three different $\text{Mg}^{2+}/\text{Ca}^{2+}$ molar ratios. An extra set of experiments was conducted for a fixed $\text{Mg}^{2+}/\text{Ca}^{2+}$ molar ratio of one to clarify the effect of temperature on the yield and chemical compositions of the carbonate precipitate. The pH of the solution was recorded continuously during the experiment. The gas inlet and outlet tubes allowed a continuous injection of pure CO_2 gas stream with a flow rate of 15 L/min at atmospheric pressure. This rate has been confirmed to be the optimum value to eliminate the external diffusion resistance [19]. The quantitative mineral speciation of solid precipitate was conducted using quantitative X - ray diffraction (QXRD) methodology, through which the amounts of crystalline and amorphous phases were determined by applying an internal standard method. The experimental method and analysis of the samples have been described elsewhere [20].

6.3.2 Modelling methods

A simplified flowchart for the modelling procedure is presented in **Figure 6.1**, with all the details given below.

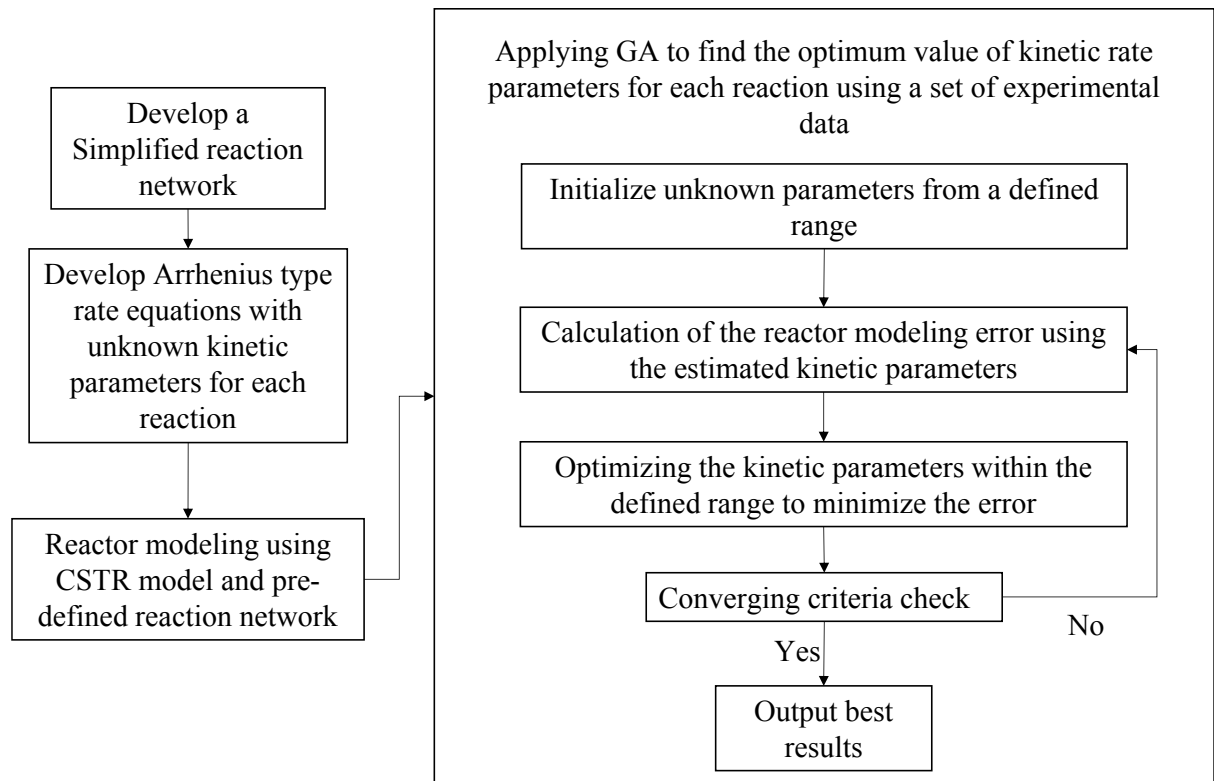
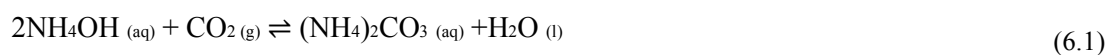


Figure 6.1 A simplified flowchart for the kinetic modelling steps and methods

6.3.2.1 Reaction network and kinetic modelling

In order to clarify the kinetics for the dissolution of CO₂ in water and the subsequent interaction of the dissolved CO₂ and Mg²⁺ and Ca²⁺ ions, a simplified reaction network was first developed. This simplified model is expected to predict the distinct time scales over which the reactions take place and to provide simple expressions for the resulting equilibrium concentration and reaction rates.

In the Mg²⁺ - Ca²⁺ - CO₂ - NH₃ - H₂O system, the overall process was divided into the following three principal stages:



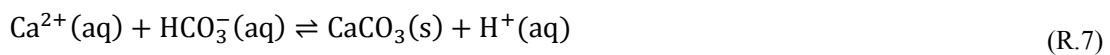
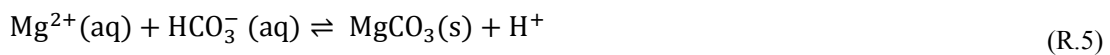
In addition, we assumed that such a system consists of a number of reversible chemical reactions (R.1 to R.10). The system is initially at its equilibrium state with all the species at low concentrations, which is then subjected to an instantaneous injection of gaseous CO₂. At a high pH value, the CO₂ transfer is dominated by the reaction path described in Equations (R.1 to R.3) [17]. The carbonation reaction initiates with the diffusion of CO₂ gas through a gas film near the gas - liquid interface (R.1). The diffusion rate depends on the type of the equipment used to bring the gas into contact with the solution [23]. According to Sun et al. (2011 and 2012), a continuous stirring at 400 rpm is sufficient for eliminating the diffusion limit for CO₂ capture in the batch-scale reactor adopted here [22,24]. The CO₂ dissolution is followed by the formation of HCO₃⁻ by Equation (R.2), which subsequently dissolves to form CO₃²⁻ by Equation (R.3).



Protonation of the pH-swing reagent is initiated according to Equation (R.4).

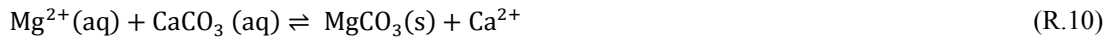
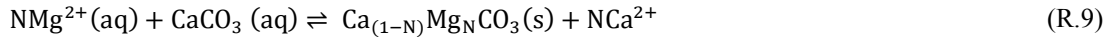


These reactions will exert a remarkable impact on the pH of the solution, which in turn determine the concentration of CO₃²⁻ that is crucial for the carbonation of Ca²⁺ and Mg²⁺ to form the respective carbonate precipitate through the Equations (R.5 to R.8) [17,22]:



Calcium carbonate consists of different polymorphs including three anhydrous crystalline phases (calcite, aragonite and vaterite), two hydrated phases (monohydrate and hexahydrate), and amorphous calcium carbonate (ACC). Calcite and aragonite are the most naturally occurring polymorphous of calcium carbonate, whereas ACC is the least stable and often transforms to a crystalline phase [25]. It has been confirmed that the temporal stabilisation of ACC can occur by the incorporation of organic molecules or magnesium ions [26,27]. Substitution of Mg²⁺ in CaCO₃ crystal lattice to form Mg-calcite was found to be the most probable reaction upon the co-existence of Ca²⁺ and Mg²⁺ in the leachate [28]. These reactions lead to the precipitation or the dissolution of different Ca²⁺ - and Mg²⁺ - carbonate. The abundance of crystal aragonite or vaterite depends on Mg²⁺/Ca²⁺ ratio, temperature and pH [29-31]. To simplify the model, we excluded the different polymorphs of calcium carbonate, assuming all the calcium carbonate precipitates possess an identical structure in the reaction model. In addition, with regard to the

inclusion of Mg^{2+} into calcite, a general form of $Mg_NCa_{(1-N)}CO_3$ referring to magnesian calcite has been confirmed [20]. The value of N is a non-monotonic function of time and the Mg^{2+}/Ca^{2+} ratio [20, 32]. At the end of the reaction, the amount of magnesium in magnesian calcite is equilibrated at a constant value for the varying Mg^{2+}/Ca^{2+} ratios [20]. In the modelling work hereafter, N was added as an unknown parameter to the model and its averaged value was estimated upon optimisation.



To account for the interaction of Mg^{2+} and Ca^{2+} in the model, the power law rate equations were applied for reactions (R.5) to (R.10). The parameters (n_i and m_j) were added as power for the reactants in the overall rate equations of each step.

6.3.2.2 Numerical methods

Kinetic modelling of such a complicated process with many reaction steps led to a set of non-linear kinetic equations. To solve such a complicated system, one of the solutions is to model the reactor and then try to find the kinetic values using an optimisation method [33]. In this method, the reactor is first modelled using the all reactions of the reaction network. Subsequently, the validated reactor model is used as an objective function in an optimisation algorithm. The optimisation algorithm iteratively optimises all the unknown rate constants by trial and error. Finally, the apparent rate constants of the kinetic model are determined.

6.3.2.2.1 Reactor modelling

The rate - based chemical reactions were modelled for a continuous stirred-tank reactor (CSTR) with a continuous CO_2 injection. In order to model this reactor, all differential equations of the reaction network and mass transfer equations were solved simultaneously from $t=0$ to reaction time with a set of ordinary differential equation (ODE). The equilibrium constants k_{eq} for all the reactions were calculated from the HSC chemistry 7.1, as summarised in **Table 6.1**. It is noteworthy that, due to the lack of data for magnesian calcite with a low magnesium-content in HSC Chemistry and in the literature, the k_{eq} for reaction (R.9) was estimated from the assumption of $N=0$. Magnesian calcite can be regarded as a dilute solution of $MgCO_3$ in the solvent $CaCO_3$ [34]. The equilibrium constants were used to calculate the inverse reaction rate according to Equation (6.4):

$$k'_i = \frac{k_i}{k_{eq,i}} \quad (6.4)$$

The kinetics of equations (R.1 to R.10) were modelled by the following rate equations, where t is time (minute), $[]$ denotes concentration (mol/L), k_1 to k_{10} and k'_1 to k'_{10} are,

respectively, the forward and reverse rate constant for the ten reactions (R.1 to R.10). In addition, n and m are the orders of reactions for the first and second reactants, respectively.

$$\frac{d[\text{CO}_2(\text{g})]}{dt} = 0 \quad (\text{R}' .1)$$

$$\frac{d[\text{CO}_2(\text{aq})]}{dt} = +k_1[\text{CO}_2(\text{g})] - k_1'[\text{CO}_2(\text{aq})] - k_2[\text{CO}_2(\text{aq})] + k_2'[\text{HCO}_3^-][\text{H}^+] \quad (\text{R}' .2)$$

$$\begin{aligned} \frac{d[\text{HCO}_3^-(\text{aq})]}{dt} = & +k_2[\text{CO}_2(\text{aq})] - k_2'[\text{HCO}_3^-][\text{H}^+] - k_3[\text{HCO}_3^-] + k_3'[\text{CO}_3^{2-}][\text{H}^+] - \\ & k_5[\text{Mg}^{2+}]^{n_5}[\text{HCO}_3^-]^{m_5} + k_5'[\text{MgCO}_3][\text{H}^+] - \\ & k_7[\text{Ca}^{2+}]^{n_7}[\text{HCO}_3^-]^{m_7} + k_7'[\text{CaCO}_3][\text{H}^+] \end{aligned} \quad (\text{R}' .3)$$

$$\begin{aligned} \frac{d[\text{CO}_3^{2-}]}{dt} = & +k_3[\text{HCO}_3^-] - k_3'[\text{CO}_3^{2-}][\text{H}^+] + k_6[\text{Mg}^{2+}]^{n_6}[\text{CO}_3^{2-}]^{m_6} - k_6'[\text{MgCO}_3] \\ & - k_8[\text{Ca}^{2+}]^{n_8}[\text{CO}_3^{2-}]^{m_8} + k_8'[\text{CaCO}_3] \end{aligned} \quad (\text{R}' .4)$$

$$\begin{aligned} \frac{d[\text{Ca}^{2+}]}{dt} = & -k_7[\text{Ca}^{2+}]^{n_7}[\text{HCO}_3^-]^{m_7} + k_7'[\text{CaCO}_3][\text{H}^+] - k_8[\text{Ca}^{2+}]^{n_8}[\text{CO}_3^{2-}]^{m_8} \\ & + k_8'[\text{CaCO}_3] + N.k_9[\text{Mg}^{2+}]^{n_9}[\text{CaCO}_3]^{m_9} \\ & - k_9'[\text{Ca}_{(1-N)}\text{Mg}_N(\text{CO}_3)]N.[\text{Ca}^+]^N + k_{10}[\text{Mg}^{2+}]^{n_{10}}[\text{CaCO}_3]^{m_{10}} \\ & - k_{10}'[\text{MgCO}_3(\text{aq})][\text{Ca}^{2+}] \end{aligned} \quad (\text{R}' .5)$$

$$\begin{aligned} \frac{d[\text{H}^+]}{dt} = & +k_2[\text{CO}_2(\text{aq})] - k_2'[\text{HCO}_3^-][\text{H}^+] - k_3[\text{HCO}_3^-] + k_3'[\text{CO}_3^{2-}][\text{H}^+] \\ & + k_4[\text{NH}_4^+] - k_4'[\text{NH}_4\text{OH}][\text{H}^+] + k_5[\text{Mg}^{2+}]^{n_5}[\text{HCO}_3^-]^{m_5} \\ & - k_5'[\text{MgCO}_3(\text{aq})][\text{H}^+] + k_7[\text{Ca}^{2+}][\text{HCO}_3^-] \\ & + k_7'[\text{Ca}^{2+}]^{n_7}[\text{HCO}_3^-]^{m_7} - k_7'[\text{CaCO}_3(\text{aq})][\text{H}^+] \end{aligned} \quad (\text{R}' .6)$$

$$\begin{aligned} \frac{d[\text{Mg}^{2+}]}{dt} = & -k_5[\text{Mg}^{2+}]^{n_5}[\text{HCO}_3^-]^{m_5} + k_5'[\text{MgCO}_3(\text{aq})][\text{H}^+] \\ & - k_6[\text{Mg}^{2+}]^{n_6}[\text{CO}_3^{2-}]^{m_6} + k_6'[\text{MgCO}_3(\text{aq})] \\ & - N.k_9[\text{Mg}^{2+}]^{n_9}[\text{CaCO}_3]^{m_9} \\ & + k_9'[\text{Ca}_{(1-N)}\text{Mg}_N(\text{CO}_3)]N.[\text{Ca}^+]^N - k_{10}[\text{Mg}^{2+}]^{n_{10}}[\text{CaCO}_3]^{m_{10}} \\ & + k_{10}'[\text{MgCO}_3(\text{aq})][\text{Ca}^{2+}] \end{aligned} \quad (\text{R}' .7)$$

$$\begin{aligned} \frac{d[\text{CaCO}_3(\text{s})]}{dt} = & +k_7[\text{Ca}^{2+}]^{n_7}[\text{HCO}_3^-]^{m_7} - k_7'[\text{CaCO}_3(\text{aq})][\text{H}^+] \\ & + k_8[\text{Ca}^{2+}]^{n_8}[\text{CO}_3^{2-}]^{m_8} - k_8'[\text{CaCO}_3] - N.k_9[\text{Mg}^{2+}]^{n_9}[\text{CaCO}_3]^{m_9} \\ & + k_9'[\text{Ca}_{(1-N)}\text{Mg}_N(\text{CO}_3)]N.[\text{Ca}^+]^N - k_{10}[\text{Mg}^{2+}]^{n_{10}}[\text{CaCO}_3]^{m_{10}} \\ & + k_{10}'[\text{MgCO}_3(\text{aq})][\text{Ca}^{2+}] \end{aligned} \quad (\text{R}' .8)$$

$$\begin{aligned} \frac{d[\text{MgCO}_3(\text{s})]}{dt} = & k_5[\text{Mg}^{2+}]^{n_5}[\text{HCO}_3^-]^{m_5} - k_5'[\text{MgCO}_3(\text{aq})][\text{H}^+] \\ & + k_6[\text{Mg}^{2+}]^{n_6}[\text{CO}_3^{2-}]^{m_6} \\ & - k_6'[\text{MgCO}_3(\text{aq})] + k_{10}[\text{Mg}^{2+}]^{n_{10}}[\text{CaCO}_3]^{m_{10}} \\ & - k_{10}'[\text{MgCO}_3(\text{aq})][\text{Ca}^{2+}] \end{aligned} \quad (\text{R}' .9)$$

$$\frac{d[\text{NH}_4^+]}{dt} = k_4[\text{NH}_4\text{OH}][\text{H}^+] - k_4'[\text{NH}_4^+] \quad (\text{R}' .10)$$

$$\frac{d[\text{NH}_4\text{OH}]}{dt} = -k_4[\text{NH}_4\text{OH}][\text{H}^+] + k_4'[\text{NH}_4^+] \quad (\text{R}' .11)$$

Equation (R'.1) was included in the system based on the assumption that CO_2 diffusion is not a limiting step for carbonation in the continuously stirred batch reactor used here [17]. In

other words, the gas concentration was assumed to remain constant in the solution, which is reasonable due to a large gas flow rate (15 L/min) compared to the volume of the reactor (0.5 L) and a continuous injection of the CO₂ gas. The initial CO₂ concentration was calculated from Henry's law constant as a function of temperature [35].

Table 6.1 Equilibrium constants for reactions 1 to 10

Reactions	log k_{eq}		
	20 °C	30 °C	70 °C
1	-1.32	-1.54	-1.77
2	-6.5	-6.45	-6.44
3	-10.36	-10.26	-10.03
4	-9.39	-9.09	-8.03
5	-5.42	-5.05	-3.73
6	4.93	5.20	6.30
7	-2.09	-1.92	-1.28
8	8.27	8.34	8.75
9	-2.47	-2.25	-1.4
10	-3.34	-3.13	-2.45

6.3.2.2.2 Optimisation method

An optimisation tool was employed to find the kinetic parameters of the reactor model by the least-square method. For objective functions with such a complex structure, traditional gradient-based algorithms are likely to fail due to getting trapped in local optima [36]. For the optimisation of complex kinetic parameters, various approaches based on the evolutionary algorithms such as genetic algorithm optimisation method have been developed. Genetic algorithm is based on the principle of evolution in which the fittest individual has the better chance to survive and pass on their genetics to the next generation. The genetic algorithm is applied to solve different types of optimisation problems, including those in which the objective function is discontinuous, stochastic or highly non-linear [37]. The decimal genetic algorithm was adopted here to estimate the rate equations based on the experimental data.

In this algorithm, the solution procedure starts with an initial set of random candidates called population. Each individual called chromosome is a complete answer for the individual variables (k_0, n, m, E). The chromosomes evolve through generations by iteratively comparing against one another according to the defined objective function. Through the use of the cross-over strategy, two chromosomes from current generation are merged or modified through mutation to find new individuals until the error is finally minimised to a satisfactory level [33]. Regarding the objective function used here, it is defined as equations (6.5) and (6.6) below for the difference

between predicted and experimental data for the precipitation percentages of Ca^{2+} and Mg^{2+} and the pH of the leachate, respectively:

$$\sum_{i=1}^m \left[\left(\frac{X_{\text{Mg-calc},i} - X_{\text{Mg-Exp},i}}{X_{\text{Mg-Exp},i}} \right)^2 + \left(\frac{X_{\text{Ca-calc},i} - X_{\text{Ca-Exp},i}}{X_{\text{Ca-Exp},i}} \right)^2 + \left(\frac{\text{pH}_{\text{calc},i} - \text{pH}_{\text{Exp},i}}{\text{pH}_{\text{Exp},i}} \right)^2 \right] \quad (6.5)$$

$$X_{\text{M,Calc}} = \frac{C_{\text{M,t}} - C_{\text{M,t}_0}}{C_{\text{M,t}_0}} \times 100 \quad (6.6)$$

In Equation (6.5), X refers to the precipitation percentages of Mg^{2+} or Ca^{2+} which is defined in Equation (6.6) and index *calc* and *exp* denotes the modelling and experimental results, respectively. The optimisation routine uses a population of 100 chromosomes, 50% of population as mating pool and probability of 15% for mutation [33]. We first used the experimental data with $\text{Mg}^{2+}/\text{Ca}^{2+}=1/1$ at different temperatures to find the activation energy (E) of each reaction. Subsequently, the activation energies of the individual reactions were employed to find the other parameters including k_0 , m and n to be satisfied for each $\text{Mg}^{2+}/\text{Ca}^{2+}$ ratio. The routine was implemented in MATLAB to carry out these modelling works.

6.3.3 Methodology for sensitivity analysis

The primary motivation of the sensitivity analysis here is to clarify how the carbonation yields and compositions differ upon the variation of the parent fly ash composition and the subsequent change in the composition of its leachate used for carbonation. In light of this, the influence of a variety of effective parameters such as initial Mg^{2+} , Ca^{2+} and ammonia concentrations and initial CO_2 pressure on carbonation reaction were investigated.

The initial parameters were manipulated according to **Table 6.2** and the concentration profile of each carbonation species was calculated by the model. In each modelling, only one parameter was changed and other parameters were kept constant according to the reference case for an $\text{Mg}^{2+}/\text{Ca}^{2+}$ molar ratio of 1/1 shown as case 3 in Table 6.2.

Table 6.2 Sensitivity analysis parameters

Case	Concentration (mol/L)			CO_2 Pressure (atm)
	Mg^{2+}	Ca^{2+}	NH_4OH	
1	0.17	0.17	0.80	0.1
2	0.34	0.34	1.59	0.5
3 ^b	0.68	0.68	3.18	1
4	1.36	1.36	6.36	2
5	2.72	2.72	12.72	3

^a For each sensitivity case, only one concentration/ CO_2 pressure was changed and the other parameters remained the same as the reference case

^b Row for the concentrations and CO_2 pressure in the reference case.

6.4 Results and Discussion

6.4.1 Calculation of the activation energies for individual reactions

The first step of kinetic modelling was performed using experimental data at different temperatures and the fixed $\text{Mg}^{2+}/\text{Ca}^{2+}$ ratio of 1 to determine the activation energies for individual reactions from R.1 to R.10. The results are summarised in **Table 6.3**, whereas the results reported by Mattila et al. (2012) [17] are presented in a separate column for comparison. Note that, the kinetic models reported in literature were only validated by the continuous pH – monitoring during the carbonation of calcium-containing steelmaking slag in a two-step pH swing process. Although the majority of the single reactions are similar for the two different feedstocks, the corresponding activation energies are different. This is an indicator of the strong dependence of carbonation reactions on the experimental condition and particularly the concentrations of Ca^{2+} and Mg^{2+} in the leachate, which are different for the different feedstock tested. The presence of Mg^{2+} in our model and the competition of Mg^{2+} and Ca^{2+} upon carbonation, compared to the carbonation of Ca^{2+} only in the aqueous carbonation of steel making slag should play an important role on the kinetics. For the reactions of (R.1) to (R.3) in **Table 6.3**, the activation energies of the diffusion of CO_2 into the solution and the subsequent dissociation into CO_3^{2-} and HCO_3^- are less than the corresponding activation energies estimated by Mattila et al. (2012). The difference should be relevant to the mixing-sensitive nature of the dissolution of the gaseous CO_2 in the solution [38]. The large CO_2 volumetric flux for a large volumetric flow rate (15 L/min) in a smaller reactor size (0.5 L) together with the fast enough stirring speed (400 rpm) in our experimental system should explain for a rapid and more homogenous distribution of CO_2 in the solution. For reference, Matilla et al., (2012) adopted the following parameters for the CO_2 transfer from gaseous phase to the aqueous solution: 2 L/min CO_2 flow rate, 1 L reactor size and 200 rpm stirring speed [17]. In addition, according to Rendeck et al. (2006), the flow rate of CO_2 affects the precipitation rate (R.5 to R.8), although it has negligible effects on the final precipitate yield and properties of the solid precipitate formed [39].

The protonation of ammonia solution via reaction (R.4) is directly related to the CO_2 dissolution and the formation of HCO_3^- and CO_3^{2-} . A relatively large difference in activation energies of the two models is partly affected by the method of analysing the kinetic data and assumptions involved. The large activation energy for this reaction indicates its large sensitivity to the reaction temperature [40]. As the CO_2 dissolution continues, the pH of the solution drops continuously, resulting in the requirement of more energy to drive the protonation of ammonia. As a result, the low activation energies for CO_2 dissolution and its subsequent dissociation are partially counteracted with the high activation energy required for the protonation of ammonia. The activation energies reported for these two models on the formation of calcium carbonate

according to reactions (R.7) and (R.8) are relatively comparable. However, the lower activation energies reported by our model suggested that the presence of Mg^{2+} in the leachate may help the Ca^{2+} to overcome the precipitation barriers.

To further validate the model, the Mg^{2+} and Ca^{2+} precipitation extents calculated by model predictions were compared and plotted with the respective experimental data in **Figure 6.2**. In this figure, the experimental and simulation data were assigned to x -axis and y -axis, respectively. As can be seen, a satisfactory agreement has been achieved, which proved a good accuracy of the model network developed here.

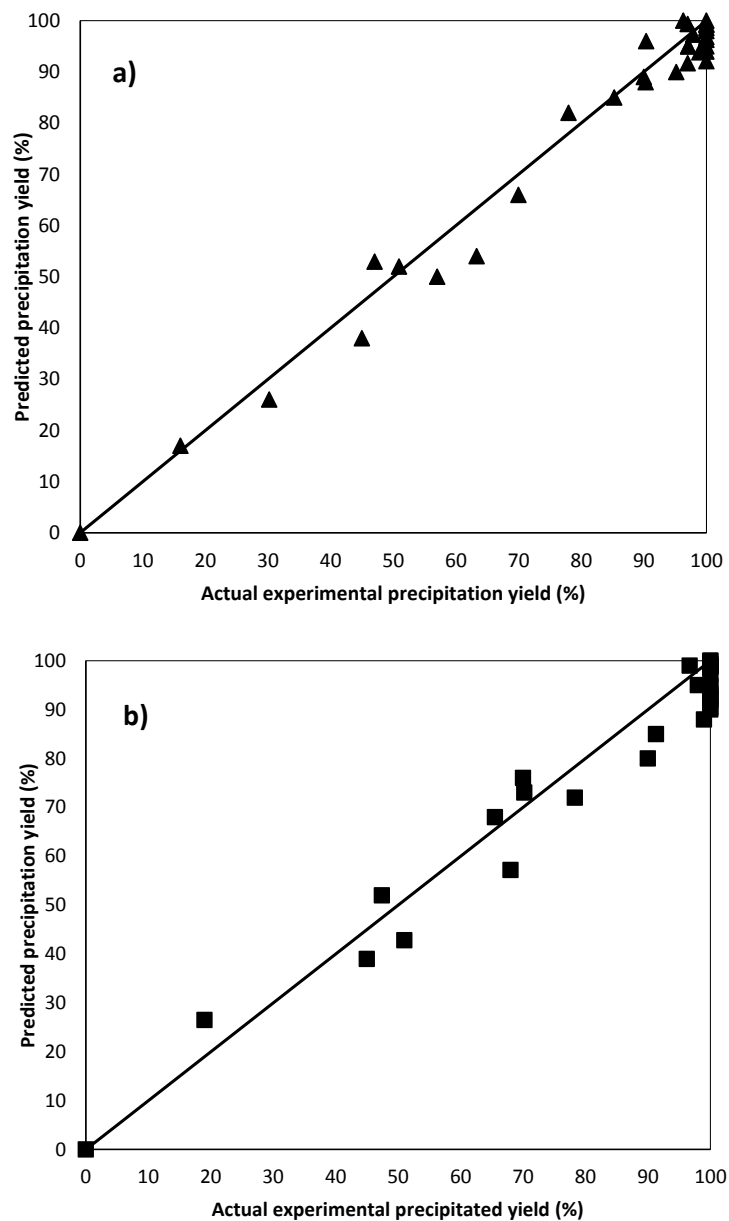


Figure 6.2 Comparison of *a)* Mg^{2+} and *b)* Ca^{2+} actual experimental precipitation yield (%) and predicted precipitation yield (%) calculated by model at different temperatures and a fixed Mg^{2+}/Ca^{2+} molar ratio of 1

Table 6.3 Activation energies of each reaction estimated by GA compared with literature [17]

Reactions	E (kJ/mol) ^a	E (kJ/mol) ^b	Remarks
R-1	3.8	15.5	CO ₂ mass transfer from the gas phase to the liquid phase
R-2	0.96	41	CO ₂ dissolution in the aqueous phase
R-3	10.5	22	HCO ₃ ⁻ dissolution
R-4	41.4	0.2	Protonation of NH ₄ OH
R-5	30.9	-	Mg ²⁺ reaction with HCO ₃ ⁻
R-6	36.9	-	Mg ²⁺ reaction with CO ₃ ²⁻
R-7	29.2	37	Ca ²⁺ reaction with HCO ₃ ⁻
R-8	2.4	6.0	Ca ²⁺ reaction with CO ₃ ²⁻
R-9	42.9	-	Magnesian calcite formation
R-10	14.75	-	Mg ²⁺ ion exchange with calcite

^a our model

^b The E values for each reaction is based on a model on simultaneous dissolution of steel making slag in an ammonium salt and its carbonation [17]

6.4.2 Calculation of the reaction constants and orders for individual reactions

The experimental data from the carbonation of different Mg²⁺/Ca²⁺ ratios were subsequently used to estimate the reaction constants for the proposed reaction scheme. The results are summarised in **Table 6.4**. As can be seen, the predicted *N* value for the averaged molecules of Mg²⁺ per mole calcite is 0.09, which is very close to the experimentally determined value ~0.1 [20]. The average value for *N* in the case of aqueous carbonation of Mg²⁺ and Ca²⁺ was found to be 0 - 0.15, depending on the reaction time, temperature, pressure and Mg²⁺/Ca²⁺ ratio as well [41,42]. Based on kinetic parameters defined in Table 6.4, the reaction rate equations are as follows:

$$r_1 = k_{01}e^{-\frac{E_1}{RT}}[\text{CO}_2(\text{g})] - k'_{01}e^{-\frac{E_2}{RT}}[\text{CO}_2(\text{aq})] \quad (\text{R}'' .1)$$

$$r_2 = k_{02}e^{-\frac{E_2}{RT}}[\text{CO}_2(\text{aq})] - k'_{02}e^{-\frac{E_2}{RT}}[\text{HCO}_3^-][\text{H}^+] \quad (\text{R}'' .2)$$

$$r_3 = k_{03}e^{-\frac{E_3}{RT}}[\text{HCO}_3^-] - k'_{03}e^{-\frac{E_3}{RT}}[\text{CO}_3^{2-}][\text{H}^+] \quad (\text{R}'' .3)$$

$$r_4 = k_{04}e^{-\frac{E_4}{RT}}[\text{NH}_4^+] - k'_{04}e^{-\frac{E_4}{RT}}[\text{NH}_4\text{OH}][\text{H}^+] \quad (\text{R}'' .4)$$

$$r_5 = k_{05}e^{-\frac{E_5}{RT}}[\text{Mg}^{2+}]^{n_5}[\text{HCO}_3^-]^{m_5} - k'_{05}e^{-\frac{E_5}{RT}}[\text{MgCO}_3(\text{aq})][\text{H}^+] \quad (\text{R}'' .5)$$

$$r_6 = k_{06}e^{-\frac{E_6}{RT}}[\text{Mg}^{2+}]^{n_6}[\text{CO}_3^{2-}]^{m_6} - k'_{06}e^{-\frac{E_6}{RT}}[\text{MgCO}_3(\text{aq})] \quad (\text{R}'' .6)$$

$$r_7 = k_{07}e^{-\frac{E_7}{RT}}[\text{Ca}^{2+}]^{n_7}[\text{HCO}_3^-]^{m_7} - k'_{07}e^{-\frac{E_7}{RT}}[\text{CaCO}_3(\text{aq})][\text{H}^+] \quad (\text{R}'' .7)$$

$$r_8 = k_{08}e^{-\frac{E_8}{RT}}[\text{Ca}^{2+}]^{n_8}[\text{CO}_3^{2-}]^{m_8} - k'_{08}e^{-\frac{E_8}{RT}}[\text{CaCO}_3(\text{aq})] \quad (\text{R}'' .8)$$

$$r_9 = k_{09}e^{-\frac{E_9}{RT}}[\text{Mg}^{2+}]^{n_9}[\text{CaCO}_3]^{m_9} - k'_{09}e^{-\frac{E_9}{RT}}[\text{Ca}_{(1-N)}\text{Mg}_N(\text{CO}_3)] \cdot [\text{Ca}^+] \quad (\text{R}'' .9)$$

$$r_{10} = k_{010}e^{-\frac{E_{10}}{RT}}[\text{Mg}^{2+}]^{n_{10}}[\text{CaCO}_3]^{m_{10}} - k'_{010}e^{-\frac{E_{10}}{RT}}[\text{MgCO}_3(\text{aq})][\text{Ca}^{2+}] \quad (\text{R}'' .10)$$

In the above equations, k_{oi} and k'_{oi} refers to the kinetic rate constant for individual reactions ($i=1$ to 10) for the forward and reverse reactions respectively. In **Table 6.4**, the k_o value calculated by genetic algorithm was used to calculate k values at room temperature using Arrhenius's equation and each individual k value was then compared with corresponding k value in the two existing kinetic models proposed for carbonation of calcium. For the two models reported in the literature, the first model was proposed by Mattila et al. (2012) on the precipitation of Ca^{2+} derived from the leaching of steelmaking slag [17], while the second one is for aqueous carbonation of Ca^{2+} in the absence of pH-swing agent [43]. Again, the discrepancy here demonstrates that different experimental facilities and conditions can substantially influence the resulting expressions for the kinetic constants [44].

The forward reaction rate constant for reaction (R.1) is considerably large in the model proposed by Mitchell et al. (2010) [43]. It was derived from a simplified assumption on an equilibrated distribution of CO_2 between the gas and aqueous phases, which resulted in a very fast reaction progression. On the other hand, the reaction constant for the same reaction in our model is four order of magnitude larger than that estimated by Matilla et al. (2012), suggesting the strong effect of the CO_2 flow rate and the mixing extent on the rate of this reaction. To reiterate, the large flow rate and small reactor used here ensured a quick dissolution of CO_2 and its subsequent dissociation to HCO_3^- and CO_3^{2-} . The k value for ammonium solution protonation is lower than the corresponding reaction constant reported by Mattila et al. (2012) [17]. This is because the CO_2 dissolution rate is faster in our experimental system, which facilitated the formation of more HCO_3^- and CO_3^{2-} in the solution that in turn increased the concentration of H^+ via reactions (R.5) and (R.7). Consequently, the reverse reaction for (R.4) was accelerated in our system. Finally, with regard to the discrepancy of the k_i values for reactions (R.7) and (R.8) in Table 6.4, it should be mainly attributed to the competition from Mg^{2+} carbonation reactions (R.5) and (R.6) which consumed and reduced the concentrations of HCO_3^- and CO_3^{2-} in the leachate, thereby slowing down the carbonation reactions (R.7) and (R.8) for Ca^{2+} .

The validity of kinetic model was further tested by the comparison of the precipitation percentages of the two cations calculated by the model with the respective experimental data for the two other $\text{Mg}^{2+}/\text{Ca}^{2+}$ ratios of 2 and 1/2, and at room temperature. The results are presented in **Figure 6.3** for Mg^{2+} (left panel) and Ca^{2+} (right panel) for a) $\text{Mg}^{2+}/\text{Ca}^{2+}$ of 2/1 and b) $\text{Mg}^{2+}/\text{Ca}^{2+}$ of 1/2. Clearly, a satisfactory agreement has been achieved between the experimental data and the kinetic model prediction. In the case of $\text{Mg}^{2+}/\text{Ca}^{2+}=2/1$, the kinetic model slightly underestimated the carbonation precipitation yields for the two cations from 20 min onwards. This may be due to that the different polymorphs of calcium carbonate and the diffusivity of magnesium in different calcium carbonate crystals were not considered. Even so, the deviation is negligible.

Table 6.4 Kinetic parameters fitted by experimental data obtained at different Mg^{2+}/Ca^{2+} ratios and comparison with the other carbonation models reported in literature

Reaction number	Our model					Literature	
	n_i^a	m_j^a	N	k_{0i} $M^{(1-m_i-n_i)} s^{-1}$	k_i $M^{(1-m_i-n_i)} s^{-1}$	k_i^b	k_i^c
1	1	-	-	23.2	5.0	$5.5 \times 10^{-4} s^{-1}$	$1 \times 10^{10} s^{-1}$
2	1	1	-	12.2	8.3	$0.52 M^{-1} s^{-1}$	-
3	1	-	-	36.9	0.53	$0.06 s^{-1}$	$3 M^{-1} s^{-1}$
4	1	1	-	1.0×10^4	5.5×10^{-4}	$0.45 M^{-1} s^{-1}$	-
5	1.4	1.2	-	7.2	2.8×10^{-5}	-	-
6	0.8	0.8	-	1.4×10^5	0.05	-	-
7	1.6	1.5	-	4.5	3.4×10^{-5}	$0.17 M^{-1} s^{-1}$	-
8	0.9	2.3	-	7.9	3.0	$72.5 M^{-1} s^{-1}$	$2 M^{-1} s^{-1}$
9	1.4	1.4	0.09	9.5×10^5	0.03	-	-
10	0.8	2.2	-	5.7	0.01	-	-

^a Reaction power coefficients for all reverse reactions are equal to 1.

^b The k value for each reaction is based on a model on simultaneous dissolution of steel making slag in an ammonium salt and its carbonation [17].

^c The k value for each reaction is derived from a model on precipitation of Ca^{2+} solution without pH-swing agent [43].

*M and s refers to Molar and second respectively.

The validated model is also able to satisfactorily predict the formation rate of magnesian calcite at the three different Mg^{2+}/Ca^{2+} molar ratios, as shown in **Figure 6.4**. The weight percentage of magnesian calcite increased rapidly, once the reaction started, and eventually levelled off. The original Mg^{2+}/Ca^{2+} molar ratio in the leachate is critical. For the Mg^{2+}/Ca^{2+} molar ratio of 1 referring to an equal concentration for the two cations in the leachate, the final yield for magnesian calcite is the highest, suggesting the strongest synergy between the two cations for their co-precipitation. Increasing the Mg^{2+}/Ca^{2+} molar ratio to 2 for an excessive presence of Mg^{2+} in the leachate resulted in a slight decrease on the magnesian calcite yield, which should be attributed to the larger solubility of magnesian calcite than calcite [32]. It also indicates a limited capacity of calcite to absorb Mg^{2+} . More interestingly, upon the halving of the Mg^{2+}/Ca^{2+} molar ratio to 0.5 for an excessive presence of Ca^{2+} , the formation of magnesian calcite was slowed down, with its final yield not levelling off even after 40 min. This should be caused by the difference in the calcite polymorph dominated by aragonite and vaterite under this Mg^{2+}/Ca^{2+} molar ratio [20].

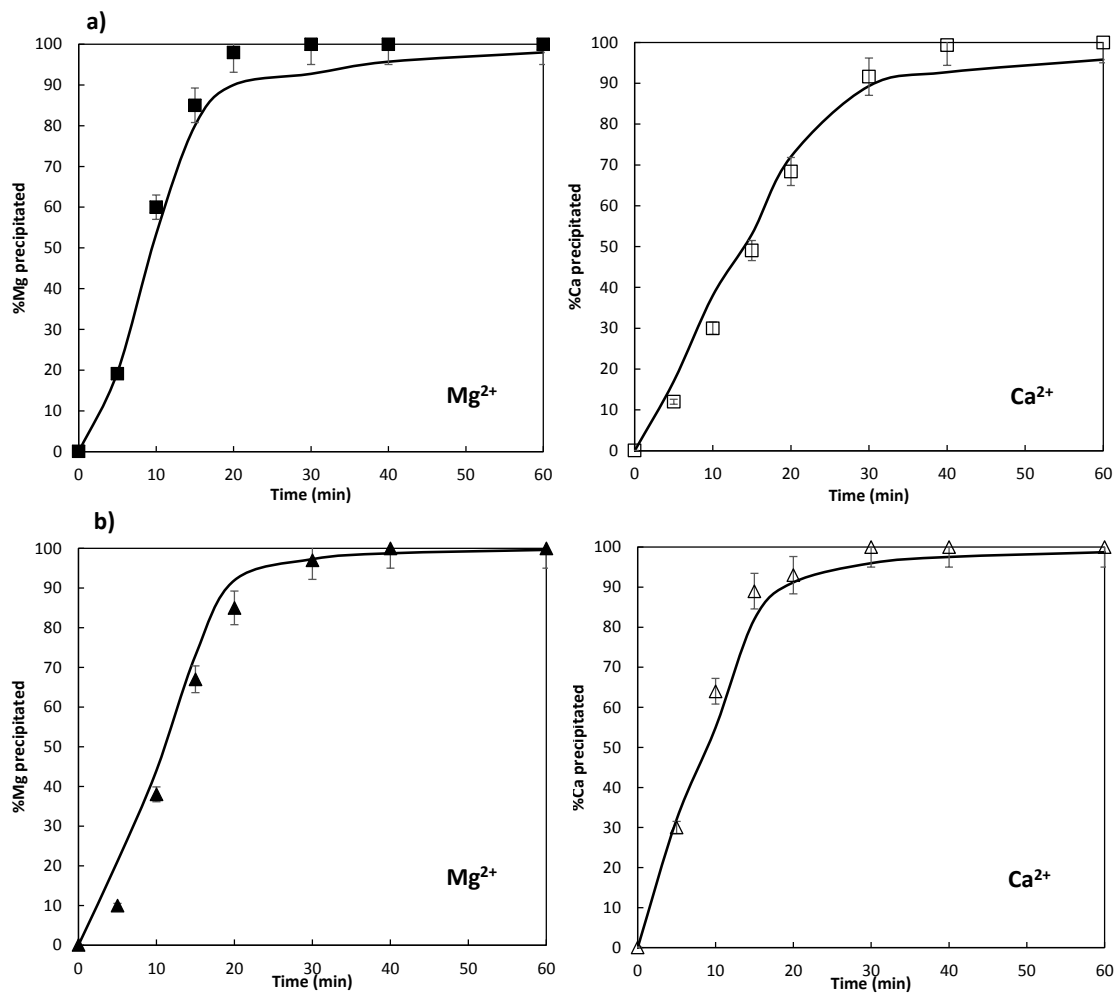


Figure 6.3 Comparison of Mg^{2+} (left panel) and Ca^{2+} (right panel) carbonation for a) $Mg^{2+}/Ca^{2+}=2/1$ and b) $Mg^{2+}/Ca^{2+}=1/2$ from experimental data (data points) and modelling data (solid lines), Experimental data are collected at room temperature.

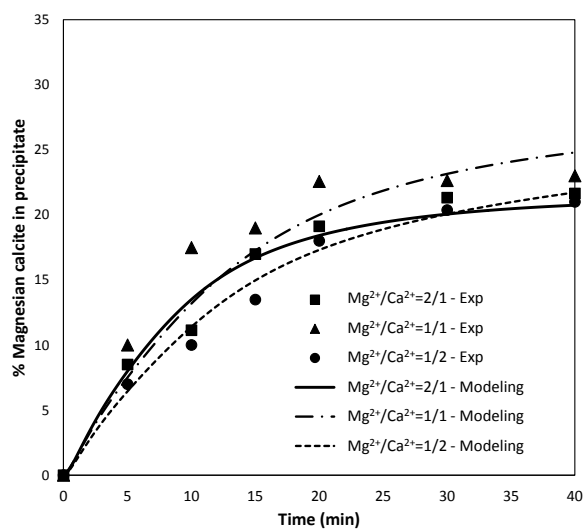


Figure 6.4 The mass fraction of magnesian calcite in the total precipitate as a function of time for Mg^{2+}/Ca^{2+} ratio of 2/1, 1/1 and 1/2 calculated by experimental (points) and modelling data (solid lines). Experimental data were collected at room temperature.

6.4.3 Concentration profiles for individual species at the Mg^{2+}/Ca^{2+} molar ratio of 1

Figure 6.5 *a-f* demonstrates the concentration profiles of individual species formed at the Mg^{2+}/Ca^{2+} ratio of 1 based on the model together with the measured pH values. Only this molar ratio was discussed hereafter, considering that it is the optimum molar ratio for the co-precipitation of the two cations as evident in the above sub-section.

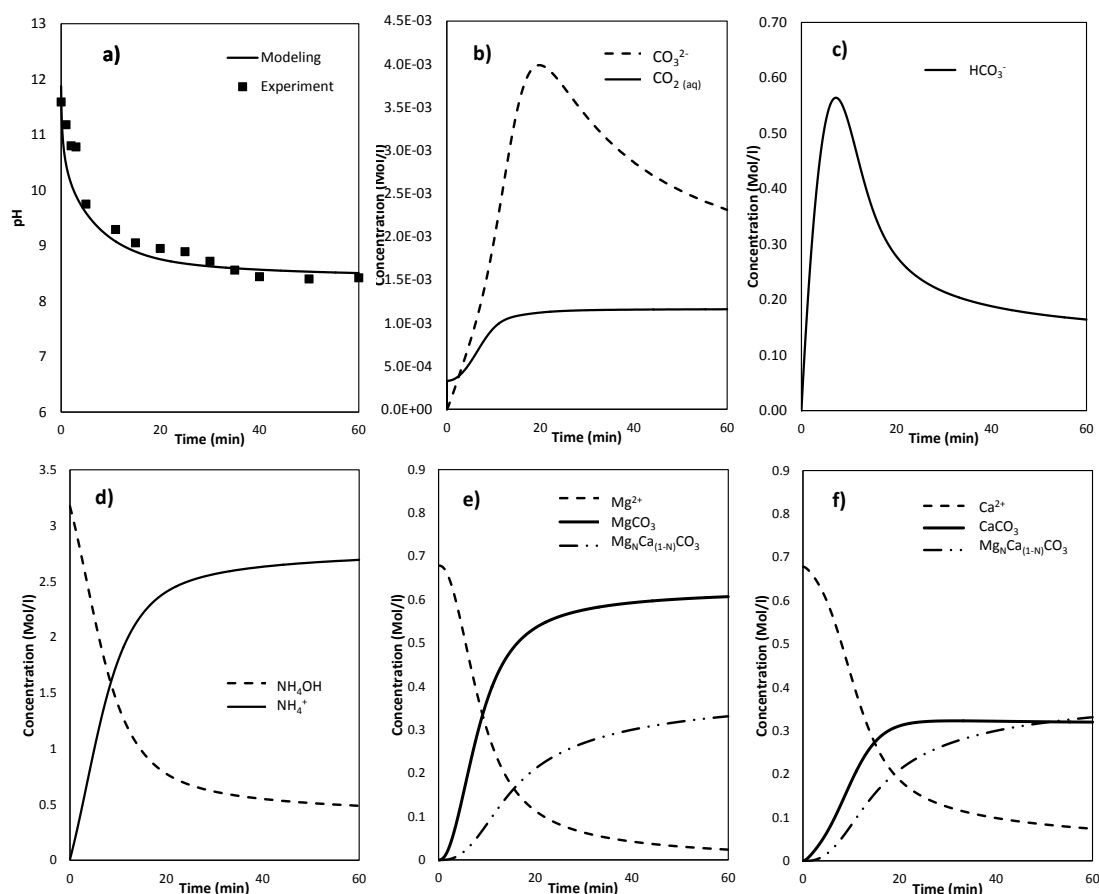


Figure 6.5 *a)* Experimental (points) and predicted pH and concentrations (line) of *b)* $CO_2(aq)$ and CO_3^{2-} , *c)* HCO_3^- , *d)* NH_4^+ and NH_4OH , *e)* Mg^{2+} , $MgCO_3$ and $Mg_NCa_{(1-N)}CO_3$, *f)* Ca^{2+} , $CaCO_3$ and $Mg_NCa_{(1-N)}CO_3$.

Here again, one can see a good agreement between the model prediction and experimentally measured pH values for the leachate. With regard to the first four panels from *a* to *d*, the results demonstrate the dissolution rate of CO_2 in ammonia water and the concentrations of the resulting aqueous species. As can be seen, the dissolution of CO_2 was stabilised from 20 min onwards, which was accompanied by a continuous consumption of NH_4OH and production of NH_4^+ in the leachate. This is due to the decomposition of NH_4OH to release NH_4^+ and OH^- to balance the H^+ in the leachate. The concentrations of HCO_3^- and CO_3^{2-} ions were maximised at 20 min and then decreased quickly onwards, due to their stabilisation into the carbonate precipitates. The

formation of these deposits is an additional driving force that can pull the reactions (R.3) and (R.4) to the right-hand side which in turn results in a continuous drop in the pH, as shown in panel *a* [45]. The model prediction suggests the increasing concentration of MgCO_3 , CaCO_3 and $\text{Mg}_x\text{Ca}_{(1-x)}\text{CO}_3$ over the reaction time, shown in panels *e* and *f*. At the beginning of the carbonation, the Mg^{2+} and Ca^{2+} ion concentrations in the solution phase are relatively high. Afterwards, they gradually decrease due to the consumption of Mg^{2+} , Ca^{2+} , HCO_3^- and CO_3^{2-} ions. However, it takes around 10 min for HCO_3^- and CO_3^{2-} to reach their maximum values. The consumption of these ions leads to more CO_2 gas being absorbed into the solution, which lowered the pH of the solution.

6.4.4 Sensitivity analysis

6.4.4.1 Effect of the initial Mg^{2+} concentration

The results for the effect of the initial Mg^{2+} concentration in the leachate are presented in **Figure 6.6** *a* and *b*, in which the Ca^{2+} concentration was fixed at 0.68 mol/L, and the reaction time was set at 30 min. In this figure, panel *a* corresponds to the resulting $\text{Mg}^{2+}/\text{Ca}^{2+}$ - bearing species (both cation and solid precipitate) and panel *b* shows the concentration of NH_4^+ , NH_4OH and HCO_3^- . In the starting level of the Mg^{2+} concentration which is 0.17 mol/L, the concentration of CaCO_3 is significantly higher than MgCO_3 . There are also sufficient HCO_3^- and CO_3^{2-} ions to precipitate the whole Mg^{2+} and Ca^{2+} in the leachate. With increasing initial Mg^{2+} concentration (*i.e.* the $\text{Mg}^{2+}/\text{Ca}^{2+}$ molar ratio) in the leachate, Mg^{2+} competes with Ca^{2+} and even absorbs CO_2 more readily than Ca^{2+} . This competition led to a rapid increase in the yield of MgCO_3 at a cost of the decrease on the yield of CaCO_3 precipitation. The similar observation has been reported elsewhere [30].

Moreover, the results here further confirmed that, increasing the initial concentration of Mg^{2+} to ~ 0.7 mol/L for an $\text{Mg}^{2+}/\text{Ca}^{2+}$ molar ratio of ~ 1 is in favour of the formation of magnesian calcite. However, upon the further rise of the concentration of Mg^{2+} , the yield of magnesian calcite decrease gradually and turns negligible in the case of an initial Mg^{2+} concentration of 2.75 mol/L for an $\text{Mg}^{2+}/\text{Ca}^{2+}$ molar ratio of ~ 4 . This is accompanied by the decrease in the yield of CaCO_3 whilst an increase in the yield for MgCO_3 . In other words, in an Mg^{2+} -rich leachate, the extent for Mg^{2+} to incorporate into calcite crystal lattice is rare. The presence of magnesian calcite was also found to mainly occur at low CaCO_3 concentrations in the leachate, as suggested by Santos et al. (2013) [32]. Moreover, according to Boyd et al. (2014), when the $\text{Mg}^{2+}/\text{Ca}^{2+}$ ratio exceeds the threshold ratio (~ 1 -2), the presence of excess Mg^{2+} can inhibit the calcite growth [30]. As result, there were insufficient calcite seeds to promote the formation of magnesian calcite.

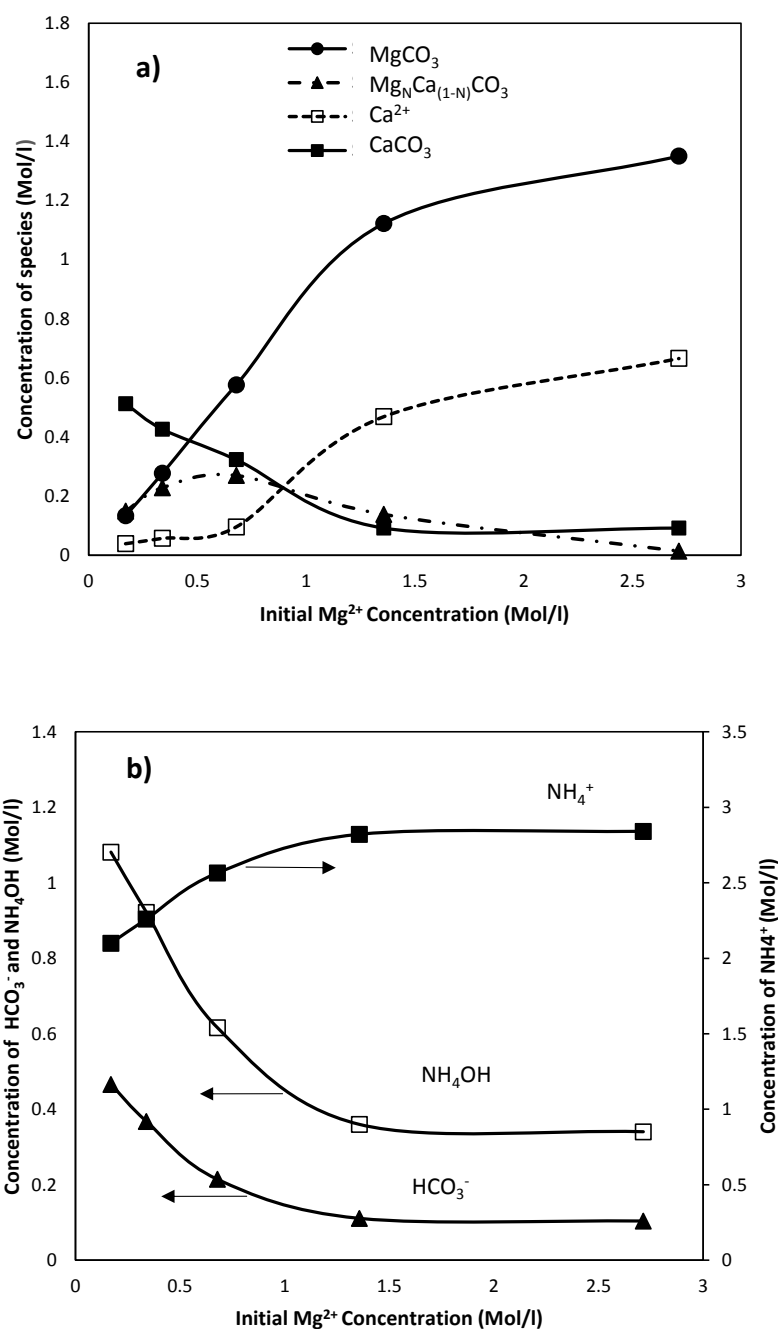
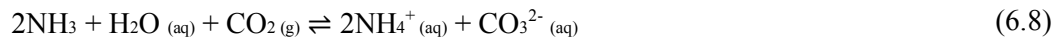
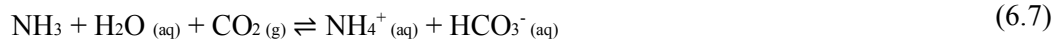


Figure 6.6 Concentrations of a) Mg/Ca-bearing species and b) NH_4^+ , NH_4OH and HCO_3^- as a function of initial Mg^{2+} concentration in the solution at 30 min reaction time (temperature, Ca^{2+} and NH_4OH concentration and CO_2 pressure remained constant at room temperature, 0.68 and 3.18 mol/L and 1 atm respectively)

With regard to the results in panel b of Figure 6.6, upon increasing the Mg^{2+} concentration from ~ 0.7 mol/L (Mg^{2+}/Ca^{2+} of 1/1) onwards, the amount of HCO_3^- ion turns insufficient to carbonate the whole Mg^{2+} . Therefore, according to the amounts of $MgCO_3$ and magnesian calcite formed, around half of the original Mg^{2+} remained unreacted in the solution. The NH_4^+

concentration shows an upward trend due to the dissociation of ammonia solution according to Equations (6.7) and (6.8) [46]. According to Reaction (R.5), the precipitation of MgCO_3 causes a sudden decrease in the pH by releasing H^+ into the solution. To establish the equilibrium, a further dissociation of ammonia has to take place. This reaction will in turn supply more HCO_3^- and CO_3^{2-} to react with the excess Mg^{2+} until the equilibrium is established again.



6.4.4.2 Effect of the initial Ca^{2+} concentration

The effect of the initial concentration of Ca^{2+} on the overall carbonation performance was studied by examining a wide range of concentration from ~ 0.17 mol/L to 2.71 mol/L, corresponding to a broad variation of the reference case by a factor of 2 to 4. The initial concentration of Mg^{2+} remained constant at 0.68 mol/L here, and the reaction time was fixed at 30 min too. **Figure 6.7** demonstrates the concentration profiles for the different species. Contrary to the detrimental effect of increasing Mg^{2+} concentration on formation of calcium carbonate, a small amount of Ca^{2+} in the leachate benefits the incorporation of Mg^{2+} into calcite. From the Ca^{2+} concentration of around 1.3 mol/L, the yields of calcium carbonate and magnesian calcite growth are rather stable, due to the insufficiency of CO_2 dissolved in the leachate, and hence, the excessive Ca^{2+} remained unreacted in the leachate.

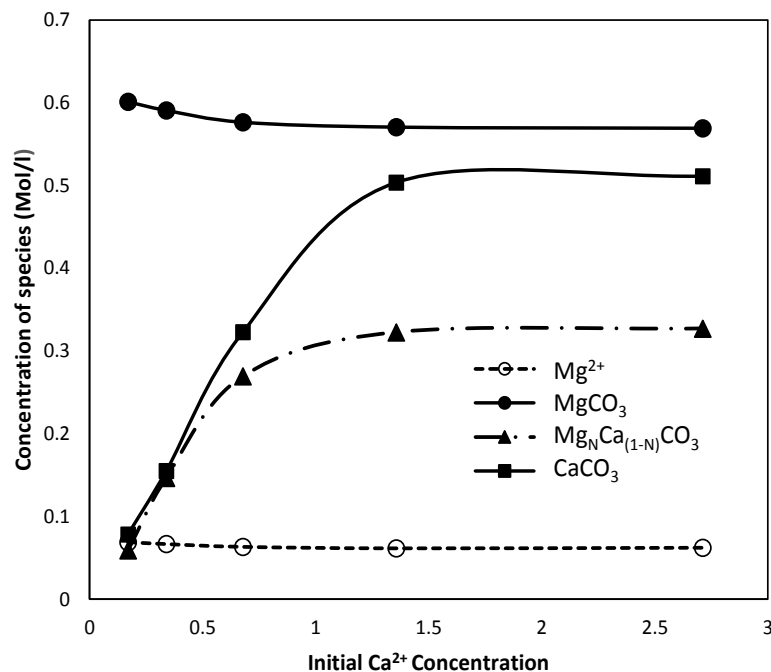


Figure 6.7 Concentrations of different Mg- and Ca-bearing species as a function of initial Ca^{2+} concentration in the leachate in 30 min (Other parameters were fixed as room temperature, initial Mg^{2+} 0.68mol/L, initial NH_4OH 3.18mol/L and CO_2 pressure 1 atm)

6.4.4.3 Effect of the initial NH₄OH concentration

The influence of the initial NH₄OH concentration (*i.e.* amount of ammonia doped in for the pH control) on the concentration of carbonate precipitates and NH₄⁺, HCO₃⁻ and CO₃²⁻ are demonstrated in **Figure 6.8 a** and **b**, respectively. Note that, the initial Mg²⁺/Ca²⁺ molar ratio and reaction time was fixed at 1 and 30 min, respectively. A rise in the initial NH₄OH concentration up to ~4 mol/L (shown in panel *a*) is clearly beneficial in accelerating the carbonation rate for both Mg²⁺ and Ca²⁺, due to the continually enhanced concentration of NH₄⁺, HCO₃⁻ and CO₃²⁻ in the leachate (shown in panel *b*). Upon a further increase of the NH₄OH concentration, the change in the yields of two pure carbonates is marginal and even negligible. More interestingly, the yield of magnesian calcite even decreases from the NH₄OH concentration of ~3.8 mol/L onwards. As presented in panel *b*, the concentration of HCO₃⁻ was increased much faster than that of CO₃²⁻ with the increase on the amount of ammonia added into the leachate.

To further examine the effect of ammonia concentration on the overall system yield, the dynamic concentration profiles for the major species in the leachate are illustrated in **Figure 6.9 a-f**. In each panel, the concentration profile obtained at the ammonia concentration equal to the reference case is shown as *x*, and the other cases are displayed by the multiplication of the reference case, which is 1/4, 1/2, 2 and 4. Note that, the ammonia concentration chosen as a reference case is equal to the amount of ammonia recovered from the leaching stage [19]. As can be seen from Figures 6.9 *a* and *b*, in the early stage of the reaction, a sudden decrease in the NH₄OH concentration occurred, due to its fast dissociation to NH₄⁺ and OH⁻. The alkalinity of the solution resulted in the absorption of more CO₂ in the solution, which was initially in the form of carbonic acid and subsequently dissociated to HCO₃⁻ and CO₃²⁻. The sudden increase in NH₄⁺ is consistent with a rapid rise in HCO₃⁻ at the same time shown in Panel *c*. As the reactions proceed, the concentrations of both NH₄⁺ and NH₄OH were stabilised. However, the time for these two concentrations to stabilise varies with the initial ammonia concentration. At a smaller ammonia concentration such as 1/2*x* or even 1/4*x*, the dissociation of ammonia was retarded in less than 10 min, due to the insufficient activities of ammonia ions in the solution. Since the concentration of ammonia in the solution is insufficient to release OH⁻ in the solution, pH dropped quickly upon the continuous feeding of CO₂ into the solution. Consequently, reaction (6.1) slowed down and eventually stopped after ~30 min. With regard to the concentration profile for HCO₃⁻ in panel *c*, it was maximised at about 10 min for the two smaller ammonia doping cases, 1/4*x* and 1/2*x*. This should be due to the insufficient amount of ammonia. The observation for the two larger ammonia doping cases is different, due to the excessive amount of ammonia used. The carbonation reactions for Ca²⁺ and Mg²⁺ were completed in 15 min (as evident in panels *d* and *e*), and thus HCO₃⁻ was not consumed afterwards. The consumption of the whole

ammonia followed by the reaction of existing with Mg^{2+} and Ca^{2+} led to the unavailability of HCO_3^- from 30 min onward as shown in panel c.

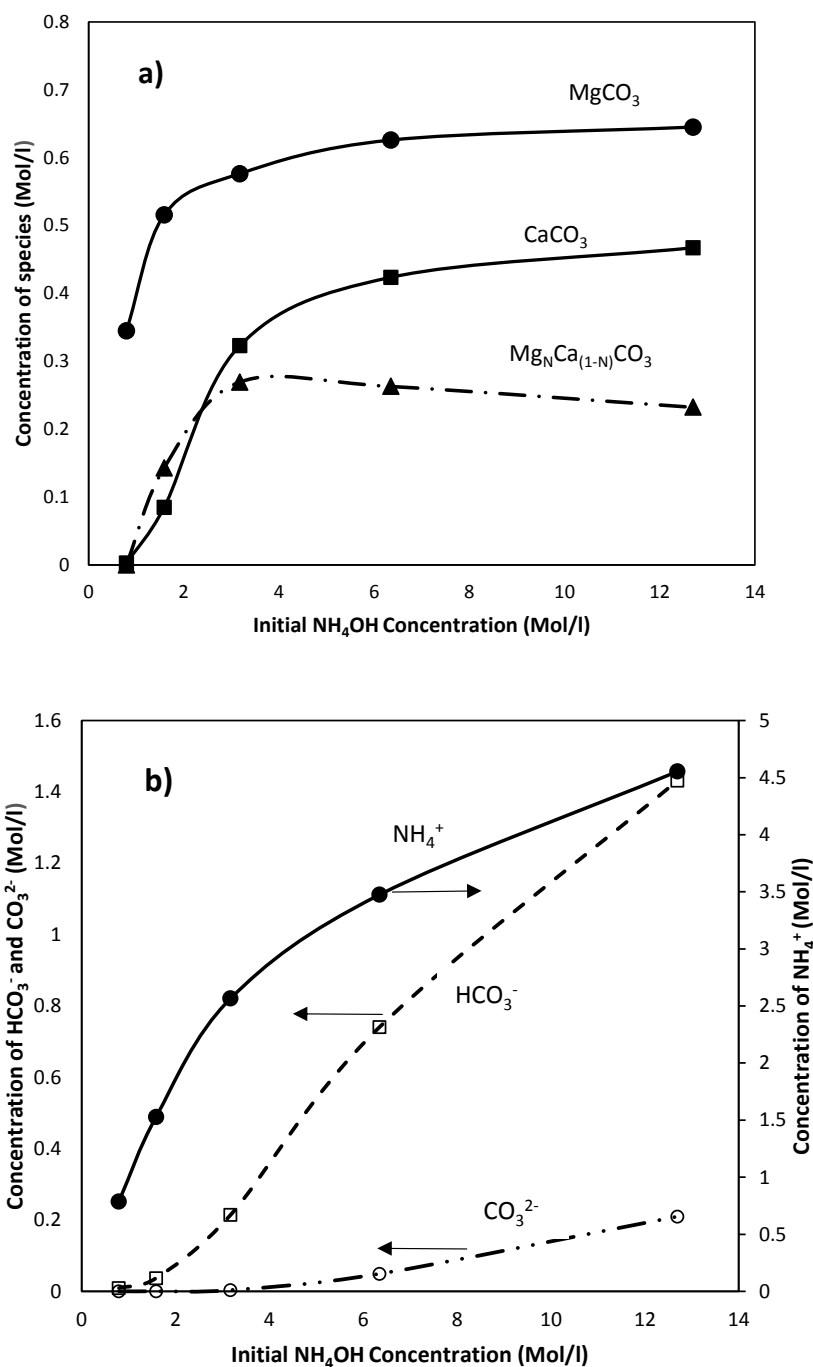


Figure 6.8 Concentrations of Mg- and Ca-bearing species in the solution at different NH_4OH concentrations at 30 min reaction time (equal Mg^{2+} and Ca^{2+} concentrations of 0.68 mol/L, room temperature and atmospheric CO_2 pressure)

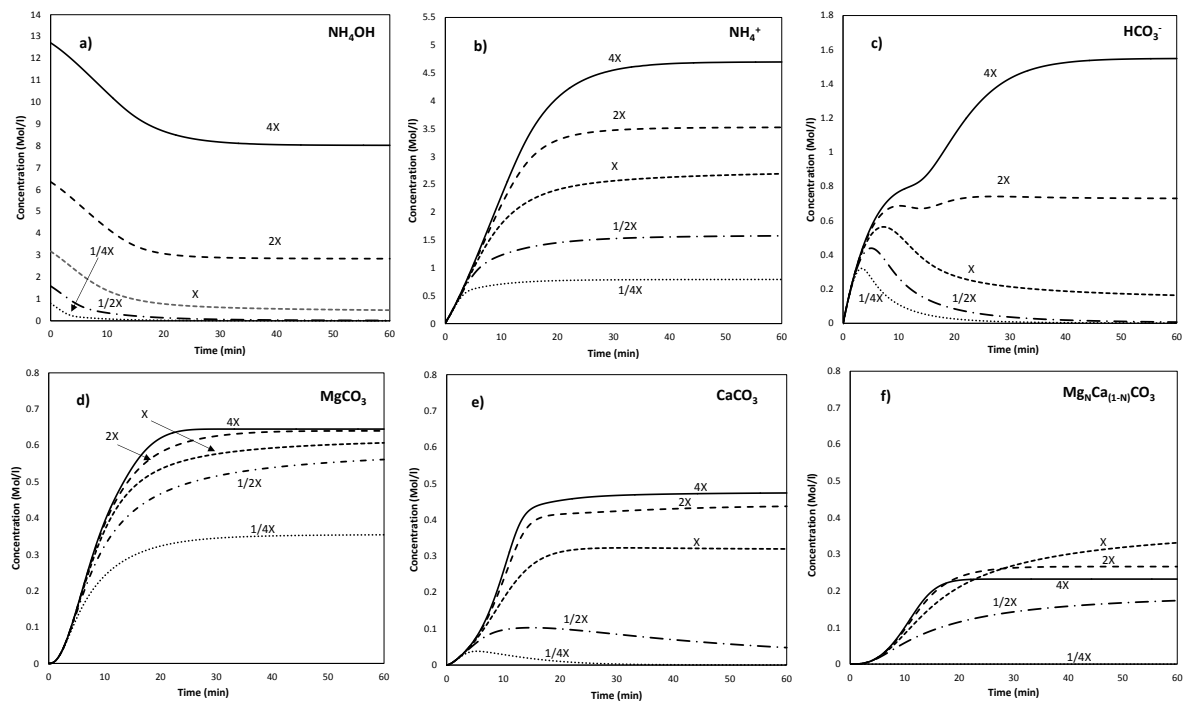


Figure 6.9 Concentration profile of a) NH_4OH , b) NH_4^+ , c) HCO_3^- , d) MgCO_3 , e) CaCO_3 and f) $\text{Mg}_N\text{Ca}_{(1-N)}\text{CO}_3$ upon the change of the initial ammonia concentration by a factor of 2, 4, 1/2 and 1/4. (equal Mg^{2+} and Ca^{2+} concentrations of 0.68 mol/L, CO_2 pressure of 1 atm, room temperature and x refers to the ammonia concentration at reference case (3.18 mol/L))

The concentration profiles of solid precipitate as presented in panels *d*, *e* and *f* can be partially explained by the availability of HCO_3^- upon the dissociation of ammonia in the solution. Irrespective of original ammonia concentration, the HCO_3^- is abundant in the early stage of the reaction, and therefore, the reaction proceeded fast. At a very low NH_4OH concentration of 1/4 of the reference case, nearly the whole Ca^{2+} remained unreacted and only half of the Mg^{2+} ions were carbonated. The amount of magnesian calcite is even negligible, indicating an extremely slow incorporation of Mg^{2+} into calcite under the low ammonia doping condition. Increase in ammonia concentration from 1/4x to x helped improve the precipitation yields of both Mg^{2+} and Ca^{2+} . However, upon a further increase on the ammonia concentration to $2x$ and $4x$, its effect on the yields of solid precipitates is marginal and even insignificant. With regard to the formation rate, a slight acceleration in the magnesian calcite growth rate was observed. The prevalence of HCO_3^- at higher ammonia concentration ($2x$ and $4x$ of the reference case) and tendency in formation of soluble $\text{Mg}^{2+}/\text{Ca}^{2+}$ -bearing bicarbonate are the most likely reasons for the reduction on the final yield of magnesian calcite. However, upon the use of excessive ammonia (*e.g.* $2x$ and $4x$ here), the time to reach equilibrium was shortened to about 15 min, relative to more than 30 min required at the reference case where the amount of ammonia added is exactly the same as that released during the leaching stage. This implies the water-soluble hydroxide is probably one intermediate formed to promote the incorporation of Mg^{2+} into calcite.

6.4.4.4 Effect of the initial CO₂ partial pressure

Figure 6.10 presents the relationship between the initial CO₂ partial pressure and the yields of carbonates at a fixed Mg²⁺/Ca²⁺ molar ratio of 1 in 30 min. The yields of all the three carbonate precipitates were found to strongly depend on the CO₂ partial pressure. Upon increasing the CO₂ partial pressure to 1 atm referring to a pure CO₂ stream at the atmospheric pressure, one can see a rather linear increase on the yields of the two pure carbonates, MgCO₃ and CaCO₃. In general, a sufficiently high CO₂ pressure increases the rate of carbonation reaction with providing more dissolved CO₂ in the solution [47] to react with Mg²⁺ and Ca²⁺. The yields of the two pure carbonates are stabilised from the pressure of 1 atm onwards. This should be due to the completion of the carbonation reaction in 30 min, irrespective of the CO₂ partial pressure. However, the yield of magnesian calcite is maximised at 2 atm, implying a slow incorporation of Mg²⁺ into the calcite crystal lattice.

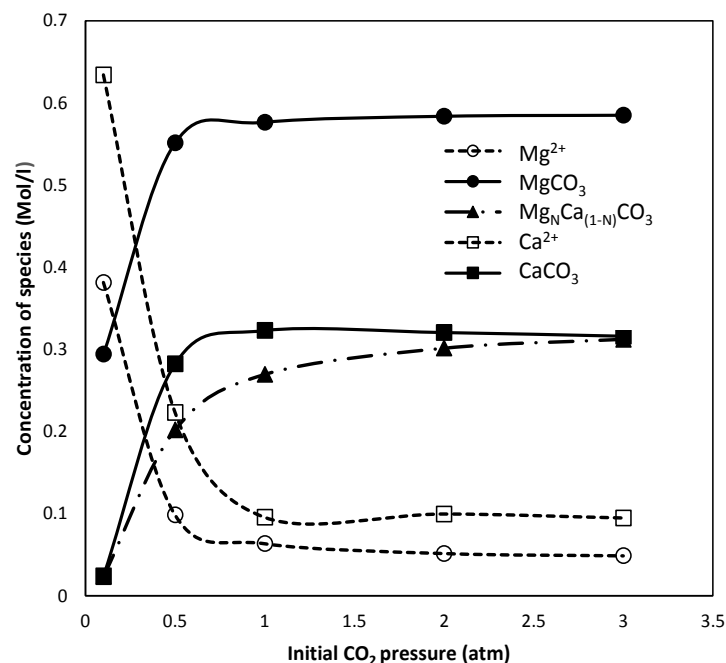


Figure 6.10 Concentrations of different Mg- and Ca-bearing species as a function of the initial CO₂ pressure in 30 min (equal Mg²⁺ and Ca²⁺ concentrations of 0.68 mol/L, room temperature and NH₄OH concentration of 3.18 mol/L)

To further explore the influence of CO₂ partial pressure, the time-resolved concentration profiles for individual species are plotted in **Figure 6.11 a-f**. For the three anions including HCO₃⁻, CO₃²⁻ and CO_{2(aq)}, one can see that these species exhibit a maximum value in the aqueous leachate. The time to reach the maximum value for these species was shortened to varying extent upon the rise of the CO₂ partial pressure. In panel *a*, the peak concentration for HCO₃⁻ was shortened to approximately 5 min, relative to a rather flat and insignificant formation of this anion at a partial pressure of 0.1 atm referring to 10% CO₂ in the atmospheric flue gas discharged

out of a furnace. A quick formation of this species is essential for the formation and precipitation of carbonate, as evident by the reaction equations (R.5) and (R.7). The similar phenomenon was observed for CO_3^{2-} shown in panel *b*. Compared to HCO_3^- , the equilibrium time for CO_3^{2-} is more sensitive to the initial CO_2 pressure. The time required to reach its peak value was shortened from around 40 min to 10 min upon the increase of the CO_2 partial pressure from 0.1 atm through to 3 atm. A rapid formation of this anion is also beneficial in accelerating the carbonate precipitation rate. For the partial pressure of 0.1 atm, the concentration of CO_3^{2-} is also much smaller than other cases and thus the carbonation rate upon the injection of flue gas with an atmospheric pressure is extremely low. As a result, the reactor has to be extremely large. For the higher initial CO_2 pressures, CO_3^{2-} also exhibits a sharp decline in its concentration towards the end of the reaction time. The concentration of $\text{CO}_{2(\text{aq})}$ for the first 10 min of the reaction follows the same trend as HCO_3^- , remaining equilibrated from ~10 min onwards. Increasing the CO_2 partial pressure speeds up its absorption in the leachate, thereby increasing the concentration of $\text{CO}_{2(\text{aq})}$. The CO_2 is also injected continuously into the leachate, and hence, the concentration of CO_2 remains constant after being stabilised.

With respect to the three carbonate precipitates, increasing the partial pressure to 3 atm is clearly beneficial in accelerating their formation rates, *i.e.* decreasing the reaction time. For the two pure carbonates, the reaction time to achieve their equilibrated yields were shortened from nearly infinite at 0.1 atm to around 40 min in 0.5 atm, which was further reduced down to 20 min in 1 atm, and around 10 min in 2-3 atm. The difference between the two highest pressures is marginal, suggesting that an initial CO_2 partial pressure of 2 atm is sufficiently high. Compared to MgCO_3 yield profile showing a relatively small variation upon the rise of CO_2 partial pressure from 0.5 to 3 atm, the yield profile for CaCO_3 is more broad and sensitive, and the reaction time for the termination of CaCO_3 formation also decreased more quickly. More interestingly, the increase in the CO_2 partial pressure is more beneficial for accelerating the incorporation of Mg^{2+} into calcite to form magnesian calcite, as evident in panel *f*. Compared to an infinite time for the maximisation of magnesian calcite at 0.1 atm, increasing the CO_2 partial pressure to 2 atm led to a rapid rise on the formation of this complex carbonate in the first 20 min. Increasing time and CO_2 partial pressure further exerted a marginal effect. Increase in the CO_2 pressure can facilitate the reordering of the magnesian calcite to attract more Mg^{2+} in its crystal lattice. Lippmann (1973) concluded that the presence of activated CO_3^{2-} in the solution resulted from increase in pressure could overcome the magnesium hydration barrier [48]. Therefore, the conversion to dolomite proceeds in the co-existence of Mg^{2+} , excess CO_3^{2-} and pre-existing calcium carbonate particle seeds.

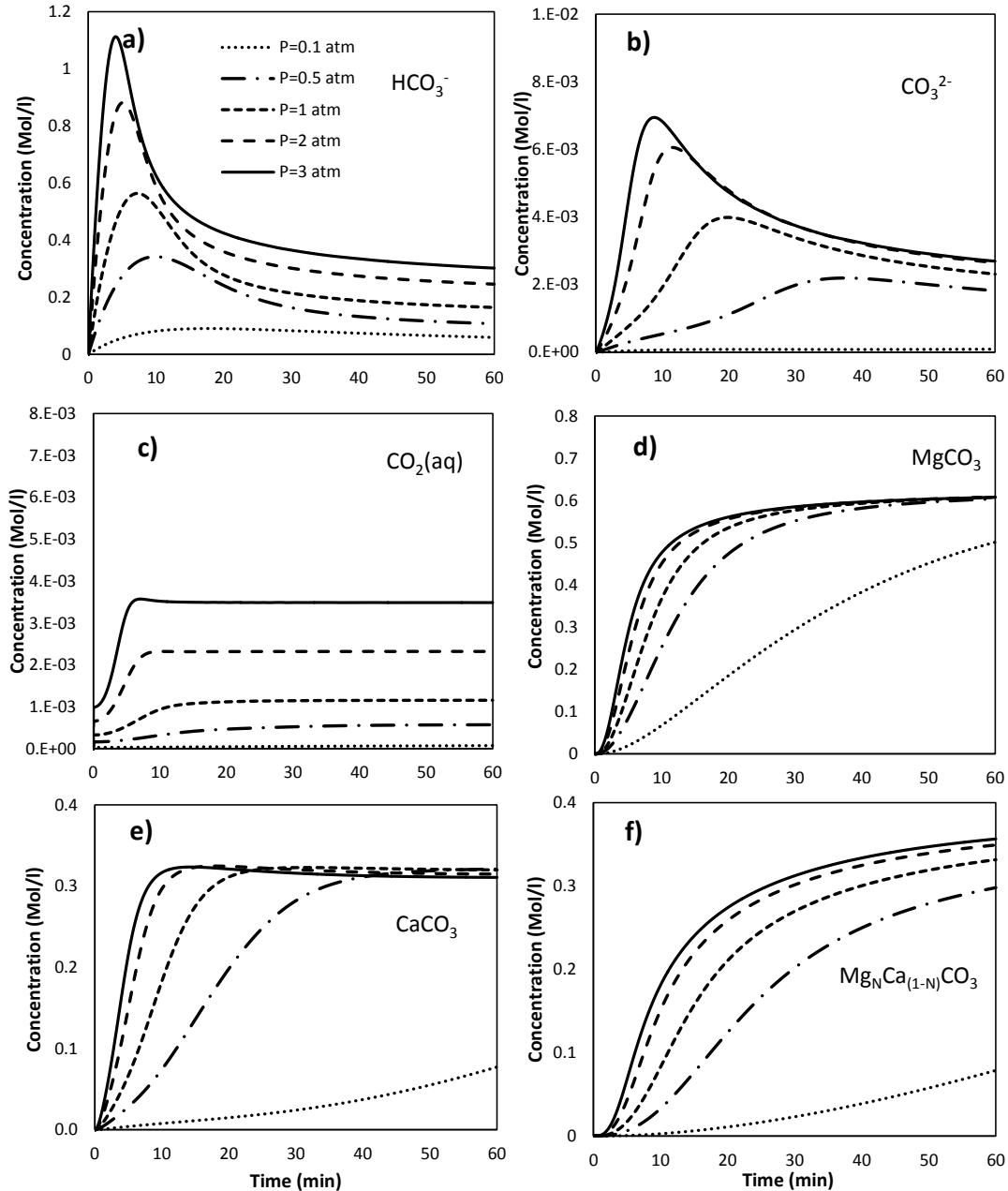


Figure 6.11 Concentration profile for *a)* HCO₃⁻, *b)* CO₃²⁻, *c)* CO₂(aq), *d)* MgCO₃, *e)* CaCO₃ and *f)* Mg_NCa_(1-N)CO₃ at different initial CO₂ pressure

(Equimolar Mg²⁺ and Ca²⁺ concentrations (0.68 mol/L), room temperature, NH₄OH concentration of 3.18 mol/L)

6.4. Conclusions

The modelling on the carbonation behaviour of Ca²⁺ and Mg²⁺ under mild conditions was performed in the co-existence of these two cations together in the leachate. Special attention was paid to establish the kinetic constants governing the formation of magnesian calcite that has yet to be explored in the literature. Moreover, based on a validated model, a sensitivity analysis was further conducted to evaluate the effect of individual operating parameters including the initial

concentrations of Mg^{2+} , Ca^{2+} and NH_4OH and CO_2 partial pressure on the formation rates and yields of individual species. The major conclusions can be drawn as follow:

- 1) After reactor modelling through the use of genetic algorithm as the optimization tool, the average value for the amount of magnesium or N value in the magnesian calcite ($Mg_NCa_{(1-N)}CO_3$) was found to be 0.09, which has been validated for a wide range of operating conditions.
- 2) Based on the sensitivity analysis, the optimum Mg^{2+}/Ca^{2+} molar ratio of one was found to achieve the highest Mg^{2+} and Ca^{2+} co-precipitation rate. Increase in Mg^{2+} concentration decelerated the rate of calcium precipitation while the presence of a certain amount of Ca^{2+} in the solution was in favour of magnesium precipitation. At the Mg^{2+}/Ca^{2+} molar ratios larger than one, the strong competition of Mg^{2+} and Ca^{2+} upon absorbing the dissolved CO_2 led to the decrease in the yields of both calcite and magnesian calcite.
- 3) The carbonation reaction rates of Mg^{2+} and Ca^{2+} were sensitive to the initial NH_4OH concentration up to ~ 4 mol/L which is equal to the amount of ammonia released from the leaching stage in a closed indirect mineral carbonation loop. The excess amount of ammonia slightly decreased the magnesian calcite yield, which, however, has little effect on the total precipitation extent for both Mg^{2+} and Ca^{2+} that remained $\sim 100\%$.
- 4) With respect to the initial CO_2 pressure, the concentration of the Mg/Ca-bearing species in the solution was highly dependent on the CO_2 pressure. At 30 min or longer reaction times, the atmospheric pressure was found to be the optimal condition to achieve the highest carbonation extent. The further increase in the pressure from atmospheric pressure to 2 atm is in favour of the co-precipitation of Mg^{2+} and Ca^{2+} in the form of magnesian calcite.

Acknowledgment

This project is supported by the Faculty of Engineering of Monash University for a 2013-2014 seed grant. The first author is also grateful to Monash Research Graduate School (MRGS) for a PhD scholarship and Faculty of Engineering for Postgraduate Publication Award (PPA). A CSIRO Flagship scholarship fund is gratefully acknowledged for additional support.

References

- [1] Jo, H.Y.; Kim, J.H.; Lee, Y.J.; Lee, M.; Choh, S.J. Evaluation of factors affecting mineral carbonation of CO_2 using coal fly ash in aqueous solutions under ambient conditions. *Chem. Eng. J.* **2012**, 183, 77-87.

- [2] Kodama, S.; Nishimoto, T.; Yamamoto, N.; Yogo, K.; Yamada, K. Development of a new pH-swing CO₂ mineralisation process with a recyclable reaction solution. *Energy* **2006**, 33(5), 776-784.
- [3] Mayoral, M.C.; Andrés, J.M.; Gimeno, M.P. Optimisation of mineral carbonation process for CO₂ sequestration by lime-rich coal ashes. *Fuel* **2013**, 106, 448-454.
- [4] Bonfils, B. ; Julcour-Lebigue, C. ; Guyot, F. ; Bodénan, F. ; Chiquet, P. ; Bourgeois, F. Comprehensive analysis of direct aqueous mineral carbonation using dissolution enhancing organic additives. *Int. J. Greenh. Gas Control* **2012**, 9, 334-346.
- [5] Dri, M.; Sanna, A.; Maroto-Valer, M.M. Dissolution of steel slag and recycled concrete aggregate in ammonium bisulphate for CO₂ mineral carbonation. *Fuel Process. Technol.* **2013**, 113, 114-122.
- [6] Sanna, A.; Dri, M.; Hall, M.R.; Maroto-Valer, M.M. Waste materials as a potential resource for carbon capture and storage by mineralisation (CCSM) in the UK context. *Appl. Energy* **2012**, 99, 545-554.
- [7] Stephens, J.C.; Keith, D.W. Assessing geochemical carbon management. *Climatic Change* **2008**, 90, 217-242.
- [8] Huijgen, W.J.J. ; Comans, R.N.J. Mineral CO₂ sequestration by carbonation of industrial residues. Literature review and selection of residues, **2005**.
- [9] Carey, J.W.; Rosen, E.P.; Bergfeld, D.; Chipera, S.J.; Counce, D.A.; Snow, M.G.; Ziock, H.J.; Guthrie, G.D. Experimental studies of the serpentine carbonation reaction. 28th International Technical Conference on Coal Utilisation & Fuel Systems, Coal Technology Association, Clearwater, FL, USA, **2003**.
- [10] Huijgen, W.J.J., Comans, R.N.J. Carbon dioxide sequestration by mineral carbonation, literature review. Energy research Centre of the Netherlands, ECN-C-03-016, Petten, The Netherlands, **2003**.
- [11] Guthrie, G.D.; Carey, J.W.; Bergfeld, D.; Byler, D.; Chipera, S.; Ziock, H.J.; Lackner, K.S. Geochemical aspects of the carbonation of magnesium silicates in an aqueous medium, NETL mineral sequestration workshop, **2001**.
- [12] Wu, J.C.S.; Sheen, J.D.; Chen, S.Y.; Fan, Y.C. Feasibility of CO₂ fixation via artificial rock weathering. *Ind. Eng. Chem. Res.* **2001**, 40/18, 3902-3905.
- [13] Baciocchi, R.; Costa, G.; Polettini, A.; Pomi, R.; Prigiobbe, V. Comparison of different reaction routes for carbonation of APC residues. *Energy Procedia* **2009**, 1, 4851-4858.

- [14] Reddy, K.J.; John, S.; Weber, H.; Argyle, M.D.; Bhattacharyya, P.; Taylor, D.T.; Christensen, M.; Foulke, T.; Fahlsing, P. Simultaneous capture and mineralisation of coal combustion flue gas carbon dioxide (CO₂). *Energy Procedia* **2011**, 4, 1574-1583.
- [15] Teir, S. Fixation of carbon dioxide by producing carbonates from minerals and steelmaking slags. Doctoral Dissertation. Helsinki University of Technology, Espoo, Finland, **2008**.
- [16] Velts, O.; Uibu, M.; Kallas, J.; Kuusik, R. CO₂ mineral trapping: modelling of calcium carbonate precipitation in a semi-batch reactor. *Energy Procedia* **2011**, 4, 771-778.
- [17] Mattila, H.P.; Grigaliunaite, I.; Zevenhoven, R. Chemical kinetics modelling and process parameter sensitivity for precipitated calcium carbonate production from steelmaking slags. *Chem. Eng. J.* **2012**, 192, 77-89.
- [18] Eloneva, S. Reduction of CO₂ emissions by mineral carbonation: steelmaking slags as raw material with a pure calcium carbonate end product. Doctoral Dissertation. Aalto University, School of Science and Technology, Espoo, Finland, **2010**.
- [19] Hosseini, T.; Selomulya, C.; Haque, N.; Zhang, L. Indirect Carbonation of Victorian Brown Coal Fly Ash for CO₂ Sequestration: Multiple-Cycle Leaching-Carbonation and Magnesium Leaching Kinetic Modelling. *Energy Fuels* **2014**, 28(10), 6481-6493.
- [20] Hosseini, T. ; Selomulya, C. ; Haque, N. ; Zhang, L. ; Investigating the Effect of Mg²⁺/Ca²⁺ Molar Ratio on the Carbonate Speciation during the Mild Mineral Carbonation Process at Atmospheric Pressure. *Energy Fuels* **2015**, 29(11), 7483-7496.
- [21] Daval, D.; Martinez, I.; Corvisier, J.; Findling, N.; Goffé, B.; Guyot, F. Carbonation of Ca-bearing silicates, the case of wollastonite: Experimental investigations and kinetic modelling. *Chem. Geol.* **2009**, 1-2, 63-78.
- [22] Sun, Y.; Parikh, V.; Zhang, L. Sequestration of carbon dioxide by indirect mineralisation using Victorian brown coal fly ash. *J. Hazard. Mater.* **2012**, 209-210, 458– 466.
- [23] Bravo, R.V.; Camacho, R.F.; Moya, V.M.; Garcia, L.A.I. Desulphurisation of SO₂-N₂ mixtures by limestone slurries. *Chem. Eng. Sci.* **2002**, 57 (11), 2047-2058.
- [24] Sun, Y.; Yao, M.S.; Zhang, J.P.; Yang, G. Indirect CO₂ mineral sequestration by steelmaking slag with NH₄Cl as leaching solution, *Chem. Eng. J.* **2011**, 173(2), 437-445.
- [25] Liu, X.Y. (ed.) Bioinspiration: From Nano to Micro Scales, Biological and Medical Physics, Biomedical Engineering, Springer, **2012**.
- [26] Loste, E.; Wilson, R.M.; Seshadri, R.; Meldrum, F.C. The role of magnesium in stabilising amorphous calcium carbonate and controlling calcite morphologies. *J. Cryst. Growth* **2003**, 254, 206–218.

- [27] Donners, J.J.J.M.; Heywood, B.R.; Meijer, E.W.; Nolte, R.J.M.; Roman, C.; Schenning, A.P.H.J.; Sommerdijk, N.A.J.M. Amorphous calcium carbonate stabilised by poly (propylene imine) dendrimers. *Chem. Commun* **2000**, 19, 1937–1938.
- [28] Xu, J.; Yan, C.; Zhang, F.; Konishi, H.; Xu, H.; Teng, H.H. Testing the cation-hydration effect on the crystallisation of Ca–Mg–CO₃ systems; Proceedings of the national academy of sciences of the United States of America, **2013**.
- [29] Althoff, P.L.. Structural refinements of dolomite and a magnesian calcite and implications for dolomite formation in the marine environment. *Am. Mineral.* **1977**, 62 (7–8), 772-783.
- [30] Boyd, V.; Yoon, H.; Zhang, C.; Oostrom, M.; Hess, N.; Fouke, B.; Valocchi, A.J.; Werth, C.J. Influence of Mg²⁺ on CaCO₃ precipitation during subsurface reactive transport in a homogeneous silicon-etched pore network. *Geochim. Cosmochim. Acta* **2014**, 135, 321-335.
- [31] Fernandez-Diaz, L.; Putnis, A. The role of magnesium in the crystallisation of calcite and aragonite in a porous medium. *J. Sediment. Res.* **1996**, 66(3), 482-491.
- [32] Santos, R.M.; Van Bouwel, J.; Vandeveld, E.; Mertens, G.; Elsen, J.; Van Gerven, T. Accelerated mineral carbonation of stainless steel slags for CO₂ storage and waste valorisation: Effect of process parameters on geochemical properties. *Int. J. Greenh. Gas Con.* **2013**, 17, 32-45.
- [33] Daneshpayeh, M.; Khodadadi, A.; Mostoufi, N.; Mortazavi, Y.; Sotoudeh-Gharebagh, R.; Talebizadeh, A. Kinetic modelling of oxidative coupling of methane over Mn/Na₂WO₄/SiO₂ catalyst. *Fuel process. Technol.* **2009**, 90 (3), 403-410.
- [34] Konigsberger, E.; Gamsjager, H. Solid-solute phase equilibria in aqueous solution: VII. A re-interpretation of magnesian calcite stabilities. *Geochim. Cosmochim. Acta* **1992**, 56, 4095-4098.
- [35] Danckwerts, P.V. Gas-liquid Reactions. McGraw-Hill Book Company, New York, **1970**.
- [36] Fatemi, S.; Masoori, M.; Boozarjomehri, R. Application of genetic algorithm in kinetic modelling and reaction mechanism studies. *Iran. J. Chem. Chem. Eng.* **2005**, 24 (4).
- [37] Vatani, A.; Jabbari, E.; Askarieh, M.; Torangi, M.A. Kinetic modelling of oxidative coupling of methane over Li/MgO catalyst by genetic algorithm. *J. Nat. Gas Sci. Eng.* **2014**, 20, 347-356.
- [38] Shah, S.I.A.; Kostiuik, L.W.; Kresta S.M. The Effects of Mixing, Reaction Rates, and Stoichiometry on Yield for Mixing Sensitive Reactions—Part I: Model Development. *Int. J. Chem. Eng.* **2012**, Article ID 750162.

- [39] Rendek, E.; Ducom, G.; Germain, P. Carbon dioxide sequestration in municipal solid waste incinerator (MSWI) bottom ash. *J. Hazard. Mater.* **2006**, B12, 873-879.
- [40] Levenspiel, O., Chemical Reaction Engineering, John Wiley and Sons, New York, **1999**.
- [41] Kitano, Y.; Hood, D.W. Calcium carbonate crystal forms formed from sea water by inorganic processes. *The Journal of the Oceanographic Society of Japan* **1962**, 18 (3), 141–145.
- [42] Santos, R.M.; Bodor, M.; Dragomir, P.N.; Vraciu, A.G.; Vlad, M.; Van Gerven, T. Magnesium chloride as a leaching and aragonite-promoting self-regenerative additive for the mineral carbonation of calcium-rich materials. *Miner. Eng.* **2014**, 59, 71–81.
- [43] Mitchell, M.J.; Jensen, O.E.; Cliffe, K.; Maroto-Valer, M.M. A model of carbon dioxide dissolution and mineral carbonation kinetics. *Proc. R. Soc. A.* **2010**, 466 (2117), 1265–1290.
- [44] Kierzkowska-Pawlak, H. Determination of kinetics in gas-liquid reaction systems. An overview. *Ecol. Chem. Eng.* **2012**, S. 19 (2), 175.196.
- [45] Lide, D.R., CRC Handbook of Chemistry and Physics, 71 ed. Boca Raton, Ann Arbor, Boston: CRC Press, **1990-1991**.
- [46] Ahn, C.K.; Lee, H.W.; Lee, M.W.; Chang, Y.S.; Han, K. Determination of ammonium salt/ion speciation in the CO₂ absorption process using ammonia solution: Modelling and experimental approaches. *Energy Procedia* **2011**, 4, 541–547.
- [47] Chang, E.E.; Pan, S.Y.; Chen, Y.H.; Chu, H.W.; Wang, C.F.; Chiang, P.C. CO₂ sequestration by carbonation of steelmaking slags in an autoclave reactor. *J. Hazard. Mater.* **2011**, 195, 107–114.
- [48] Lippmann, F. Sedimentary Carbonate Minerals, Minerals, Rocks and Inorganic Materials, Monograph Series of Theoretical and Experimental Studies. v. 4: Berlin, Springer-Verlag, p. 228, **1973**.

Monash University

Declaration for Thesis Chapter 7

Declaration by candidate

In the case of Chapter 7, the nature and extent of my contribution to the work was the following:

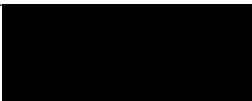
Nature of contribution	Extent of contribution (%)
Key idea, Simulation, techno-economic analysis using software and hand calculation, writing up	100 %

The following co-authors contributed to the work. If co-authors are students at Monash University, the extent of their contribution in percentage terms must be stated:

Name	Nature of contribution	Extent of contribution (%) for student co-authors only
Lian Zhang	Editing paper, comments and feedback	Supervisor
Cordelia Selomulya	Editing paper, comments and feedback	Supervisor
Nawshad Haque	Editing paper, comments and feedback	Supervisor

The undersigned hereby certify that the above declaration correctly reflects the nature and extent of the candidate's and co-authors' contributions to this work*.

Candidate's Signature		Date 12/11/2015
--------------------------	---	--------------------

Main Supervisor's Signature		Date 12/11/2015
-----------------------------------	---	--------------------

*Note: Where the responsible author is not the candidate's main supervisor, the main supervisor should consult with the responsible author to agree on the respective contributions of the authors.

Chapter 7

Simulation and techno-economic analysis of the overall process

In the previous chapters, leaching and carbonation sub-processes were examined experimentally. From the experimental results, the possibility of utilisation of Victorian brown coal fly ash through indirect mineral carbonation was confirmed. This chapter further discusses the process from technical and economical point of view. Four different scenarios, two aiming in selection of the best leaching agent and the last two, targeting waste minimisation with modification of the main process, were considered. The concepts based on experimental data were modelled and simulated using process flow-sheeting software Aspen Plus[®]. Then, the mass and energy balances results were used to assess the preliminary economic analysis using Aspen process economic analyser. This chapter has been reformatted from the following submitted manuscript to Applied Energy Journal: **T. Hosseini**, N. Haque, C. Selomulya, L. Zhang, Mineral Carbonation of Victorian Brown Coal Fly Ash Using Regenerative Ammonium Chloride – Process Simulation and Techno-economic Analysis.

7.1 Abstract

This report examined the technical and economic feasibility of four process scenarios for the mineral carbonation of Victorian brown coal fly ash. The first two design scenarios aimed to compare the performance of two leaching agents, namely, ammonium chloride (NH_4Cl) and a mixture of ammonium chloride and hydrochloric acid ($\text{NH}_4\text{Cl}+\text{HCl}$), on product yields and cost, whereas the other two scenarios were designed to recycle the leaching residue *via* single or multi-stage leaching steps to co-produce a carbonate precipitate and cement additive-grade by-product. Detailed designs were developed in Aspen Plus to determine the technical and economic potential of the selected process configurations and identify the concept with the lowest overall costs relative to the product yields. As has been confirmed, the overall production costs and carbon dioxide (CO_2) capture cost of the evaluated process scenarios range from ~\$61 to 333 per tonne of product and from \$135 to 1091 per tonne of CO_2 , respectively. The process scenario that used $\text{NH}_4\text{Cl}+\text{HCl}$ as the leaching reagent had a significantly larger cost and a higher carbonation conversion compared to the other scenarios. The process configuration that recycled the leaching residue resulted in the lowest cost per tonne of fly ash and the lowest CO_2 capture cost among the four proposed scenarios. The largest net present value (NPV) and the internal rate of return (IRR) as well as the shortest payback period for this scenario further confirmed its highest profitability. The NPV, IRR and payback period of \$49 million, 53.4% and 2.3 years, respectively, could be achieved using Victorian brown coal fly ash in this scenario. A sensitivity analysis suggests that the change in the ammonium chloride price exerts the largest effect on the production cost. A 50% increase in the ammonium chloride cost could result in the production cost increasing by 29.5%. Additionally, the selling price of the carbon precipitate product and the production cost strongly affect the financial indices. However, the production of the cement-additive by-product exerts a marginal role on the process profit. The extra income created from the cement-additive by-product is counteracted by the larger cost related to the purchase and consumption of hydrochloric acid used in the final leaching stage.

7.2 Introduction

Fossil fuel combustion was responsible for approximately 31 Gt of CO_2 emissions into the atmosphere in 2011, and this amount is expected to increase to 57 Gt in 2050 [1]. Due to the significant concerns for global warming, carbon dioxide capture and storage (CCS) is considered to be one of the potential options for addressing the increase of CO_2 concentration in the atmosphere and climate change mitigation. [2-5]. Although CO_2 geological storage is the only option that has been practically used in the industry [2], storing CO_2 as a mineral carbonate has received increased attention due to its numerous advantages, particularly its small environmental load in terms of product disposal [6,7]. Furthermore, the resultant carbonate can be used in a

value-added way. The growing interest in the development of mineral carbonation methods still requires intensive investigation to reduce its cost and demonstrate potential applications for these technologies in existing power plants [8].

In mineral carbonation, carbon dioxide is fixed with divalent metal oxides, such as magnesium and calcium, from natural minerals or industrial wastes to produce stable carbonate as an end product [2,9]. Despite the intrinsic advantages of mineral carbonation, it still suffers from two major drawbacks: prohibitive energy consumption and poor economic aspects [10]. Efforts to accelerate the kinetic reaction and reduce the required activation energies have motivated the development of an indirect mineral carbonation process using two separate steps for mineral leaching and CO₂ capture [10,11]. Indirect mineral carbonation involves the extraction of the reactive minerals prior to carbonation [12]. This method is appealing due to the possibility of occurring under mild operating conditions (*i.e.*, temperature <100°C and pressure up to 5 bar) and producing high-purity carbonate with a high market value [13]. To ensure that this process is economically and environmentally sustainable, the chemicals used in the process need to be regenerated within the process itself [14]. The leaching media for the dissolution of calcium and magnesium in the minerals are either strong or weak acidic reagents, ammonium salts, or alkaline solutions [15-17]. Among them, the ammonium extraction process appears to be a favourable technique, given its potential for reagent recovery and the relatively large selectivity of magnesium and calcium over other elements [17,18].

Coal-fired power plants, which provide ~ 40% of the world's electricity and annually generate 12,000 Mt of CO₂ and 600 Mt of fly ash (FA) [19], could benefit from this option by using its own by-products, *i.e.*, fly ash for CO₂ sequestration. Generally, approximately 30% of the fly ash produced in coal power plants, which has a high content of calcium (Ca), aluminium (Al) and silicate (Si), is used for construction materials [3,19]. The maximum CO₂ sequestration potential of bituminous coal fly ash is relatively low (~9%); however, it could reach as high as 43-49% for Ca-rich lignite or low-rank coal fly ash [19,20]. The high-Ca fly ash (>20%) produced from lignite or sub-bituminous coals is comprised of Ca-Al-Si glass and a wide variety of crystalline phases. These crystalline phases can react with water and harden due to the formation of cementitious hydration products, which causes the fly ash to react more rapidly than low-Ca ash and renders the fly ash both pozzolanic and hydraulic [21]. However, excessive amounts of magnesia (MgO) or free lime (CaO) in the cementitious materials may cause undesirable volume changes when these materials are used in concrete [21]. It was determined that an MgO content of up to 5% in cement is useful for modifying the shrinkage behaviour of concrete [22]. A prior removal of free MgO and CaO out of the fly ash in a mineral carbonation process can selectively remove and convert free MgO and CaO into carbonates. In addition to the above-mentioned benefits for a typical mineral carbonation process, this process is also

beneficial for the production of cement additive-grade by-products. The development of an appropriate mineral carbonation technology using fly ash as feedstock may help enhance the economic, technological and environmental benefits of fly ash [23].

Currently, only a few commercial technologies are available for the carbonation of industrial wastes [24,25]. Thus far, the most comprehensively studied process for fly ash carbonation is the direct route, which involves high temperature and CO₂ pressure in the range of 100 to 500°C and 10-20 bar, respectively [3, 20,26-29]. Montes-Hernandez et al. (2009) achieved a carbonate conversion of 82% and a carbon sequestration capacity of 26 kg CO₂/t ash at 30°C and 10 bar initial CO₂ pressure over 18 h in water [20]. Uliasz-Bochenczyk et al. (2009) achieved a maximum carbon sequestration capacity of 7.85 g CO₂/100 g ash at ambient temperatures and 10 bar CO₂ initial pressure over 24 h in water [26]. There is a noticeable lack of published techno-economic feasibility studies in this area that could potentially support the feasibility of these processes [19,30]. It is envisioned that mineral carbonation demonstration plants of up to 1Mt CO₂ per annum may be operational as early as 2020 [31].

We previously tested the possibility of the application of Victorian brown coal fly ash in the indirect mineral carbonation process [13]. This process involved the use of ammonium chloride (NH₄Cl), which initially extracted the free MgO and CaO in the fly ash into an aqueous form *via* the substitution reaction of $\text{NH}_4^+ + \text{Ca/MgO} = \text{NH}_3(\text{g}) + \text{Ca}^{2+}/\text{Mg}^{2+}$. The resulting Ca²⁺ and Mg²⁺ cations were subsequently carbonated *via* a continuous bubbling of CO₂-containing flue gas and ammonia (NH₃) for pH control. These ammonium salt solvents were found to be recyclable, although minor losses of ammonia were noted [13]. The objectives of the research presented here is to evaluate whether the proposed mineral carbonation method could be scaled up to a relative large scale for both the CO₂ capture and the production of high-purity carbonate products to be sold to compensate for the high cost of the process. Process flow-sheeting was initially schemed using Aspen Plus[®] based on our earlier experimental studies. Subsequently, four different scenarios were established to optimise the process integration to minimise the process energy consumption. Then, an economic analysis was conducted using the US-based economic analysis package as well as a modified version to assess the cost for different contexts in the world. Lastly, a sensitivity analysis was performed to examine the variation in the production cost with different operating and economical parameters, and a cash flow analysis was performed to clarify the profitability of the process by determining its net present value (NPV), internal rate of return (IRR) and payback period.

7.3 Methodology

7.3.1 Process description

The block diagram of the proposed mineral carbonation process using regenerative ammonia chloride is presented in **Figure 7.1**, including the system boundaries of this study. The mineral carbonation plant was assumed to be located next to the Victorian brown coal-fired power plant, which produces both fly ash and flue gas in Latrobe Valley, Australia. The overall process consists of two major areas: fly ash leaching and carbonation. Fly ash was assumed to be supplied free, as slurry, at the battery limits. In this study, the fly ash produced by the International Power Hazelwood power plant was used as a feedstock. The typical fresh and weathered fly ash compositions used for simulation as well as the variation range of individual species are presented in **Table 7.1** [32]. Depending on the ageing extent and the heterogeneity of the coal, the composition of the fly ash is considerably variable. Due to the limitations of the model to consider all of these changes, an average composition of a typical fresh and weathered fly ash was used as the input data. Despite the potential uncertainties in the production yield when changing the fly ash composition, a sensitivity analysis can predict a few of these changes and provide more flexibilities to link the model to actual cases.

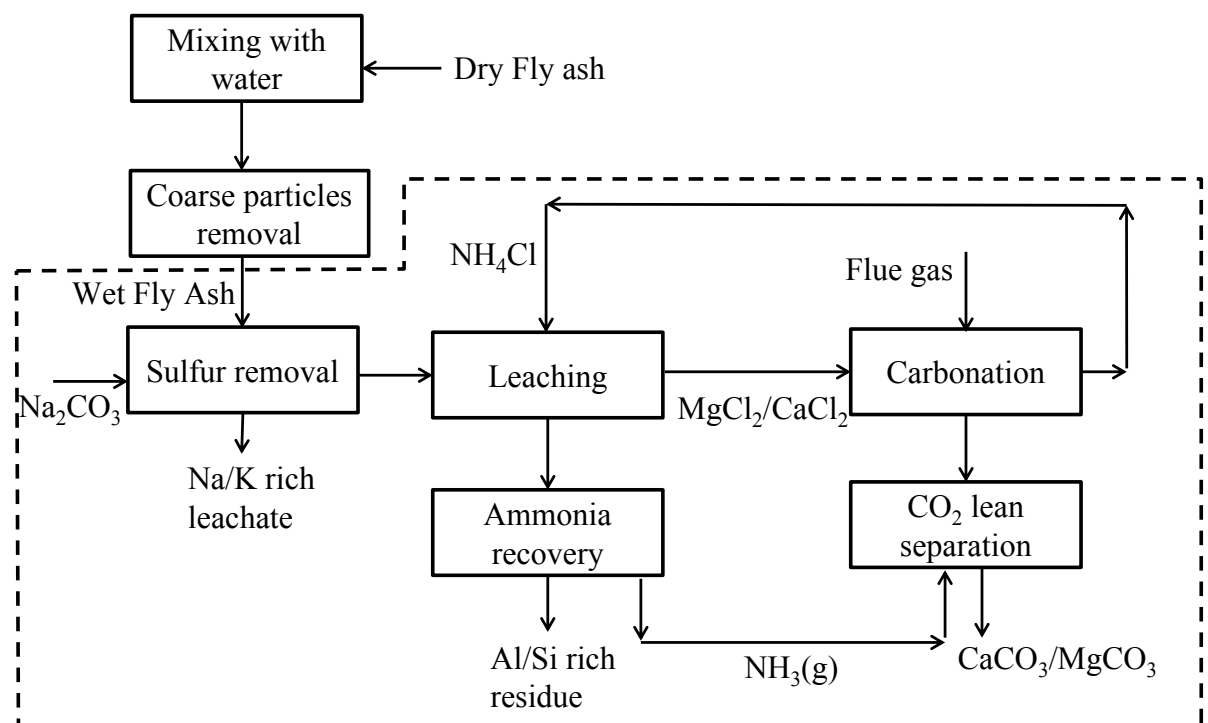
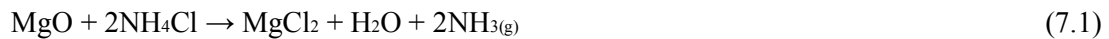


Figure 7.1 Proposed block flow diagram and system boundary for mineral carbonation of Victorian brown coal fly ash

Table 7.1 Typical compositions of Hazelwood fly ash

Components	Composition (wt.%)		
	Fresh fly ash	Weathered fly ash	Variation range
SiO ₂	5	4	1-5
CaFe ₂ O ₅	12	1.5	2-15
Al ₂ O ₃	2	-	2-5
Fe ₂ O ₃	6	6.5	6-8
CaO	16	5	5-20
MgO	30	25	20-30
MgCO ₃	0	5	0-5
CaCO ₃	10	25	10-25
CaSO ₄	18	18	10-20
Water	1	10	0-10

In the mineral carbonation process, the dry fly ash first undergoes sieving to remove silica and unburnt carbon particles. Subsequently, it is mixed with water and pumped to the leaching reactor. The flow rate of the ash-water slurry was assumed to be 25 tonne/h for a plant capacity of ~100,000 tonne/year of products. In the leaching stage, the fly ash can be mixed with an NH₄Cl solution in the leaching reactor to extract the free MgO and CaO [13] as follows:



The heat required for these two reactions can be provided by the low-pressure steam from the adjacent power plant and partly from the hot, recycled ammonium chloride in the carbonation tank. The solution exhibits alkalinity due to the continuous production of ammonia vapour in the above equations [18], which can be trapped by water into a liquid phase in a flash separator at 100°C. After the solid-liquid separation, the leachate rich in Ca²⁺ and Mg²⁺ passes to the carbonation reactor, where the leachate comes into contact with the CO₂-containing flue gas for carbonation. Meanwhile, the ammonia water derived from the leaching step is also added into the carbonation tank to increase the alkalinity of the solution [14,18]. Consequently, based on equations (7.3) and (7.4), Ca²⁺ and Mg²⁺ precipitate as solid carbonates whereas NH₄Cl is regenerated [13].



7.3.2 Model development

The continuous process was implemented in Aspen Plus[®] V8.4 using its solid modelling capabilities to establish material balances as well as energy and utility requirements. The fresh ash, whose composition is indicated in Table 7.1, was first simulated to optimise the process integration. Subsequently, the weathered fly ash was simulated to evaluate the process robustness upon the variation in the fly ash composition. For the fresh fly ash, it was confirmed that nearly all Mg was in the form of MgO while Ca was present in CaO, CaCO₃, CaSO₄ and CaFe₂O₅; furthermore, the remaining feedstock consisted of Si, Fe and Al in oxide form [32].

Due to the presence of ionic species in the system and considering the non-ideality of the liquid phase, the liquid and vapour properties were computed using the NRTL (Non-Random Two Liquid) method, which is an activity-coefficient based model. This model uses Henry's Law to calculate the solubility of CO₂ and NH₃ in water [33]. The equilibrium constant for the precipitates were regressed from the solubility data extracted from the Aspen model. The chemistry feature was used to define different components as soluble salts, non-soluble or partially soluble for the vapour-liquid-solid tertiary equilibrium [34]. HSC chemistry was used to estimate the missing properties in the Aspen database. If necessary, DHSFORM (solid heat of formation) was added into the Aspen database for a conventional solid.

The leaching and carbonation reactors were modelled using a stoichiometric reactor block (RStoic) [35]. The reaction stoichiometry was specified for each component as well as the fractional conversion of the relevant components. It was assumed that under this condition, 33% and 36% of MgO and CaO were leached, respectively, based on our previous experimental results [13]. Because reaction (7.1) in the leaching stage is endothermic, a jacketed agitated reactor with steam coils was used to maintain the reactor at 80°C. Ammonia vapour released during the leaching reactions is collected through a vapour-liquid flash separator at 100°C. The resulting leachate is separated from the unreacted solid residue using a solid-liquid separation filter and pumped into the carbonation reactor. Flue gas from the adjacent power plant, which contains 15% CO₂ at 150°C, is fed to the continuously cooled carbonation reactor, as the carbonation reaction is highly exothermic [36]. The reactor temperature is set at 60°C, which was proven to be the optimum carbonation temperature [37,38]. The hot regenerated ammonium chloride stream, after being mixed with the fly ash and make-up stream for ammonium chloride, is used to pre-heat the inlet streams of the leaching reactor. The unreacted hot flue gas passes through the solution and leaves the reactor from its top. In simulation, this step is depicted by a flash separator due to the limitations of RStoic (it should be noted that in reality, this separation can take place inside the reactor due to the continuous injection of hot gas in the reactor). The solid product is separated from the liquid phase by filtration, and the regenerated ammonium

chloride is recycled. The ammonium chloride make-up is added into the process to ensure an identical flow rate of ammonium chloride in each pass. A purge is used in both the liquid and main gas recycles to avoid the probable accumulation of impurities (*i.e.*, soluble salts leached from the feedstock and gaseous impurities in the CO₂ feed, such as N₂) [34]. **Table 7.2** summarises all of the assumptions used in the simulation.

Table 7.2 Assumptions used within the Aspen Plus simulation for the unit operations

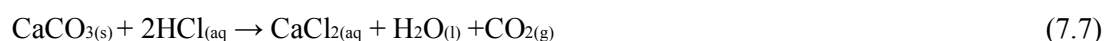
Unit operation	Assumptions
Pumps	Centrifugal pump for liquids and rotary lobe pump for slurries
Pump efficiency (%)	75
Reactors	Stoichiometric reactor
pressure drop	1 bar [39]
Leaching	
MgO leaching %	33 [13]
CaO leaching %	36 [13]
Carbonation	
Mg carbonation %	99 [13,38]
Ca carbonation %	99 [13,38]
Separators	pressure filters
separation efficiency for solid %	98 [39]
separation efficiency for liquid %	98 [39]
Flash separators	vertical process vessels
pressure drop	0.5 bar

7.3.3 Four proposed scenarios with different process integration

Four scenarios were proposed for the integration of the individual steps in this study, as depicted in **Figure 7.2**. The first two scenarios were proposed to examine the effects of the leaching reagent (NH₄Cl versus NH₄+HCl mixture) on the overall performance of the process.

Scenario 1 is the simplest process, which represents the leaching of fly ash with regenerative ammonium chloride followed by the carbonation reaction. In principle, the use of ammonium salt for the leaching process is superior over acidic leaching because it can be recovered readily and reused in a closed loop [40]. However, the ammonium salt leaching capacity is limited when the target metals are bound with other metallic compounds in a stable structure [32,41]. Even for the free MgO and CaO, the extent of leaching in the ammonium salt is low due to the gradual increase in the pH of the leachate upon the dissolution of MgO and CaO [13]. Thus, it was

postulated that maintaining a constant pH by doping concentrated HCl (*i.e.*, pH-controlled leaching) would be beneficial in improving the leaching yields of the target elements as well as creating a residue with minimal free oxides [32]. Furthermore, HCl can rapidly attack the unreacted CaO, MgO and CaCO₃ particles, which are deeply embedded in the ash matrix. However, HCl regeneration is not easy, and its consumption imposes a remarkable expense on the process [42]. Therefore, there is a trade-off between the additional raw material costs and the product yield. To examine the effects of the addition of HCl on the product rate as well as its cost, 20 t/h of HCl (based on a constant pH of ~4-4.5 [32]) was initially added to the ammonium chloride solution in the leaching stage; this process was simulated as *Scenario 2*. In addition to reactions (7.1) and (7.2), three extra reactions occur inside the leaching reactor as follows:



The mass yields of each reaction were determined to match the experimentally determined total yield of 50% and 45% for Ca and Mg, respectively [32]. Based on the thermodynamic calculation and Gibbs free energy of reaction, CaFe₂O₅ and CaSO₄ react with neither HCl nor NH₄Cl at low temperatures. For both scenarios, the leached solid residue after separation from the leachate is returned to the ash pond.

In Scenario 2, which uses NH₄Cl mixed with HCl as a leaching reagent, room temperature is sufficient, and it is not necessary to preheat the feed for the leaching stage [32]. However, at such a low temperature, *i.e.*, room temperature, the solubility of the ammonia gas is very high, and the produced ammonia from equations (7.1 and 7.2) remains in the aqueous phase. Kodama et al. (2008) used Aspen Plus to calculate the water-solubility of NH₃ under atmospheric pressure by following the Peng-Robinson method. They determined that the solubility decreased when the temperature increased from 40 to 90°C [18]. Therefore, the ammonia recovery step is eliminated. However, because the pH of the resulting leachate is not high enough for the carbonation reaction, the make-up stream of ammonia solution (30% ammonia) is still necessary. Instead, the make-up of ammonium chloride is not required.

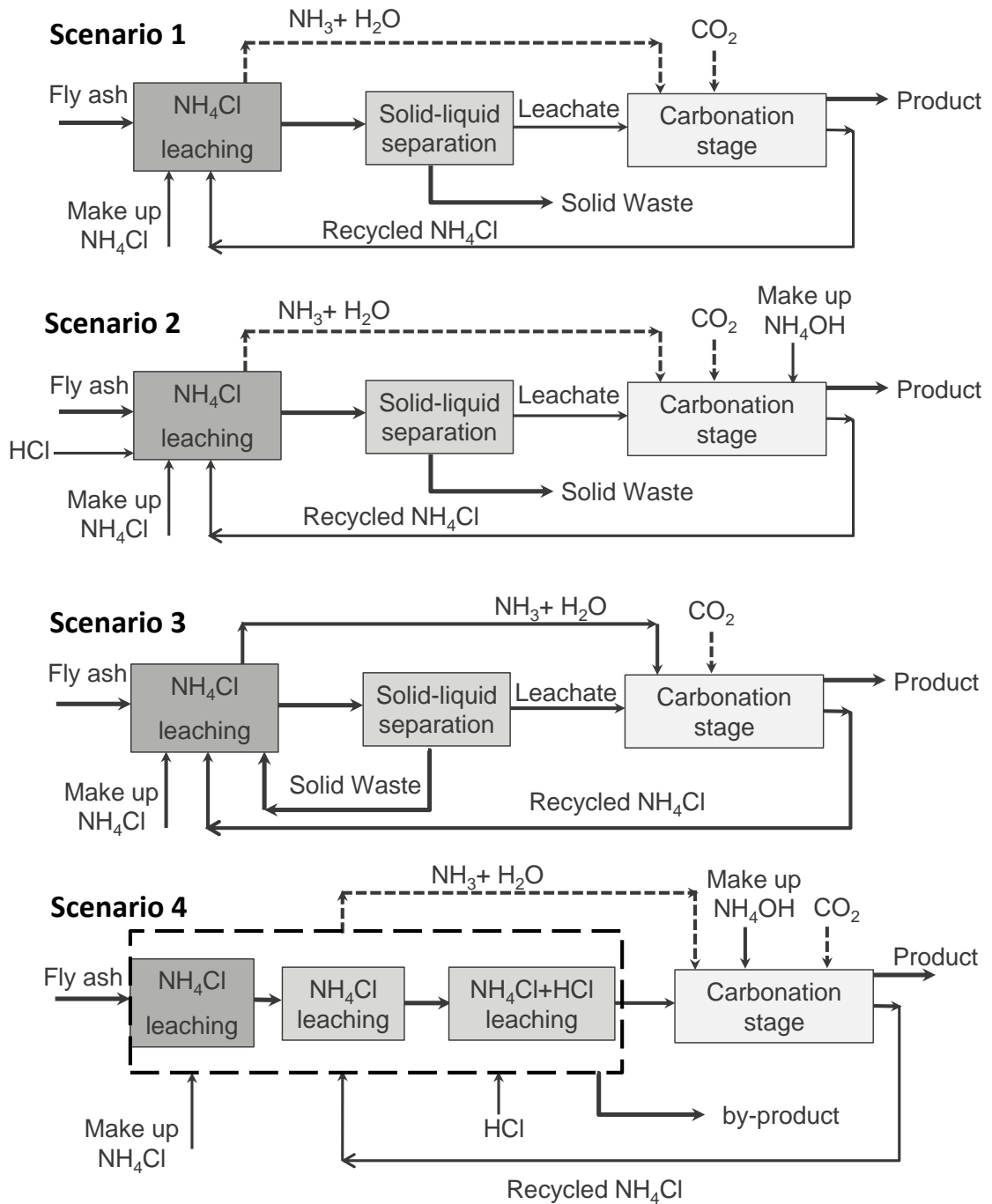


Figure 7.2 Simplified diagram for Scenario 1 (NH_4Cl leaching), Scenario 2 ($\text{NH}_4\text{Cl} + \text{HCl}$ leaching), Scenario 3 (NH_4Cl leaching with leaching waste recycling) and Scenario 4 (Multiple cycle leaching)

Scenarios 3 and 4 were further designed to modify the ammonium chloride leaching process, targeting the minimisation of waste/residue and the production of a cement additive-grade by-product leaching residual. *Scenario 3* was aimed to extract the maximum amount of free CaO and MgO out of the fly ash. This process is based on repeatedly recycling the leached residue back to the leaching tank until the contents of these two free oxides are reduced to 5%, which is the maximum allowable oxide content in a cement additive. To use the same size leaching tank

as in Scenario 1, the original fresh fly ash flow rate was decreased in this scenario. Moreover, an extra pump was added to recycle the leaching residue back into the leaching tank. In this scenario, the effects of the decrease in the initial fly ash flow rate on the final carbonation product yield was examined.

Scenario 4 consists of a multi-stage leaching process in which the initial fresh fly ash flow rate remains the same as in Scenario 1. The original fly ash and its leaching residues are leached separately in different tanks rather than in the same one, as proposed in Scenario 3. The solid residue derived from the first leaching tank undergoes two more leaching steps in separate tanks using fresh NH_4Cl and $\text{NH}_4\text{Cl}+\text{HCl}$ in tanks 2 and 3, respectively. Each step includes a leaching tank, filtration unit and ammonia recovery flash separator. Adding HCl to the last leaching stage attempts to reduce the free MgO and CaO in the solid residue to the level required by the cement additive.

7.3.4 Cost estimation methodology

The Aspen Process Economic Analyser (APEA) software claims to have been field-tested for more than 30 years on commercial plants and is used worldwide by engineering design firms [43]. In this study, the APEA was combined with Aspen Plus to estimate the costs using the output results from the Aspen Plus simulations.

The hypothetical plant location was set as Melbourne, Australia, and all data were reported in AU dollar (A\$) using an exchange rate of 0.76 to the US dollar (based on November 2015 data). The geographical location affects certain costs, such as freight, taxes, wage rates and workforce productivities [44]. Next, general specifications were defined for the starting date of the plant, process description and complexity, plant type (*e.g.*, green field), currency, necessary utilities, designating raw material and product streams. A key step in integrated economics is mapping the unit operation models from the simulation to equipment models in the APEA. The APEA maps unit operations from the Aspen Plus flow sheet to equipment cost models, which then size the equipment based on the relevant design codes and estimate the equipment purchase costs based on the vendor quotes. The specific types and materials of the process equipment were defined and sized based on guidelines specified elsewhere [39,42,45]. Identical economic assumptions were applied for all four scenarios. **Table 7.3** summarises the assumptions as well as the prices of raw materials and utilities in A\$ specified in the APEA. To reiterate, the feedstock for all of the evaluated cases is fly ash. The mineral carbonation facility is considered to be part of the power plant, and fly ash is thus considered to be free of charge. The prices of bulk ammonium chloride, hydrochloric acid and ammonium hydroxide were obtained online [46]. The amount of raw material was calculated based on the amount of the leaching reagent required to run a single-step process plus a make-up of each cycle.

Table 7.3 Economic inputs to Aspen process economic analyser (APEA)

General economic parameters		Cash flow analysis parameters	
Plant location	Melbourne, AU	Tax rate	30%
Currency conversion rate	A\$/USD 0.76	Discount rate	10%
Project type	Green field	Interest rate	10%
Source of utilities	Across the fence	Economic life of project	20 years
Project fluids	Liquids and solids	Depreciation	5% per year
Operating hours per year	8000	Depreciation method	Straight line
Start date for engineering	1-Jan-16	Working capital	6.7% of the fixed capital cost
Raw material process		Utilities	
Ammonium chloride	200 A\$/t ^b	Electricity	0.1 A\$ per KW h ^a
Hydrochloric acid (30%)	200 A\$/t ^b	Water	2.5 A\$ per cubic meter
Ammonium hydroxide (30%)	280 A\$/t ^b	LP steam	34.57 A\$ per MW h ^a
Fly ash	Not costed		
Flue gas	Not costed		

^a: APEA default values (country base: USA), ^b: Online resources

A number of methods are available for estimating the plant cost. They require different degrees of detail and engineering expertise for the data input and result in different levels of accuracy. These results are applicable for several purposes but are not limited to economic planning, feasibility studies and optimising the design of a process. For an initial feasibility study involving the consideration of alternative process routes, an accuracy of $\pm 30\%$ may be satisfactory [47]. In addition to using the APEA, an in-house resource and methodology [48] established by the Commonwealth Scientific and Industrial Research Organisation (CSIRO) was also used. This method has been successfully applied in the cost estimation of numerous research projects within Australia. Although there are location differences in the components of the plant cost for the different states and regions of Australia, they are generally minor in terms of overall plant cost for most industrial locations within Australia. This method calculates the capital expenditure items as a percentage of the Equipment Purchase Cost (EPC) and Direct Equipment Cost (DEC). The total operating costs were considered as the summation of the raw material costs, utilities, total fixed charges, depreciation and capital. The last two items are estimated as a percentage of the capital cost. In this study, the cost of each scenario was first estimated using the APEA, and the best scenario was thus selected. Subsequently, the CSIRO methodology was applied to the best scenario to refine the cost to be more reasonable in the Australian context.

7.4 Results and Discussion

7.4.1 Comparison of leaching agents in Scenarios 1 and 2

The process flowsheets for Scenario 1 and 2 are illustrated in **Figures 7.3** and **7.4**, respectively. In Scenario 1, an additional ~2% ammonium chloride make-up was added to each cycle to compensate for its loss. Eloneva et al. (2012) determined that approximately 1 wt.% of the solution was lost during the carbonation of slag. In their calculation, a 2 wt.% loss was considered to ensure a higher reliability [49].

Table 7.4 presents the material and energy balance for Scenarios 1 and 2 in which the original fly ash mass flow rate remains identical. Using ammonium chloride as the leaching reagent, Scenario 1 produces 4.98 and 4.85 tonne/h of MgCO_3 and CaCO_3 , respectively. Simultaneously, approximately 0.17 tonne of CO_2 per tonne of fly ash is captured. Scenario 2 is more complicated, with an efficiency that is highly dependent on the mass flow rate of HCl. With the addition of 20 tonne/h of HCl to control the pH of the leachate in the range of 4 to 4.5, the MgCO_3 and CaCO_3 yields increased to 9.12 and 7.25 tonne/h, respectively. Furthermore, approximately 0.3 tonne of CO_2 per tonne of fly ash is captured, which is nearly double that of Scenario 1 due to the enhanced leaching of both free CaO and MgO out of the fly ash. However, such increases are counteracted by the increased consumption of HCl and ammonium hydroxide (NH_4OH). Additionally, the total electricity requirement for Scenario 2 is considerably higher than that in the first scenario, even though the leaching is conducted at room temperature. This result occurs due to the circulation of larger amounts of chemicals in each loop, which causes a rise in both the size and the power consumption of the agitators and filter separators. Clearly, from a technical point of view, Scenario 2, which uses a mixture of $\text{NH}_4\text{Cl}+\text{HCl}$, is more efficient. However, from an economic perspective, an opposing situation is valid due to the increased energy consumption and capital cost of Scenario 2, which will be discussed later.

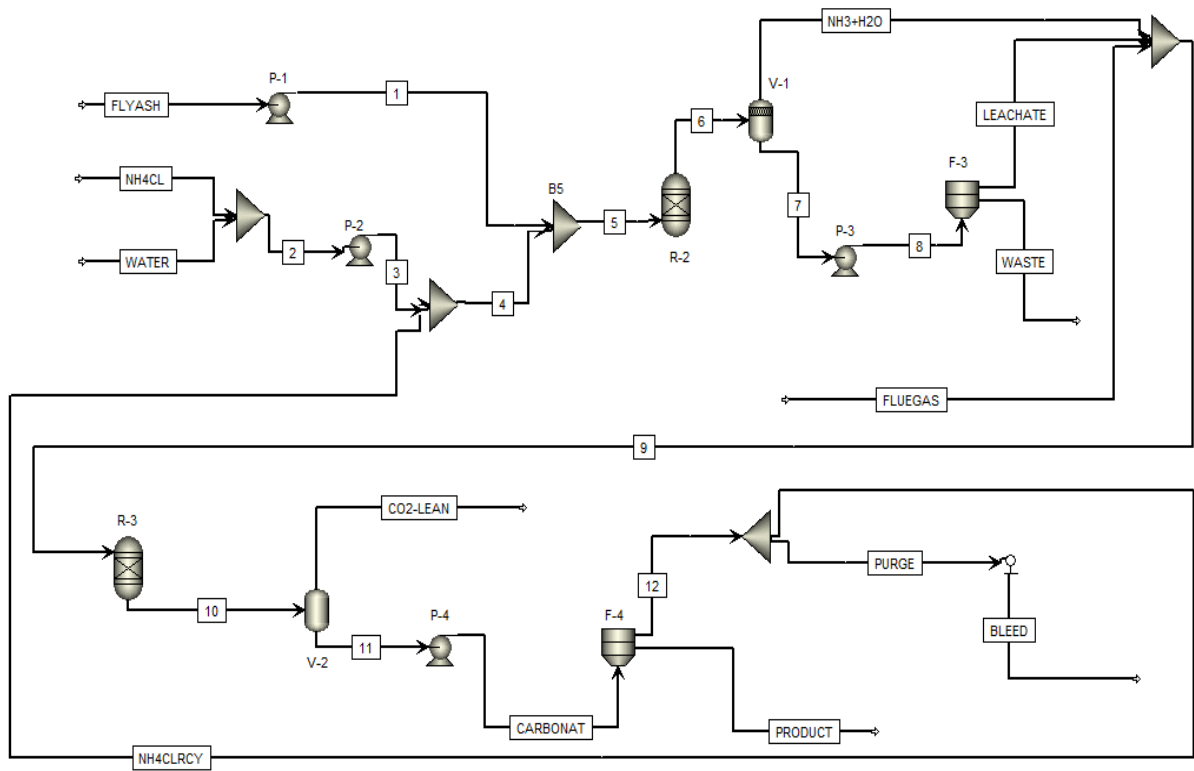


Figure 7.3 Aspen Plus flowsheet for Scenario 1

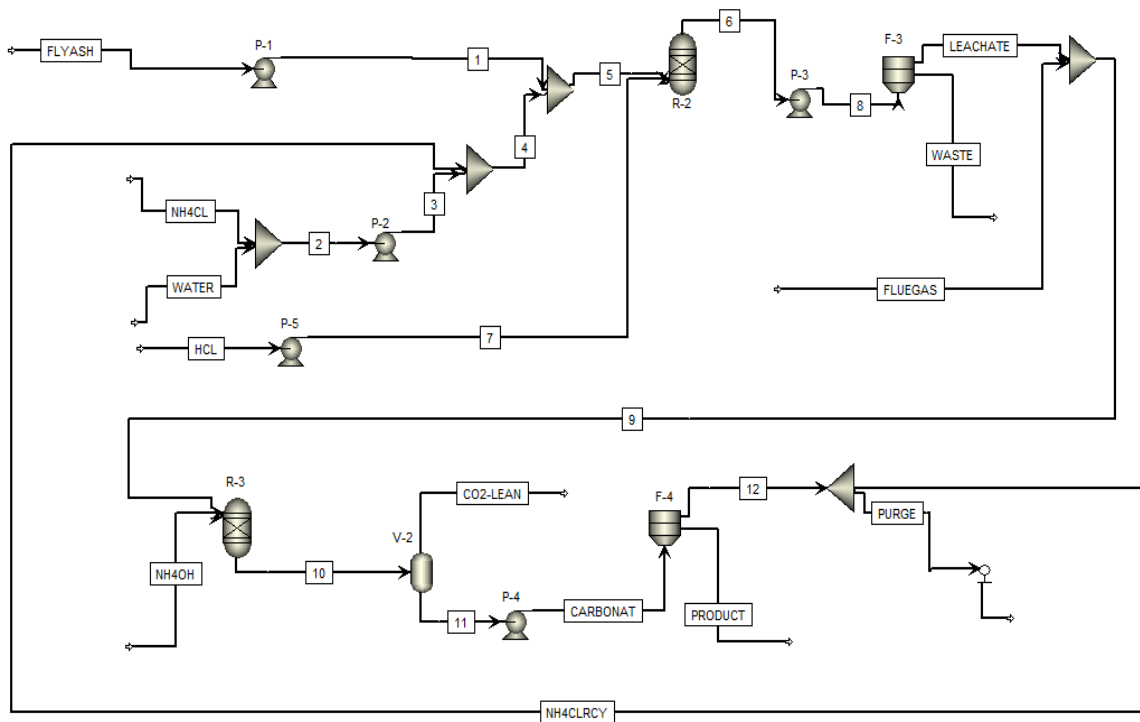


Figure 7.4 Aspen Plus flowsheet for Scenario 2

Table 7.4 Material and energy balance for Scenarios 1 (NH₄Cl leaching) and 2 (NH₄Cl+HCl leaching)

	Scenario 1	Scenario 2
Plant input (t/h)		
Fly ash	25	25
NH ₄ Cl make-up	1.1	0
HCl	-	20
NH ₄ OH	-	7.5
Water	2.04	19.34
Hot utility (MW)	2.5	0.15
Cold utility (MW)	15.2	16.4
Power (MW)	0.33	1.5
CO ₂ IN by streams	16.5	16.5
Plant output (t/h)		
Product		
MgCO ₃	4.98	9.2
CaCO ₃	4.85	7.12
Water	1.37	5.04
Other	0.7	1.83
Waste		
CaSO ₄	4.41	4.41
CaCO ₃	2.54	1.3
MgO	4.93	2.87
CaO	1.18	0.59
SiO ₂	1.23	1.23
Fe ₂ O ₃	1.47	1.47
CaFe ₂ O ₅	3.43	3.43
Other	1.76	6.9
CO ₂ OUT by streams	11.7	9.00
CO ₂ OUT by utilities	0.6	0.05
Net CO ₂ capture (t/h)	4.21	7.45
Net CO ₂ capture (tonne/tonne fly ash)	0.17	0.3

7.4.2 Comparison of different process integrations in Scenarios 1, 3 and 4

Figure 7.5 demonstrates the effects of the fresh fly ash flow rate of the two carbonation production yields on recycling the leached residue back into the same leaching tank, *i.e.*, Scenario 3. For comparison, the production yields for Scenario 1 with an initial fly ash flow rate of 25 t/h are also presented in Figure 7.5. Clearly, in the case that the fresh fly ash flow rate remains constant at 25 t/h, the product yields increases for both MgCO₃ and CaCO₃ in Scenario 3. The product yield for CaCO₃ increased from ~4.98 t/h in Scenario 1 to approximately 7.1 t/h for Scenario 3. Interestingly, the production yield for MgCO₃ is nearly tripled, increasing from 4.85 t/h in Scenario 1 to ~12.4 t/h in Scenario 3. Clearly, recycling the leaching residue is

beneficial for enhancing the extraction yield of free MgO in the fly ash. This result most likely occurs due to the presence of a larger quantity of free MgO in the fresh fly ash and the leaching residue (see **Table 7.4**). However, the size of the leaching tank must be considerably increased to accommodate both the original fly ash and the leached residue. To use the same size leaching reactor as in Scenario 1, it can be inferred from Figure 7.5 that decreasing the initial fly ash flow rate to ~16 t/h is essential to achieve the same calcium carbonate yield. Nevertheless, the corresponding MgCO₃ product yield from this flow rate is still significantly higher than that of Scenario 1, which feeds 25 t/h of fresh fly ash without recycling the residue.

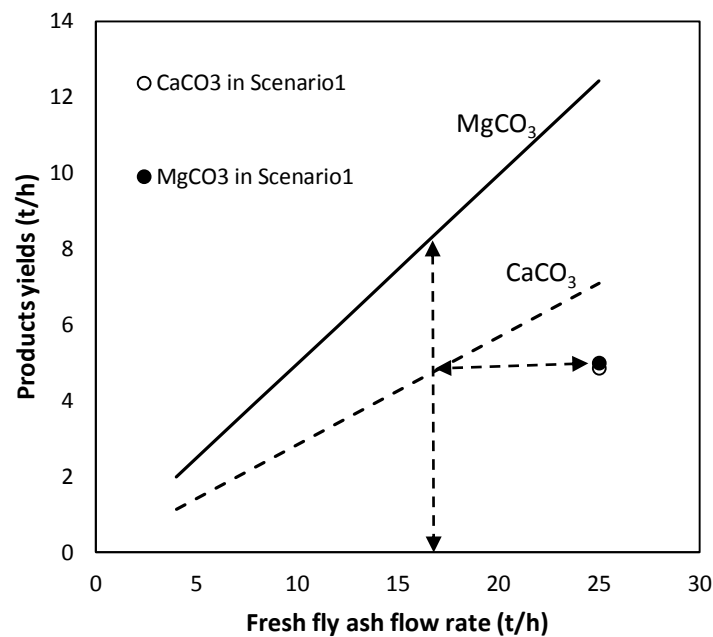


Figure 7.5 Product yield as a function of the fresh fly ash flow rate in the case of recycling the leaching waste (Scenario 3) compared with the case without recycling (Scenario 1- indicated by two single points at 25 t/h)

To reiterate, Scenario 4 targets the co-production of carbonates and cement additive-grade by-products using the ASTM C618 specification [21] of leached residue. Hence, an extra 9 t/h of HCl is used in the final leaching stage. The mass percentage of each component in the solid waste obtained from the final leaching stage is presented in **Figure 7.6**. The figure indicates that the mass fractions of free MgO and CaO decreased to less than 5% and 1%, respectively. The calculated loss on ignition (LOI) accounts for 8.5% based on the amount of CO₂ in the MgCO₃ and CaCO₃, which is also in accordance with the limit of 12% for the cement additive [21].

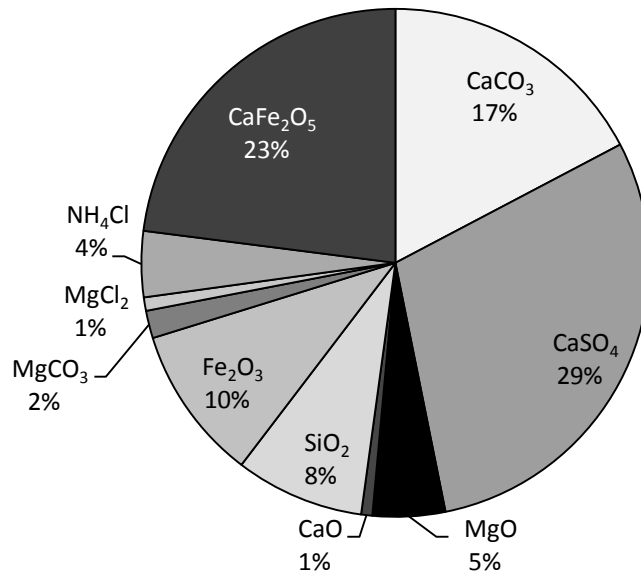


Figure 7.6 Chemical composition of the solid waste obtained from the final leaching stage of Scenario 4

The product yields and amount of chemicals consumed for this scenario are further compared with Scenarios 1 and 2 in **Figure 7.7**. Clearly, using three-stage leaching in Scenario 4 is the most beneficial for the production of MgCO₃ and CaCO₃ among the three scenarios. It consumes considerably lesser amounts of HCl and NH₄OH than Scenario 2. This is because HCl is used to attack only the hard-to-dissolve fractions whereas the easily dissolved fraction is attacked by the use of regenerative NH₄Cl.

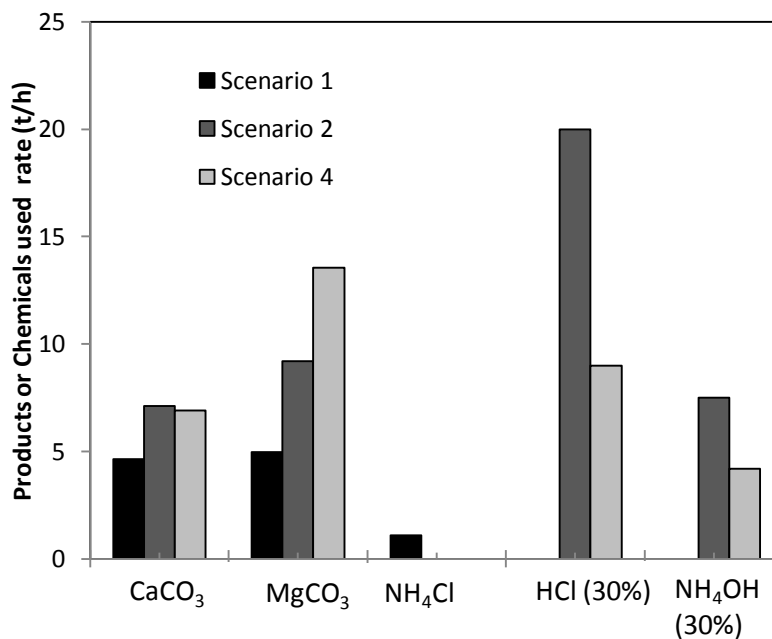


Figure 7.7 Comparison of the amount of products and chemicals used for Scenarios 1, 2 and 4

7.4.3 Economic analysis

7.4.3.1 Operating and capital costs

To estimate the capital cost, the specific types and materials for construction of the process equipment were defined and sized based on the principles outlined in the literature and recommendations in the APEA. Rotary lobe pumps were selected for handling the fly ash and other solid streams [50]. Centrifugal pumps were used for pumping the ammonium chloride solution and hydrochloric acid. The continuous stirred-tank reactors (CSTR) were specified as agitated, enclosed, jacketed tanks. Based on the residence time of 30 min and 40 min for the leaching and carbonation processes, respectively [13,38], the reactor sizes were consequently determined. For Scenario 1, the leaching tank was sized to an internal diameter (ID) of 3.7 m and a liquid depth of 12.8 m whereas the carbonation tank had an ID of 3.4 m and a liquid depth of 11.6 m. A pressure filter was used for the solid-liquid separation [51]. A vertical vessel configuration was used to size of the ammonia recovery flash drum. For all equipment in contact with ammonium chloride and hydrochloric acid, a SS 316 material was used to minimise corrosion.

Figure 7.8 depicts the breakdown of the capital costs for the major parts and the total capital cost of the four scenarios. It should be noted that for all of the scenarios, except No. 3, the fly ash flow rate remains constant at 25 t/h. For Scenario 3, the optimised fly ash flow rate obtained in the last section, *i.e.*, 16 t/h in Figure 7.5, was used for the cost calculation. The total capital cost is the summation of the direct field costs, indirect field costs and non-field costs. The calculated total capital cost is expressed in Australian dollars (A\$) based on the 2015 cost index. This cost was estimated to be \$10.1 million for Scenario 1. Scenario 2 is associated with the highest total capital cost because of the larger total flow rate and larger equipment size due to the use of additional HCl. Scenario 4 is the second most expensive scenario due to the additional bundle of equipment for the three-stage leaching. Scenarios 1 and 3 exhibit nearly the same capital costs due to their similar flow rate and equipment size.

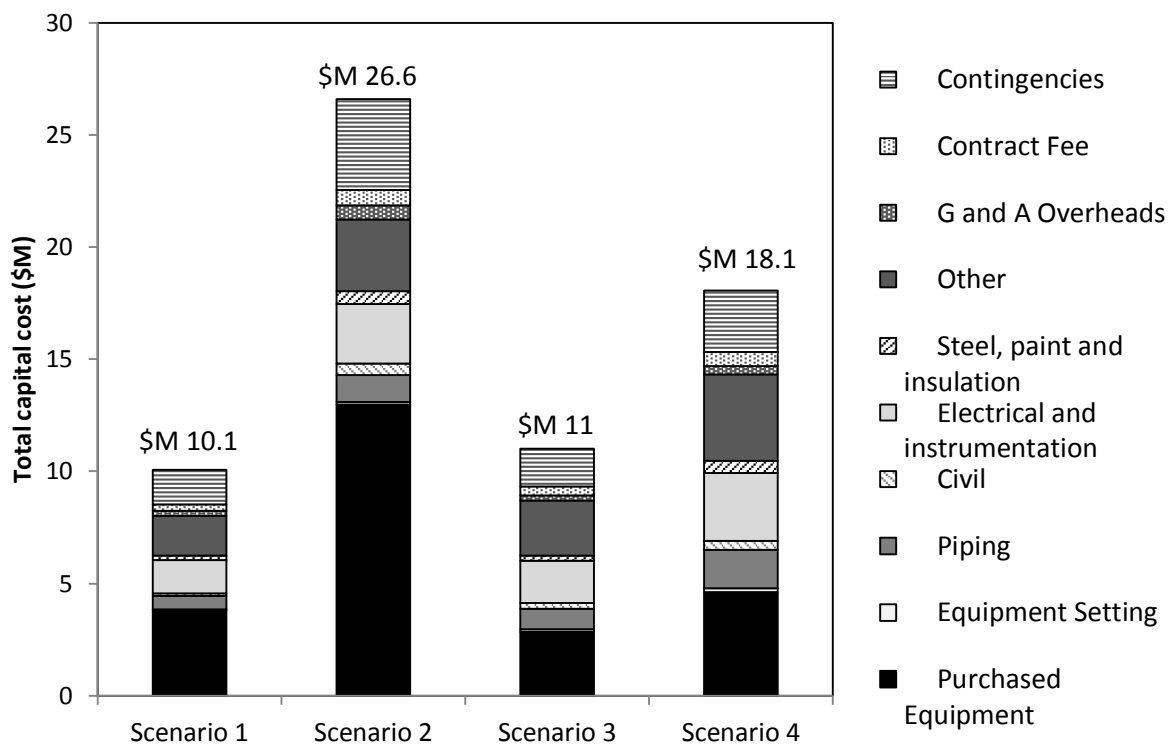


Figure 7.8 Breakdown of the capital costs for the different scenarios

The annual operating cost and its breakdown are summarised in **Figure 7.9**. The annual operating cost includes expenditures for chemicals (*e.g.*, leaching agents), utilities (*e.g.*, electricity and natural gas for heating), labour and maintenance cost, operating charges and plant overhead [51]. Reagent costs are the largest contributor to the operating cost, especially for Scenario 2, which consumes a large amount of HCl. Details of the raw material consumptions and cost per hour as well as the total annual cost of each scenario are summarised in **Table 7.5**. The ammonium chloride start-up cost was calculated based on the amount required to run the process for the first time, assuming a total of 5 hours for a single-step operation. Based on these results, it is evident that the amount of HCl used in Scenario 2 is critical for the production costs.

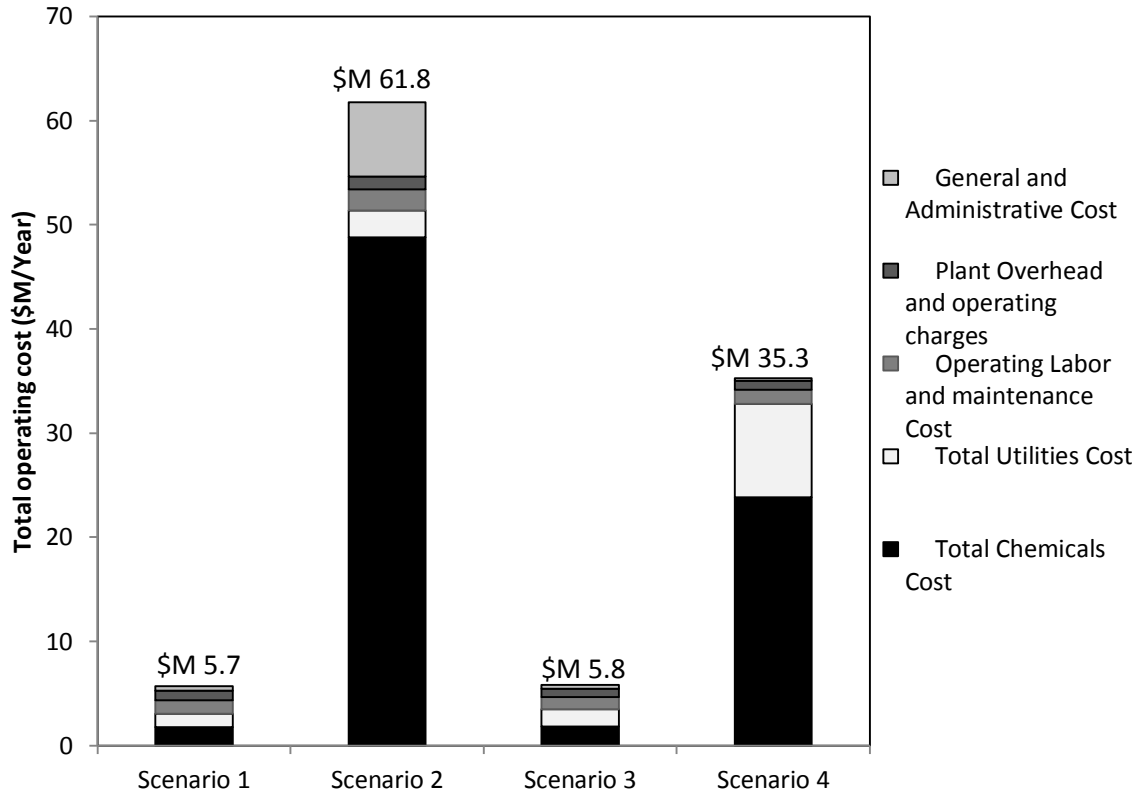


Figure 7.9 Total operating cost and breakdown for the operating items per year in the evaluated scenarios

Table 7.5 Chemical consumption and purchasing cost of the evaluated scenarios

Raw materials	Consumption (t/h)				Total cost/year (\$)			
	Scenario 1	Scenario 2	Scenario 3	Scenario 4	Scenario 1	Scenario 2	Scenario 3	Scenario 4
NH ₄ Cl start-up	61.5	61.5	61.5	61.5	61,500	61,500	61,500	61,500
NH ₄ Cl make-up	1.1	0	1.1	0	1,760,000	-	1,760,000	-
NH ₄ OH (30%)	0	7.5	0	4.2	-	16,800,000	-	9,408,000
HCl (30%)	0	20	0	9	-	32,000,000	-	14,400,000
Total	62.6	89	62.6	74.7	1,821,500	48,861,500	1,821,500	23,869,500

With reference to **Figure 7.9**, the total operating cost of the different scenarios ranged from \$5.7 million for Scenario 1 to \$61.8 million for Scenario 2. Scenarios 1 and 3 have a similar operating cost of \$5.7-5.8 M due to the similarity of these two processes and lower chemical costs. For a comparison between Scenarios 2 and 4, the utility consumption cost for using the NH₄Cl+HCl mixture in Scenario 2 is considerably lower compared to that achieved using NH₄Cl for the first two steps in Scenario 4. This is because the addition of HCl decreases the leaching

temperature requirement to room temperature compared to 80°C when using NH₄Cl as the leaching agent. However, the utility consumption for Scenario 2 is still higher than those of Scenarios 1 and 3. The reason this result occurs is the large volume of materials handled in each loop and, consequently, the higher electricity requirement for the pumps and reactors.

The operating cost per tonne of fly ash as well as the produced and captured CO₂ was further calculated, as indicated in **Table 7.6**. Scenario 3 has the lowest production and carbon capture cost at \$42.8 and \$135 per tonne, respectively, due to its lower operating cost when compared with the other three scenarios. The second best option is Scenario 1 at \$60.5 and \$169.3 cost per tonne of produced and captured CO₂, respectively. Scenarios 2 and 4 are associated with the highest production costs at \$333.3 and \$168.4, respectively. The primary reason for this result is that these two scenarios consume a large amount of HCl.

Table 7.6 Operating cost per tonne of fly ash as well as the produced and captured CO₂ for the different scenarios evaluated

	Operating cost per tonne of fly ash (\$)	Operating cost per tonne of product (\$)	Operating cost per tonne of CO ₂ captured (\$)
Scenario 1	28.5	60.5	169.3
Scenario 2	307.8	333.3	1036.4
Scenario 3	29.1	42.8	135.0
Scenario 4	176.3	168.4	1091.2

7.4.3.2 Effects of HCl amount and flow rate

For Scenario 2 and Scenario 4, the cost of the required HCl is most critical in determining the feasibility of these scenarios from an economic perspective. To reiterate, the operating cost of Scenario 2 is ten-fold larger than that of Scenario 1. Conversely, the capital cost of this scenario increases three-fold when compared to Scenario 1. Therefore, a sensitivity analysis was conducted by assessing the cost and production yield of Scenario 2 versus the mass flow rate of HCl from 0 tonne/h (Scenario 1) to 20 tonne/h. The results for the total chemical costs per tonne of fly ash or per tonne of product are displayed in **Figure 7.10**. It is evident that with an increase in the HCl flow rate, the cost of chemical per tonne of fly ash as well as per tonne of products increases linearly. The steep slope for the cost per tonne of product compared to the cost per tonne of fly ash indicates that the rate of increase in the chemical cost is faster than the incremental increase in the production yield.

The total cost, CO₂ capture and steam utility consumption were further compared for both the lowest and highest HCl flow rates examined in the above sensitivity analysis (1 tonne/h and 20/tonne h). The results are presented in **Table 7.7**. Using 20 tonne/h of HCl in the process resulted in a magnesium carbonate and calcium carbonate yield of 9.19 and 7.12 tonne/h,

respectively, compared to 6.21 and 4.89 tonne/h for 1 tonne/h of HCl. By decreasing the HCl flow rate from 20 tonne/h to 1 tonne/h, the total capital cost and the total operating cost decreased from \$26.6 M to \$8.72 M and \$ 61.74 M to \$ 8.04 M, respectively.

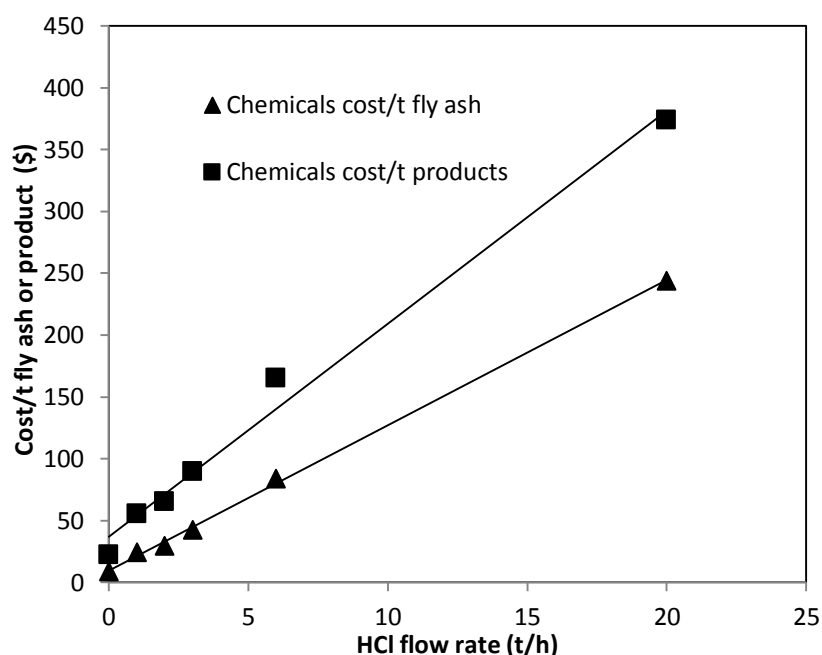


Figure 7.10 Chemical cost per tonne of fly ash or per tonne of product as a function of the HCl flow rate

Table 7.7 Comparison of the operational parameters and cost of the lowest and highest HCl flow rates evaluated in this study

	Lowest HCl rate (1 tonne/h)	Highest HCl rate (20 tonne/h)
CO₂ capture		
CO ₂ captured (kg/h)	5467	7448
CO ₂ captured (t/t fly ash)	0.22	0.30
Total cost		
Total capital cost (\$M)	8.72	26.60
Equipment cost (\$M)	2.06	11.52
Total operating cost (\$M)	8.04	61.74
Cost of chemicals (\$M)	4.87	48.80
Operating cost/t CO ₂ captured	183.79	1036.25
Product yield		
Calcium carbonate Production rate (t/h)	4.89	7.12
Magnesium carbonate Production rate (t/h)	6.21	9.19
Utilities		
Steam utility (MW)	0.03	0.15
Cooling utility (MW)	9.8	16.4

7.4.3.3 Effects of fly ash composition

The capacity of the fly ash to sequester CO₂ depends directly on the proportion of free oxides (CaO and MgO) and/or hydroxides (Ca(OH)₂) and Mg(OH)₂) within it. Considering the heterogeneity of the fly ash composition, the composition of the weathered fly ash, which has more inert species due to ageing (as mentioned in **Table 7.1**), was further used for simulation. A comparison of the total cost, CO₂ capture and steam utility using the fresh and weathered fly ash as feedstock in Scenario 1 is presented in **Table 7.8**. It is clear from this table that the production cost and CO₂ capture cost per tonne of fly ash for the weathered fly ash is more expensive due to its lower production yield. Moreover, due to the relatively low production yield using NH₄Cl, it can be inferred that using a mixture of NH₄Cl+HCl is preferential when using weathered fly ash for mineral carbonation.

Table 7.8 Comparison of the operational parameters and cost of fresh and weathered fly ash leaching using NH₄Cl as the leaching agent (Scenario 1)

	Fresh fly ash	Weathered fly ash
CO₂ capture		
CO ₂ captured (t/h)	4.21	2.69
CO ₂ captured (t/t fly ash)	0.17	0.11
Total cost		
Total capital cost (\$M)	10.1	7.7
Equipment cost (\$M)	3.36	1.57
Total operating cost (\$M)	5.7	5.2
Cost of raw materials (\$M)	1.82	1.34
Operating cost/t CO ₂ captured	169.3	357.8
Product yield		
Calcium carbonate production rate (t/h)	4.85	1.62
Magnesium carbonate production rate (t/h)	4.98	4.51
Utilities		
Steam utility (MW)	2.5	2.7
Cooling utility (MW)	15.2	12.2

7.4.3.4 Comparison of CO₂ capture capacity and cost with other mineral carbonation processes

The CO₂ capture and utilisation options are at different levels of technological development and market maturity [52]. Mineral carbonation using natural minerals has been implemented in a few demonstration plants across the world. Similarly, only a few projects based on industrial wastes have advanced to the commercial evaluation phase or demonstration scale [19]. Due to the lack of industrial applications, the cost assessments reported in the literature are merely rough estimates based on lab-scale or pilot-scale results. The profitability of these processes are currently uncertain because a large number of factors, such as profit margins, applicable taxes,

governments subsidies and CO₂ capture credits, remain unknown [1]. There are few detailed cost analyses of mineral CO₂ sequestration available. In the literature review conducted by Sipla et al., (2007), the cost of a mineral carbonation plant for the best scenarios from 2005 to 2007 was reported as €38-77 (~\$48-97) per tonne of CO₂ [53]. The most reliable cost of the *ex-situ* mineral carbonation route using natural minerals was developed by the National Energy Technology Laboratory (NETL) [19]. Based on their calculations, the sequestration costs of a direct process with pre-treatment ranges from \$50-210 per tonne of CO₂ for olivine, wollastonite and serpentine, which is considerably higher than other CCS methods, such as geological storage [54]. Using the indirect aqueous route with value-added products, such as precipitated calcium carbonate (PCC) produced from slag, the cost of the chemicals is estimated to be approximately \$600-4500 per tonne of CO₂ if they are not regenerated [19]. Clearly, the cost of CO₂ capture for the proposed process using Scenarios 1 and 3 is in the range of the costs estimated for natural minerals. Furthermore, it is cheaper than the cost estimated for industrial wastes in the literature.

A comparison between the CO₂ capture capacity of Victorian brown coal fly ash and other fly ashes is summarised in **Table 7.9**. The capacity to sequester CO₂ for Victorian brown coal fly ash is clearly higher than the other types of ashes reported in the literature. However, compared to the extremely low cost (*e.g.*, \$11-21 per tonne of CO₂ captured) of using black coal fly ash, the cost of using Victorian brown coal fly ash is still extremely high. Thus, the utilisation of the carbonation products has to be considered to compensate for the large CO₂ capture cost.

Table 7.9 Comparison of the CO₂ capture capacity of various fly ashes with Victorian brown coal fly ash

Carbonation condition	Fly ash type	CO ₂ capture capacity (t CO ₂ /t ash)	Cost per t of CO ₂ captured
0.115 bar, 48-57°C, 2 h	Black coal fly ash [24]	0.1-0.2	\$11-21 ^a
30°C 40 bar, 2 h with brine	Black coal fly ash [55]	0.0718	NA
10 bar, 36°C, 579 h	Lignite ash [56]	0.046	NA
10 bar, 60°C, 1h	VBC FA ^c [37]	0.264	NA
1 bar, 60°C, 40 min	VBC FA ^c (this study)	0.215	\$102.6 ^b

^a Cost is based on 2010

^b Our process; the cheapest scenario (Scenario 3) with an exchange rate of 0.76 to convert A\$ to US\$

^c Victorian brown coal fly ash

7.4.3.5 Modified cost for Australian context

The new cost alternative method based on the Australian local market price was used to modify the operating and capital cost obtained from the APEA. The comparison between the APEA and the new cost calculation alternative is presented in **Figure 7.11**. For both costs, the new method prediction demonstrates the same sequence as that predicted by the APEA, *i.e.*, Scenario 2 has the largest cost followed by No. 4, 1 and 3 in a descending sequence. This result suggests that all of the comparisons made for the four scenarios in the previous sections are

reasonable. In terms of the detailed cost estimate for each scenario, the capital cost of Scenario 1 nearly increases by 50% when using the new cost alternative. For Scenario 2, its new capital cost is nearly double the result obtained from the APEA. However, the changes in the capital costs for Scenarios 3 and 4 are insignificant. The primary factors contributing to these variations include local regulations, taxes, and availability and productivity of construction labour [42]. The fluctuating exchange rate, which spiked from 1.07 to 0.72 in the last five years, is another factor affecting the cost in the Australian context. As an example, details on calculating the capital cost and the operating cost for all assumptions in Scenario 1 (reference case) are presented in **Tables 7.10** and **7.11**, respectively.

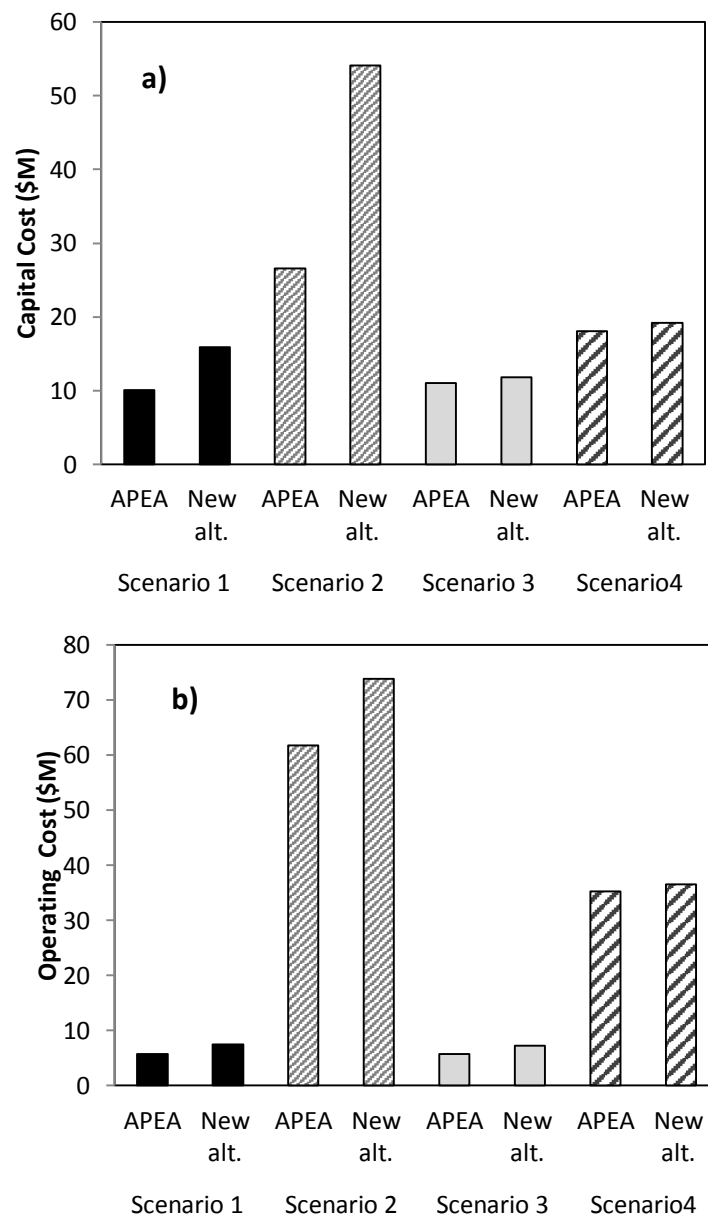


Figure 7.11 Comparison of the a) capital cost and b) operating cost calculated from the Aspen process economic analyser (APEA) and the new cost alternative method for the different scenarios

Table 7.10 Capital cost of Scenario 1 (NH₄Cl leaching) using the new cost alternative based on the Australian local market price

Capital cost items	Basis	Cost (\$M ex. GST)
Direct Plant Costs		
Equipment Purchase	EPC ^a	3.36 ^c
Freight	10 % of EPC	0.34
Direct equipment cost (DEC)	EPC + Freight	3.69
Installation	45 % of DEC ^b	1.66
Instrumentation	25 % of DEC	0.92
Minor piping	16 % of EPC	0.54
Structural	15% of EPC	0.50
Electrical	25 % of DEC	0.92
Buildings	25 % of EPC	0.84
Yard Improvements	15 % of EPC	0.5
Service Facilities	40 % of EPC	1.34
HSE Functions	10 % of EPC	0.34
Total Indirect Costs		
Engineering Supervision	50 % of DEC	1.85
Legal Expenses	4 % of DEC	0.15
Construction Expenses	40 % of DEC	1.48
Working Capital		
Working Capital	8% of Direct plant cost + Total indirect costs	1.18
Total Capital (ex GST)		15.90

^a: EPC: Equipment purchased cost, ^b: DEC: Direct equipment cost

^c: Equipment purchase cost is derived from APEA

To further evaluate the variation in the cost of the proposed process, a sensitivity analysis was conducted for a $\pm 50\%$ change in the base case value for the capital cost and the primary operating cost contributors: labour, electricity, natural gas and ammonium chloride cost. Here, Scenario 1 was used as an example. As indicated in **Figure 7.12**, the production cost has the largest sensitivity towards the variation in the cost of ammonium chloride. In the case for an ammonium chloride price increase from \$200/t to \$300/t, an increase of 29.5% in the production cost of is observed. Conversely, for a decrease in the ammonium chloride price by 50%, the production cost drops from ~\$79/t (base case) to \$56/t, and a change in the labour cost results in the smallest change in the production cost. In the case of a 50% increase in the labour cost, the production cost only increases by 13%. A 50% decrease in the labour cost merely drops the production cost from \$79/t to \$69/t. The capital cost was found to exert the second highest impact on the production cost.

Table 7.11 Operating cost of Scenario 1 (NH₄Cl leaching) using the new cost alternative based on the Australian local market price

Item	Total cost (\$M)	Amount used	Price per unit
Raw Materials			
Fly ash	0	2.12 (t/t product)	free
Ammonium chloride start-up	-	-	-
Ammonia chloride make-up	1.76	0.09 (t/t product)	\$200 /t
Flue-gas	-	0.41 (t/t product)	free
Water	0.02	0.18 (cum/ t product)	\$1 /cum
HCl (30%)	0	-	\$200 /t
Utilities			
Electricity	0.262		\$0.1/ kWh
Natural Gas	0.42		\$5 /GJ
Total fixed charges		Assumptions	
Labour	1.96		\$25/t product
Maintenance and repairs	0.8	5% of total capital cost	NA
Operating supplies	0.16	1% of total capital cost	NA
Taxes (property)	0.32	2% of total capital cost	NA
Insurance	0.16	1% of total capital cost	NA
Depreciation & Capital			
Fixed Capital Depreciation	0.8	5% of total capital cost	NA
Interest on capital	0.8	5% of total capital cost	NA
Total product cost	7.44		
Operating cost per tonne of fly ash			\$37.2
Operating cost per tonne of product			\$78.9
Operating cost per tonne of CO ₂ captured			\$221

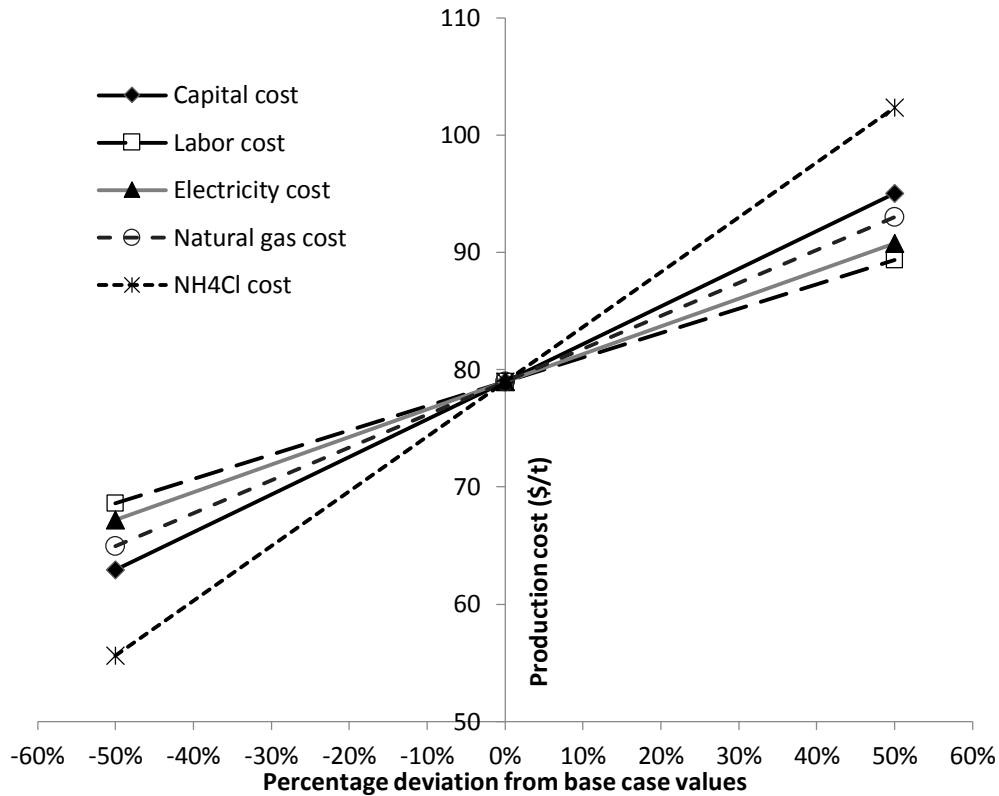


Figure 7.12 Production cost sensitivity to the economic parameters for Scenario 1

7.4.4 Product utilisation

7.4.4.1 NPV, IRR and payback period analysis

The utilisation of mineral carbonation products were considered in this section. Industrial applications of the obtained carbonate products can be divided into two categories: low-end high-volume uses and high-end low-volume uses. Construction and filler applications are the most probable users of low-end high-volume products [19]. In our process, the product is a mixture of magnesium carbonate and calcium carbonate in varying proportions with less than 8% impurities, which is a similar composition to dolomite. Considerable variations in the dolomite composition are found in nature, which relate to lime and magnesia percentages as well as impurities [57], thus overshadowing the change in the compositions of the product due to variations in the fly ash composition or leaching reagent. This product can be considered to be a primary source of magnesium for agricultural and pharmaceutical applications. Dolomite is widely used as a refractory and fettling material in steel melting as well as a fluxing material for blast furnace operation in primary and secondary steel and ferromanganese production [57].

In the case that the carbonate products of this process are used in a value-added way, a portion of the costs and energy consumption associated with the proposed mineral carbonation process can be recovered [58]. With an approximate cost for dolomite of \$130/t in the local market in Australia [46], in terms of cost per tonne of product, Scenarios 1 and 3 are clearly most attractive. In addition to the primary products, the by-product of Scenario 4 can also be utilised as an additive to cement. The reported price of fly ash as a supplementary cementing material ranges from \$90-140 per tonne in Australia [59].

Based on these considerations, a cash flow analysis was developed to determine the net present value (NPV), internal rate of return (IRR) and payback period. Income is generated from the sale of the product as synthetic dolomite with an average selling price of \$130/t in the local market for all four scenarios as well as an additional average of \$110/t of leaching waste as a supplementary cementing material for Scenario 4.

Figure 7.13 illustrates the variation in the cumulative discounted cash flow over the lifetime of the project for all of the scenarios, except Scenario 2. The reason for excluding Scenario 2 is that its cash flow is always negative due to its high chemical cost. In other words, this scenario is not economically feasible. The NPV, IRR and payback period results for Scenarios 1, 3 and 4 are further summarised in **Table 7.12**. Clearly, with a project lifetime of 20 years, Scenario 3, which recycles the leaching residue, demonstrates the best economic performance, exhibiting the highest cumulative discounted cash flow and the shortest payback period, *i.e.*, 2.3 years. The NPV and the IRR of this scenario can reach as high as \$49 million and 53.4%, respectively. Scenario 1 is the second most efficient scenario with an NPV, IRR and payback period of \$13 million, 19.8% and 7.2 years, respectively. For Scenario 4, the cumulative cash flow becomes positive within 12.7 years, and a small NPV of \$5 million indicates the high investment risk in this process. Despite the extra income from the side-product in Scenario 4, this scenario does not appear attractive due to the low selling price of leaching waste as a cement additive material.

Table 7.12 Financial indices calculated using the cash flow analysis for Scenario 1 (NH₄Cl leaching), Scenario 3 (waste recycling) and Scenario 4 (multi-stage leaching)

	Scenario 1	Scenario 3	Scenario 4
Net present value (NPV) \$M	13	49	5
Internal rate of return (IRR) %	19.8	53.4	13.0
Payback period (Year)	7.2	2.3	12.7

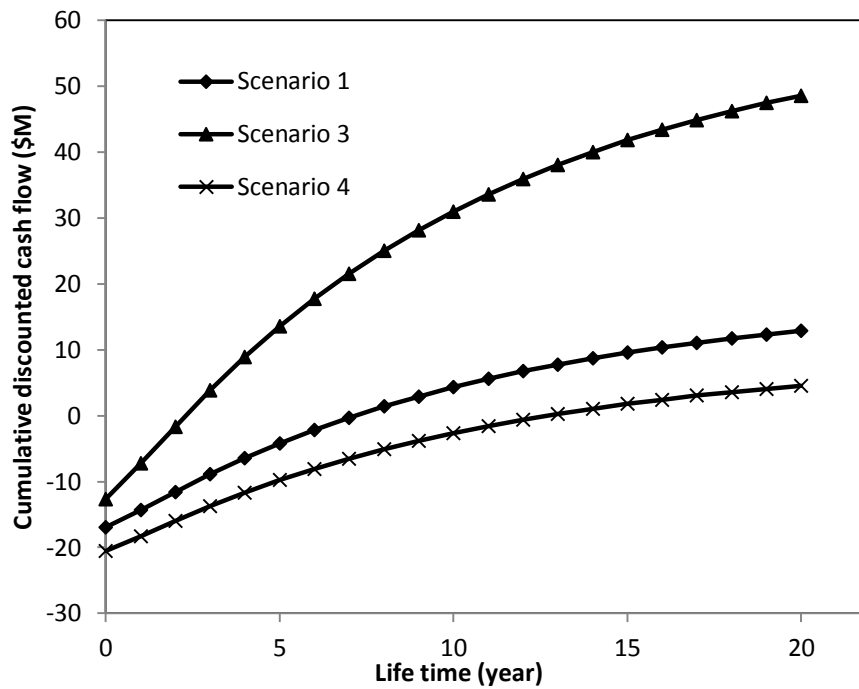


Figure 7.13 Cumulative discounted cash flow analysis over the lifetime of the project for Scenario 1 (NH₄Cl leaching), Scenario 3 (waste recycling) and Scenario 4 (multi-stage leaching)

7.4.4.2 Sensitivity analysis of the effects of the major variables on the NPV, IRR and payback period

Furthermore, considering the fluctuation of the market prices and uncertainties for the products, particularly the carbonate precipitates, a sensitivity analysis was performed to assess the sensitivity of the NPV, IRR and payback period to the variation in the input parameters. The parameters under investigation include the selling price of the product, production cost and capital cost. The input parameters were varied $\pm 50\%$ for Scenario 1 to calculate the NPV, IRR and payback period values, and the results are presented in **Figure 7.14 a, b and c**, respectively. As indicated in panel *a*, the NPV is highly sensitive towards the variation in the selling price of the carbonate product. For a 50% rise in the selling price of the carbonate (caused by its improved purity and fineness), the NPV could reach \$48 million. Conversely, decreasing the selling price by 17% of the base value could result in a negative NPV. This case could occur due to the increased contents of impure elements within the carbonate precipitates. Furthermore, an increase in the production cost up to 30% can result in a significant decrease in the NPV value from \$13 million to nil. With a further rise in the production cost, the process results in a negative NPV value. The change in the capital cost exerts the lowest impact on the NPV value, as evident by the least steep slope for the variation in the NPV for a change in the capital cost. With respect to the IRR, a minimum selling price of \$89/t (~32% lower than the base value) for the carbonate

precipitate appears to be necessary for a positive IRR. A 50% increase in the selling price of the product can improve the IRR from 19.8% to 42.8%. This result suggests that further experimental studies on the production of high-quality carbonates (e.g., highly pure and ultra-fine/nano-particle carbonates) should be prioritised in the future. The production cost is the second most sensitive parameter, which varies the IRR from 19.8% to 34% and 1.5% for a of -50% and +50%, respectively. A decrease in the capital cost from the base case value by 50% results in the formation of a steeper slope for the IRR, thus suggesting the remarkable benefit of reducing the capital cost.

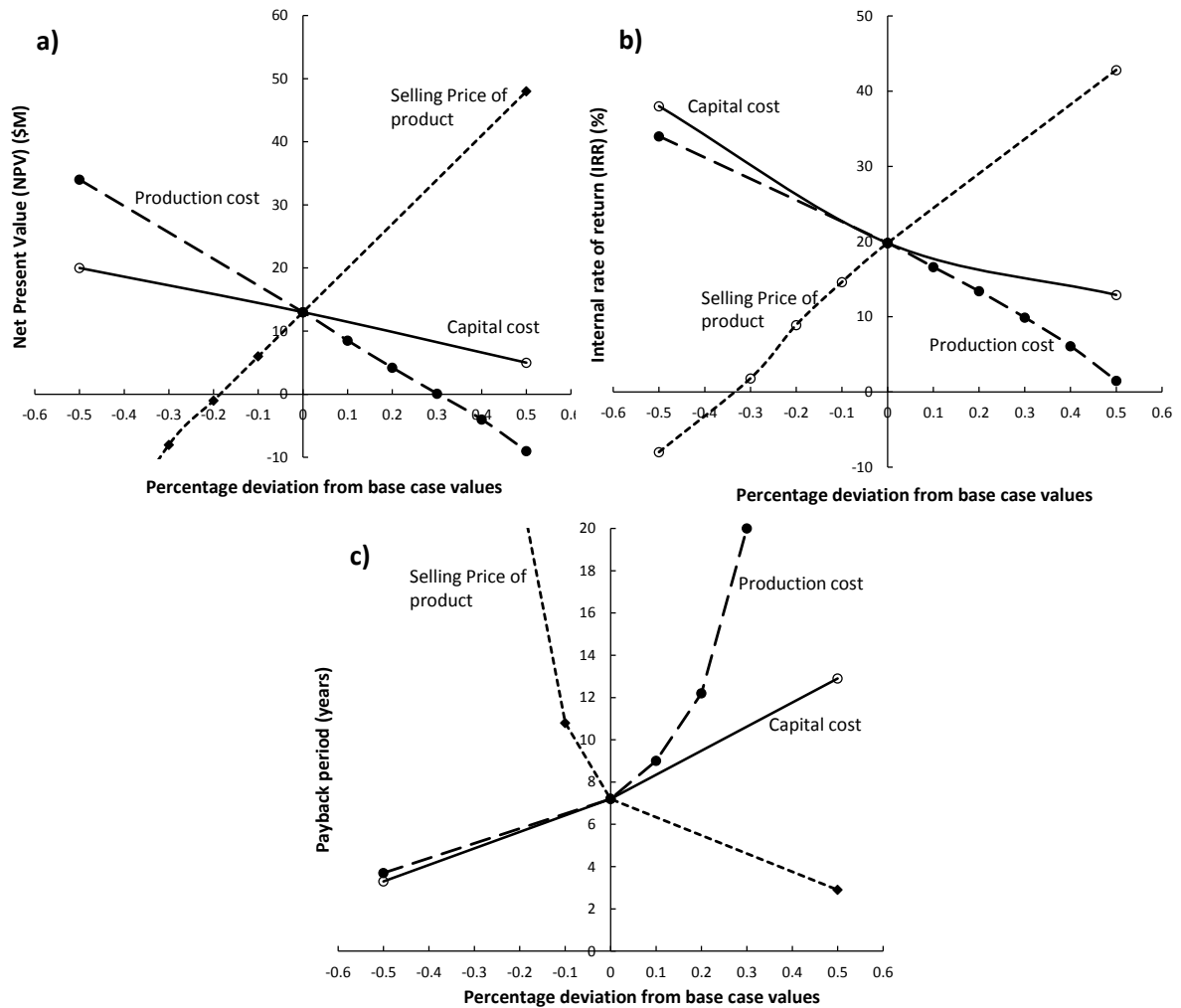


Figure 7.14 Sensitivity analysis on the effects of the production cost, selling price of the product and capital cost on the a) NPV; b) IRR; and c) Payback period for Scenario 1

Furthermore, as indicated in Figure 7.14 c, the payback period is mostly susceptible to a decrease in the selling price of the product as well as an increase in the production cost. A decrease in the selling price of the product by 22% results in the project being non-profitable, yielding a payback period that is even longer than the lifetime of the project. Conversely, an increase in the selling price by 50% could shorten the payback period to 2.9 years. With respect

to the production cost, an increase by 30% increases the payback period from 7.2 to 20 years. A further increase in the production cost beyond 30% increases the payback period to infinity, thus indicating the non-profitability of this process. A variation in the capital cost exerts the least impact on the payback period. For a change of -50% and +50% on the capital cost, the payback period only varies from 7.2 (base case) to 3.3 and 12.9 years, respectively.

7.5 Conclusions

This paper examined the technical and economic feasibility of four process scenarios for the mineral carbonation of Victorian brown coal fly ash. The first two design scenarios aimed to compare the performance of two leaching agents NH_4Cl and $\text{NH}_4\text{Cl}+\text{HCl}$ on product yields and cost whereas the two scenarios were designed to recycle the leaching residue *via* single or multi-stage leaching steps to co-produce a carbonate precipitate and cement additive-grade by-product. Detailed designs were developed in Aspen Plus to determine the technical and economic potential of the selected process configurations as well as identify the concept with the lowest overall costs relative to the product yields. The primary conclusions can be drawn as follows:

- 1) The overall production costs and the CO_2 capture cost of the evaluated process scenarios range from ~\$61-333 per tonne of product and \$135-1091 per tonne of CO_2 , respectively. The process scenario that uses $\text{NH}_4\text{Cl}+\text{HCl}$ as a leaching reagent has significantly large costs but a higher carbonation conversion compared to the other scenarios. The primary reasons for this are the high cost of HCl and the larger equipment size, which result from the treatment and circulation of a large mass flow rate of chemicals.
- 2) The process configuration incorporating the recycling of leaching residue results in the lowest cost per tonne of fly ash and the lower CO_2 capture cost among the four proposed scenarios. The largest NPV and IRR values as well as the shortest payback period for this scenario further confirmed its highest profitability. The NPV, IRR and payback period of \$49 million, 53.4% and 2.3 years, respectively, could be achieved when using Victorian brown coal fly ash in this scenario.
- 3) A sensitivity analysis confirmed the mild sensitivity of the production cost towards the capital cost and operating cost items. The change in the ammonium chloride price exerts the largest effect on the production cost. A 50% rise in the ammonium chloride cost could lead to the production cost increasing by 29.5%.
- 4) The selling price of the product and the production cost strongly affects the financial indices. For a 50% rise in the selling price of the carbonate precipitate, a large improvement in NPV, IRR and payback period could be achieved. The NPV and IRR could increase from \$13

million and 19.8% (base value) to \$48 million and 42.8%, respectively. Conversely, decreasing the selling price of the carbonate precipitate by 17% could lead to a negative NPV over the project lifetime. The production of the cement-additive by-product exerts a marginal role on the process profit, and the extra income created from the cement-additive by-product is counteracted by the larger cost related to the purchase and consumption of hydrogen chloride used in the final leaching stage.

Acknowledgment

This project is supported by the Faculty of Engineering of Monash University for a 2013-14 seed grant. Additionally, the first author is grateful to the Monash Research Graduate School (MRGS) for a PhD scholarship and the Faculty of Engineering for a Postgraduate Publication Award (PPA). The CSIRO Flagship scholarship fund is gratefully acknowledged for additional support.

References

- [1] Dimitriou, I.; García-Gutiérrez, P.; Elder, R.H.; Cuellar-Franca, R.; Azapagic, A.; Allen, R.W.K. Carbon dioxide utilisation for production of transport fuels: process and economic analysis, *Energy Environ. Sci.* **2015**, 8, 1775-1789.
- [2] Eloneva, S.; Said, A.; Fogelholm, C.J.; Zevenhoven, R. Preliminary Assessment of a Method Utilising Carbon Dioxide and Steelmaking Slags to Produce Precipitated Calcium Carbonate. *Appl. Energy* **2012**, 90, 329-334.
- [3] Sanna, A.; Dri, M.; Hall, M.R.; Maroto-Valer, M.M. Waste materials as a potential resource for carbon capture and storage by mineralisation (CCSM) in the UK context, *Appl. Energy* **2012**, 99, 545-554.
- [4] Lee, J.; Han, S.J.; Wee, J.H. Synthesis of dry sorbents for carbon dioxide capture using coal fly ash and its performance, *Appl. Energy* **2014**, 131, 40-47.
- [5] Jiang L. A review of physical modelling and numerical simulation of long-term geological storage of CO₂. *Appl. Energy* **2011**, 88, 3557-3566.
- [6] Han, S.J.; Im, H.J.; Wee, J.H. Leaching and indirect mineral carbonation performance of coal fly ash-water solution system, *Appl. Energy* **2015**, 142, 274-282.
- [7] Dri, M.; Sanna, A.; Maroto-Valer, M.M. Mineral carbonation from metal wastes: Effect of solid to liquid ratio on the efficiency and characterisation of carbonated products, *Appl. Energy* **2014**, 113, 515-523.
- [8] Pettinau, A.; Ferrara, F.; Amorino, C. Techno-economic comparison between different technologies for a CCS power generation plant integrated with a sub-bituminous coal mine in Italy, *Appl. Energy* **2012**, 99, 32-39.

- [9] Sanna, A.; Dri, M.; Hall, M.R.; Maroto-Valer, M.M. Waste materials as a potential resource for carbon capture and storage by mineralisation (CCSM) in the UK context, *Appl. Energy* **2012**, 99, 545-554.
- [10] Nduagu, E.; Romão, I.; Fagerlund, J.; Zevenhoven, R. Performance assessment of producing Mg(OH)₂ for CO₂ mineral sequestration, *Appl. Energy* **2013**, 106, 116–126.
- [11] Bobicki, E.R.; Liu, Q.; Xu, Z.; Zeng, H. Carbon capture and storage using alkaline industrial wastes. *Prog. Energ. Combust. Sci.* **2012**, 38(2): 302-320.
- [12] Teir, S.; Eloneva, S.; Fogelholm C.J.; Zevenhoven, R. Fixation of carbon dioxide by producing hydromagnesite from serpentinite. *Appl. Energy* **2009**, 86,214-218.
- [13] Hosseini, T.; Selomulya, C.; Haque, N.; Zhang, L. Indirect Carbonation of Victorian Brown Coal Fly Ash for CO₂ Sequestration: Multiple-Cycle Leaching-Carbonation and Magnesium Leaching Kinetic Modelling. *Energy Fuels* **2014**, 28(10), 6481–6493.
- [14] Wang, X.; Maroto-Valer, M.M. Optimisation of carbon dioxide capture and storage with mineralisation using recyclable ammonium salts, *Energy* **2013**, 51, 431-438.
- [15] Bao, W.J.; Li, H.Q.; Zhang, Y. Selective leaching of steelmaking slag for indirect CO₂ mineral sequestration, *Ind. Eng. Chem. Res.* **2010**, 49, 2055-2063.
- [16] Teir, S.; Eloneva, S.; Fogelholm, C.J.; Zevenhoven, R. Dissolution of steelmaking slags in acetic acid for precipitated calcium carbonate production, *Energy* **2007**, 32, 528-539.
- [17] Sun, Y.; Yao, M.S.; Zhang, J.P.; Yang, G. Indirect CO₂ mineral sequestration by steelmaking slag with NH₄Cl as leaching solution. *Chem Eng J* **2011**, 173(2), 437-445.
- [18] Kodama, S.; Nishimoto, T.; Yamamoto, N.; Yogo, K.; Yamada, K. Development of a new pH-swing CO₂ mineralisation process with a recyclable reaction solution. *Energy* **2008**, 33, 776-784.
- [19] Sanna, A.; Uibu, M.; Caramanna, G.; Kuusik, R.; MarotoValer, M.M. A Review of Mineral Carbonation Technologies to Sequester CO₂. *Chem. Soc. Rev.* **2014**, 43: 8049-8080.
- [20] Montes-Hernandez, G.; Pérez-López, R.; Renard, F.; Nieto, J.M.; Charlet, L. Mineral sequestration of CO₂ by aqueous carbonation of coal combustion fly-ash, *J Hazard Mater* **2009**, 161,1347-1354.
- [21] Thomas M.D.A. Optimising the use of fly ash in concrete, IS548. Skokie, IL: Portland Cement Association, **2007**,24.
- [22] Mo, L.; Deng, M.; Tang, M.; Al-Tabbaa, A. MgO expansive cement and concrete in China: Past, present and future. *Cem. Concr. Res.* **2014**, 57, 1-12.

- [23] Pan, S.Y.; Chang, E.E.; Chiang, P.C.; CO₂ Capture by Accelerated Carbonation of Alkaline Wastes: A Review on Its Principles and Applications, *Aerosol and Air Quality Res.* **2012**, 12, 770-791.
- [24] Reddy, K.J.; John, S.; Weber, H.; Argyle, M.D.; Bhattacharyya, P.; Taylor, D.T.; Christensen, M.; Foulke, T.; Fahlsing, P. Simultaneous capture and mineralisation of coal combustion flue gas carbon dioxide (CO₂), *Energy Procedia* **2011**, 4, 1574-1583.
- [25] GCCS, Accelerating the Uptake of CCS: Industrial Use of Captured Carbon Dioxide, P. Brinckerhoff, **2011**, p. 279.
- [26] Uliasz-Bochenczyk, A.; Mokrzycki, E.; Piotrowski, Z.; Pomyka, R. Estimation of CO₂ sequestration potential via mineral carbonation in fly ash from lignite combustion in Poland. *Energy Procedia* **2009**, 1, 4873-4879.
- [27] Muriithi, G.N.; Petrik, L.F.; Fatoba, O.; Gitari, W.M.; Doucet, F.J.; Nel, J.; Nyale, S.M.; Chuks, P.E. Comparison of CO₂ capture by ex-situ accelerated carbonation and in in-situ naturally weathered coal fly ash, *J. Environ. Manag.* **2013**, 127, 212–220.
- [28] Ukwattage, N.L.; Ranjith, P.G.; Wang, S.H. Investigation of the potential of coal combustion fly ash for mineral sequestration of CO₂ by accelerated carbonation, *Energy* **2013**, 52, 230-236.
- [29] Bauer, M.; Gassen, N.; Stanjek, H.; Peiffer, S. Carbonation of lignite fly ash at ambient T and P in a semi-dry reaction system for CO₂ sequestration, *Appl. Geochemistry* **2011**, 26, 1502–1512.
- [30] Giannoulakis, S.; Volkart, K.; Bauer, C. Life cycle and cost assessment of mineral carbonation for carbon capture and storage in European power generation, *Int. J. Greenh. Gas Control* **2014**, 21, 140-157.
- [31] Zevenhoven, R.; Fagerlund, J.; Songok, K.J. CO₂ mineral sequestration: developments toward large-scale application. *Greenhouse Gases Sci. Technol.* **2011**, 1, 48-57.
- [32] Hosseini, T.; Han, B.; Selomulya, C.; Haque, N.; Zhang, L. Chemical and Morphological Changes of Weathered Victorian Brown Coal Fly Ash and its Leaching Characteristic upon the Leaching in Ammonia Chloride and Hydrochloric Acid, *Hydrometallurgy* **2015**, 157, 22-32.
- [33] Strube, R.; Pellegrini, G.; Manfrida, G. The environmental impact of post-combustion CO₂ capture with MEA, with aqueous ammonia, and with an aqueous ammonia-ethanol mixture for a coal-fired power plant, *Energy* **2011**, 36, 3763-3770.
- [34] Aspen plus User guide.

- [35] Zhang, C.; Jun, K.W.; Gao, R.; Lee, Y.J.; Chang, S. Efficient utilisation of carbon dioxide in gas-to-liquids process: Process simulation and techno-economic analysis, *Fuel* **2015**, 157, 285–291.
- [36] Chang, E.E.; Chen, C.H.; Chen, Y.H.; Pan, S.Y.; Chiang, P.C. Performance evaluation for carbonation of steel-making slags in a slurry reactor, *J. Hazard. Mater.* **2011**, 186, 558-564.
- [37] Sun, Y.; Parikh, V.; Zhang, L. Sequestration of carbon dioxide by indirect mineralisation using Victorian brown coal fly ash, *J. Hazard. Mater.* **2012**, 209-210, 458–466.
- [38] Hosseini, T.; Selomulya, C.; Haque, N.; Zhang, L. Investigating the Effect of Mg^{2+}/Ca^{2+} Molar Ratio on the Carbonate Speciation during the Mild Mineral Carbonation Process at Atmospheric Pressure. *Energy Fuels* **2015**, 29(11), 7483-7496.
- [39] Huijgen, W.J.J.; Ruijg, G.J.; Comans, R.N.J; Witkamp, G.J. Energy Consumption and Net CO₂ Sequestration of Aqueous Mineral Carbonation. *Ind. Eng. Chem. Res.* **2006**, 45, 9184-9194.
- [40] Teir, S.; Revitzer, H.; Eloneva, S.; Fogelholm, C.J.; Zevenhoven, R. Dissolution of natural serpentinite in mineral and organic acids. *Int. J. Miner. Process.* **2007**, 83,36-46.
- [41] Fagerlund J, Nduangu E, Zevenhoven R. Recent developments in the carbonation of serpentinite derived $Mg(OH)_2$ using a pressurised fluidised bed, *Energy Procedia* **2011**, 4, 4993–5000.
- [42] Huijgen, W.J.J.; Comans, R.N.J. Carbon dioxide sequestration by mineral carbonation, literature review; Energy research Centre of the Netherlands, ECN-C-03-016, Petten, The Netherlands, **2003**.
- [43] Seider, W.D.; Seader, D.; Lewin, D.R. Product and process design principles: synthesis, analysis, and evaluation. New Jersey: Wiley; **2004**.
- [44] Lee, S. Process simulation, economic analysis and synthesis of biodiesel from waste vegetable oil using supercritical methanol, Master of applied science thesis, University of British Columbia, **2010**.
- [45] Brennan, D. sustainable process engineering. Pan Stanford publishing. CRC press, Taylor & Francis Group; **2012**.
- [46] Alibaba Group, <http://www.alibaba.com/>.
- [47] Brennan, D. Process industry economics. UK: IChemE; **1998**.
- [48] Haque, N.; Bruckard, W.; Cuevas, J. A techno-economic comparison of pyrometallurgical and hydrometallurgical options for treating high-arsenic copper concentrates, *IMPC* **2012**, 17, 1908-1923.

- [49] Eloneva, S.; Said, A.; Fogelholm, C.J.; Zevenhoven, R. Preliminary assessment of a method utilising carbon dioxide and steelmaking slags to produce precipitated calcium carbonate, *Appl. Energy* **2012**, 90, 329-334.
- [50] Maschinenbau, H.V. Injection housing - optimising rotary lobe pumps for liquids with high solids content. *World pumps* **2007**, 489, 36-38.
- [51] Irfan Anwar, H.M. Simulation of Solid Processes by Aspen Plus, Master's thesis, Lappeenranta University of Technology, **2011**.
- [52] Pérez-fortes, M.; Bocin-dumitriu, Andrei.; Tzimas, E. Techno-Economic Assessment of Carbon Utilisation Potential in Europe, *Chem Eng Trans* **2014**, 39, 1453-1458.
- [53] Sipilä, J.; Teir, S.; Zevenhoven, R. Carbon dioxide sequestration by mineral carbonation Literature review update 2005 – 2007. Abo Academi University, **2008**.
- [54] Gerdemann, S.J.; O'Connor, W.K.; Dahlin, D.C.; Penner, L.R.; Rush, H. Ex situ aqueous mineral carbonation, *Environ. Sci. Technol.* **2007**, 41, 2587-2593.
- [55] Nyambura, M.; Mugera, G.; Felicia, P.; Gathura, N. Carbonation of brine impacted fractionated coal fly ash: implications for CO₂ sequestration, *J. Environ. Manage.* **2011**, 92, 655-664.
- [56] Galan, I.; Andrade, C.; Mora, P.; Sanjuan, M.A. Sequestration of CO₂ by concrete carbonation, *Environ. Sci. Technol.* **2010**, 44, 3181-3186.
- [57] <http://www.mineralszone.com/minerals/dolomite.html>.
- [58] Stolaroff, J.K.; Lowry, G.V.; Keith, D.W. Using CaO- and MgO-rich industrial waste streams for carbon sequestration; *Energ. Convers. Manag.* **2004**, 46(5), 687-699.
- [59] http://www.sydneyconstructionmaterials.com.au/mk_pozzolan.html

Chapter 8

Conclusions and future works

This closing chapter compiles and summarises the major conclusions derived from prior working chapters and also provides recommendations for future works.

8.1 Conclusions

This thesis conducted a comprehensive study on possibility of utilisation of Victorian brown coal fly ash *via* indirect mineral carbonation process for the first time. Through this study, an overall closed-loop leaching-carbonation using regenerative ammonium chloride as leaching agent at mild operating condition (temperature $< 80^{\circ}\text{C}$ and atmospheric pressure) was developed. Apart from parametric investigation over the influence of time and temperature on once-through leaching experiments, five closed leaching-carbonation loops using two different types of Victorian brown coal fly ash have been performed to explore the reusability of the leaching reagent as well as the accumulation of impurities upon recycling (Chapter 3).

Following further investigations on the leaching process, the properties and leaching characteristics of weathered fly ash was compared with fresh fly ash. To improve leaching yield of magnesium and calcium, a mixture of $\text{NH}_4\text{Cl}+\text{HCl}$ was used and results were compared with sole HCl leaching. (Chapter 4).

Given the fact that the compositions of both calcium and magnesium in fly ash varies broadly, the competition between the two cations, Ca^{2+} and Mg^{2+} extracted in the leachate can be regarded as the most critical parameter affecting their carbonation rate, as well as the final carbonate product properties. In light of this result, a synthetic leachate was employed and the $\text{Mg}^{2+}/\text{Ca}^{2+}$ ratio was varied between two extremes for pure Ca^{2+} or Mg^{2+} cation to examine their competition in the carbonation process. In addition, the carbonation of the mixed solutions was conducted as a function of reaction temperature and time at atmospheric pressure (Chapter 5).

Due to the complexity of the reactions, none of the available kinetic models for Mg or Ca carbonation can be considered as appropriate model. This required the estimation of optimum kinetic parameters with the aid of simulation and optimisation techniques. A simplified reaction network for Mg^{2+} - Ca^{2+} - CO_2 - NH_3 - H_2O system was developed and the genetic algorithm was used to optimise k values.

Ultimately, the overall simulation and techno-economic analysis of the overall process was performed. The conceptual design of four different scenarios utilising 25 t/h of fly ash using sole NH_4Cl as a reference case scenario and mixture of $NH_4Cl+HCl$ as leaching reagent with different leaching configuration, were implemented with the aid of Aspen plus software. Then the process was techno-economically evaluated.

8.1.1 Multiple cycle leaching-carbonation

Leaching and carbonation percentage of magnesium and calcium decreased upon increasing the cycle number, due to the loss of ammonium chloride by crystallisation and its interaction with dissolved magnesium forming complex precipitates. The optimum conditions, for leaching of magnesium from pure MgO within the range studied here, were found to be at 80°C, reaction time of 30 min, liquid/solid ratio of 6, and ammonium chloride concentration of 4 M. It was found that ammonium chloride is not able to extract magnesium from Yallourn fly ash with a chemically stable magnesia ferrite. On the contrary, Hazelwood fly ash rich in MgO and CaO showed acceptable magnesium and calcium leaching extent. From experimental leaching data, a kinetic model was developed to predict magnesium leaching from Hazelwood fly ash.

8.1.2 Leaching kinetic modelling

It was shown that, the leaching of magnesium in this fly ash follows two different kinetic models. For the first 30 min of reaction, it follows a pseudo-second order reaction with a non-constant ammonium chloride concentration while the second step showed good fit to the diffusion control process. The activation energy for the leaching of MgO was found to be ~20.7 kJ/mol from the start of reaction toward 30 min after reaction. This activation energy is consistent with the values obtained for the reaction control kinetic modelling.

8.1.3 Properties and leaching propensity of weathered fly ash

In comparison to the fresh fly ash rich in oxides, the weathered fly ash is dominated by hydrates and carbonate forms which were formed in aqueous landfilling system. These species were mostly poorly crystallised, and even loosely agglomerated into the clusters. Irrespective of the leaching reagent, the target Ca and Mg in the weathered fly ash were more easily extracted

than in the fresh ash under the same leaching conditions. This is due to the association of these two metals with the amorphous species.

8.1.4 Selective leaching of Mg and Ca by NH₄Cl+HCl solution

It was found that the use of NH₄Cl+HCl is superior over sole HCl, due to the buffering property of NH₃ and its complexing capability to prevent the dissolution of impure elements. Instead, the use of sole HCl even at the same pH value as the mixture of NH₄Cl + HCl, resulted in a deep penetration of protons into particles. The intense breakage of the ash cluster, and hence, the simultaneous dissolution of plenty of impure elements occurred.

8.1.5 Effect of Mg²⁺/Ca²⁺ molar ratio and reaction time on carbonation

Under the ambient conditions, an initial pH of ~11, and the CO₂ flow rate of 15 L/min (large enough to eliminate the diffusion resistance in this study), the carbonation of sole Ca²⁺ or Mg²⁺ can be completed in 10 min and 30 min, respectively. Upon the blending of two cations and the increase in the Mg²⁺/Ca²⁺ molar ratio, the carbonation time for Ca²⁺ was increased. On the contrary, the time was shortened noticeably for Mg²⁺. In terms of the carbonation reactivity, the reactivity of Ca²⁺ was decreased linearly upon increasing the Mg²⁺/Ca²⁺ ratio, whereas Mg²⁺ achieved its maximum reactivity at Mg²⁺/Ca²⁺ molar ratio of 2. This is due to the trapping of Mg²⁺ into the calcite lattice to form magnesian calcite

8.1.6 Composition of carbonate precipitates

The metastable phase of vaterite is predominant for the case of sole Ca²⁺, which is mainly formed upon the shell damage of aragonite. The amorphous phase accounts for less than 20 wt% of the total carbonate. In contrast, the carbonate formed from sole Mg²⁺ is mainly unidentifiable upon XRD speciation, which is presumably hydromagnesite. The blending of Ca²⁺ and Mg²⁺ induced the formation of magnesian calcite caused by the substitution of a portion of Ca²⁺ by Mg²⁺ in the calcite lattice. The formation of this complex is also favoured upon increasing the Ca²⁺/Mg²⁺ molar ratio.

8.1.7 Effect of temperature on carbonation

Increasing the temperature is in favour of the carbonation of both ions particularly Ca²⁺ before 60°C. The increase of temperature from 60°C results in the reduction of the carbonation reactivity of Mg²⁺, due to the decreased solubility of CO₂. Upon the elevation of the reaction temperature, the Ca-bearing carbonate changes its crystal from trigonal-rhombohedral calcite to orthorhombic aragonite. The resulting aragonite is not in favour of the formation of magnesian calcite. As a result, the amorphous structure dominated by Mg²⁺ is dominant in the high temperature carbonate precipitate.

8.1.8 Techno-economic analysis of different scenarios

The overall production costs and CO₂ capture cost for base case scenario was estimated as ~\$72.5 per tonne of product and \$162.3 per tonne of CO₂, respectively. The process scenario, implemented NH₄Cl+HCl as leaching reagent, resulted in significantly higher costs and higher carbonation conversion than other scenarios. The primary reasons were the high cost of HCl and the larger size of equipment resulting from treatment and circulation of the large volume of raw materials. The cost of CO₂ capture for this process considering only scenarios 1 and 3 is in the range for natural minerals mineralisation and potentially be cheaper than few cost estimations done so far for industrial wastes. However, in addition to capture CO₂, this process has another advantage which is decreasing the amount of waste fly ash in the landfills.

8.2 Recommendations

The research findings reported in this thesis have demonstrated the feasibility of utilisation of Victorian brown coal fly ash *via* indirect mineral carbonation process. This research has primarily been conducted as a fundamental study regarding the effects of variation of operating parameters on magnesium and calcium leaching and carbonation, along with multiple-cycle test. A techno-economic evaluation of this process shows that cost per tonne of CO₂ captured in this process is in the range of typical mineral carbonation processes developed on pilot scale and demonstration scales. Although the cost per tonne of CO₂ in this process is high compared to the other carbon capture methods such as underground storage, but this process has another advantage which is the utilisation of the fly ash and emptying the ash ponds. Future work is recommended to better understand the phenomena observed in this study. An environmental impact evaluation of this flowsheet using life cycle assessment (LCA) is also recommended.

8.2.1 Investigating the leaching capability and crystallisation affinity of other ammonia salts

To overcome the problems of crystallisation of ammonia chloride, other ammonium salts such as ammonium acetate or ammonia carbonate can be examined. Ammonium acetate is supposed to be able to extract alkaline earth metals as well; it also possesses higher solubility in water (about 3-4 times higher than ammonium chloride at the same temperature). Hence, its crystallisation is supposed to be unlikely in the proposed process. The final decision should be taken after the investigation of extraction capability of ammonium acetate, feed and operation cost and crystallisation affinity of this solvent in high concentration of magnesium and calcium chloride.

8.2.2 Pilot scale research

An important next step in aqueous mineral carbonation research is a pilot-scale process under continuous feeding of solid (fly ash) and the process of liquid (leachate) at a larger scale. Pilot-scale research should provide more insight in the technically feasible range of reactor conditions and may improve the leaching extent due to the circulating fresh leaching reagent. The amount of heat required in a jacketed reactor and the heat loss to environment can be investigated which is important for reducing the energy consumption and the cost of the current process. In addition, the heat integration of exothermic and endothermic sub-processes through pinch analysis can be undertaken in the future.

8.2.3 Research on application or purification of carbonation products

Research on the re-use possibilities of carbonation products is recommended, particularly with regard to determination of the value and volume of possible markets. The beneficial utilisation of these products can contribute to a substantial reduction of sequestration costs. The purification of product through pH adjustment prior to the carbonation or post-purification process might be helpful if higher purity products are required.

8.2.4 Research on regeneration of HCl

Further research on HCl regeneration through electrolysis processes seems warranted given significantly lower production cost. Such research may focus on the possible route for the production of HCl from $MgCl_2$ solution which may need high energy. However the heat integration of the whole process can reduce the total heat consumption and consequently the cost of the process and make this process economically viable. This suggestion has, however, not yet been experimentally verified.

8.2.5 Utilisation of other industrial wastes through this process

Given the fact that this process could be applied easily on a fly ash rich in Mg and Ca in the free oxide or hydroxide form, it is worthwhile to conduct more research on the application of this process on other potentially suitable industrial wastes such as steel-making slag and municipal solid waste incinerator ash (MSWI). Preliminary research using steel-making slag as the feedstock for this process confirmed possibility of utilisation of this waste through this process.

Appendix

The following appendices comprise the individual experimental chapter's supplementary material; it is intended to complement the results reported within each chapter.

Appendix A: Supplementary material – Chapter 5

Appendix B: Supplementary material – Chapter 6

Appendix C: Supplementary material – Chapter 7

Appendix D: Online version of published papers

Appendix A.

Supplementary material – Chapter 5

- Q-XRD reliability experiments

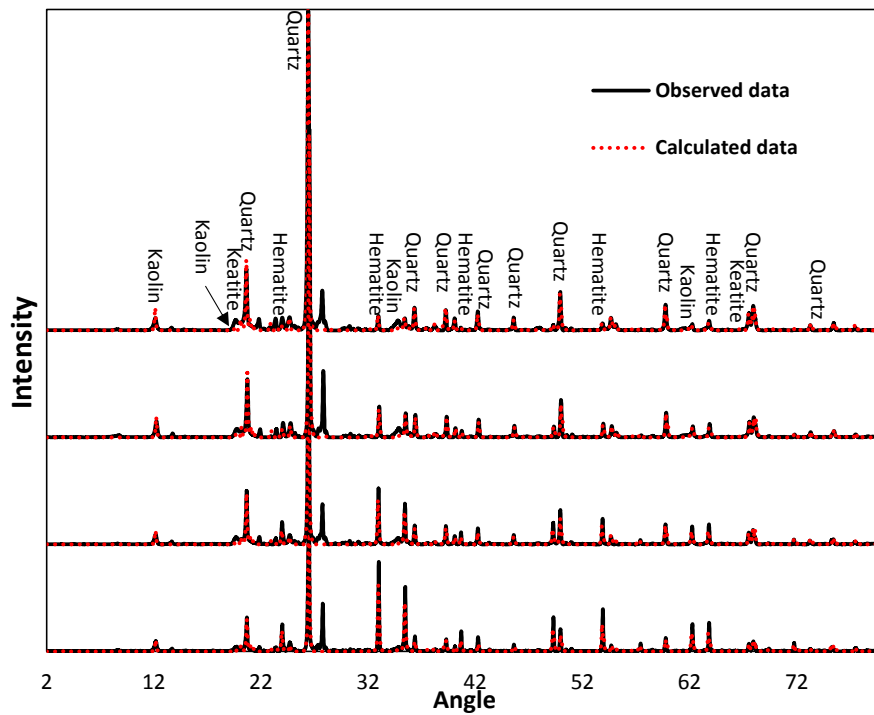


Figure A.1 XRD spectrum for Fe₂O₃ and SiO₂ mixture at different mass ratios (From top to bottom SiO₂ + 2.5%, 5%, 10% and 20% Fe₂O₃); black solid line represents observed data and red dot line shows Siroquant fitting

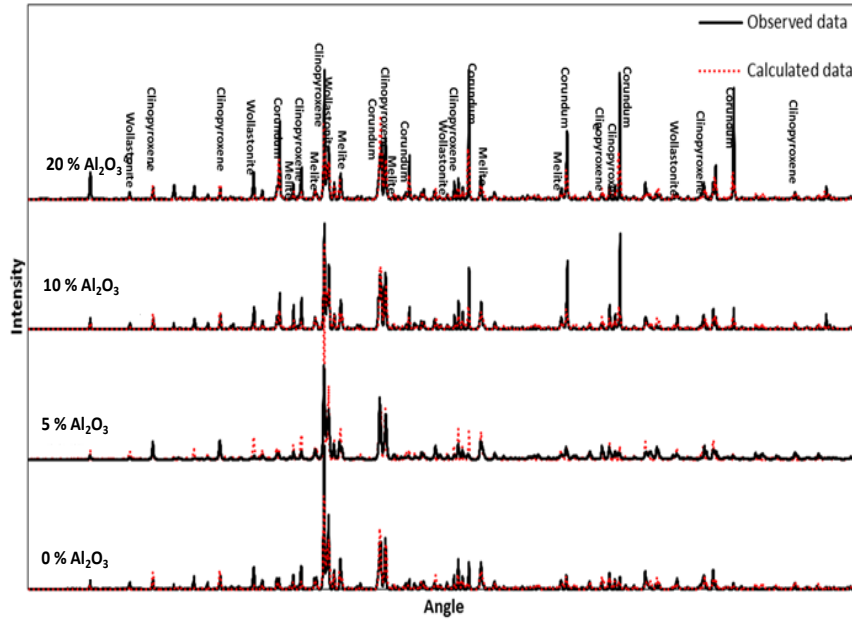


Figure A.2 XRD spectrum for fly ash mixed with different proportions of corundum

Table A.1 QXRD and XRF results of fly ash mixed with different percentage of Al₂O₃ and amorphous amount calculated

Elements	MgO(wt%)		Al ₂ O ₃ (wt%)		SiO ₂ (wt%)		CaO(wt%)		Fe ₂ O ₃ (wt%)		Amorphous wt%
	XRD	XRF	XRD	XRF	XRD	XRF	XRD	XRF	XRD	XRF	
Fly ash + 0% Al ₂ O ₃	8.74	11.24	12.33	8.567	35.38	31.82	24.36	21.92	3.86	12.9	-
Fly ash + 5% Al ₂ O ₃	8.03	9.44	17.85	10.91	33.86	32.63	23.23	21.13	4.18	12.45	15.7
Fly ash + 10% Al ₂ O ₃	6.28	7.88	30.54	13.22	26.77	33.38	19.94	20.42	5.08	11.97	57.2
Fly ash + 20% Al ₂ O ₃	4.2	4.77	49.38	18.29	17.77	35.06	13.22	19.01	7.58	10.32	65.7

Appendix B.

Supplementary material – Chapter 6

Contents:

1. Genetic algorithm codes in MATLAB
2. Objective function
3. Genetic algorithm objective function
4. K_{eq} function
5. Henry coefficients function

- **Genetic algorithm codes in MATLAB**

```
clc;
clear;
load 'Z:\F\Kinetic Modeling\Parameters.mat';
reply = input('Do you want to load last population?\nEnter: No\n1: Yes\n2: Only the best population\n','s');
if isempty(reply)
    reply = 'N';
end
population=20;
Iteration=3000;
format long;
S=size(Params);
ParamDim=S(1);
S=size(CarbonationExpData);
ExperDim=S(1);
Fitness=zeros(1,population);
if reply == 'N'
    X=(rand(ParamDim,population));
    for i=1:population
        X(:,i)=X(:,i).*(Params(:,3)-Params(:,2))+Params(:,2);
    end
    X(:,1)=Params(:,1);
end
if reply == '1'
    load 'Z:\F\Kinetic Modeling\LastPup.mat';
end
if reply == '2'
    load 'Z:\F\Kinetic Modeling\LastPup.mat';
    BestX=X(:,1);
    X=(rand(ParamDim,population));
    for i=1:population
        X(:,i)=X(:,i).*(Params(:,3)-Params(:,2))+Params(:,2);
    end
    X(:,1)=BestX;
end
FitnessArray=zeros(Iteration,2);
PupStart=1;
for IterationCount=1:Iteration
    for PupCount=PupStart:population
        KineticPar=X(:,PupCount);
        m_F=0;
        for ExpCount=1:ExperDim
            KineticExpdata=CarbonationExpData(ExpCount,:);
            [m_Fitness, time, C_Results]=ObFunc1(KineticPar, KineticExpdata);
            m_F=m_F+m_Fitness;
        end
    end
end
```

```

if(m_F<0.0)
    m_F=1000;
end
Fitness(PupCount)=m_F;
end
PupStart=fix(population/2)+1;
%sorting
for i=1:population
    for j=1:population-1
        if(Fitness(j)>Fitness(j+1))
            Ftemp=Fitness(j);
            Fitness(j)=Fitness(j+1);
            Fitness(j+1)=Ftemp;
            temp=X(:,j);
            X(:,j)=X(:,j+1);
            X(:,j+1)=temp;
        end
    end
end
%breeding and mutation
for i=fix(population/2)+1:2:population
    I=fix(rand(1)*population/2);
    J=fix(rand(1)*population/2);
    if(round(rand(1)*20)==10)
        I=1;
        J=1;
    end
    if(I==0) I=1; end
    if(J==0) J=1; end
    p1=X(:,I);
    p2=X(:,J);
    for c=1:ParamDim
        if(round(rand(1))==1)
            off1(c)=0.8*p1(c)+0.2*p2(c);
            off2(c)=0.8*p2(c)+0.2*p1(c);
        else
            off1(c)=0.8*p2(c)+0.2*p1(c);
            off2(c)=0.8*p1(c)+0.2*p2(c);
        end
        if(round(rand(1)*6)==3)
            off1(c)=rand(1)*(Params(c,3)-Params(c,2))+Params(c,2);
            off2(c)=rand(1)*(Params(c,3)-Params(c,2))+Params(c,2);
        end
    end
    X(:,i)=off1';
    X(:,i+1)=off2';
end
FitnessArray(IterationCount,1)=Fitness(1);
FitnessArray(IterationCount,2)=mean(Fitness);
% if(round(IterationCount/10)*10==IterationCount)
    fprintf('Iteration=%d Best Fitness=%d Mean
Fitness=%d\n',IterationCount,FitnessArray(IterationCount,1),FitnessArray(IterationCount,2));
    save('LastPup','X');
% end
end

```

- **Objective function**

```

function [Fitness time C_Results]=ObFunc1(Params, Expdata)
Kvalues=0;
Evalues=0;
Nvalues=0;
Mvalues=0;
Kvalues=Params(1:11);

```

```

Evalues=Params(11:22);
Nvalues=Params(23:44);
Mvalues=Params(45);
CO2Pressure=1; %atm
Temperature=Expdata(1); %kelvin
Time=Expdata(4);
ExppH=Expdata(7);
V=0.05+0.016; %reactor volume
CCO2g=1;
C_Mg=Expdata(2);
C_Ca=Expdata(3);
C_Mg0=Expdata(2);
C_Ca0=Expdata(3);
C_NH4OH=0;
C_NH4=0;
C_OH=10^-7;
C_H=10^-7;
C_CO2aq=0;
C_CO2g=0;
C_HCO3=0;
C_CO3=0;
C_CaCO3=0;
C_MgCO3=0;
C_CaMgCO3_2=0;
C_M_1CaMMgCO3=0;
Keq=0;
Keq(1)=GetKeq(1, Temperature);
Keq(2)=GetKeq(2, Temperature);
Keq(3)=GetKeq(3, Temperature);
Keq(4)=GetKeq(4, Temperature);
Keq(5)=GetKeq(5, Temperature);
Keq(6)=GetKeq(6, Temperature);
Keq(7)=GetKeq(7, Temperature);
Keq(8)=GetKeq(8, Temperature);
Keq(9)=GetKeq(9, Temperature);
Keq(10)=GetKeq(10, Temperature);

%initial concentrations
C_CO2g=CO2Pressure; %Atm

M_NH4OH=0.21; %mol of amonia added at first of reaction
C_NH4OH_before_Reaction=M_NH4OH/V;
C_NH4OH=C_NH4OH_before_Reaction;

%calculation of ammonia equilibrium before reaction
KbNH3=1.77*10^-5;
syms c_x positive; % remain NH4OH after equilbirium
[cc]=solve(c_x^2+c_x*KbNH3-C_NH4OH_before_Reaction*KbNH3);
C_NH4OH=C_NH4OH_before_Reaction-double(cc);
C_NH4=double(cc);
C_OH=double(cc);
C_H=10^-14/C_OH;

I=0; %sumation of ions concentration
C_CO2aq0=CO2Pressure/Henry(Temperature,I);
%C_CO2aq0=CO2Pressure/Henry(298,I);

tt=0:Time;

[t,C]=ode23s(@(t,C) GA1ODEFunc(t,C,Kvalues,Evalues,Nvalues,Mvalues,Keq,C_CO2aq0, Temperature)
,tt,[C_H,C_NH4OH,C_NH4,C_CO2aq,C_HCO3,C_CO3,C_Ca,C_CaCO3,C_Mg,C_MgCO3,C_CaMgCO3_2
C_M_1CaMMgCO3]);

% 1- H+
% 2- NH4OH
% 3- NH4
% 4- CO2aq

```

```

% 5- HCO3
% 6- CO3
% 7- Ca
% 8- CaCO3
% 9- Mg
% 10- MgCO3
C_Results=C;
time=t;
C_H=C(:,1);
% C_NH4OH=C(:,2);
% C_NH4=C(:,3);
% C_CO2aq=C(:,4);
% C_HCO3=C(:,5);
% C_CO3=C(:,6);
pH=-log10(C_H(end));

C_Ca=C(:,7);
C_Mg=C(:,9);

CalcCaCarbonation=0;
CalcMgCarbonation=0;

if C_Ca0>0 CalcCaCarbonation=(C_Ca0-C_Ca(end))/C_Ca0; end
if C_Mg0>0 CalcMgCarbonation=(C_Mg0-C_Mg(end))/C_Mg0; end
if ExppH==0
    ExppH=pH;
end

Fitness=(CalcMgCarbonation-Expdata(5))^2+(CalcCaCarbonation-Expdata(6))^2;
%+((pH-ExppH)/5)^2
%(CalcMgCarbonation-Expdata(5))^2;

```

- **Genetic algorithm objective function:**

```

function DC = GA1ODEFunc( t, C, K_values, E_values, N_values, Mvalues, Keq, C_CO2g, Temp)
%UNTITLED2 Summary of this function goes here
% Detailed explanation goes here

C_H= C(1); % 1- H+
C_NH4OH= C(2); % 2- NH4OH
C_NH4= C(3); % 3- NH4
C_CO2aq= C(4); % 4-CO2aq
C_HCO3=C(5); % 5-HCO3
C_CO3=C(6); % 6-CO3
C_Ca=C(7); %7-Ca
C_CaCO3=C(8); %8-CaCO3
C_Mg=C(9); %9-Mg
C_MgCO3=C(10); %10-MgCO3
C_CaMgCO3_2=C(11); %11-CaMg(CO3)2
C_M_1CaMMgCO3=C(12); %12-CaMgn(CO3)2

R=8.314;
K_1=K_values(1)*exp(-E_values(1)/(R*Temp));
K_2=K_values(2)*exp(-E_values(2)/(R*Temp));
K_3=K_values(3)*exp(-E_values(3)/(R*Temp));
K_4=K_values(4)*exp(-E_values(4)/(R*Temp));
K_5=K_values(5)*exp(-E_values(5)/(R*Temp));
K_6=K_values(6)*exp(-E_values(6)/(R*Temp));
K_7=K_values(7)*exp(-E_values(7)/(R*Temp));
K_8=K_values(8)*exp(-E_values(8)/(R*Temp));
K_9=K_values(9)*exp(-E_values(9)/(R*Temp));
K_10=K_values(10)*exp(-E_values(10)/(R*Temp));
K_11=K_values(11)*exp(-E_values(11)/(R*Temp));

```

```

m=Mvalues(1);

%N_values(:)=1;
n1A=N_values(1);
n1B=N_values(2);
n2A=N_values(3);
n2B=N_values(4);
n3A=N_values(5);
n3B=N_values(6);
n4A=N_values(7);
n4B=N_values(8);
n5A=N_values(9);
n5B=N_values(10);
n6A=N_values(11);
n6B=N_values(12);
n7A=N_values(13);
n7B=N_values(14);
n8A=N_values(15);
n8B=N_values(16);
n9A=N_values(17);
n9B=N_values(18);
n10A=N_values(19);
n10B=N_values(20);
n11A=N_values(21);
n11B=N_values(22);

KspCaCO3=2.8e-9;
KspMgCo3=3.5e-8;

r1=K_1*C_NH4;
r1r=K_1/Keq(1)*C_NH4OH*C_H;
r2=K_2*C_CO2g;
r2r=K_2/Keq(2)*C_CO2aq;
r3=K_3*C_CO2aq;
r3r=K_3/Keq(3)*C_HCO3*C_H;
r4=K_4*C_HCO3;
r4r=K_4/Keq(4)*C_CO3*C_H;
r5=K_5*C_Ca^n5A*C_CO3^n5B;
r5r=K_5/Keq(5)*C_CaCO3*KspCaCO3;
r6=K_6*C_Ca^n6A*C_HCO3^n6B;
r6r=K_6/Keq(6)*C_CaCO3*KspCaCO3*C_H;
r7=K_7*C_Mg^n7A*C_CO3^n7B;
r7r=K_7/Keq(7)*C_MgCO3*KspMgCo3;
r8=K_8*C_Mg^n8A*C_HCO3^n8B;
r8r=K_8/Keq(8)*C_MgCO3*KspMgCo3*C_H;
r9=K_9*C_Mg^n9A*C_CaCO3^n9B;
r9r=K_9/Keq(9)*C_M_1CaMMgCO3*KspMgCo3*C_Ca;
r10=K_10*C_Mg^n10A*C_CaCO3^n10B;
r10r=K_10/Keq(10)*C_MgCO3*KspMgCo3*C_Ca;
r11=K_11*C_Ca^n11A*C_MgCO3^n11B;
r11r=0;

% 1- H+
DC(1)=r1+r3+r4+r6+r8-(r1r+r3r+r4r+r6r+r8r);
% 2- NH4OH
DC(2)=r1-r1r;
% 3- NH4
DC(3)=r1+r1r;
% 4-CO2aq
DC(4)=r2+r3r-(r3+r2r);
%HCO3
DC(5)=r3+r4r+r6r+r8r-(r3r+r4r+r6r+r8r);
%6-CO3
DC(6)=r4+r5r+r7r-(r4r+r5r+r7r);
%7-Ca
DC(7)=r5r+r6r+(1-m)*r9r+r10r+r11r-(r5r+r6r+(1-m)*r9r+r10r+r11r);
%8-CaCO3

```

```

DC(8)=r5+r6+r9*(1-m)+r10r-(r5r+r6r+(1-m)*r9+r10);
%9-Mg
DC(9)=r7+r8r+m*r9r+r10r-(r7+r8r+m*r9+r10);
%10-MgCO3
DC(10)=r7+r8+r10+2*r11r-(r7r+r8r+r10r+2*r11);
%11-CaMg(CO3)2
DC(11)=r11-r11r;
%12-CaMgn(CO3)2
DC(12)=r9-r9r;

DC=DC';

end

```

- **K_{eq} function:**

```

function [ output_args ] = GetKeq( Index,Temp )
%UNTITLED Summary of this function goes here
% Detailed explanation goes here
output_args=1;

if Index==1
    output_args=10^-14/spline([273 20+273 40+273 50+273],[1.374*10^-5 1.71*10^-5 1.86*10^-5 1.89*10^-5],Temp);
end

if Index==2
    output_args=10^spline([20+273 30+273 70+273],[-1.406 -1.526 -1.860],Temp);
end

if Index==3
    output_args=(10^spline([20+273 30+273 70+273],[-6.384 -6.327 -6.274],Temp));
end

if Index==4
    output_args=(10^spline([20+273 30+273 70+273],[-10.376 -10.289 -10.106],Temp));
end

if Index==5
    output_args=(spline([20+273 30+273 70+273],[185491381.255513 217257233.79653 567591431.645492],Temp));
end
if Index==6
    output_args=(spline([20+273 30+273 70+273],[0.00818861672178954 0.0120382201844934 0.0527302713919156],Temp));
end
if Index==7
    output_args=(spline([20+273 30+273 70+273],[85672.2577033279 160093.617741763 2009521.45237608],Temp));
end
if Index==8
    output_args=(spline([20+273 30+273 70+273],[3.78204786267979E-06 8.87078504512493E-06 0.000186688180342105],Temp));
end
if Index==9
    output_args=(spline([20+273 30+273 70+273],[0.021491079878748 0.0271456275803566 0.0595015676606316],Temp));
end
if Index==10
    output_args=(spline([20+273 30+273 70+273],[0.000461866514354729 0.000736885096731417 0.00354043655407272],Temp));
end
end
end

```

- **Henry coefficient function**

```
function [ output_args ] = Henry( Temperature,I)
%UNTITLED Summary of this function goes here
% Detailed explanation goes here

output_args=29.41*exp(-2400*(1/Temperature-1/298.15))*10^(-0.138*I);% atm/(mole/liter)
end
```

Appendix C.

Supplementary material – Chapter 7

Contents:

1. Aspen plus simulation
2. Equipment design

- **Aspen plus simulation**

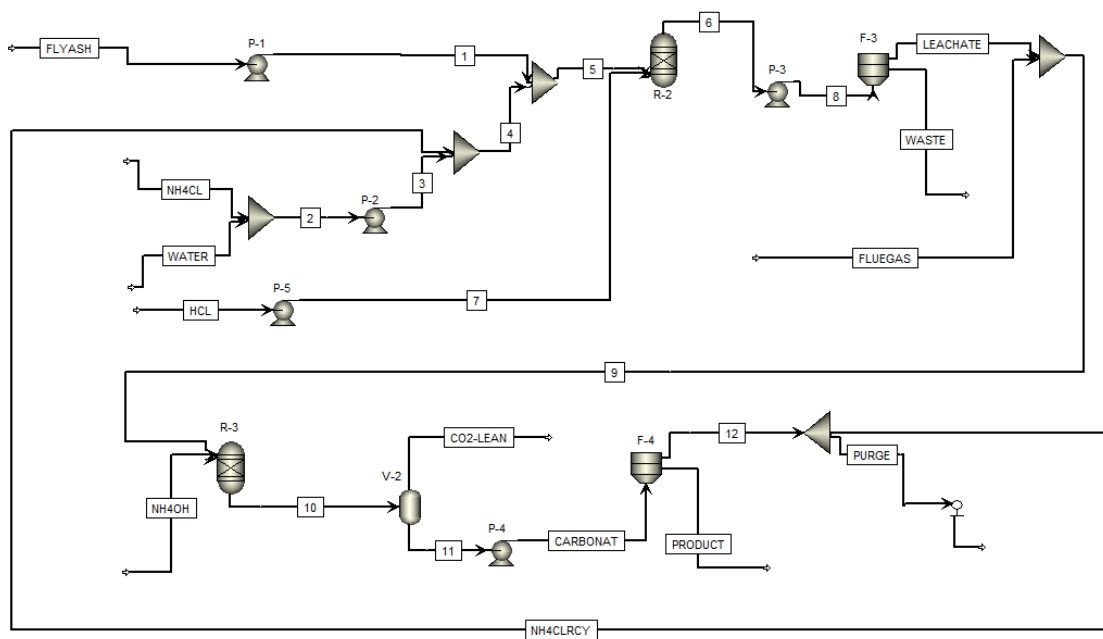


Figure C.1 Aspen simulation for scenario 2 ($\text{NH}_4\text{Cl}+\text{HCl}$ leaching)

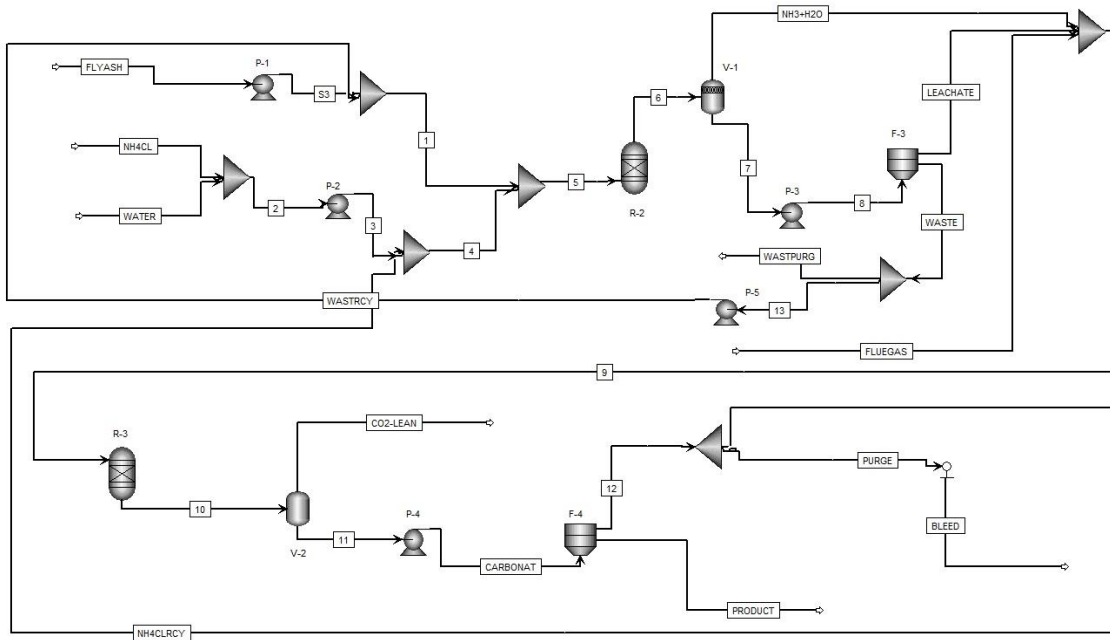


Figure C.2 Aspen simulation for scenario 3 (leaching waste recycling)

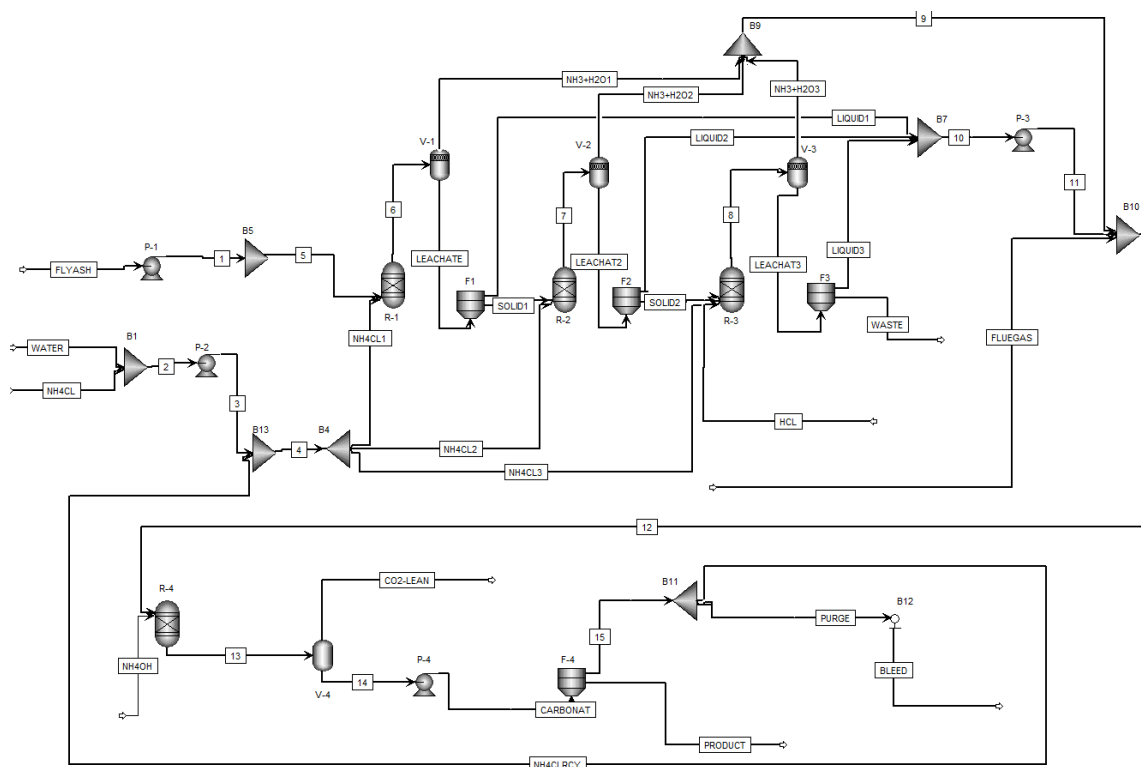


Figure C.3 Aspen simulation for scenario 4 (multi-stage leaching)

- **Equipment design**

Table C.1 Pump sizing and detailed design for the first scenario

Equip	Equip Description	No.	Tag	Property	Value	Units
NH ₄ Cl Recycle Pump	Sanitary rotary lobe pump	2	P-4	Casing material	SS 316	
				Design gauge pressure	1300	KPAG
				Driver power	37.500	KW
				Fluid viscosity	0.5	MPA-S
				Impeller speed	254.000	RPM
				Liquid flow rate	23.000	L/S
				Material	SS316	
				Pump size selection	520-8	
				Relief cover type	0	
				Seal type	MECH	
				Source of quote	SG	
				Total weight	2200	KG
leachate Pump	Sanitary rotary lobe pump	1	P-3	Casing material	SS 316	
				Design gauge pressure	1300	KPAG
				Driver power	75	KW
				Fluid viscosity	0.5	MPA-S
				Impeller speed	378	RPM
				Liquid flow rate	41.221	L/S
				Material	SS316	
				Pump size selection	520-8	
				Relief cover type	0	
				Seal type	MECH	
				Source of quote	SG	
				Total weight	2400	KG
NH ₄ Cl Pump	Centrifugal single or multi-stage pump	1	P-2	Casing material	SS316	
				Design gauge pressure	468.671	KPAG
				Design temperature	125	DEG C
				Driver power	1.5	KW
				Driver type	motor	
				Fluid head	107.5	M
				Fluid viscosity	0.5	MPA-S
				Liquid flow rate	3.3718	L/S
				Seal type	SNGL	
				Source of quote	SG	
				Speed	3000	RPM
				Total weight	570	KG
Fly ash Pump	Centrifugal single or multi-stage pump	1	P-1	Casing material	SS 316	
				Design gauge pressure	1300	KPAG
				Driver power	11	KW
				Fluid viscosity	0.5	MPA-S
				Impeller speed	470	RPM
				Liquid flow rate	5.9335	L/S
				Material	SS316	
				Pump size selection	130-3	
				Relief cover type	0	
				Seal type	MECH	
				Source of quote	SG	
				Total weight	330	KG

Table C.2 Reactor sizing and detailed design for the based case scenario

Equip	Equip Description	No.	Tag	Property	Value	Units
Leaching reactor	Agitated tank - enclosed, jacketed	1	R-2	Agitator power	90.000	KW
				Application	CONT	
				Base material thickness	26.000	MM
				Design gauge pressure	243.671	KPAG
				Design temperature	125.000	DEG C
				Fluid depth	12.802	M
				Impeller speed	347.000	RPM
				Jacket design gauge pressure	620.001	KPAG
				Jacket type	FULL	
				Liquid volume	137.711	M3
				Shell material	SS316	
				Source of quote	SG	
				Total weight	77300	KG
				Vessel diameter	3.6576	M
				Vessel tangent to tangent height	13.106	M
Carbonation reactor	Agitated tank - enclosed, jacketed	1	R-3	Agitator power	75.000	KW
				Application	CONT	
				Base material thickness	26.000	MM
				Design gauge pressure	243.671	KPAG
				Design temperature	125.000	DEG C
				Fluid depth	11.582	M
				Impeller speed	373.000	RPM
				Jacket design gauge pressure	620.001	KPAG
				Jacket type	FULL	
				Liquid volume	104.951	M3
				Shell material	SS316	
				Source of quote	SG	
				Total weight	62500	KG
				Vessel diameter	3.3528	M
				Vessel tangent to tangent height	11.887	M

Table C.3 Separation unit sizing and detailed design for the based case scenario

Equip Category	Equip Description	No.	Tag No	Property	Value	Units
carbonation step solid-liquid Separation	Pressure leaf-wet filter	1	F4	Item type	LEAF WET	
				Material	SS316	
				Source of quote	SG	
				Surface area	26.245	M2
				Total weight	1600	KG
Leaching step solid-liquid Separation	Pressure leaf-wet filter	2	F3	Item type	LEAF WET	
				Material	SS316	
				Source of quote	SG	
				Surface area	55.000	M2
				Total weight	2700	KG

Table C.4 Vessel sizing and detailed design for the based case scenario

Equip Category	Equip Description	No.	Tag No	Property	Value	Units
Ammonia recovered flash separator	vertical process vessel	1	V-1	Application	CONT	
				Base material thickness	5	MM
				Design gauge pressure	243.671	KPAG
				Design temperature	130	DEG C
				Liquid volume	18.793	M3
				Shell material	SS316	
				Source of quote	SG	
				Total weight	2600	KG
				Vessel diameter	1.9812	M
				Vessel tangent to tangent height	6.0960	M

Appendix D.

Published versions of thesis chapters

Chapter 3

T. Hosseini, C. Selomulya, N. Haque, L. Zhang, Indirect Carbonation of Victorian Brown Coal Fly Ash for CO₂ Sequestration: Multiple-Cycle Leaching-Carbonation and Magnesium Leaching Kinetic Modelling, *Energy & Fuels*, 2014, 28(10), pp 6481–6493.

Chapter 4

T. Hosseini, C. Selomulya, N. Haque, L. Zhang, Chemical and Morphological Changes of Weathered Victorian Brown Coal Fly Ash and its Leaching Characteristic upon the Leaching in Ammonia Chloride and Hydrochloric Acid, *Hydrometallurgy*, 2015, 157, pp 22-32.

Chapter 5

T. Hosseini, C. Selomulya, N. Haque, L. Zhang, Investigating the Effect of Mg²⁺/Ca²⁺ Molar Ratio on the Carbonate Speciation during the Mild Mineral Carbonation Process at Atmospheric Pressure, *Energy & Fuels*, 2015, 29 (11), pp 7483–7496.

Indirect Carbonation of Victorian Brown Coal Fly Ash for CO₂ Sequestration: Multiple-Cycle Leaching-Carbonation and Magnesium Leaching Kinetic Modeling

Tahereh Hosseini,[†] Cordelia Selomulya,[†] Nawshad Haque,[‡] and Lian Zhang^{*,†}

[†]Department of Chemical Engineering, Monash University, Clayton, GPO Box 36, Victoria 3800, Australia

[‡]Process Science and Engineering Division, CSIRO, Clayton, Victoria 3168, Australia

ABSTRACT: In this paper, a closed-loop multistep process which allows leaching and precipitation of magnesium and calcium as carbonate from Victorian brown coal fly ash has been examined. Victorian brown coal fly ash has a distinctively high concentration of alkaline earth metals and low amounts of aluminum and silica. The main objective here is to clarify the dissolution kinetics of magnesium and calcium in regenerative ammonium chloride and subsequent carbonation of dissolved cations. Instead of a once-through test with fresh ammonium chloride, multiple locked circuits were adopted to assess the leaching capability of regenerated ammonium salt, as well as the accumulation of impurities upon the recycling and reuse of the leaching agent. As has been revealed, upon increasing cycles of ammonium chloride use, the extraction yields of both target cations decreased significantly. Their extraction by ammonium chloride was favored by the presence of the oxide form in the original ash sample, with the extraction of calcium occurring much faster than that of magnesium. Both phenomena were in agreement with the thermodynamic equilibrium prediction on the lowest Gibbs function for the dissolution of oxides, especially calcium oxide in ammonium chloride solution. Carbonation results dropped gradually upon the increase in the cycle number; meanwhile, the size and morphology of precipitates were changed from the first to last cycle. By fitting the observed results with a shrinking core model, it was shown that the extraction of Mg²⁺ followed a pseudo-second-order reaction with a nonconstant ammonium chloride concentration in the film layer on the surface of a solid particle. The activation energy of 20.7 kJ mol⁻¹ was obtained for the dissolution of magnesium from both Hazelwood fly ash and pure MgO in ammonium chloride solution.

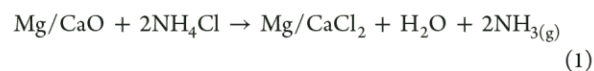
1. INTRODUCTION

Mineral carbonation or mineralization is one of the most promising processes for carbon capture, storage, and utilization (CCSU) to combat the climate change. In this process, carbon dioxide (CO₂) reacts with alkaline oxides or hydroxides, specifically magnesium and/or calcium in natural minerals or industrial waste, to convert into thermodynamically stable carbonates, thus avoiding the necessity of the costly monitoring of CO₂ leakage during transportation and storage.¹

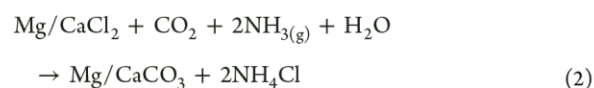
Mineral carbonation technologies can be divided into single-step (direct) and multiple-step (indirect) categories. The single-step method involves a direct reaction of feedstock material with CO₂ in a single reactor maintained at controlled temperature and pressure which generally fall in the ranges 100–500 °C and 10–20 bar, respectively.² In contrast, the multistep indirect carbonation is initiated by the dissolution of a mineral species in an aqueous medium to extract the alkaline earth metals within it. The resulting cations are subsequently carbonated through bubbling the CO₂-containing flue gas into the leachate. Both leaching and carbonation take place under relatively mild conditions, e.g., 20–80 °C and 1–5 bar.

The leaching media for the dissolution of calcium and magnesium in minerals are either strong or weak acidic reagents, ammonium salts, or alkaline solutions.³ Of those, the ammonium extraction process appears to be a favorable technique, given its potential for reagent recovery and the relatively large selectivity of magnesium and calcium over other elements,⁴ as demonstrated by the reactions below:

Extraction:



Carbonation:



To date, various types of minerals rich in alkaline earth metals, either natural species or man-made industry waste, have been tested for their carbonation propensities. These include serpentine,⁵ olivine and wollastonite,⁶ fly ash derived from coal combustion and municipal solid waste incineration (MSWI),^{3,7} blast furnace, and steelmaking slag.^{1,8} Brown coal fly ash is a potentially appropriate source, as it is rich in magnesium and/or calcium. The fly ash is generated on-site with CO₂ together in a power plant. It possesses a particle size distribution with the majority falling in the micron or even submicron scale, thereby requiring no comminution prior to utilization. In addition, the conversion of fly ash from zero value waste into value-added high-purity carbonates could create extra income stream for power plants, thereby offsetting the carbon tax to be implemented in the carbon-constrained future.^{3,9–12} The

Received: June 26, 2014

Revised: September 9, 2014

Published: September 9, 2014

Table 1. Waste Minerals Elemental Quantification (XRF)

	composition (%)									
	SiO ₂	Al ₂ O ₃	Fe ₂ O ₃	CaO	MgO	Na ₂ O	K ₂ O	P ₂ O ₅	SO ₃	
Hazelwood fly ash	5.82	3.01	14	32.4	29.3	0.2	0.17	0.41	12.8	
Yallourn fly ash	8.92	5.92	42.3	9.4	27.9	0.56	0.16	0.11	2.84	

capacity to sequester CO₂ for fly ash depends directly on the proportion of binary oxides (CaO and MgO) and/or hydroxides (Ca(OH)₂ and Mg(OH)₂) contained in the waste matrix. For example, a fly ash containing a high percentage of free magnesium in oxide form can be carbonated more readily than a fly ash with the same magnesium content but in the form of silicates. Thus, it is difficult to directly compare the efficiency of various fly ashes for mineral carbon sequestration.¹³

Brown coal is the single largest energy source in the state of Victoria, Australia, meeting >85% of its electricity need. The combustion of brown coal yields up to 1.3 million tons of fly ash annually, nearly all of which was simply dumped in ash ponds. Victorian brown coal fly ash has a chemical composition dominated by magnesium, calcium, iron, and sulfur and is classified as being a strongly alkaline fly ash that is not suitable as cement's additive.³ Due to its high moisture content, the brown coal combustion generates a high CO₂ emission rate relative to the high-rank black coal and natural gas in Australia.¹⁴ A cost-effective carbon capture process is pivotal for the sustainability of brown coal in the carbon-constrained future. Moreover, with the continuous increase in the amount of fly ash generated, it incurs the increasing demand on the use of vast land for landfills, which also contaminates the soil, ground, and water simultaneously.¹⁵ On the assumption of a full conversion of magnesium and calcium to carbonate for a typical Victorian brown coal fly ash containing around 32% CaO and 29% MgO (Table 1), the carbonation reaction is expected to capture 278 kg of CO₂ per ton of raw fly ash, which is equivalent to a total amount of 0.36 million tons of CO₂ captured per annum. Sun et al. (2012) compared the CO₂ sequestration capacity of Victorian brown coal fly ash with other fly ashes and found 264 kg of CO₂ per ton of raw fly ash at 60 °C, 10 bar, and 1 h reaction time, which is remarkably higher than lignite and black coal fly ashes.³ Although this number is much smaller than the total amount of CO₂ released, it is expected that the industrial mineral wastes can act as a supplement to the natural minerals for CO₂ capture.

Considering the broad variation of fly ash properties, the methods developed in the literature are generally not applicable to different samples. To date, the majority of studies on fly ash utilization have focused on direct carbonation under a high CO₂ partial pressure with a rather long reaction time.^{16–18} However, reports on utilization of coal fly ash are limited with

Table 2. NH₄Cl Concentration at the Start Point of Each Cycle for MgO, MgO + CaO, MgO+Fe₂O₃, and Hazelwood Fly Ash

cycle	NH ₄ Cl concentration (M)			
	MgO	MgO + CaO	MgO+Fe ₂ O ₃	Hazelwood Fly ash
1	4	4	4	4
2	3.47	3.52	3.58	3.38
3	3.02	3.04	3.01	2.99
4	2.81	2.84	2.86	2.85
5	2.67	2.73	2.76	2.72

the research target set only to optimize the conditions for once-through leaching and carbonation stages. The integration of leaching and carbonation stages and the recovery of leaching reagent are yet to be discussed. Moreover, the mechanisms underpinning the dissolution of magnesium upon leaching of fly ash are rarely reported.¹⁹ Few papers reported leaching kinetics of different elements including Al, Fe, and Ca and trace elements like Cr, Zn, and As from coal fly ash.^{20,21}

Elemental leaching from fly ash is a complex process, which involves dissolution, diffusion, adsorption, and mineral precipitation. Leaching of ash takes place through dissolution of constituents inside or on the surface of ash particles and transport through the pore structure to the surrounding solution. For solid–fluid reactions, the shrinking core kinetic model²² has been used widely. Ranjitham et al. (1990),²³ Raschman (2000),²⁴ and Atashi et al. (2010)²⁵ have successfully applied this model to the leaching kinetics of calcined magnesite in ammonium chloride with a concentration of about 1 M. Paul et al. (2004) indicated that the kinetics of acid consumption for different types of Turkish fly ashes consist of an initially fast process followed by a slower period.¹⁹ To reiterate, all of these studies only focused on the once-through fresh leaching reagent.

In this study, two types of Victorian brown coal fly ash were tested in multiple cycles of the leaching-carbonation closed loop using regenerative ammonium chloride as the leaching reagent. The aim is to clarify the extraction and carbonation mechanisms of magnesium (as well as calcium) in an industrially relevant process. That is, rather than the use of fresh reagent for once-through investigation, a multicycle experiment has been conducted to reveal the recyclability of a regenerative reagent, ammonia chloride. As a comparison to fly ash, pure oxide compounds of predominant elements (MgO, CaO, and Fe₂O₃) and their mixtures were also examined in the multicycle mode to evaluate the influence of impurities in fly ash on the extraction of target oxides. Furthermore, a detailed modeling on the leaching of magnesium from pure oxide and fly ash was conducted by assessing the applicability of various models, so as to provide an accurate model for future scale-up.

2. MATERIALS AND EXPERIMENTAL METHODS

2.1. Materials Preparation. Two coal fly ash samples were collected as dry powders from the electrostatic precipitator in International Power Hazelwood and Energy Australia Yallourn power plant located at the Latrobe Valley, Victoria, Australia. Once being delivered to the laboratory, each fly ash sample was initially washed with water with a liquid to solid (L/S) mass ratio of 10 to remove the unburnt carbon and water-soluble species such as sodium and potassium sulfate. Subsequently, the water-washed fly ash samples were dried in an oven at 120 °C overnight and crushed mildly below 150 μm prior to use. Pure MgO and CaO samples were prepared by calcination of magnesium carbonate and calcium carbonate (purchased from Sigma-Aldrich), respectively. The temperature and time for calcination in a muffle furnace were fixed at 800 °C and 12 h, respectively.²³ The resulting MgO and CaO obtained were analyzed by thermogravimetric analysis (TGA) to ensure a complete calcination of the carbonates. Pure Fe₂O₃ was purchased from Sigma-Aldrich in

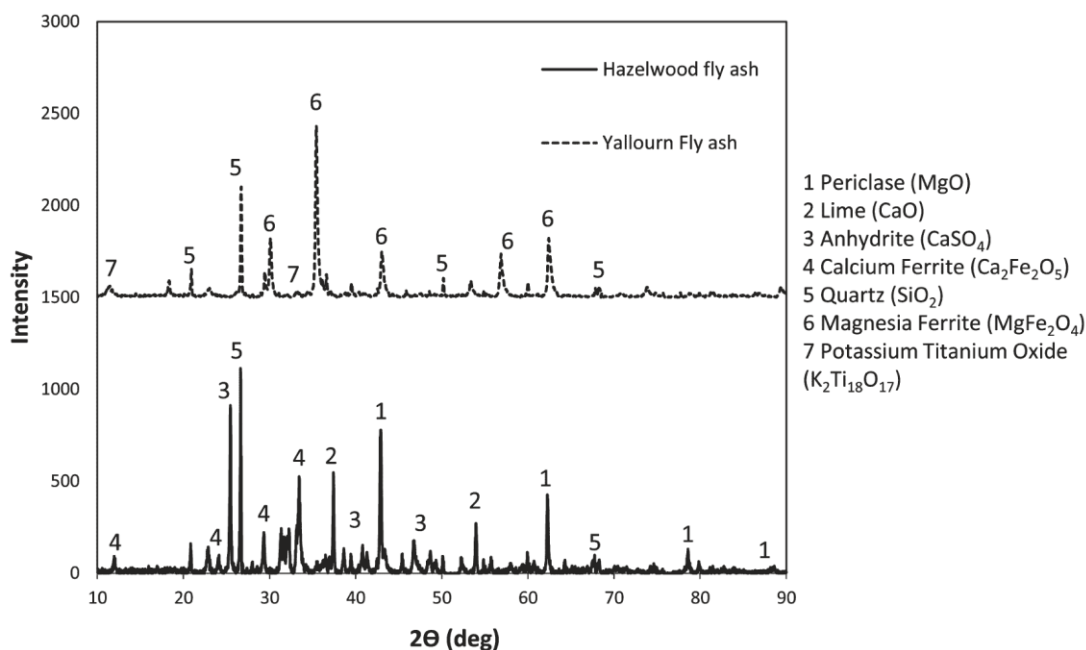


Figure 1. XRD spectra for Hazelwood fly ash and Yallourn fly ash.

oxide form. In addition, the analytical grade ammonium chloride was purchased from Merck with a purity of 98%.

For the comparison to fly ash samples, the pure oxide and their mixtures were also tested on multiple leaching-carbonation cycles, including pure MgO, mixtures of MgO + CaO (mass ratio 1:1), and mixtures of MgO + Fe₂O₃ (mass ratio 1:4). These ratios were selected on the basis of molecular weights and weight percentages of these metals in the two fly ash samples.

2.2. Materials Characterization. The elemental composition of a raw sample, its leaching residues, and precipitated carbonates were determined by a precalibrated X-ray fluorescence spectroscopy (XRF, Spectro iQ II). About 3–4 g of a representative sample was finely ground and stored in a sample holder for the XRF analysis. The leaching percentage of each element was calculated on the basis of the difference between its mass in raw washed sample and solid residue after drying. The produced carbonates were dried overnight at 105 °C and weighted to determine the conversion. The mineralogical composition of raw fly ash and few leaching residues and carbonates was determined by X-ray diffraction analysis (XRD, Rigaku, Miniflex), under a scanning speed of 1° min⁻¹ from 2 to 90°, 40 kV and 15 mA. The peak identification was achieved by search-match function in the JADE software.

Scanning electron microscopy (SEM) was employed for morphology observation of carbonate precipitates. The sample powder was dispersed into a carbon-taped sample holder stub and platinum coated. Each carbonate precipitate was characterized by randomly selecting 3–4 fields of view and examining all the fly ash particles observed within the selected fields. The SEM microscope used is a JEOL JSM-7001F equipped with energy dispersive X-ray spectroscopy (EDX). SEM imaging studies were performed at 15 kV at a working distance of 10 mm.

2.3. Thermodynamic Equilibrium Calculation. The different species and phases, which were known to exist, were specified into the reaction equation module of HSC Chemistry 7.1 to calculate multicomponent equilibrium compositions for the heterogeneous systems. The heat capacity, enthalpy, entropy, and Gibbs energy of a single species and reaction systems of pure substances were provided by the built-in database in the HSC Chemistry.²⁶ The Gibbs free energy of the reactions of various Mg- and Ca-bearing species with ammonium chloride were calculated in a wide temperature range.

2.4. Single Leaching Conditions. For each run, 10 g of a sample in dried powder form was mixed with 60 mL, 4 M ammonium chloride at a L/S ratio of 6. The liquid to solid ratio and ammonium chloride concentration were fixed throughout this study. Instead, a broad range of temperature (25, 40, 60, and 80 °C) and time (10–60 min) was varied and three replications were carried out for each condition. The temperature was not increased further due to the limitation of operation at higher temperatures in industry and to avoid evaporation of aqueous solutions that might increase the concentration of ammonium chloride, thus causing the dissolved ammonium chloride to precipitate back in leaching residue. In addition, the study on leaching behavior of calcined magnesite carried out by Ranjitham and Khangaonkar (1990) showed an insignificant change of leaching progress at temperatures above 80 °C.²³

Batch leaching tests were performed in a glass sealed beaker equipped with two connections, one for feeding air of 1 L·min⁻¹ and another tube for releasing ammonia vapor that is then trapped in a conical flask containing distilled water. The reaction temperature (40–80 °C) was controlled by immersing the reactor in a thermostat-controlled water bath. A magnetic stirrer bar with a stirring speed of 350 rpm enabled the solution to be fully agitated with minimal spillage. The resulting residue after filtration was dried at 120 °C overnight in an oven, weighed, and quantified by XRF for elemental compositions to determine the leaching percentages of individual elements, particularly magnesium and calcium. The resulting ammonium water was titrated by acetic acid (1 M) to determine the amount of the ammonia recovered from the leaching step.

2.5. Single Carbonation Conditions. Following the leaching experiment, the resulting leachate was subsequently carbonated under the conditions of the pH of the 9–10⁸ through the doping of ammonia–water (NH₃, generated from the leaching step), a continuous injection of pure (grade 4.5) CO₂ at 15 L·min⁻¹ for 20 min. The amount of ammonia added in the carbonation tank is exactly the same as that evaporated from the leaching step to ensure a closure of the whole process in NH₃ balance. These conditions were optimized in our previous works. According to reactions 1 and 2, the Mg²⁺ and Ca²⁺ cations in the leachate are expected to fully precipitate out as solid carbonate, which in turn results in the regeneration of ammonia chloride to be used in the next round. The resulting carbonate was filtered and dried overnight in the oven, and its mass was recorded.

2.6. Five-Cycle Leaching-Carbonation Conditions. Once a cycle of leaching-carbonation is finished, the regenerated ammonia chloride is tested again for a total of five cycles in this study. The experiments for all the leaching and carbonate exactly follow the above-mentioned conditions, except that a small amount of fresh hydrochloric acid (2 M) was doped into the regenerated chloride to reduce its pH back to the original value of 4.5. The increase in the pH of ammonia chloride is attributed to the accumulation of unreacted alkali and alkaline earth metal cations after carbonation.

3. RESULTS AND DISCUSSION

3.1. Properties of Fly Ashes. Table 1 tabulates XRF results in oxide form for as-received and washed Hazelwood and Yallourn fly ash samples. The major elements are Mg, Ca, and Fe. Hazelwood fly ash is rich in MgO and CaO (29.3 and 32.4%, respectively) and also includes 14% Fe₂O₃, whereas the predominant elements in Yallourn fly ash are Fe₂O₃ and MgO (42.3 and 27.9%, respectively) with only 9.4% CaO. Figure 1 depicts the XRD spectra for Hazelwood and Yallourn fly ash. As can be seen, periclase (MgO) is the only Mg-bearing crystal species in Hazelwood fly ash, which is accompanied by Ca-bearing species including anhydrite (CaSO₄), lime (CaO), calcium ferrite (CaFe₂O₄), and silicate. Only two major crystalline phases were found in Yallourn fly ash, with magnesite ferrite showing the strongest intensity and quartz with a medium peak height. Interestingly, calcium (9.4% in its oxide form) in Yallourn fly ash was present as an amorphous structure that was undetectable by XRD analysis.

3.2. Single Leaching Results. The solid lines in Figure 2 illustrate the leaching percentage of pure MgO as a function of

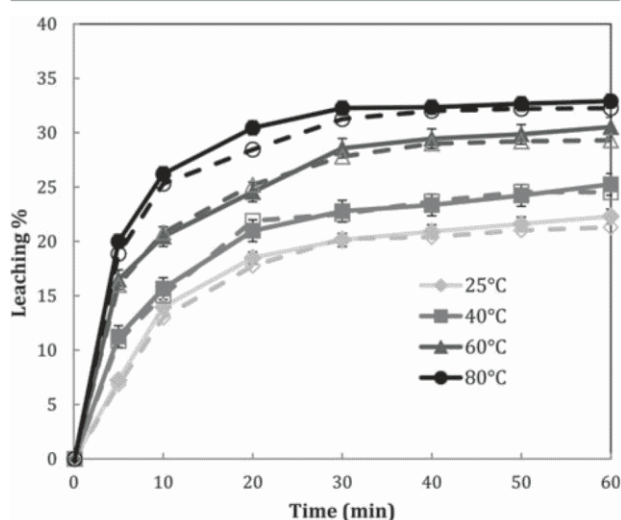


Figure 2. Effect of time and temperature on leaching of magnesium. Solid lines represent leaching from pure MgO, and dashed lines refer to Hazelwood Fly ash.

temperature and time. In contrast, the dashed lines show the magnesium leaching percentage from Hazelwood fly ash. The error bars refer to standard deviations from measured values of three replicates. The nearly identical results for magnesium extraction from both pure MgO and Hazelwood fly ash can be confirmed for the same condition. This substantiates the presence of the majority of magnesium as free oxide in Hazelwood fly ash and the insignificant influence of impurities and the other forms of magnesium in this fly ash, if any. The leaching temperature was influential, as it improved the

equilibrium fraction of magnesium leached in 1 h from around 20% at 25 °C to 32% at 80 °C. The increasing trend of temperature is consistent with the observation of Ranjitham and Khangaonkar (1990) on the leaching of calcined magnesite with temperature up to 80 °C. However, they achieved around 43% magnesium extraction at 80 °C and 30 min reaction time with an L/S of 20. The lower pH of their solution emerging from using a significant amount of leaching agent is the likely cause of discrepancy.²³

At a given temperature, the leaching fraction of magnesium increased exponentially over time, reaching its maximum at around 30 min. The leaching of magnesium was nearly ceased from 30 min onward. The probable explanation for this phenomenon is the crystallization of ammonium chloride and the possible reaction of free Mg²⁺ with OH⁻ from ammonium hydroxide on the surface of ash at high pH, creating a passive layer on the surface of particles to block the continued leaching of magnesium.

To validate the above proposed hypothesis, the thermal decomposition of leaching residue obtained from conditions of 80 °C and 1 h for the use of pure MgO was conducted by TGA, at a heating rate of 5 °C/min from room temperature to 800 °C. Figure 3 illustrates a three-step mass loss for the residue tested. The first loss was commenced before 200 °C, which can be assigned to hydrate; the second one at around 330 °C is attributed to the decomposition of ammonium chloride crystals which is 338 °C for the pure compound;²⁷ and the last one at about 490 °C was due to the decomposition of magnesium hydroxide. A significant decrease in weight of leaching residue after washing with water was another proof for the existence of ammonium chloride crystal, which accounted for around 48% of the total residue. Such a phenomenon has been confirmed by Wang et al. (2012)²⁸ who has observed that the crystallization of NH₄Cl occurs from the NH₄Cl-rich solution when the concentration of MgCl₂ within it is increased up to 2.5–2.7 mol·L⁻¹. The concentration of MgCl₂ in the leachate achieved in our study reaches 2.62 mol·L⁻¹, which falls in the above range.

The theoretical and practical ammonia recovery as a function of leaching time and temperature are presented in Figure 4. The theoretical ammonia recovery was calculated according to eq 1, based on the amount of magnesium cation extracted. Increasing temperature favors the recovery of ammonia. This was expected, since the solubility of ammonia will decrease at elevated temperatures. However, the practical ammonia recovery is much lower than the corresponding theoretical value, indicating that a certain fraction of evaporated ammonia gas is still present in the leachate. This may not be a big issue, as the ammonia is essential for the subsequent carbonation of the dissolved Ca²⁺ and Mg²⁺ cations.

3.3. Five Leaching-Carbonation Cycles. **3.3.1. Leaching Results.** The leaching percentages of magnesium in pure oxide compounds upon the reuse of ammonia chloride in the five cycles are presented in panel a of Figure 5, and panel b shows the results of the two fly ashes tested. For pure oxide mixtures, the extraction yield of magnesium is relatively constant for the three mixtures, regardless of the cycle number. This is an indicator of the independence of magnesium extraction on the mass of MgO in a solid sample mixture. For all of the pure oxide mixtures, the total mass of each solid remained the same while the mass of MgO is different because its content is different for the three mixtures. For each pure species, upon the increase on cycle number, the extraction yield of magnesium

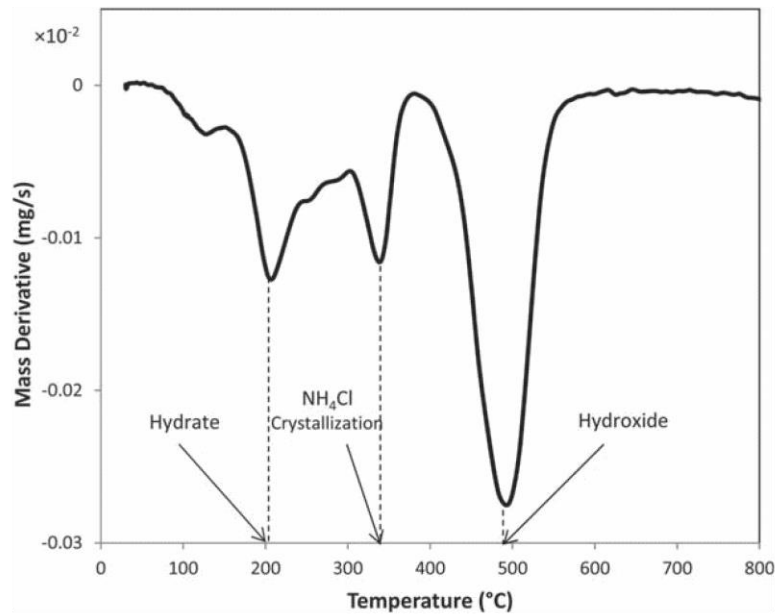


Figure 3. Derivative mass loss of dried residue against temperature running TGA ($T = 80\text{ }^{\circ}\text{C}$, $t = 1\text{ h}$).

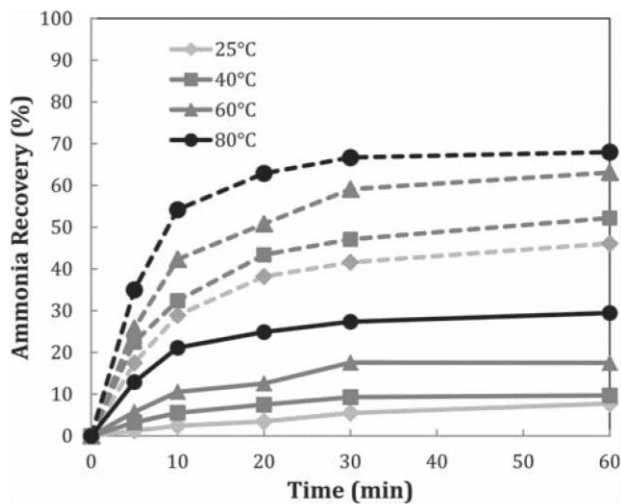


Figure 4. Theoretical and practical ammonia recovery. Dashed lines are related to theoretical ammonia recovery, and solid lines correspond to practical ammonia recovery.

drops slowly from $\sim 35\%$ in the first cycle to 30% in the fifth cycle. A similar observation was confirmed for Hazelwood fly ash. However, for Yallourn fly ash, the leaching yield of magnesium reached only 25% in the first three cycles. Its leaching and carbonation were fully stopped from the third cycle (results for the fourth and fifth cycles are not shown). This should be due mainly to a strong association of most of magnesium with iron in the form of magnesite ferrite in this fly ash. Accordingly, the ammonia salt was too weak to break the strong association of MgO and Fe_2O_3 .

The leaching percentage of calcium from the $\text{MgO} + \text{CaO}$ mixtures has also been compared to the two fly ash samples. The results are presented in Figure 6. Compared to a rather constant extraction yield of around 80% for calcium from the $\text{MgO} + \text{CaO}$ mixture, the leaching yield of calcium out of two fly ashes is much lower and decreases dramatically upon

increasing the cycle number. The calcium leaching yields from two fly ash samples reach 32% for the first cycle and only 10% at the fifth cycle for Hazelwood fly ash, and from 37 to 3% for Yallourn fly ash during the three cycles tested. This was attributed to different modes of occurrence of calcium in two fly ash samples, i.e., an abundance of a mixture of anhydrite, lime, and calcium ferrite in Hazelwood fly ash, and undetectable amorphous calcium aluminosilicate in Yallourn coal fly ash.

The dissolution rates of both magnesium- and calcium-bearing species in ammonium chloride were compared using thermodynamic equilibrium calculation (Figure 7). For the dissolution of MgO in ammonium chloride, its ΔG turns negative from $80\text{ }^{\circ}\text{C}$ onward, suggesting the spontaneity of the forward reaction to occur at this temperature. This is consistent with our results for the leaching of pure MgO and Hazelwood fly ash summarized in Figure 2. The lower magnesium leaching percentage of Yallourn fly ash rich in magnesite ferrite can also be explained by the positive ΔG for this reaction from room temperature to $200\text{ }^{\circ}\text{C}$ in Figure 7. For both calcium oxide and portlandite ($\text{Ca}(\text{OH})_2$), their dissolution ΔG is always lower than the other Ca-/Mg-bearing compounds, substantiating the spontaneous dissolution of these two species in ammonium chloride at every temperature. This supports the experimental observation for higher calcium extraction percentage from the mixture of $\text{MgO} + \text{CaO}$ than the two real fly ash samples.

The decreasing trend upon the five cycles suggests that the ammonium chloride leaching capability has declined upon recycling. It is hypothesized that increasing the concentration of dissolved magnesium and calcium ions in leachate favored two side reactions: 1 - reaction of ammonium chloride with dissolved Mg^{2+} cation to form a complex precipitate, 2 - ammonium chloride crystallization during carbonation. The second hypothesis has been proven by the leaching residue mass loss profile upon heating in Figure 3. To further support the first hypothesis, XRD analysis results for the leaching residue and carbonate from the first cycle of multiple-cycle leaching-carbonation of pure MgO are presented in Figure 8. The presence of a Mg-Cl complex in the untreated leaching

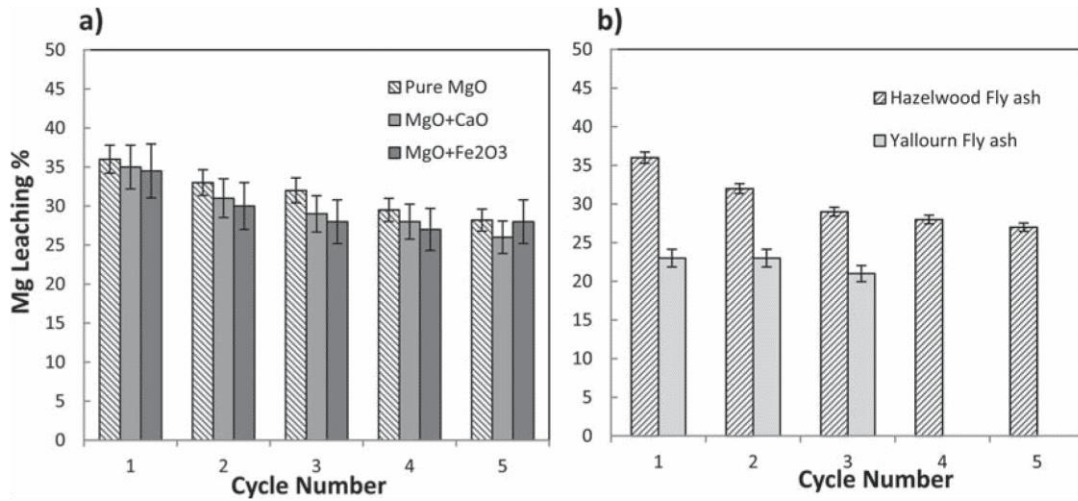


Figure 5. Leaching % for Mg during five-cycle leaching-carbonation at optimum conditions ($T = 80\text{ }^{\circ}\text{C}$, $t = 30\text{ min}$). (a) Pure MgO, MgO + CaO, and MgO+Fe₂O₃. (b) Hazelwood and Yallourn fly ash.

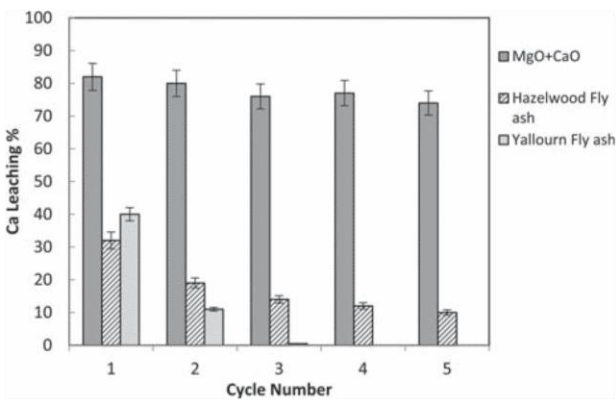


Figure 6. Leaching % for Ca during five-cycle leaching-carbonation at optimum conditions ($T = 80\text{ }^{\circ}\text{C}$, $t = 30\text{ min}$), in MgO + CaO and Hazelwood and Yallourn fly ash.

residue was verified. XRD results show that the peak characteristic of Mg–Cl complex disappeared after water washing. Similarly, the ammonium chloride crystals in carbonate products were confirmed too, which again vanished upon water washing. Similar results were confirmed for the leaching residues and carbonates generated in the other cycles (XRD data not shown). Moreover, on the basis of the assumption of producing 1 mol of Mg–Cl complex upon consumption of 1 mol of ammonium chloride, the weight loss after washing can be further derived for the fractionation of ammonium chloride complex coupled with dissolved magnesium. The results are depicted in Figure 9. For the pure MgO and its mixture with CaO, the crystallization extent of ammonium chloride is more significant than the fraction of solid complex formed. The crystallization extent also increases noticeably upon increasing the cycle number. Such a trend was however not found for the solid complex. In contrast, the solid complex formed has a comparable and even higher fraction than that of ammonium chloride crystal for the pure mixture of

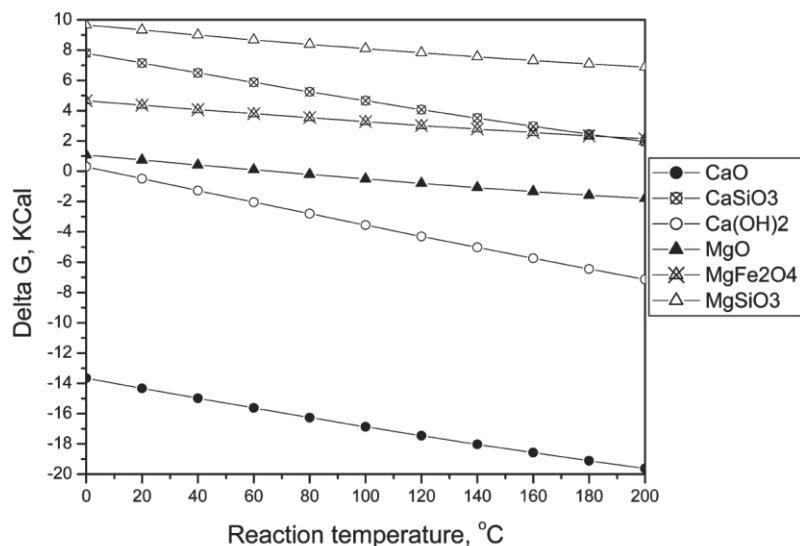


Figure 7. Thermodynamic equilibrium calculation for different Mg- and Ca-bearing species in ammonium chloride solution.

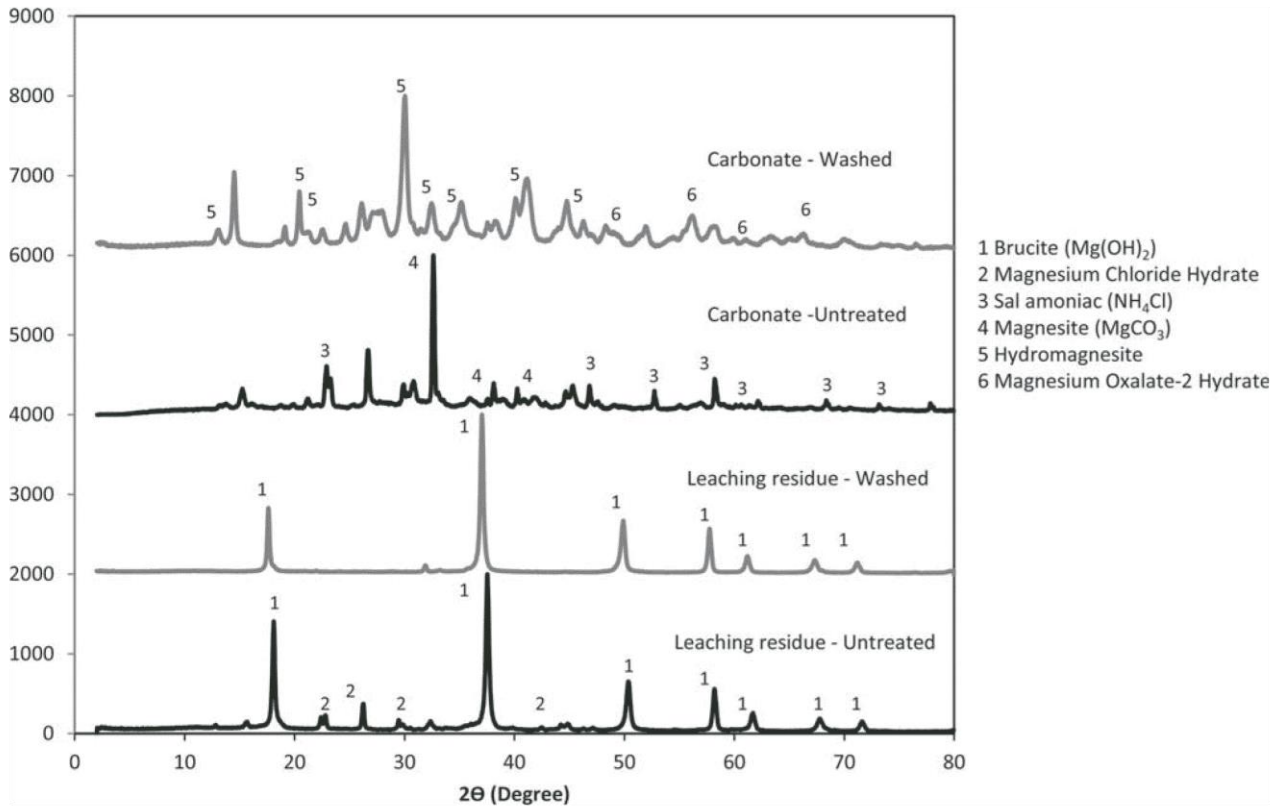


Figure 8. XRD results for first-cycle leaching residue and carbonate before and after washing for pure MgO.

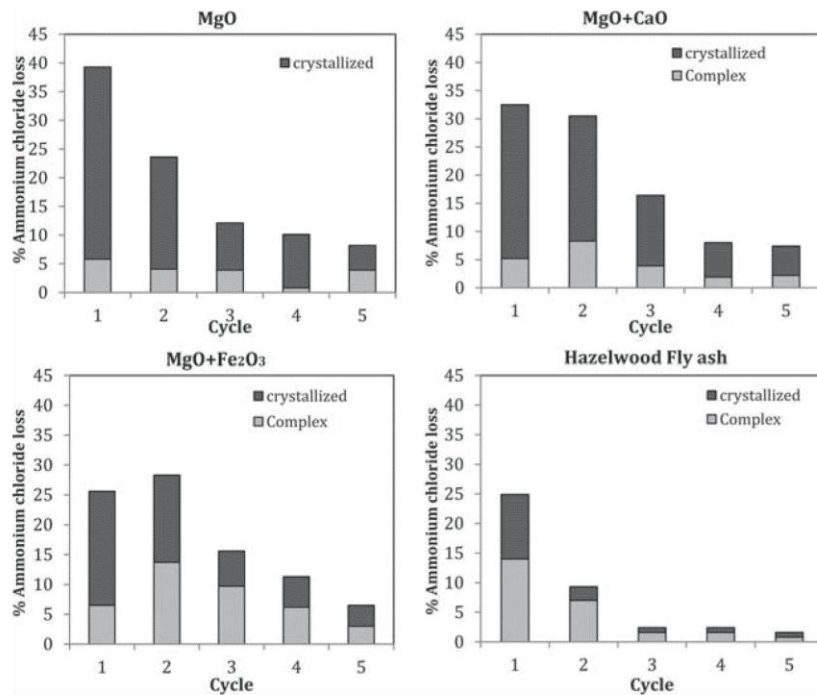


Figure 9. Loss percentage of NH_4Cl at each cycle breaking down to crystallized and complex formed for MgO, MgO + CaO, MgO + Fe_2O_3 , and Hazelwood fly ash. Water washing was conducted at room temperature, $L/S = 10$ and $t = 1$ h.

MgO + Fe_2O_3 and Hazelwood fly ash. This suggests that Fe_2O_3 and other impurities in fly ash are in favor of the combination of ammonium and MgO into complex solid. This explains the

extremely low extraction yield for magnesium out of MgO + Fe_2O_3 mixture and Yallourn coal fly ash. Moreover, the concentration of ammonium chloride at each cycle were also

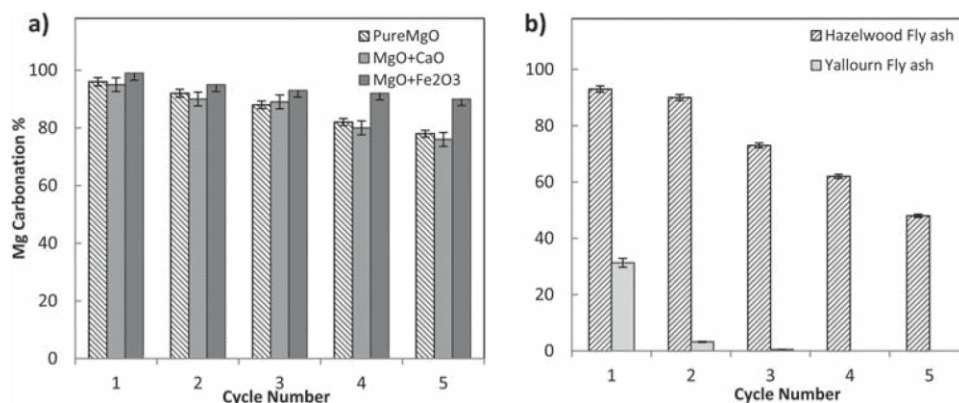


Figure 10. Carbonation % for Mg during five-cycle leaching-carbonation at optimum conditions ($T = RT$, $t = 20$ min). (a) Pure MgO, MgO + CaO, and MgO + Fe₂O₃. (b) Hazelwood and Yallourn fly ash.

calculated and summarized in Table 2. As can be seen that, for all of the four leachates examined, ammonium chloride concentration was decreased gradually from first cycle to last cycle. It is another direct evidence for the loss of ammonium chloride from the solution upon recycling.

3.3.2. Carbonation Results. Figure 10 demonstrates the carbonation percentage of Mg from the leachates of (a) different mixtures of pure oxides and (b) two fly ashes. Panel a indicates that, irrespective of the oxide mixture type, the carbonation percentage of magnesium reaches nearly 100% at the first cycle, and drops gradually upon the increase in the cycle number. For the two fly ash samples in panel b, magnesium in the Hazelwood Fly ash leachate was nearly fully carbonated in the first cycle. Its carbonation yield, however, was dropped quickly to only 50% in the fifth round. This is clearly faster than the pure oxide compounds shown in panel a. Moreover, the performance of Yallourn fly ash leachate is even worse, with the carbonation degrees for Mg²⁺ cations decreasing sharply from 31% in the first cycle to nearly zero in the third cycle. These results link with the aforementioned phenomenon on the loss of ammonium and magnesium into solid complex and crystallization species in the leaching residues.

The carbonation percentages of calcium in MgO + CaO, Hazelwood fly ash, and Yallourn fly ash are presented in Figure 11. Compared to Mg²⁺ cation in the leachate from the mixture

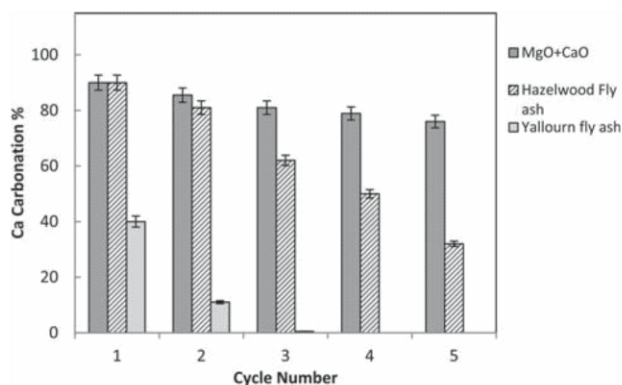


Figure 11. Carbonation % for Ca during five-cycle leaching-carbonation at optimum conditions ($T = RT$, $t = 20$ min) in MgO + CaO and Hazelwood and Yallourn fly ash.

of MgO + CaO, Ca²⁺ cation showed a slightly low carbonation extent, with a similar trend of decreasing slightly from 90% in the first cycle to 76% in the last cycle. The Ca²⁺ cation in the leachate of Hazelwood fly ash shows the same calcium carbonation behavior as the mixture of oxide (MgO + CaO) in the first and second cycles. However, its carbonation extent was decreased sharply after the second cycle and reached 32% at the fifth cycle. Similarly, the Yallourn fly ash carbonation percentage is the lowest among the samples tested, dropping from 40% to a negligible value at the third cycle.

The availability of calcium and magnesium cations in a solution is one of the significant factors influencing their carbonation.²⁹ The competition between ions present in solution can influence the nature and morphology of precipitated carbonates.³⁰ Figure 12 and Table 3 illustrate a suite of typical SEM images and the respective elemental analysis for single spots in the carbonate precipitates from the first and last cycles of (a) pure MgO, (b) MgO + CaO, (c) MgO + Fe₂O₃, and (d) Hazelwood fly ash. Being complementary to the SEM observation, XRD results on the major Mg- and Ca-bearing carbonate minerals are summarized in Table 4.

In the case of pure MgO demonstrated in Figure 12a, its first cycle carbonate is dominated by discrete rosettes of magnesite (MgCO₃). Under the natural (i.e., ambient) conditions, hydromagnesite or other metastable phases such as nesquehonite and lansfordite can be formed, depending on the availability of Mg²⁺ ions in solution in relation to the availability of other cations such as Ca²⁺.³¹ In addition, the transformation of nesquehonite to magnesite or amorphous magnesium carbonate at 70–100 °C was reported by Hollingbery et al. (2010), which could occur during drying in the oven at a temperature of 110 °C.³² Instead, the last cycle precipitates showed aggregates of small round particles. Such a discrepancy should be caused by the decreased concentration of magnesium cation in the leachate in the last cycle, which preferred to precipitate into small crystals that are too dilute to agglomerate together. This is consistent with the observation of Case et al. (2011) that concluded a higher concentration of magnesium ion in solution along with adding substrate increases the nucleation rate of magnesium precipitates.³³ Upon the initial central nuclei or hydroxide formed, the formation of magnesite and its nucleation growth can be accelerated significantly.³⁴

Regarding the case of the MgO + CaO mixture, its carbonate precipitates in Figure 12b suggest a polymorph of round

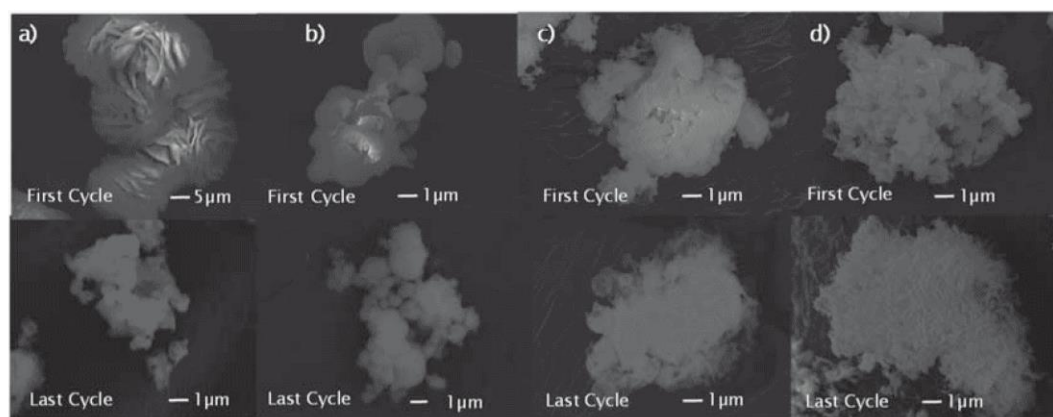


Figure 12. SEM images of carbonate obtained from the first and last cycles of multiple-cycle leaching-carbonation: (a) Pure MgO; (b) MgO + CaO; (c) MgO + Fe₂O₃; (d) Hazelwood fly ash.

Table 3. SEM-EDX Elemental Analysis of Representative Precipitate Particles Obtained from the First and Last Cycles of Five-Cycle Leaching-Carbonation of Pure MgO, MgO + CaO, MgO + Fe₂O₃, and Hazelwood Fly Ash

sample	cycle	elemental composition (wt %)					
		Ca	Mg	Fe	S	Cl	O
pure MgO	first		26			21	53
	last		4			8	68
MgO + CaO	first	34	2			8	56
	last	14	20			13	53
MgO + Fe ₂ O ₃	first		24			20	56
	last		30			5	65
Hazelwood fly ash	first	16	20			13	51
	last	23	14		2	7	54

particles for the first cycle while in the last cycle an aggregate of rhombohedral platy particles was observed. EDX mapping indicates the scattering of magnesium spots among the calcium-rich particles. Along with this, strong peaks were formed for magnesite and lansfordite in the XRD spectra. All of these suggest the incursion of magnesium ion into the internal layers of the calcite lattice. The sensitivity of calcium carbonate crystallization to the presence of magnesium ions has been reported by several investigators.^{30,35} Roques and Girou (1974) have reported that calcium carbonate precipitation was markedly reduced by the presence of a small amount of magnesium ions in the solution. The ions of Mg stabilize amorphous, unstable, and hydrated phases and thus decrease the quantity of well crystallized carbonates.³⁶

The crystalline structures of carbonate precipitates from the first and last cycles of MgO + Fe₂O₃ are present in Figure 12c. In comparison to the precipitates from MgO leachate (Figure 12a), the presence of iron in the leachate apparently changed the morphology of the magnesium carbonate particles to a relatively porous structure. However, there is not a significant difference observed between the first and last cycles. The smallest drop in the carbonation extent of MgO + Fe₂O₃ from the first to last cycle in comparison to other mixtures is consistent with a negligible change in carbonation morphology of magnesium through recycling. This can be attributed to an inferior concentration of magnesium ion in the leachate and a low tendency of iron to compete with magnesium to form carbonate or precipitate in the pH range 7–9.5.

Carbonate precipitates obtained from first and last cycle leaching-carbonation of Hazelwood fly ash are present in panel d of Figure 12. As can be seen, significant changes occur for the particle shape as the cycle number shifts from first to last. First cycle precipitates show randomly oriented polycrystalline aggregates, while at the last cycle formation of submicron rod shape particles coalesced and settled in the irregular shaped agglomerates was observed. XRD results for the first cycle precipitates showed incorporation of both magnesium and calcium in the crystal lattice in the form of calcite magnesium ((Ca,Mg)CO₃). The calcium sulfate peak in the last cycle XRD spectra shows an affinity of the calcium ion to react with a high concentration of sulfate ion in the leachate to form solid precipitate. Bischoff and Fyfe (1968) reported inhibition of calcite formation strongly by the presence of magnesium and less strongly by sulfate ions.³⁵ The increased concentration of

Table 4. Different Mg- and Ca-Bearing Minerals Detected by XRD for the First and Last Cycles of Carbonation Obtained from Multiple-Cycle Leaching-Carbonation of Pure MgO, MgO + CaO, MgO + Fe₂O₃, and Hazelwood Fly Ash^a

cycle	pure MgO	MgO + CaO	MgO + Fe ₂ O ₃	Hazelwood fly ash
first cycle	magnesite (MgCO ₃)	magnesite (MgCO ₃)	magnesite (MgCO ₃)	magnesian calcite [(Ca, Mg)CO ₃]
		Lansfordite [MgCO ₃ ·5(H ₂ O)]		
		calcite (CaCO ₃)		
last cycle	hydromagnesite [Mg ₅ (CO ₃) ₄ (OH) ₂ ·4(H ₂ O)]	magnesite (MgCO ₃)	magnesite (MgCO ₃)	magnesite (MgCO ₃)
		Lansfordite [MgCO ₃ ·5(H ₂ O)]		
		calcite (CaCO ₃)		
				calcium sulfate (CaSO ₄)

^aOven drying at 110 °C may cause the formation of magnesite from the conversion of nesquehonite.

interfering ions concentration in leachate upon recycling clearly affected the morphology of carbonate.

3.4. Kinetic Modeling of Magnesium Leaching. In comparison to an obvious time dependence of the leaching of magnesium in Figure 2, the leaching of calcium in the form of oxide is much faster, which was proven in Figure 13 to be

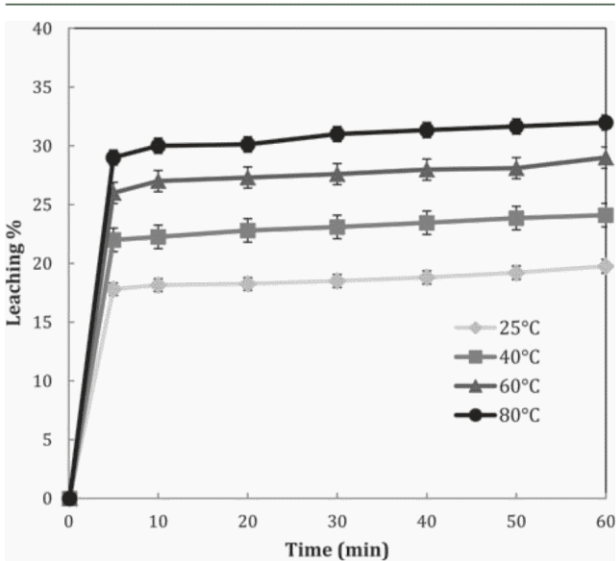


Figure 13. Effect of time and temperature on leaching of calcium from Hazelwood fly ash.

finished in less than 5 min, irrespective of the leaching temperature. Clearly, the leaching of calcium in the form of oxide is mainly thermodynamically controlled, whereas its reaction rate is fast enough. In other words, for the coexistence of magnesium and calcium in a sample such as Hazelwood fly ash, the leaching of magnesium out of the solid matrix is the limiting step for the overall extraction. In this sense, the kinetic modeling for magnesium was further performed in this paper.

For the noncatalytic reaction of particles with surrounding fluid, two simple idealized models can be considered, the progressive-conversion model (PCM) and the shrinking unreacted-core model (SCM). In the PSM, it is assumed that the reactant enters and reacts through the particle at all times; thus, solid reactant is converted continuously and progressively throughout the particles. Instead, the SCM assumes the reaction occurs first at the outer skin of the particle and the reaction zone then moves into the solid, leaving behind partly or completely converted material and inert solid which can precipitate back on the surface of the particle. Thus, at any time during the reaction, there exists an unreacted core of material which shrinks in size. Back to Figure 2, it is clear that the leaching process was controlled either by diffusion of reactant through the solution boundary, through a solid product layer, or by the surface chemical reaction rate.²² Therefore, the shrinking core model for magnesium leaching is considered here. In the model, a solid particle *B* immersed in a fluid *A* reacts with the fluid by eq 3:



We assume MgO as solid *B* and ammonium chloride as fluid *A*, and according to eq 1, the stoichiometric coefficient of *a* can be set as 2. When the first-order surface chemical reaction is the

slowest step, the following expression of the shrinking core model can be used to describe the dissolution kinetics:

$$1 - (1 - X_B)^{1/3} = \frac{K_C M_B C_A}{\rho_B a r_0} = k_r t \quad (4)$$

Vice versa, in the case that the diffusion of magnesium ion through the ash layer is the rate controlling step, the following equation can be used:

$$1 - \frac{2}{3} X_B - (1 - X_B)^{2/3} = \frac{2 D M_B V_A}{\rho_B a r_0^2} t = K_d t \quad (5)$$

In eqs 4 and 5, X_B is the fraction of solid reacted, K_C is the kinetic constant, M_B is the molecular weight of the solid, C_A is the concentration of dissolved lixiviant *A* in the bulk of solution, ρ_B is the density of solid, *a* is the stoichiometric coefficient of the reagent in the leaching reaction, r_0 is the initial radius of the solid particle, *t* is the reaction time, *D* is the diffusion coefficient in the porous product layer, and K_r , K_d are the rate constants which are calculated from eqs 4 and 5, respectively.³⁷

The rate of dissolution of magnesium was tested against diffusion control (eq 4) and chemical control (eq 5). For this purpose, the left sides of these equations were plotted with respect to reaction time. The fitting level of these models was evaluated using correlation coefficient (R^2) values. The slopes of these plots were used as the apparent rate constants (K_r and K_d). Table 5 summarizes the diffusion control and chemical

Table 5. Dissolution Rate and R^2 Using the Reaction Controlled Model, Diffusion Control Model, and Mixed Reaction and Diffusion Control Model

<i>T</i> (°C)	reaction controlled model		diffusion controlled model	
	$1 - (1 - X_B)^{1/3}$		$1 - (2/3)X_B - (1 - X_B)^{2/3}$	
	R^2	$K_r \times 10^3 \text{ (min}^{-1}\text{)}$	R^2	$K_d \times 10^4 \text{ (min}^{-1}\text{)}$
25	0.7482	1.142	0.8458	2.944
40	0.7543	1.333	0.8551	4.010
60	0.7054	1.663	0.7973	5.984
80	0.5779	1.728	0.6104	6.676

control models of leaching reaction in terms of rate constant and correlation coefficient. Clearly, the correlation coefficients are mostly below 0.8, which are too poor to be accepted. In other words, the above approaches based on the classical shrinking core model are inaccurate. A careful examination of the leaching results in Figure 2 reveals that the magnesium concentration in the bulk liquid solution initially increased very fast and then leveled off at an equilibrium value in each temperature. Furthermore, the previous discussions have confirmed the crystallization of ammonium chloride and the formation of complex mixture as solid residues. They grow steadily upon the gradual dissolution of magnesium into the leachate. As a result, the resistance against diffusion of ions through the boundary should increase gradually, which eventually leads to the full termination of the reaction. For simplification, the leaching of magnesium was simulated by two steps, the first 30 min for step 1 and the remaining 30 min for step 2 where the leaching is rather stopped.

The kinetic data for the first step were matched well by the fitting of an empirical pseudo-second-order reaction with nonconstant ammonium chloride concentration in the outer surface of MgO particles, as presented in eq 6. This model is

also consistent with the stoichiometric coefficient of ammonium chloride in eq 1 and the decreasing trend of the magnesium leaching results from multiple-cycle leaching-carbonation of pure MgO and Hazelwood fly ash presented in Figure 5. To reiterate, the reason for a decreased extraction of magnesium upon multiple cycles is due to the decreased concentration of free ammonium chloride. To reflect this point, the concentration of ammonium chloride was introduced into the left-hand side of eq 6, as a nonconstant term and as a function of time and temperature. By further dividing both the left- and right-hand sides by C_A , the concentration of ammonium chloride at time t , the effect of the initial concentration of ammonium chloride on leaching is further added into the model. C_A can be substituted in terms of initial concentration and conversion.

$$\frac{(1 - X_B)^{-1}}{C_{A0} - 2C_{B0}X_B} = \frac{K_C M_B}{\rho_B \alpha r_0} = K_1 t \quad (6)$$

The diffusion control model presented in eq 5 was proven to fit the kinetic data for the second step satisfactorily. In summary, Figure 14 shows the R^2 values of two proposed models for (a) the first step and (b) the diffusion control model for the second step. One can see the much better correlation coefficients for the newly developed model. The Arrhenius

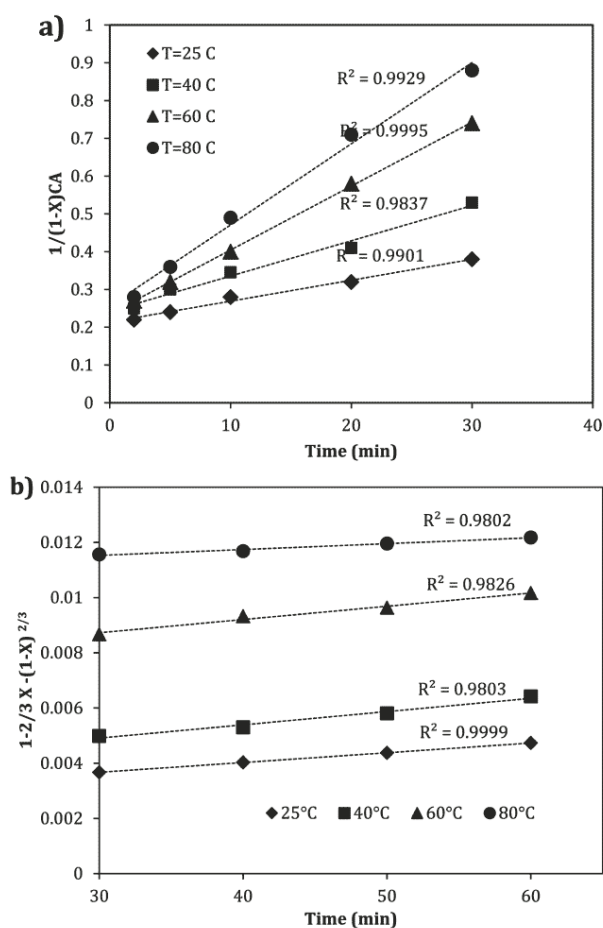


Figure 14. Plots for (a) pseudo-second-order reaction for the first 30 min of reaction and (b) product layer diffusion for the last 30 min of reaction.

plots of $\ln(K)$ versus the reciprocal of temperature for the pseudo-second-order reaction model (eq 6) further indicate an activation energy of 20.7 kJ mol^{-1} for the leaching of magnesium in the first 30 min, as demonstrated in Figure 15.

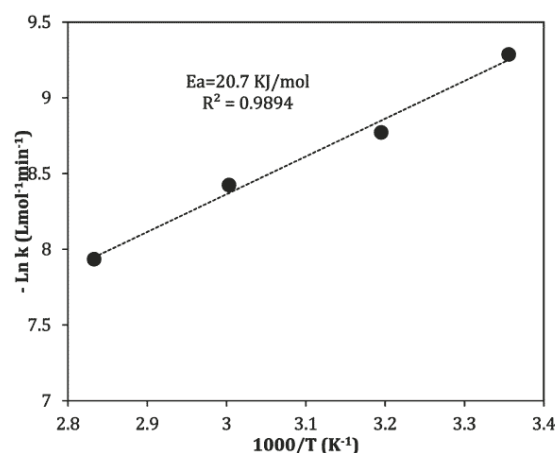


Figure 15. Arrhenius plot for leaching of MgO with ammonium chloride using the pseudo-second-order reaction model.

Ranjitham et al. (1990),²³ Raschman (2000),²⁴ and Atashi et al. (2010)²⁵ reported activation energies of 43.2, 48.5, and 42.2 kJ mol^{-1} , respectively, for the leaching of calcined magnesite, all of which are relatively higher than our result. This may be due to a much smaller fly ash size examined here. Luo et al. (2013)³⁸ concluded activation energies of 32, 28, and 19 kJ mol^{-1} for dissolution of aluminum, calcium, and iron, respectively, from calcined Chinese coal fly ash in hydrochloric acid, which is clearly comparable with present work. Figure 16 further

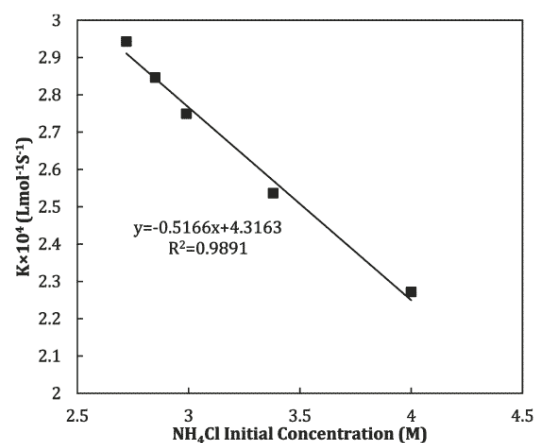


Figure 16. K values fitting the second-order model for different cycles of Hazelwood fly ash.

demonstrates a linear dependence of the K value on the initial/free concentration of ammonium chloride for the leaching of magnesium from Hazelwood fly ash/pure MgO. This further confirmed the applicability of this model for predicting magnesium leaching kinetics in the multiple-cycle leaching-carbonation.

4. CONCLUSION

A comprehensive investigation on the leaching propensity of dominant oxides (MgO and CaO) in two different types of brown coal fly ash (Hazelwood and Yallourn) using ammonium chloride has been conducted. Apart from the parametric investigation over the influence of time and temperature on the once-through leaching experiment, five closed leaching-carbonation loops have been performed to explore the reusability of the leaching reagent, as well as the accumulation of impurities upon recycling. The optimum conditions for leaching of magnesium from pure MgO within the range studied here were found to be at 80 °C, a reaction time of 30 min, a liquid/solid ratio of 6, and an ammonium chloride concentration of 4 M.

Identical results for magnesium leaching yields have been observed for all samples, except for Yallourn coal fly ash with a chemically stable magnesia ferrite (MgFe₂O₄). The leaching and carbonation percentage of magnesium and calcium decreased upon increasing cycle number, due to the loss of ammonium chloride by crystallization and its interaction with dissolved magnesium forming complex precipitates. The leaching of calcium in the form of oxide is much faster than magnesium, which can be finished in less than 5 min at a given temperature. Instead, the leaching of magnesium in Hazelwood fly ash was slow in the first 30 min, following a pseudo-second-order reaction with a nonconstant ammonium chloride concentration, while the kinetic data for the second step showed a good fit to the diffusion-controlled process. The activation energy for the leaching of MgO was found to be about 20.7 kJ mol⁻¹ from the start of reaction toward 30 min after the reaction, which is consistent with the value obtained for the reaction control kinetic modeling.

■ AUTHOR INFORMATION

Corresponding Author

*Phone: +61-3-9905-2592. Fax: +61-3-9905-5686. E-mail: lian.zhang@monash.edu.

Notes

The authors declare no competing financial interest.

■ ACKNOWLEDGMENTS

This project is supported by the Faculty of Engineering of Monash University for a 2012–2013 seed grant. The first author is also grateful to Monash Research Graduate School (MRGS) for a Ph.D. scholarship.

■ REFERENCES

- (1) Eloneva, S.; Teir, S.; Salminen, J.; Fogelholm, C. J.; Zevenhoven, R. Fixation of CO₂ by carbonating calcium derived from blast furnace slag. *Energy* **2008**, *33*, 1461–1467.
- (2) Sanna, A.; Dri, M.; Hall, M. R.; Maroto-Valer, M. Waste materials for carbon capture and storage by mineralisation (CCSM) – A UK perspective. *Appl. Energy* **2012**, *99*, 545–554.
- (3) Sun, Y.; Parikh, V.; Zhang, L. Sequestration of carbon dioxide by indirect mineralization using Victorian brown coal fly ash. *J. Hazard. Mater.* **2012**, *209–210*, 458–466.
- (4) Teir, S.; Revitzer, H.; Eloneva, S.; Fogelholm, C. J.; Zevenhoven, R. Dissolution of natural serpentinite in mineral and organic acids. *Int. J. Miner. Process.* **2007**, *83*, 36–46.
- (5) Maroto-Valer, M. M.; Kuchta, M. E.; Zhang, Y.; Andrésen, J. M.; Fauth, D. J. Comparison of physical and chemical activation of serpentine for enhanced CO₂ sequestration. *Prepr. Pap. - Am. Chem. Soc., Div. Fuel Chem.* **2004**, *49* (1), 373–375.

(6) Gerdemann, S. J.; O'Connor, W. K.; Dahlin, D. C.; Penner, L. R.; Rush, H. Ex Situ Aqueous Mineral Carbonation. *Environ. Sci. Technol.* **2007**, *41*, 2587–2593.

(7) Hong, K. J.; Tokunaga, S.; Kajiuchi, T. Extraction of heavy metals from MSW incinerator fly ash using saponins. *J. Hazard. Mater.* **2000**, *75*, 57–73.

(8) Sun, Y.; Yao, M. S.; Zhang, J. P.; Yang, G. Indirect CO₂ mineral sequestration by steelmaking slag with NH₄Cl as leaching solution. *Chem. Eng. J.* **2011**, *173* (2), 437–445.

(9) Nyambura, M. G.; Mugeru, W. G.; Felicia, P. L.; Gathura, N. P. Carbonation of brine impacted fractionated coal fly ash: implications for CO₂ sequestration. *J. Environ. Manage.* **2011**, *92*, 655–664.

(10) Montes-Hernandez, G.; Pérez-López, R.; Renard, F.; Nieto, J. M.; Charlet, L. Mineral sequestration of CO₂ by aqueous carbonation of coal combustion fly-ash. *J. Hazard. Mater.* **2009**, *161* (2–3), 1347–1354.

(11) Huijgen, W. J. J.; Witkamp, G. J.; Comans, R. N. J. Mineral CO₂ sequestration by steel slag carbonation. *Environ. Sci. Technol.* **2005**, *39* (24), 9676–9682.

(12) Bonenfant, D.; Kharoune, L.; Sauvé, S.; Hausler, R.; Niquette, P.; Mimeault, M. CO₂ Sequestration potential of steel slags at ambient temperature and pressure. *Ind. Eng. Chem. Res.* **2008**, *47* (20), 7610–7616.

(13) Bobicki, E. R.; Liu, Q.; Xu, Z.; Zeng, H. Carbon capture and storage using alkaline industrial wastes. *Prog. Energy Combust. Sci.* **2012**, *308*, 302–320.

(14) Johnson, T. R. In *Future Options for Brown Coal based Electricity Generation – the role of IDGCC*, Proceedings of the ANZSES Destination Renewable Conference, Melbourne, November 26th–29th, 2003; 371–380.

(15) Wu, C. Y.; Yu, H. F. Extraction of aluminum by pressure acid-leaching method from coal fly ash. *Trans. Nonferrous Met. Soc. China* **2012**, *22*, 2282–2288.

(16) Huang, K.; Inoue, K.; Harada, H. Leaching of heavy metals by citric acid from fly ash generated in municipal waste incineration plants. *J. Mater. Cycles Waste Manage.* **2011**, *13*, 118–126.

(17) Kersch, C.; Pereto; Ortiza, S.; Woerlee, G. F.; Witkampa, G. J. Leachability of metals from fly ash: leaching tests before and after extraction with supercritical CO₂ and extractants. *Hydrometallurgy* **2004**, *72*, 119–127.

(18) Soco, E.; Kalemkiewicz, J. Investigations of sequential leaching behaviour of Cu and Zn from coal fly ash and their mobility in environmental conditions. *J. Hazard. Mater.* **2007**, *145*, 482–487.

(19) Paul, M.; Seferinoglu, M.; Aygik, G. A.; Sandström, A.; Paul, J. Acid leaching of coal and coal-ash: kinetics and dominant ions. American Chemical Society, *228th National Meeting Conference proceeding*, 2004.

(20) Seidel, A.; Zimmels, Y. Mechanism and kinetics of aluminum and iron leaching from coal fly ash by sulfuric acid. *Chem. Eng. Sci.* **1998**, *53* (22), 3835–3852.

(21) Zhu, Z. Characterization and modeling of toxic fly ash constituents in the environment. Ph.D. Thesis, University of Tennessee, 2011.

(22) Levenspiel, O. *Chemical Reaction Engineering*; John Wiley and Sons: New York, 1972.

(23) Ranjitham, A. M.; Khangaonkar, P. R. Leaching Behaviour of Calcined Magnesite with Ammonium Chloride Solutions. *Hydrometallurgy* **1990**, *23*, 177–189.

(24) Raschman, P. Leaching of calcined magnesite using ammonium chloride at constant pH. *Hydrometallurgy* **2000**, *56*, 109–123.

(25) Atashi, H.; Fazlollahi, F.; Tehranirad, S. Leaching Kinetics of Calcined Magnesite in Ammonium Chloride Solutions. *Aust. J. Basic Appl. Sci.* **2010**, *4*, 5956–5962.

(26) Pickles, C. A. Thermodynamic modelling of the formation of zinc-manganese ferrite spinel in electric arc furnace dust. *J. Hazard. Mater.* **2010**, *179*, 309–317.

(27) <http://www.chem.unep.ch/irptc/sids/OECD/SIDS/12125029.pdf>.

- (28) Wang, D.; Li, Z. Study of Crystallization Kinetics of Ammonium Carnallite and Ammonium Chloride in the $\text{NH}_4\text{Cl-MgCl}_2\text{-H}_2\text{O}$ System. *Ind. Eng. Chem. Res.* **2012**, *51*, 2397–2406.
- (29) Han, Y. S.; Hadiko, G.; Fuji, M.; Takahashi, M. Effect of flow rate and CO_2 content on the phase and morphology of CaCO_3 prepared by bubbling method. *J. Cryst. Growth* **2005**, *276*, 541.
- (30) Reddy, M. M.; Nancollas, G. H. The crystallization of calcium carbonate: iv. The effect of magnesium, strontium and sulfate ions. *J. Cryst. Growth* **1976**, *35*, 33–38.
- (31) Frost, R. L.; Hales, M. C.; Locke, A. J.; Kristof, J.; Horvath, E. Vagvolgyi, Controlled rate thermal analysis of hydromagnesite. *J. Therm. Anal. Calorim.* **2008**, *92*, 893–897.
- (32) Hollingbery, L. A.; Hull, T. R. The Thermal Decomposition of Huntite and Hydromagnesite - A Review. *Thermochim. Acta* **2010**, *509*, 1–11.
- (33) Case, D. H.; Wang, F.; Giammar, D. E. Precipitation of Magnesium Carbonates as a Function of Temperature, Solution Composition, and Presence of a Silicate Mineral Substrate. *Environ. Eng. Sci.* **2011**, *28*, 881–889.
- (34) Langmuir, D. Stability of Carbonates in the System $\text{MgO-CO}_2\text{-H}_2\text{O}$. *J. Geol.* **1965**, *73*, 73.
- (35) Bischoff, J. L.; Fyfe, W. S. Catalysis, inhibition and the calcite-aragonite problem. *Am. J. Sci.* **1968**, *266*, 65–79.
- (36) Roques, H.; Girou, A. Kinetics of the formation conditions of carbonate tartars. *Water Res.* **1974**, *8*, 907–920.
- (37) Dehghan, R.; Noaparast, M.; Kolahdoozan, M. Leaching and kinetic modelling of low-grade calcareous sphalerite in acidic ferric chloride solution. *Hydrometallurgy* **2009**, *96*, 275–282.
- (38) Luo, Q.; Chen, G.; Sun, Y.; Ye, Y.; Qiao, X.; Yu, J. Dissolution kinetics of aluminum, calcium and iron from circulating fluidized bed combustion fly ash with hydrochloric acid. *Ind. Eng. Chem. Res.* **2013**, *52*, 18184–18191.



Chemical and morphological changes of weathered Victorian brown coal fly ash and its leaching characteristic upon the leaching in ammonia chloride and hydrochloric acid



Tahereh Hosseini^a, Boyoung Han^a, Cordelia Selomulya^a, Nawshad Haque^b, Lian Zhang^{a,*}

^a Department of Chemical Engineering, Monash University, Clayton, GPO Box 36, Victoria 3800, Australia

^b Minerals Resources Flagship, CSIRO, Clayton, Victoria 3168, Australia

ARTICLE INFO

Article history:

Received 14 April 2015

Received in revised form 7 July 2015

Accepted 22 July 2015

Available online 26 July 2015

Keywords:

Weathered Victorian brown coal fly ash

Leaching

NH₄Cl + HCl

Sole HCl

ABSTRACT

In this paper, the properties and leaching propensity of weathered Victorian brown coal fly ash have been investigated. This study was conducted to assess if the weathered ash could replace fresh fly ash in mineral carbonation process. Through the use of a variety of advanced instruments, the mineralogical properties of weathered fly ash have been investigated. In addition, the leaching of such a fly ash in the mixture of ammonium chloride and sole hydrochloric acid has been examined. As has been confirmed, the weathered fly ash is dominated by hydrates and carbonates which were formed in aqueous landfilling system. These species were mostly poorly crystallized, and even loosely agglomerated into clusters in the weathered fly ash. Irrespective of the leaching reagent, the target Ca and Mg in weathered fly ash were more easily extracted than in the fresh ash counterpart under the same leaching conditions. In addition, for the use of either leaching agent, the temperature and time played little or marginal role on the extraction of target Ca and Mg out of the weathered fly ash sample. Decreasing the pH of the leaching agent is beneficial in enhancing the extraction of Ca and Mg, at a cost of a gradually lowered selectivity due to the simultaneous elution of impure elements. The optimum pH value was found to be around 4 for the mixture of NH₄Cl + HCl, which maximized the extraction yields of Ca and Mg close to ~70% at a minimal elution of the impurities. This is attributed to the buffering property of NH₃ and its complexing capability to prevent the dissolution of impure elements. Instead, the use of sole HCl even at the same pH value as the mixture of NH₄Cl + HCl resulted in a deep penetration of protons into particle inside, the intense breakage of ash cluster, and hence, the simultaneous dissolution of plenty of impurities.

© 2015 Elsevier B.V. All rights reserved.

1. Introduction

Coal-fired power stations around the world produce enormous quantities of coal fly ash annually. Since the consumption of fly ash to make value-added products is poorly low, the large amount of fly ash is disposed in storage ponds (Yeheyis et al., 2009). This induces the environmental concerns related to land and subsurface water contamination upon the dissolution of toxic and non-degradable elements (Ahmaruzzaman, 2010).

The management of long-term fly ash disposal or its utilization needs proper understanding of the weathered fly ash properties (Eze et al., 2013). Regarding the coal ash characteristics, they vary broadly with the properties of the raw coal, combustion technology used to generate electricity, as well as the wet processing and environmental exposure in storage (Ahmaruzzaman, 2010). Natural weathering process occurs via hydration, carbonation, dissolution and so forth, leading to the changes in physical, chemical and mineralogical properties of a fly

ash sample (Eze et al., 2013; Muriithi et al., 2013; Yeheyis et al., 2009). Upon the decrease of the pH of fly ash-water slurry, it has been confirmed that the soluble salt content was reduced remarkably as well (Baba et al., 2008; Ward et al., 2009).

The utilization of coal fly ash has been receiving increased attention, since it is an effective means of reducing the amount of this waste product that otherwise has to be landfilled. Considering the increasing trend of demand for fly ash in different applications, the landfilled fly ash, as a supplement to the fresh ash derived from a power plant, has also been considered so as to empty the historical ash landfilled site (Baker et al., 2015). Compared to the conventional methods such as the use of fly ash as additive to cement, the use of fly ash to supplement natural minerals for CO₂ mineralization has been receiving increased attention (Jo et al., 2012; Montes-Hernandez et al., 2009; Nyambura et al., 2011; and Sun et al., 2011). The brown coal fly ash is unsuitable for cement industry, because it is predominated by alkali and alkaline earth metals that are highly soluble in rain water (Hosseini et al., 2014). Regarding the CO₂ mineralization process, one primary method, namely indirect carbonation is to first separate alkaline earth metals via aqueous leaching out of solid fly ash. The resulting leachate is

* Corresponding author.

E-mail address: lian.zhang@monash.edu (L. Zhang).

Table 1
Summary of leaching experiments conditions carried out for fly ash.

Material	Leaching agent	Condition	pH range	Description
Weathered and fresh fly ash	NH ₄ Cl + HCl	T = 80 °C, t = 30 min L/S = 6, 60 ml NH ₄ Cl 4 M HCl 4 M added during leaching	pH ~ 5–5.5 pH < 4.5	Comparison of leaching characteristic of fresh and weathered fly ash
Weathered fly ash		T = 25, 40, 60, 80 °C t = 30, 40, 50, 60 min Initial L/S = 2, 3, 4, 5, 6	pH < 4.5	Optimization of condition
Weathered fly ash		T = 25 °C t = 40 min Initial L/S = 6	0.5–6	Effect of pH and selectivity
Weathered and fresh fly ash	Sole HCl	T = 25 °C t = 30 min 60 mL HCl 1 M, L/S = 6	Without control pH	Comparison of leaching characteristic of fresh and weathered fly ash
Weathered fly ash		T = 25, 40, 60, 80 °C t = 30, 40, 50, 60 min	Without control pH	Optimization of condition
Weathered fly ash		T = 25 °C t = 30 min 60 mL HCl 1 M, L/S = 6	0.5–6	Effect of pH and selectivity

subsequently bubbled with CO₂-bearing flue gas to precipitate the alkaline earth cations out as carbonates (Sun et al., 2012). For such a purpose, the fly ash rich in alkaline earth metals collected from brown coal combustion process is an ideal source.

As a continuation of our previous works focusing on the use of dried fresh fly ash collected from the electrostatic precipitator in a Victorian brown coal combustion power plant (Hosseini et al., 2014), this paper aims to further examine the applicability of weathered Victorian brown coal fly ash upon indirect leaching process. The motivation of us lies in the fact that the Victorian brown coal fly ash has been stored in ash pond for the past decades, which thus possesses a huge amount and potentially distinct properties when compared with the fresh fly ash. It raises the concern if the results based on fresh fly ash can be applied to its weathered counterpart. It is still unclear how the weathering would affect the modes of occurrence of alkaline earth metals in a fly ash and their leaching behavior in acidic reagent prior to carbonation. As far as the authors are aware, there are very limited papers that have touched down the leaching characteristics of different types of weathered fly ash (Andrade et al., 1989; Mudd and Kodikara, 2000; Singh et al., 2014; Żygadło and Woźniak, 2010). In particular, there is no information available on the properties of weathered Victorian brown coal fly ash and its potential for utilization through CO₂ sequestration process.

In principle, the use of ammonium salt for the leaching process is superior over acidic leaching, since it can be recovered readily and

reused in a closed loop (Teir et al., 2007). However, ammonia and ammonium ion constitute a pH buffer solution which is not in favor of the extraction of alkaline earth metals requiring a low pH for the solution. On the other hand, the use of strong acids such as hydrochloric acid has been reported to improve the extraction yields of target elements. However, the selectivity of target elements is usually poor, because the undesirable elements are also extracted simultaneously (Berry et al., 1986). In this paper, we modified the ammonium chloride solution by combining with acid via pH control leaching, so as to improve both the extraction yields and selectivity of calcium and magnesium over other metals in a fly ash matrix. A one-year old weathered Hazelwood fly ash was used for such a test. Initially, it was compared with the fresh ash sample collected from the electrostatic precipitator (ESP) of the same power plant. For such a purpose, the modes of occurrence of individual metals in both fly ash samples were characterized by quantitative X-ray diffraction (QXRD) for mineralogical identification and quantification. Subsequently, the leaching characteristics of the two fly ash samples in ammonia chloride solution, with and without pH control using sole hydrochloric acid (HCl) were examined. The aim here is to maximize both leaching yields and selectivity of magnesium and calcium from weathered Victorian brown coal fly ash. The optimization of process parameters including temperature and time has been conducted intensively. The results achieved are expected to shed light in understanding the mechanisms underpinning the synergetic interaction between ammonia chloride and hydrochloric acid in the extraction of individual elements out of ash matrix, and in broadening the methods for a value-added utilization of landfilled Victorian brown coal fly ash, an otherwise valueless waste which is of environmental concern.

2. Materials and experimental methods

2.1. Materials preparation

The fresh coal fly ash sample was collected as dry powders from the ESP in International Power Hazelwood power plant located at the Latrobe Valley, Victoria, Australia. One-year old wet weathered fly ash was collected from the top of the ash pond in the same power plant, and dried in ambient air prior to being tested. Although the ash from different depths of the ash pond was not sampled, it is presumed that the top surface ash collected is representative, since its properties are broadly in agreement with the previously reported ash pond samples

Table 2
Elemental quantification of major elements in fresh fly ash, weathered fly ash, synthesized fly ash 1 (from synthetic weathering of fresh fly ash) and synthesized fly ash 2 (from synthetic weathering of weathered fly ash).

Elements	Elemental composition (wt.%)			
	Fresh fly ash	Synthesized fly ash 1	Weathered fly ash	Synthesized fly ash 2
SiO ₂	5.82	5.62	3.86	4.09
Al ₂ O ₃	3.01	2.54	3.65	3.36
Fe ₂ O ₃	14	17.14	16.8	17.2
CaO	32.4	33.72	30.97	31.19
MgO	29.3	29.29	32.51	32.1
Na ₂ O	0.2	0.24	2.35	2.21
K ₂ O	0.17	0.18	0.15	0.15
SO ₃	12.8	8.63	9.44	9.23

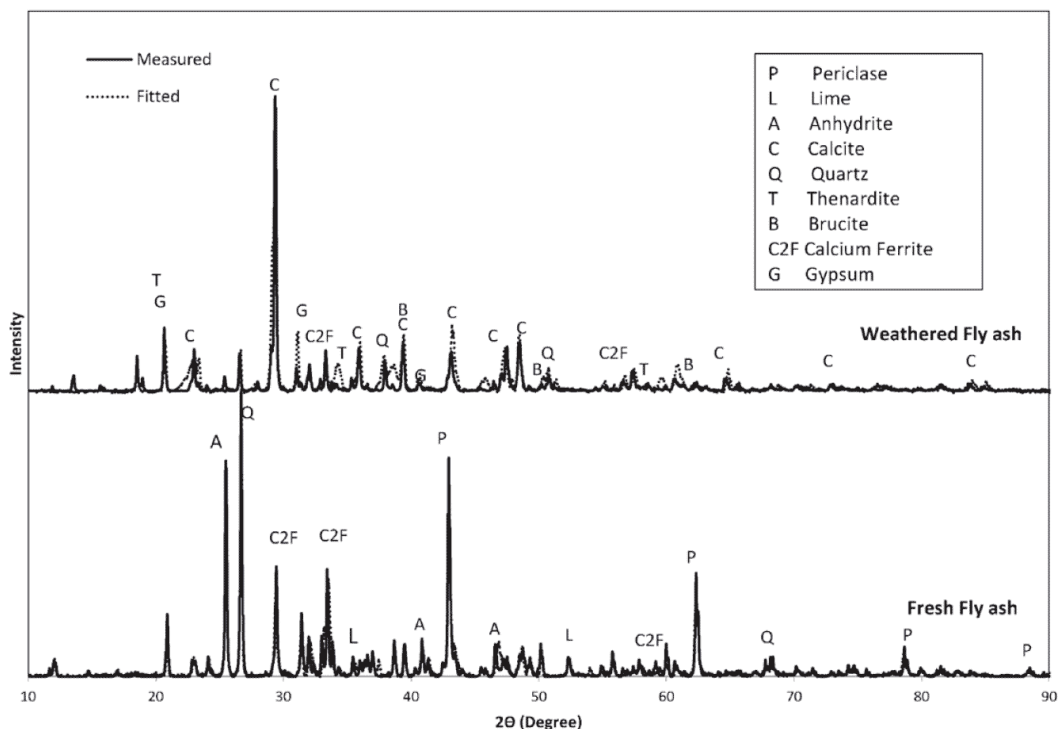


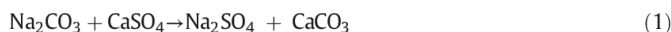
Fig. 1. Measured and fitted XRD pattern by SIROQUANT software for fresh and weathered fly ash.

(Mudd and Kodikara, 2000). The previous study also confirmed insignificant variation in composition of ash and leachate with sites and depths of the ash dam (Mudd and Kodikara, 2000).

In order to estimate the degree of weathering of fly ash collected from ash dump, two complementary experiments were performed on the synthesis of weathered fly ash through the use of fresh and weathered sample collected. For each sample, it was immersed into milli-Q water and left in the laboratory for two weeks. This is to mimic the natural environment in the ash dam. Obtained samples (herein after synthesized fly ash 1 and 2 respectively) were dried overnight in the oven at 110 °C and analyzed by XRF and QXRD.

A portion of fly ash was prewashed with sodium carbonate solution (0.3 M) to remove sulfur and soluble salts. A 100 g sample of dried fly

ash was mixed together with sodium carbonate solution in a beaker and stirred at room temperature for around 1 h. This is to ensure the production of high-purity carbonate that could be used as a value-added product. The sulfur in fly ash (mainly in form of calcium sulfate) was washed by sodium carbonate according to the following equation (Sharma, 2001):



After vacuum filtration, the filter cake was dried in oven at 120 °C overnight and analyzed by both XRF and XRD.

2.2. Materials characterization methodologies

The elemental composition of a raw and sodium carbonate washed fly ash and leaching residues were determined by a pre-calibrated X-ray fluorescence spectroscopy (XRF, Spectro iQ II). The leaching percentage of each element was calculated based on the difference between its mass in raw washed sample and leaching residue after drying.

The mineralogical composition of fly ash samples and its leaching residues were determined by X-ray diffraction analysis (XRD, Rigaku, MiniFlex 600), under the condition of scanning speed 1°/min from 2 to 90°, 40 kV and 15 mA. The peak identification and crystalline mineral phase quantification was achieved by SIROQUANT. Based on the Rietveld method, SIROQUANT generates a synthetic X-ray pattern from crystallographic information of the built-in mineral database and adjusts the pattern interactively through refinement procedure to minimize the chi-square value (Ward et al., 1999). To quantify the amount of amorphous species within a sample, 20 wt.% corundum (Sigma–Aldrich >99.5%, powder) was added as internal standard into a sample and the mixture was re-measured by XRD, following the method proposed elsewhere (Williams and Van Riessen, 2010).

The cross-sectional scanning electron microscopy (SEM) images of particles was observed by mounting the sample in epoxy resin and polishing using silicon carbide and diamond papers. Each fly ash sample

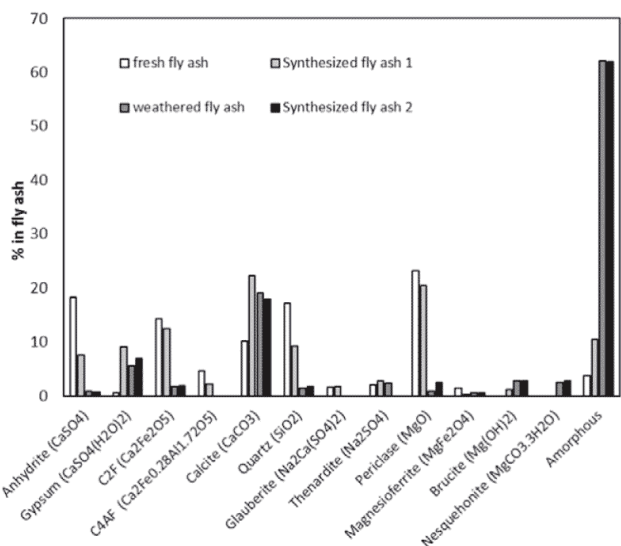


Fig. 2. Composition of fresh fly ash, synthesized fly ash 1 (from synthetic weathering of fresh fly ash), weathered fly ash and synthesized fly ash 2 (from synthetic weathering of weathered fly ash) calculated by QXRD and internal standard method.

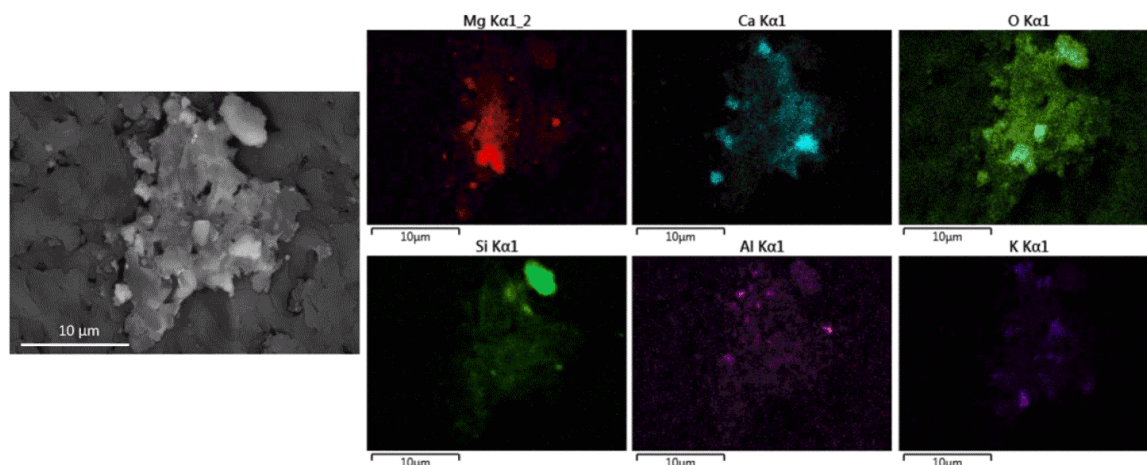


Fig. 3. BSE image (magnification 4000 \times) and EDX elemental maps of representative particle of weathered fly ash. Elemental maps of Mg (red), Ca (light blue), O (light green), Si (dark green), Al (purple) and K (dark blue).

was characterized by randomly selecting 3–4 fields of view and examining all the fly ash particles observed within the selected fields. The SEM microscopes used are a JEOL JSM-7001F equipped with backscattered electron detectors (BSE) coupled with Energy Dispersive X-ray Spectroscopy (EDX). SEM imaging studies were performed at 15 kV at a working distance of 10 mm.

Iron Mössbauer spectroscopy analyses were also conducted. Approximate loadings of 60–94 mg/cm² were weighed out into piston type perspex absorber holders for the Mössbauer analyses. The

experiments were carried out with both the source and absorber at room temperature with a high and low velocity resolution. The samples were exposed to a beam of γ radiation. The γ ray emitted by the source pass through an absorber and the transmitted gamma rays are detected by a radiation detector. In the resulting spectra, γ -ray intensity was plotted as a function of the source velocity. All spectra have been fitted with Voigtian line-shapes, which is a Lorentzian with Gaussian broadening due to variation in the local coordination of the iron atoms.

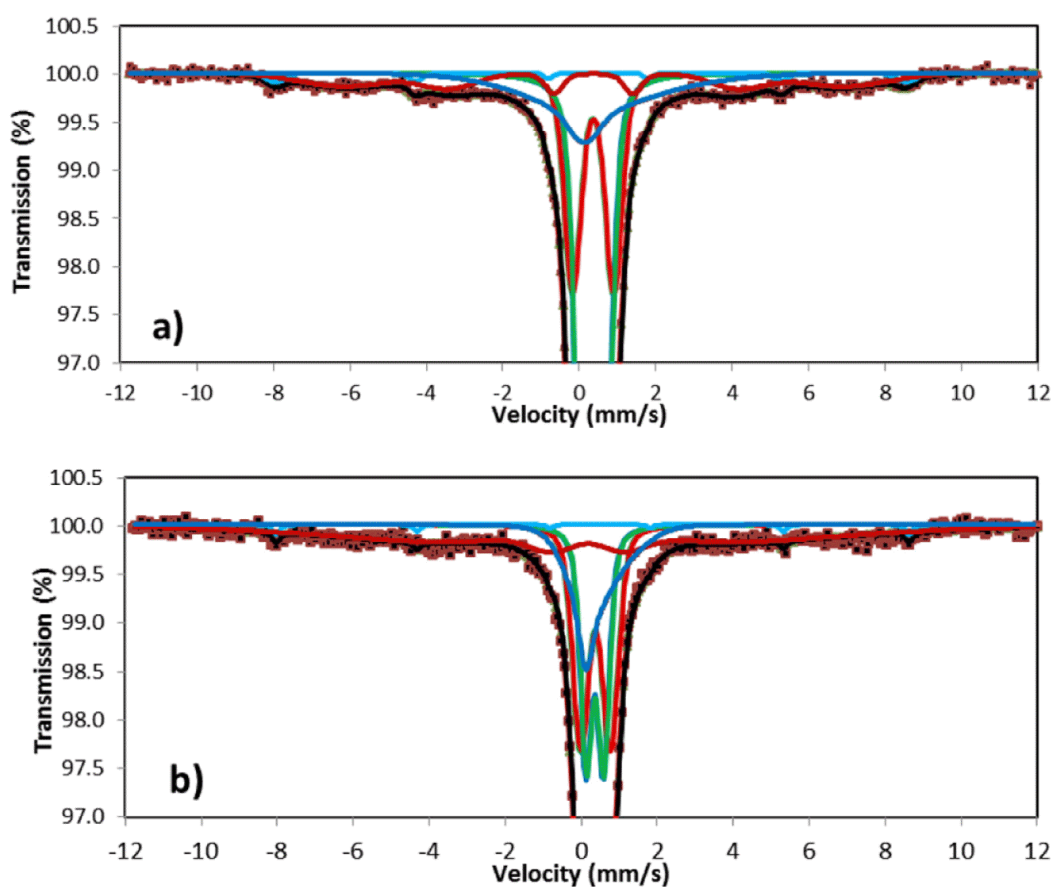


Fig. 4. Mössbauer spectroscopy fitting results a) fresh fly ash; b) weathered fly ash 3 sextets + 2 doublets.

Table 3
Hyperfine parameters determined by Mössbauer spectrum fitting for fresh and weathered fly ash.

Sample	Sextets				Doublet 1 (magnesioferrite)			Doublet 2 (spinel)		
	IS	QS (ϵ)	Area	phase	IS	QS (Δ)	Area	IS	QS (Δ)	Area
	mm/s	mm/s	%		mm/s	mm/s	%	mm/s	mm/s	%
Fresh FA	0.40	-0.12	2	HEM	0.35	0.58	39	0.34	1.05	24
	0.29	0	8	CAF/MAF						
	0.35	0	17	MAF						
	0.35	0.25	9	MAF						
Weathered FA	0.38	-0.1	1.3	HEM	0.35	0.46	22	0.36	0.78	27
	0.16	0	31	CAF/MAF						
	0.35	0.25	18	MAF						

2.3. Leaching experiments procedure

Since the kinetics of leaching of minerals is highly dependent upon the activity of hydrogen ion (i.e. H^+) in a leachate, the influence of leachate pH was examined here. The pH of a leachate was varied by either using ammonium chloride solution which has its pH regulated by continuously dropping HCl, namely the mixture of $NH_4Cl + HCl$ at the two pH ranges (5–5.5 and <4.5), or the use of sole HCl without pH control. In both series of leaching experiments, the initial condition was selected based on optimized condition found in our previous work (Hosseini et al., 2014). To maximize both yield and selectivity of calcium and magnesium, the weathered fly ash leaching condition was further varied for different final pH in the leaching system of $NH_4Cl + HCl$ and sole HCl. The leaching conditions are summarized in Table 1.

Batch leaching tests were performed in a glass sealed beaker equipped with four connections, one for feeding air of 1 L/min, one tube for the release of ammonia vapor to be trapped in a conical flask containing distilled water, one connection for pH meter entrance and another one for acid injection to solution. The pH was controlled at pre-set value over the entire testing period by continuous measurement and automatic doping of acid into the leachate. Reaction temperature was controlled by having the reactor immersed in a thermostat controlled water bath. After the temperature reached its set point, 10 g of sodium carbonate washed fly ash was added to the solution. A magnetic stirrer bar with a stirring speed of 350 rpm enabled the solution to be fully agitated with minimal spillage. The resulting residue after filtration were dried at 120 °C overnight in an oven, weighed and quantified by XRF for elemental compositions to determine the leaching percentages of individual elements, particularly magnesium and calcium.

3. Results and discussions

3.1. Characterization of raw weathered fly ash

3.1.1. XRF, QXRD and SEM results

Table 2 tabulates the composition of raw fresh fly ash, weathered fly ash and synthesized fly ash 1 and 2. Note that, synthesized fly ash 1 refers to the fresh ash which has been soaked into water for two weeks in the laboratory, whereas synthesized fly ash 2 denotes the weathered fly ash that was immersed into water for two weeks in the laboratory. It can be found that the major elements available in both fly ashes are quite similar with a deviation of $\pm 3\%$ for each element. This confirms that these samples are derived from the identical coal, although they underwent natural or simulated weathering conditions. The most noticeable change is the amount of sulfur that showed reduction between a synthesized sample and its respective original sample. This indicates the dissolution of sulfur upon weathering. In particular, the fresh fly ash is highly active upon weathering, the sulfur content in which was decreased considerably. In contrast, the weathered fly ash collected from ash dam is rather stable.

Full-pattern fitting and major peaks identification for QXRD analysis of fresh and weathered fly ash are summarized in Fig. 1. Note that, a Chi-square value of 4.63 and 20.44 has been achieved for the fresh and weathered fly ash, respectively.

The abundance of individual mineralogical species in fresh fly ash, weathered fly ash and synthetic fly ash 1 and 2 determined by QXRD is summarized in Fig. 2. For the fresh fly ash, the amorphous species only accounts for 3.75 wt.%, suggesting the high crystallization extent

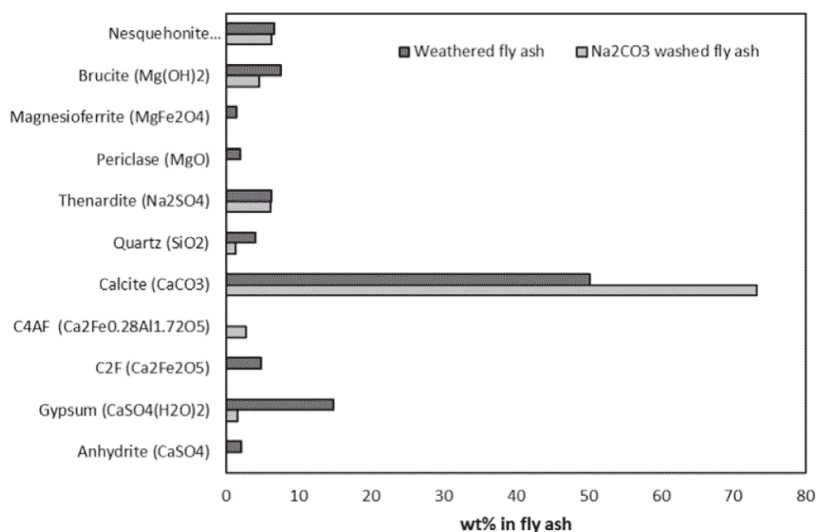


Fig. 5. Percentage of different minerals in crystalline phase (amorphous phase was not considered) before and after sodium carbonate washing of weathered fly ash calculated by QXRD.

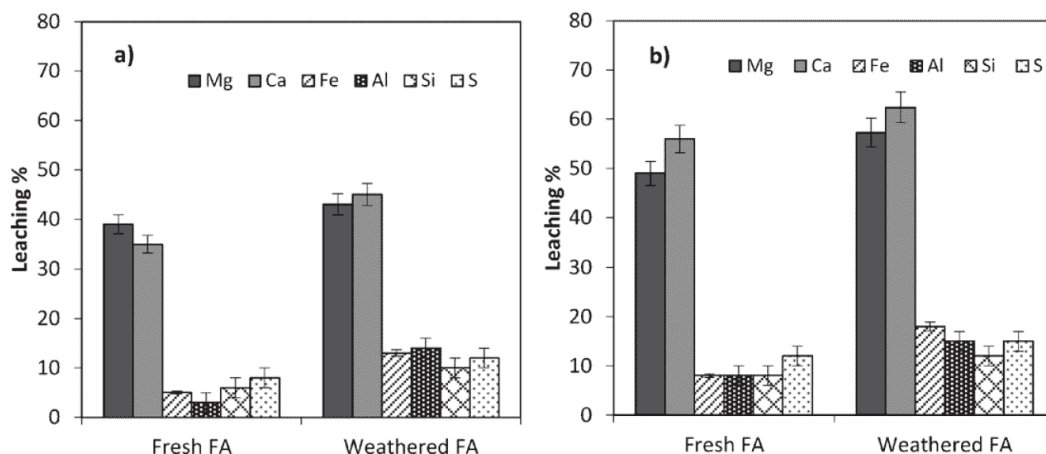


Fig. 6. Leaching yields of Mg and Ca (target elements) and Fe, Al, Si and S (interfering elements) from fresh fly ash and weathered fly ash using NH_4Cl 4 M, $T = 80^\circ\text{C}$ and $t = 30$ min at a) pH 5–5.5 and b) <4.5.

of the mineral species within it. Periclase (MgO) is the only Mg-bearing species while anhydrite (CaSO_4), C_2F ($\text{Ca}_2\text{Fe}_2\text{O}_5$) and a few amount of calcite (CaCO_3) are the major Ca-bearing species within it. Moreover, quartz (SiO_2) was found to be the major form for silicon within the fresh dried ash sample. The results for synthesized fly ash 1 indicate that, although the weathering time is only two weeks, the change on ash properties occurred quickly, leading to the increase in the amount of amorphous species, hydrated compound and carbonate as well. In the meanwhile the amount of anhydrous sulfate was decreased considerably and gypsum ($\text{CaSO}_4 \cdot \text{H}_2\text{O}$) was formed instead. For the weathered fly ash collected from ash dam, the quantity of its amorphous species was increased to 62.1 wt.%, which is a clear sign of the strong secondary reactions occurred in the aqueous system during long-term disposal of fly ash. The increased amount for calcite suggested the complete carbonation reaction in the landfill. The amount of periclase (MgO) was reduced significantly, which was replaced by abundant brucite ($\text{Mg}(\text{OH})_2$) and nesquehonite ($\text{MgCO}_3 \cdot 3\text{H}_2\text{O}$). For anhydrite, quartz (SiO_2) and C_4AF ($\text{Ca}_2\text{Fe}_{0.28}\text{Al}_{1.72}\text{O}_5$) which were the predominant Si and Al bearing species in the fresh fly ash, their quantities were reduced to a trivial level in the weathered fly ash. Clearly, most of these species interacted in the aqueous system to convert into poorly crystalline species that are undetectable by XRD. Negligible changes of composition upon second synthetic weathering process suggested that the weathered fly ash collected is fully stabilized in ash dam, bearing no any propensity to change upon weathering.

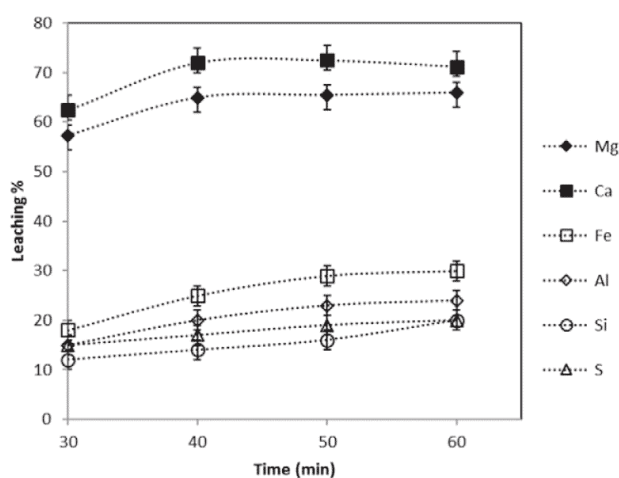


Fig. 7. Leaching of major elements from weathered fly ash as a function of leaching time (ammonium chloride pH controlled condition pH <4.5, $T = 80^\circ\text{C}$).

The typical cross-sectional image observed by SEM suggests a strong affinity of various species together within the weathered fly ash, as illustrated in Fig. 3. X-ray mapping shows that this particle consists of multiple elements including Ca, Mg, O, Si and S. The particle of quartz (SiO_2) on top part of the particles was observed while the particles around the corners are rich in Ca bounded with evenly dispersed O and C in the form of calcite which is the most predominant mineral in XRD spectra. Mg is dispersed mostly in the middle parts and associated with C and O to form hydroxide or carbonate forms specially brucite or nesquehonite.

3.1.2. Mössbauer results for the speciation of iron

As suggested by QXRD in Fig. 2, iron in a fly ash sample is mostly bound to other elements which potentially increase the difficulty for the extraction of target magnesium or calcium. The exact lattice position of the iron ions, however, is difficult to determine. The Mössbauer provides an excellent spectroscopic method for studying iron cation positions in different minerals (Taylor et al., 1968). The fitted Mössbauer spectra for fresh and weathered fly ash are illustrated in Fig. 4. All the hyperfine parameters are summarized in Table 3 and *Area%* refers to proportion of total iron in each of the phases.

Each of the full spectra in Fig. 4 consists of a relatively weak, poorly structured magnetic component and a much stronger non-magnetic component in the center of the spectrum. The weak sharp features visible at -8 , $+5.5$ and $+8.8$ mm/s fitted in light blue, which are the signature peaks of hematite (Fe_2O_3). The remainder of the magnetic sub-spectrum, as fitted in red, can be assigned as aluminum substituted

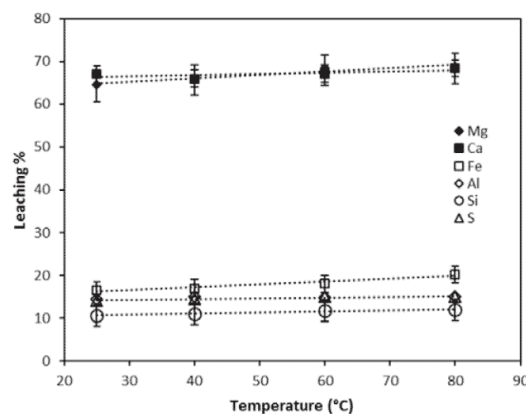


Fig. 8. Leaching of major elements from weathered fly ash as a function of temperature (ammonium chloride pH controlled condition pH <4.5, $t = 40$ min).

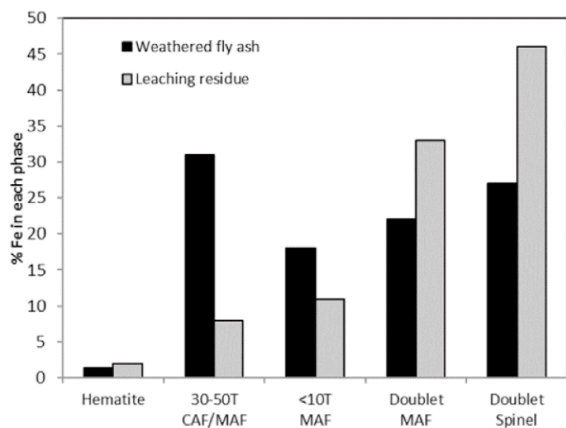


Fig. 9. Fe speciation before and after leaching of weathered fly ash, taken from Mössbauer spectra.

calcium ferrite, CAF ($\text{Ca}_2\text{Fe}_{2-x}\text{Al}_x\text{O}_5$), and/or magnesioferrite, MAF ($\text{MgFe}_{2-x}\text{Al}_x\text{O}_4$). The central doublet in all spectra was not symmetrical, indicating the co-existence of two or more doublets with slightly different centers (isomer shifts). The quadrupole splitting < 0.75 mm/s were classified as magnesioferrite and those > 0.75 mm/s were classified as spinel (also possibly including iron substituted periclase, $\text{MgO}:\text{Fe}^{3+}$ which has the same parameters). Any possible superparamagnetic CAF would have a quadrupole splitting of ~ 1.5 mm/s (Murad and Cashion, 2004). From Table 3, one can clearly see that most of the iron in fresh fly ash is in the magnesioferrite phase (39%) while around 50% of total iron in the weathered fly ash is in the MAF/CAF phase. This indicates the interaction between dissolved aluminum and magnesioferrite in the aqueous system. The other species including hematite (HEM) and doublet 2 for a spinel structures are highly stable and resistant against weathering. This is consistent with the previous observation (Kukier et al., 2003).

3.2. Sulfur removal upon sodium carbonate washing

In Fig. 5, the QXRD results for raw and sodium carbonate washed weathered fly ash is presented. Note that, the amorphous amount was not considered here. It is obvious that huge amounts of anhydrite and gypsum were removed and replaced by calcite formed upon Eq. (1). In addition, the amount of thenardite (Na_2SO_4) was found remaining unchanged, which implies that such a water-soluble species should be highly embedded within the fly ash matrix and hence, it was not easily accessed during the sodium carbonate washing process.

3.3. Fresh and weathered fly ash leaching characteristic

3.3.1. Leaching in $\text{NH}_4\text{Cl} + \text{HCl}$

Fig. 6a and b illustrate the extraction of target elements (Mg and Ca) and interfering ions (Fe, Al, Si and S) from sodium carbonate washed fresh and weathered fly ashes in the mixture of NH_4Cl and HCl at the two pH ranges of 5–5.5 and < 4.5 , respectively. The leaching temperature and time were fixed at 25 °C and 30 min here. As can be seen, the leaching yields of all elements from weathered fly ash are slightly higher than the respective elements in fresh fly ash. The leaching yields of individual element also show notable dependence upon pH for a more efficient dissolution of all the elements at lower pH, as expected. At the pH range of 5–5.5, 43% Mg, 45% Ca and 13% Fe were extracted from weathered fly ash, which were further increased to 57%, 62% and 18% upon decreasing the pH to < 4.5 .

The influences of leaching time and temperature were examined and plotted in Figs. 7 and 8, respectively. Note that, all the experiments in these two figures were conducted under the pH-control for a final pH < 4.5 for the leachate. As evident in Fig. 7, the influence of leaching time varies with the elemental type. Instead, the influence of temperature is insignificant for all the elements, as demonstrated in Fig. 8. From Fig. 7 it is clear that the leaching time of approximately 40 min at 80 °C is sufficient to maximize the extraction of target Mg and Ca out of the weathered fly ash, reaching 65% and 70% respectively. Interestingly, such values are just slightly higher than the room temperature results shown in Fig. 6b, 59% and 62% for Ca and Mg respectively. Again, this witnesses an insignificant influence of the leaching temperature. For the interfering elements including Al, Si and S, the increment on their elution yields with leaching time is less than that observed for the two target elements. This reflects a rather refractory association of these elements in the washed fly ash. To reiterate, the unwashed thenardite (as shown in Fig. 5) should be highly embedded within the amorphous matrix of the fly ash, otherwise it should be extracted readily upon either washing by sodium carbonate or $\text{NH}_4\text{Cl}/\text{HCl}$. For both Al and Si, the majority should be present as host species for the affiliation of others to form amorphous species.

Fe leaching is more time-dependent, reaching approximately 30 wt.% in 50 min. The quantified speciation information for iron before and after leaching is summarized in Fig. 9. Note that, the original Mössbauer spectroscopy spectra and the respective fitting curves are plotted in Fig. 10. Fig. 9 indicates that, hematite is least eluted upon the leaching, whereas the percentages of the 30–50 T CAF/MAF and the < 10 T MAF species were reduced dramatically after the leaching. Since the percentages of the other two were increased, it is inferable that, calcium in the CAF was preferentially extracted over the MAF and magnesioferrite upon the attack from the mixed NH_4Cl and HCl reagent. The difficulty for the breakage of the latter two species in acid has been reported previously (Choo et al., 2014).

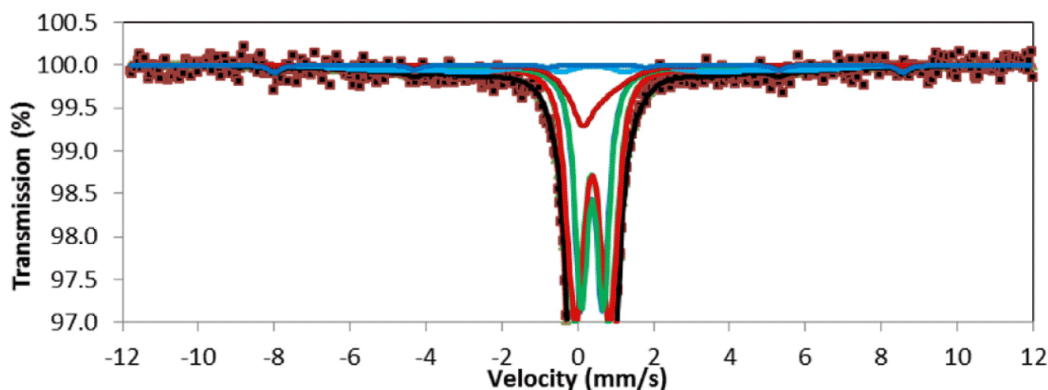


Fig. 10. Mössbauer spectroscopy fitting results $\text{NH}_4\text{Cl} + \text{HCl}$ leached residue.

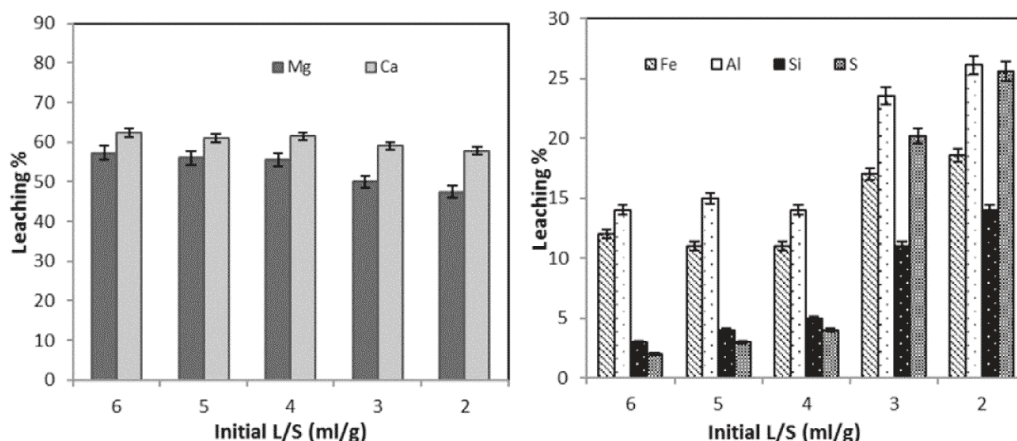


Fig. 11. Leaching yields of a) Mg and Ca (target elements) and b) Fe, Al, Si and S (Interfering elements) as a function of initial L/S ratio from weathered fly ash using NH_4Cl 4 M, $T = \text{RT}$ and $t = 40$ min at $\text{pH} < 4.5$.

The influence of liquid to solid (L/S) ratio was examined for the leaching of the weathered fly ash. As demonstrated in Fig. 11, the optimum L/S ratio was found to be 4. A lower L/S ratio resulted in a rapid increase in the extraction of interfering elements, whereas the extraction of two target elements was reduced.

3.3.2. Leaching in sole HCl

Leaching experiments were further conducted using pure HCl (without pH control) to increase the extraction yields of the two target elements. Despite a very low pH of around 0.8 for HCl used, its pH was increased quickly to ~7 once mixed with fly ash. Subsequently, the pH of the leachate fluctuated and was stabilized at ~6 in 10 min. In light of this, the results of using HCl can be compared with the pH-controlled leaching experiments using $\text{NH}_4\text{Cl} + \text{HCl}$ for a final pH value of 5–5.5. Fig. 12 shows the leaching yields of major and interfering elements in sole HCl 1 M. Similar to the pH controlled condition for the use of ammonia chloride (Fig. 6a), the leaching of both major and interfering ions from weathered fly ash is slightly higher than fresh fly ash. About 43% and 44% of Mg and Ca were extracted from weathered fly ash, relative to 41% and 41% respectively from fresh fly ash. This further indicates the abundant amorphous species in weathered fly ash are easier to be cracked than the highly crystallized species in the fresh ash. In other words, the weathering of fly ash is beneficial in improving its leaching propensity. The effect of temperature on the leaching of Mg, Ca and Fe in sole HCl was further examined and demonstrated in Fig. 13. Again, similar with the leaching results for $\text{NH}_4\text{Cl} + \text{HCl}$ in

Fig. 8, the temperature is insignificant on the extraction rates of Mg and Ca while the leaching of interfering ions was enhanced slightly.

3.4. Selective leaching of Mg and Ca over Fe, Al, Si and S by $\text{NH}_4\text{Cl} + \text{HCl}$ solution

The effect of pH on leaching behavior of individual elements from weathered fly ash was further investigated in the two leaching systems of $\text{NH}_4\text{Cl} + \text{HCl}$ and sole HCl. Note that, both two systems were pH controlled at various values show as x-axis in Fig. 14. The results for both two leaching systems were also plotted in each panel for the comparison purpose.

As expected, decreasing pH resulted in a rapid increase in the dissolution of all the metals in both $\text{NH}_4\text{Cl} + \text{HCl}$ and sole HCl solution. However, the two leaching systems performed considerably different upon the variation of pH. For the two target elements Ca and Mg shown in panel a, although the sole HCl is slightly better in terms of the yields of the two elements below the pH of 3.0, the use of $\text{NH}_4\text{Cl} + \text{HCl}$ solution is clearly superior at the higher pH values, leading to the extraction of 71% Mg and 66% Ca relative to only 50% of the two metals extracted in sole HCl at the same pH value of 4. With a further increase of pH from 4 to 5.5, the discrepancy between the two leaching systems was decreased and eventually vanished. For the interfering elements shown in panel b, increasing the pH value of the leachate is clearly beneficial in reducing their yields, which were stabilized at the pH of ~4.5 for both two leaching systems. Clearly, the pH value of 4.5 is the optimum/maximum value to be chosen for either leaching system.

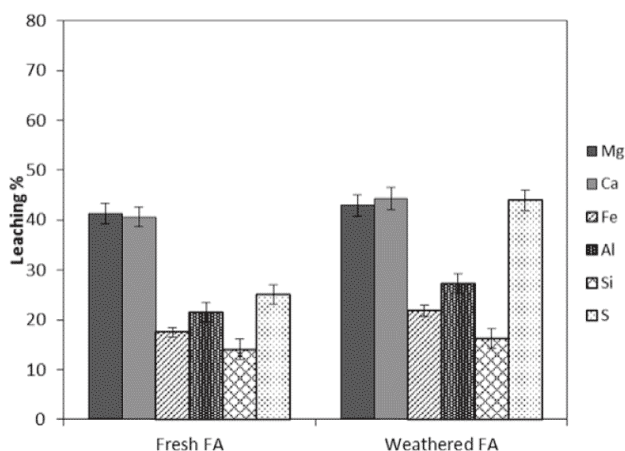


Fig. 12. Leaching yields of Mg, Ca, Fe, Al, Si and S from fresh fly ash and weathered fly ash using HCl 1 M without control pH ($T = \text{RT}$ and $t = 30$ min and $L/S = 6$).

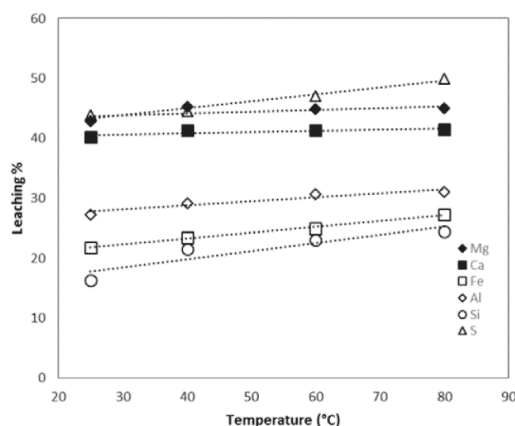


Fig. 13. Effect of temperature on hydrochloric acid leaching of Mg, Ca and Fe from weathered fly ash ($L/S = 6$, $t = 30$ min, $\text{HCl} = 1$ M).

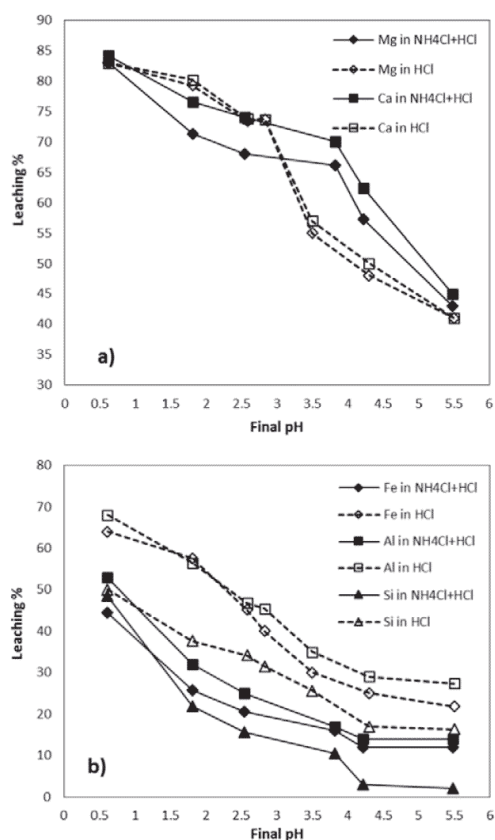


Fig. 14. Leaching behavior of a) Mg and Ca and b) other metals Fe, Si and Al in different pH of $\text{NH}_4\text{Cl} + \text{HCl}$ and sole HCl solution.

Moreover, the use of $\text{NH}_4\text{Cl} + \text{HCl}$ was confirmed superior against the sole HCl in the leaching of impure elements. In other words, the use of $\text{NH}_4\text{Cl} + \text{HCl}$ mixture facilitates a selective leaching of Ca and Mg over other elements out of fly ash.

It is inferred that cationic metal ions are chemically adsorbed on the surface of fly ash particles, especially weathered fly ash and hence, they are highly reactive. The release of metallic ions aqueous solution is assisted by the aid of hydrogen ions of acids or salts according to a cation exchange mechanism (Huang et al., 2011). Therefore, maintaining a high level of in the leach liquor using HCl is in favor of enhancing the reaction kinetics. For the fly ash studied here, the H^+ ion should penetrate into its internal layers to break the refractory associations such as CAF. Consequently, the elution of both target and interfering ions was improved. The positive role of NH_4Cl here is easier pH adjustment and restricting H^+ concentration through its buffer property (Künkül et al., 2013). Though HCl was added drop-wise to both NH_4Cl and HCl solution but fluctuation of pH from ~1 to 5 in the case of sole HCl could favors partial dissolution of substantial amount of iron, silicon and sulfur which can be released into the solution at lower pH range.

In addition, ammonium chloride has proven to be able to isolate metals or groups of metals from a polymetallic solution. As has been mentioned by Smith and Martell (1974), ammonia can selectively form a complex with magnesium and calcium and no other ions in a solution. The addition of an ammonium salt increases the solubility of the complexed species of Mg and Ca, which thus allows a much broader range of pH where the interfering ions precipitate rather dissolving into the leachate. Lalancette et al. (2014) has used hydrochloric acid as the leaching agent to dissolve desirable ions like magnesium, zinc and arsenic. Consequently they used ammonium chloride as complex agent to precipitate iron and prevent co-precipitation of other ions.

Table 4

XRD quantification of $\text{NH}_4\text{Cl} + \text{HCl}$ and sole HCl residues from leaching of weathered fly ash.

Minerals	Composition (wt.%)	
	NH_4Cl leached residue	HCl leached residue
Anhydrite (CaSO_4)	–	0.6
Gypsum ($\text{CaSO}_4(\text{H}_2\text{O})_2$)	1.0	1.2
C_2F ($\text{Ca}_2\text{Fe}_2\text{O}_5$)	–	2.2
C_4AF ($\text{Ca}_2\text{Fe}_{0.28}\text{Al}_{1.72}\text{O}_5$)	–	0.3
Calcite (CaCO_3)	11.5	15.8
Quartz (SiO_2)	1.2	1.2
Cristobalite (SiO_2)	0.3	0.4
Thenardite (Na_2SO_4)	–	1.6
Magnesioferrite (MgFe_2O_4)	–	1.8
Brucite ($\text{Mg}(\text{OH})_2$)	0.4	0.8
Nesquehonite ($\text{MgCO}_3 \cdot 3\text{H}_2\text{O}$)	0.7	0.7
Hematite (Fe_2O_3)	–	1.6
Ettringite ($\text{Ca}_6\text{Al}_2(\text{SO}_4)_3(\text{OH})_{12} \cdot 26\text{H}_2\text{O}$)	0.6	–
Tschermigite ($\text{NH}_4\text{AlSO}_4 \cdot 12(\text{H}_2\text{O})$)	1.2	–
Magnesite (MgCO_3)	10.2	–
Mascagnite ($\text{NH}_4(\text{SO}_4)_2$)	0.7	–
Amorphous amount	71.8%	71.6%

The XRD results for weathered fly ash $\text{NH}_4\text{Cl} + \text{HCl}$ and HCl leached residues are tabulated in Table 4. The leaching residues were obtained from the same final pH (around 5.5) for both leaching systems under the same experiment condition, (80 °C, 30 min and L/S ratio of 6). The results confirmed the formation of new minerals including ettringite ($\text{Ca}_6\text{Al}_2(\text{SO}_4)_3(\text{OH})_{12} \cdot 26\text{H}_2\text{O}$), tschermigite ($\text{NH}_4\text{AlSO}_4 \cdot 12(\text{H}_2\text{O})$) and mascagnite ($\text{NH}_4(\text{SO}_4)_2$) in $\text{NH}_4\text{Cl} + \text{HCl}$ system. It is evident that ammonium chloride inhibited the dissolution of Al and Si into the leachate through precipitation. No differences were observed in terms of amorphous amounts from two leaching reagents. It is also clear that there is more amorphous present in the leaching residue, around 71%, compared to only 62% in the original fly ash.

The SEM cross-sectional images taken from $\text{NH}_4\text{Cl} + \text{HCl}$ and sole HCl leaching residues further show the different particle compositions. Fig. 15a shows SEM images of typical particles (L1 and L2) in $\text{NH}_4\text{Cl} + \text{HCl}$ leaching residue while part b demonstrates the representative particles from HCl leaching residue (L3 and L4). Elemental composition of closed area on surface of particles calculated from EDX analysis is summarized in Table 5. The particle L1 shown is the combination of Fe, Ca and Mg that might be mixture of CAF, MAF or hematite in amorphous form. Abundance of O and C in all of the particles confirms the presence of oxide, hydroxide or carbonates of Mg. L2 shows significant amount of Fe, Mg, Si and Al which can be attributed to quartz, hematite or magnesioferrite along with magnesium hydroxide or carbonates. Both two particles are rather dense with fewer pores inside, indicating a weak penetration of ammonium ion into the particle for the extraction of the elements embedded in depth. Instead, L3 shows a large cluster which are composed of fine agglomerates that are made up of Fe, C, O and Mg. Brucite, periclase, nesquehonite, magnesioferrite and hematite are possible minerals existing in this particle. The rather loose packing of the particle aggregates indicates the breakage of original coarse particles upon the severe attack of protons. The particle L4 is different in shape and texture, which is flat in shape and is exclusively made up of Al, Fe and Mg. It can be inferred as Fe-bearing spinel that is even difficult to dissolve in sole acid (Choo et al., 2014).

4. Conclusion

This work for the first time has examined the properties and leaching propensity of weathered Victorian brown coal fly ash collected from ash pond. The leaching conditions for the target metals Ca and Mg were also optimized. The major conclusions achieved are summarized as follows:

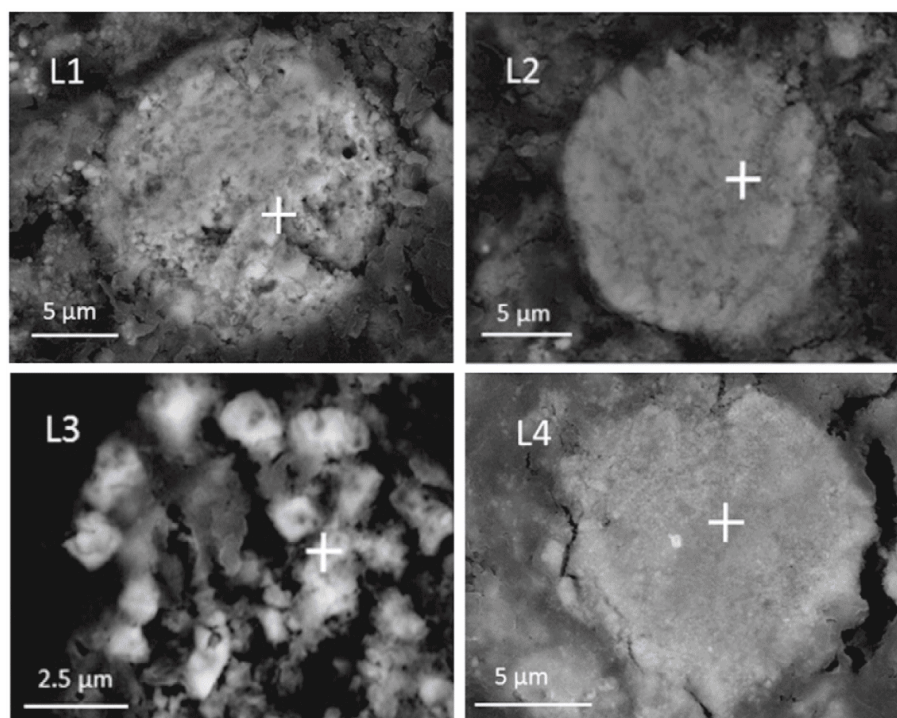


Fig. 15. BSE images magnification 5000 \times of typical particles L1 and L2 obtained from NH_4Cl + HCl (top) and L3 and L4 from sole HCl (bottom) leaching residue of weathered fly ash.

- 1) In comparison to fresh fly ash rich in oxides, the weathered fly ash is dominated by hydrates and carbonate forms formed in aqueous landfilling system. These species were mostly poorly crystallized, and even loosely agglomerated into clusters. Irrespective of the leaching reagent, the target Ca and Mg in weathered fly ash were more easily extracted than in the fresh ash counterpart under the same leaching conditions, due to the association of these two metals with amorphous species.
- 2) For the use of either leaching agent, the temperature and time played little or marginal role on the extraction of target Ca and Mg out of the weathered fly ash sample. In contrast, the liquid to solid ratio is crucial. The optimum value of 4 was found beneficial for maximizing the selectivity of Ca and Mg.
- 3) The optimum pH value was found to be around 4 for the mixture of NH_4Cl + HCl, which reduced the extraction yields of impure elements to the lowest value, whereas the leaching extent of two target elements was still reasonably high, $\sim 70\%$. However, this is not the case observed for the sole HCl, the use of which resulted in a lower selectivity of Ca and Mg at the pH of 4.
- 4) The use of NH_4Cl + HCl is superior over sole HCl, due to the buffering property of NH_3 and its complexing capability to prevent the dissolution of impure elements. Instead, the use of sole HCl even at the same pH value as the mixture of NH_4Cl + HCl resulted in a deep penetration of protons into particle inside, the intense breakage of ash cluster, and hence, the simultaneous dissolution of plenty of impure elements.

Table 5

Elemental composition of representative leaching residue particles L1 and L2 (NH_4Cl + HCl leached) and L2 and L3 (HCl leached) determined by EDX.

Sample	Size (μm)	Elemental composition (wt.%)								
		Ca	Mg	Fe	Si	Al	S	Cl	Na	O
L1	10–15	23	13	28	+	3	+	+	ND	32
L2	10–15	3	9	33	8	6	+	2	+	38
L3	10–15	2	6	53	3	5	ND	2	ND	24
L4	8–10	2	15	15	+	18	+	+	ND	44

+: not significant, ND: not detected.

Acknowledgment

This project was supported by the Faculty of Engineering of Monash University for 2012–13 seed grant. The first author is grateful to Monash Research Graduate School (MRGS) for PhD tuition fee award and CSIRO Flagship scholarship. The invaluable comments from Jim Siemon in Latrobe Magnesium Co. Ltd are also acknowledged.

References

- Ahmaruzzaman, M., 2010. A review on the utilization of fly ash. *Prog. Energ. Combust.* 36, 327–363.
- Andrade, A., Coenegracht, Y.M.A., Hollman, G.G., Janssen-Jurkovicova, M., Pietersen, H.S., Vriend, S.P., Schuiling, R.D., 1989. Leaching characteristics of fly ash after four years of natural weathering. *MRS online proceeding library* 178.
- Baba, A., Gurdal, G., Sengunalp, F., Ozay, O., 2008. Effects of leachant temperature and pH on leachability of metals from fly ash. A case study: can thermal power plant, province of Canakkale, Turkey. *Environ. Monit. Assess.* 139, 287–298.
- Baker, L., Gupta, A., Gasiowski, S., 2015. Triboelectrostatic beneficiation of landfilled fly ash. *World of Coal Ash (WOCA) Conference*. May 5–7, Nashville, USA.
- Berry, E.E., Hemmings, R.T., Golden, D.M., 1986. Enhanced resource recovery by beneficiation and direct acid leaching of fly ash. *Mat. Res. Soc. Symp. Proc.* 86. *MRS online proceedings library*, Pittsburgh, PA, pp. 365–382.
- Choo, T.K., Song, Y., Zhang, L., Selomulya, C., Zhang, L., 2014. Mechanisms underpinning the mobilization of iron and magnesium cations from Victorian brown coal fly ash. *Energy Fuels* 28 (6), 4051–4061.
- Eze, C.P., Nyale, S.M., Akinyeye, R.O., Gitari, W.M., Akinyemi, S.A., Fatoba, O.O., Petrik, L.F., 2013. Chemical, mineralogical and morphological changes in weathered coal fly ash: a case study of a brine impacted wet ash dump. *J. Environ. Manag.* 129, 479–492.
- Hosseini, T., Selomulya, C., Haque, N., Zhang, L., 2014. Indirect carbonation of Victorian brown coal fly ash for CO_2 sequestration: multiple-cycle leaching-carbonation and magnesium leaching kinetic modelling. *Energy Fuels* 28 (10), 6481–6493.
- Huang, K., Inoue, K., Harada, H., Kawakita, H., Ohtto, K., 2011. Leaching of heavy metals by citric acid from fly ash generated in municipal waste incineration plants. *J. Mater. Cycles Waste Manage.* 13, 118–126.
- Jo, H.Y., Ahn, J.H., Jo, H., 2012. Evaluation of the CO_2 sequestration capacity for coal fly ash using a flow-through column reactor under ambient conditions. *J. Hazard. Mater.* 242, 127–136.
- Kukier, U., Ishak, C.F., Sumner, M.E., Miller, W.P., 2003. Composition and element solubility of magnetic and non-magnetic fly ash fractions. *Environ. Pollut.* 123, 255–266.
- Künkül, A., Gülezgin, A., Demirkiran, N., 2013. Investigation of the use of ammonium acetate as an alternative lixiviant in the leaching of malachite ore. *Scientific Paper. Inonu University, Malatya, Turkey*.
- Lalancette, J.M., Dubreuil, B., Lemieux, D., 2014. Method for selective precipitation of iron, arsenic and antimony, US Patent 2014/0120012.

- Montes-Hernandez, G., Pérez-López, R., Renard, F., Nieto, J.M., Charlet, L., 2009. Mineral sequestration of CO₂ by aqueous carbonation of coal combustion fly-ash. *J. Hazard. Mater.* 161 (2–3), 1347–1354.
- Mudd, G.M., Kodikara, J., 2000. Field studies of the leachability of aged brown coal ash. *J. Hazard. Mater.* 76 (2–3), 159–192.
- Murad, E., Cashion, J., 2004. *Mössbauer Spectroscopy of Environmental Materials and Their Industrial Utilization*. Kluwer Academic Publishers, Dordrecht.
- Muriithi, G.N., Petrik, L.F., Fatoba, O., Gitari, W.M., Doucet, F.J., Nel, L., Nyale, S.M., Chucks, P.E., 2013. Comparison of CO₂ capture by ex-situ accelerated carbonation and in situ naturally weathered coal fly ash. *J. Environ. Manag.* 127, 212–220.
- Nyambura, M.G., Mugeru, W.G., Felicia, P.L., Gathura, N.P., 2011. Carbonation of brine impacted fractionated coal fly ash: implications for CO₂ sequestration. *J. Environ. Manag.* 92, 655–664.
- Sharma, B.K., 2001. *Soil And Noise Pollution*. Goel publishing house, Meerut.
- Singh, R.K., Gupta, N.C., Guha, B.K., 2014. pH dependence leaching characteristics of selected metals from coal fly ash and its impact on ground water quality. *Int. J. Chem. Environ. Eng.* 5, 218–222.
- Smith, R.M., Martell, A.E., 1974. *Critical stability constants. Volume 4: Inorganic Complexes*. Plenum Press, New York.
- Sun, Y., Yao, M.S., Zhang, J.P., Yang, G., 2011. Indirect CO₂ mineral sequestration by steel-making slag with NH₄Cl as leaching solution. *Chem. Eng. J.* 173 (2), 437–445.
- Sun, Y., Parikh, V., Zhang, L., 2012. Sequestration of carbon dioxide by indirect mineralization using Victorian brown coal fly ash. *J. Hazard. Mater.* 209–210, 458–466.
- Taylor, G.R., Ruotsala, A.P., Keeling, R.O., 1968. Analysis of iron in layer silicates by Mössbauer spectroscopy. *Clay Clay Miner.* 16, 381–391.
- Teir, S., Revitzer, H., Eloneva, S., Fogelholm, C.J., Zevenhoven, R., 2007. Dissolution of natural serpentinite in mineral and organic acids. *Int. J. Miner. Process.* 83, 36–46.
- Ward, C.R., Taylor, J.C., Cohen, D.R., 1999. Quantitative mineralogy of sandstones by x-ray diffractometry and normative analysis. *J. Sediment. Res.* 69 (5), 1050–1062.
- Ward, C., French, D., Jankowski, D., Dubikova, M., Li, Z., Riley, K., 2009. Element mobility from fresh and long-stored acidic fly ashes associated with an Australian power station. *Int. J. Coal Geol.* 80, 224–236.
- Williams, R.P., Van Riessen, A., 2010. Determination of the reactive component of fly ashes for geopolymer production using XRF and XRD. *Fuel* 89 (12), 3683–3692.
- Yeheyis, M., Shang, J., Yanful, E., 2009. Chemical and mineralogical transformations of coal fly ash after landfilling. *World Of Coal Ash (WOCA) Conference*. May 4–7, Lexington, USA.
- Żygadło, M., Woźniak, M., 2010. Processes of coal fly ash weathering in waste deposits. *Environ. Prot. Eng.* 36 (2), 17–29.

Investigating the Effect of the Mg²⁺/Ca²⁺ Molar Ratio on the Carbonate Speciation during the Mild Mineral Carbonation Process at Atmospheric Pressure

Tahereh Hosseini,[†] Cordelia Selomulya,[†] Nawshad Haque,[‡] and Lian Zhang^{*,†}

[†]Department of Chemical Engineering, Monash University, GPO Box 36, Clayton, Victoria 3800, Australia

[‡]Minerals Resources Flagship, Commonwealth Scientific and Industrial Research Organisation (CSIRO), Clayton, Victoria 3168, Australia

Supporting Information

ABSTRACT: Aqueous mineral carbonation of industrial wastes, such as fly ash, is a promising sequestration technology to reduce CO₂ emissions in small-/medium-sized plants. In this paper, the carbonation capacity of a leachate rich in Mg²⁺ and Ca²⁺ contents was examined to clarify the competition between the carbonation of these two cations and the speciation of the resulting carbonate precipitate, under the mild carbonation conditions using 20–80 °C and atmospheric pressure. As confirmed, the carbonation precipitation of the two cations was completed in 30–40 min. At room temperature, increasing the Mg²⁺/Ca²⁺ molar ratio was in favor of the carbonation rate of Mg²⁺, which is maximized at the Mg²⁺/Ca²⁺ molar ratio of 2. In contrast, the carbonation rate of Ca²⁺ was decreased monotonically as a result of the competition from Mg²⁺. For both cations, their carbonation rate was maximized at 60 °C. In comparison to the formation of predominant calcite and vaterite in the presence of sole Ca²⁺ in the leachate, the coexistence of two cations resulted in the preferential formation of amorphous species, aragonite and magnesian calcite. The quantity of the amorphous phase was increased remarkably upon increasing the Mg²⁺/Ca²⁺ molar ratio at room temperature. An increase in the carbonation temperature further deteriorated the crystallization of the carbonation precipitate, resulting in the increase of the amount of amorphous species and the phase change of calcium carbonate from calcite to aragonite.

1. INTRODUCTION

Mineral carbonation is a process that involves the sequestration of CO₂ by converting the Ca- and/or Mg-bearing solid residue wastes into carbonates, which are thermodynamically stable.^{1–3} The main drawback of mineral carbonation technologies that use natural mineral resources, such as serpentine, wollastonite, and olivine, as feedstock is the large effort that has been exerted in mining and milling of raw material to achieve a small size and large specific surface area.⁴ The utilization of alkaline solid wastes, such as fly ash, has several advantages, including a low cost of sequestration, a close proximity to the place which CO₂ is emitted, and an abundance of fine and uniform particle size, which circumvents the comminution cost. Moreover, alkaline solid wastes are typically more reactive with CO₂ than natural minerals as a result of their chemical instability.⁵

Fly ash is a valueless waste derived from the combustion of coal and municipal solid waste (MSW), containing magnesium (Mg) and calcium (Ca) at varying proportions. The characteristics of fly ash differ substantially according to the coal type and combustion conditions. Fly ash derived from low-rank lignite or sub-bituminous coal generally consists of more than 20% CaO and MgO in total, which are essential for mineral carbonation.⁶ The typical Victorian brown coal fly ash, from Victoria, Australia, is composed of 29.3% MgO and 32.4% CaO, which has proven to be an appropriate feedstock for mineral carbonation.^{7,8}

Because the fly ash rich in alkali and alkaline earth metals is unsuitable for being used as an additive in cement, the use of

this kind of fly ash to supplement natural minerals for CO₂ mineralization has been receiving increased attention.^{9–11} To date, the majority of studies on fly ash utilization has focused on direct carbonation under a high CO₂ partial pressure with a rather long reaction time.^{10,12} Little work has been performed on an indirect carbonation fashion, i.e., a prior leaching for the extraction of Ca and Mg into an aqueous leachate with subsequent precipitation of solid carbonate by contacting the liquor with a CO₂-laden flue gas.^{11,13,14} The advantages of this method lie in the fact that mild conditions (25–80 °C and atmospheric pressure) are good enough for both leaching and carbonation. The resulting carbonation products are also of high purity that can be used as a substitution for the natural carbonates.

To date, the majority of works on the indirect carbonation of industrial wastes focused on the optimization of process conditions to maximize the yield of calcium carbonate as a result of the less amount of Mg in certain solid wastes.^{4,5,9,15} In the case of solid wastes with a high Ca/Mg ratio, such as steel-making slag, it is mostly preferred to minimize Mg contamination in the leachate and, consequently, achieve high-purity calcium carbonate by adjusting the leaching or carbonation parameters.^{16–18} In some cases, however, studies on the carbonation of aqueous resources, including seawater,

Received: July 15, 2015

Revised: October 1, 2015

Table 1. Summary of Different Ratios of Mg²⁺/Ca²⁺ in Carbonation Experiments

case	material	[Mg ²⁺]/[Ca ²⁺]	concentration	description
1	MgCl ₂ ·6H ₂ O	[Mg ²⁺]/[Ca ²⁺] = 1:0	MgCl ₂ (0.0646 g/mL)	only Mg ²⁺ in solution
2	MgCl ₂ ·6H ₂ O + CaCl ₂ ·2H ₂ O	[Mg ²⁺]/[Ca ²⁺] = 2:1	MgCl ₂ (0.0646 g/mL) + CaCl ₂ (0.03762 g/mL)	[Mg ²⁺] kept constant in the solution and CaCl ₂ doubled in each case
3	MgCl ₂ ·6H ₂ O + CaCl ₂ ·2H ₂ O	[Mg ²⁺]/[Ca ²⁺] = 1:1	MgCl ₂ (0.0646 g/mL) + CaCl ₂ (0.07524 g/mL)	
4	MgCl ₂ ·6H ₂ O + CaCl ₂ ·2H ₂ O	[Mg ²⁺]/[Ca ²⁺] = 1:2	MgCl ₂ (0.0646 g/mL) + CaCl ₂ (0.15048 g/mL)	
5	CaCl ₂ ·2H ₂ O	[Mg ²⁺]/[Ca ²⁺] = 0:1	CaCl ₂ (0.07524 g/mL)	only Ca ²⁺ in solution

subsurface brine, and industrial effluents, have focused on the carbonation of both Ca²⁺ and Mg²⁺.^{19,20} Although over 90% of Mg²⁺ and Ca²⁺ in seawater can precipitate in their carbonate forms through raising the pH of the leachate or CO₂ partial pressure,²¹ the coexistence of Mg²⁺ and Ca²⁺ in the leachate has proven to exert a remarkable effort on the precipitation behavior of Ca²⁺.^{21–24} Roques and Girou have reported that the Ca²⁺ precipitation extent was significantly reduced by the presence of even a small amount of Mg²⁺ in the leachate. They concluded that the cations having atomic radii smaller than that of Ca²⁺ and hydration energy higher than that of Ca²⁺ can orient to aragonite (CaCO₃), a deposit normally made up of calcite.²¹ Kitano has observed that the initial concentration ratio of Mg²⁺/Ca²⁺ greater than 3 yielded a precipitate that is composed mainly of aragonite (CaCO₃).²³

Although a limited number of studies have been mentioned about the co-precipitation of Mg and Ca in the aqueous mineral carbonation process, the competition of Mg and Ca cations on the carbonation rate and carbonate precipitate composition has yet to be achieved. This is the motivation for this study. Given the fact that the compositions of both calcium and magnesium in fly ash vary broadly, the competition between the two cations Ca²⁺ and Mg²⁺ extracted in the leachate can be regarded as the most critical parameter affecting their carbonation rate as well as the final carbonate product properties. In light of this, we have varied the Ca²⁺/Mg²⁺ ratio between two extremes for pure Ca²⁺ or Mg²⁺ cation to examine their competition in the carbonation process. The pure CaCl₂ and MgCl₂ solutions were used to mimic the leachates achieved from leaching processes of Mg- and Ca-rich industrial wastes or natural minerals, which usually have a broad Ca²⁺ to Mg²⁺ molar ratio upon the variation of the feedstock. In addition, the carbonation of the mixed solutions was conducted as a function of the reaction temperature and time at atmospheric pressure. Here, the partial pressure of CO₂ and its flow rate was fixed at 1 atm and 15 L min⁻¹, respectively, which were large enough to eliminate both external and internal diffusion resistances. By doing this, the effect of CO₂ partial pressure was ruled out in this study. The precipitated solid products from the carbonation process were analyzed delicately using quantitative X-ray diffraction (Q-XRD), to establish the mineral phase diagram for both cations upon atmospheric carbonation. The accuracy of the Q-XRD has been validated through the use of pure compound mixtures. An internal standard method was also established by use of the Q-XRD to quantify the amount of both amorphous and individual crystallized species. This study aims to provide an overall mineral phase diagram for mild indirect carbonation and, therefore, enhance the understanding on properties of carbonate upon the competition between two cations and their potential value-added utilization as well.

2. MATERIALS AND METHODS

2.1. Materials. Experiments were performed using mixtures of MgCl₂ and CaCl₂ solutions to mimic fly ash leachates. Analytical-grade reagents MgCl₂·6H₂O, CaCl₂·2H₂O, and aqueous ammonia (28%) were used as the source of Mg²⁺, Ca²⁺, and pH swing agent, respectively. The carbonation experiment conditions are summarized in Table 1. The first and last experiments correspond to two extremes for the presence of sole Mg²⁺ and Ca²⁺ in the solution, respectively. The initial concentration of 0.065 g mL⁻¹ MgCl₂ (0.0163 g mL⁻¹ Mg²⁺) was chosen on the basis of the leachate achieved from the leaching of a brown coal fly ash in ammonium chloride solution in our previous work.⁷ For all of the remaining experiments, the concentration of Mg²⁺ remained constant, where Ca²⁺ with different ratios relative to Mg²⁺ was added to the solution. An extra set of complementary experiments was conducted at a Mg²⁺/Ca²⁺ molar ratio of 1 to clarify the effect of the temperature on the carbonation yield and the quantity of precipitates. Note that the concentration range for Mg²⁺ and Ca²⁺ in the simulated leachates studied here is broadly consistent with the respective ranges for the man-made mineral-derived leachates that have been studied.^{8,11,25}

For each carbonation experiment, the predetermined amounts of MgCl₂·6H₂O and CaCl₂·2H₂O were dissolved in distilled water. Before carbonation, 16 mL of ammonia solution (28%) was added to synthesized solution to adjust the pH value to 10–11. The resulting solution was placed immediately into a sealed glass beaker under magnetic stirring at 400 rpm. The gas inlet and outlet tubes allowed for a continuous pure CO₂ gas stream with a constant flow rate of 15 L min⁻¹ at atmospheric pressure. This rate has been confirmed to be the optimum value in terms of eliminating the external diffusion resistance. It is also high enough to stir the leachate thoroughly to eliminate the internal diffusion but causes no splash of the solution. In theory, the optimized flow rate depends upon the size of the reactor, volume of solution, and pH.⁵ The role of CO₂ partial pressure is out of scope for this study. Moreover, although the flow rate of CO₂ is influential in affecting the carbonation rate, it has been confirmed affecting little on the final yield and properties of the final carbonate products.²⁶

The aqueous carbonation experiments were conducted with a reaction time up to 1 h. Eventually, the solution was filtered using a vacuum filter, and the resulting solid powders were dried at 110 °C overnight and stored. The solid dry residue was further washed with distilled water for around 1 h at a liquid/solid ratio of 10 to remove any crystallized ammonium chloride.⁷

2.2. Characterization of Solid Precipitates. The elemental compositions of carbonate precipitates were determined using precalibrated X-ray fluorescence spectroscopy (XRF, Spectro iQ II). The X-ray diffraction (XRD, Rigaku, Miniflex 600) pattern for each precipitate was recorded from 2 to 90° 2θ at 40 kV and 15 mA using a rate of 2° min⁻¹ with Cu Kα radiation. Mineral identification was conducted in MDI Jade 6, whereas Q-XRD was performed using Siroquant, version 4.0. Through the least-squares fitting refinement of the Rietveld parameters, Siroquant is able to create a theoretical XRD profile to fit the measured XRD pattern, through iteratively minimizing the χ². The Rietveld method has been applied successfully to determine crystalline phase composition of pure and complex substances. It was applied successfully to analyze National Institute of Standards and Technology (NIST) fly ash standard reference material, and the total average error was found to be only 4%.²⁷ In this

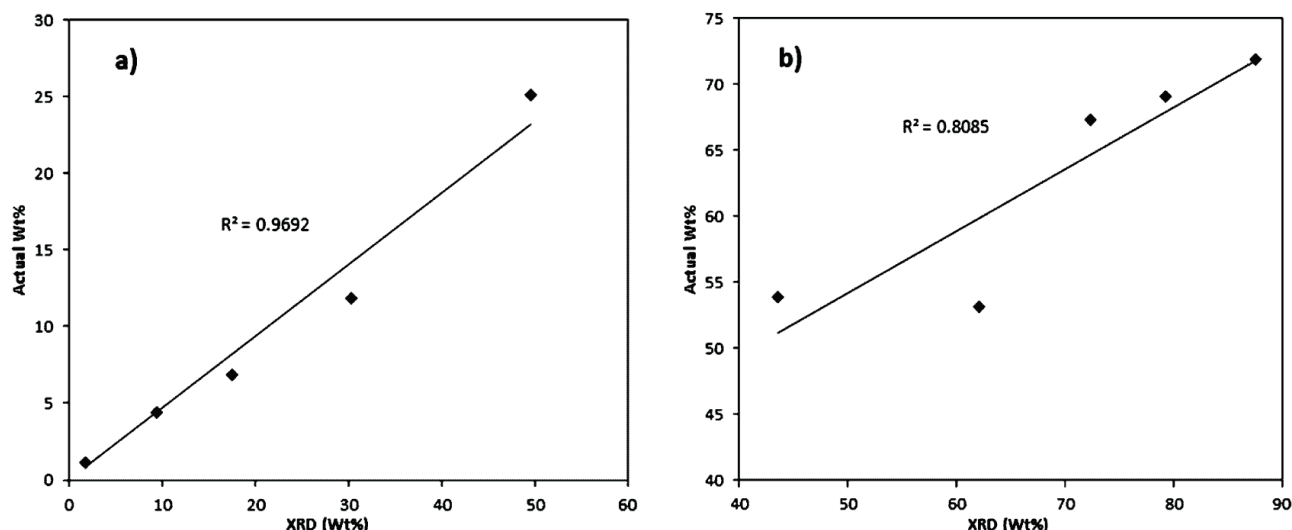


Figure 1. Comparison of Q-XRD results to actual mass percentages for two pure oxides in their mixtures: (a) Fe₂O₃ and (b) SiO₂ at different mixing ratios.

study, we also ground each carbonate precipitate down to <10 μm through the use of a SPEX Mixer/Mill 8000D. The adequate reduction of the particle size will eliminate preferred orientation and obtain a uniformly sized, randomly oriented fine power specimen, which accurately reflects the structure and composition of phases.²⁸ To validate the Q-XRD results in the quantification of oxide compositions, the mixtures of superpure silica (SiO₂, >99%, Sigma-Aldrich) were mixed with iron oxide (Fe₂O₃, >99%, Sigma-Aldrich) at different mass ratios and were analyzed by the Q-XRD first. Figure S1 of the Supporting Information provides the measured XRD patterns for the mixtures and their respective fitting curves. On the basis of the Rietveld method, the Q-XRD is further able to deliver the mass percentage of these two oxides. Figure 1 is the corresponding scatter charts for the comparison of Q-XRD results and the actual values for different mixtures of SiO₂ and Fe₂O₃. Clearly, one can see a good accuracy for the Q-XRD, yielding linear regression R² values of 0.8085 and 0.9692 for SiO₂ and Fe₂O₃, respectively. This echoes a χ² error no larger than 50 for the Q-XRD fitting in Figure S1.

On the basis of the fact that the amorphous species is undetectable in XRD, we further extend the Q-XRD methodology for the quantification of the amount of species, through the use of an internal standard, high-purity corundum α-Al₂O₃ crystal powder (>99.5%, Sigma-Aldrich). The amount of amorphous species upon Q-XRD analysis was determined on the basis of the mass percentage ($W_{\text{Al}_2\text{O}_3, \text{Q-XRD}}$) of the internal standard, with corundum quantified by Q-XRD, by eq 1^{29–31}

$$W_{\text{Al}_2\text{O}_3, \text{Q-XRD}} = \left(\frac{W_{\text{Al}_2\text{O}_3} \times 100}{(100 - W_{\text{Al}_2\text{O}_3} \times 100 - X)} \right) \times 100 \quad (1)$$

where $W_{\text{Al}_2\text{O}_3}$ is the original mass percentage of Al₂O₃ added to its mixture with the real sample to be analyzed and X stands for the mass amount of amorphous species in the sample with a mass of $100 - W_{\text{Al}_2\text{O}_3} \times 100$. The value of $W_{\text{Al}_2\text{O}_3, \text{Q-XRD}}$ must be larger than that for $W_{\text{Al}_2\text{O}_3}$ as a result of the presence of amorphous species, which cannot be detected by the XRD.

Figure 2 demonstrates a variation of the quantity of the amorphous species with the amount of the internal standard added in real fly ash samples collected from a coal-fired power plant. The elemental composition of the fly ash sample mixed with different ratios of corundum calculated by XRD and XRF as well as amorphous amounts calculated by eq 1 are presented in Table S1 of the Supporting Information. The XRD patterns for its mixture with corundum are given in Figure S2. It is clear that a minimum amount of 10 wt % is

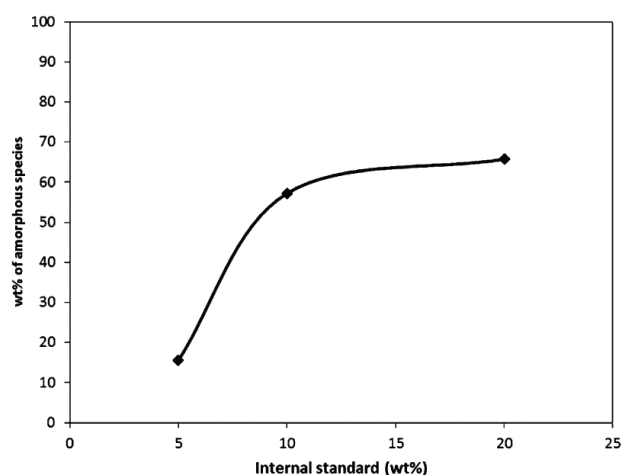


Figure 2. Amorphous percentage inside the fly ash sample based on different amounts of internal standard.

essential for the internal standard; otherwise, its peaks are strongly superimposed by the species in the fly ash sample, as demonstrated in Figure S2. To maximize the accuracy of the Q-XRD results, we hereafter fixed the internal standard amount at 20 wt %. Such a value has also proven highly accurate elsewhere.³² It is also noteworthy that the amorphous fraction (~61 wt %) is broadly consistent with that reported for a NIST fly ash reference sample.²⁷ This is another evidence supporting the high accuracy of the Q-XRD method developed here.

The thermal characteristics of the carbonation precipitate and loss on ignition (LOI) were examined with a thermogravimetric analyzer (TGA, Shimadzu). Approximately 5–10 mg of the solid precipitate were placed inside a quartz crucible and heated at a heating rate of 50 °C min⁻¹ in a nitrogen flow rate of 100 mL min⁻¹.

The following equations were used to calculate the percentage of Mg and Ca precipitated:

$$\text{Mg (\%)} = \frac{(W_{\text{ws}} - \text{LOI})\text{Mg(XRF \%)}}{W_{\text{Mg}}} \times 100 \quad (2)$$

$$\text{Ca (\%)} = \frac{(W_{\text{ws}} - \text{LOI})\text{Ca(XRF \%)}}{W_{\text{Ca}}} \times 100 \quad (3)$$

C

DOI: 10.1021/acs.energyfuels.5b01609
Energy Fuels XXXX, XXX, XXX–XXX

In the above equations, W_{ws} refers to the weight of a solid precipitate after washing by water to remove ammonia chloride residue and W_{Mg} and W_{Ca} are the absolute amounts of Mg^{2+} and Ca^{2+} , respectively, which were calculated on the basis of their concentration in the leachate. Calcium carbonation conversion for some cases was also calculated on the basis of the following equation and was compared to results from eq 3. The error was around 2–3%, which can confirm the presence of whole Ca in the carbonate form.

$$\text{Ca (\%)} = \frac{\frac{\text{CO}_2 \text{ (wt \%)} \cdot \text{MW}_{\text{Ca}}}{100 - \text{CO}_2 \text{ (wt \%)} \cdot \text{MW}_{\text{CO}_2}}}{W_{\text{Ca}}} \quad (4)$$

CO_2 (wt %) in eq 4 was derived from the weight loss observed in the TGA at a temperature range of ~620–780 °C, which is the characteristic temperature for the decomposition of calcium carbonate. MW_{Ca} and MW_{CO_2} are the molar weights of Ca and CO_2 in kg mol^{-1} , respectively, and W_{Ca} is the total Ca content of leachate in kg kg^{-1} .³³

2.3. Geochemical Modeling. Thermodynamic equilibrium speciation modeling was carried out using Visual MINTEQ, a Windows version of the MINTEQA2 geochemical speciation code. VMINTEQ is an equilibrium speciation model that is useful for calculating the equilibrium mass distribution among dissolved species and multiple solid phases under a variety of conditions, including a gas phase with constant partial pressure.³⁴ The degree of undersaturation or oversaturation of a leachate with respect to a particular mineral is determined as the saturation index (SI), according to eq 5

$$\text{SI} = \log \frac{\text{IAP}}{K_{\text{sp}}} \quad (5)$$

where IAP is the ion activity product and K_{sp} is the solubility constant for a particular mineral.³⁵ In the case of the SI value greater than 0, the leachate solution was deemed oversaturated with respect to that particular mineral and that mineral will spontaneously precipitate. In this study, the dissolved concentration of each species was set as input for the modeling. The partial pressure of CO_2 was introduced as a fixed parameter, and a pH value of 11 was chosen for the carbonation reaction. The Davis method was used to estimate the fugacity coefficients.

3. RESULTS AND DISCUSSION

3.1. Effect of the $\text{Mg}^{2+}/\text{Ca}^{2+}$ Molar Ratio and Reaction Time on Carbonation at Room Temperature. Panels a and b of Figure 3 depict the precipitation rate of Mg^{2+} and Ca^{2+} cations as a function of the molar ratio of $\text{Mg}^{2+}/\text{Ca}^{2+}$ at room temperature, respectively. The data show that, regardless of the molar ratio of $\text{Mg}^{2+}/\text{Ca}^{2+}$, the precipitation rate of two cations was increased exponentially over time and was completed in 40 min. This is consistent with our previous findings for tests on real leachates derived from ammonia chloride leaching of fly ash.⁷ Moreover, the molar ratio of two cations was found to play a noticeable role on the precipitation rate of each cation. For the sole Mg^{2+} cation in Figure 3a, it shows the slowest precipitation rate, whereas the case for a molar $\text{Mg}^{2+}/\text{Ca}^{2+}$ ratio of 2 exhibits the fastest precipitation rate. More interestingly, upon the decrease on the molar ratio of $\text{Mg}^{2+}/\text{Ca}^{2+}$, the precipitation rate of Mg^{2+} was decreased considerably. The results for Ca^{2+} in Figure 3b show an opposite trend. That is, the existence of sole Ca^{2+} in the leachate exhibits the highest precipitation rate, whereas its precipitation rate decreases quickly upon increasing the molar ratio of $\text{Mg}^{2+}/\text{Ca}^{2+}$ in the leachate.

To further quantitatively compare the precipitation rates of two cations in different cases, a parameter $1/\tau_{50}$ for the reverse of the reaction time required to reach a 50 wt % precipitation extent was plotted versus the molar ratio of $\text{Mg}^{2+}/(\text{Mg}^{2+} +$

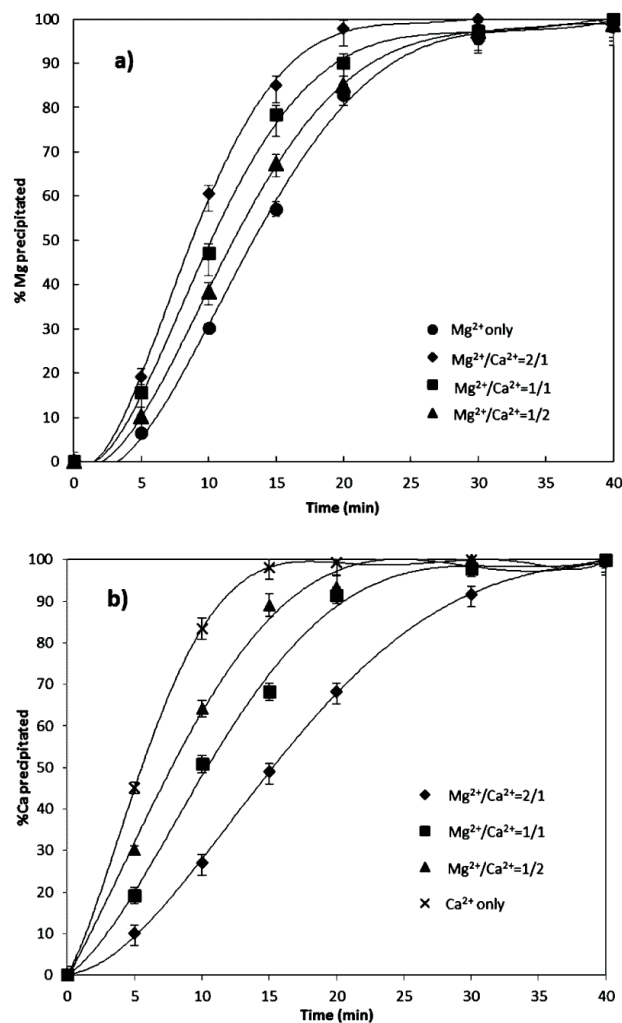


Figure 3. (a) Mg and (b) Ca carbonation yields of different $\text{Mg}^{2+}/\text{Ca}^{2+}$ ratios at room temperature as a function of time.

Ca^{2+}) and shown in Figure 4. Such a ratio was used as the x axis to avoid the appearance of infinity for the molar ratio of $\text{Mg}^{2+}/\text{Ca}^{2+}$ in the case of sole Mg^{2+} . Here, a value of 0 for $\text{Mg}^{2+}/(\text{Mg}^{2+} + \text{Ca}^{2+})$ refers to the case of sole Ca^{2+} in the leachate, whereas the unity value denotes the case of sole Mg^{2+} for the carbonation reaction. The values of τ_{50} were inferred from the simulated curves in the two panels in Figure 3. Clearly, the precipitation rate of Ca^{2+} decreases monotonically upon introducing and increasing the Mg^{2+} cation in the leachate. This is a direct sign of the competition between the two cations in reacting with CO_2 dissolved in the leachate. On the contrary, the precipitation rate of Mg^{2+} reaches a peak at the value of 0.67 for the molar ratio of $\text{Mg}^{2+}/(\text{Mg}^{2+} + \text{Ca}^{2+})$, which corresponds to the case when the concentration of Mg^{2+} is twice that of Ca^{2+} in the leachate. The precipitation rate of Mg^{2+} at such a peak value is even higher than that of Ca^{2+} . Such a unique phenomenon can be explained by the promoting effect of Ca^{2+} on the carbonation rate of Mg^{2+} when they coexist. There have been several studies to support this phenomenon. Calcite in a supersaturated solution can precipitate by nucleation in an early stage and subsequent growth in later stages. The presence of Mg^{2+} in the solution, however, inhibits the calcite nucleation kinetics by poisoning

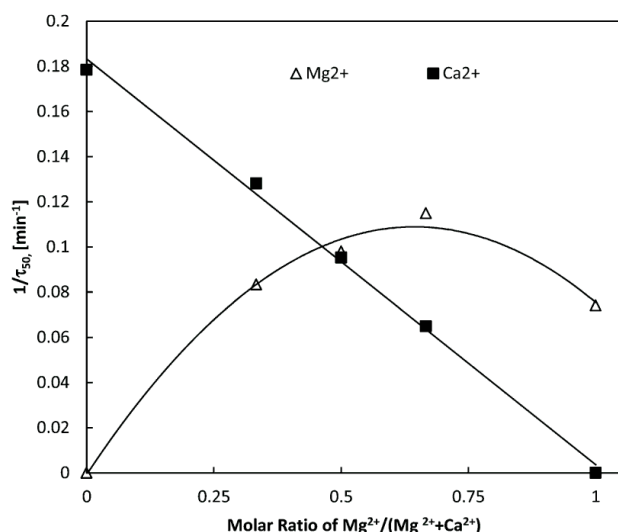


Figure 4. Correlation between the molar ratio of $\text{Mg}^{2+}/(\text{Mg}^{2+} + \text{Ca}^{2+})$ and $1/\tau_{50}$ for the precipitation of two cations.

the active growth sites of the pre-critical nuclei through the incorporation of Mg^{2+} into the calcite lattice.^{9,36–38} Both the rate of the diffusion and the composition of the products are also strongly dependent upon the initial $\text{Mg}^{2+}/\text{Ca}^{2+}$ in the solution.³⁹ Upon further increasing of the Ca^{2+} concentration over the optimum value for the peak precipitation rate of Mg^{2+} , Ca^{2+} competes with Mg^{2+} and attracts CO_3^{2-} and HCO_3^- more readily, thereby leading to a longer equilibrium time for Mg^{2+} precipitation.

The monotonic decrease on the precipitation rate of Ca^{2+} upon the increase of the Mg^{2+} concentration is not unusual. Fernandez-Diaz et al. have reported inhibition of calcite crystal growth in the presence of Mg with the concentration higher than 25 mg kg^{-1} . This has been attributed to the incorporation of Mg^{2+} cation into the calcite crystal lattice and a 20% higher dehydration energy of Mg^{2+} than Ca^{2+} , resulting in a slower growth of calcite nuclei.³⁶ Moreover, it was found that the variation in the Mg^{2+} carbonation rate is rather narrower than that for Ca^{2+} , which is a strong indicator for a greater inhibitory influence of Mg^{2+} on calcite formation. For the case of the concentration of Mg^{2+} equaling twice that of Ca^{2+} , the promotion effect of Ca^{2+} on Mg^{2+} is clearly much greater than the reserve inhibitory influence of Mg^{2+} on Ca^{2+} ; therefore, the precipitation rate of Mg^{2+} is nearly double that of Ca^{2+} .

3.2. Characterization of Solid Precipitates Formed at Room Temperature. **3.2.1. Precipitates from Sole Mg^{2+} Leachate.** Carbonation of sole Mg^{2+} resulted in the formation of an unidentified precipitate, the XRD pattern of which cannot be matched by any database that we have. As an instance, the XRD pattern for the precipitate obtained after 10 min of reaction time as well as the standard database in MDI Jade software with unmatched potential Mg-bearing components is depicted in Figure 5. For the $\text{Mg}-\text{CO}_2-\text{H}_2\text{O}$ system, the thermodynamically stable phase is either magnesite (MgCO_3) or brucite [$\text{Mg}(\text{OH})_2$]. However, in practice, these two species are mostly preceded or usurped by the metastable phases.⁴⁰ Several unidentified magnesium carbonates have been detected, some of which possess amorphous structures.^{41,42} Botha and Strydom obtained an unidentified structure, which shows

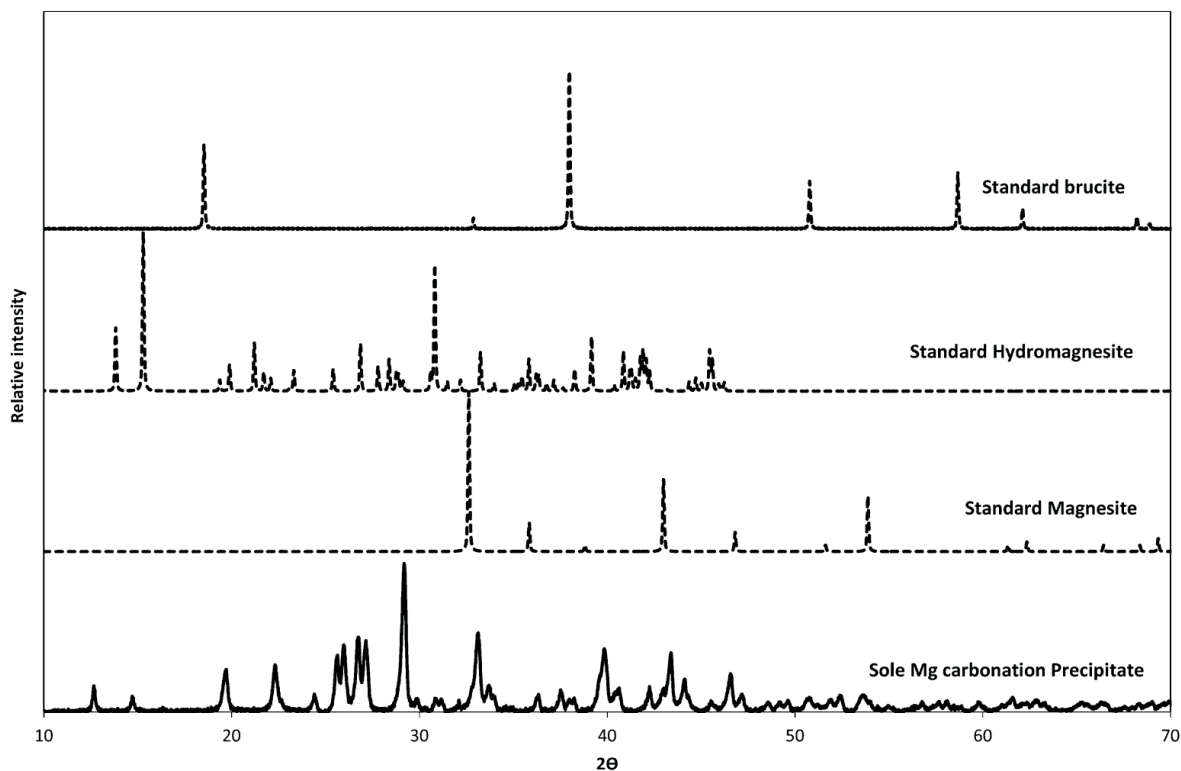


Figure 5. XRD pattern for the carbonation precipitate of sole Mg^{2+} after 10 min of reaction time, unfitted with potential Mg-bearing minerals from the MDI Jade database.

similarities to hydromagnesite $[\text{Mg}_5(\text{CO}_3)_4(\text{OH})_2 \cdot 4\text{H}_2\text{O}]$ and appears to be an intermediate phase between nesquehonite $(\text{MgCO}_3 \cdot 3\text{H}_2\text{O})$ and hydromagnesite $[\text{Mg}_5(\text{CO}_3)_4(\text{OH})_2 \cdot 4\text{H}_2\text{O}]$. They have confirmed that the carbonate product dried at 80–120 °C is unidentified amorphous, which is consistent with our experimental observations here.⁴¹

The precipitation potential of minerals that could form in the Mg–H₂O–CO₂ system was further assessed by MINTEQA and demonstrated in Table 2. As seen, four species including

Table 2. Log IAP and SI Calculated by MINTEQA for Possible Minerals in Precipitate Obtained from Carbonation of Sole Mg²⁺

mineral	log IAP	SI
artinite $[\text{Mg}_2(\text{CO}_3)(\text{OH})_2 \cdot 3\text{H}_2\text{O}]$	12.758	3.158
brucite $[\text{Mg}(\text{OH})_2]$	15.453	−1.647
hydromagnesite $[\text{Mg}_5(\text{CO}_3)_4(\text{OH})_2 \cdot 4\text{H}_2\text{O}]$	4.671	13.437
magnesite (MgCO_3)	−2.696	4.764
nesquehonite $(\text{MgCO}_3 \cdot 3\text{H}_2\text{O})$	−2.696	1.974
periclase (MgO)	15.453	−6.131

artinite $[\text{Mg}_2(\text{CO}_3)(\text{OH})_2 \cdot 3\text{H}_2\text{O}]$, hydromagnesite $[\text{Mg}_5(\text{CO}_3)_4(\text{OH})_2 \cdot 4\text{H}_2\text{O}]$, magnesite (MgCO_3) , and nesquehonite $(\text{MgCO}_3 \cdot 3\text{H}_2\text{O})$ can thermodynamically be formed and precipitate under the experimental conditions employed here. However, none of them has been confirmed by the XRD analysis. This hints that the unknown species, such as metastable hydrated magnesium carbonate phases, could be formed instead. Metastable phases interfere with the production of magnesite or well-ordered crystals as a result of their fast nucleation and growth rate compared to magnesite

crystals.⁴³ Metastable arrangements are common when minerals are grown rapidly at low temperature.⁴⁴

3.2.2. Precipitates from the Mixture of Mg²⁺ + Ca²⁺ and Sole Ca²⁺. The measured XRD patterns for the precipitates formed from the coexistence of two cations and sole Ca²⁺ have been matched satisfactorily by Siroquant. As an example, the measured and fitted XRD patterns for the precipitates obtained at 5 min of different Mg²⁺/Ca²⁺ ratios (except sole Mg²⁺) carbonation are presented in Figure 6. The χ^2 values for the final fitting of XRD patterns for the reaction times of 5 and 60 min areas are summarized in Table 3, suggesting that all of the errors have been minimized to a very low and acceptable level.⁴⁵

Table 3. χ^2 Value for Selected Siroquant Fitting

case	χ^2 value	
	$t = 5$ min	$t = 60$ min
Mg ²⁺ /Ca ²⁺ = 2:1	11.9	18
Mg ²⁺ /Ca ²⁺ = 1:1	8.1	22.8
Mg ²⁺ /Ca ²⁺ = 1:2	27.1	17.9
sole Ca ²⁺	9.7	9.3

The presence of sole Ca²⁺ in the solution led to the formation of different polymorphs of pure Ca carbonates, calcite (CaCO₃), aragonite (CaCO₃), and vaterite (CaCO₃). Calcite is generally the most common mineral species formed in most of the Ca-bearing solutions.⁴⁶ Examination of the XRD patterns from co-precipitation of Mg²⁺ and Ca²⁺ revealed the broadening of the peak positioned ~29–30.5°, which overlaps with calcite, dolomite $[\text{CaMg}(\text{CO}_3)_2]$, and magnesian calcite $(\text{Mg}_n\text{Ca}_{1-n}\text{CO}_3)$, typically with $n \ll 1$) on the same hkl plane

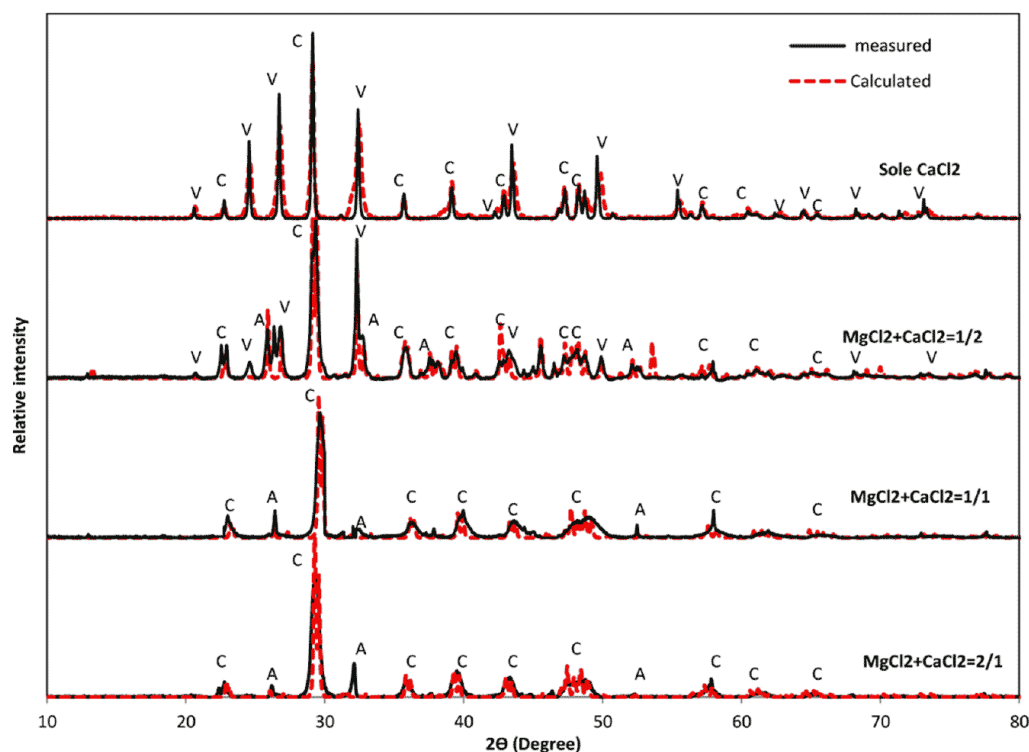


Figure 6. Measured and calculated XRD patterns for the carbonation of different molar ratios of Mg²⁺/Ca²⁺ at 5 min of reaction time (V, vaterite; C, calcite and magnesian calcite; and A, aragonite).

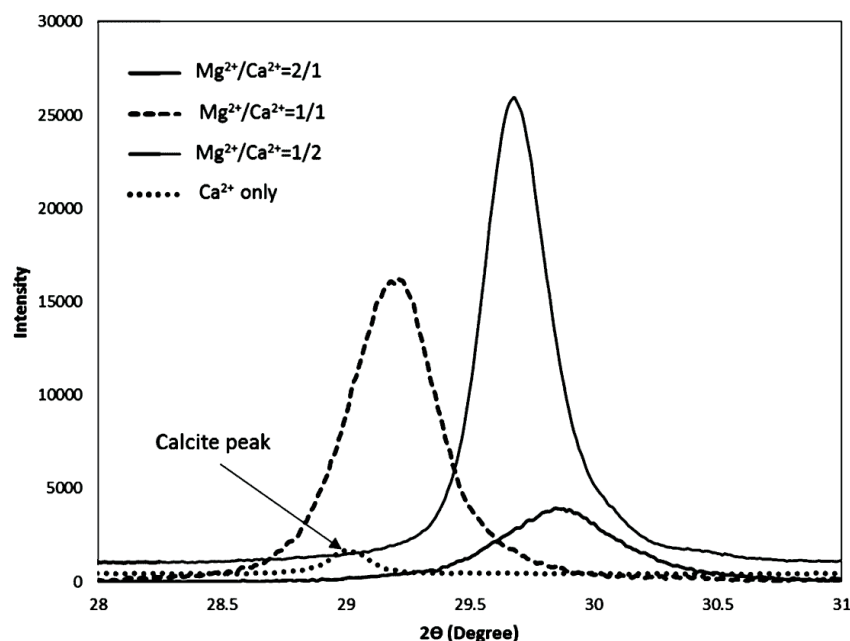


Figure 7. Enlarged XRD patterns for magnesian calcite peak positions for different $\text{Mg}^{2+}/\text{Ca}^{2+}$ ratios compared to pure calcite after 10 min of reaction time.

Table 4. XRD Fitting Parameters of the Major Peak at ($2\theta \sim 28.5\text{--}31^\circ$) Extracted from Jade for Precipitates at Different Mg/Ca Ratios and Sole Ca at 10 min of Reaction Time

case	2θ (deg)	d (Å)	centroid	skew	fwhm	breadth
$\text{Mg}^{2+}/\text{Ca}^{2+} = 2:1$	29.861	2.9897	29.861	-0.004	0.584	0.739
$\text{Mg}^{2+}/\text{Ca}^{2+} = 1:1$	29.183	3.0575	29.189	-0.056	0.418	0.522
$\text{Mg}^{2+}/\text{Ca}^{2+} = 1:2$	29.645	3.011	29.668	-0.31	0.284	0.384
sole Ca^{2+}	28.997	3.0768	28.988	0.219	0.153	0.211

of 104. The Rietveld refinement using both calcite and magnesian calcite showed better fitting and a lower χ^2 value compared to the sole presence of any of the three phases mentioned above. Diagnostic X-ray spacing and a typical diffractogram are another two criteria that can be used to differentiate calcite from dolomite. The peak at $\sim 28.5\text{--}29.5^\circ$ with a space diameter of ~ 0.304 nm represents calcite. A skewing or displacement of the calcite peak toward lower spacing will denote the presence of magnesian calcite as well. Generally, the presence of magnesian calcite shifts the overlapped calcite and magnesian calcite peak toward higher 2θ . This is evident in Figure 7, which displays the enlarged XRD pattern of $28\text{--}31^\circ$ for magnesian calcite peak positions formed at different $\text{Mg}^{2+}/\text{Ca}^{2+}$ ratios after 10 min of reaction time. The calcite peak from carbonation of sole Ca^{2+} is also presented for comparison.

The main feature of dolomite is that it occurs at higher 2θ ($\sim 30.6\text{--}31.4^\circ$) compared to calcite and magnesian calcite with a space diameter of 0.289 nm.⁴⁷ In this study, the differentiation of these species has been successfully performed through the use of two software programs. As depicted in Table 4, it is clear that 2θ for the mixture of Mg and Ca has been shifted to higher angles and lower spacing upon the increase of the molar ratio of $\text{Mg}^{2+}/\text{Ca}^{2+}$ in the leachate. Such a distinct feature echoes the presence of magnesian calcite in the samples. In addition, it is noteworthy that the dolomite [$\text{CaMg}(\text{CO}_3)_2$] peak was not observed in any of the $\text{Mg}^{2+}/\text{Ca}^{2+}$ ratios in the leachate. Dolomite occurs mostly at earth surfaces through a

dissolution–precipitation reaction, in which a calcium carbonate precursor is replaced by dolomite through interaction with magnesium-rich solution.³⁹ In the aqueous environment, hydration of magnesium and cation ordering prevent dolomite precipitation and metastable magnesian calcite forms instead. An increase in pressure favors dolomitization of magnesian calcite as a result of the tendency of atoms to approach an ideal arrangement.³⁷

The phase diagram derived from Q-XRD for all of the precipitates formed as a function of the reaction time are summarized in panels a–d of Figure 8. From panels c and d of Figure 8 related to the least $\text{Mg}^{2+}/\text{Ca}^{2+}$ ratio and sole Ca^{2+} , respectively, the metastable form of CaCO_3 , vaterite, was detected and is even predominant in the sole Ca^{2+} case. Calcite is the second largest Ca-bearing species for calcium. The presence of Mg^{2+} in the leachate ($\text{Mg}^{2+}/\text{Ca}^{2+}$ molar ratio of 1:2) led to the transformation of whole vaterite to calcite toward the end of the reaction time. Upon the increase of the $\text{Mg}^{2+}/\text{Ca}^{2+}$ ratio in the leachate, the fractions of aragonite, magnesian calcite, and even the amorphous species were increased remarkably. The increased formation of aragonite growth with increasing Mg^{2+} concentrations was also observed by Boyd et al.³⁸

Figure 9 further demonstrates the percentages of two major compounds, amorphous phase and magnesian calcite, in solid precipitates as a function of the $\text{Mg}^{2+}/\text{Ca}^{2+}$ molar ratio and reaction time at room temperature. For the amorphous species depicted in Figure 9a, its amount formed in the case of sole

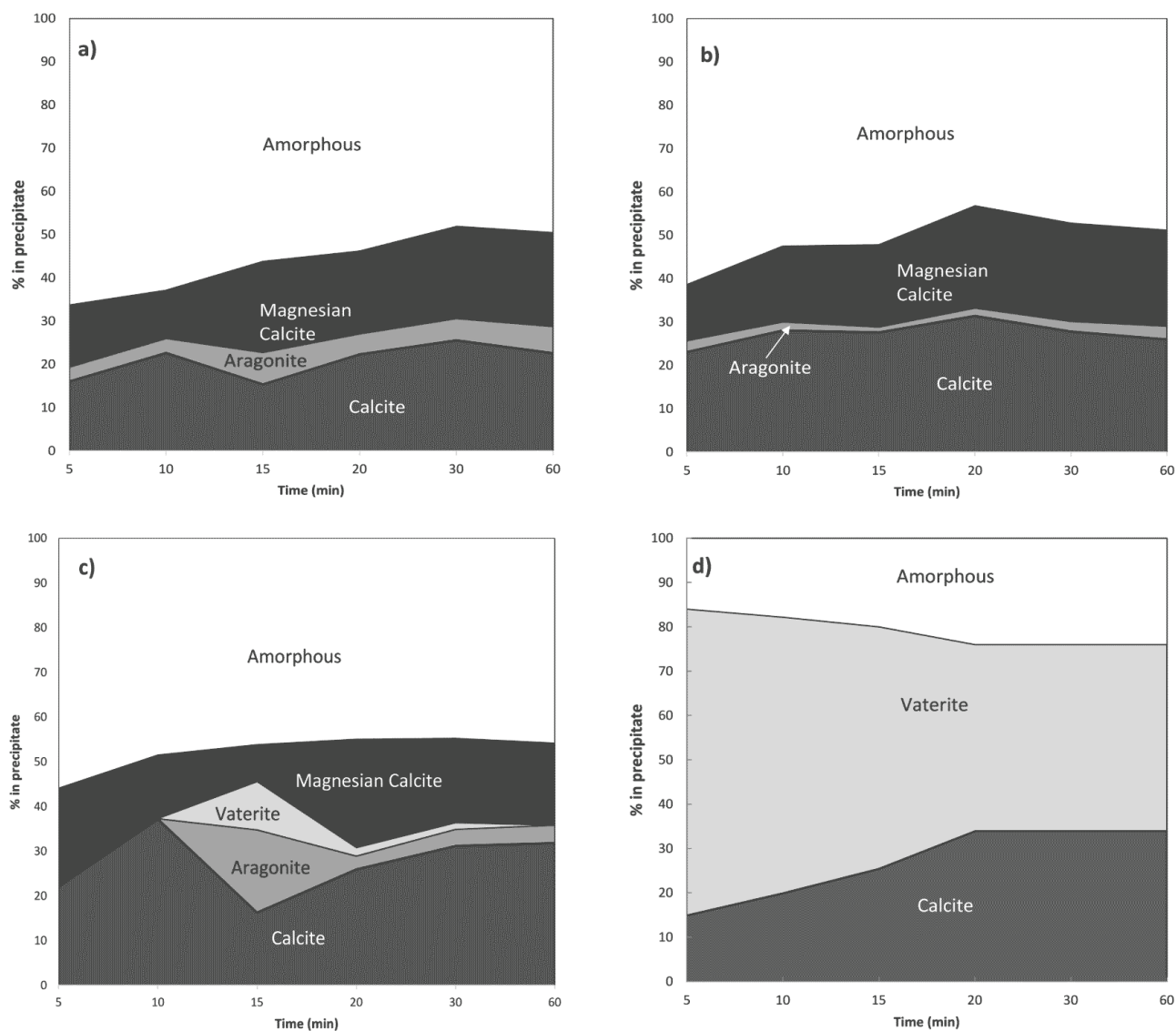


Figure 8. Solid precipitate composition of carbonation of (a) $\text{Mg}^{2+}/\text{Ca}^{2+} = 2:1$, (b) $\text{Mg}^{2+}/\text{Ca}^{2+} = 1:1$, (c) $\text{Mg}^{2+}/\text{Ca}^{2+} = 1:2$, and (d) sole Ca^{2+} , at room temperature calculated by Q-XRD and an internal standard method.

Ca^{2+} is the lowest, reaching the maximum of ~ 20 wt % at around 10 min and stabilized afterward. Upon the increase of $\text{Mg}^{2+}/\text{Ca}^{2+}$ in the leachate, the amount of amorphous formed was increased dramatically in the first 10 min, reaching around 50 and 65 wt % for the two medium $\text{Mg}^{2+}/\text{Ca}^{2+}$ ratios and the highest ratio, respectively. Xu et al. have also confirmed exclusive formation of amorphous magnesian calcite and magnesite in high $\text{Mg}^{2+}/\text{Ca}^{2+}$ ratios and sole Mg^{2+} leachate, respectively.⁴⁸ With respect to magnesian calcite shown in Figure 9b, it was found that the $\text{Mg}^{2+}/\text{Ca}^{2+}$ ratio of 1:1 is the optimum ratio for the maximized formation of this species in the carbonate precipitate. Its amount was maximized in 20 min, irrespective of the $\text{Mg}^{2+}/\text{Ca}^{2+}$ molar ratio in the leachate. Upon the further increase of time, this species levels off for the cases of $\text{Mg}^{2+}/\text{Ca}^{2+}$ equaling 1 and 2. However, it decreases continuously for the case with the least $\text{Mg}^{2+}/\text{Ca}^{2+}$ ratio. This phenomenon indicates a complicated reordering of the magnesian calcite crystal lattice in the leachate. It is very likely

that a portion of Mg^{2+} could elute out of the calcite matrix upon increasing its residence time in the leachate.

To further clarify this phenomenon, the percentage of MgCO_3 or n in magnesian calcite formula ($\text{Mg}_n\text{Ca}_{1-n}\text{CO}_3$) as a function of time for various $\text{Mg}^{2+}/\text{Ca}^{2+}$ molar ratios is further shown in Figure 10. This percentage was estimated from a semi-quantitative method based on the position of the magnesian calcite peak with respect to the calcite peak.⁴⁷ With regard to the optimum $\text{Mg}^{2+}/\text{Ca}^{2+}$ of 1 discussed above, the lowest MgCO_3 content was confirmed in magnesian calcite, which reaches only 15 wt % in 20 min. Such a value is close to around 17 wt % observed for $\text{Mg}^{2+}/\text{Ca}^{2+}$ of 1:2 but lower than the case of the molar ratio of $\text{Mg}^{2+}/\text{Ca}^{2+}$ equaling 2. This fluctuation suggests that, under certain conditions, Mg^{2+} is trapped in the calcite crystal lattice, leading to the increase in the solubility of the solid precipitate as a result of the creation of strains on the crystalline structure.⁴⁹ Moreover, irrespective of the $\text{Mg}^{2+}/\text{Ca}^{2+}$ molar ratio, the fraction of MgCO_3 in magnesian calcite reached a plateau at $\sim 10\%$ MgCO_3 in the

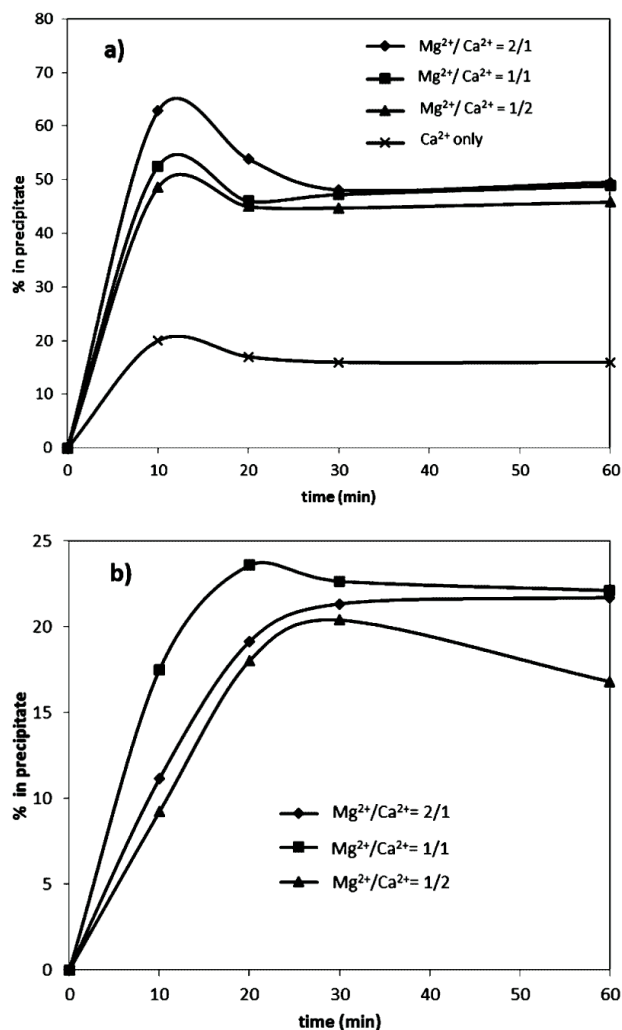


Figure 9. Percent of (a) amorphous phase and (b) magnesian calcite in precipitates formed from the carbonation of different ratios of $\text{Mg}^{2+}/\text{Ca}^{2+}$ as a function of the reaction time.

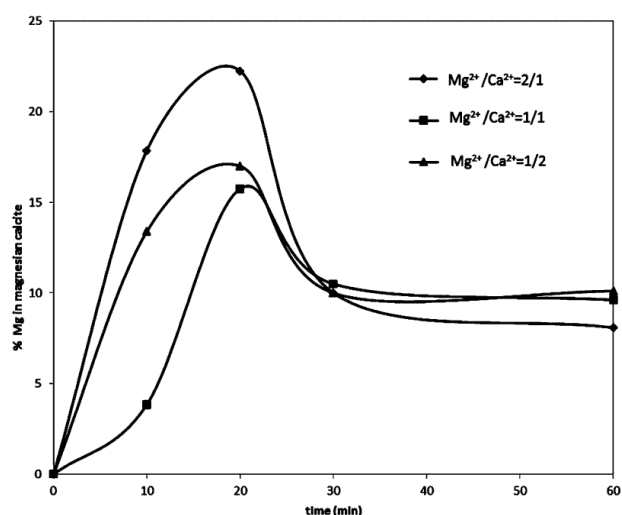


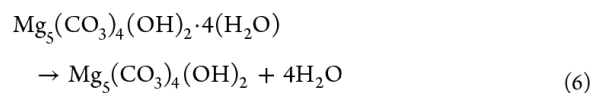
Figure 10. Mass fraction of MgCO_3 in magnesian calcite for different ratios of $\text{Mg}^{2+}/\text{Ca}^{2+}$ as a function of the reaction time.

calcite lattice. Such a value has been confirmed to be the highest limit for the amount of MgCO_3 in thermodynamically stable magnesian calcite.⁵⁰ In marine environments, coprecipitation of magnesium generally results in calcite with up to ~10% MgCO_3 , whereas in natural skeletal calcite, the magnesium content can increase up to ~30%.⁵¹ However, crystallization experiments using artificial or real seawater-produced calcite with a magnesium content up to 22% along with other carbonate phases have been reported in the literature.⁵² The Mg content in inorganically formed calcite is limited as a result of the formation of aragonite, the saturation degree of calcite lattice, and the reaction temperature as well.⁵¹

In addition, to reveal the probable structure for the abundant amorphous species observed in Figures 8 and 9, thermogravimetry–differential thermogravimetry (TG–DTG) analysis of the thermal behavior of carbonation precipitates was further conducted for the samples received after 20 min of carbonation. The results are depicted in Figure 11. In the lower panel of this figure is the DTG curves for pure MgCO_3 and $\text{Mg}(\text{OH})_2$. Clearly, the carbonate precipitates formed from the leachate rich in Mg^{2+} (i.e., $\text{Mg}^{2+}/\text{Ca}^{2+} = 1$ and 2) show the closer resemblance with $\text{Mg}(\text{OH})_2$ in terms of the decomposition temperatures, implying the strong hydration extent of these precipitate. The peak for MgCO_3 is rather small, suggestive of the minor content for this crystal species in these precipitates. Moreover, the mass loss curves for each $\text{Mg}^{2+}/\text{Ca}^{2+}$ ratio are close in decomposition temperatures but different in the weight loss, suggesting the presence of different moles of CO_2 and H_2O molecules in the solid precipitates. The weight loss between temperatures of ~600–800 °C is contributed mainly by the decomposition of CaCO_3 .⁵³ Increasing the $\text{Mg}^{2+}/\text{Ca}^{2+}$ ratio slightly reduced the calcium carbonate decomposition temperature, which should be attributed to the association of calcite with magnesium. At this temperature range, the weight loss percentage for the case of the $\text{Mg}^{2+}/\text{Ca}^{2+}$ ratio equaling 1:2 is most significant as a result of the presence of a larger amount of calcium carbonate polymorphs along with calcium-carbonate-rich magnesian calcite in the solid residue. For the broad temperature range of ~200–600 °C, it can be due to the release of chemically bound water or carbon dioxide from a general formula of $(\text{MgO})_x(\text{CO}_2)_y(\text{H}_2\text{O})_n$ for hydrated Mg carbonates in the amorphous form. The large discrepancy between Q-XRD and XRF in the quantification of the MgO content, as tabulated in Table 5, confirmed the abundance of amorphous Mg-bearing species that cannot be detected by XRD.

Three major peaks were observed for the precipitate from the case of the $\text{Mg}^{2+}/\text{Ca}^{2+}$ ratio of 2:1. These temperatures closely resemble the presence of nesquehonite ($\text{MgCO}_3 \cdot 3\text{H}_2\text{O}$). For nesquehonite, the first peak observed at around 200 °C was attributed to the loss of two water molecules of water. Another endothermic peak detected at 440 °C is related to the loss of the remaining water molecule. Finally, at ~550 °C, decarbonation of magnesium carbonate takes place.⁵⁴

The decomposition curve for the $\text{Mg}^{2+}/\text{Ca}^{2+}$ ratio of 1:1 resembles the presence of hydromagnesite [$\text{Mg}_5(\text{CO}_3)_4(\text{OH})_2 \cdot 4\text{H}_2\text{O}$]. Todor reported that, between 210 and 395 °C, the four water molecules of hydromagnesite are released according to eq 6.



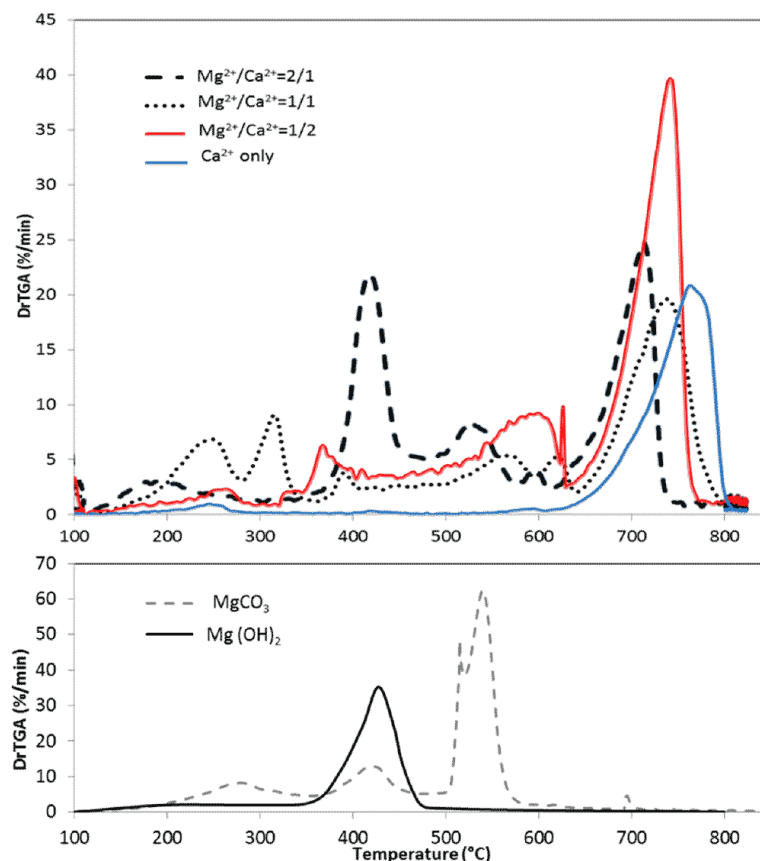
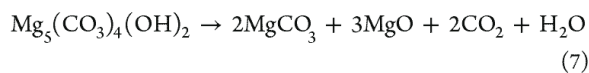


Figure 11. TG–DTG mass loss curves of solid carbonate precipitates compared to pure MgCO_3 and $\text{Mg}(\text{OH})_2$ decomposition after 20 min of reaction time.

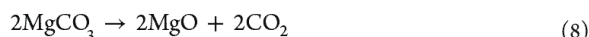
Table 5. Comparison of Q-XRD and XRF Results for the MgO Contents in the Carbonate Precipitates Formed from Different $\text{Mg}^{2+}/\text{Ca}^{2+}$ Ratios at 30 min of Reaction Time

$\text{Mg}^{2+}/\text{Ca}^{2+}$ ratio	XRF (wt %)	Q-XRD (wt %)	χ^2 value for Q-XRD
$\text{Mg}^{2+}/\text{Ca}^{2+} = 2:1$	59.8	7.18	36.14
$\text{Mg}^{2+}/\text{Ca}^{2+} = 1:1$	33.5	6.7	23.84
$\text{Mg}^{2+}/\text{Ca}^{2+} = 1:2$	28.9	5.5	17.01

Following the loss of the four water molecules, the loss of a carbon dioxide molecule occurs between 395 and 460 °C, which is further followed by a reorganization of the crystal structure. Between 460 and 515 °C, a fifth molecule of water is released as a result of the decomposition of the hydroxide group and a further carbon dioxide molecule.



Finally, over the temperature range of 515–640 °C, further two carbon dioxide molecules are released to leave a magnesium oxide residue.⁵⁵



3.3. Effect of the Temperature on Carbonation. Figure 12 illustrates the influence of the temperature on the precipitation rate of two cations for the $\text{Mg}^{2+}/\text{Ca}^{2+}$ molar ratio of 1. For each cation, its precipitation rate was increased remarkably upon the elevation of the carbonation temperature. In comparison to the duration of 30 min required at room

temperature, the completion of carbonation was shortened to 20 min at the other three temperatures. However, for the three high temperatures tested, the carbonation rate of each cation was not increased monotonically upon the rise of the reaction temperature. For Mg^{2+} shown in Figure 12a, its carbonation rate was maximized at 60 °C and slightly reduced at 80 °C, especially before the residence time of 10 min. A similar phenomenon was observed for Ca^{2+} for a maximum carbonation rate at 60 °C, as evident in Figure 12b. This is consistent with our previous observation using coal fly-ash-derived leachate.⁸ The reaction temperature affects several parameters, including the reaction rate and CO_2 solubility, simultaneously. Although the carbonation reaction rate is favored upon the rise of the reaction temperature, the solubility of CO_2 decreases oppositely. Moreover, because of the exothermicity of the carbonation reaction, the equilibrium constant based on Le Chatelier's principle is decreased upon the elevation of the temperature.⁵⁶ To further quantitatively compare the precipitation rates of two cations at different temperatures, $1/\tau_{50}$ as the reverse of the reaction time required to reach a 50 wt % precipitation extent was plotted versus the temperature and shown in Figure 13. This figure indicates that, except room temperature, the rate of Ca^{2+} is nearly 2 times higher than that of Mg^{2+} at each of the other three temperatures.

3.4. Characterization of the Solid Precipitate at Different Temperatures. The time-dependent composition of carbonate precipitates at different temperatures is illustrated in panels a–d of Figure 14. This figure shows that, in

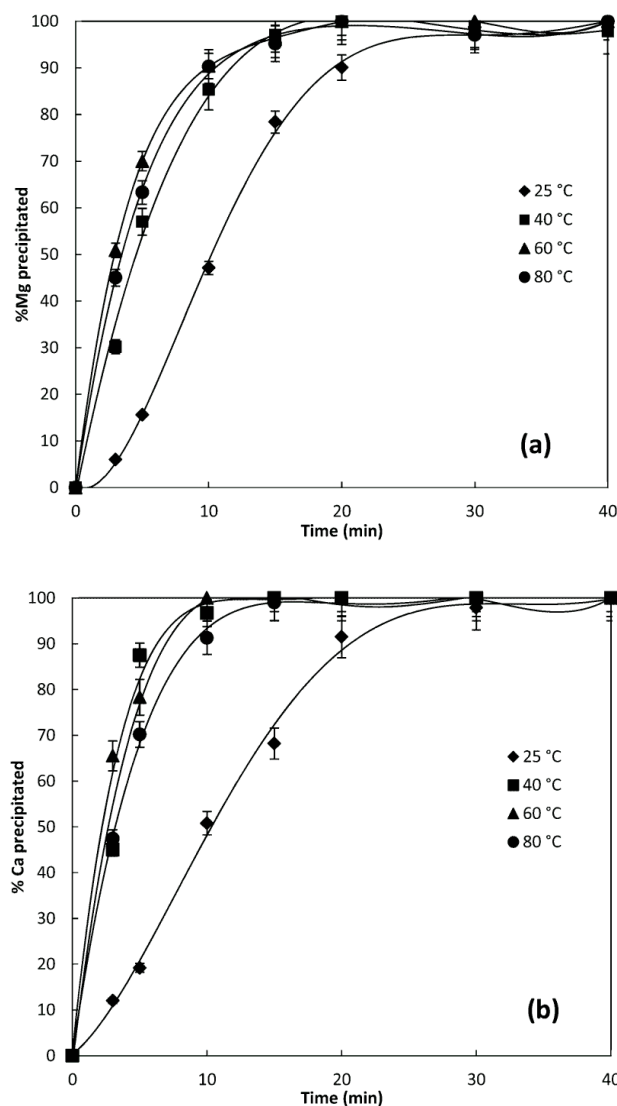


Figure 12. Effect of the temperature and time on (a) Mg and (b) Ca carbonation for case 3 ($\text{Mg}^{2+}/\text{Ca}^{2+}$ equal to 1:1).

comparison to the reaction time, increasing the carbonation temperature is more influential in altering the mineral speciation. Figure 15 further plots the variation of the percentages of individual species as a function of the reaction temperature, with the time fixed at 10 min. Increasing the temperature led to the loss of crystals and the transformation of crystals to the amorphous phase. For the dominant calcite formed at room temperature, the decrease in its amount is accompanied by the increase in the fraction of its counterpart, aragonite, which exhibits the highest amount at 60 °C. This indicates the reordering of the calcium carbonate crystal lattice structure at the elevated temperatures. In comparison to calcite bearing a trigonal-rhombohedral structure, aragonite is in an orthorhombic system with acicular crystals and easily fragile as well. Such an observation has also been confirmed by Rodriguez-Blanco et al., who have confirmed that, at temperatures of <30 °C, pure amorphous calcium carbonate (ACC) converts into calcite via vaterite, while at temperatures of >40 °C, pure ACC is prone to transfer into aragonite via vaterite.⁵⁷ Another obvious change is the reduction on the amount of

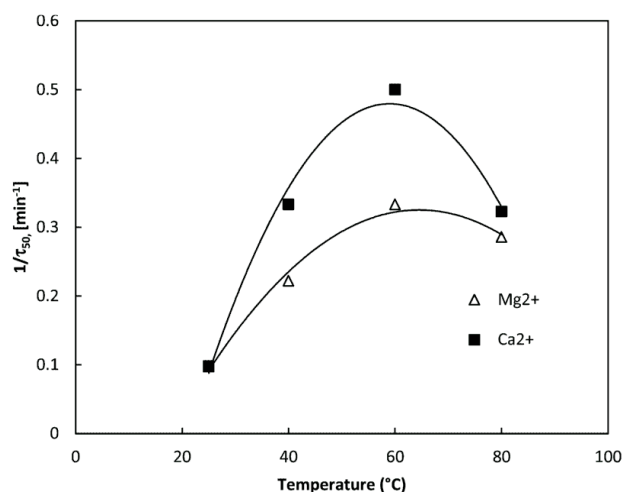


Figure 13. Influence of the temperature on $1/\tau_{50}$ (carbonation rate to achieve 50 wt % precipitation extents) of two cations at a molar ratio of 1 in solution.

magnesian calcite upon the rise of the reaction temperature up to 60 °C. Such a change should be partially caused by the above-mentioned change on the lattice structure of calcium carbonate. The lattice structure of aragonite is not easily accessible to Mg^{2+} .³⁸ Consequently, the carbonation of Mg^{2+} alone is promoted, which has the propensity to form an amorphous structure, as discussed before. Apparently, at 60 °C, the formation of aragonite and amorphous Mg-bearing carbonates are the main reasons for achieving the highest carbonation rate at this temperature.

4. CONCLUSION

This paper has investigated the competition between Ca^{2+} and Mg^{2+} ions during the mild carbonation process and its impacts on the optimum conditions and carbonate precipitate structure. The major conclusions can be drawn as follows: (1) Under the ambient conditions, an initial pH of ~11 and CO_2 flow rate of 15 L min^{-1} (large enough to eliminate the diffusion resistance in this study), the carbonation of sole Ca^{2+} or Mg^{2+} can be completed in 10 and 30 min, respectively. Upon the blending of two cations and the increase in the $\text{Mg}^{2+}/\text{Ca}^{2+}$ molar ratio, the carbonation time for Ca^{2+} was increased. In contrast, the time was shortened noticeably for Mg^{2+} . In terms of the carbonation reactivity, the reactivity of Ca^{2+} was decreased linearly upon increasing the $\text{Mg}^{2+}/\text{Ca}^{2+}$ ratio, whereas Mg^{2+} achieved its maximum reactivity at the $\text{Mg}^{2+}/\text{Ca}^{2+}$ molar ratio of 2. This is due to the trapping of Mg^{2+} into the calcite lattice to form magnesian calcite. (2) With regard to the structure of carbonation precipitate, the metastable phase of vaterite is predominant for the case of sole Ca^{2+} , which is mainly formed upon the shell damage of aragonite. The amorphous phase accounts for less than 20 wt % of the total carbonate. In contrast, the carbonate formed from sole Mg^{2+} is mainly unidentifiable upon XRD speciation, which is presumably hydromagnesite. The blending of Ca^{2+} and Mg^{2+} induced the formation of magnesian calcite caused by the substitution of a portion of Ca^{2+} by Mg^{2+} in the calcite lattice. The formation of this complex is also favored upon increasing the $\text{Ca}^{2+}/\text{Mg}^{2+}$ molar ratio. (3) Increasing the temperature is in favor of the carbonation of both ions, particularly Ca^{2+} before 60 °C. The increase of the temperature from 60 °C results in the reduction

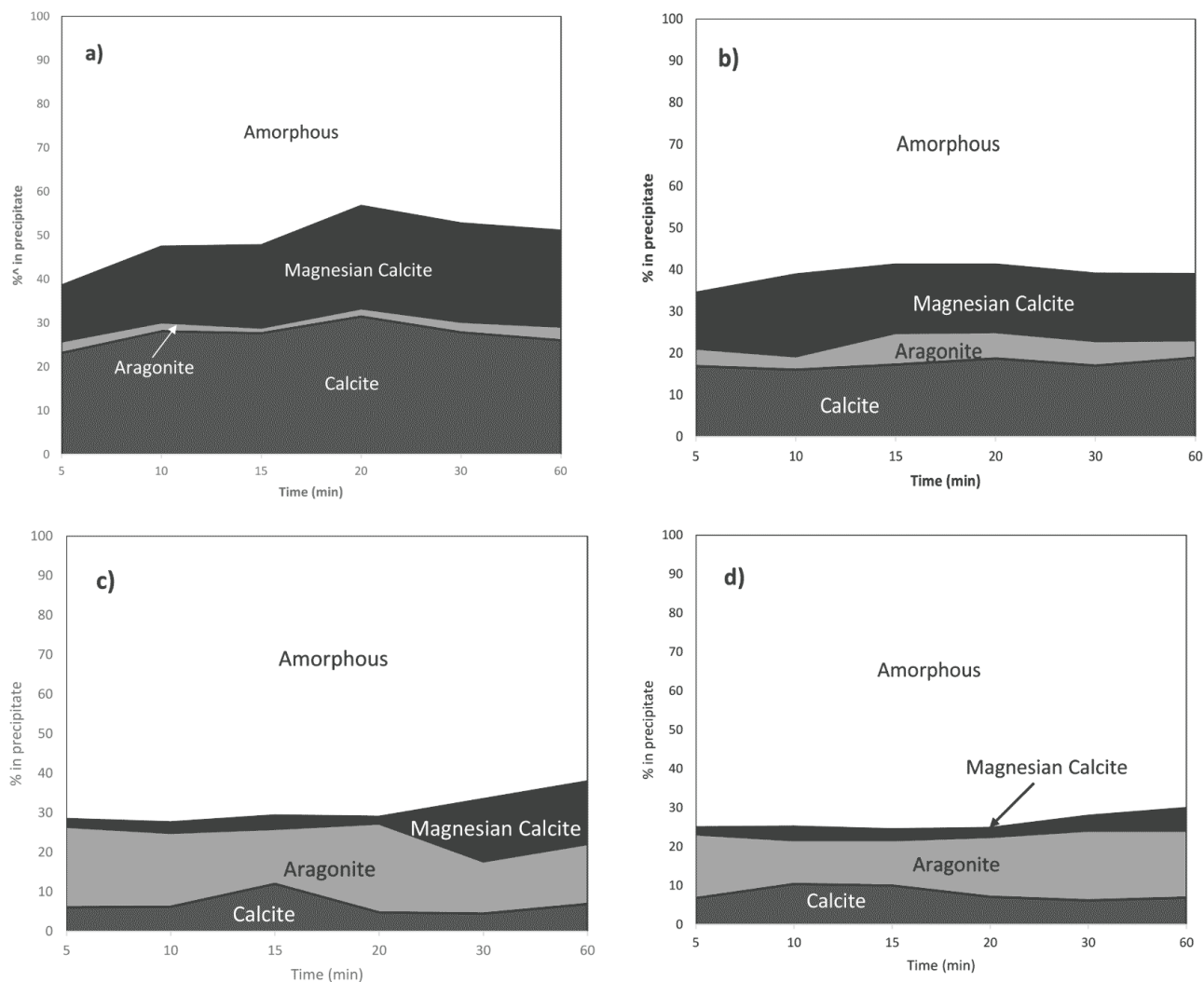


Figure 14. Solid precipitate composition of carbonation of $\text{Mg}^{2+}/\text{Ca}^{2+} = 1:1$ at different temperatures: (a) 25 °C, (b) 40 °C, (c) 60 °C, and (d) 80 °C, calculated by Q-XRD and an internal standard method.

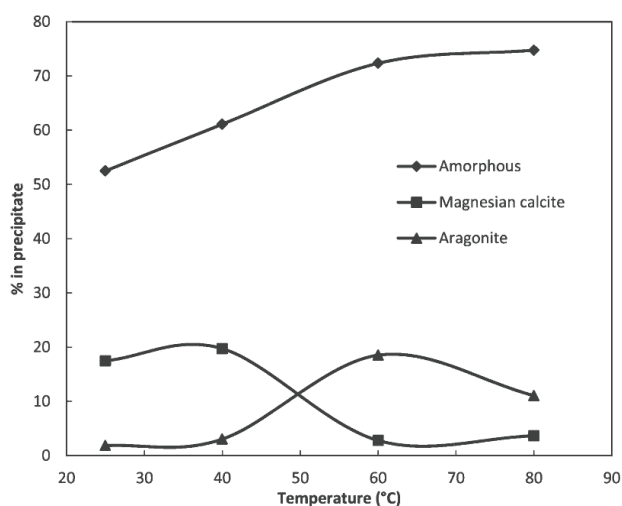


Figure 15. Mass fractions of amorphous, magnesian calcite, and aragonite in the solid precipitate as a function of the temperature at the fixed reaction time of 10 min.

of the carbonation reactivity of Mg^{2+} as a result of the decreased solubility of CO_2 . Upon the elevation of the reaction temperature, the Ca-bearing carbonate changes its crystal from trigonal-rhombohedral calcite to orthorhombic aragonite. Resulting aragonite is not in favor of the formation of magnesian calcite. As a result, the amorphous structure dominated by Mg^{2+} is dominant in the high-temperature carbonate precipitate.

■ ASSOCIATED CONTENT

Supporting Information

The Supporting Information is available free of charge on the ACS Publications website at DOI: 10.1021/acs.energyfuels.Sb01609.

Extra explicit details on the Q-XRD methods (PDF)

■ AUTHOR INFORMATION

Corresponding Author

*Telephone: +61-3-9905-2592. Fax: +61-3-9905-5686. E-mail: lian.zhang@monash.edu.

Notes

The authors declare no competing financial interest.

ACKNOWLEDGMENTS

This project is supported by the Faculty of Engineering of Monash University for a 2013–2014 seed grant. The first author is also grateful to Monash Research Graduate School (MRGS) for a Ph.D. scholarship. A CSIRO Flagship scholarship fund is gratefully acknowledged for additional support. The authors also thank Dashen Dong and Wang Zhao for their contribution to the Q-XRD reliability confirmation experiments.

REFERENCES

- (1) Lackner, K. S.; Wendt, C. H.; Butt, D. P.; Joyce, E. L.; Sharp, D. H. Carbon dioxide disposal in carbonate minerals. *Energy* **1995**, *20*, 1153–1170.
- (2) Baciocchi, R.; Polettini, A.; Pomi, R.; Prigiobbe, V.; Von Zedwitz, V. N.; Steinfeld, A. CO₂ sequestration by direct gas-solid carbonation of air pollution control (APC) residues. *Energy Fuels* **2006**, *20*, 1933–1940.
- (3) Hänchen, M.; Prigiobbe, V.; Storti, G.; Seward, T. M.; Mazzotti, M. Dissolution kinetics of forsteritic olivine at 90 – 150 °C including effects of the presence of CO₂. *Geochim. Cosmochim. Acta* **2006**, *70*, 4403–4416.
- (4) Mayoral, M. C.; Andrés, J. M.; Gimeno, M. P. Optimization of mineral carbonation process for CO₂ sequestration by lime-rich coal ashes. *Fuel* **2013**, *106*, 448–454.
- (5) Jo, H. Y.; Kim, J. H.; Lee, Y. J.; Lee, M.; Choh, S. J. Evaluation of factors affecting mineral carbonation of CO₂ using coal fly ash in aqueous solutions under ambient conditions. *Chem. Eng. J.* **2012**, *183*, 77–87.
- (6) Wee, J. H. A review on carbon dioxide capture and storage technology using coal fly ash. *Appl. Energy* **2013**, *106*, 143–151.
- (7) Hosseini, T.; Selomulya, C.; Haque, N.; Zhang, L. Indirect carbonation of Victorian brown coal fly ash for CO₂ sequestration: Multiple-cycle leaching-carbonation and magnesium leaching kinetic modeling. *Energy Fuels* **2014**, *28* (10), 6481–6493.
- (8) Sun, Y.; Parikh, V.; Zhang, L. Sequestration of carbon dioxide by indirect mineralization using Victorian brown coal fly ash. *J. Hazard. Mater.* **2012**, *209–210*, 458–466.
- (9) Montes-Hernandez, G.; Pérez-López, R.; Renard, F.; Nieto, J. M.; Charlet, L. Mineral sequestration of CO₂ by aqueous carbonation of coal combustion fly-ash. *J. Hazard. Mater.* **2009**, *161* (2–3), 1347–1354.
- (10) Nyambura, M. G.; Mugeru, W. G.; Felicia, P. L.; Gathura, N. P. Carbonation of brine impacted fractionated coal fly ash: implications for CO₂ sequestration. *J. Environ. Manage.* **2011**, *92*, 655–664.
- (11) Sun, Y.; Yao, M. S.; Zhang, J. P.; Yang, G. Indirect CO₂ mineral sequestration by steelmaking slag with NH₄Cl as leaching solution. *Chem. Eng. J.* **2011**, *173* (2), 437–445.
- (12) Uliasz-Bochenczyk, A.; Mokrzycki, E.; Piotrowski, Z.; Pomykała, R. Estimation of CO₂ sequestration potential via mineral carbonation in fly ash from lignite combustion in Poland. *Energy Procedia* **2009**, *1*, 4873–4879.
- (13) Pundsack, F. L.; Somerville, N. J. *Recovery of Silica, Iron Oxide and Magnesium Carbonate from the Treatment of Serpentine with Ammonium Bisulfate*; Johns-Manville Corporation: New York, 1963.
- (14) Kodama, S.; Nishimoto, T.; Yamamoto, N.; Yogo, K.; Yamada, K. Development of a new pH-swing CO₂ mineralization process with a recyclable reaction solution. *Energy* **2008**, *33* (5), 776–784.
- (15) Jo, H. Y.; Ahn, J. H.; Jo, H. Evaluation of the CO₂ sequestration capacity for coal fly ash using a flow-through column reactor under ambient conditions. *J. Hazard. Mater.* **2012**, *241–242*, 127–136.
- (16) Dri, M.; Sanna, A.; Maroto-Valer, M. Dissolution of steel slag and recycled concrete aggregate in ammonium bisulfate for CO₂ mineral carbonation. *Fuel Process. Technol.* **2013**, *113*, 114–122.
- (17) Huijgen, W. J. J.; Comans, R. N. J. Carbonation of steel slag for CO₂ sequestration: Leaching of products and reaction mechanisms. *Environ. Sci. Technol.* **2006**, *40*, 2790–2796.
- (18) Teir, S.; Eloneva, S.; Fogelholm, C. J.; Zevenhoven, R. Dissolution of steelmaking slags in acetic acid for precipitated calcium carbonate production. *Energy* **2007**, *32*, 528–539.
- (19) Wang, W.; Liu, X.; Wang, P.; Zheng, Y.; Wang, M. Enhancement of CO₂ mineralization in Ca²⁺/Mg²⁺-rich aqueous solutions using insoluble amine. *Ind. Eng. Chem. Res.* **2013**, *52*, 8028–8033.
- (20) Ainscow, W. S.; Gadgil, B. B. Process for producing magnesium oxide. U.S. Patent 4,720,375 A, Jan 19, 1988.
- (21) Roques, H.; Girou, A. Kinetics of the formation conditions of carbonate tartars. *Water Res.* **1974**, *8*, 907–920.
- (22) Reddy, M. M.; Nancollas, G. H. The crystallization of calcium carbonate: iv. The effect of magnesium, strontium and sulfate ions. *J. Cryst. Growth* **1976**, *35*, 33–38.
- (23) Kitano, Y. A study of the polymorphic formation of calcium carbonate in thermal springs with an emphasis on the effect of temperature. *Bull. Chem. Soc. Jpn.* **1962**, *35*, 1980–1985.
- (24) Bischoff, J. L.; Fyfe, W. S. Catalysis, inhibition and the calcite-aragonite problem. *Am. J. Sci.* **1968**, *266*, 65–79.
- (25) Yoo, K.; Kim, B. S.; Kim, M. S.; Lee, J. C.; Jeong, J. Dissolution of Magnesium from Serpentine Mineral in Sulfuric Acid Solution. *Mater. Trans.* **2009**, *50*, 1225–1230.
- (26) Rendek, E.; Ducom, G.; Germain, P. Carbon dioxide sequestration in municipal solid waste incinerator (MSWI) bottom ash. *J. Hazard. Mater.* **2006**, *128*, 73–79.
- (27) Winburn, R. S.; Grier, D. G.; McCarthy, G. J.; Peterson, R. B. Rietveld quantitative X-ray diffraction analysis of NIST fly ash standard reference materials. *Powder Diffr.* **2000**, *15* (3), 163–172.
- (28) Hillier, S. Accurate quantitative analysis of clay and other minerals in sandstones by XRD; comparison of a Rietveld and a reference intensity ratio (RIR) method and the importance of sample preparation. *Clay Miner.* **2000**, *35* (1), 291–302.
- (29) Ward, C. R.; Taylor, J. C.; Cohen, D. R. Quantitative mineralogy of sandstones by x-ray diffractometry and normative analysis. *J. Sediment. Res.* **1999**, *69* (5), 1050–1062.
- (30) Williams, R. P.; Van Riessen, A. Determination of the reactive component of fly ashes for geopolymer production using XRF and XRD. *Fuel* **2010**, *89* (12), 3683–3692.
- (31) Chancey, R. T.; Stutzman, P.; Juenger, M. C. G.; Fowler, D. W. Comprehensive phase characterization of crystalline and amorphous phases of a Class F fly ash. *Cem. Concr. Res.* **2010**, *40* (1), 146–156.
- (32) Ward, C. R.; Taylor, J. C. Quantitative mineralogical analysis of coals from the Callide Basin, Queensland, Australia using X-ray diffractometry and normative interpretation. *Int. J. Coal Geol.* **1996**, *30* (3), 211–229.
- (33) Chang, E.-E.; Chen, C.-H.; Chen, Y.-H.; Pan, S.-Y.; Chiang, P.-C. Performance evaluation for carbonation of steel-making slags in a slurry reactor. *J. Hazard. Mater.* **2011**, *186*, 558–564.
- (34) United States Environmental Protection Agency (U.S. EPA). *Exposure Assessment Model: MINTEQ2*; U.S. EPA: Washington, D.C., 1993.
- (35) Drever, J. I. *The Geochemistry of Natural Waters: Surface and Groundwater Environments*, 3rd ed.; Prentice Hall: Upper Saddle River, NJ, 1997.
- (36) Fernandez-Diaz, L.; Putnis, A. The role of magnesium in the crystallization of calcite and aragonite in a porous medium. *J. Sediment. Res.* **1996**, *66* (3), 482–491.
- (37) Althoff, P. L. Structural refinements of dolomite and a magnesium calcite and implications for dolomite formation in the marine environment. *Am. Mineral.* **1977**, *62* (7–8), 772–783.
- (38) Boyd, V.; Yoon, H.; Zhang, C.; Oostrom, M.; Hess, N.; Fouke, B.; Valocchi, A. J.; Werth, C. J. Influence of Mg²⁺ on CaCO₃ precipitation during subsurface reactive transport in a homogeneous silicon-etched pore network. *Geochim. Cosmochim. Acta* **2014**, *135*, 321–335.

- (39) Kaczmarek, S. E.; Sibley, D. F. On the evolution of dolomite stoichiometry and cation order during high-temperature synthesis experiments: an alternative model for the geochemical evolution of natural dolomites. *Sediment. Geol.* **2011**, *240*, 30–40.
- (40) Hanchen, M.; Prigiobbe, V.; Baciocchi, R.; Mazzotti, M. Precipitation in the Mg-carbonate system-effects of temperature and CO₂ pressure. *Chem. Eng. Sci.* **2008**, *63*, 1012.
- (41) Botha, A.; Strydom, C. A. Preparation of a magnesium hydroxy carbonate from magnesium hydroxide. *Hydrometallurgy* **2001**, *62*, 175–183.
- (42) Botha, A.; Strydom, C. A. DTA and FT-IR analysis of the rehydration of basic magnesium carbonate. *J. Therm. Anal. Calorim.* **2003**, *71*, 987–996.
- (43) Swanson, E. J.; Fricker, K. J.; Sun, M.; Park, A.-H. A. Directed Precipitation of Hydrated and Anhydrous Magnesium Carbonates for Carbon Storage. *Phys. Chem. Chem. Phys.* **2014**, *16*, 23440–23450.
- (44) Fyfe, W. S. *Geochemistry of Solids*; McGraw-Hill: New York, 1964.
- (45) Toby, H. B. R factors in Rietveld analysis: How good is good enough? *Powder Diffr.* **2006**, *21* (1), 67–70.
- (46) Morse, J. W.; Arvidson, R. S.; Lüttge, A. Calcium carbonate formation and dissolution. *Chem. Rev.* **2007**, *107* (2), 342–382.
- (47) St. Arnaud, R. J.; Herbillon, A. J. Occurrence and genesis of secondary magnesium-bearing calcite in soils. *Geoderma* **1973**, *9*, 279–298.
- (48) Xu, J.; Yan, C.; Zhang, F.; Konishi, H.; Xu, H.; Teng, H. H. Testing the cation-hydration effect on the crystallization of Ca–Mg–CO₃ systems. *Proc. Natl. Acad. Sci. U. S. A.* **2013**, *110*, 17750–17755.
- (49) Santos, R. M.; Van Bouwel, J.; Vandeveld, E.; Mertens, G.; Elsen, J.; Van Gerven, T. Accelerated mineral carbonation of stainless steel slags for CO₂ storage and waste valorization: Effect of process parameters on geochemical properties. *Int. J. Greenhouse Gas Control* **2013**, *17*, 32–45.
- (50) Long, X.; Ma, Y.; Qi, L. In vitro synthesis of high Mg calcite under ambient conditions and its implication for biomineralization process. *Cryst. Growth Des.* **2011**, *11*, 2866–2873.
- (51) *Ion Partitioning in Ambient-Temperature Aqueous Systems*; Prieto, M., Stoll, H., Eds.; Mineralogical Society: Twickenham, U.K., 2011; EMU Notes in Mineralogy, Vol. 10, ISBN: 978-0903056-26-7.
- (52) Ma, Y. R.; Cohen, S. R.; Addadi, L.; Weiner, S. Sea urchin tooth design: an “all-calcite” polycrystalline reinforced fiber composite for grinding rocks. *Adv. Mater.* **2008**, *20*, 1555–1559.
- (53) Vassilev, S. V.; Vassileva, C. G. Central methods for characterization of composition of fly ashes from coal-fired power stations: A critical overview. *Energy Fuels* **2005**, *19*, 1084–1098.
- (54) Lanás, J.; Alvarez, J. I. Dolomitic lime: thermal decomposition of nesquehonite. *Thermochim. Acta* **2004**, *421*, 123–132.
- (55) Todor, D. N. *Thermal Analysis of Minerals*; Abacus Press: Kent, U.K., 1976.
- (56) Chang, E. E.; Pan, S. Y.; Chen, Y. H.; Tan, C. S.; Chiang, P. C. Accelerated carbonation of steelmaking slags in a high-gravity rotating packed bed. *J. Hazard. Mater.* **2012**, *227–228*, 97–106.
- (57) Rodriguez-Blanco, J. D.; Shaw, S.; Benning, L. G. The kinetics and mechanisms of amorphous calcium carbonate (ACC) crystallization to calcite, via vaterite. *Nanoscale* **2011**, *3*, 265–271.